

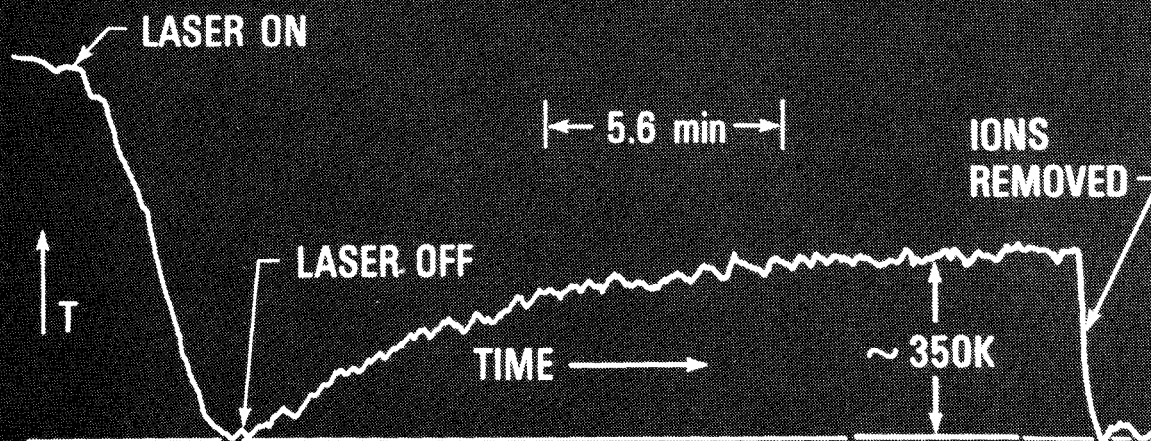


NBS TECHNICAL NOTE 1086

U.S. DEPARTMENT OF COMMERCE / National Bureau of Standards

Trapped Ions and Laser Cooling

Selected publications of the Ion Storage Group of the Time and Frequency Division, NBS, Boulder, Colorado



Edited by
David J. Wineland
Wayne M. Itano
James C. Bergquist
John J. Bollinger

T

he National Bureau of Standards¹ was established by an act of Congress on March 3, 1901. The Bureau's overall goal is to strengthen and advance the nation's science and technology and facilitate their effective application for public benefit. To this end, the Bureau conducts research and provides: (1) a basis for the nation's physical measurement system, (2) scientific and technological services for industry and government, (3) a technical basis for equity in trade, and (4) technical services to promote public safety. The Bureau's technical work is performed by the National Measurement Laboratory, the National Engineering Laboratory, the Institute for Computer Sciences and Technology, and the Center for Materials Science.

The National Measurement Laboratory

Provides the national system of physical and chemical measurement; coordinates the system with measurement systems of other nations and furnishes essential services leading to accurate and uniform physical and chemical measurement throughout the Nation's scientific community, industry, and commerce; provides advisory and research services to other Government agencies; conducts physical and chemical research; develops, produces, and distributes Standard Reference Materials; and provides calibration services. The Laboratory consists of the following centers:

- Basic Standards²
- Radiation Research
- Chemical Physics
- Analytical Chemistry

The National Engineering Laboratory

Provides technology and technical services to the public and private sectors to address national needs and to solve national problems; conducts research in engineering and applied science in support of these efforts; builds and maintains competence in the necessary disciplines required to carry out this research and technical service; develops engineering data and measurement capabilities; provides engineering measurement traceability services; develops test methods and proposes engineering standards and code changes; develops and proposes new engineering practices; and develops and improves mechanisms to transfer results of its research to the ultimate user. The Laboratory consists of the following centers:

- Applied Mathematics
- Electronics and Electrical Engineering²
- Manufacturing Engineering
- Building Technology
- Fire Research
- Chemical Engineering²

The Institute for Computer Sciences and Technology

Conducts research and provides scientific and technical services to aid Federal agencies in the selection, acquisition, application, and use of computer technology to improve effectiveness and economy in Government operations in accordance with Public Law 89-306 (40 U.S.C. 759), relevant Executive Orders, and other directives; carries out this mission by managing the Federal Information Processing Standards Program, developing Federal ADP standards guidelines, and managing Federal participation in ADP voluntary standardization activities; provides scientific and technological advisory services and assistance to Federal agencies; and provides the technical foundation for computer-related policies of the Federal Government. The Institute consists of the following centers:

- Programming Science and Technology
- Computer Systems Engineering

The Center for Materials Science

Conducts research and provides measurements, data, standards, reference materials, quantitative understanding and other technical information fundamental to the processing, structure, properties and performance of materials; addresses the scientific basis for new advanced materials technologies; plans research around cross-country scientific themes such as nondestructive evaluation and phase diagram development; oversees Bureau-wide technical programs in nuclear reactor radiation research and nondestructive evaluation; and broadly disseminates generic technical information resulting from its programs. The Center consists of the following Divisions:

- Inorganic Materials
- Fracture and Deformation³
- Polymers
- Metallurgy
- Reactor Radiation

¹Headquarters and Laboratories at Gaithersburg, MD, unless otherwise noted; mailing address Gaithersburg, MD 20899.

²Some divisions within the center are located at Boulder, CO 80303.

³Located at Boulder, CO, with some elements at Gaithersburg, MD.

Trapped Ions and Laser Cooling

Selected publications of the Ion Storage Group of the Time and Frequency Division, NBS, Boulder, Colorado

Edited by
David J. Wineland
Wayne M. Itano
James C. Bergquist
John J. Bollinger

Time and Frequency Division
Center for Basic Standards
National Measurement Laboratory
National Bureau of Standards
Boulder, Colorado 80303

Supported in part by
U.S. Office of Naval Research
800 North Quincy
Arlington, VA 22217
and
U.S. Air Force Office of Scientific Research
Bolling Air Force Base, DC 20332



U.S. DEPARTMENT OF COMMERCE, Malcolm Baldrige, Secretary

NATIONAL BUREAU OF STANDARDS, Ernest Ambler, Director

Issued June 1985

National Bureau of Standards Technical Note 1086
Natl. Bur. Stand. (U.S.), Tech Note 1086, 192 pages (July 1985)
CODEN: NBTNAE

U.S. GOVERNMENT PRINTING OFFICE
WASHINGTON: 1985

For sale by the Superintendent of Documents, U.S. Government Printing Office, Washington, DC 20402

PREFACE

This collection of papers represents the work on stored atomic ions (initiated in the Fall of 1977) by the Time and Frequency Division of the National Bureau of Standards. Although the primary goal of this research has been the development of techniques necessary for achieving better time and frequency standards, we have also been able to investigate related areas of research.

Papers 15, 20, 21, 24, 25, A5, A8 and A13 were intended to be more general reviews of the subject and include discussion of experiments by other groups. Papers listed with the prefix A are not included here but can be obtained on request. We intend to update this publication periodically to include new work not contained here. We hope this collection of papers will be useful to our colleagues in this and related fields.

We gratefully acknowledge the support of the U.S. Office of Naval Research and the U.S. Air Force Office of Scientific Research.

David J. Wineland
Wayne M. Itano
James C. Bergquist
John J. Bollinger

Boulder, Colorado
July 1985

CONTENTS

		Page
1.	"Radiation-Pressure Cooling of Bound Resonant Absorbers," D. J. Wineland, R. E. Drullinger, and F. L. Walls.....	TN-1
2.	"Laser Cooling of Atoms," D. J. Wineland and W. M. Itano.....	TN-5
3.	"Laser-to-Microwave Frequency Division Using Synchrotron Radiation," D. J. Wineland.....	TN-25
4.	"Laser to Microwave Frequency Division Using Synchrotron Radiation II," J. C. Bergquist and D. J. Wineland.....	TN-30
5.	"Frequency and Time Standards Utilizing Laser Cooled Ions," W. M. Itano and D. J. Wineland.....	TN-34
6.	"Laser Induced Magnetron Compression (Expansion) of Ions Stored in a Penning Trap," D.J. Wineland, R.E. Drullinger, J.C. Bergquist, and W.M. Itano..	TN-35
7.	"High-Resolution Optical Spectra of Laser Cooled Ions," R. E. Drullinger, D. J. Wineland, and J. C. Bergquist.....	TN-36
8.	"Double-Resonance and Optical-Pumping Experiments on Electromagnetically Confined, Laser Cooled Ions," D.J. Wineland, J.C. Bergquist, W.M. Itano, and R.E. Drullinger..	TN-40
9.	"Spectroscopy of a Single Mg^+ Ion," D. J. Wineland and W. M. Itano.....	TN-43
10.	"Proposed Stored $^{201}Hg^+$ Ion Frequency Standards," D. J. Wineland, W. M. Itano, J. C. Bergquist, and F. L. Walls...	TN-47
11.	"Precision Measurement of the Ground-State Hyperfine Constant of $^{25}Mg^+$," W. M. Itano and D. J. Wineland.....	TN-57
12.	"Laser Cooling of Ions Stored in Harmonic and Penning Traps," W. M. Itano and D. J. Wineland.....	TN-67
13.	"Shift of $^2S_{1/2}$ Hyperfine Splittings Due to Blackbody Radiation," W. M. Itano, L. L. Lewis, and D. J. Wineland.....	TN-87
14.	"Laser Cooled, Stored Ion Experiments at NBS and Possible Applications to Microwave and Optical Frequency Standards," D. J. Wineland, J. C. Bergquist, R. E. Drullinger, H. Hemmati, W. M. Itano, and F. L. Walls.....	TN-90

	Page
15. "Spectroscopy of Stored Ions," D. J. Wineland.....	TN-97
16. "Magnetic Field Dependence of (s,ℓ) Electron Configurations," D. J. Wineland and W. M. Itano.....	TN-107
17. "Laser Cooling and Double Resonance Spectroscopy of Stored Ions," W. M. Itano and D. J. Wineland.....	TN-108
18. "Generation of Continuous-Wave 194-nm Radiation by Sum- Frequency Mixing in an External Ring Cavity," H. Hemmati, J. C. Bergquist, and W. M. Itano.....	TN-117
19. "Laser Fluorescence Mass Spectroscopy," D. J. Wineland, J. J. Bollinger, and W. M. Itano.....	TN-120
20. "Time and Frequency Standards Based on Charged Particle Trapping," W. M. Itano, D. J. Wineland, H. Hemmati, J. C. Bergquist, and J. J. Bollinger.....	TN-125
21. "Frequency Standard Research Using Stored Ions," D. J. Wineland, W. M. Itano, J. C. Bergquist, J. J. Bollinger, and H. Hemmati.....	TN-128
22. "Precision Measurements of Laser Cooled ${}^9\text{Be}^+$ Ions," J. J. Bollinger, D. J. Wineland, W. M. Itano, and J. S. Wells...	TN-132
23. "Hyperfine Structure of the $2p^2P_{1/2}$ State in ${}^9\text{Be}^+$," J. J. Bollinger, J. S. Wells, D. J. Wineland, and W. M. Itano...	TN-137
24. "Trapped Ions, Laser Cooling, and Better Clocks," D. J. Wineland.....	TN-141
25. "Spectroscopy of Stored Atomic Ions," D. J. Wineland, W. M. Itano, J. C. Bergquist, J. J. Bollinger, and J. D. Prestage.....	TN-147
26. "Strongly Coupled Nonneutral Ion Plasma," J. J. Bollinger and D. J. Wineland.....	TN-172
27. "Laser-Cooled-Atomic Frequency Standard," J. J. Bollinger, J. D. Prestage, W. M. Itano, and D. J. Wineland.....	TN-176
28. "Limits for Spatial Anisotropy by Use of Nuclear-Spin- Polarized ${}^9\text{Be}^+$ Ions," J. D. Prestage, J. J. Bollinger, W. M. Itano, and D. J. Wineland.....	TN-180

Additional publications of the Time and Frequency
Division Ion Storage Group not included in this technical note.

- A1. "New Possibilities for Frequency Standards Using Laser Cooling and Detection of Stored Ions," F. L. Walls, D. J. Wineland, and R. E. Drullinger. Proc. 32nd Annual Symp. on Frequency Control, June 1978, p. 453-459. (Copies available from: Annual Frequency Control Symposium, c/o Electronic Industries Assoc., 2001 Eye St., Washington, DC, 20006).
- A2. "Laser Cooling of Ions Bound to a Penning Trap," R. E. Drullinger and D. J. Wineland, in: Laser spectroscopy IV, Eds. H. Walther and K. W. Rothe, (Springer, Berlin, 1979) p. 66-72. Same title by D. J. Wineland and R. E. Drullinger, Proc. 6th Vavilov Conf. on Non-Linear Optics, Novosibirsk, Springer, June 1979.
- A3. "The Isolated Electron," Philip Ekstrom and David Wineland, Sci. American 243, no. 2, p. 105-121, August 1980.
- A4. "Shift of $^2S_{1/2}$ Hyperfine Splittings Due to Blackbody Radiation and Its Influence on Frequency Standards," Wayne M. Itano, L. L. Lewis, and D. J. Wineland, J. de Physique, Colloque C8, suppl. to no. 12, vol. 42, Dec. 1981, p. C8-283-287.
- A5. "Prospects for Stored Ion Frequency Standards," D. J. Wineland, Proc. 13th Ann. Precise Time and Time Interval (PTTI) Applications and Planning Meeting, Naval Research Laboratory, Washington, DC, Dec. 1981. NASA Conf. Publ. 2220., p. 579-592.
- A6. "Progress Toward a Stored Ion Frequency Standard at NBS," Wayne M. Itano, D. J. Wineland, J. C. Bergquist, and F. L. Walls. Proc. Conf. on Precision Measurements and Fundamental Constants; Gaithersburg, MD June 1981; Precision Measurement and Fundamental Constants II, B.N. Taylor and W. D. Phillips, eds. National Bureau of Standards (US) Spec. Publ. 617 (1984), p. 93-97.
- A7. "High Power Second Harmonic Generation of 257 nm Radiation in an External Ring Cavity," J. C. Bergquist, H. Hemmati, and W. M. Itano, Opt. Commun. 43, 437-442 (1982).
- A8. "High Resolution Spectroscopy of Stored Ions," D. J. Wineland, Wayne M. Itano and R. S. Van Dyck Jr., in Advances in Atomic and Molecular Physics, Vol. 19, ed. by Bederson & Bates, (Academic Press, Aug. 1983), p. 135-186.
- A9. "Laser Cooled $^9\text{Be}^+$ Accurate Clock," J. J. Bollinger, Wayne M. Itano, and D. J. Wineland, Proc. 37th Annual Symp. Freq. Control, 1983, p. 37-41 (copies available from Systematics General Corp., Brinley Plaza, Rt. 38, Wall Township, NJ 07719.)
- A10. "Spectroscopy of Stored Ions Using Fluorescence Techniques," D. J. Wineland, Wayne M. Itano, J. C. Bergquist, and H. Hemmati, S.P.I.E., Vol. 426-Laser Based Ultrasensitive Spectroscopy and Detection V, Society of Photo-Optical Instrumentation Engineers, 1983, p. 65-70.

- A11. "Frequency and Time Standards Based on Stored Ions," J. J. Bollinger, D. J. Wineland, W. M. Itano, J. C. Bergquist and J. D. Prestage, Proc. 16th Ann. Precise Time and Time Interval (PTTI) Applications and Planning Meeting, Naval Research Laboratory, Washington, DC., Dec. 1984, to be published.
- A12. "Measurements of the g_J - Factors of the $6s\ ^2S_{1/2}$ and $6p\ ^2P_{1/2}$ States in $^{198}\text{Hg}^+$," W. M. Itano, J. C. Bergquist, and D. J. Wineland, J. Optical Soc. Am., to be published.
- A13. "Optical Pumping of Stored Atomic Ions," D. J. Wineland, W. M. Itano, J. C. Bergquist, J. J. Bollinger, and J. D. Prestage, Proc. Symp. Alfred Kastler, Paris, Jan. 1985., to be published.
- A14. "Angular Momentum of Trapped Atomic Particles," D. J. Wineland, J. J. Bollinger, W. M. Itano, and J. D. Prestage, J. Opt. Soc. Am. B, Special issue on "The Mechanical Effects of Light", to be published.

Radiation-Pressure Cooling of Bound Resonant Absorbers

D. J. Wineland, R. E. Drullinger, and F. L. Walls

Time and Frequency Division, National Bureau of Standards, Boulder, Colorado 80303

(Received 26 April 1978)

We report the first observation of radiation-pressure cooling on a system of resonant absorbers which are elastically bound to a laboratory fixed apparatus. Mg II ions confined in a Penning electromagnetic trap are cooled to < 40 K by irradiating them with the 8- μ W output of a frequency doubled, single-mode dye laser tuned to the low-frequency side of the Doppler profile on the $^2S_{1/2} \leftarrow ^2P_{3/2}$ ($M_J = +\frac{1}{2} \leftarrow M_J = +\frac{3}{2}$ or $M_J = -\frac{1}{2} \leftarrow M_J = -\frac{3}{2}$) transitions. Cooling to approximately 10^{-3} K should be possible.

Any scheme to improve fundamentally the resolution and accuracy of high-resolution spectroscopy (rf as well as optical) beyond the present limits must incorporate sub-Doppler techniques and a means to suppress substantially the second-order and residual first-order Doppler effects. In the following we report the first experimental evidence that bound absorbers can be cooled via radiation pressure thereby fundamentally reducing both the first- and second-order Doppler effects. The use of radiation pressure for cooling was independently suggested for the case of a gas of neutral atoms¹ and for ions bound in an electromagnetic trap² and has also been incorporated into the suggested schemes for optical trapping.^{3,4} Methods for significantly cooling electrons and ions contained in electromagnetic traps via radiation damping or collisions with cold gas have been known for some time⁵⁻⁷; however, these techniques do not provide cooling of atomic ions much below room temperature. It has recently been demonstrated⁸ that the magnetron motion of electrons in a Penning trap can be cooled by nonlinear excitation of the other degrees of freedom. The method of radiation-pressure cooling demonstrated here offers the possibility to cool substantially all degrees of freedom.

The method is outlined for the case of a harmonically bound resonant absorber (resonance frequency ν_0) which is constrained to move along the x axis. We assume that its velocity is given by $v_x = v_0 \cos 2\pi\nu_0 t$ where ν_0 is its vibrational frequency and that the natural linewidth ($\Delta\nu$) is less than ν_0 . The observed spectrum of the absorber in the laboratory contains the central resonance line with first-order-Doppler-effect-generated sidebands separated by ν_0 having intensity $J_n^2(\nu_0\nu_0/c\nu_0)$ (with n a positive or negative integer) when observed in the direction of motion; here, J_n is the Bessel function of order n . If we irradiate the absorber with photons of frequency $\nu_L = \nu_0$

$+n\nu_0$, the frequencies of the resonantly scattered photons occur at ν_0 and symmetrically around ν_0 at the sideband frequencies $\nu_0 \pm \nu_0, \nu_0 \pm 2\nu_0, \dots$. Therefore, although photons of energy $h(\nu_0 + n\nu_0)$ are absorbed, on the average photons of energy $h\nu_0$ are reemitted; when n is negative, this energy difference causes the kinetic energy of the absorber to decrease by $nh\nu_0$ per scattering event. In our experiments, $\Delta\nu \gg \nu_0$; however, the above conclusion is still valid. An alternative explanation is that when $\nu_L < \nu_0$, the absorber predominantly interacts with the incident radiation when it moves towards the source of radiation and Doppler shifts the frequency into resonance, i.e., when $\nu_L(1 + v_x/c) = \nu_0$. In the absorption process, the photon momentum is first transferred to the absorber causing its momentum to change by h/λ ($\lambda\nu_L = c$) and since the emission occurs symmetrically in the $\pm x$ directions, the net effect is to change the velocity of the absorber by $\Delta v_x = h/M\lambda$ ($M =$ mass of absorber). If $\Delta v_x \ll v_x$, then the kinetic energy of the absorber decreases by an amount $Mv_x \Delta v_x = nh\nu_0$. Through the harmonic binding force, virtually all of the photon recoil momentum is eventually transferred to the "lattice" (trap structure in this case); however, since the mass of this lattice is very large, the energy change occurs in the vibrational motion. Note that, when $\Delta\nu < \nu_0$, scattering of photons with energy $h\nu_0$ is equivalent to the Mössbauer effect.

In our experiments we store approximately 5×10^4 Mg II ions (density approximately $2 \times 10^7/\text{cm}^3$) in a copper Penning trap with hyperbolic electrodes of characteristic dimensions^{5,6} $r_0 = 1.64z_0 = 0.63$ cm. Typical operating parameters are $\nu_0 = 7$ V and $B_0 = 1.3$ T. The motion of an ion in the trap is comprised of a harmonic oscillation along the axial (z) direction (frequency ν_z) plus a composite of circular cyclotron motion (frequency ν_c') superimposed upon a circular magnetron motion (frequency ν_m) in the x - y plane. In the notation of

Byrne and Farago,⁹

$$\begin{aligned} \vec{r} &= x + iy = \vec{r}_c + \vec{r}_m \\ &= \vec{r}_{c_0} \exp(i\omega_c t) + \vec{r}_{m_0} \exp(i\omega_m t), \end{aligned} \quad (1)$$

where $\omega = 2\pi\nu$. For the above operating parameters, $\nu_c \approx 205$ kHz, $\nu_c' \approx 798$ kHz, and $\nu_m \approx 26$ kHz.

The trap apparatus is mounted in an enclosure at high vacuum allowing observed ion thermalization times due to collisions with the background gas as long as 30 min and storage times of approximately 1 day. Mg is emitted from an oven and ions are formed by an electron beam coincident with the trap axis. Because the oven is approximately 0.5 cm from the trap, the temperature of the trap and therefore of the background gas is elevated above room temperature. Thermal motion of the ions induces currents in the trap electrodes yielding a signal proportional to NT (N = ion number, T = ion temperature).^{5,6} Since the time for the cooling experiments is much less than the ion storage time and since observations confirm that the laser does not eject ions from the trap, N can be assumed constant. Therefore the signal provides a direct measurement of ion temperature.

The radiation for the experiments is derived from the frequency-doubled output of a single-mode, c.w., Rhodamine-110 dye laser. In the spectral region of interest (~ 560 nm), this laser has a power output of approximately 250 mW in a 1-MHz bandwidth when pumped with 3 W of 514.5-nm radiation from an Ar⁺ laser. The dye laser can be continuously tuned across 30 GHz and is frequency doubled into the uv with a 90°-phase-matched AD*P (deuterated ammonia dihydrogen phosphate) crystal. This allows us to tune across the ${}^2S_{1/2} \leftarrow {}^2P_{3/2}$ ($M_J = \pm \frac{1}{2} \leftarrow M_J = \pm \frac{3}{2}$) transitions in one sweep. The uv output (up to 40 μ W) is confined in a 1-2-mm-diam beam and is polarized perpendicular to the trap/magnet axis. It is introduced to and exits from holes in the ring electrode of the trap.

In a magnetic field the ${}^2S_{1/2} \leftarrow {}^2P_{3/2}$ transition splits according to the electronic Zeeman effect. The laser radiation is nearly uncoupled from the $\Delta M = 0$ transitions due to the polarization; moreover, all of the $|M_J| = \frac{1}{2} \leftarrow |M_J| = \frac{1}{2}$ transitions optically pump the ground state. However, the $M_J = \pm \frac{1}{2} \leftarrow M_J = \pm \frac{3}{2}$ transitions can be driven many times in succession and provide the transitions for cooling. Figure 1(a) shows an experimental trace of ion temperature versus uv frequency

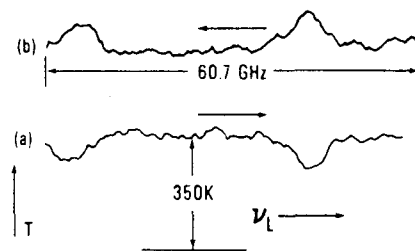


FIG. 1. Ion temperature vs swept laser frequency. Arrows above the traces show the direction of the sweep. The two resonance curves correspond to the ${}^2S_{1/2} \leftarrow {}^2P_{3/2}$ ($M_J = -\frac{1}{2} \leftarrow M_J = -\frac{3}{2}$ and $M_J = +\frac{1}{2} \leftarrow M_J = +\frac{3}{2}$) transitions. When the laser frequency sweep is positive, the transitions are indicated by a temperature decrease; when the sweep is negative the transitions are indicated by an increase in temperature. Curve b is displaced upward and the baseline is not shown.

when the laser is swept from low to high frequencies through the ${}^2S_{1/2} \leftarrow {}^2P_{3/2}$ manifold. A decrease in temperature is observed at two frequencies corresponding to the separation of the $+\frac{1}{2} \leftarrow +\frac{3}{2}$ and $-\frac{1}{2} \leftarrow -\frac{3}{2}$ transitions. As the radiation frequency is swept up through the low-frequency side of the Doppler profile on either transition, it cools the ions. When line center is reached, cooling stops; and as the laser sweeps through the high-frequency side of the Doppler profile, heating occurs. Conversely, if the laser frequency is swept down through the transitions, heating appears first and then cooling. [See Fig. 1(b).]

The rate of heat extraction (addition) per ion is given by

$$dQ/dt = Ch(\nu_L - \nu_0)\sigma_s(\nu_L)I(\nu_L)/h\nu_L, \quad (2)$$

where $I(\nu_L)$ is the laser flux (W/cm^2) and C is a factor ≤ 1 describing the overlap of the laser beam with the ion cloud. The cross section $\sigma_s(\nu_L)$ is given by the convolution of the natural line shape with the Doppler profile. When $\Delta\nu$ is much less than the Doppler width, $\sigma_s(\nu_L)$ can be given by

$$\sigma_s(\nu_L) \approx \sigma_0 \frac{\Delta\nu\sqrt{\pi}}{2\nu_D} \exp\left[-\left(\frac{\nu_L - \nu_0}{\nu_D}\right)^2\right], \quad (3)$$

where σ_0 is the resonance scattering cross section ($\frac{4}{3}\pi\lambda^2$ for the transitions here) and where $\nu_D \equiv (2kT/M)^{1/2}\nu_0/c$. The monitored signal is proportional to the temperature of the strongly coupled cyclotron and axial motions but not to the magnetron motion.^{5,6} Moreover the laser only weakly couples to the magnetron motion (see below) and therefore each ion has a specific heat of $2k$ (k = Boltzmann's constant). Using Eqs. (2)

and (3) the rate of temperature change is therefore

$$\frac{dT}{dt} = \frac{1}{2k} \frac{dQ}{dt} = C \frac{I(\nu_L) \sigma_c \Delta \nu \sqrt{\pi} (\nu_L - \nu_0)}{4 \nu_D \nu_L k} \exp \left[- \left(\frac{\nu_L - \nu_0}{\nu_D} \right)^2 \right] \quad (4)$$

When the laser frequency is swept across the line so that $\nu_L - \nu_0 = \dot{\nu} t$ ($\dot{\nu} \equiv d\nu_L/dt$) and when $I(\nu_L)$ equals a constant value I_0 , then in the limit of small cooling (heating) where ν_D is nearly constant, Eq. (4) can be integrated from $-\infty$ to t to give

$$T(t) = T(\nu_L - \nu_0) \approx \mp C I_0 \sigma_c \frac{\sqrt{\pi} \Delta \nu \nu_D}{8 \dot{\nu} \nu_0 k} \exp \left[- \left(\frac{\nu_L - \nu_0}{\nu_D} \right)^2 \right], \quad (5)$$

where the sign is negative for sweeping up and positive for sweeping down. The maximum cooling rate is expected when $\nu_L - \nu_0 = \nu_D \sqrt{2}$. Note that for small temperature changes the observed line shape (temperature versus frequency) should reproduce the normal Doppler line shape. For the curves in Fig. 1, $I_0 \approx 4 \mu\text{W}/\text{mm}^2$ for the $-\frac{1}{2} \rightarrow -\frac{3}{2}$ and $6 \mu\text{W}/\text{mm}^2$ for the $+\frac{1}{2} \rightarrow +\frac{3}{2}$ transitions, $C \approx 0.5$, $\dot{\nu} = 0.1 \text{ GHz}/\text{sec}$, and¹⁰ $\Delta \nu \approx 43 \text{ MHz}$, yielding a factor 250 K in front of the exponential in Eq. (5). The ambient (trap) temperature was measured to be approximately $350 \pm 50 \text{ K}$ by infrared means. The observed cooling (heating) ($\sim 100 \text{ K}$) is not as strong as predicted which may be caused by the observed presence of other ions in trap which reduces the net effect or by too high an estimate of C . The observed splitting of the lines ($\approx 37 \text{ GHz}$) agrees with the value predicted based on magnetic field measurements to about 3%. The mean frequency of the two lines agrees with the reported value¹¹ to within 0.02 cm^{-1} by comparison of the dye-laser output to the spectrum of I_2 . The observed width of the lines (4.5 GHz) is larger than that predicted from the ambient temperature (2.9 GHz) and is partially caused by the magnetron-motion Doppler broadening and possibly the slightly shifted resonances of the ^{25}Mg and ^{26}Mg isotopes (about 10% each). We note, however, that if we cool the ions to one-half of their equilibrium temperature, and then sweep through the transition, the linewidth decreases by a factor of approximately 1.5 as expected.

In Fig. 2 a plot of temperature versus time is shown for the case when $\nu_L - \nu_0$ is constant and the laser is turned on for a fixed time as shown. The ions had previously been heated with the laser to about 700 K. Laser cooling is then implemented for a fixed time showing the ion temperature approaching 0 K with an upper bound of 40 K determined by the noise. After the laser is turned off, the ions rethermalize as shown. With $I_0 = 8 \mu\text{W}$, $\nu_L - \nu_0 \approx -(2 \pm 1) \text{ GHz}$, we measure

a cooling rate of 5 K/sec but predict a rate of $15 \pm \frac{5}{10} \text{ K}/\text{sec}$ based on Eq. (4) evaluated at $T = 350 \text{ K}$. For this trace the background gas pressure was purposely made higher to reduce the thermalization time.

The laser can couple to the magnetron motion and we must estimate this effect. If we use Eq. (1) and its time derivative we can relate a given velocity change, Δv , to a change in magnetron radius by the expression $\Delta \vec{r}_m = i \Delta \vec{v} / (\omega_c' - \omega_m)$. For each scattering event $\Delta \vec{v} = \hat{x} \hbar / M \lambda$ which causes the magnetron orbit size to change by $|\Delta \vec{r}_m| \approx 1 \times 10^{-6} \text{ cm}$. If we irradiate the ion cloud uniformly, $|\vec{r}_m|$ increases in a random walk with step size $|\Delta \vec{r}_m|$; this is a small effect. Moreover, if one irradiates the cloud preferentially on the side of the trap where the magnetron motion recedes from the laser, the magnetron vector should become smaller. This can be used to overcome the diffusion of ions out of the trap due to collisions and therefore indefinite confinement should be possible. We have mapped the ion cloud shape by measuring the cooling (heating) signal strengths as a function of laser beam position and found: $r_m(\text{max}) \approx 1 \text{ mm}$ and $z(\text{max}) \approx 0.5 \text{ mm}$.

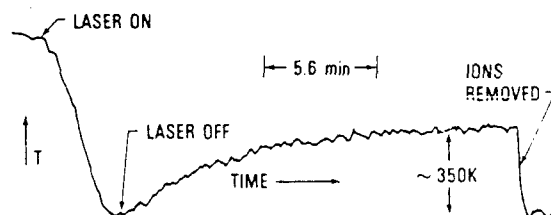


FIG. 2. Ion temperature vs time when laser cooling is applied for fixed $\nu_L - \nu_0$. The ions were initially heated above equilibrium temperature with the laser. Laser cooling was then applied on the $-\frac{1}{2} \rightarrow -\frac{3}{2}$ transition for a fixed time until a temperature approaching 0 K ($< 40 \text{ K}$) was achieved. After the laser is turned off, the ions rethermalize to the ambient temperature.

The ultimate limit on cooling is determined by a competition of the damping rate on the vibrational energy due to laser cooling and the "noise" excitation of the vibrational energy due to the random occurrence (in time) of the photon impulses. In the limit where $\nu_0 \ll \Delta\nu$ and when one tunes for maximum cooling ($\nu_L - \nu_0 = -\frac{1}{2}\Delta\nu$), the resulting kinetic energy is approximately equal to $h\Delta\nu/8$ corresponding to $T \approx 0.5 \times 10^{-3}$ K for the transitions discussed here. One can use the scattered photons from the cooling process as a monitor in a double-resonance experiment. Since the laser is not needed for trapping, it can be turned off for a relatively long time while the resonance of interest is probed. The possibility also exists to use a mixture of ions—one kind which can be laser cooled and by collisions cools the other kind which are the ions of spectroscopic interest. We note that the cooling method is quite general and can in principle be applied to other cases such as ions or nuclei bound in solid lattice.

The authors wish to acknowledge the help of the other members of the Time and Frequency Division, in particular the support and leadership of H. Hellwig, and electronics construction by C. Klepper. The basic trap structure was built by one of the authors (D.J.W.) and R. S. VanDyck, Jr., at the University of Washington and was used with the kind permission of H. G. Dehmelt. The cooling limit was estimated with key input from E. M. Purcell and D. J. Larson, Harvard University. This work was funded in part

by the U. S. Office of Naval Research under Contract No. N00014-77-F-0046.

¹T. W. Hänsch and A. L. Schawlow, *Opt. Commun.* **13**, 68 (1975).

²D. J. Wineland and H. Dehmelt, *Bull. Am. Phys. Soc.* **20**, 637 (1975).

³A. Ashkin, *Phys. Rev. Lett.* **24**, 156 (1970), and **25**, 1321 (1970), and **40**, 729 (1978).

⁴V. S. Letokhov, *Comments At. Mol. Phys.* **6**, 119 (1977), and many earlier references contained herein.

⁵H. G. Dehmelt and F. L. Walls, *Phys. Rev. Lett.* **21**, 127 (1968); H. Dehmelt, in *Advances in Atomic and Molecular Physics*, edited by D. R. Bates and I. Esterman (Academic, New York, 1967, 1969), Vols. 3 and 5; D. J. Wineland and H. G. Dehmelt, *J. Appl. Phys.* **46**, 919 (1975).

⁶R. A. Heppner, F. L. Walls, W. T. Armstrong, and G. H. Dunn, *Phys. Rev. A* **13**, 1000 (1976).

⁷D. A. Church and H. G. Dehmelt, *J. Appl. Phys.* **40**, 3421 (1969).

⁸R. S. VanDyck, Jr., P. B. Schwinberg, and H. G. Dehmelt, in *Proceedings of Orbis Scientiae*, Coral Gables, 1978 (Plenum, New York, to be published).

⁹J. Byrne and P. S. Farago, *Proc. Phys. Soc. (London)* **86**, 801 (1965).

¹⁰W. L. Wiese, M. W. Smith, and B. M. Miles, *Atomic Transition Probabilities*, U. S. National Bureau of Standards, National Standards Reference Data Series—22 (U. S. GPO, Washington, D. C., 1969), Vol. II.

¹¹S. Bashkin and J. O. Stoner, Jr., *Atomic Energy Levels and Grotrian Diagrams* (North-Holland, Amsterdam, 1975).

Laser cooling of atoms

D. J. Wineland

Frequency and Time Standards Group, National Bureau of Standards, Boulder, Colorado 80303

Wayne M. Itano*

Department of Physics, Harvard University, Cambridge, Massachusetts 02138

(Received 16 May 1979)

Various aspects of the laser cooling of atoms are investigated theoretically. More generally, the authors investigate a process through which the kinetic energy of a collection of resonant absorbers can be reduced by irradiating these absorbers with near-resonant electromagnetic radiation. The process is described here as anti-Stokes spontaneous Raman scattering. Cooling mechanisms, rates, and limits are discussed for both free and bound atoms.

I. INTRODUCTION

In the past few years, there has been increasing interest in the use of near-resonant photon scattering to cool a collection of atoms, ions, or molecules. This interest is motivated in part by the practical need to reduce first- and second-order Doppler shifts in ultra-high-resolution spectroscopy and in part by the esthetic appeal of controlling the positions and velocities of a collection of atomic particles to within the limits imposed by quantum fluctuations. Recent proposals and experiments using narrow-band tunable lasers suggest that such control may soon become a reality. It is not difficult to imagine that the concepts and techniques which are being developed may have application in a variety of areas not initially anticipated.

Current interest in the possibility of cooling began with independent proposals to reduce the temperature of a gas of neutral atoms¹ or ions which are bound in an electromagnetic "trap"² with near-resonant laser radiation. This method of cooling has subsequently been incorporated into the interesting schemes for trapping of particles using near-resonant optical fields.³ The first demonstration⁴ of cooling using the basic techniques described here was made for a slightly modified situation; specifically, the magnetron motion of an electron bound in a Penning trap was "cooled" by a technique called motional sideband excitation,⁵ which is formally equivalent to the laser cooling of atoms. Cooling of ions bound in an electromagnetic trap was more recently demonstrated.^{6,7} The cooling which is potentially achievable should permit spectroscopy of unprecedented resolution and accuracy.

As discussed below, the technique can variously be described in terms of radiation pressure, motional sideband excitation, optical pumping, or

anti-Stokes spontaneous Raman scattering; this last concept is the one primarily used here because of its generality. It should be mentioned that cooling by Raman scattering is not a new idea; "lumino-refrigeration" was hypothesized as early as 1950 by Kastler.⁸ We also note that other cooling processes are possible; for example, one could use optical pumping followed by collisional relaxation, as discussed in Sec. II, or cooling by collisionally aided fluorescence.⁹ The process described in this paper is, however, more direct and does not rely on atom-atom collisions to alter the atom kinetic energy.

The paper is divided as follows. In Sec. II we describe the general aspects of the cooling process and treat the problem combining simple classical and quantum ideas. Section III introduces the concepts and notation of the quantum-mechanical treatment which is then applied to free atoms in Sec. IV and bound atoms in Sec. V. In order to make the problem somewhat more tractable, we limit the discussion to simple systems which exhibit the salient features of the process.

II. SIMPLE DESCRIPTION OF THE COOLING PROCESS

A. Analogy with optical pumping

The basic features of the cooling process have been outlined previously (Refs. 1, 2, 5, 6, 7). The attempt is made here to describe the qualitative aspects of the problem more completely; however, the general problem becomes quite complicated, and therefore several limiting cases will be treated.

First, recall that in optical pumping we have a way of drastically altering the temperature of a specific degree of freedom in an atom or molecule. Assume, for example, that we have an alkali-like atom which has ground-state "hyperfine" structure. This atom can also have many

excited electronic states, but we assume that we have a narrow-band laser which can excite the atom from one of the ground states to only one excited electronic state. The relevant levels are shown in Fig. 1.

Without laser irradiation, the atoms eventually reach thermal equilibrium by collisions or interaction with the background blackbody radiation. Therefore, the ratio of the number of atoms in state 2 to those in state 1 is given by the Boltzmann law:

$$N_2/N_1 = \exp[-(E_2 - E_1)/k_B T], \quad (1)$$

where k_B = Boltzmann's constant, T = temperature, and E_1 , E_2 and N_1 , N_2 are the respective energies and numbers of atoms in the states. For simplicity we assume that the ground state has only two nondegenerate energy levels; hence statistical weight factors are absent in Eq. (1).

If we now apply the laser radiation to the atoms, optical pumping occurs. Atoms are excited to level 3, but can decay into either ground state. If we neglect the finite frequency widths of the laser and of the optical transition, this process continues until all of the atoms are in level 1. They remain there until another process (say, the collisions) depopulates this level. However, in the pumping process, $N_2/N_1 \rightarrow 0$, and, via Eq. (1), we may say that $T \rightarrow 0$ also. In this simple example, we see that we can cool an internal degree of freedom of the atom (the hyperfine structure) by optical pumping. In principle, we could continue this optical pumping process and, using collisions to transfer kinetic energy to the internal degree of freedom, could reduce the translational temperature of the gas if there were sufficient isolation from the rest of the environment. The process of laser cooling discussed below is very similar to the optical pumping case except that the translational degrees of freedom are optically pumped directly.

B. Laser cooling of free atoms

Assume that we have an unbound gas of atoms (or resonant absorbers in general) which possess

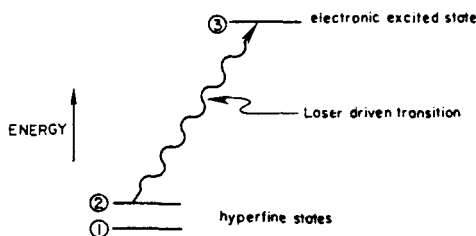


FIG. 1. Levels of interest in a hypothetical alkali-like atom. Optical pumping into state 1 occurs while driving the $2 \rightarrow 3$ transition with a laser.

a resonant electric dipole transition (frequency, ν_0) in some convenient spectral region with radiative linewidth $\gamma/2\pi$ (full width at half-intensity points). Now suppose that we irradiate these atoms with monochromatic, directed, low intensity radiation tuned near, but slightly lower than, the resonance frequency. We assume that the intensity is well below that which would cause saturation (the case of saturation is treated in Ref. 10), and that the thermalizing collision rate γ_c between atoms is much less than the natural linewidth γ , but is larger than the optical absorption rate ($\gamma \gg \gamma_c \gg$ absorption rate, see Sec. V F). Those atoms of a particular velocity class moving against the radiation are Doppler shifted toward the resonant frequency ν_0 and scatter the incoming light at a higher rate than those atoms moving with the radiation which are Doppler shifted away from resonance. For each scattering event, the atom receives a momentum impulse $\hbar \vec{k}$ (\vec{k} is the photon wave vector) in the absorption process. For an atom which is moving against the radiation, this impulse retards its motion. This retardation can also be described in terms of radiation pressure.^{1,10} The average momentum per scattering event transferred to the atom by the reemitted photons is zero, because of the randomness of the photons' directions (if we neglect terms of second order in $|\vec{v}|/c$, where \vec{v} is the atom velocity and c is the speed of light). The average net effect then is that the atomic velocity is changed by an amount $\Delta \vec{v} \cong \hbar \vec{k}/M$ per scattering event, where M is the atomic mass. When \vec{v} and \vec{k} are antiparallel, this leads to a net cooling, provided $|\vec{v} + \Delta \vec{v}| < |\vec{v}|$.¹ (See Fig. 2.) In a practical cooling experiment it would be desirable to irradiate the atoms from all sides with radiation that covered the entire lower half of the Doppler profile.¹ Alternatively, narrow-band laser schemes might be employed where the laser frequency is swept from some very low value to a value approaching the rest frequency.³ This requirement is substantially relaxed if the

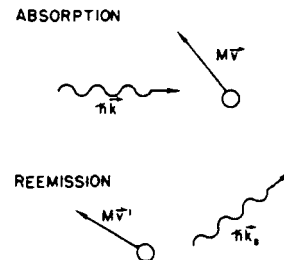


FIG. 2. Qualitative description of radiation-pressure cooling. In the absorption process, the atomic velocity is changed (reduced for $\vec{k} \cdot \vec{v} < 0$) by an amount $\Delta \vec{v} = \hbar \vec{k}/M$. In the reemission process, the average change in velocity is zero. Therefore in the overall scattering process, the kinetic energy can be reduced.

atoms are bound, as is described later. (See Sec. II C.)

The above argument gives the essence of the cooling process but neglects residual heating effects due to recoil. For example, in the re-emission process, as explained below, the average momentum transfer is zero (neglecting terms of order $|\vec{v}|^2/c^2$); however, the atom undergoes a random walk in momentum space because of the finite momentum transfer in each emission. Thus, the limiting kinetic energy for a single atom in the cooling process must be at least the recoil energy $R = (\hbar k)^2/2M$, and, as we will see below, may be considerably larger than the recoil energy. To be more quantitative, we first write the *resonance* absorption and spontaneous emission frequencies, which are given by:

$$\omega_{\text{abs}} = \omega_0 + \vec{k}_{\text{abs}} \cdot \vec{v} - \frac{1}{2}\omega_0\beta^2 + R/\hbar, \quad (2a)$$

$$\omega_{\text{em}} = \omega_0 + \vec{k}_{\text{em}} \cdot \vec{v}' - \frac{1}{2}\omega_0\beta^2 - R/\hbar, \quad (2b)$$

where $\omega_0 = 2\pi\nu_0$, $|\vec{k}_{\text{abs}}| = \omega_{\text{abs}}/c$, $|\vec{k}_{\text{em}}| = \omega_{\text{em}}/c$, \vec{v} = atom velocity in the ground state, \vec{v}' = atom velocity in excited state, c = speed of light, $\beta = |\vec{v}|/c$, $\hbar \cdot 2\pi$ = Planck's constant. These equations, valid to order β^2 in the atom velocity, and to first order $R/\hbar\omega_0$ in the recoil energy, can be obtained by invoking conservation of energy and momentum in the absorption and emission processes. The second term on the right-hand side of these equations is the ordinary first-order Doppler shift, the third term is the second-order Doppler or time dilation shift, and the last term is usually called the recoil shift. We will use the nonrelativistic approximation and therefore neglect the third term in Eq. 2. Also, as explained in Sec. III, the net effect of averaging over all possible directions of reemission, is equivalent to setting the second term in Eq. 2(b) equal to zero (neglecting terms of order β^2 and higher). Hence, the average energy change of the photon per resonant spontaneous scattering event is given by

$$\Delta E(\text{photon}) = \hbar(\omega_{\text{em}} - \omega_{\text{abs}}) = -\hbar\vec{k}_{\text{abs}} \cdot \vec{v} - 2R.$$

Here we note that this equation applies to both resonant and nonresonant scattering and can also be simply derived in general by considering conservation of energy and momentum in the overall scattering process. For this more general case, \vec{k}_{abs} is replaced by \vec{k} . The change in photon energy is accounted for by a change in atom kinetic energy per scattering event

$$\Delta E_K(\text{atom}) = \hbar\vec{k} \cdot \vec{v} + 2R. \quad (3)$$

This leads to a net average cooling as long as $\hbar\vec{k} \cdot \vec{v} < -2R$, and net heating for the opposite con-

dition. As an example, suppose we have an atom with $M = 100$ amu, $\nu_0 = 5 \times 10^{14}$ Hz ($\lambda = 600$ nm) at thermal energies ($T = 300$ K), then $v_{\text{rms}} = 2.2 \times 10^4$ cm/s, $\hbar|\vec{k}|v_{\text{rms}} = 2.5 \times 10^{-18}$ ergs, $2R = 7.3 \times 10^{-23}$ ergs. Clearly, the recoil heating does not play a significant role until very low temperatures are achieved. Of course, at higher frequencies ν_0 it becomes more important. If we interpret the energy changes in terms of temperature changes by the relation $\Delta E_K = \frac{3}{2}k_B\Delta T$, then $\Delta T \cong 0.012$ K per scattering event at $T = 300$ K, and it therefore takes on the order of 10^4 scattering events to do substantial cooling at optical frequencies.

1. Cross section and cooling rates

The atomic cross section for absorption, neglecting saturation,¹⁰ has the form

$$\sigma(\omega) = \sigma_0 \frac{(\frac{1}{2}\gamma)^2}{[(\omega - \omega_{\text{abs}})^2 + (\frac{1}{2}\gamma)^2]}, \quad (4)$$

where σ_0 is the resonance scattering cross section ($\sigma_0 = 2\pi\lambda^2$ for unpolarized atoms). Therefore, if the radiation is incident along the x direction, the rate of kinetic energy change is, using Eq. (3):

$$\frac{dE}{dt} = \frac{I}{\hbar\omega} \sigma(\omega) (\hbar kv_x + 2R), \quad (5)$$

where I is the energy flux of the laser beam (ergs/sec cm²) and where σ is given by Eq. (4). (This expression will be more fully justified in Sec. III.) Equation (5) gives the cooling (heating) rate for a single atom. If we consider an ensemble of atoms we must average v_x over the velocity distribution. If, for example, the distribution is given by a Maxwell-Boltzmann distribution, Eq. (4) becomes a Voigt profile:

$$\sigma(\omega) = \sigma_0 \int_{-\infty}^{\infty} \frac{\exp[-(v_x/u)^2]}{\sqrt{\pi}u} \times \frac{dv_x}{1 + [(2/\gamma)(\omega - \omega'_0 - kv_x)]^2}, \quad (6)$$

where $u = (2k_B T/M)^{1/2}$ and $\omega'_0 = \omega_0 + R/\hbar$. Similarly, Eq. (5) becomes

$$\frac{dE}{dt} = \frac{I\sigma_0}{\hbar\omega} \int_{-\infty}^{\infty} \frac{\hbar kv_x + 2R}{1 + [(2/\gamma)(\omega - \omega'_0 - kv_x)]^2} \times \frac{\exp[-(v_x/u)^2]}{\sqrt{\pi}u} dv_x. \quad (7)$$

Equation (7) can also be written in the form

$$\frac{dE}{dt} = \frac{I\sigma_0\gamma^2}{4ku\omega} \left[\text{Re } Z(F, Q) + \frac{2}{\gamma} \left(\omega'_0 - \omega - \frac{2R}{\hbar} \right) \text{Im } Z(F, Q) \right],$$

where $F \equiv (\omega'_0 - \omega)/(ku)$, $Q \equiv \gamma/(2ku)$, and $Z(F, Q)$

is sometimes called the plasma dispersion function¹¹ defined as

$$Z(F, Q) = \pi^{-1/2} \int_{-\infty}^{\infty} \frac{dx e^{-x^2}}{x - F - iQ}$$

for $Q > 0$. We can numerically solve Eq. (7) for dE/dt ; however, when γ and R/\hbar are much less than the Doppler width we can approximate the integral and the cooling rate by

$$\frac{dE}{dt} = \frac{I\sigma_0}{\hbar\omega} [\hbar(\omega - \omega_0) + R] \frac{\gamma\sqrt{\pi}}{2\omega_D} \exp\left[-\left(\frac{\omega - \omega_0'}{\omega_D}\right)^2\right], \quad (8)$$

where $\omega_D = \omega_0\mu/c$.

For the case of unbound atoms, radiation incident along only one direction would retard the motion only in that direction and heat the motion in the other directions due to recoil. Therefore, in a practical situation we might irradiate the atoms with six narrow-band laser beams directed along the $\pm x$, $\pm y$, and $\pm z$ directions of a Cartesian coordinate system. In this case we must sum terms like Eq. (5) for each laser beam. If (i) the frequencies of the lasers are equal giving standing waves, or (ii) if the waves are not plane, we must consider the effect of the induced dipole forces responsible for optical trapping.³ In order to disregard this effect we will assume that the incident (plane-wave) radiation has low enough power—that is, the limiting kinetic energy is larger than the potential energy “hills” created by the standing-wave-induced dipole force. In this limit, the induced forces average to zero. When the atoms are bound this complication need not arise, since one laser beam may be sufficient to cool all degrees of freedom.

2. Cooling limit

We can estimate the limit on cooling with the following argument whose general features were advanced by Purcell.¹² Assume that substantial cooling has already taken place so that the Doppler width of the atomic transition is smaller than the natural linewidth γ . We further assume that we irradiate the unpolarized atoms with six laser beams as described above, which are tuned near the lower half-power point of the optical resonance, $\omega - \omega_0 \cong -\frac{1}{2}\gamma$. Considering the rate of energy change in the x direction, we can write

$$\frac{dE_x}{dt} = \frac{I}{\hbar\omega} [\sigma_+ (\hbar kv_x + 2R) + \sigma_- (-\hbar kv_x + 2R)], \quad (9)$$

where I is the energy flux of each laser beam and where σ_+ (σ_-) is the scattering cross section for the laser light moving with (against) the atomic motion.

With the approximation that the Doppler width

is much less than the natural width, we can show that the maximum cooling rate is achieved when $\omega = \omega_0' - \frac{1}{2}\gamma$. In this case Eq. (9) reduces to

$$\frac{dE_x}{dt} = \frac{2I\sigma_0}{\hbar\omega} \left(-\frac{\hbar k^2 \langle v_x^2 \rangle}{\gamma} + R \right). \quad (10)$$

We find the minimum kinetic energy (E_K) when $dE_x/dt = 0$, in which case

$$\langle E_{Kx} \rangle_{\min} = \frac{1}{4} \hbar \gamma, \quad (11)$$

which is independent of intensity. In a real situation, of course, other causes of heating would be present, making high intensity desirable. (See, however, Sec. V F). Note that Eq. (11) holds for a single atom or an ensemble of weakly thermalized atoms. If the atoms have a Maxwell-Boltzmann distribution, then $E_{Kx} = \frac{1}{2} k_B T$. If $\gamma = 2\pi \cdot 10$ MHz, we find $T_{\min} \cong 2.4 \times 10^{-4}$ K.

From Eq. (11) the rms velocity $v_{rms} = (\langle v_x^2 \rangle)^{1/2}$ can be used to arrive at an approximate Doppler broadening $\Delta\omega_D \cong \omega_0 v_{rms}/c$. In deriving Eq. (11), we have assumed that this Doppler broadening is much less than the natural linewidth, which then implies that $R \ll \hbar\gamma$. In our example, $\hbar\gamma \cong 0.7 \times 10^{-19}$ ergs $\gg R \cong 4 \times 10^{-23}$ ergs, and our assumption is justified. However, for weakly allowed transitions in light atoms, this condition will be violated and the minimum kinetic energy will be limited as shown below to approximately the recoil energy R .

When the condition $R \ll \hbar\gamma$ is not satisfied we must accurately evaluate Eq. (7) to find the cooling limit. Assuming the thermalizing collision rate between atoms is large compared to the optical absorption rate, we can evaluate the plasma dispersion function to find the average energy

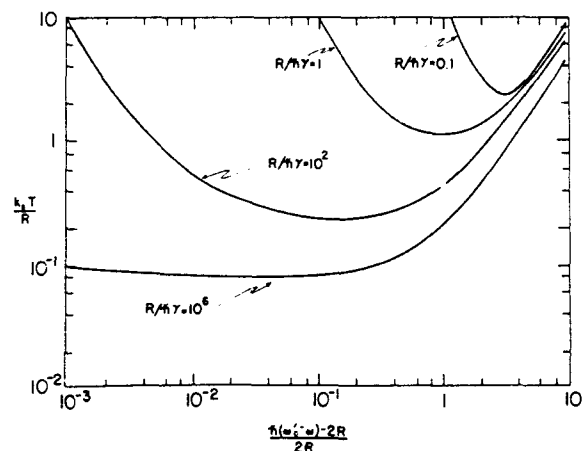


FIG. 3. Plots of $k_B T_{\min}$ versus $\hbar(\omega_0' - \omega)/R$ for four values of $R/\hbar\gamma$. We have assumed that the thermalizing collision rate (γ_c) is much greater than the optical absorption rate.

which makes Eq. (7) vanish for particular values of $\omega'_0 - \omega$, R , and γ . (We note that cooling is possible only if $(\omega'_0 - \omega) > 2R/\hbar$.) In Fig. 3 we show the minimum energy thus obtained for various values of $\hbar(\omega'_0 - \omega)/R$ and $R/\hbar\gamma$. We note that it is possible to cool to an average energy less than the recoil energy; however, we must also note the difficulty in obtaining the proper conditions under which these results hold. In particular, free atoms cannot really be thermalized amongst themselves. Therefore some kind of confinement is required, in which case the required degree of thermal isolation from the environment would be difficult to achieve. (Ideally, we would like a transparent box whose walls have zero heat capacity.) This situation can be nearly realized for electromagnetically bound ions, in which case we might be able to obtain temperatures less than R/k_B when $\gamma < R/\hbar$. For the atoms described in the previous example ($R \cong 4 \times 10^{-23}$ ergs), this would imply $T < 2.7 \times 10^{-7}$ K, when the natural linewidth of the transition $\gamma/2\pi$ was less than 6 kHz. We also note that practical limitations on laser power would occur for the case of free atoms since the diffusion of the atoms during the cooling process would require large volumes ($\gg 1$ cm³).

C. Laser cooling of bound atoms

For the case of bound atoms we consider the special situation where they are harmonically bound in all dimensions. The assumption of harmonic binding is not essential, but it allows a simple interpretation and exhibits the most important features found in any bound system. For simplicity, we consider an atom constrained in the x , y , and z directions by springs of negligible mass as shown in Fig. 4. Of course, in a real situation, the springs might be replaced by electromagnetic restoring forces. We assume that the springs are attached to a massive block and that they act independently and may have different

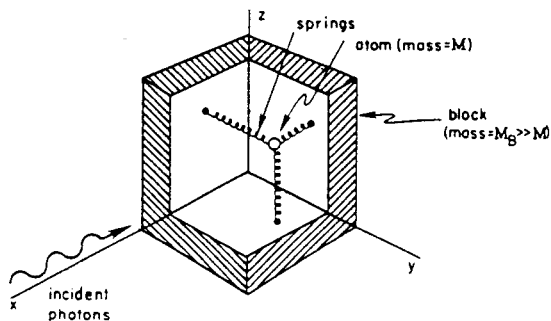


FIG. 4. Idealized representation of bound atom. In this picture the binding forces are due to (massless) springs; in an actual experiment these springs might be replaced by electromagnetic restoring forces.

spring constants giving rise to different frequencies of oscillation Ω_x , Ω_y , and Ω_z in the three directions, where we assume $\{\Omega_i\} \ll \omega_0$, $i = x, y, z$.

1. Strong binding

When the binding is "strong", ($\gamma \ll \{\Omega_i\}$), the gross features of the absorption spectrum are significantly altered. We can see this by considering the optical electrical field seen by a particular atom. If the incident (plane-wave) radiation is directed along the x axis,

$$\vec{E}_{\text{atom}} = \vec{E}_0 \sin(kx - \omega t), \quad (12)$$

where x is the atomic x coordinate and k and ω are the wave vector and frequency of the incident radiation. Now

$$x = x_a \sin(\Omega_x t + \phi_x),$$

where x_a is the oscillation amplitude and ϕ_x is a phase factor. Choosing $\phi_x = 0$, we have

$$\vec{E}_{\text{atom}} = \vec{E}_0 \sin(kx_a \sin \Omega_x t - \omega t). \quad (13)$$

This expression is familiar as the signal derived from an oscillator of frequency ω which is frequency modulated at frequency Ω_x with modulation index kx_a . Equation (13) can be expanded in terms of a series of Bessel functions and gives rise to the spectrum shown in Fig. 5(a) when $kx_a = 1.5$. We note that the atom sees a spectrum comprised of a "carrier" at frequency ω with equally spaced first-order Doppler effect gen-

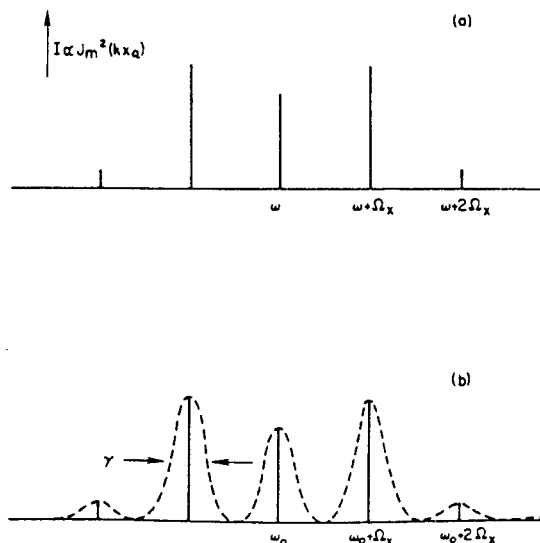


FIG. 5. Radiation spectrum when $\Omega_x \gg \gamma$. Part (a) illustrates the spectrum of an incident wave $\vec{E} = \vec{E}_0 \sin(kx - \omega t)$ as seen by an atom which oscillates according to $x = x_a \cos \Omega_x t$, where we have chosen $kx_a = 1.5$. Part (b) shows the emission spectrum as observed in the laboratory including the broadening due to the lifetime of the upper electronic state.

erated sidebands at the frequencies $\omega - m\Omega_x$ ($m = \pm 1, \pm 2, \pm 3, \dots$) having intensities proportional to $J_m^2(kx_a)$. Similarly, the spectrum of the atom as seen by an observer in the laboratory will have the same character as in Fig. 5(a), but each component will be broadened by the natural linewidth γ as shown in Fig. 5(b).

To approximate the cooling rate, we note that when $\gamma \ll \Omega_x$ we can tune the incident radiation to one of the resolved lower sidebands. Thus, an atom can be made to absorb photons predominantly of energy $\hbar(\omega_0 + m\Omega_x)$ where m is a (negative) integer. Photons of average energy approximately equal to $\hbar\omega_0$ are reemitted, leading to a net cooling.² One can, therefore, approximate the cooling rate to be:

$$\frac{dE}{dt} = (\hbar m \Omega_x) \frac{I \sigma_0}{\hbar \omega} J_m^2(kx_a). \quad (14)$$

In Sec. V we will see that this expression is strictly valid only when the recoil effect is negligible. For this approximation, as an example, suppose $\Omega_x/2\pi = 12.5$ MHz, $M = 100$ amu, $\lambda = 600$ nm, and $m = -28$. Let $\gamma/2\pi = 1.0$ MHz, and suppose that the intensity is such that $\sigma_0 I/\hbar\omega_0 = 5$ MHz. If the x motion initially has an energy corresponding to room temperature, so that $\frac{1}{2}M\Omega_x^2 \langle x^2 \rangle = \frac{1}{2}M\Omega_x^2 x_a^2 = \frac{1}{2}k_B T$ ($T = 300$ K) then $x_a \cong 2.8 \times 10^{-4}$ cm, $kx_a \cong 30$, $J_{28}^2(kx_a) \cong 0.046$ and $dE/dt \cong 0.3$ eV/sec, $I = 2.7$ mW/cm². We therefore see that when the atom is bound, rather substantial cooling can be achieved with modest incident power tuned to a single frequency. (We have, however, chosen a strong sideband). Additionally, we can simultaneously cool all degrees of freedom with a single laser beam if the incident radiation is directed along, for example, the $\hat{i} + \hat{j} + \hat{k}$ direction when the vibration frequencies are related by rational numbers (but are not equal), or if, as in a cloud of ions, the long-range electrostatic forces tend to thermalize all degrees of freedom. This technique² has been called "cooling by motional sideband excitation."⁵

In a collection of bound atoms that are weakly thermalized (i.e., the collision rate $\gamma_c \ll \gamma$) a more realistic estimate of the cooling can be obtained if we average Eq. (14) over a thermal distribution. We have

$$\left\langle \frac{dE}{dt} \right\rangle = (\hbar m \Omega_x) \frac{I \sigma_0}{\hbar \omega} \times \left(\frac{1}{k_B T} \int \exp\left(\frac{-E}{k_B T}\right) J_m^2(kx_a) dE \right).$$

Since $E = \frac{1}{2}M\Omega_x^2 x_a^2$ the factor in parentheses can be integrated to give the result

$$\left\langle \frac{dE}{dt} \right\rangle = (\hbar m \Omega_x) \frac{I \sigma_0}{\hbar \omega} \exp(-k^2 \langle x^2 \rangle) \times I_m(k^2 \langle x^2 \rangle), \quad (15)$$

where I_m is the modified Bessel function of order m and $k^2 \langle x^2 \rangle = 2Rk_B T / (\hbar \Omega_x)^2$. If we assume that we irradiate somewhere within the Doppler profile, then we can show [see Eq. (41)] that $|m| \leq k \langle x^2 \rangle^{1/2}$. In the high-temperature or short-wavelength limit, $k \langle x^2 \rangle^{1/2} \gg 1$. Therefore we can use the following asymptotic expansion¹³ of I_m :

$$I_m(z) - (2\pi z)^{-1/2} \exp(z - m^2/2z) \quad z \gg m \gg 1 \quad (16)$$

and we obtain

$$\left\langle \frac{dE}{dt} \right\rangle = (\hbar m \Omega_x) \frac{I \sigma_0}{\hbar \omega} \frac{\Omega_x}{\sqrt{\pi} \omega_D} \exp\left(-\frac{(\omega - \omega_0)^2}{\omega_D^2}\right), \quad (17)$$

where $\omega - \omega_0 = m\Omega_x$. The last factor shows the Doppler profile. For the above conditions, $\langle dE/dt \rangle \cong 0.057$ eV/sec.

The above description is not quite correct because we have not considered in detail momentum and energy conservation in the process of absorption and reemission. It happens that the absorption and emission spectra are also altered by recoil. Qualitatively we can say that in the emission spectrum, for example, components occur at frequencies ω_0 and $\omega_0 + m\Omega_x$, but the spectrum is now slightly skewed. For example, suppose we look at the emissions at $\omega_0 \pm \Omega_x$ when $kx_a < 1$. For photon emission at frequency $\omega_0 - \Omega_x$, conservation of energy tells us that the energy of oscillatory motion must increase; hence, during the emission, kx_a increases and so also does the amplitude of the spectral component at $\omega_0 - \Omega_x$. The opposite argument holds for the component at $\omega_0 + \Omega_x$ and, consequently, the average energy spectrum is shifted to a value slightly below $\hbar\omega_0$. The solution to this problem is straightforward when quantum mechanics is used and, therefore, we defer discussion to Sec. V. It has been treated by a semiclassical approach⁷ when $kx_a \ll 1$.

A further complication arises when we ask for the cooling limit when $\gamma \ll \Omega_x$. We find that the minimum kinetic energy achieved from a classical treatment is less than the zero-point energy of the harmonic oscillator and therefore we defer this discussion to the quantum-mechanical treatment.

At this point we can see the similarity of this problem (when $\gamma \ll \Omega_x$) to the Mössbauer effect. Indeed, when $kx_a \lesssim 1$, the central peak or "carrier" becomes dominant; excitation at this central peak is equivalent to absorption on the Mössbauer line—the main difference being that at γ -ray energies the recoil plays a much larger role. As

we will see below, the quantum-mechanical treatment of laser cooling can use some of the same formalism as the treatment of the Mössbauer effect.

Finally, another picture which provides a connection with a familiar situation is given by considering the "molecule" formed by the block and the atom bound to it. Cooling of the vibrational motion is achieved by anti-Stokes Raman scattering. However, the ordinary selection rules for vibrational transitions do not apply in general since the "molecular" dimensions may be considerably larger than the optical wave length.

2. Weak binding

When $\gamma \gg \Omega_i$, the period of the atomic center-of-mass oscillation is much larger than the optical decay time. Therefore, during one oscillation period the atomic velocity gradually reaches the value where the incident radiation is shifted into resonance; scattering occurs, and for each scattering event Eq. (3) holds. In this limit we have treated the interaction of the radiation with the atom as occurring at an instant of time. This is reasonable since the atom loses optical phase memory during one oscillation period and therefore coherence during successive oscillations (which gives rise to the resolved sidebands) can be neglected. An important difference from the free-atom case is that the momentum of the photon is transferred to the center-of-mass motion of the block and atom. In the limit that the mass of the block becomes infinite, the change in velocity of the center of mass, per scattering event, goes to zero and the energy change must occur in the kinetic energy of the bound atom.

Therefore, in the weak binding limit we may apply Eq. (5) and find the average cooling rate by averaging v_x over one center-of-mass oscillation period. In an ensemble of weakly thermalized atoms Eqs. (7) and (8) therefore also apply. Neglecting recoil, we obtain Eqs. (2) and (3) of Ref. 6. However, if we assume only one laser beam is present to do the cooling we must assume that the transition rate is small enough to avoid heating by recoil in directions perpendicular to the laser beam. (See Sec. V F). If three mutually perpendicular laser beams are used to do the cooling this restriction is not necessary, but the power must be held low enough to avoid the effects of the induced dipole force. Note that the estimated cooling limit given in Ref. 6 is too low by a factor of 2. This is because only the recoil heating in the absorption process was considered and not the contribution from reemission.

D. Generalization of the cooling process

In this paper we address a rather specific problem, that is, the laser cooling of atoms. Abstracting the problem slightly, we have excited one "oscillator"—the atom's internal electronic resonance at frequency ω_0 —with radiation at a lower frequency ω . In the frame of the harmonically bound atom, this excitation occurs due to one or more of the upper sidebands shown in Fig. 5(a). For the free atom these "sidebands" become a single line.

Instead of the internal atomic "oscillator," consider an electron (or in general a charged particle) which is constrained like the atom shown in Fig. 4. Further suppose that the resonance frequencies Ω_y, Ω_z are very high so that $\hbar\Omega_y, \hbar\Omega_z \gg \hbar\Omega_x$. If incident radiation is polarized along the z axis and is directed along the x axis at frequency $\Omega_z - \Omega_x$, then the z oscillation is excited much the same way that the electronic transition in the atom was excited by the frequency $\omega_0 - \Omega_x$. Thus, cooling of the x motion can be achieved at the expense of driving (heating) the z motion. This is the essence of "magnetron" cooling which was demonstrated for an electron bound in a Penning trap.⁴ Treating this problem classically is reasonably straightforward,^{5,14,15} but a general quantum-mechanical treatment is complicated by two things. (a) Recall that for the laser cooling of atoms, the electronic states can be assumed to comprise a two-level system which is not saturated; this is a good approximation for many practical situations. However, when the atomic transition is replaced by the harmonic oscillator, many levels are involved and saturation between levels can occur. (b) In addition, the condition $k_B T \ll \hbar\Omega_y, \hbar\Omega_z$ is not generally satisfied and one must contend with the effects of thermal background radiation. Nevertheless, certain cases of this more general problem can be treated.¹⁶ Fortunately, these two problems usually do not occur for the laser cooling of atoms and many aspects of the quantum-mechanical treatment are quite straightforward.

We remark that the velocity selectivity provided by the narrow-band (laser) source might be provided by other means. For example, assume the atom is polarized in the z direction and is constrained to move along the x axis. If white light irradiates the atom at an angle with respect to the x axis, then, because the absorption rate is dependent on the angle the radiation is received (in the frame of the atom), we obtain a differential effect which is dependent on the atom velocity as is required above. This is analogous to the state selectivity provided by optical polarization in the

case of ordinary optical pumping.

We note that in terms of the above description we are discussing the case of a nearly ideal refrigerator: for each scattering event (i) we extract an amount of energy $\hbar\Omega_x$ from the "x reservoir" at temperature T_x , (ii) we supply an amount of energy $\hbar(\Omega_z - \Omega_x)$, and (iii) we transfer the amount of energy $\hbar(\Omega_z - \Omega_x) + \hbar\Omega_x = \hbar\Omega_z$ to the "z reservoir" at temperature T_z . The second law of thermodynamics then implies that the minimum obtainable temperature T_x is given by the relation¹⁷

$$T_x/T_z \geq \Omega_x/\Omega_z. \quad (18)$$

The competing heating mechanism which gives rise to this limit arises because the thermally excited z motion (frequency Ω_z) modulates the Lorentz force due to the incoming radiation (frequency $\Omega_z - \Omega_x$) and gives a component at frequency Ω_x which then excites the x motion.¹⁸

In the following we will assume that $T_z = 0$; equivalently, we will assume that the atoms are normally in their ground electronic state and the background blackbody radiation is negligible. Then the minimum temperature achieved will be determined by recoil effects. We must, however, keep the thermodynamic limit in mind in certain cases.

We further remark that in terms of the above description, the cooling process is entirely analogous to the Overhauser effect where the flipping of an electron spin in a solid is accompanied by a flipping of the nuclear spin system.¹⁷

We also note that cooling by the technique of collisionally aided fluorescence⁹ shares many similarities with cooling described here. When collisions are present, the atoms' absorption spectrum is broadened, and, if the collisions were very regular like the ion "collisions" with the electric restoring forces in an electromagnetic trap, then the spectrum might appear as in Fig. 5(b). Of course, for the general case of collisions the line broadening is not so regular; however, the cooling principle still applies, so that if we irradiated the atom at a frequency lower than the center of gravity of its emission spectrum, cooling would occur.

Finally, we observe that the cooling process can be described in terms of radiation pressure. The radiation pressure force on atoms has usually been developed in terms of scattering^{1,10}; however, we note that an alternative approach sometimes used in elementary texts¹⁹ describes the radiation pressure force on a conductor in terms of the Lorentz force interaction of the oscillating magnetic field with the induced current. For the atomic case, a dynamic polarization is established

which is usually given in terms of the susceptibility. This atomic polarization interacts with the magnetic component of the radiation field via the Lorentz force leading to a force in the direction of the radiation:

$$\vec{F} = \frac{d\vec{p}}{dt} = \frac{I}{\hbar\omega} \sigma \hbar \vec{k}.$$

The effects of recoil must be added separately in this approach. The treatment of the problem as scattering has the advantage of completeness and is therefore used in the following. We finally remark that the interest in radiation pressure forces has had a long history. Some of the very early experimental and theoretical papers have been summarized by Nichols and Hull.²⁰ The first experiment observing radiation pressure on atoms was reported by Frisch.²¹

III. QUANTUM-MECHANICAL TREATMENT—GENERAL ASPECTS

For the quantum-mechanical treatment we will make some simplifying assumptions in order to illustrate the basic features of the problem. We can, however, assume that the atom (or molecule, or resonant absorber in general) moves in three dimensions. We assume that the motions in the different directions are independent, although it will sometimes be convenient to assume for a collection of atoms that they are thermalized with each other by some relatively weak long-range forces yielding a collision rate $\gamma_c \ll \gamma$. It is also assumed that the time required for the kinetic energy to thermalize with the outside environment is extremely long. This situation is closely approximated for a cloud of ions stored in an electromagnetic trap, for example. We further assume that the internal structure of the atom comprises a two-level system with ground-state energy E_g and excited-state energy E_e such that $E_e - E_g \gg k_B T$, where T is the ambient temperature. Within the limits imposed by thermodynamics (Sec. II D) this allows us to neglect the effects of background blackbody radiation; that is, in the absence of laser irradiation, we assume that the atoms are in the ground state. Finally, we assume that the incident radiation is highly monochromatic (spectral width $\ll \gamma$) and that the intensity is well below saturation.

In the following we will assume that the Hamiltonian for the system can be written

$$H = H_0 + H',$$

where H_0 is the unperturbed Hamiltonian and H' describes the interaction of the radiation with the atom. We have

$$H_0 = H_a + H_f + H_{rad}$$

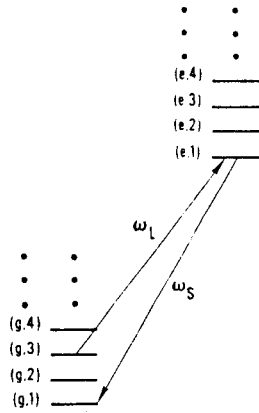


FIG. 6. Pictorial representation of electronic [ground (*g*) and excited (*e*)] energy states and translational energy states (denoted by integers) for an atom. When the atom is very weakly bound or unbound the spacing between translational energy levels goes to zero. The cooling can be described as anti-Stokes Raman scattering or optical pumping where the frequency (ω_s) of the scattered photon is greater than the frequency (ω_L) of the "laser" photon.

where H_a is the Hamiltonian for the two internal states of the atom, H_t is the Hamiltonian for the translational degrees of freedom, and H_{rad} is the Hamiltonian of the radiation field. Assuming that the various degrees of freedom are not coupled in the absence of H' , we write the total wave function as a direct product:

$$\frac{d\sigma_{l \rightarrow f}}{d\omega_s d\Omega} = \sum_s \frac{\omega_s}{\omega} \left(\frac{r_e}{m\hbar} \right)^2 \left| \sum_j \frac{\langle f | \hat{\epsilon}_s \cdot \vec{P}_{el} \exp(-i\vec{k}_s \cdot \vec{R}_{el}) | j \rangle \langle j | \hat{\epsilon} \cdot \vec{P}_{el} \exp(i\vec{k} \cdot \vec{R}_{el}) | l \rangle}{\omega_j - \omega - \frac{1}{2}i\gamma} \right|^2 \times \delta(\omega - \omega_s - [E_f(\text{trans}) - E_l(\text{trans})]/\hbar), \quad (19)$$

where $d\Omega$ is the differential element of solid angle into which the photons are scattered, ω is the incident photon frequency ($|\vec{k}| = \omega/c$), $\hbar\omega_j = \hbar\omega_0 + E_j(\text{trans}) - E_l(\text{trans})$, r_e is the classical electron radius e^2/mc^2 , subscript *s* denotes the two possible directions of the polarization of the scattered photon, *j* denotes the intermediate state, and where the wave functions now describe only the electronic and translational degrees of freedom

$$|j\rangle = |\text{int}(j)\rangle |\text{trans}(j)\rangle.$$

The δ function in Eq. (19) ensures conservation of energy for the scattering process; that is, $\hbar(\omega_s - \omega) = E_l(\text{trans}) - E_f(\text{trans})$. The operator in the matrix elements of Eq. (19) is proportional to H' . From this equation we see qualitatively that the process is described as the absorption of a photon which promotes the atom to a distribution of possible intermediate (virtual) states $\{j\}$ (where

$$|\psi\rangle = |\text{int}\rangle |\text{trans}\rangle |\text{rad}\rangle.$$

In the absence of the radiation field, the internal and translational energy levels are depicted in Fig. 6. In the nonrelativistic limit, and assuming low intensity, we make the usual approximation

$$H' \approx (e/mc) \vec{P}_{el} \cdot \vec{A}(\vec{R}_{el}),$$

where \vec{P}_{el} and \vec{R}_{el} are the momentum and position of the optically active electron, \vec{A} is the vector potential of the radiation field evaluated at the position of the electron, and m is the electron mass. We have neglected the \vec{A}^2 term in the Hamiltonian.²²

For the cooling problem, we are primarily interested in a scattering process that changes the translational and radiation states but leaves the internal atomic state unchanged. In particular, we can formulate the problem by asking for the cross section for scattering a photon of wave vector \vec{k} and polarization $\hat{\epsilon}$ where the translational energy has changed from $E_l(\text{trans})$ to $E_f(\text{trans})$ and where the scattered photon has wave vector \vec{k}_s and polarization $\hat{\epsilon}_s$. The differential cross section for this process can be obtained as a particular result from the Kramers-Heisenberg formula, which can be derived from time-dependent perturbation theory.²² Specifically, the differential scattering cross section for scattering from initial state *l* to final state *f* can be written

energy need not be conserved) followed by spontaneous reemission. The denominator indicates that a resonance is involved in the absorption. This is the main cause for the cooling, since a resonance can occur when the kinetic energy of the atom changes, that is, when $\omega = \omega_0 + [E_j(\text{trans}) - E_l(\text{trans})]/\hbar$. Equation (19) can, of course, also describe ordinary Raman and Rayleigh scattering.²²

To evaluate the matrix elements in Eq. (19), it is useful to express the electron position and momentum as functions of the atomic center-of-mass position and momentum \vec{x} and \vec{P} , the position of the electron relative to the atomic core \vec{r} , and the velocity of the electron relative to the atomic core \vec{p}/m , (m , in this expression is the electron reduced mass given by $m(1 + m/M_c)^{-1}$, where M_c is the mass of the core. In the approximation that $m \ll M_c$ we have:

$$\vec{R}_{el} = \vec{x} + \vec{r}, \quad (20a)$$

$$\vec{P}_{el} = \frac{m}{M} \vec{P} + \vec{p}, \quad (20b)$$

where $M = M_c + m$.

Before applying Eq. (19), we make the qualitative observation that the cooling process can be represented as in Fig. 6, where we have illustrated a process involving specific initial, intermediate, and final states. In general we must, of course, sum over all possible intermediate states, average over the initial-state distribution, and sum over all final states to get the net result. We see, however, that the cooling process can be described as spontaneous anti-Stokes Raman scattering or as a type of optical pumping as described in Sec. II.

IV. LASER COOLING OF FREE ATOMS

A. Matrix elements

For a free atom we have

$$H_t = \frac{\vec{P}^2}{2M}$$

and the spatial eigenfunctions are

$$|\text{trans}\rangle = C_N \exp(i\vec{K} \cdot \vec{x}) \equiv |\vec{K}\rangle,$$

where C_N is a normalization constant and

$$\langle \vec{K} | \vec{P} | \vec{K} \rangle = \hbar \vec{K}, \quad \langle \vec{K} | H_t | \vec{K} \rangle = (\hbar K)^2 / 2M,$$

$$\langle \vec{K}' | \vec{K} \rangle = \delta(\vec{K}', \vec{K}),$$

where δ denotes the Kronecker δ .

Using Eqs. (20), the matrix elements in Eq. (19) take the form:

$$\begin{aligned} \langle j | \hat{\epsilon} \cdot \vec{P}_{el} \exp(i\vec{k} \cdot \vec{R}_{el}) | l \rangle \\ = \langle \vec{K}' | \hat{\epsilon} \cdot \frac{m}{M} \vec{P} \exp(i\vec{k} \cdot \vec{x}) | \vec{K} \rangle \langle e | \exp(i\vec{k} \cdot \vec{r}) | g \rangle \\ + \langle \vec{K}' | \exp(i\vec{k} \cdot \vec{x}) | \vec{K} \rangle \langle e | \hat{\epsilon} \cdot \vec{p} \exp(i\vec{k} \cdot \vec{r}) | g \rangle, \end{aligned} \quad (21)$$

where e and g denote the internal atomic excited and ground states, respectively.

Qualitatively, the first term in Eq. (21) represents a transition of the center-of-mass motion which is caused by a field component resulting from the laser field "modulated" by the internal electronic oscillation. The second term represents an electronic transition which is caused by a field component of the laser field which has been Doppler shifted by the motion. For both terms, however, a simultaneous change in electronic and kinetic energy state has occurred.

We have

$$[\hat{\epsilon} \cdot \vec{P}, \exp(i\vec{k} \cdot \vec{x})] = 0 \quad (\text{Coulomb gauge}).$$

Therefore,

$$\langle \vec{K}' | \hat{\epsilon} \cdot \frac{m}{M} \vec{P} \exp(i\vec{k} \cdot \vec{x}) | \vec{K} \rangle = (m/M) \hbar \vec{K} \cdot \hat{\epsilon} \delta(\vec{K} + \vec{k}, \vec{K}'), \quad (22a)$$

$$\langle \vec{K}' | \exp(i\vec{k} \cdot \vec{x}) | \vec{K} \rangle = \delta(\vec{K} + \vec{k}, \vec{K}'), \quad (22b)$$

$$\langle e | \exp(i\vec{k} \cdot \vec{r}) | g \rangle \approx i\vec{k} \cdot \langle \vec{r} \rangle, \quad (22c)$$

$$\langle e | \hat{\epsilon} \cdot \vec{p} \exp(i\vec{k} \cdot \vec{r}) | g \rangle \approx im\omega_0 \hat{\epsilon} \cdot \langle \vec{r} \rangle, \quad (22d)$$

where we have made the usual dipole approximation ($1/|\vec{k}| \gg$ atomic dimensions) and have defined $\langle \vec{r} \rangle = \langle e | \vec{r} | g \rangle$. The ratio of the first term to the second term in Eq. (21) can be written:

$$\frac{\hbar(\vec{K} \cdot \hat{\epsilon}) \vec{k} \cdot \langle \vec{r} \rangle}{M\omega_0 \hat{\epsilon} \cdot \langle \vec{r} \rangle} \approx \frac{v}{c}.$$

In the nonrelativistic approximation used here, the first term is therefore negligible and Eq. (19) becomes:

$$\frac{d\sigma_{1 \rightarrow f}}{d\omega_s d\Omega} = C \sum_s \frac{\omega_s}{\omega} |\hat{\epsilon}_s \cdot \langle \vec{r} \rangle|^2 |\hat{\epsilon} \cdot \langle \vec{r} \rangle|^2 \left| \sum_j \frac{\langle \vec{K}_f | \exp(-i\vec{k}_s \cdot \vec{x}) | \vec{K}_j \rangle \langle \vec{K}_j | \exp(i\vec{k} \cdot \vec{x}) | \vec{K}_i \rangle}{\omega_0 - \omega + (\hbar/2M)(K_j^2 - K_i^2) - \frac{1}{2}i\gamma} \right|^2 \delta(\omega - \omega_s - (\hbar/2M)(K_f^2 - K_i^2))$$

or equivalently:

$$\frac{d\sigma_{1 \rightarrow f}}{d\omega_s d\Omega} = C \sum_s \frac{\omega_s}{\omega} |\hat{\epsilon}_s \cdot \langle \vec{r} \rangle|^2 |\hat{\epsilon} \cdot \langle \vec{r} \rangle|^2 \frac{\delta(\vec{K}_f + \vec{k}_s, \vec{K}_i + \vec{k}) \delta(\omega - \omega_s - (\hbar/2M)(K_f^2 - K_i^2))}{[\omega_0 - \omega + (\hbar/2M)(k^2 + 2\vec{k} \cdot \vec{K}_i)]^2 + \frac{1}{4}\gamma^2}, \quad (23)$$

where $C = (r_e m \omega_0^2 / \hbar)^2$. The δ functions in this equation express conservation of momentum and energy in the scattering process. We set $\vec{K}_f = \vec{K}_i + \vec{k} - \vec{k}_s$. After some manipulation, which is outlined in Ref. 23, Eq. (23) can be put in the form

$$\begin{aligned} \frac{d\sigma_{1 \rightarrow f}}{d\omega_s d\Omega} \\ = \frac{C \sum_s (\omega_s / \omega) |\hat{\epsilon}_s \cdot \langle \vec{r} \rangle|^2 |\hat{\epsilon} \cdot \langle \vec{r} \rangle|^2 N \delta(\omega_s - \omega_+)}{[\omega_0 - \omega + (\hbar/2M)(k^2 + 2\vec{k} \cdot \vec{K}_i)]^2 + \frac{1}{4}\gamma^2}, \end{aligned} \quad (23a)$$

where N is an angular factor of order unity which depends on the angles between \vec{k} , \vec{k}_s , and \vec{K}_i . An exact expression for N is given in Ref. 23. Neglecting terms of order $R/\hbar\omega_0$, β^2 and higher, we have

$$N \approx 1 + \beta_1 \cos \theta_{1s}, \quad (23b)$$

where θ_{1s} is the angle between \vec{K}_i and \vec{k}_s and $\beta_1 = \hbar K_i/Mc$. ω_+ is the frequency of the scattered photon²³ and, neglecting the same order of terms as above, is given approximately by

$$\omega_+ \approx \omega - (2R/\hbar)(1 - \cos \theta_s) - \beta_1 \omega (\cos \theta_i - \cos \theta_{1s}), \quad (23c)$$

where θ_s is the angle between \vec{k} and \vec{k}_s and θ_i is the angle between \vec{k} and \vec{K}_i .

B. Cross sections

The total cross section for scattering of the laser light by an atom in the translational state $|\vec{K}_i\rangle$, obtained by integrating the differential cross section obtained from Eq. (23a) over all angles of the scattered photon, is (neglecting terms of order $R/\hbar\omega_0$, β^2 , and $(\omega - \omega_0)/\omega_0$)

$$\frac{d\sigma_{i \rightarrow f}}{d\omega_s d\Omega} = C \sum_s \frac{\omega_s}{\omega} |\hat{\epsilon}_s \cdot \langle \vec{r} \rangle|^2 \sum_m \frac{|\hat{\epsilon}_m \cdot \langle \vec{r} \rangle|^2 \delta(\vec{K}_i + \vec{k}_s, \vec{K}_i + \vec{k}_m) \delta(\omega - \omega_s - (\hbar/2M)(K_i^2 - K_f^2))}{[\omega_0 - \omega + (\hbar/2M)(k^2 + 2\vec{k}_m \cdot \vec{K}_i)]^2 + \frac{1}{4}\gamma^2}, \quad (25)$$

where the sum over m represents the sum over the directions of the six laser beams.

C. Cooling rates and limits

For each scattering event, the average change in the kinetic energy of an atom initially in the state $|\vec{K}_i\rangle$ is the negative of the average change in energy of the scattered photon and is equal to [with σ_i given by Eq. (24)]

$$\int d\Omega_s \hbar(\omega - \omega_s) \frac{d\sigma_{i \rightarrow f}}{d\Omega_s} / \sigma_i = 2R + \hbar \vec{k} \cdot \vec{v}_i, \quad (26)$$

in agreement with Eq. (3). Again, smaller terms of order $\beta_1^2 \hbar\omega_0$, $\beta_1 R$, and higher have been neglected. This same result was obtained in Sec. II by averaging over all possible directions of the scattered photon. The net cooling rate is given by

$$\begin{aligned} & \left\langle \frac{d(E_f - E_i)}{dt} \right\rangle \\ &= \frac{I}{\hbar\omega} \int d\Omega \sum_{f,i} P_i(E_f - E_i) \frac{d\sigma_{i \rightarrow f}}{d\Omega}, \end{aligned} \quad (27)$$

$$\begin{aligned} \sigma_i &= \int d\Omega d\omega_s \frac{d\sigma_{i \rightarrow f}}{d\omega_s d\Omega} \\ &= \frac{C \frac{8}{3} \pi |\hat{\epsilon} \cdot \langle \vec{r} \rangle|^2 |\langle \vec{r} \rangle|^2}{(\omega_{abs} - \omega)^2 + \frac{1}{4}\gamma^2}, \end{aligned}$$

where ω_{abs} is given by Eq. (2a) (neglecting the β^2 term). Since γ is equal to $4c^2 |\langle \vec{r} \rangle|^2 \omega_0^3 / (3\hbar c^3)$, then

$$\sigma_i = 6\pi \lambda^2 |\hat{\epsilon} \cdot \langle \vec{r} \rangle|^2 (\frac{1}{2}\gamma)^2 / [(\omega_{abs} - \omega)^2 + (\frac{1}{2}\gamma)^2], \quad (24)$$

where $\langle \vec{r} \rangle$ is the unit vector corresponding to $\langle \vec{r} \rangle$. If the orientation of the atom with respect to the polarization vector $\hat{\epsilon}$ is random, the average value of $|\hat{\epsilon} \cdot \langle \vec{r} \rangle|^2$ is $\frac{1}{3}$, and we arrive at Eq. (4). However, in a particular experimental situation, the orientation of $\langle \vec{r} \rangle$ and $\hat{\epsilon}$ may be fixed, in which case this averaging should not be performed.

We will assume as in Sec. II that we have six laser beams of equal intensity directed along the $\pm x, \pm y, \pm z$ directions. To avoid the effects of the induced dipole forces we must make the same approximations as in the classical treatment. In this case the initial wave function describing the radiation field becomes:

$$\begin{aligned} |n(\vec{k})\rangle &= |n(\vec{k}_x), n(-\vec{k}_x), n(\vec{k}_y), \\ & n(-\vec{k}_y), n(\vec{k}_z), n(-\vec{k}_z)\rangle \end{aligned}$$

where the occupation numbers are the same and $|\vec{k}_i| = k$. Equation (23) then becomes

where I is the intensity of each laser beam, P_i is the probability for an atom to be in the initial state $|\vec{K}_i\rangle$, and $d\sigma_{i \rightarrow f}/d\Omega$ is given by Eq. (25). With the help of Eq. (26), we can write

$$\begin{aligned} \left\langle \frac{d(E_f - E_i)}{dt} \right\rangle &= \frac{I\sigma_0}{2\hbar\omega} \sum_{m,i} |\hat{\epsilon}_m \cdot \langle \vec{r} \rangle|^2 |G_{m,i}|^2 \\ & \times \left(2R + \frac{\hbar^2 \vec{K}_i \cdot \vec{k}_m}{M} \right) P_i, \end{aligned}$$

where

$$(1/\gamma') G_{m,i} \equiv [\omega_0 + (\hbar/2M)(k_m^2 + 2\vec{k}_m \cdot \vec{K}_i) - \omega - \frac{1}{2}i\gamma]^{-1}$$

and $\gamma' = \frac{1}{2}(1 - i)\gamma$. If we assume that the Doppler width is smaller than the natural width ($\hbar \vec{k}_m \cdot \vec{K}_i / M \ll \gamma$) and write $\omega = \omega_0 + R/\hbar - \frac{1}{2}\gamma + \Delta\omega$ we can write when $\Delta\omega \ll \gamma$

$$G_{m,i} \approx 1 + \Delta\omega/\gamma' - (\hbar \vec{k}_m \cdot \vec{K}_i)/\gamma' M.$$

Assuming P_i is isotropic, the cooling rate is given by Eq. (10) (maximum cooling for $\Delta\omega = 0$) and the corresponding limit by Eq. (11). Similarly if the Doppler width is not negligible com-

pared to the natural width, we obtain Eq. (7), if P_i is given by a Maxwell-Boltzmann distribution. Consequently, the limits of Fig. 3 are also obtained. Thus the fully quantum-mechanical treatment is not necessary to describe the cooling for the case of free atoms. We shall see, however, that it is necessary for an accurate description of bound atoms.

V. LASER COOLING OF BOUND ATOMS

A. Matrix elements

To study the cooling process when the atoms are bound we will assume for simplicity that the atoms are harmonically bound in three dimensions as discussed in Sec. II. This case may not be realized in practical systems, but it may be a close approximation; moreover, it illustrates the important features of the problem. Thus we have

$$H_i = \frac{\vec{P}^2}{2M} + \frac{1}{2}M(\Omega_x^2 x^2 + \Omega_y^2 y^2 + \Omega_z^2 z^2).$$

The solution for the eigenstates of a harmonic oscillator appears in many texts; using the operator formalism we have

$$H_i = \sum_{i=x,y,z} \hbar\Omega_i(N_i + \frac{1}{2}), \quad N_i = a_i^\dagger a_i,$$

where a_i and a_i^\dagger are the lowering and raising operators for the states satisfying $[a_i, a_i^\dagger] = \delta_{ij}$. The position and momentum operators are given by

$$x = x_0(a_x + a_x^\dagger), \quad p_x = ix_0M\Omega_x(a_x^\dagger - a_x), \\ x_0 = (\hbar/2M\Omega_x)^{1/2}, \quad (28)$$

and similarly for y and z . We have $\Psi = \Psi_x\Psi_y\Psi_z$, where in the above representation

$$\Psi_i = |n_i\rangle \quad \langle n_i | n_j \rangle = \delta_{n_i n_j} \delta_{ij} \\ a_i |n_i\rangle = (n_i)^{1/2} |n_i - 1\rangle \quad \Psi = |n_x\rangle |n_y\rangle |n_z\rangle \\ a_i^\dagger |n_i\rangle = (n_i + 1)^{1/2} |n_i + 1\rangle \quad i, j = x, y, z$$

and in the Schrödinger representation²⁴:

$$|n_x\rangle = (2^{n_x} n_x! \pi^{1/2})^{-1/2} \exp(-M\Omega_x x^2/2\hbar) \\ \times H_{n_x}[(M\Omega_x/\hbar)^{1/2} x], \quad (29)$$

where H_{n_x} is the Hermite polynomial of order n_x .

From Eqs. (19) and (20) we will be interested in matrix elements of the form

$$\langle n' | \hat{\epsilon} \cdot (m/M) \vec{P} \exp(i\vec{k} \cdot \vec{x}) | n \rangle \langle e | \exp(i\vec{k} \cdot \vec{r}) | g \rangle \\ + \langle n' | \exp(i\vec{k} \cdot \vec{x}) | n \rangle \langle e | \hat{\epsilon} \cdot \vec{p} \exp(i\vec{k} \cdot \vec{r}) | g \rangle, \quad (30)$$

and therefore we are interested in harmonic oscillator matrix elements of the form

$$\langle n' | \exp(i\vec{k} \cdot \vec{x}) | n \rangle \\ = \langle n'_x | \exp(ik_x x) | n_x \rangle \langle n'_y | \exp(ik_y y) | n_y \rangle \\ \times \langle n'_z | \exp(ik_z z) | n_z \rangle.$$

Therefore, in general, we are interested in matrix elements of the type $\langle n' | \exp(ikx) | n \rangle$, where we have dropped the subscripts.

These matrix elements can be straightforwardly evaluated from the explicit form of the wave functions given in Eq. (29) or by the following operator method. Since

$$e^{A+B} = e^A e^B e^{-[A,B]/2}$$

when

$$[A, [A, B]] = [B, [A, B]] = 0,$$

we have

$$\exp(ikx) = \exp[ikx_0(a^\dagger + a)] \\ = \exp[-\frac{1}{2}(kx_0)^2] \exp(ikx_0 a^\dagger) \\ \times \exp(ikx_0 a).$$

Since

$$a^m |n\rangle = \begin{cases} [n!/(n-m)!]^{1/2} |n-m\rangle & m \leq n \\ 0 & m > n \end{cases}$$

then

$$\exp(ikx_0 a) |n\rangle \\ = \sum_{m=0}^n \frac{(ikx_0)^m}{m!} \left(\frac{n!}{(n-m)!} \right)^{1/2} |n-m\rangle.$$

Thus the matrix elements can be written

$$\langle n' | \exp(ikx) | n \rangle \\ = \exp[-\frac{1}{2}(kx_0)^2] \\ \times \langle n' | \exp(ikx_0 a^\dagger) \exp(ikx_0 a) | n \rangle.$$

Operating to the right with $\exp(ikx_0 a)$ and to the left with $\exp(ikx_0 a^\dagger)$ and using orthogonality, we obtain

$$\langle n' | \exp(ikx) | n \rangle \\ = \exp[-\frac{1}{2}(kx_0)^2] (n! n'!)^{1/2} (ikx_0)^{\Delta n} \\ \times \sum_{m=0}^{n_c} \frac{(-1)^m (kx_0)^{2m}}{m! (m + \Delta n)! (n_c - m)!},$$

where $\Delta n = |n' - n|$ and n_c is the lesser of n and n' . From the explicit form of the generalized Laguerre polynomial

$$L_m^\alpha(X) = \sum_{m=0}^n (-1)^m \binom{n+\alpha}{n-m} \frac{X^m}{m!}$$

we have

$$\begin{aligned} & \langle n' | \exp(ikx) | n \rangle \\ &= \exp\left[-\frac{1}{2}(kx_0)^2\right] [n_c! / (n_c + \Delta n)!]^{1/2} \\ & \times (ikx_0)^{\Delta n} L_{n_c}^{\Delta n} [(kx_0)^2]. \end{aligned} \quad (31)$$

In the following we will see that the cooling problem for bound absorbers shares many similarities with the Mössbauer effect; therefore, some of the same mathematics^{25,26} can be employed. In the study of the Mössbauer effect, one typically looks at the absorption and emission processes separately; for the cooling problem we recall that we are primarily interested in a scattering process. Nevertheless, it will be useful to look at the absorption and emission processes separately in the cooling problem as well. With the help of Eqs. (22c) and (22d), Eq. (30) reduces to

$$im\omega_0 \langle n' | \exp(i\vec{k} \cdot \vec{x}) (\hat{\epsilon} \cdot \langle \vec{r} \rangle - \frac{\vec{k} \cdot \langle \vec{r} \rangle}{M\omega_0} \hat{\epsilon} \cdot \vec{P}) | n \rangle$$

and this expression can be substituted into Eq. (19) to obtain the cross section.

B. Spontaneous emission

With the approximation of low laser intensity used here, the scattered photon results from spontaneous emission. Therefore, if we look at the emission process separately, we are interested in amplitudes which are matrix elements

$$\begin{aligned} \langle n_j | A_{sp}^\dagger [H_t, A_{sp}] | n_j \rangle &= R(\hat{\epsilon}_s \cdot \langle \vec{r} \rangle)^2 + R \left(\frac{\vec{k}_s \cdot \langle \vec{r} \rangle}{M\omega_0} \right)^2 \langle (\hat{\epsilon}_s \cdot \vec{P})^2 \rangle_j - \frac{2\hbar}{M^2\omega_0} \hat{\epsilon}_s \cdot \langle \vec{r} \rangle \vec{k}_s \cdot \langle \vec{r} \rangle \langle (\hat{\epsilon}_s \cdot \vec{P})(\vec{k}_s \cdot \vec{P}) \rangle_j \\ &+ \frac{i\hbar}{M\omega_0^2} (\vec{k}_s \cdot \langle \vec{r} \rangle)^2 \langle \hat{\epsilon}_s \cdot \vec{P} \left(\sum_{m=x,y,z} \Omega_m^2 \chi_m \epsilon_{sm} \right) \rangle_j, \end{aligned} \quad (34)$$

where, for an operator J ,

$$\langle J \rangle_j \equiv \langle n_j | J | n_j \rangle,$$

and $|\vec{k}_s| \approx |\vec{k}|$.

The third term in Eq. (34) is approximately equal to

$$|\langle \vec{r} \rangle|^2 (RE_K / \hbar\omega_0) \approx \hbar\omega_0 \beta^2 |\langle \vec{r} \rangle|^2,$$

and the fourth term is approximately equal to $|\langle \vec{r} \rangle|^2 R(\Omega/\omega_0)^2$. The fourth term is clearly negligible with respect to the first, and the third term is negligible when $E_K \ll \hbar\omega_0$, which is reasonable and is assumed here.

With the above approximations and noting that

$$\begin{aligned} & (\hat{\epsilon}_s \cdot \langle \vec{r} \rangle)^2 + \left(\frac{\vec{k}_s \cdot \langle \vec{r} \rangle}{M\omega_0} \right)^2 \langle (\hat{\epsilon}_s \cdot \vec{P})^2 \rangle_j \\ &= \sum_j \langle n_j | A_{sp} | n_j \rangle^2, \end{aligned} \quad (35)$$

we have

of the operator:

$$A_{sp} \equiv \exp(-i\vec{k}_s \cdot \vec{x}) [\hat{\epsilon}_s \cdot \langle \vec{r} \rangle + (\vec{k}_s \cdot \langle \vec{r} \rangle) \hat{\epsilon}_s \cdot \vec{P}] / (M\omega_0). \quad (32)$$

Strictly speaking, we must sum over all amplitude contributions of the intermediate states n_j as in Eq. (19); however, if only one intermediate state n_j is excited, which is a good approximation when $\gamma \ll \Omega_i$, then the probability for reemission is proportional to $|\langle n_j | A_{sp} | n_j \rangle|^2$.

It is instructive to first look at the average energy change of the translational energy states in the emission process. We have

$$\langle E_f - E_i \rangle = \frac{\int d\Omega \sum_{s,f} \sum_{s,f} (E_f - E_i) |\langle n_f | A_{sp} | n_j \rangle|^2}{\int d\Omega \sum_{s,f} \sum_{s,f} |\langle n_f | A_{sp} | n_j \rangle|^2},$$

where we can write

$$\begin{aligned} & \sum_j (E_f - E_i) |\langle n_f | A_{sp} | n_j \rangle|^2 \\ &= \sum_j \langle n_j | A_{sp}^\dagger | n_j \rangle \langle n_f | [H_t, A_{sp}] | n_j \rangle \\ &= \langle n_j | A_{sp}^\dagger [H_t, A_{sp}] | n_j \rangle. \end{aligned}$$

Using the expression

$$\begin{aligned} & [H_t, \exp(-i\vec{k}_s \cdot \vec{x})] \\ &= [\exp(-i\vec{k}_s \cdot \vec{x}) / 2M] (\hbar^2 k_s^2 - 2\hbar \vec{k}_s \cdot \vec{P}) \end{aligned} \quad (33)$$

we have

$$\langle E_f - E_i \rangle = R, \quad (36)$$

which is independent of the intermediate state. This is a familiar result from the studies of the Mössbauer effect and shows that a fundamental limit to the cooling process is caused by the recoil heating upon reemission. It also agrees with Eq. (2b) (averaged over emission angles) for the free atom case (neglecting β^2 terms). At this point we note that

$$[(\vec{k}_s \cdot \langle \vec{r} \rangle) / M\omega_0]^2 \langle (\hat{\epsilon}_s \cdot \vec{P})^2 \rangle_j \approx |\langle \vec{r} \rangle|^2 \beta^2,$$

and therefore we will neglect the second term in Eqs. (32) and (35) in what follows.

We can arrive at a better understanding of the emission spectrum by asking for the second moment of translational energy change in the emission process. This is interesting because it gives the spread of photon energies in the emission process. We have

$$\begin{aligned}\langle(\Delta E)^2\rangle &= \langle(E_f - E_j - \langle E_f - E_j \rangle)^2\rangle \\ &= \langle(E_f - E_j)^2\rangle - R^2,\end{aligned}$$

where we have used Eq. (36). We have

$$\langle(E_f - E_j)^2\rangle = \int d\Omega \sum_{s,j} (E_f - E_j)^2 |\langle n_f | \exp(-i\vec{k}_s \cdot \vec{x}) | n_j \rangle|^2 / \int d\Omega \sum_{s,j} |\langle n_f | \exp(-i\vec{k}_s \cdot \vec{x}) | n_j \rangle|^2.$$

Writing

$$\begin{aligned}(E_f - E_j)^2 |\langle n_f | \exp(-i\vec{k}_s \cdot \vec{x}) | n_j \rangle|^2 \\ = |\langle n_f | [H_f, \exp(-i\vec{k}_s \cdot \vec{x})] | n_j \rangle|^2,\end{aligned}$$

using Eqs. (28) and (33), and assuming the atoms to be unpolarized, we obtain

$$\langle(\Delta E)^2\rangle = \frac{2}{3}R\langle H_f \rangle. \quad (37)$$

If the motion is characterized by the Maxwell-Boltzmann distribution, this is just the expression

for broadening due to the Doppler effect. Below we will show that in the classical limit the profile of the emission spectrum observed in a particular direction is a shifted Gaussian. In this case, for the recoil energy R approximately equal to the atom kinetic energy, the spectrum is shown in Fig. 7. We note that Eqs. (36) and (37) are also valid for the case of the free atom (neglecting terms of order β^2), since Eq. (33) holds for both cases; however, the spectrum is continuous and is shown by the dotted line in Fig. 7.

C. Absorption cross section

For the case of bound atoms, Eq. (19) becomes

$$\frac{d\sigma_{i \rightarrow f}}{d\omega_s d\Omega} = C \sum_s \frac{\omega_s}{\omega} |\hat{\epsilon}_s \cdot \langle \vec{r} \rangle|^2 |\hat{\epsilon} \cdot \langle \vec{r} \rangle|^2 \left| \sum_j \frac{\langle n_j | \exp(-i\vec{k}_s \cdot \vec{x}) | n_i \rangle \langle n_j | \exp(i\vec{k} \cdot \vec{x}) | n_f \rangle}{\omega_0 - \omega + (E_j - E_i)/\hbar - \frac{1}{2}i\gamma} \right|^2 \delta\left(\omega - \omega_s - \frac{E_f - E_i}{\hbar}\right). \quad (38)$$

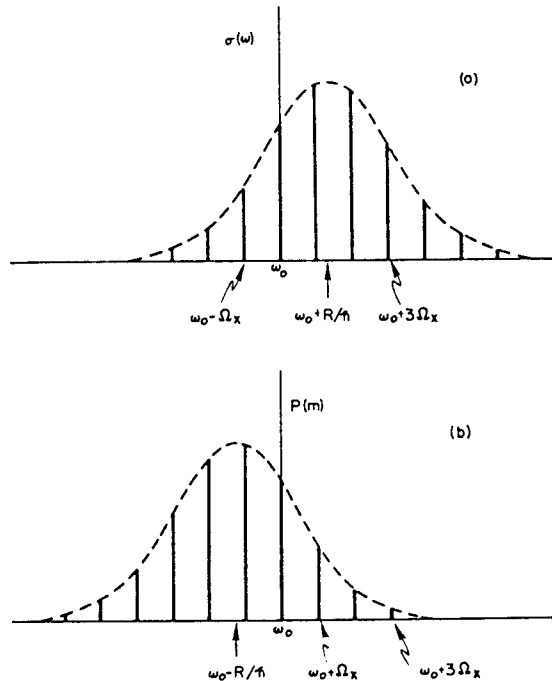


FIG. 7. Atomic spectra in classical limit ($\hbar\Omega_x \ll k_B T$) when $R \lesssim \hbar\omega_D$. Part (a) shows the absorption cross section for a laser directed along the x axis for the case when $\gamma \ll \Omega_x$ (giving the discrete lines) and when $\Omega_x \rightarrow 0$ (dashed curve) which is also the case for free atom. Part (b) shows the emission spectrum observed along the x direction for the same two cases.

We can obtain the absorption cross section by summing over the final states and integrating over possible scattered photon states. Following the procedure used to obtain Eq. (24), we have

$$\begin{aligned}\sigma_i &= 6\pi \lambda^2 |\hat{\epsilon} \cdot \langle \vec{r} \rangle|^2 \\ &\times \sum_j \left| \frac{\langle n_j | \exp(-i\vec{k} \cdot \vec{x}) | n_i \rangle \frac{1}{2}\gamma}{\omega_0 - \omega + (E_j - E_i)/\hbar - \frac{1}{2}i\gamma} \right|^2.\end{aligned} \quad (39)$$

1. Strong binding

Equation (39) clearly shows the sideband structure in the absorption spectrum when $\Omega_i \gg \gamma$. For this case, essentially only one term contributes to the sum over j when the resonance condition $[\omega_0 - \omega + (E_j - E_i)/\hbar = 0]$ is met. For simplicity, assume that the atoms are unpolarized and that the laser radiation is incident along the x axis, so that $\omega = \omega_0 + m\Omega_x$ ($m = 0, \pm 1, \pm 2, \dots$) that is, we are tuned to the m th sideband. Then Eq. (39) becomes

$$\sigma_i \approx \sigma_0 |\langle n_i + m | \exp(i\vec{k} \cdot \vec{x}) | n_i \rangle|^2, \quad (40)$$

where we have dropped the x subscripts in the wave functions.

It is useful to examine Eq. (40) when $R \ll k_B T$ and where n_i is approximately equal to the mean occupation number, i.e.,

$$n_l = n^* \approx \langle n \rangle = (H_l) / (\hbar\Omega_x) - \frac{1}{2}.$$

For the case of interest, the laser frequency must lie somewhere within the Doppler profile of the atomic resonance (i.e., $|m|\hbar\Omega_x \leq \beta\hbar\omega_0$). In this case, we can show that $|m| \ll n^*$. We have

$$\begin{aligned} |m|\hbar\Omega_x &\leq \hbar\omega_0 \Omega_x \langle x^2 \rangle^{1/2} / c \\ &= \hbar\Omega_x k \langle x^2 \rangle^{1/2} \end{aligned} \quad (41)$$

and so

$$\frac{|m|}{n^*} \leq \frac{k \langle x^2 \rangle^{1/2}}{n^*} \approx \left(\frac{R}{n^* \hbar\Omega_x} \right)^{1/2} \approx \left(\frac{R}{k_B T} \right)^{1/2} \ll 1.$$

If n^* is large ($\hbar\Omega_x/E_x \ll 1$), we can approximate the Laguerre polynomial in the matrix element by its asymptotic form.²⁷ Dropping the • superscript, we have

$$\begin{aligned} \exp[-\frac{1}{2}(kx_0)^2] (kx_0)^{|m|} L_{n-|m|}^{|m|} |_{|m|} \langle (kx_0)^2 \rangle \\ \approx \frac{\Gamma(n+1) J_{|m|} [kx_0(4n-2|m|+2)^{1/2}]}{(n_1 - \frac{1}{2}|m| + \frac{1}{2})^{|m|/2} (n-|m|)!}. \end{aligned}$$

Since $n \gg |m|$, then

$$\begin{aligned} (n-|m|)! &= n! [n(n-1)(n-2)\dots(n-|m|+1)]^{-1} \\ &\approx n! n^{-|m|} \end{aligned}$$

and

$$(n - \frac{1}{2}|m| + \frac{1}{2})^{|m|/2} \approx n^{|m|/2}$$

so that

$$\begin{aligned} \sigma(m) &= \sigma_0 \left[1 - \exp\left(\frac{-\hbar\Omega_x}{k_B T}\right) \right] \sum_{n_l=-m}^{\infty} \exp\left(\frac{-n_l \hbar\Omega_x}{k_B T}\right) |\langle n_l + m | e^{ikx} | n_l \rangle|^2 \\ &= \sigma_0 \left[1 - \exp\left(\frac{-\hbar\Omega_x}{k_B T}\right) \right] \exp\left[-(kx_0)^2 + \left(\frac{m \hbar\Omega_x}{k_B T}\right)\right] (kx_0)^{-2m} \sum_{n=0}^{\infty} \exp\left(\frac{-n \hbar\Omega_x}{k_B T}\right) \frac{n!}{(n-m)!} [L_n^{-m}(k^2 x_0^2)]^2, \end{aligned}$$

where we have used Eq. (31). We obtain a similar result for $m \geq 0$. These sums can be evaluated with the generating function²⁸

$$\begin{aligned} \sum_{n=0}^{\infty} \frac{n!}{\Gamma(n+\alpha+1)} L_n^\alpha(x) L_n^\alpha(y) z^n \\ = (1-z)^{-1} \exp\left[-z\left(\frac{x+y}{1-z}\right)\right] \\ \times (xyz)^{-\alpha/2} I_\alpha\left(\frac{2(xy z)^{1/2}}{1-z}\right). \end{aligned}$$

If we let

$$z = \exp(-\hbar\Omega_x/k_B T), \quad x = y = (kx_0)^2, \quad \alpha = |m|,$$

and noting that $I_m = I_{-m}$, then

$$\begin{aligned} \exp[-\frac{1}{2}(kx_0)^2] (kx_0)^{|m|} L_{n-|m|}^{|m|} |_{|m|} \langle (kx_0)^2 \rangle \\ \approx n^{|m|/2} J_{|m|} (2n^{1/2} kx_0). \end{aligned}$$

Therefore

$$\begin{aligned} \langle n^* - |m| | \exp(i\vec{k} \cdot \vec{x}) | n^* \rangle \\ \approx (i)^{|m|} J_{|m|} (2n^{*1/2} kx_0) \end{aligned}$$

and since

$$n^* x_0^2 \approx \frac{1}{2} \langle x^2 \rangle = \frac{1}{4} x_a^2,$$

where x_a is the amplitude of the classical oscillatory motion, then Eq. (40) can be written

$$\sigma_l \approx \sigma_0 J_{|m|}^2(kx_a),$$

which is equivalent to the cross section used in Eq. (14).

In general, we must average the absorption cross section over a distribution of initial state values. This averaged cross section is then given by:

$$\sigma(m) = \sum_l P_l \sigma_l, \quad (42)$$

where σ_l is given by Eq. (40) and where P_l is the probability of the atom initially being in the state l . In this more general case we can arrive at an expression for the cross section by assuming that P_l is given by a thermal distribution. That is,

$$P_l = [1 - \exp(-\hbar\Omega_x/k_B T)] \exp(-n_l \hbar\Omega_x/k_B T),$$

so that when $m \leq 0$

$$\begin{aligned} \sigma(m) &= \sigma_0 \exp\left[\frac{m}{2} \frac{\hbar\Omega_x}{k_B T} - 2(kx_0)^2\right] \\ &\quad \times \left(\frac{1}{2} - \frac{1}{1 - \exp(-\hbar\Omega_x/k_B T)}\right) \\ &\quad \times I_m\left(\frac{2(kx_0)^2 \exp(-\frac{1}{2}\hbar\Omega_x/k_B T)}{1 - \exp(-\hbar\Omega_x/k_B T)}\right). \end{aligned}$$

Noting that

$$\langle x^2 \rangle = 2x_0^2 \langle n \rangle + \frac{1}{2},$$

where $\langle n \rangle$ is the mean occupation number

$$\langle n \rangle = \sum_n n P_n = \left[\exp\left(\frac{\hbar\Omega_x}{k_B T}\right) - 1 \right]^{-1}, \quad (43)$$

then

$$\sigma(m) = \sigma_0 \exp\left[\frac{1}{2}m(\hbar\Omega_x/k_B T) - k^2\langle x^2 \rangle\right] \\ \times I_m[\exp(\hbar\Omega_x/2k_B T)2(kx_0)^2\langle n \rangle]. \quad (44)$$

Examination of Eq. (44) shows the skewing of the cross section to high-energy values, i.e., $m > 0$. This is plausible because, for example, in the low-temperature limit ($k_B T \approx R$) the atom more easily gains energy rather than losing it in the scattering process. (When $T = 0$ it is impossible for it to lose energy.)

A result similar to Eq. (44) is obtained when one looks for the probability of emission at a certain sideband frequency. From Sec. VB we write a general expression for the probability of emission of a photon of frequency $\omega_0 + m\Omega_x$, which we call $P(m)$. We have

$$P(m) = \sum_j \langle n_j - m | \exp(-i\vec{k}_s \cdot \vec{x}) | n_j \rangle|^2 P_j,$$

where P_j is the probability of the atom being in the translational energy level j when in the excited state. $P(m)$ is normalized to unity as can be verified by summing over m . If we observe the emitted light in the x direction, then $\vec{k}_s \cdot \vec{x} = k_s x$. If P_j is given by a Maxwell-Boltzmann distribution then we find

$$P(m) = \exp\left[-\frac{1}{2}m(\hbar\Omega_x/k_B T) - k^2\langle x^2 \rangle\right] \\ \times I_m[\exp(\hbar\Omega_x/2k_B T)2(kx_0)^2\langle n \rangle]. \quad (45)$$

This same result was derived by an alternative method and is given by Eq. (3.66a) of Ref. 26. Equation (45) clearly shows the skewing to low-energy values.

In a high-resolution experiment with lasers used to probe a bound atom, we might be particularly interested in the cross section for absorption on the unshifted carrier given by Eq. (44) for $m = 0$. We have

$$\sigma(m=0) = \sigma_0 \exp(-k^2\langle x^2 \rangle) \\ \times I_0[\exp(\hbar\Omega_x/k_B T)2(kx_0)^2\langle n \rangle].$$

A special case is when $\langle n \rangle = 0$, yielding the cross section:

$$\sigma(0-0) = \sigma_0 \exp(-k^2\langle x_0^2 \rangle).$$

The exponential factor is known as the Debye-Waller factor and is familiar in studies of x-ray scattering and the Mössbauer effect. It shows the

suppression of the cross section due to zero-point vibrations.

It is interesting to evaluate Eq. (44) in the classical limit, that is, when $\hbar\Omega_x \ll k_B T$. In this case, if we apply Eq. (16) we obtain

$$\sigma(m) = (\sigma_0 \Omega_x / \sqrt{\pi} \omega_D) \exp\{-[(\omega - \omega'_0)/\omega_D]^2\}, \quad (46)$$

where $\omega - \omega'_0 = m\Omega_x - R/\hbar$. This expression is analogous to the cross section used in Eq. (17), but now shows the dependence on recoil. We note that the envelope of the cross section for the sidebands has a normal Doppler shape; however, the center of gravity of this Doppler profile is shifted to the frequency $\omega'_0 = \omega_0 + R/\hbar$. Similarly, we can also find the expression for the emission spectrum which then has the same form as Eq. (46) except that $\omega'_0 - \omega''_0 = \omega_0 - R/\hbar$. Thus, we obtain a Doppler profile whose center of gravity is shifted to the frequency $\omega_0 - R/\hbar$ as indicated in Fig. 7.

2. Weak binding

When the condition $\gamma \ll \Omega_x$ is not satisfied, we must return to the cross section given in Eq. (42), where σ_1 is given by Eqs. (38) or (39). Assuming the atoms are thermalized and unpolarized, we have:

$$\sigma(\omega) = \sum_{m=-\infty}^{\infty} \frac{\sigma(m)}{1 + [(2/\gamma)(\omega_0 - \omega + m\Omega_x)]^2}, \quad (47)$$

where $\sigma(m)$ is given by Eq. (44). In the classical limit ($\hbar\Omega_x \ll k_B T$), we can use Eq. (46) and convert the sum in Eq. (47) to an integral to obtain

$$\sigma(\omega) = \frac{\sigma_0}{\sqrt{\pi} \omega_D} \int_{-\infty}^{\infty} \frac{\exp[-(\Omega/\omega_D)^2]}{1 + [(2/\gamma)(\omega'_0 - \omega + \Omega)]^2} d\Omega,$$

which is identical to Eq. (6). Thus we see that the absorption cross section for a bound atom approaches that of the free atom in the limit of weak binding.

D. Cooling rate

The cooling rate can be derived from the differential cross section by means of Eq. (27), where $d\Omega_{i \rightarrow f}/d\Omega$ is given by Eq. (38). After some simplification, and assuming the atoms are unpolarized, we can write

$$\left\langle \frac{d(E_f - E_i)}{dt} \right\rangle = \frac{I\sigma_0}{\hbar\omega} \sum_{i,j} P_i \left((R + E_j - E_i) \frac{\langle n_j | \exp(i\vec{k} \cdot \vec{x}) | n_i \rangle|^2}{1 + \{(2/\gamma)[\omega_0 - \omega + (E_j - E_i)/\hbar]\}^2} \right). \quad (48)$$

In this form we have separated out the effect due to reemission (R term) and the effect due to absorption ($E_j - E_i$ term).

1. Strong binding

In the limit $\gamma \ll \Omega_x$, and assuming we are tuned to resonance ($\omega = \omega_0 + m\Omega_x$), then only one term of the sum in Eq. (48) is important, and we obtain

$$\left\langle \frac{d(E_f - E_i)}{dt} \right\rangle_m = \frac{I\sigma(m)}{\hbar\omega} [R + m\hbar\Omega_x], \quad (49)$$

where $\sigma(m)$ is given by Eq. (42) or by Eq. (44) when P_i is given by a Maxwell-Boltzmann distribution. In the classical limit $\sigma(m)$ is given by Eq. (46) and we obtain

$$\left\langle \frac{d(E_f - E_i)}{dt} \right\rangle_m = \frac{I\sigma_0\Omega_x}{\hbar\sqrt{\pi}\omega_0\omega_D} [R + m\hbar\Omega_x] \times \exp[-(\omega - \omega_0')^2/\omega_D^2], \quad (50)$$

which is analogous to Eq. (17) but now includes the effect due to recoil.

2. Weak binding

When the condition $\gamma \ll \Omega_x$ is not satisfied, we must perform the sum in Eq. (48). In the classical limit $\hbar\Omega_x \ll k_B T$ we obtain

$$\left\langle \frac{d(E_f - E_i)}{dt} \right\rangle = \frac{I}{\hbar\sqrt{\pi}\omega_0\omega_D} \times \int_{-\infty}^{\infty} \frac{(2R + \hbar\Omega) \exp[-(\Omega^2/\omega_D^2)] d\Omega}{1 + [(2/\gamma)(\omega_0' - \omega + \Omega)]^2},$$

which is identical to Eq. (7).

E. Cooling limits

It is also interesting to estimate the limits to the cooling processes; that is, what are the minimum temperatures which can be achieved by the technique? As explained in Sec. II, the limit is obtained when the heating rate due to recoil equals the cooling rate.

1. Strong binding

We first examine the case when $\Omega_x \gg \gamma$. We will assume that substantial cooling has already taken place, and therefore the spectrum of the atom consists of the "carrier" at frequency ω_0 and sidebands at $\omega_0 \pm \Omega_x$; that is, $k(x^2)^{1/2} \ll 1$. Note also that for this model to work, we must require $R \ll \hbar\Omega_x$ or else the reemission spectrum does not satisfy the simple picture of a "carrier" and two adjacent sidebands; however, this seems to be a most interesting case in the optical domain. The case when $R \gg \hbar\Omega_x$ could be easily treated. For

maximum cooling the incident radiation is tuned to $\omega = \omega_0 - \Omega_x$, i.e., the lower sideband. In Eq. (49) we have included the effect of only the resonant sideband in arriving at a cooling rate. However, to obtain the cooling limit, we will include the effect of both upper and lower sidebands and the carrier. From Eq. (48) we therefore find near the cooling limit:

$$\left\langle \frac{dE}{dt} \right\rangle = \frac{I\sigma_0}{\hbar\omega} R \left(\frac{5}{16} \frac{\gamma^2}{\Omega_x^2} - \langle n_x \rangle \right), \quad (51)$$

which is independent of initial-state distribution but assumes that the y and z degrees of freedom are thermalized with the x degree of freedom and therefore have the same distribution. We might be tempted to apply Eq. (51) to the case of a single isolated atom, but we note that if the laser is directed along the x axis, then the y and z degrees of freedom are heated without bound by the recoil upon reemission. If the frequencies $\{\Omega_i\}$ are degenerate then this argument applies regardless of the direction of the laser since there are no unique axes for the bound atom. If the frequencies $\{\Omega_i\}$ are unequal, then Eq. (51) cannot hold for a single laser directed along, say, the $\hat{i} + \hat{j} + \hat{k}$ direction, because the laser frequency cannot simultaneously coincide with the first lower sidebands for the three independent oscillations. Each specific case is easily treated; for simplicity, however, we will assume as above that we have a collection of weakly thermalized atoms such that the collision rate between atoms is much larger than the optical transition rate. (See Sec. V F). To find the minimum energy possible, we set $\langle dE/dt \rangle = 0$ and obtain

$$\langle n_x \rangle = \frac{5}{16} (\gamma^2/\Omega_x^2) \ll 1.$$

Note that this expression differs from that of Ref. 7. The difference appears to be due to the neglect of the heating effect due to recoil in the direction perpendicular to the laser beam in Ref. 7. That is, if the unshifted emission in the direction perpendicular to the laser beam is considered (the source of the "1 + 1" factor), then the heating due to recoil in this direction must also be considered.

The minimum energy is of course limited to the zero-point energy $\frac{1}{2}\hbar\Omega_x$; however, this can presumably be accurately determined if Ω_x is known, and therefore the uncertainty in energy will be on the order of $\langle n_x \rangle \hbar\Omega_x$. In this limit, if the atoms have a Maxwell-Boltzmann distribution, then the temperature of the atoms is given by Eq. (43). If $\Omega_x/2\pi = 12.5$ MHz and $\gamma/\Omega_x = 0.1$, then $T \cong 10^{-4}$ K; however, the fractional uncertainty in this minimum energy is about 3×10^{-3} . In this simple case where the absorption

spectrum consists of a strong carrier with weak adjacent sidebands ($k\langle x^2 \rangle^{1/2} \ll 1$), we remark that if the incident radiation were tuned to ω_0 we would see in the scattered light a strong component at frequency ω_0 , a weak Stokes line at $(\omega_0 - \Omega_x)$, and a weak anti-Stokes line at $(\omega_0 + \Omega_x)$. However, since the incident radiation is tuned to $\omega_0 - \Omega_x$, the scattered light will contain a component at this frequency, but a much stronger component at frequency ω_0 . Because of this we might regard the cooling process as anti-Stokes or *inverse-Stokes* spontaneous resonance Raman scattering.

2. Weak binding

When the condition $\gamma \ll \Omega_x$ is not satisfied, there are two interesting cases to discuss. For both cases we will assume that γ_c is much larger than the transition rate or that we irradiate the atoms with three mutually perpendicular laser beams. (See Sec. V F.) In the first case we will assume that substantial cooling has already taken place so that the Doppler width is much less than the natural width (which as before requires $R \ll \hbar\gamma$). Maximum cooling will be obtained when $\omega - \omega_0 \approx -\frac{1}{2}\gamma$ and we can expand the denominator in Eq. (48) to obtain

$$\frac{dE}{dt} = \left\langle \frac{d(E_t - E_i)}{dt} \right\rangle = \frac{I\sigma_0}{2\hbar\omega} \sum_I P_I \langle n_i | A(\vec{k})^\dagger (R A(\vec{k}) + [H_t, A(\vec{k})]) | n_i \rangle,$$

where

$$A(\vec{k}) = \exp(i\vec{k} \cdot \vec{x}) + (1/\hbar\gamma') [\exp(i\vec{k} \cdot \vec{x}), H_t].$$

After some simplification we obtain

$$\frac{dE}{dt} \approx \frac{I\sigma_0}{\hbar\omega} R \left(1 - \frac{2\langle E_x \rangle}{\hbar\gamma} \right),$$

which does not depend on the distribution of initial states and therefore holds for an isolated atom if we use three mutually perpendicular laser beams. Minimum kinetic energy is obtained when $dE/dt = 0$, and we obtain Eq. (11) ($\langle E_{K_x} \rangle_{\min} = \frac{1}{4}\hbar\gamma$). It should be noted here that the total energy of a harmonic oscillator is, on the average, equally divided between the kinetic and potential energies.

The second case to discuss is when $R \gg \hbar\gamma$. In this limit we have shown that Eq. (7) applies when P_i is given by a Maxwell-Boltzmann distribution leading to the limits in Fig. 3.

F. Energy distribution for low thermalization rate

We are interested in the kinetic energy distribution when we use a single laser beam to cool a

collection of bound atoms. For simplicity we discuss a particular example; other cases could be similarly treated.

Suppose we have a single laser beam incident along the x axis and consider the limit $\gamma \gg \{\Omega_i\}$. If we ask for the cooling limit, then we want $\omega - \omega_0 \approx -\frac{1}{2}\gamma$ when $R \ll \hbar\gamma$. For this case the equation analogous to Eq. (10) is

$$\frac{dE_x}{dt} = \gamma_i \left(-\frac{4RE_x}{\hbar\gamma} + \frac{4}{3}R \right) + \gamma_c \left(\frac{E_y}{2} + \frac{E_z}{2} - E_x \right),$$

where $\gamma_i \equiv I\sigma_0/(2\hbar\omega)$ and where we have included the transfer of energy between degrees of freedom (via the "collision" rate γ_c) and have assumed for simplicity that the recoil upon reemission is distributed equally over the three degrees of freedom. Note, however, that this simple assumption is violated even for unpolarized atoms. For the y and z directions we have

$$\frac{dE_y}{dt} = \gamma_i \frac{R}{3} + \gamma_c \left(\frac{E_x}{2} + \frac{E_z}{2} - E_y \right),$$

$$\frac{dE_z}{dt} = \gamma_i \frac{R}{3} + \gamma_c \left(\frac{E_x}{2} + \frac{E_y}{2} - E_z \right).$$

In steady state, $dE_i/dt = 0$, and we have $E_x = \frac{1}{2}\hbar\gamma$, which is identical to Eq. (11), and $E_y = E_z = \frac{1}{2}\hbar\gamma + \frac{2}{3}R\gamma_i/\gamma_c$. Hence if $\gamma_c \ll \gamma_i$, the other degrees of freedom are substantially heated by recoil; for a single isolated atom they are heated without bound.

VI. SUMMARY

We have discussed laser cooling of atoms from the standpoint of anti-Stokes spontaneous Raman scattering. To isolate the essential features of the problem we have made several simplifying assumptions. We have assumed that the internal states of the atoms comprise a simple two-level structure and that radiative transitions between these two levels proceed via pure electric dipole transitions. We assume that the plane-wave radiation source (laser) has spectral width $\ll \gamma$ and power much less than that required for saturation. We also assume that the power is small enough to avoid the effects of the induced dipole force³; this is particularly important for the free-atom case where it is desirable to have several laser beams in order to cool in all directions (Sec. II B 1). Finally, we assume that the laser power is low enough to avoid the effects of recoil heating in directions perpendicular to the laser beam when only one beam is used. The treatment has been nonrelativistic; hence we have neglected terms of order $\beta^2\hbar\omega_0$ and βR in the energy.

The cooling rates for free atoms are given in Eq. (5) (one laser beam in x direction), Eq. (7)

(one laser beam in x direction, atoms thermalized), and Eq. (8) [approximation of Eq. (7) when $\gamma, R/\hbar \ll \omega_D$]. These formulas are justified in Sec. IV. For bound atoms, the most general expression for the cooling rate (for one laser beam) is given in Eq. (48). Cooling rates for various approximations are given in Eq. (49) ($\gamma \ll \Omega_x$, one laser beam directed along the x axis and tuned to $\omega = \omega_0 + m\Omega_x$, where m is an integer), Eq. (50) [Eq. (49) in classical limit $\hbar\Omega_x \ll k_B T$], and Eq. (7) (classical limit when $\gamma \gg \Omega_x$, one laser beam directed along the x axis).

As an example, for $M = 100$ amu, $\nu_0 = 5 \times 10^{14}$ Hz ($\lambda = 600$ nm), $\gamma = 2\pi \times 10$ MHz, $I = 50$ mW/cm², $\sigma_0 = 5.7 \times 10^{-10}$ cm², the cooling rate for "free" or weakly bound atoms ($\Omega_x \ll \gamma$) is given by Eq. (8) when the atoms are thermalized. This gives a rate $dE/dt \approx -1.4$ eV/sec. We have assumed that the laser is tuned to $\omega - \omega_0 = -\omega_D/\sqrt{2}$; this is the condition for maximum cooling when $\gamma \ll \omega_D$. This result is independent of temperature as long as $\gamma \ll \omega_D$. (Note, however, that the laser must be swept closer to the line center as the atoms cool to satisfy the condition $\omega - \omega_0 = -\omega_D/\sqrt{2}$.) Equation (8) will also be invalid when $\omega_D \lesssim 10\gamma$ in this example due to saturation of the op-

tical transition.

When the atom is tightly bound ($\Omega_x \gg \gamma$) we may apply Eq. (50) in the classical limit ($\hbar\Omega_x \ll k_B T$). We note that for the same approximate detuning (i.e., assuming the laser is tuned to the sideband which is closest to satisfying the condition $m\hbar\Omega_x = -\omega_D/\sqrt{2}$), the cross section is equal to the cross section in Eq. (8) times $2\Omega_x/(\pi\gamma)$, which results from the compression of the full Doppler profile into discrete sidebands. The cooling rate is increased by the same factor.

It is particularly interesting to examine the cooling limits for various cases. These are summarized in Table I. In each case the mechanism which limits the cooling is the recoil effect; however, this may not be apparent from the expressions. The limits given in Table I assume that there are no other heating mechanisms present; in particular, we have avoided the thermodynamic limits caused by blackbody radiation (Sec. IID) by assuming that blackbody radiation from the surroundings is absent.

For our example atom above, since $R/\hbar \ll \gamma$, the first limit for both free and bound atoms applies. (The assumption is that $\Omega \ll 2\pi \times 10$ MHz, which is usually the case for electromagnetically

TABLE I. Cooling limits for various limiting cases.

Case	Limit	Assumptions
Free atoms	$\langle E_{Kx} \rangle_{\min} = \frac{1}{4} \hbar \gamma$	$R/\hbar \ll \gamma$. Six laser beams in $\pm x$, $\pm y$, and $\pm z$ directions, tuned to $\omega = \omega_0 + R/\hbar - \gamma/2$. (Atoms need not be thermalized via collisions.) $\gamma/2\pi$ is the full width at half-maximum for the optical transition.
	$k_B T \lesssim R$ (Fig. 3)	$R/\hbar \sim \gamma$. Ensemble of atoms assumed to be thermalized with Maxwell-Boltzmann distribution.
Bound atoms	$\langle E_{Kx} \rangle_{\min} = \frac{1}{4} \hbar \gamma$	$R/\hbar, \Omega \ll \gamma$. Laser(s) tuned to $\omega = \omega_0 + R/\hbar - \gamma/2$. If atoms are thermalized only one laser beam need be present. If atoms are not thermalized we must have 3 mutually perpendicular laser beams or one laser beam along $\hat{i} + \hat{j} + \hat{k}$ direction when $\Omega_x \neq \Omega_y, \neq \Omega_z \neq \Omega_x$.
	$k_B T \lesssim R$ (Fig. 3)	Same as for free atom. ($\gamma \gg \Omega_x$)
	$\langle n_x \rangle = 5\gamma^2/16\Omega_x^2$	$\gamma, R/\hbar \ll \Omega_x$. One laser beam directed along x axis and tuned to $\omega_0 - \Omega_x$, atoms thermalized. Same limit for noncolliding atoms if $\Omega_x = \Omega_y = \Omega_z$ and 3 mutually perpendicular beams are used.

confined ions, for example.) We have $\langle E_{rx} \rangle_{\min} \approx 10^{-8}$ eV or, if the atoms are thermalized, $T_{\min} \approx 2.4 \times 10^{-4}$ K. If the atomic transition was only very weakly allowed (given by the condition $\gamma \leq R/\hbar$), then the limits given in Fig. 3 apply. This would imply $T \approx 2.7 \times 10^{-7}$ K for $M = 100$ amu, $\nu_0 = 5 \times 10^{14}$ Hz. However, for this limit to apply we must have $\gamma/2\pi < 6$ kHz. This condition could be realized on an intercombination line, for example. Finally, if the atom was tightly bound, we could realize the last limit in Table I. In this case the minimum energy is given by the zero-point energy, but as discussed in Sec. V E, the uncertainty in this energy could be quite small.

ACKNOWLEDGMENTS

The authors are particularly indebted to J. C. Bergquist (National Bureau of Standards), J. Cooper (University of Colorado), D. J. Larson (University of Virginia), and F. L. Walls (National Bureau of Standards) for the critical reading of the manuscript and several important suggestions for improvement. We thank S. Jarvis, Jr. for the computer solution of the plasma dispersion function and E. DeWeese for careful manuscript preparation. One of us (D.J.W.) wishes to acknowledge partial support by the Office of Naval Research.

*Present address: Frequency and Time Standards Group, National Bureau of Standards, Boulder, Col. 80303.

¹T. W. Hänsch and A. L. Schawlow, *Opt. Commun.* **13**, 68 (1975).

²D. J. Wineland and H. Dehmelt, *Bull. Am. Phys. Soc.* **20**, 637 (1975).

³See, for example, J. E. Bjorkholm, R. R. Freeman, A. Ashkin, and D. B. Pearson, *Phys. Rev. Lett.* **41**, 1361 (1978); A. Ashkin, *Phys. Rev. Lett.* **40**, 729 (1978); V. S. Letokhov, V. G. Minogin, and B. D. Pavlik, *Zh. Eksp. Teor. Fiz.* **72**, 1328 (1977) [*Sov. Phys. JETP* **45**, 698 (1977)]; A. P. Kazantsev, *Usp. Fiz. Nauk.* **124**, 113 (1978) [*Sov. Phys. Usp.* **21**, 58 (1978)]; A. Ashkin and J. P. Gordon, *Opt. Lett.* **4**, 161 (1979).

⁴R. S. Van Dyck, Jr., P. B. Schwinberg, and H. G. Dehmelt, in *New Frontiers in High-Energy Physics*, edited by B. M. Kursunoglu, A. Perlmutter, and L. F. Scott (Plenum, New York, 1978), p. 159.

⁵H. G. Dehmelt, *Nature* **262**, 777 (1976); D. Wineland and H. Dehmelt, *Int. J. Mass Spectrometry Ion Phys.* **16**, 338 (1975); **19**, 251(E) (1976).

⁶D. J. Wineland, R. E. Drullinger, and F. L. Walls, *Phys. Rev. Lett.* **40**, 1639 (1978).

⁷W. Neuhauser, M. Hohenstatt, P. Toschek, and H. Dehmelt, *Phys. Rev. Lett.* **41**, 233 (1978).

⁸A. Kastler, *J. Phys. Radium* **11**, 255 (1950).

⁹For a summary, see P. R. Berman and S. Stenholm, *Opt. Commun.* **24**, 155 (1978).

¹⁰A. Ashkin, *Phys. Rev. Lett.* **24**, 156 (1970); **25**, 1321 (1970).

¹¹B. D. Fried and S. D. Conte, *The Plasma Dispersion Function* (Academic, New York, 1961).

¹²E. M. Purcell (private communication).

¹³W. Magnus, F. Oberhettinger, and R. P. Soni, *For-*

mulas and Theorems for Special Functions of Mathematical Physics (Springer-Verlag, New York, 1966), p. 140.

¹⁴D. J. Wineland, *J. Appl. Phys.* **50**, 2528 (1979).

¹⁵Ya. B. Zel'dovich, *Pis'ma Zh. Eksp. Teor. Fiz.* **19**, 120 (1974) [*JETP Lett.* **19**, 74 (1974)].

¹⁶S. P. Vyatchanin, *Dokl. Akad. Nauk. SSSR* **234**, 1295 (1977); *Sov. Phys. Dokl.* **22**, 321 (1977).

¹⁷See, for example, F. Reif, *Fundamentals of Statistical and Thermal Physics* (McGraw-Hill, New York, 1965).

¹⁸H. G. Dehmelt (private communication).

¹⁹See, for example, D. R. Corson and P. Lorrain, *Introduction to Electromagnetic Fields and Waves* (Freeman, San Francisco, 1962), p. 396 or D. Halliday and R. Resnick, *Physics, Part II*, 2nd ed. (Wiley, New York, 1962), p. 995.

²⁰E. E. Nichols and G. F. Hull, *Phys. Rev.* **17**, 26 (1903).

²¹R. Frisch, *Z. Phys.* **86**, 42 (1933).

²²See, for example, Rodney Loudon, *The Quantum Theory of Light* (Oxford University, London, 1973) or W. Heitler, *The Quantum Theory of Radiation*, 3rd ed. (Clarendon, Oxford, 1954).

²³J. F. Lam and P. R. Berman, *Phys. Rev. A* **14**, 1683 (1976).

²⁴See, for example, D. Bohm, *Quantum Theory* (Prentice-Hall, New Jersey, 1951), p. 296.

²⁵See, for example, H. Frauenfelder, *The Mössbauer Effect* (Benjamin, New York, 1962).

²⁶H. J. Lipkin, *Quantum Mechanics* (North-Holland, Amsterdam, 1973), Chaps. 2-4.

²⁷*Higher Transcendental Functions*, edited by A. Erdelyi (McGraw-Hill, New York, 1953), Vol. II, p. 199.

²⁸See Ref. 27, p. 189.

Laser-to-microwave frequency division using synchrotron radiation

D. J. Wineland

Time & Frequency Division, National Bureau of Standards, Boulder, Colorado 80303
(Received 28 July 1978; accepted for publication 25 September 1978)

Calculations are made to demonstrate the feasibility of obtaining one-step frequency division from optical or infrared laser frequencies to a subharmonic in the microwave spectral region. The cyclotron orbit of a single relativistic electron in a Penning trap is driven with a Gaussian laser beam focused to a spot diameter $\sim \lambda$; the laser subharmonic frequency is measured from the electron synchrotron radiation. The uncertainty in orbit dimensions is limited to $\lambda/2$ by radiative cooling and the technique of motional sideband excitation.

PACS numbers: 42.65.Cq, 42.60. - v

I. INTRODUCTION

The need for precise frequency measurement in the infrared and optical regions is well known.¹ Present successful techniques¹ use the method of harmonic mixing to intercompare optical and infrared laser frequencies and to compare these laser frequencies with the more conventional microwave frequency standards. It would of course be desirable to simplify this process as much as possible; for example, if the most stable and accurate frequency sources are eventually realized in the infrared or optical regions, one needs to translate the frequency to very low values to obtain precise and accurate timing. With this in mind, it is suggested that frequency translation from the infrared or optical region to the microwave region might be accomplished by a single device which is a type of frequency divider as described below.

II. PRINCIPLE OF FREQUENCY DIVISION

The more conventional techniques of frequency multiplication or harmonic mixing use the harmonic generation and mixing properties resulting from a nonlinear device (e.g., crystal with nonlinear response for harmonic generation) which is driven by one or more linear excitations.¹ It is noted, however, that harmonic response can also be obtained by driving a purely harmonic oscillator by a nonlinear (spatially inhomogeneous) field. This technique has been used in high-energy particle accelerators for many years.² For example, particles in synchrotrons are sometimes driven by radiation from microwave cavities (localized to a small portion of the cyclotron orbit) at frequencies which are higher harmonics of the cyclotron orbit frequency. It is suggested then, to carry this technique to its practical limit; that is, one can drive the cyclotron orbit of a charged particle (electron) in a magnetic field at a very high harmonic of the cyclotron frequency. The power supplied by the harmonic excitation is balanced by the synchrotron radiation. If the orbit is stable, then the cyclotron frequency is an exact submultiple of the driving frequency and can be measured from the emitted synchrotron or cyclotron radiation.

To illustrate this technique, consider the example of Fig. 1. Radiation from a collimated Gaussian laser beam

(polarized in the x direction) travels in the $-z$ direction and is focused to a spot diameter S_0 (beam-waist diameter at focal point). The center of the beam waist is made to coincide with the orbit path of a single electron confined to the x, y plane (see Sec. III). As the electron passes through this region it experiences an electric field whose amplitude in the x direction can approximately³ be given by

$$E_x = \phi \left(\frac{2}{\pi} \right)^{1/2} \frac{2}{S_0} \exp \left(- \frac{4(x^2 + y^2)}{S_0^2} \right) \cos(\omega t + \delta), \quad (1)$$

where $\omega_l = 2\pi c/\lambda = 2\pi\nu_l$ is the laser angular frequency, t is the time (where $t = 0$ coincides with the electron crossing the y axis), δ is the phase factor, and ϕ is the amplitude factor (in volts). Assuming the change in energy (ΔW) for one pass through the laser field is small compared to the total electron energy and that the spot size is small compared to the orbit diameter, we have

$$\Delta W \cong \int_{-\infty}^{\infty} eE_x dx = \sqrt{2}e\phi \cos\delta \exp \left[- \left(\frac{\pi c S_0}{2 \nu \lambda} \right)^2 \right], \quad (2)$$

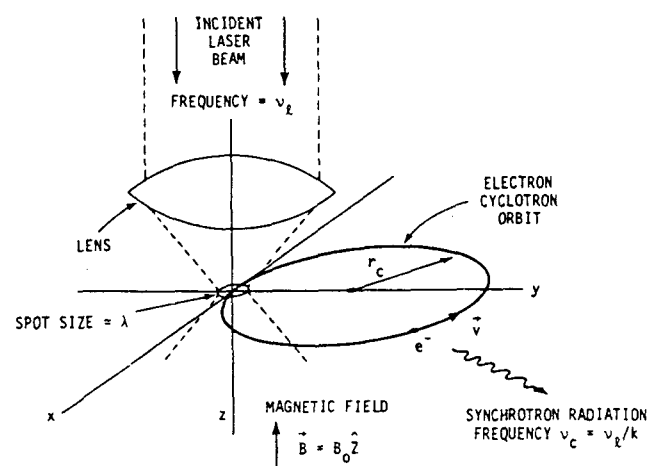


FIG. 1. Schematic depicting the principle of the synchrotron frequency divider. The electron-cyclotron orbit is stabilized by balancing the synchrotron radiation (frequency ν_c) with power supplied by the focused laser beam (frequency ν_l). For the phase-lock condition, the measured cyclotron frequency is an exact submultiple (k) of the laser frequency.

where the substitution $t = x/v$ (v is the electron velocity) has been used. We can write the incident laser power in the form

$$P_I = \frac{c v_I}{4\pi} \int_{A'} \int_{t=0}^{1/v_I} E_x^2 dA dt = \frac{c}{8\pi} \phi^2.$$

If $P_I = 1$ mW, then $\phi = 0.87$ V, and for $v = 0.8c$ and $S_0 = \lambda$, $\Delta W = 4.1 \times 10^{-21}$ (cos δ) J/pass. If the cyclotron frequency $\nu_c = 50$ GHz ($r_c = 0.076$ cm), then the power (P_e) absorbed by the electron is $P_e = 2 \times 10^{-10}$ (cos δ) W. In steady state, this same power is radiated by the electron, and it is assumed that a substantial fraction can be coupled out at frequency ν_c . Note in Eq. (2) that ΔW depends critically on the ratio $cS_0/(v\lambda)$; this expresses the fact that ΔW is small unless the electron experiences a nearly constant phase of the laser field as it passes through the interaction region. If the extent of this interaction region could be made substantially less than λ (for example with some kind of cavity), then the speed of the electron could be made correspondingly less.

III. ELECTRON CONFINEMENT

The electron-cyclotron orbit can be provided by a static magnetic field $\mathbf{B} = B_0 \hat{z}$ ($2\pi\nu_c = eB_0/mc$, m is the electron mass). However, deviations from the circular electron orbit path must be $\lesssim \frac{1}{2}\lambda$, or ΔW averages to zero after several passes. This can be accomplished by confining the electron in a Penning trap with hyperbolic electrodes.⁴ The electric potential inside such a trap is given by $\psi = V_0[r^2 - 2(z^2 - Z_0^2)]/(R_0^2 + 2Z_0^2)$, where r is the radial coordinate, R_0 and Z_0 are the characteristic dimensions of the trap,⁴ and V_0 is the voltage applied between the trap electrodes. The axially symmetric trap is formed with two "end-cap" electrodes which conform to $\psi = 0$ equipotentials and a "ring" electrode which conforms to the equipotential $\psi = V_0$. In the nonrelativistic limit, the motion is comprised of purely harmonic motion along the axial (z) direction at frequency ν_z and the motion in the xy plane is described by the sum of the two vectors \mathbf{r}_c and \mathbf{r}_m , which rotate at frequencies ν_c' and ν_m . These frequencies are given by $\nu_z = [eV_0/m(R_0^2 + 2Z_0^2)]^{1/2}/\pi$, and ν_c' and ν_m are solutions of the equation $\nu^2 - \nu_c\nu + \frac{1}{2}\nu_z^2 = 0$. When $\nu_c \gg \nu_z$, then $\nu_m \approx \nu_c^2/2\nu_c$ and $\nu_c' \approx \nu_c$.

To include relativistic effects, consider only the case where $|\mathbf{r}_m|$ and $z \lesssim \frac{1}{2}\lambda$, which can be accomplished by radiatively cooling⁴ the axial (z) motion and suppressing the magnetron motion by the technique of motional sideband excitation.^{5,6} The electron orbit is then nearly circular with frequency ν_c' ; however, the above expressions must take into account that the electron mass is the relativistic mass $m = \gamma m_0$, where m_0 is the electron rest mass and $\gamma = [1 - (v/c)^2]^{-1/2}$. Note that this special solution is possible when $|\mathbf{r}_m|$ and $z \lesssim \frac{1}{2}\lambda$ only because the electron velocity (and therefore γ) are nearly constant.

Treating the problem quantum mechanically, one can show that the amplitudes of the axial and magnetron motion are given by⁷

$$z_n = [\hbar(n + \frac{1}{2})/\pi\nu_z\gamma m_0]^{1/2}$$

and

$$|\mathbf{r}_m| = r_q = [\hbar(q + \frac{1}{2})/\pi(\nu_c - 2\nu_m)\gamma m_0]^{1/2},$$

where n and q are the axial and magnetron-oscillation quantum numbers, respectively. Expressed in terms of temperature (T_z) we have (when $\hbar\nu_z \ll kT_z$)

$$\hbar\nu_z(n + \frac{1}{2}) = kT_z = m\omega_z^2 \langle z^2 \rangle.$$

The axial motion can be thermalized to the ambient temperature, which could be that of liquid He. The magnetron motion could be "cooled" by the technique of motional sideband excitation.^{5,6} Treating the problem classically (see the Appendix) the magnetron radius can be shrunk to a value

$$r_m^2 \approx 2(\omega_m/\omega_z) \langle z^2 \rangle,$$

where $\langle z^2 \rangle$ is the mean-square thermally excited axial amplitude. Assuming $R_0 = 1.6Z_0 = 0.1$ cm, $V_0 = 10$ kV, $v/c = 0.8$, $S_0 = \lambda$, $\nu_c = 50$ GHz, and $T_z = 4$ K, we have $\nu_z = 7.8$ GHz, $n \approx 10.3$, $z_{10.3} = 175$ nm, $r_m \approx 50$ nm, and $B_0 \approx 3.0$ T. Hence the path of the orbit can be confined to $< \frac{1}{2}\lambda$ provided $\lambda \gtrsim 700$ nm in this example.

IV. CYCLOTRON ORBIT STABILITY

Under the proper conditions, the cyclotron orbit will phase lock to a subharmonic of the laser frequency. This is generally true if the condition $\frac{1}{2}\pi > \delta > 0$ is satisfied and if the laser has rather modest frequency and amplitude stability. Consider that $\delta = \frac{1}{4}\pi$ initially. Then $P_e \approx 1.4 \times 10^{-10}$ W, and this same power must be dissipated by the synchrotron radiation. The power radiated by an electron orbiting in a magnetic field in free space is²

$$P_f = \frac{4\pi\nu_c}{3} \frac{e^2}{r_c} \left(\frac{v}{c}\right)^3 \gamma^4.$$

For the example conditions discussed above, $P_f = 2.5 \times 10^{-13}$ W. To achieve the necessary increase in damping rate, it would be necessary to split the ring electrode along a plane containing the z axis and couple the two halves to a microstrip which is then made to resonate at frequency ν_c' ($Q \approx 500$). This circuit would then be coupled into frequency-measurement electronics to determine ν_c' . One could alternatively reduce the laser power but it is desirable to couple the maximum power out in order to maximize the signal-to-noise ratio.

Stability is achieved because if the energy of the electron increases slightly, due for example to increased laser power or reduction in Q of the microwave resonator, then the cyclotron frequency of the electron decreases slightly (due to the increase in relativistic mass) and it arrives at the laser spot experiencing a slightly advanced phase on the next pass, i.e., δ in Eq. (1) increases slightly. From Eq. (2) this implies ΔW decreases slightly and therefore the electron energy decreases. In this sense the electron-cyclotron frequency phase locks to the laser frequency. To be more specific, suppose that the division factor $\nu_I/\nu_c' = k$. (In the above example if $\lambda = 600$ nm, $k = 10\,000$.) We now consider the response of the electron cyclotron frequency to various instabilities in the system.

A. Laser frequency stability requirements

An obvious upper limit for the phase fluctuations in the laser is given by the condition that $|\delta| \lesssim \frac{1}{2}\pi$ in a time less than the cyclotron orbit time. A stronger limit is, however, given by the condition that the cyclotron frequency be able to track the laser frequency as it jitters or drifts. An approximate limit on how fast the cyclotron frequency can slew is given by the rate at which the cyclotron energy decays. (This is also approximately equal to the maximum rate at which the energy can increase, which is the condition when $\delta \rightarrow 0$.) In a more thorough treatment of the problem one must consider the effect of stimulated emission.⁸ This would actually create a stronger tendency to lock as the cyclotron frequency became less; for simplicity we neglect stimulated emission here. We have

$$\frac{d\nu_c'}{dt} = -\frac{\nu_c'}{E} \frac{dE}{dt} \approx -\frac{\nu_c'}{E} P_e,$$

where E is the total relativistic electron energy. In the phase-lock condition, $\nu_l = k\nu_c'$; therefore to maintain phase lock, the maximum rate of frequency change that can be tolerated by the laser is

$$\left| \frac{d\nu_l}{dt} \right|_{\max} = k \frac{\nu_c'}{E} P_e,$$

which equals 5×10^{17} Hz/sec for the example parameters chosen above. Stabilized lasers⁹ have shown frequency slew rates as small as 50–500 kHz/sec, and therefore this condition is satisfied.

B. Laser amplitude stability requirements

Similarly, rather modest amplitude stability requirements are imposed on the laser. When the laser input power is "matched" to the extracted power, ($\delta \approx \frac{1}{2}\pi$) then phase lock is maintained except for extremely large amplitude fluctuations in a time $< 1/\nu_c'$. Over longer times, if the laser power decreases by more than a factor of 2 from the matched condition [$\phi < \sqrt{2}\phi(\text{matched})$], then ΔW becomes too small to maintain phase lock.

In the phase-locked condition, we note that amplitude changes cause phase fluctuations given by the condition that ΔW must remain constant. From Eq. (2), we note that changes in ϕ must therefore be accompanied by changes in δ . This implies that the change in phase at the output frequency (ν_c') is equal to $\Delta\delta/k$.

C. Magnetic field stability requirements

If the magnetic field strength changes, then phase lock will still be maintained since the cyclotron radius (r_c) will change to keep ν_c' constant. This is true to the extent that the cyclotron orbit path continues to pass through the laser spot. From the expression $\omega_c = eB/(\gamma m_0 c)$ we find that for ν_c' to remain constant we have

$$\frac{dr_c}{r_c} = \left(\frac{v}{c} \gamma \right)^{-2} \frac{dB_0}{B_0}.$$

If we require $dr_c < 0.1\lambda$, then for the example discussed

above we must have $dB_0/B_0 < 7.4 \times 10^{-5}$, which is easily satisfied. The limit on how fast B_0 can change is given by how fast the energy can change for constant ω_c' . We have

$$\frac{1}{B_0} \frac{dB_0}{dt} = \frac{1}{E} \frac{dE}{dt} \approx \frac{1}{E} P_e.$$

For the example conditions, the maximum fractional rate of change of B_0 is equal to $10^3/\text{sec}$, which is easily satisfied.

Similar stability requirements are imposed on the trap electric potentials, but the requirements are relaxed by the ratio $\sim \nu_m/\nu_c'$.

D. Determination of k

The division factor k may be determined two ways: (1) by a prior knowledge of ν_l to an accuracy of better than $1/k$ and a measurement of ν_c' , or (2) a measurement of ν_c' for two different values of k . It is interesting to ask if a given geometrical arrangement can support different values of k . This is true if the cyclotron orbit passes through the laser spot for different k values. From the expression $\omega_c' = v/r_c$, it follows that

$$\frac{dr_c}{r_c} = -\frac{d\omega_c'}{\omega_c'} \left(\frac{c}{v} \right)^2.$$

In the above example, for k to change by 1, $d\omega_c'/\omega_c' = 10^{-4}$ and we have $dr_c = 119 \text{ nm} < S_0$. Therefore the same geometrical configuration will support division by a few values of k .

E. Radiation pressure

In addition to the force on the electron along the x direction as it passes through the laser field, there are forces along the other directions as well. For example, the distortion of the laser fields for tight focusing⁷ causes a force along the z direction. A larger force in the z direction is due to radiation pressure; this is the force due to the $\mathbf{v} \times \mathbf{B}$ term experienced by the electron passing through the laser spot. The corresponding energy gained per pass, ΔW_z , is much smaller than ΔW because the electron axial velocity is extremely small. For the example above, $\Delta W_z \ll \hbar\omega_z$; moreover, this force is periodic with frequency ν_c' , not ν_z , and therefore its effect is negligible.

F. Background gas pressure

Clearly, any collisions with background gas will cause the electron to either be scattered out of the trap or, for example, receive sufficient axial energy that ΔW averages to zero over many passes and phase lock is lost. In an apparatus at liquid-helium temperatures, pressures of $\lesssim 1.3 \times 10^{-11}$ Pa (10^{-13} Torr) should be obtainable, and the primary background gas constituent should be He. For $v/c = 0.8$, the electron-He total scattering cross section (σ) is estimated to be¹⁰ 2.4×10^{-19} cm², yielding a total "destructive" collision rate (R) of

$$R = n(\text{He})v\sigma \lesssim 2.2 \times 10^{-5}/\text{sec},$$

where $n(\text{He})$ is the He density. Therefore, continuous operation for a time $\gtrsim 4 \times 10^4$ sec could be expected, which is long enough to complete a precise frequency measurement.

V. SCENARIO OF OPERATION

A single electron could be provided in the Penning trap by using established procedures.^{4*} The relativistic cyclotron orbit could be initialized by using an external drive (across the split ring electrodes) at frequency ν_c' . Note that this external drive frequency must be swept down as the electron energy increases due to the relativistic mass shift; for the example above $\nu_c(\text{final}) = 0.6\nu_c(\text{initial})$. With microwave electric field strengths of 1V/cm at the cyclotron orbit, this "run-up" time can be less than 1 msec. With the external cyclotron drive held at $\nu_c(\text{final})$, the inhomogeneous excitation at frequency $\nu_z + \nu_m$ must then be applied in order to "freeze out" the magnetron oscillations. The laser can then be turned on and the ν_c' drive turned off and phase locking should occur. Note that the inhomogeneous excitation at $\nu_z + \nu_m$ must be continuously applied or the magnetron motion will be excited by the background thermal radiation. The focused laser beam could be projected through the trap if, for example, the endcaps are made of mesh with hole size $\gg \lambda$.

VI. OPERATION AT LONGER LASER WAVELENGTHS

Experimental conditions (traps size, etc.) are considerably relaxed by using lower laser frequencies and therefore reducing confinement constraints. For example, if $\nu_c = 25$ GHz, $R_0 = 1.6Z_0 = 0.2$ cm, $V_0 = 500$ V, $v/c = 0.8$, $S_0 = \lambda$, and $T_z = 4$ K, then $\nu_z = 866$ MHz, $n = 96$, $z_{96} = 1.57$ μm , and $r_m = 200$ nm, which is suitable for CO₂ laser wavelengths (10 μm).

VII. DISCUSSION

The use of a type of frequency divider as discussed here potentially has important advantages over presently used techniques. First, the divider could replace in a single device the elements in a frequency synthesis chain which may use several multipliers and intermediate oscillators. It should be able to divide over a continuous range of laser frequencies being limited only by the frequency sensitivity of the focusing lens. Also, we note that in frequency multipliers of order k , the noise spectral density increases as k^2 relative to the carrier. For high-order multiplication this may mean that the carrier becomes completely lost in the noise unless an oscillator with very high spectral purity is used as the input oscillator. With a type of frequency divider as discussed here, this problem does not occur. The noise spectral density decreases relative to the carrier, being limited by the added instrumental noise in the ν_c' detection electronics.

ACKNOWLEDGMENTS

The author wishes to thank his colleagues R. Barger, J. Bergquist, R. Drullinger, G. Dunn, K. Evenson, J. Hall, H. Hellwig, D. Jennings, J. Levine, K. Persson, R. Petersen, E. Smith, S. Stein, and F. Walls for useful comments and discussion. The author also thanks J. Baker and E. DeWeese for manuscript preparation.

APPENDIX

Doppler-effect-generated optical sideband cooling^{5,11}

and magnetron cooling^{5,6} are formally identical, but for the sake of conciseness only the specific case of magnetron cooling is examined. Briefly, the technique works as follows: To reduce the magnetron oscillation amplitude, the axial motion can be driven by an inhomogeneous rf field at the sideband frequency $\nu_z + \nu_m$; however, the axial motion predominantly reradiates at frequency ν_z . The energy difference per scattered microwave photon $h[\nu_z - (\nu_z + \nu_m)] = -h\nu_m$ must come from the magnetron energy; therefore, the oscillation amplitude decreases. Qualitatively, the cooling is limited because the magnetron motion is excited by the noise generated from the thermal axial motion via the inhomogeneous rf field.¹² This noise has the same spectral shape as that of the axial oscillation, but is centered around frequency ν_m .

To estimate the cooling limit classically, assume that the electron in the Penning trap is subjected to an inhomogeneous rf field

$$E(t) = E(r) \cos(\omega_z + \omega_m)t, \quad (\text{A1})$$

where

$$E(r) = E_0 + \hat{i} \left(\frac{\partial E_x}{\partial x} x + \frac{\partial E_x}{\partial z} z \right) + \hat{k} \left(\frac{\partial E_z}{\partial x} x + \frac{\partial E_z}{\partial z} z \right),$$

and the x coordinate of the electron motion can be written

$$x = r_c \cos(\omega_c t + \phi_c) + r_m \cos(\omega_m t + \phi). \quad (\text{A2})$$

Substituting Eq. (A2) into (A1) we find that the axial motion is driven by a resonant rf electric field

$$E_z(t) = \frac{\partial E_z}{\partial x} \frac{r_m}{2} \cos(\omega_z t - \phi_m),$$

and the driven axial resonance has the form¹³

$$z_d(t) = b_z \cos(\omega_z t - \phi_m - \frac{1}{2}\pi), \quad (\text{A3})$$

where $b_z = eE_z \tau_z / (2m\omega_z)$, and τ_z is the amplitude-damping time constant. The power delivered to the external damping resistance is¹³

$$\begin{aligned} \frac{dE_z}{dt} &= \frac{mb_z^2 \omega_z^2}{\tau_z} = \frac{(eE_z)^2 \tau_z}{(4m)} \\ &= \left(e \frac{\partial E_z}{\partial x} r_m \right)^2 \tau_z (16m)^{-1}. \end{aligned}$$

The corresponding rate of magnetron energy change is

$$\frac{dE_m}{dt} = \frac{\omega_m}{\omega_z} \frac{dE_z}{dt} = \frac{\omega_m}{\omega_z} \left(e \frac{\partial E_z}{\partial x} r_m \right)^2 \tau_z (16m)^{-1}. \quad (\text{A4})$$

Note that for the magnetron motion, r_m becomes smaller as E_m increases since most of the magnetron energy is electric field potential energy.

The axial motion can be described by

$$z(t) = z_d(t) + z_n, \quad (\text{A5})$$

where $z_d(t)$ is given by Eq. (A3) and z_n is the thermally ex-

cited noise oscillation. Substituting Eq. (A5) into Eq. (A1) we find that the magnetron motion is driven by the rf electric field

$$E_x(t) = \frac{\partial E_x}{\partial z} (z_d(t) + z_n) \cos(\omega_z + \omega_m) t. \quad (\text{A6})$$

The first term is the "damping" term which resulted in the magnetron energy change given by Eq. (A4). The second term is responsible for the magnetron noise excitation. To estimate the effect of this term we consider the following: If the undamped magnetron motion is driven by a resonant electric rf field the resulting amplitude contains a term which grows according to¹⁴

$$r_m(t) \cos(\omega_m t + \zeta) = \frac{eE_x}{2m} \frac{\omega_m t}{(\frac{1}{2}\omega_z^2 - \omega_m^2)} \cos(\omega_m t + \zeta).$$

When excited by noise, the amplitude grows in this fashion only for a time τ_c , where τ_c is the coherence time of the noise. In this case the coherence time is determined by the bandwidth of the axial oscillation, and we have $\tau_c = 2\tau_z$. After t/τ_c coherence times the amplitude has grown in a random-walk fashion and we have

$$\langle r_m^2 \rangle = \left(\frac{eE_x \omega_m \tau_c}{2m(\frac{1}{2}\omega_z^2 - \omega_m^2)} \right)^2 \frac{t}{\tau_c}. \quad (\text{A7})$$

The total magnetron energy can be written as

$$E_m = \frac{1}{2} m r_m^2 (\omega_m^2 - \frac{1}{2}\omega_z^2). \quad (\text{A8})$$

Using Eqs. (A6)–(A8) we obtain

$$\frac{dE_m}{dt} = - \frac{\tau_z [e(\partial E_x / \partial z)]^2 \langle z^2 \rangle \omega_m^2}{16m(\frac{1}{2}\omega_z^2 - \omega_m^2)}. \quad (\text{A9})$$

Balance between "cooling" [Eq. (A4)] and "heating" [Eq. (A9)] is obtained when

$$r_m^2 = \frac{(\omega_z \omega_m)}{(\frac{1}{2}\omega_z^2 - \omega_m^2)} \langle z^2 \rangle, \quad (\text{A10})$$

where we have assumed that the rf magnetic field is negligible and have used Faraday's law. When $\omega_m \ll \omega_z$ we have

$$r_m \cong [(2\omega_m / \omega_z) \langle z^2 \rangle]^{1/2}. \quad (\text{A11})$$

¹⁴K.M. Evenson, D.A. Jennings, F.R. Peterson, and J.S. Wells, *Proc. Third Int. Conf. on Laser Spectroscopy*, Edited by J.L. Hall and J.L. Carlsten (Springer-Verlag, Heidelberg, 1977), Vol. 7, p. 56; D.J.E. Knight and P.T. Woods, *J. Phys. E* 9 898 (1976).

¹⁵H. Semat and J.R. Albright, *Introduction to Atomic and Nuclear Physics*, 5th ed. (Holt, Rinehart and Winston, New York, 1972), Chap. 12; B.A. Mamyrin, N.N. Aruev, and S.A. Alekseenko, *Zh. Eksp. Teor. Fiz.* 63, 3 (1972); *Sov. Phys.-JETP* 36, 1 (1973).

¹⁶For the case of tight focusing discussed here the fields become distorted near the focal point; however, this distortion is small enough that it is disregarded here. See D.J. Innes and A.L. Bloom, *Spectra Physics Laser Tech. Bull.* No. 5, 1966 (unpublished).

¹⁷H.G. Dehmelt and F.L. Walls, *Phys. Rev. Lett.* 21, 127 (1968); H. Dehmelt, in *Advances in Atomic and Molecular Physics*, edited by D.R. Bates and I. Esterman (Academic, New York, 1967, 1969), Vols. 3 and 5; D.J. Wineland, P. Ekstrom, and H. Dehmelt, *Phys. Rev. Lett.* 31, 1279 (1973). Note that in general one needs only axially symmetric electrodes; for simplicity the case of hyperbolic electrodes is discussed here.

¹⁸D. Wineland and H. Dehmelt, *Bull. Am. Phys. Soc.* 20, 637 (1975); H.G. Dehmelt, *Nature* 262, 777 (1976).

¹⁹R.S. VanDyck, Jr., P.B. Schwinberg, and H.G. Dehmelt, to appear in *Proc. of Orbis Scientiae* (Plenum, New York, to be published).

²⁰A. Sokolov and Y. Pavlenko, *Opt. Spectrosc.*, 22, 1 (1967); G. Graff, E. Klempt, and G. Werth, *Z. Phys.*, 222, 201 (1969).

²¹J. Schneider, *Phys. Rev. Lett.* 2, 504 (1959).

²²J.L. Hall, *Proc. Esfahan Symp. on Fund. and Appl. Laser Phys.*, edited by M.S. Feld, A. Javan, and N.A. Kurnitt (Wiley, New York, 1973), p. 469.

²³The total cross section is the sum of elastic (σ_{el}) and inelastic (σ_{in}) cross sections. We have $\sigma_{el} \cong 7.3 \times 10^{-21}$ cm². See: M. Inokuti and M.R.C. McDowell, *J. Phys. B.* 7, 2382 (1974); $\sigma_{in} \cong 2.35 \times 10^{-19}$ cm²; see M. Inokuti, Y.K. Kim, and R.L. Platzman, *Phys. Rev.* 164, 55 (1967).

²⁴D.J. Wineland, R.E. Drullinger, and F.L. Walls, *Phys. Rev. Lett.* 40, 1639 (1978); W. Neuhauser, M. Hohenstatt, P. Toschek, and H. Dehmelt, *Phys. Rev. Lett.* 41, 233 (1978).

²⁵H.G. Dehmelt (private communication).

²⁶L.D. Landau and E.M. Lifshitz, *Mechanics* (Pergamon, New York, 1960), Chap. V.

²⁷S. Jarvis, Jr. (unpublished).

LASER TO MICROWAVE FREQUENCY DIVISION
USING SYNCHROTRON RADIATION II

J. C. Bergquist and D. J. Wineland
Frequency and Time Standards Group
National Bureau of Standards
Boulder, CO 80303
(303) 499-1000, ext. 4459

Abstract

We present a review of theoretical calculations which demonstrate the feasibility of obtaining one step frequency division from optical or infrared laser frequencies to a subharmonic in the microwave spectral region, and include current experimental designs toward a practical realization of this goal. We plan to drive the cyclotron orbit of a single relativistic electron, which is confined in a Penning ion trap, with a laser beam focused to a spot diameter $\sim \lambda$. This method is an extension of a common technique used in cyclotrons and synchrotrons where the orbit of high energy particles is driven at a harmonic of the orbit frequency. Our experiment is designed to measure this orbit frequency which is then a subharmonic of the driving (laser) frequency. This technique requires that the uncertainty in the electron orbit dimensions be limited to $\leq \lambda/2$, which is possible by radiative cooling and the method of motional side-band excitation. The possibility of a unified optical wavelength/frequency standard is evident.

Introduction

It is our intent in this paper to summarize and extend the theoretical analysis of a broadband laser to microwave frequency divider proposed earlier.¹ We also give a brief description of experimental designs being considered for the realization of this division. The importance of accurate frequency division from the optical spectrum derives primarily from frequency (time) and wavelength metrology and the extreme likelihood that the most accurate, reproducible, and stable oscillators may be realized in that part of the electromagnetic spectrum. Certainly, there is great value of such a device in the area of atomic and molecular spectroscopy.

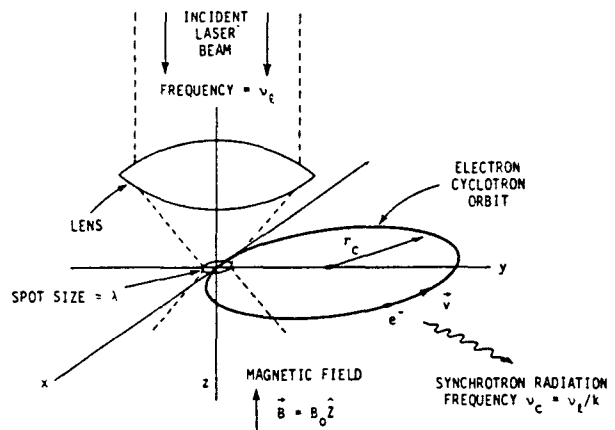
Principle of Operation

The proposed synchrotron divider is based on the principle that a purely harmonic oscillator can be coherently driven (pumped) by a spatially non-uniform, higher order harmonic driving field. This method has been used for years in cyclotrons, synchrocyclotrons, and synchrotrons to accelerate charged particles to relativistic speeds. In these devices, particles are frequently driven by radiation from microwave cavities, which is localized to a small portion of the cyclotron orbit, at frequencies integrally related to the cyclotron orbit

frequency. For a significant transfer of energy from the RF driving field into the cyclotron orbit it is necessary that the interaction time of the charged particles with the radiation field be comparable to or less than one-half period of the RF frequency. Longer interaction times quickly average the transfer of energy to zero.

It would seem possible to straightforwardly extend this technique to driving fields of shorter wavelengths in order to drive the cyclotron orbit of a single electron in a magnetic field at a very high harmonic of the cyclotron frequency. Theoretically, this is the case, however, shorter wavelengths entail special practical considerations discussed below. If the orbit is stable then the power absorbed by the electron from the harmonic excitation is balanced by the emitted synchrotron radiation. The cyclotron frequency is then a phase-locked submultiple of the driving frequency.

We illustrate the important features of the proposed method in fig. 1.



SYNCHROTRON FREQUENCY DIVIDER

Radiation from a well collimated, Gaussian laser beam, linearly polarized in the x direction and traveling in the -z direction is focused into a spot with diameter $\sim \lambda$ by a lens. If it is possible to provide that the electron orbit, which is confined to lie in the x,y plane, pass through this focus, then the electron will absorb energy from

Proc. 33rd Annual Symp. on Frequency Control, 1979, p. 494-497. Copies available from: Annual Frequency Control Symposium, c/o Electronic Industries Assoc., 2001 Eye St., Washington, D.C., 20006.

the radiation field. Assuming that the envelope for the electric field vector is approximately Gaussian and that the absorbed energy per pass (ΔW) is small compared to the total electron energy, we have

$$\Delta W \cong \int_{-\infty}^{\infty} eE_x dx = \sqrt{2} eA \cos \delta \exp \left\{ -\left[\frac{\pi c S_0}{2v\lambda} \right]^2 \right\} \quad (1)$$

where

- A = field amplitude factor
- δ = phase of laser field
- v = electron's velocity
- S₀ = actual diameter of focused line ($\sim \lambda$)
- c⁰ = speed of light

Note that ΔW shows a double exponential dependence on the ratio $cS_0/\lambda v$. Thus the energy transferred to the electron is extremely small unless this ratio is approximately equal to one. This is because the oscillating driving field will rapidly average the energy transfer to zero unless we can arrange that the electron spend approximately one cycle or less in the radiation field. If the extent of the interaction region could be made substantially less than λ then the speed of the electron could be made correspondingly less while maintaining an effective energy transfer. A possibility may be a dielectric waveguide with transverse dimensions less than λ that is projected into the trap and is cut off within about λ of the electron orbit.

Confinement of the circular electron orbit path to $\leq \lambda/2$, which is necessary to prevent $\Delta W \rightarrow 0$, is accomplished by trapping the electron in a Penning trap with hyperbolic electrodes immersed in a static magnetic field $\vec{B} = B_0 \hat{z}$. The electrostatic potential is given by $\psi = V_0 (r^2 - 2(z - z_0)^2) / (r_0^2 + 2z_0^2)$ where r is the radial coordinate, z is the axial coordinate, r_0 and z_0 are the characteristic dimensions of the trap,² and V_0 the voltage applied between the trap electrodes. The axially symmetric, static electromagnetic trap is thus formed with two endcap electrodes which are constructed to lie on the $\psi = 0$ equipotential surface and a ring electrode which conforms to the equipotential $\psi = V_0$. The motion of the electron is given by the synthesis of three separate oscillations. First there is the harmonic motion parallel to the z axis at frequency $\nu_z = (eV_0/m\pi^2(r_0^2 + 2z_0^2))^{1/2}$ due solely to the applied electric field. In the radial plane the motion is comprised of the sum of two vectors \vec{r}_c and \vec{r}_m which rotate at frequencies ν_c' and ν_m . These frequencies are approximated by $\nu_m \cong \nu_z^2/(2\nu_c)$ and $\nu_c' \cong \nu_c = (eB_0/2\pi mc)$, when $\nu_c \gg \nu_z$. In order to satisfy our requirement to confine the electron orbit path to $\leq \lambda/2$, $|\vec{r}_m|$ and z must be held to $\leq \lambda/4$. This can be

accomplished by radiatively cooling the axial (z) motion and suppressing the magnetron (r_m) motion by the method of motional sideband excitation.^{1,3} The electron orbit is then nearly circular with cyclotron frequency ν_c' .

The minimum r_m is given by¹

$$r_m^2 \cong 2 (\omega_m/\omega_z) \langle z^2 \rangle \quad (2)$$

where $\langle z^2 \rangle$ is the mean square thermally excited axial amplitude. As a quantitative example, assume that $r_0 \cong 1.6 z_0 = 0.1$ cm, $V_0 = 10$ kV, $v/c = 0.8$, $S_0 = \lambda$, $B_0 \cong 1$ T with $\nu_c \sim 15$ GHz, and $T_z = 4$ K. These conditions will give $\nu_z \cong 7.8$ GHz, $\sqrt{\langle z^2 \rangle} \cong 175$ nm, and $r_m \sim 150$ nm and an orbit confined to less than $\lambda/2$ provided $\lambda \geq 700$ nm. We note that V_0 is extremely large in order to confine the axial z excursions to $\leq \lambda/4$. This requirement is greatly reduced if the focus is a cylindrical line parallel to z rather than a spot of dimensions λ on all sides. This focus ($\lambda \times \lambda \times 20\lambda$) could be obtained with a softly focused beam followed by a strong focusing cylindrical lens. A smaller value of V_0 reduces the likelihood of spurious field emission currents which could give rise to extraneous trapped electrons. Since $\langle z^2 \rangle \propto V_0^{-1}$ and $\nu_z \propto V_0^{1/2}$, a reduction of V_0 by 10^2 increases $\sqrt{\langle z^2 \rangle}$ by 10 and reduces ν_z by the same factor. From Eq. 2, the minimum value of r_m increases by only a factor of three. Thus, this change in V_0 to 100 V, allowed by the cylindrical lens focus, gives $\nu_z \cong 780$ MHz, $\sqrt{\langle z^2 \rangle} \sim 1.75$ μ m, and $r_m = 0.45$ μ m, permitting $\lambda \geq 600$ nm. (It is further noted that the electron orbit confinement problem is greatly reduced by choosing longer wavelength lasers).

If we now provide an energy balance, the energy absorbed by the electron is lost through synchrotron radiation. If sufficiently coupled out to the frequency measurement electronics, the the cyclotron frequency will phase lock to a subharmonic of the laser frequency. Given that the laser has only minimum amplitude and frequency stability,¹ the phase lock condition will occur for $0 < \delta < \pi/2$. Consider that $\delta = \pi/4$ initially and that the laser power incident on the cylindrical lens is approximately 20 mW. The power absorbed and subsequently radiated by the electron, confined as described above, is about 1.4×10^{-10} W.

Feedback

Stability of the phase lock is automatically achieved since, for example, an increase in the energy of the electron results in a corresponding

decrease in the cyclotron frequency owing to the increase in relativistic mass. The electron thus experiences a slightly advanced phase of the laser on the next pass through the focus. This implies that ΔW decreases slightly and therefore the electron energy decreases. It is in this manner that the electron phase locks to the laser frequency.

We note that if initially, or at any later time, an energy imbalance exists between the energy absorbed and the energy radiated, then the automatic tracking of the electron to the balance point is not critically damped. Rather, the electron slews to the lock point in a slowly damped oscillatory fashion with a time constant equal to the trap coupled radiative decay time¹ of approximately 1 ms.

To be more quantitative, we write the change of phase of the microwave field (ϕ) as

$$\frac{d\phi(t)}{dt} = \dot{\phi}(t) + \omega_c'$$

where $\dot{\phi}(t)$ is the frequency deviation from the normal "locked" cyclotron frequency ω_c' . We have

$$\dot{\phi}(t) = \Delta\omega(t) = \Delta\omega_{fb}(t) + \Delta\omega_d(t) \quad (3)$$

where $\Delta\omega_{fb}$ is the instantaneous frequency deviation of the electron from ω_c' due to the energy imparted by the laser, and $\Delta\omega_d$ is the frequency deviation due to the radiation decay. Writing $\delta = \pi/2 - \theta$ and assuming we are in the high power limit of the laser then the nominal value of $\delta = \pi/2$ so that Eq. (1) becomes $\Delta W \approx W_0 \theta$, where $W_0 \approx \sqrt{2} eA \exp[-(\pi c S_0 / 2v\lambda)^2]$. Now $\theta = k\phi$ where k is the division factor v_e/v_c' so that $\Delta W \approx W_0 k\phi$.

Noting that

$$\frac{d(\Delta\omega_{fb})}{dt} \approx -\frac{\omega_c'}{E} \left(\frac{dE}{dt} \right)_{fb}$$

where E is the total energy of the electron, then

$$\frac{d(\Delta\omega_{fb})}{dt} = -\omega_c' \left(\frac{W_0 v_c'}{E} \right) \phi \quad (4)$$

To estimate $\frac{d(\Delta\omega_d)}{dt}$ we first note that

$$\frac{d(\Delta\omega_d)}{dt} \approx -\frac{\omega_c'}{E} \left(\frac{dE}{dt} \right)_d$$

An accurate expression for the energy decay due to synchrotron radiation $(dE/dt)_d$ in the absence of coupling structures is given in Ref. 1. Using this expression, we can find the dependence of $d(\Delta\omega_d)/dt$ on the difference frequency ($\Delta\omega$) and obtain

$$\frac{d(\Delta\omega_d)}{dt} \approx -\left(\frac{4e^2 \gamma^2 \omega_c'^2}{3Ec} \right) \Delta\omega \approx -\frac{2}{\tau} \Delta\omega \quad (5)$$

where τ is approximately equal to the damping time at low energy. We will assume that this expression is also valid when τ is decreased by coupling the electron to the trap electrodes. Differentiating Eq. 3 with respect to time and using Eqs. (4) and (5) we obtain

$$\ddot{\phi} + \frac{2}{\tau} \dot{\phi} + (\omega_\phi)^2 \phi = 0 \quad (6)$$

where $\omega_\phi \approx (\omega_c' v_c' W_0 / E)^{1/2}$. Thus phase oscillations around the nominal "locked" phase occur at frequency ω_ϕ and are damped with approximately the radiation damping time. For a laser power of 200 mW ($\lambda = 3.39 \mu\text{m}$) in the above example $W_0 \approx 1.8 \times 10^{-13}$ ergs, and $\omega_\phi / 2\pi \approx 1.7 \times 10^8$ Hz.

Spread of the electron wave packet

To estimate the restrictions placed on the model by quantum mechanics we start with the uncertainty relation $\Delta\phi \Delta n \geq 1$, where $\Delta\phi$ is the uncertainty in phase of the cyclotron orbit of the electron and Δn represents the corresponding uncertainty in energy for the electron. Neglecting the electric field and electron spin, the electron energy is given by

$$E = [(mc^2)^2 + mc^2 h \omega_c' (n + \frac{1}{2})]^{\frac{1}{2}} \quad (7)$$

We want to build a wave packet which has its phase defined with an accuracy $\Delta\phi < (2\pi\lambda/10)/(2\pi r_c) \approx 1.3 \times 10^{-4}$ rad. From the uncertainty relation this requires a spread in energy quantum number of $\Delta n < 0.75 \times 10^4$. From Eq. (7) this corresponds to a range of natural frequencies $\Delta\omega \approx \omega_c' \Delta n/n \approx 1.3 \times 10^{-6} \omega_c'$. Classically, if we assume that the initial conditions for Eq. 6 are given by these values of $\Delta\phi$ and $\Delta\omega$, then we see that the phase is bound and initially oscillates with amplitude 1.75×10^{-4} rad. Quantum mechanically, it therefore seems likely that the electron will phase lock if the initial wave packet has a limited range of values of n and ϕ . Clearly this treatment is not rigorous and a more careful analysis of the quantum fluctuations must be made.

Acknowledgments

The authors acknowledge input from others; in particular we thank Wayne M. Itano and P. L. Bender for useful discussions concerning the uncertainty problem and S. R. Stein for helpful input on the electronics problems.

References

1. D. J. Wineland, J. Appl. Phys. 50, 2528 (1979).

2. H. G. Dehmelt and F. L. Walls, Phys. Rev. Lett. 21, 127 (1968); H. Dehmelt, in Advances in Atomic and Molecular Physics, D. R. Bates and I. Esterman, eds. (Academic, New York, 1967, 1969), Vols. 3 and 5. D. J. Wineland, P. Ekstrom and H. Dehmelt, Phys. Rev. Lett. 31, 1279 (1973). Note that in general one needs only axially symmetric electrodes, for simplicity the case of hyperbolic electrodes is discussed here.
3. R. S. Van Dyck, Jr., P. B. Schwinberg, and H. G. Dehmelt, in New Frontiers in High-Energy Physics, Kursunoglu, Perlmutter, and Scott, eds., (Plenum, New York, 1978) p. 159.

Abstract Submitted
for the Houston DEAP Meeting of the
American Physical Society
10-12 December, 1979

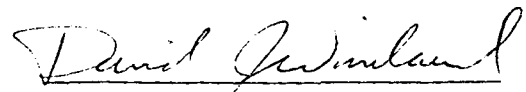
Physics and Astronomy
Classification Scheme
Number 32

Suggested title of session
in which paper should be placed
Atom-Photon Interactions

Bull. Am. Phys. Soc. 24, 1185 (1979).

Frequency and Time Standards Utilizing Laser-Cooled Ions.* Wayne M. Itano and D. J. Wineland, Frequency and Time Standards Group, N.B.S.--Frequency (and time) standards could be based on microwave transitions (where precise synthesis is currently possible, as opposed to optical transitions) in stored ions. Laser cooling to $\lesssim 0.1$ K reduces the second-order Doppler shift to $\lesssim 10^{-16}$. Transitions can be detected with near unit efficiency by repeated laser scattering [1]. Schemes using a single laser for both cooling and detection are possible only for ions with a strong optical transition and no intermediate metastable level e.g., He^+ , Be^+ , Mg^+ , Zn^+ , and Cd^+ . A simple scheme could use the $(M_J=1/2, M_I=5/2) \leftrightarrow (M_J=1/2, M_I=3/2)$ transition in $^{67}\text{Zn}^+$ ($\nu \approx 1\text{GHz}$) which has an extremum at $H_0 \approx 80$ kG with $|\delta\nu/\nu_0| \approx 10^{-2}(\Delta H/H_0)^2$. The ions could be cooled and simultaneously optically pumped into the $(M_I=5/2)$ level. Depletion of this level by microwaves would be detected as a decrease in the photon scattering rate. For 10^6 ions the shot-noise-limited S/N ratio is 10^3 . For an interrogation time τ of 100 s, $Q \approx \pi\tau\nu_0 \approx 3 \times 10^{11}$, and $\sigma_\nu(100\text{s}) \approx [Q(S/N)]^{-1} \sim 3 \times 10^{-15}$. Experimental work is being initiated on Cd^+ . *Supported in part by AFOSR. [1] D.J. Wineland, R.E. Drullinger, and F.L. Walls, Phys. Rev. Lett. 40, 1639 (1978).

- Prefer Poster Session
- Prefer Standard Session
- No Preference



David J. Wineland
Time and Frequency Division
National Bureau of Standards
Boulder, CO 80303

Address

Abstract Submitted
for the Houston DEAP Meeting of the
American Physical Society
10-12 December, 1979

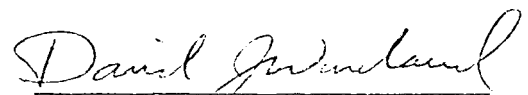
Physics and Astronomy
Classification Scheme
Number 35

Suggested title of session
in which paper should be placed
Atom-Photon Interactions

Bull. Am. Phys. Soc. 24, 1185 (1979).

Laser Induced Magnetron Compression (Expansion)
of Ions Stored in a Penning Trap.* D.J. Wineland, R.E.
Drullinger, J.C. Bergquist, and Wayne M. Itano, Time and
Frequency Division, N.B.S.-As conjectured earlier [1]; we
have been able to shrink (or expand) the magnetron orbits
of ions stored in a quadrupole Penning trap with radia-
tion pressure. In the axially symmetric trap, the radial
motion of the ions can be expressed as $\vec{r}(t) = \vec{r}_c(0)\exp$
 $(-i\omega_c t) + \vec{r}_m(0)\exp(-i\omega_m t)$ where the x(y) coordinate cor-
responds to the real (imaginary) part in this notation
and where ω_c and ω_m are the cyclotron and magnetron fre-
quencies. When $\omega_m, \omega_c \ll \gamma$ (the natural linewidth of the
ion optical transition) the scattering of a photon may be
viewed as a point-like interaction which imparts momentum
change $\Delta\vec{p} = \hbar\vec{k}$ to the ion. (\vec{k} is the photon wave vector).
Hence $\Delta\vec{r}_m = i\hbar\vec{k}(M(\omega_m - \omega_c))^{-1}$ and $\Delta\vec{r}_c = i\hbar\vec{k}(M(\omega_c - \omega_m))^{-1}$ per
scattering event. We present data illustrating the re-
sulting shrinking or expanding of \vec{r}_m ; the corresponding
effect for \vec{r}_c was described earlier [1]. Such effects
could also be realized by other means of momentum transfer
(e.g. atomic beam or coupling \vec{r}_m to negative resistance).
*Supported in part by ONR.
[1] D.J. Wineland, R.E. Drullinger, F.L. Walls, Phys.
Rev. Lett. 40, 1639 (1978).

- Prefer Poster Session
 Prefer Standard Session
 No Preference



David J. Wineland
Time and Frequency Division
National Bureau of Standards
Boulder, CO 80303

Address

High-Resolution Optical Spectra of Laser Cooled Ions

R. E. Drullinger, D. J. Wineland, and J. C. Bergquist

Time and Frequency Division, National Bureau of Standards, Boulder, CO 80303, USA

Received 25 February 1980/Accepted 29 April 1980

Abstract. We obtain essentially Doppler free spectra of the naturally occurring isotopes of Mg^+ , which are bound in a Penning trap, by using a frequency stabilized laser to continuously cool the ions, while the scatter rate from a second, frequency swept laser is monitored. We show that the magnetron motion as well as the cyclotron and axial motion can be minimized. Line position measurements yielding resonance transition energy, isotope and hyperfine shifts are reported.

PACS: 32

Radiation-pressure cooling to substantially reduce Doppler broadening, shifts, and residual velocity effects to all orders [1, 2] represents an important step in the study of ultra-narrow, lifetime limited transitions. The method reported here investigates the full Doppler width of the quantum absorber studied; but, because the absorbers are substantially cooled by radiation pressure, the line width can be dominated by the natural resonance width. Furthermore, in contrast to conventional sub-Doppler techniques, this method directly reduces all velocity effects.

Recently, cooling of a sample of bound resonant absorbers by radiation pressure has been demonstrated [1, 2]. In [1] Mg^+ ions were confined to a room temperature Penning trap and were irradiated near the $^2S_{1/2} - ^2P_{3/2}$ resonance transition (280 nm) with the output of a frequency doubled cw dye laser. In (such) a two-level system, the process of absorption followed by re-emission returns the atom to the original internal state; but, in general, a different kinetic energy state. After many such scattering events, the collective momentum of the absorbed photons can be made to cancel the thermal momentum of the absorber, whereas the recoil momenta from the randomly re-emitted photons cancel to first order [3]. In this paper, we describe some of the interesting features of electromagnetically trapped ions which are cooled by this technique and also report the first high-resolution spectra obtained on a laser cooled species. Preliminary results of this work are reported in [4].

Briefly, the eigenmotions of ions in a Penning trap [5] are a simple harmonic oscillation in the electrostatic well along the trap axis, a cyclotron orbit in the plane perpendicular to the trap axis, and a magnetron drift orbit also in that plane. The axial vibration and the cyclotron orbital motions are thermal and coupled through the long range coulomb collisions between ions in the trap, whereas the magnetron motion is nonthermal and not strongly coupled to the other motions [1, 5]. In fact, the magnetron motion is in an unstable equilibrium in the trap, but the confinement time of unperturbed ions is observed to be days.

Experiment

In our present experiments, the laser beam (diameter $\approx 100 \mu\text{m}$) crosses the trap normal to the horizontal trap axis (**B** field axis) and is also linearly polarized perpendicular to the trap axis. With this configuration, the laser directly interacts with both the cyclotron and magnetron motion. These motions can be represented as [6]

$$\mathbf{r} = x + iy = \mathbf{r}_c + \mathbf{r}_m = \mathbf{r}_{c0} e^{-i\omega_c t} + \mathbf{r}_{m0} e^{-i\omega_m t}, \quad (1)$$

where \mathbf{r}_c and \mathbf{r}_m are the cyclotron and magnetron radius vectors, respectively, and ω_c , ω_m the associated angular frequencies. If the ions undergo an incremental change in velocity, Δv , per scattering event, we find

0340-3793/80/0022/0365/\$01.00

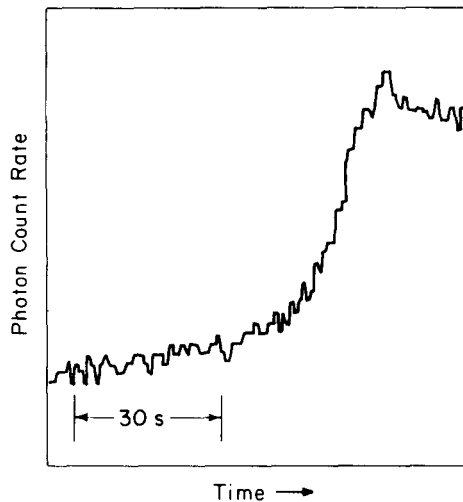


Fig. 1. Scatter rate vs. time after the laser has been blocked for 5 min. On unblocking the laser, the ion cloud which has begun to spread and heat, yields a low scatter rate at first, but returns to its previous value in approximately 1 min

that there is a corresponding incremental change in the radius vector given by

$$\Delta \mathbf{r}_c = \frac{i}{\omega_c - \omega_m} \Delta \mathbf{v} \quad \text{and} \quad \Delta \mathbf{r}_m = \frac{-i}{\omega_c - \omega_m} \Delta \mathbf{v}. \quad (2)$$

By irradiating the side of the ion cloud which recedes from the laser with photons of frequency $\omega_L < \omega_0$, both \mathbf{r}_c and \mathbf{r}_m can be made smaller. This effect is demonstrated below.

A cloud of $\lesssim 10^2 \text{ Mg}^+$ ions is loaded into the trap. The static magnetic field is 0.976 tesla and the electric potential is $\approx 7 \text{ V}$. The laser beam is initially positioned about $600 \mu\text{m}$ below the trap center; that is, where the magnetron motion carries the ions in the direction away from the laser. The laser frequency is swept up to and held at approximately the half-intensity point of the resonance transition which is Doppler shifted by the magnetron motion. Photons which are backscattered into an $f/4$ cone are collected and counted. The overall detection efficiency is $\approx 3 \times 10^{-5}$. The scatter rate is observed to decrease in time indicating that the ions move closer to trap center. This process is repeated by moving the laser beam toward trap center in $100 \mu\text{m}$ steps. When the beam reaches a position of $\approx 100 \mu\text{m}$ below trap center, the scatter rate remains constant, which indicates a stable cloud configuration (dia: $\leq 200 \mu\text{m}$) has been obtained.

Additionally, if the laser radiation is blocked, the ions begin to heat and spatially spread; however, the low entropy ion cloud can be reconstituted at trap center by simply unblocking the laser. This is indicated in Fig. 1, where a plot of scatter rate vs. time is shown, after

the laser had been blocked for 5 min. The signal rises and then stabilizes at the previous scatter rate, indicating that the ions have returned to the preblocked configuration at trap center. If the laser beam is positioned above trap center, the cloud is “blown-out” to a large radius, but still remains confined to the trap. Once again, we can reform a small, cold ion cloud by spatially stepping the laser below trap center and repeating the above procedure.

If the ions are localized and cooled and the laser beam maintained about $50 \mu\text{m}$ below trap center, an estimate of ion temperature can be obtained by rapidly scanning the laser through the optical transition and recording the scatter rate as a function of laser frequency. The broken curve (circles) in Fig. 2 shows a typical plot of scatter rate vs. laser frequency. As the frequency is swept into resonance, the ions are maintained cold and a nearly Lorentzian line shape is produced. However, even at our low laser power ($\approx 8 \mu\text{W}$) and rapid sweep (700 MHz/s), the scattering process at laser frequencies blue of resonance significantly heats the ions which results in the observed line asymmetry. The half-width at half-maximum (HWHM) of the cooled side of the line is $\approx 40 \text{ MHz}$ corresponding to a temperature of $\approx 0.5 \text{ K}$. It is to be noted however, that the laser beam, which has non-zero extent, interacts with a spread of magnetron orbits and velocities. The magnitude of the resulting Doppler broadening is a function of the cloud size and charge density, but it is expected to result in the major portion of the observed 40 MHz half width. This indicates that the cyclotron and axial motions may be substantially colder than 0.5 K . This residual Doppler effect due to magnetron motion could be avoided by interrogating the ions with the laser directed along the trap axis.

To help overcome the effects of heating as the laser is scanned through the line, a second, frequency-doubled, ring dye laser is introduced into the trap. The ring laser is frequency-stabilized by locking to a saturated absorption hyperfine feature in iodine whose doubled frequency is nearly coincidental with but to the low frequency side of $^{24}\text{Mg}^+$. The stabilized laser serves to keep the sample cold as the first laser is scanned at reduced power. For reasons not fully understood at this time, the half line-widths obtained in this fashion are a factor of two broader than those obtained with one laser if all other parameters are unchanged. If the static magnetic field is increased from the previous ≈ 1.0 to $\approx 1.4 \text{ Tesla}$, the two laser scheme also produces narrow lines corresponding to temperatures $\approx 0.5 \text{ K}$. In Fig. 2, we show the line profile of the two laser generated signal (solid curve).

Equally important, the second fixed frequency laser allows us to do high-resolution spectroscopy of like or

dissimilar ionic species. The magnesium used in these experiments had a natural isotopic mixture containing approximately 80% $^{24}\text{Mg}^+$ and 10% each $^{25,26}\text{Mg}^+$. The $^{25,26}\text{Mg}^+$ lines are positioned in the high frequency wings of $^{24}\text{Mg}^+$. Thus, scanning these lines heats $^{24}\text{Mg}^+$, which in turn heats $^{25}\text{Mg}^+$ and $^{26}\text{Mg}^+$ by Coulomb collisions. This is in addition to the heating caused by scanning to the high frequency side of $^{25}\text{Mg}^+$ and $^{26}\text{Mg}^+$. These heating effects are largely eliminated by the frequency stabilized laser. Whereas $^{24}\text{Mg}^+$ is cooled directly by the fixed frequency laser, $^{25}\text{Mg}^+$ and $^{26}\text{Mg}^+$ are cooled and maintained cold by Coulomb interactions with the cooled $^{24}\text{Mg}^+$. This confirms an earlier conjecture [1] that one ion (in this case, $^{24}\text{Mg}^+$) can be used to cool other ions of spectroscopic interest.

Monitoring the scatter rate of the low power, frequency swept laser results in the spectrum shown in Fig. 3. $^{24}\text{Mg}^+$ and $^{26}\text{Mg}^+$ have zero nuclear spin and yield single lines, while $^{25}\text{Mg}^+$ has nuclear spin $I=5/2$ and would ordinarily exhibit six lines. However, the nuclear hyperfine components are optically pumped such that nearly all of the ^{25}Mg ions are in the $M_I = -5/2$ state. Hence, $^{25}\text{Mg}^+$ is also observed as a single line. The relative positions of the observed lines depend upon the isotope shifts and (in the case of $^{25}\text{Mg}^+$) the hyperfine coupling constants. The isotope shift of the $^2S_{1/2} - ^2P_{3/2}$ line in MgII is measured to be

$$\Delta\nu(^{24}\text{Mg} - ^{26}\text{Mg}) = 3.050 \pm 0.1 \text{ GHz}. \quad (3)$$

Combining this result with the mass shift formula, which is a good approximation for low Z elements such as Mg^+ , we calculate that the isotope shift for $^{25}\text{Mg}^+$ is

$$\Delta\nu(^{26}\text{Mg} - ^{25}\text{Mg}) = 1.461 \pm 0.1 \text{ GHz}. \quad (4)$$

The frequency difference between $^{25}\text{Mg}(m_I = -5/2, m_J = -3/2 \leftrightarrow m_I = -5/2, m_J = -1/2)$ and $^{26}\text{Mg}(m_J = -3/2 \leftrightarrow m_J = -1/2)$ optical transitions is

$$\Delta f = 772.1 \pm 60 \text{ MHz}. \quad (5)$$

From this result, we obtain the hyperfine coupling constant, a_{3S} , for the $^2S_{1/2}$ state of $^{25}\text{Mg}^+$

$$a_{3S} = -607.8 \pm 50 \text{ MHz}. \quad (6)$$

This is in fair agreement with earlier works of Crawford [7] and Weber [8]. For this calculation, we first estimated the $^2P_{3/2}$ coupling constant to be $a_{3P} = -19.1 \pm 5 \text{ MHz}$ using the Goudsmit formula and the known fine structure separation [9]. The uncertainty in this value of $\pm 5 \text{ MHz}$ contributes an uncertainty $\pm 15 \text{ MHz}$ in the value calculated for a_{3S} . We expect to substantially improve the accuracy in the a value for both states with a double resonance technique presently being pursued.

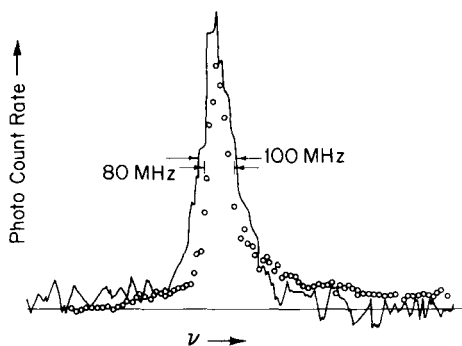


Fig. 2. Scatter rate vs. laser frequency. The curve shown in circles is with one laser only. The solid curve uses one laser to produce cooling while a second scans the line profile

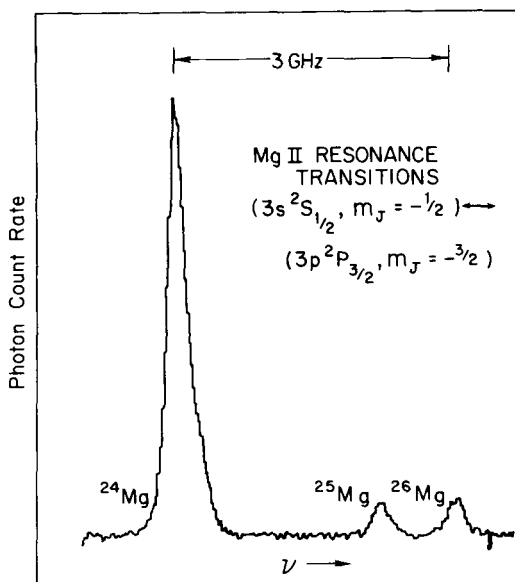


Fig. 3. Spectra of one Zeeman component of laser cooled $^{24,25,26}\text{Mg}^+$. The room temperature Doppler width of these lines is about 3 GHz. Only the $^{24}\text{Mg}^+$ is directly laser cooled. The $^{25}\text{Mg}^+$ hyperfine structure has been optically pumped resulting in the observation of a $(m_J = -1/2, m_I = -5/2) \leftrightarrow (m_J = -3/2, m_I = -5/2)$ component

By measuring the frequency difference between the center of the Doppler broadened I_2 line and the particular hyperfine component to which the stabilized ring laser is locked, we are able to reference the $^{24}\text{Mg}^+$ $3^2S_{1/2} \leftrightarrow 3^2P_{3/2}$ resonance transition to the known iodine spectra [10]. Subtracting out the linear Zeeman shift, we determine the $3^2S_{1/2} \leftrightarrow 3^2P_{3/2}$ resonance transition to be $35,760.834 \pm 0.004 \text{ cm}^{-1}$. This compares favorably to the accepted value of $35,760.88 \text{ cm}^{-1}$ [11].

Conclusion

In conclusion, we have presented high-resolution spectroscopy of laser cooled Mg^+ ions electromagnetically confined to a Penning trap. We have demonstrated a

general two laser scheme which provides both radiation pressure cooling and high-resolution spectroscopy on the cooled species. Additionally, we have demonstrated sympathetic cooling of a second species by long range Coulomb cooling (i.e. $^{25}\text{Mg}^+$ and $^{26}\text{Mg}^+$ by $^{24}\text{Mg}^+$). We have minimized the motions of the trapped ions yielding a temperature <0.5 K; but, most likely, substantially colder for the axial and cyclotron motions. We make the observation that the present experiments are limited in accuracy and resolution by the broadening and shift of the optical resonances due to residual magnetron motion. This limitation can be removed by probing the cooled ions with a laser directed along the trap axis.

Acknowledgements. The authors wish to thank W. M. Itano for assistance in parts of the experiment. We thank Dr. Itano and other members of the Frequency and Time Standards Group for helpful discussions during the course of this work. We acknowledge partial support by the Office of Naval Research and the Air Force Office of Scientific Research.

References

1. D.J. Wineland, R.E. Drullinger, F.L. Walls: Phys. Rev. Lett. **40**, 1639-1642 (1978)
2. W. Neuhauser, M. Hohenstatt, P. Toschek, H. Dehmelt: Phys. Rev. Lett. **41**, 233-236 (1978)
3. D.J. Wineland, W.M. Itano: Phys. Rev. A **20**, 1521-1540 (1979)
4. R.E. Drullinger, D.J. Wineland: In *Laser Spectroscopy IV*, ed. by H. Walther and K.W. Rothe, Springer Series Opt. Sci. **21** (Springer, Berlin, Heidelberg, New York 1979)
5. H.G. Dehmelt, F.L. Walls: Phys. Rev. Lett. **21**, 127-130 (1968); H. Dehmelt: In *Advances in Atomic and Molecular Physics*, ed. by D.R. Bates and I. Esterman (Academic Press, New York 1967, 1969), Vols. **3**, 53-72 and **5**, 109-154; D.J. Wineland, H.G. Dehmelt: J. Appl. Phys. **46**, 919-930 (1975)
6. J. Byrne, P.S. Farago: Proc. Phys. Soc. (London) **86**, 801-815 (1965)
7. M.F. Crawford, F.M. Kelly, A.L. Schawlow, W.M. Gray: Phys. Rev. **76**, 1527-1528 (1949)
8. E. Weber: University of Heidelberg, private communication
9. Average of values obtained from Eqs. (III.84) and (III.86) of N.F. Ramsey: *Molecular Beams* (Oxford University Press 1956) p. 75
10. S. Gerstenkorn, P. Luc: Rev. Phys. Appl. **14**, 791-794 (1979)
11. P. Risberg: Ark. Fys. **9**, 483 (1955)

Double-resonance and optical-pumping experiments on electromagnetically confined, laser-cooled ions

D. J. Wineland, J. C. Bergquist, Wayne M. Itano, and R. E. Drullinger

Frequency and Time Standards Group, National Bureau of Standards, Boulder, Colorado 80303

Received March 3, 1980

Experiments illustrating advantages and unique features of double-resonance and optical pumping on electromagnetically confined, laser-cooled ions are discussed. In certain cases, scattered light from the cooling transition can be used as a monitor in double-resonance experiments to give nearly 100% detection efficiency. Nonradiative relaxation rates are extremely small for stored ions, permitting nearly complete optical pumping, even in extremely weak pumping schemes.

If one hopes to improve accuracy and resolution substantially in spectroscopic studies beyond the present state of the art,¹ then one must address the problems of observation time (i.e., line Q), and first- and second-order Doppler effects. With this in mind, experiments have been carried out at the National Bureau of Standards² and Heidelberg University³ to cool substantially by radiation pressure (to less than 1 K) ions that are stored in room-temperature, macroscopic electromagnetic traps. In this Letter, we point out further advantages of using laser-cooled, trapped ions in high-resolution, double-resonance schemes and demonstrate some of these features with preliminary data. In some cases, high- Q microwave or optical transitions can be detected with nearly 100% efficiency; in addition, nearly complete optical pumping can be obtained, even in very weak pumping schemes.

More than a decade ago, Dehmelt and his co-workers pointed out advantages of using stored ions for high-resolution spectroscopy.⁴ Storage times of ions can be extremely long (days), and perturbations to the measured frequency from ion-ion collisions and confinement can be very small (less than 1 part in 10^{16}). This is to be contrasted with experiments on confined neutral atoms, in which spin exchange, buffer gas, and wall shifts can limit the accuracy achieved at the parts-in- 10^{12} level. Progress on stored-ion spectroscopy has been slowed somewhat because the number of ions that can be stored is rather small (typically $\lesssim 10^6$), thus yielding a small signal-to-noise ratio in double-resonance experiments. Because the ions are confined, the Dicke criterion is satisfied at microwave wavelengths; thus first-order Doppler shifts and broadening can be eliminated. Unfortunately, the temperature of ions in the trap is often above the ambient temperature, thus causing significant second-order Doppler effects. The cooling that has been achieved^{2,3} minimizes the second-order Doppler shift, and, as discussed below, the use of lasers in high-resolution, double-resonance experiments can increase the signal-to-noise ratio, limited only by the statistical fluctuations in the number of ions that have made the transition.

For high-resolution spectroscopic experiments on

laser-cooled ions, the use of double-resonance schemes may be a natural choice. This is because, for cooling, one prefers to drive a strongly allowed electric dipole transition repeatedly, whereas for the high-resolution spectroscopy, a microwave or weakly allowed optical transition is desired. In a few interesting cases, the ions are also forced by selection rules to return to the original ground-state sublevel on re-emission from the excited state. Thus the cooling can be performed without the necessity for mixing ground-state sublevels. Although this type of repopulation pumping has been realized in conventional optical-pumping experiments using, for example, circularly polarized light, the experiments discussed below have additional advantages.

Small clouds ($10^2 \lesssim N \lesssim 10^4$; cloud diameter $\sim 200 \mu\text{m}$ to $\sim 1 \text{mm}$) of Mg^+ ions are stored in a Penning trap.² The confining axial (z) magnetic field (0.978 T) splits the $^{24}\text{Mg}^+$ energy levels, as shown in Fig. 1. Light ($\sim 5 \mu\text{W}$ focused to a spot diameter $\approx 100 \mu\text{m}$; $\lambda \approx 280 \text{nm}$) from a frequency-doubled dye laser incident along the y axis and polarized in the x direction is tuned slightly lower ($\sim 100 \text{MHz}$) than the ($3p \ ^2P_{3/2}$, $M_J = -3/2$) \leftarrow ($3s \ ^2S_{1/2}$, $M_J = -1/2$) transition frequency. This cools the ions (to less than 1 K for the smallest clouds) and simultaneously pumps them into the $M_J = -1/2$ ground state. This repopulation pumping can be explained as follows: Ions in the $M_J = +1/2$ ground

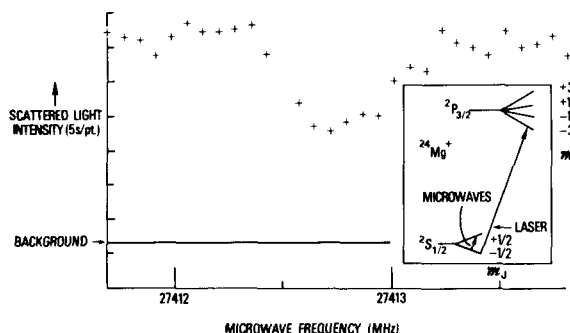


Fig. 1. Microwave-optical double resonance in $^{24}\text{Mg}^+$. Inset shows relevant microwave and optical pumping transitions.

state are driven weakly in the wings of the $(-1/2) \leftarrow (+1/2)$ transition (we denote the excited- and ground-state M_J values by the numbers in the first and second parentheses, respectively). On re-emission, the ion decays with $2/3$ probability to the $(-1/2)$ ground state, which thus tends to populate this state. Once in the $(-1/2)$ ground state, the ion is driven with high probability to the $(-3/2)$ excited state, from which it can only decay to the $(-1/2)$ ground-state level. Depopulation of the $(-1/2)$ ground state can occur because we are pumping in the wings of the $(+1/2) \leftarrow (-1/2)$ transition. Even though this transition frequency is about 36.6 GHz away from the laser frequency, it is driven at a rate that far exceeds the nonradiative relaxation rate in the ground state. However, the $(-1/2) \leftarrow (+1/2)$ transition frequency is only about 9.15 GHz away from the laser frequency, and therefore we should expect the population in the $(-1/2)$ ground state to be about 16 times larger than that in the $(+1/2)$ ground state. This is confirmed by a simple rate-equation analysis.

If we now drive a high- Q transition (here called a clock transition), which has as its ground state the same repopulated level from the laser cooling, this level will be depleted and the transition will be indicated by a decrease in the fluorescence scattering on the cooling transition.⁵ This simple double-resonance principle is illustrated in our experiments, in which the clock transition is represented by the ground-state Zeeman transition (Fig. 1). In these experiments, we observed the backscattered light in an $f/4$ cone; the net collection efficiency was 3×10^{-5} . The poor resolution in the present experiment is due to poor magnetic-field stabilization, that is, the field fluctuates about 10 parts in 10^6 in the time taken to trace the resonance. In a similar fashion, we have observed the $(-1/2) \leftarrow (-1/2)$ and $(+1/2) \leftarrow (-1/2)$ optical transitions by driving them with a second, low-power, frequency-swept laser.

We can observe the repopulation pumping process by first equalizing the ground-state populations with microwave radiation (indicated by the fluorescence signal's dropping to about 50% of its initial value). We then turn off the microwave radiation and observe that the fluorescence signal returns to its original value with a time constant characteristic of the repopulation pumping described above (Fig. 2). A simple rate-equation analysis (assuming we are well below saturation) indicates that the time constant for this is given by $\tau = 24/(17BR)$, where B is the rate for scattering on

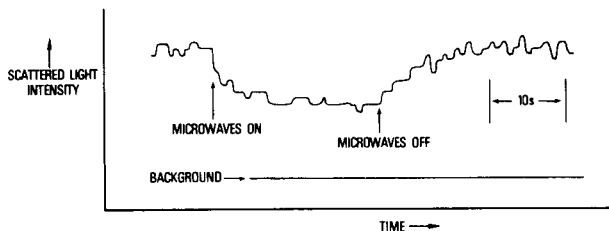


Fig. 2. Fluorescence scattering rate versus time, showing repumping into the $M_J = -1/2$ ground state on $^{24}\text{Mg}^+$. The laser is tuned to the $(M_J = -3/2) \leftarrow (M_J = -1/2)$ optical transition.

the $(-1/2) \leftarrow (+1/2)$ transition for an ion in the laser beam [recall that the laser is tuned to the $(-3/2) \leftarrow (-1/2)$ transition] and R is the geometrical fractional overlap of the laser beam with the ion cloud. For the conditions in Fig. 2, we estimated that $B \cong 30/\text{sec}$, $R \cong 0.5 \times 10^{-2}$ ($N \cong 10^3$ to 10^4), resulting in $\tau \cong 10$ sec.

Although they are similar to conventional optical pumping schemes, double-resonance experiments on laser-cooled, stored ions differ in some important respects:

1. Laser cooling, in addition to reducing Doppler shifts on the clock transition,^{2,3} can reduce the Doppler broadening of the cooling-optical-pumping transition to less than the natural width. As a consequence, the scattering cross section for all ions is approximately equal to the *resonant cross section*, thus greatly increasing the scattering rate. This is important for many types of ions that have first resonance lines in the ultraviolet, where only small power is available. These high scatter rates can permit the observation of many cooling-pumping photons for each microwave (or optical) photon absorbed on the clock transition.⁶ (Actually, in the above scheme, we observe the *absence* of many scattered cooling-pumping photons when the clock transition is driven, but the optimum signal-to-noise ratio will be the same.) In schemes in which depopulation pumping occurs in the ground state,⁶ the ratio of scattered (detection) photons to absorbed photons on the clock transition is somewhat limited; for the case in which the ion is forced by selection rules to return to the original ground state, as discussed here, the ratio can be $\gg 10^6$. This large ratio can help to make up for the losses in detection that are due to small collection solid angle, small detection quantum efficiency, etc., so that the high- Q transition can be monitored with nearly *unit-detection efficiency*.

2. *Relaxation times* of ions in the ion trap are *essentially indefinite* (>1 h). This allows one to realize nearly complete optical pumping in weak optical-pumping schemes. For the case of $^{24}\text{Mg}^+$ discussed above, the repopulation pumping occurs because we are driving weakly in the wings of the $(-1/2) \leftarrow (+1/2)$ transition. This rate is rather small (Fig. 2), but it far exceeds any other relaxation between ground-state levels.

Perhaps more importantly, we have observed nearly complete optical pumping of the $(M_J = -1/2, M_I = -5/2)$ ground state in $^{25}\text{Mg}^+$. In this case, pumping into the $M_J = -1/2$ ground states occurs as in the case of $^{24}\text{Mg}^+$. Pumping into the $M_J = -3/2$ excited states occurs from ground states that to a first approximation have the same value of M_J . However, because of the hyperfine coupling, the excited states (except for the $M_I = -5/2$ state) have a small admixture of nuclear states with lower M_J ; hence, when they decay, there is a slight probability (about 10^{-6} to 10^{-5} at a field of ~ 1 T) that M_I is reduced. After many scattering events, the ions become "trapped" in the $M_I = -5/2$ state. This pumping into individual hyperfine states should permit a double-resonance measurement of the $^{25}\text{Mg}^+$ hyperfine structure and possibly the realization of certain types of frequency standards.⁷

3. The extremely small spatial extent of the ion clouds possible with the stored-ion technique^{2,3} can be a benefit in many spectroscopic studies; we mention the additional advantage for Zeeman frequency measurements that the problem of field homogeneity is greatly reduced.

The example of $^{24}\text{Mg}^+$ is perhaps not so interesting from the high-resolution standpoint; however, it illustrates the general features of a class of experiments that hold promise for significantly improving accuracy and resolution in the future. Conceptually simple schemes^{7,8} for high-resolution, double-resonance experiments are not without practical difficulties; however, some of the advantages discussed here can be realized in other experiments without undue complication.

This work was supported in part by the U.S. Air Force Office of Scientific Research and the Office of Naval Research.

References

1. J. L. Hall, "Stabilized lasers and precision measurements," *Science* **202**, 147 (1978); A. L. Schawlow, "Laser spectroscopy of atoms and molecules," *Science* **202**, 141 (1978); H. Hellwig, K. M. Evenson, and D. J. Wineland, "Time, frequency, and physical measurement," *Phys. Today* **31**(12), 23 (1978); D. J. Wineland, "Limitations on long-term stability and accuracy in atomic clocks," in *Proceedings of 11th Annual Precise Time and Time Interval Application and Planning Meeting* (Goddard Space Flight Center, Greenbelt, Md., 1980), to be published.
2. D. J. Wineland, R. E. Drullinger, and F. L. Walls, "Radiation pressure cooling of bound resonant absorbers," *Phys. Rev. Lett.* **40**, 1639 (1978); R. E. Drullinger and D. J. Wineland, "Laser cooling of ions bound to a Penning trap," in *Laser Spectroscopy IV*, H. Walther and K. W. Rothe, eds. (Springer-Verlag, Heidelberg, 1979), p. 66.
3. W. Neuhauser, M. Hohenstatt, P. Toschek, and H. Dehmelt, "Optical-sideband cooling of visible atom cloud confined in parabolic well," *Phys. Rev. Lett.* **41**, 233 (1978); "Preparation, cooling, and spectroscopy of single, localized ions," in *Laser Spectroscopy IV*, H. Walther and K. W. Rothe, eds. (Springer-Verlag, Heidelberg, 1979), p. 73.
4. H. G. Dehmelt, "Radio frequency spectroscopy of stored ions, I and II," in *Advances in Atomic and Molecular Physics*, D. R. Bates and I. Esterman, eds. (Academic, New York, 1967 and 1969), Vols. 3 and 5.
5. To avoid light shifts and broadening, the laser could be turned off while the clock transition is driven.
6. F. L. Walls, D. J. Wineland, and R. E. Drullinger, "New possibilities for frequency standards using laser cooling and detection of stored ions," in *Proceedings of 32nd Annual Symposium on Frequency Control* (U.S. Army Electronics Command, Fort Monmouth, N.J., 1978), p. 453.
7. W. M. Itano and D. J. Wineland, "Frequency and time standards utilizing laser cooled ions," *Bull. Am. Phys. Soc.* **24**, 1185 (1979).
8. H. G. Dehmelt, "Proposed $10^{14} \Delta\nu < \nu$ laser fluorescence spectroscopy on Tl^+ mono-ion oscillator, I and II," *Bull. Am. Phys. Soc.* **18**, 1521 (1973); **20**, 60 (1975).

SPECTROSCOPY OF A SINGLE Mg^+ ION [☆]

D.J. WINELAND and Wayne M. ITANO

Frequency and Time Standards Group, Time and Frequency Division, National Bureau of Standards, Boulder, CO 80303, USA

Received 1 December 1980

A single $^{24}\text{Mg}^+$ ion has been laser cooled in a Penning trap and its optical spectrum observed by a double resonance technique. Residual Doppler line broadening implies a cyclotron–magnetron temperature of 50 ± 30 mK.

Laser cooling of ions bound in electromagnetic traps was first demonstrated [1] in 1978. More recently, this technique has been used in experiments that detect the fluorescence of, photograph, and observe a Raman transition on a single, laser-cooled Ba^+ ion in an RF trap [2]. This ability to localize single cold particles approaches the experimentalist's ideal of obtaining unperturbed systems at rest. In this letter, we report the isolation and double resonance detection [3] of a single, laser-cooled Mg^+ ion in a Penning trap. The primary differences of this work from that of ref. [2] are: (1) the requirements for localization and cooling of an ion in a Penning trap are substantially different than for the case of the RF trap, (2) we derive a kinetic "temperature" for the ion from the measured Doppler broadening of the optical spectrum rather than from the cloud size, (3) the intensity of fluorescence from a single ion is determined by destruction of individual ions by charge exchange rather than by creation by ionization.

The basic configuration of the experiment has been described elsewhere [1,3,4]. Briefly, in the present experiments, approximately three $^{24}\text{Mg}^+$ ions are loaded into the trap ($V_0 \approx 2$ V, $B_0 \approx 1$ T), laser cooled, and localized [4] at the center of the trap. V_0 and B_0 are the applied static trap potential and magnetic field. The laser beam (power approximately $5 \mu\text{W}$) is weakly focused near the center of the trap to spot size $w_0 \approx 25 \mu\text{m}$ and is incident at an angle $\theta = 82^\circ$ with

respect to the \hat{z} (B field) axis. This provides both axial and radial laser cooling. Typically, the laser beam is positioned approximately $15 \mu\text{m}$ radially from trap center in a direction such that the magnetron velocity is in the same direction as the laser beam. Typical detuning of the laser frequency is about -25 MHz from the non-Doppler-shifted ($3p^2P_{3/2}, M_J = -3/2$) \leftarrow ($3s^2S_{1/2}, M_J = -1/2$) $^{24}\text{Mg}^+$ transition. This combination of frequency detuning and spatial positioning ensures both magnetron and cyclotron cooling [4].

Fluorescence from the $^{24}\text{Mg}^+$ ions is observed while a ^{25}Mg oven is heated at a low level and the resulting atomic beam directed at the $^{24}\text{Mg}^+$ ions. The fluorescence is observed to decrease as a function of time as shown in fig. 1. We attribute the step decreases in fluorescence intensity to the occurrence of single charge exchange events ($^{24}\text{Mg}^+ + ^{25}\text{Mg} \rightarrow ^{24}\text{Mg} + ^{25}\text{Mg}^+$) eliminating the $^{24}\text{Mg}^+$ ions, one at a time. The trapped $^{25}\text{Mg}^+$ ions are ejected from the trap in about 0.2 s by cyclotron–magnetron RF excitation.

We note that the steps are of unequal size, but this is not unexpected since the magnitude of the fluorescence will depend on the spatial overlap of the ions and laser beam (which depends on ion number) and the magnetron Doppler shift, which depends on the Coulomb interaction between ions as well as applied trap voltage. We also remark that fig. 1 is *not* a "typical" curve because it shows only charge exchange events. Elastic collisions ($^{24}\text{Mg}^+ + ^{25}\text{Mg} \rightarrow ^{24}\text{Mg}^+ + ^{25}\text{Mg}$) can also be observed. These are indicated by a sudden drop

[☆] Contribution of National Bureau of Standards.

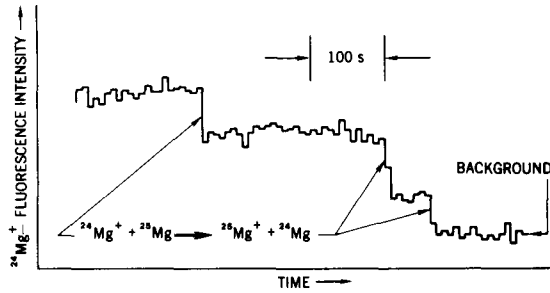


Fig. 1. $^{24}\text{Mg}^+$ ion fluorescence versus time when a ^{25}Mg atomic beam is directed at trap center. Fluorescence is integrated for 10 s on each experimental point. The large steps are attributed to single charge exchange events ($^{24}\text{Mg}^+ + ^{25}\text{Mg} \rightarrow ^{24}\text{Mg} + ^{25}\text{Mg}^+$) which remove the $^{24}\text{Mg}^+$ ions, one at a time. The last plateau is due to a single $^{24}\text{Mg}^+$ ion at trap center.

in fluorescence (a step down) as a $^{24}\text{Mg}^+$ ion is heated by the collision, causing its fluorescence to decrease due to its large Doppler width and orbit sizes. However, after some time (up to a few hundred seconds), it is again cooled down and localized at trap center and we see a step increase in the fluorescence to the former value. More important, one might suspect that the steps could be due to two or more ions: i.e., one $^{24}\text{Mg}^+$ ion is removed by charge exchange and during the time the $^{25}\text{Mg}^+$ ion is still in the trap, it has some probability (although estimated to be very small) that it heats the remaining $^{24}\text{Mg}^+$ ions by Coulomb collisions.

Since the goal of the experiment was to observe a single $^{24}\text{Mg}^+$ ion, the above difficulties could be avoided as follows: The $^{24}\text{Mg}^+$ loading conditions were scaled down so that after careful searching, fluorescence was observed on only 20% of the loads. Statistically, this meant that if any fluorescence was observed, it was, with high probability, from a single ion. At this time, the double resonance experiments (described below) were performed, after which, we looked for a single step after the ^{25}Mg oven was turned on. Immediately after this step was observed, the ^{25}Mg oven was turned off and a careful search was made to find any remaining $^{24}\text{Mg}^+$ ions. Since none were found, we concluded that, with high probability, we had a single ion.

The features of the optical spectrum of a single ion (fig. 2) could be recorded by using a simple optical pumping, double resonance scheme [3]. Briefly, a "high-power" laser (power approximately equal to $5 \mu\text{W}$) is used to keep the ion cold and at trap center;

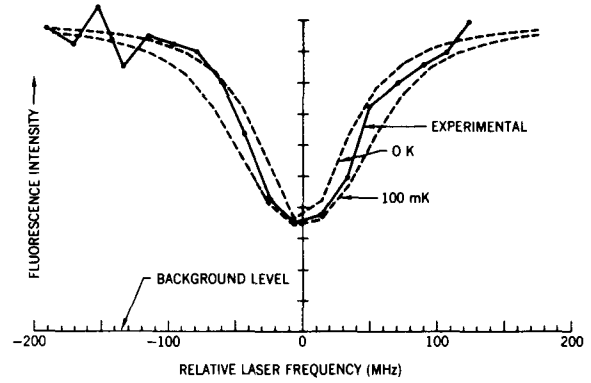


Fig. 2. Double resonance curve of a single $^{24}\text{Mg}^+$ ion. On the vertical axis is the fluorescence from a fixed frequency laser (power approximately $5 \mu\text{W}$) tuned to the $(^2\text{P}_{3/2}, M_J = -3/2) \leftarrow (^2\text{S}_{1/2}, M_J = -1/2)$ transition. Each point represents a 10 s integration; the connecting lines are only for clarity. The horizontal axis is the frequency of the low-power ($\ll 5 \mu\text{W}$) laser which is continuously scanned across the $(^2\text{P}_{3/2}, M_J = -1/2) \leftarrow (^2\text{S}_{1/2}, M_J = -1/2)$ transition. The dashed curves are simulations of fluorescence at $T = 0 \text{ K}$ and 100 mK (no added noise). The solid curve is experimental data. From these data, we conclude $T = 50 \pm 30 \text{ mK}$.

this laser also optically pumps the ion [3] so that it spends about 94% of its time in the $(^2\text{S}_{1/2}, M_J = -1/2)$ ground state Zeeman sublevel and about 6% of its time in the $(^2\text{S}_{1/2}, M_J = +1/2)$ level. If the frequency of a second lower-power ($\ll 5 \mu\text{W}$) laser beam (coincident spatially with the first laser beam) is swept through the $(^2\text{P}_{3/2}, M_J = -1/2) \leftarrow (^2\text{S}_{1/2}, M_J = -1/2)$ transition, the resonance condition will be indicated by a decrease in fluorescence due to the first laser. Specifically, the observed fluorescence is proportional to the fraction of time, $f_{-1/2}$, the ion spends in the $(M_J = -1/2)$ ground state sublevel, which is approximately equal to

$$f_{-1/2} = \frac{1}{17} [1 + 8R_1/(17R_2)]^{-1}, \quad (1)$$

where R_1 is the $(^2\text{P}_{3/2}, M_J = -1/2) \leftarrow (^2\text{S}_{1/2}, M_J = -1/2)$ transition rate, due to the low-power laser, and R_2 is the $(^2\text{P}_{3/2}, M_J = -1/2) \leftarrow (^2\text{S}_{1/2}, M_J = +1/2)$ transition rate, due to off-resonance scattering by the high-power laser. This method is superior to a previous method [4], since the signal is due to the higher scattering by the high-power laser; also the ion temperature is not significantly perturbed by the low-power laser. The experimental resonance curve in fig. 2 can be compared to the two other curves which were simulated,

assuming the ion kinetic energy had a Maxwell–Boltzmann distribution in time. The width of the 0 K curve is due to the 43 MHz natural width [5]. It is slightly broadened because of the detailed nature of the fluorescence intensity as given by eq. (1) and because the laser is continuously swept during the integration period. It is slightly asymmetric since the integration periods are not symmetric about line center. From this kind of data, we conclude that the cyclotron–magnetron “temperature” was 50 ± 30 mK. The axial temperature, T_z , can be estimated by lowering the axial well depth by lowering V_0 and noting the decrease in fluorescence as the axial excursions become comparable to the laser spot size. With $V_0 = 1$ V, the fluorescence signal drops to about half its value for $V_0 \approx 7$ V, which implies $T_z \approx 600$ mK. The Doppler broadening information is relatively insensitive to the axial temperature because θ is close to 90° . Assuming the cyclotron–magnetron temperature is zero, this yields an axial temperature of 2.6 ± 1.5 K. Thus, we conclude that the Doppler broadening is primarily a measure of cyclotron–magnetron temperature. We also note that experimentally, for a single ion, the radial extent is significantly less than the laser spot diameter.

Cyclotron–axial cooling and magnetron “cooling” in a Penning trap are fundamentally different in nature. Here, cooling is defined as reducing the *kinetic* energy in the three (cyclotron, axial, and magnetron) degrees of freedom. Previous treatments [6] apply to the harmonic axial motion. If we define the potential energy to be zero at trap center, then we can write the total energy (kinetic and potential) in the magnetron and cyclotron degrees of freedom as

$$\begin{aligned} E_m &= \frac{1}{2} M r_m^2 (\omega_m^2 - \frac{1}{2} \omega_z^2), \\ E_c &= \frac{1}{2} M r_c^2 (\omega_c'^2 - \frac{1}{2} \omega_z^2), \end{aligned} \quad (2)$$

where

$$\omega_z^2 = 4eV_0/M(r_0^2 + 2z_0^2), \quad (3)$$

ω_m , ω_c' , and ω_z are the magnetron, cyclotron, and axial frequencies and r_m and r_c are the magnetron and cyclotron radii. The dependence of the potential energy [second terms in eq. (2)] on the applied trap potential V_0 and trap dimensions r_0 and z_0 is apparent in eq. (3). Since $\omega_m < \omega_z/\sqrt{2} < \omega_c'$ for trapping, then

$E_c > 0$, but $E_m < 0$. To reduce r_m and thereby the magnetron kinetic energy, we must therefore increase the total magnetron energy. Conversely, to reduce r_c and thereby the cyclotron kinetic energy, we must *decrease* the total cyclotron energy. (The cyclotron case is analogous to the harmonic binding case described in ref. [6].) If we view laser scattering events as point interactions (valid since $\omega_z, \omega_m, \omega_c' \ll \gamma$, where γ is the optical linewidth) then the requirements for cooling are that we preferentially scatter photons when the magnetron motion recedes from the laser and the cyclotron motion approaches the laser. Since the direction of circulation is the same for both degrees of freedom, it might appear that these conditions cannot simultaneously be satisfied, but they can if the laser intensity is higher on the side of trap center where the magnetron motion recedes from the laser [4,7]. This is accomplished in our experiments by working on the slope of the nearly gaussian laser beam profile.

We have theoretically modeled the cooling of a single ion in a Penning trap [7], and when applied to our experimental conditions, these calculations can be used to predict minimum temperatures. If we define

$$\begin{aligned} T_m &= M\omega_m^2 r_m^2 / (2k), \quad T_c = M\omega_c'^2 r_c^2 / (2k) \\ T_z &= M \langle v_z^2 \rangle / k, \end{aligned}$$

where k is Boltzmann's constant, then we find minimum temperatures $T_m \approx 1.3 \times 10^{-6}$ K, $T_c \approx 0.99$ mK, $T_z \approx 11$ mK. At this time, we do not understand why our measured temperature appears higher than these predictions, but we have ruled out obvious effects, such as background gas collisions, laser frequency jitter, etc. We note, however, that if we conservatively estimate $r_m(\text{max}) = 15 \mu\text{m}$, this gives $T_m(\text{max}) \approx 1$ mK. Therefore, the observed temperature would appear to be due to “hot” cyclotron motion. We also note that the predicted and experimental values of T_c/T_z approximately agree.

One serious shortcoming of the present apparatus [3,4] is that the net detection efficiency of the scattered light (fraction of scattered photons which are counted) is only about 10^{-5} , therefore limiting signal-to-noise ratio. A new apparatus with significantly improved detection efficiency is being constructed. This will improve signal-to-noise ratio in the double resonance experiments; moreover, it should allow simpler identification of a single ion because, over short

time intervals, the fluorescence should maintain a steady value when the ion is in the $M_J = -1/2$ ground state and be totally absent when the ion is in the $M_J = +1/2$ ground state. We also note that when the Doppler width of the optical lines is less than the natural width, the *spectrum* of the scattered light is broadened only by the Doppler effect and not the natural width. If the laser linewidth is assumed negligible, the spectrum of the scattered light is composed of discrete lines, one at the laser frequency, and sidebands at $p\omega_z + q\omega_m + s\omega'_c$ where p , q , and s are positive and negative integers. For example, if we assume that only the cyclotron motion is excited and has a Maxwell-Boltzmann distribution in time, then the profile of these sidebands for light scattered in the backward direction is a gaussian with full width at half maximum = $4(2 \ln 2 \cdot kT/M\lambda^2)^{1/2}$ where λ is the wavelength of the light (this is twice the normal Doppler broadening). The centroid is shifted from the laser frequency by $\Delta\omega = -4R/\hbar$ where $R = \hbar^2/2M\lambda^2$. This spectrum could then give a more sensitive measure of the temperature ^{#1}.

^{#1} The case of resolved sidebands in the Lamb-Dicke regime has been treated by Javanainen [8].

We gratefully acknowledge the contributions of J.C. Bergquist in the laboratory and in the course of numerous discussions. We appreciate a critical reading of the manuscript by J.C. Bergquist, L. Lewis and G. Dunn. We also acknowledge the support of the Air Force Office of Scientific Research and the Office of Naval Research. One of us (W.M.I.) held an NRC Postdoctoral Research Associateship during this work.

References

- [1] D.J. Wineland, R.E. Drullinger and F.L. Walls, Phys. Rev. Lett. 40 (1978) 1638; W. Neuhauser, M. Hohenstatt, P. Toschek and H. Dehmelt, Phys. Rev. Lett. 41 (1978) 233.
- [2] W. Neuhauser, M. Hohenstatt, P.E. Toschek and H. Dehmelt, Phys. Rev. A22 (1980) 1137.
- [3] D.J. Wineland, J.C. Bergquist, W.M. Itano and R.E. Drullinger, Opt. Lett. 5 (1980) 245.
- [4] R.E. Drullinger, D.J. Wineland and J.C. Bergquist, Appl. Phys. 22 (1980) 365.
- [5] W.L. Wiese, M.W. Smith and B.M. Miles, Atomic transition probabilities, U.S. National bureau of Standards, National Standards Reference Data Series 22, Vol. II (US GPO, Washington, DC, 1969).
- [6] D.J. Wineland and W.M. Itano, Phys. Rev. A20 (1979) 1521; J. Javanainen and S. Stenholm, Appl. Phys. 21 (1980) 283; J. Javanainen, Appl. Phys. 23 (1980) 175.
- [7] W.M. Itano and D.J. Wineland, to be published.
- [8] J. Javanainen, Opt. Commun. 34 (1980) 375.

PROPOSED STORED $^{201}\text{Hg}^+$ ION FREQUENCY STANDARDS*

D. J. Wineland, Wayne M. Itano, J. C. Bergquist,
and F. L. Walls

Frequency and Time Standards Group
Time and Frequency Division
National Bureau of Standards
Boulder, Colorado 80303

Summary

In this paper, we discuss the performance potential and the problems of implementing a microwave frequency (and time) standard and an optical frequency standard utilizing $^{201}\text{Hg}^+$ ions stored in a Penning trap. Many of the discussions apply to ion storage-based frequency standards in general. Laser cooling, optical pumping, and optical detection of the microwave or optical clock transition could be achieved using narrowband radiation at the $194.2\text{ nm } 6p\ ^2P_{1/2} + 6s\ ^2S_{1/2}$ transition, while selectively mixing the ground-state hyperfine levels with appropriate microwave radiation. A first-order field-independent microwave clock transition, which is particularly well-suited to the use of the Penning ion trap is the $25.9\text{ GHz } (F, M_F) = (2, 1) \leftrightarrow (1, 1)$ hyperfine transition at a magnetic field of 0.534 T . The two-photon Doppler-free $5d^9\ 6s^2\ ^2D_{5/2} \leftrightarrow 5d^{10}\ 6s\ ^2S_{1/2}$ transition at 563 nm is a possible candidate for an optical frequency standard. Both standards have the potential of achieving absolute accuracies of better than one part in 10^{15} and frequency stabilities of less than 10^{-16} .

Introduction

In this paper, a specific proposal is made for a $^{201}\text{Hg}^+$ stored ion microwave frequency (and time) standard which could have an absolute fractional uncertainty of less than 10^{-15} . We also discuss the possibilities for a $^{201}\text{Hg}^+$ optical frequency standard. A future stored ion frequency standard may not take the exact form described here; nevertheless, it is useful to investigate a specific proposal, since many of the same generic problems will be encountered in any standard based on stored ions.

Since the pioneering work of Dehmelt and co-workers, who first developed the stored ion

method for high-resolution spectroscopy,¹ it has been clear that these techniques provide the basis for an excellent time and frequency standard.²⁻¹⁰ This conjecture is based primarily on the ability to confine the ions for long periods of time without the usual perturbations associated with confinement (e.g., "wall shift" as in the hydrogen maser). Starting with the work of Major and Werth⁵ reported in 1973, groups at Mainz⁷ and Orsay¹⁰ and at least one commercial company¹¹ have sought to develop a frequency standard based on $^{199}\text{Hg}^+$ ions stored in an rf trap. The choice of Hg^+ ions for a microwave stored ion frequency standard is a natural one because its ground-state hyperfine structure is the largest of any ion which might easily be used in a frequency standard, and its relatively large mass gives a small second-order Doppler shift at a given temperature. This work has been developed to a fairly high level; the group at Orsay¹⁰ has made a working standard whose stability compares favorably to that of a commercial cesium beam frequency standard. However, the full potential of the stored ion techniques has yet to be realized; this appears to be due to two problems: (1) Historically, it has been difficult to cool the ions below the ambient temperature; this is made more difficult in the rf trap by "rf heating"¹ —a process not clearly understood, but one that makes it difficult to cool even to the ambient temperature.¹² For both the rf and Penning traps, the inability to cool below the ambient temperature means that one must contend with the frequency shift from the second-order Doppler or time-dilation effect. Although it is possible to calculate this shift from the measured Doppler (sideband) spectra, to

*Contribution of the National Bureau of Standards not subject to copyright.

do so with the required accuracy may be difficult for ions near room temperature. (2) A second problem is that the number of ions that can be stored in a restricted volume (dimensions $\lesssim 1$ cm) is typically rather small ($\lesssim 10^6$). This, coupled with the somewhat poor signal-to-noise ratios realized with conventional lamp sources, causes the short-term stability in a frequency standard based on ions to be degraded, even though the Q's realized are quite high.

In the past two or three years, both of these problems have been addressed in experiments and the results suggest viable solutions. In 1978, groups at the National Bureau of Standards (NBS) and Heidelberg demonstrated^{13,14} that radiation pressure from lasers could be used to cool ions to temperatures < 1 K, thereby reducing the second-order Doppler shifts by 2-3 orders of magnitude below the room temperature case. As discussed below, the cooling is most favorable for very small numbers of ions (down to one ion), so that there is a trade-off between the maximum number of ions we can use and the minimum second-order Doppler shift that can be achieved.

To improve signal to noise, we note that in certain optical-pumping, double-resonance experiments, it is possible to scatter many optical photons from each ion for each microwave photon absorbed.⁹ This can allow one to make up for losses in detection efficiency due to small solid angle, small quantum efficiency in the photon detector, etc., so that the transition probability for each ion can be measured with unity detection efficiency. This means that the signal-to-noise ratio need be limited only by the statistical fluctuations in the number of ions that have made the transition.¹⁵ This is discussed in a simple example in Appendix A.

More recently, the narrow linewidths anticipated for the stored ion technique have been observed. A resonance linewidth of about 0.012 Hz at 292 MHz has been observed for the $(m_I, m_J) = (-3/2, 1/2) \leftrightarrow (-1/2, 1/2)$ hyperfine transition of $^{25}\text{Mg}^+$ at a magnetic field of about 1.24 T where the first derivative of the transition frequency with respect to magnetic field is zero.¹⁶ (The

Ramsey interference method was implemented by applying two rf pulses of 1 s duration separated by 41 s). These narrow linewidths should be preserved with hyperfine transitions of higher frequency, such as in $^{201}\text{Hg}^+$, but, of course, more attention must be paid to field homogeneity and stability.

These results have encouraged us to begin studies on the $^{201}\text{Hg}^+$ system and although this ion may not provide the "final answer," it appears to provide a case where inaccuracies significantly smaller than 10^{-13} can be achieved. The discussion here is largely devoted to a microwave frequency standard with a design goal of accuracy better than 10^{-15} ; however, the possibilities for a stored ion optical frequency standard in $^{201}\text{Hg}^+$ are also briefly included.^{17,32} For a given interaction time, the Q of a transition will scale with the frequency. Therefore, in principle, an optical frequency standard would have clear advantages over a microwave frequency standard. Our decision to work on a microwave frequency standard (as well as an optical standard) is motivated largely by practical considerations: (1) Before the full potential of an ion-storage optical frequency standard could be realized, tunable lasers with suitable spectral purity must become available. This problem may be nearing solution.²⁰ (2) If an optical frequency standard is to provide time, the phase of the radiation must be measured. This appears to present a much more formidable problem.^{18,19} Both of these problems are already solved in the microwave region of the spectrum—thus, the attraction for investigating a microwave frequency standard.

$^{201}\text{Hg}^+$ Stored Ion Microwave Frequency Standard

$^{201}\text{Hg}^+$ ions will be stored in a Penning trap. The choice of the Penning trap over the rf trap is motivated primarily because it appears easier to cool a cloud of ions in a Penning trap than in an rf trap. Residual heating mechanisms in the Penning trap are quite small¹³ whereas in the rf trap (where "rf heating" occurred), they can be substantial.¹⁴ Of course, this problem does not

exist for the rf trap if single ions are used, but for a microwave frequency standard, it is desirable to use as many ions as possible in order to increase signal-to-noise ratio. Use of a Penning trap means that one must use transitions that are independent of magnetic field to first order^{8,9,16}; this limits the number of transitions available, but need not be an absolute restriction. The $^{199}\text{Hg}^+$ isotope is therefore not considered, since there are no frequency extrema at practical fields.

The energy level structure²¹ of the $^{201}\text{Hg}^+$ ion vs. magnetic field is shown in Fig. 1. The

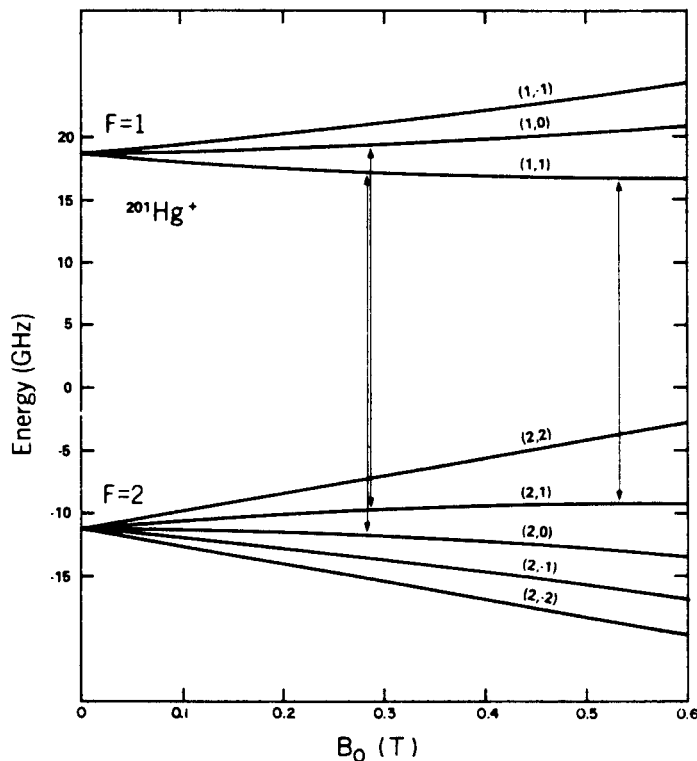


Figure 1. Ground state hyperfine energy levels of $^{201}\text{Hg}^+$ vs. magnetic field. States are designated by the (F, m_F) representation. Three transitions are indicated at the fields where the transition frequencies are independent of magnetic field to first order.

possible field independent "clock transitions" are the $(F, m_F) = (2,0) \leftrightarrow (1,1)$ and $(2,1) \leftrightarrow (1,0)$ transitions at about 0.29 T, the $(2,1) \leftrightarrow (1,1)$ transition at 0.534 T, the $(1,1) \leftrightarrow (1,0)$ transi-

tion at 3.91 T and the $(1,0) \leftrightarrow (1,-1)$ transition at 28.1 T. In principle, one desires to work at the highest microwave frequency possible (for highest Q) at the highest attainable magnetic field (to maximize the number of ions). The choice seems to be between the 25.9 GHz $(2,1) \leftrightarrow (1,1)$ transition at 0.534 T and the 7.72 GHz $(1,1) \leftrightarrow (1,0)$ transition at 3.91 T. At these magnetic fields, where the transition frequency is independent of magnetic field to first order, the second-order field dependence is given by $\Delta\nu/\nu_0$ ($(2,1) \leftrightarrow (1,1)$) = $1/6 (\Delta H/H_0)^2$ and $\Delta\nu/\nu_0$ ($(1,1) \leftrightarrow (1,0)$) $\cong .04(\Delta H/H_0)^2$. The remaining part of the proposal is modeled around the $(2,1) \rightarrow (1,1)$ transition at 0.534 T because of its higher frequency. From the second-order field dependence noted above, it is necessary to control the field stability and homogeneity over the ion cloud to better than 10^{-7} in order to achieve 10^{-15} accuracy. This is an important problem, of course, but not insurmountable—we note that the free-running stability of the magnetic field must be better than 10^{-7} over the clock transition time; in longer term it can be stabilized to this level by locking the field to a Zeeman transition in the ions.¹⁶

We will assume that a laser can be tuned to the $6p \ ^2P_{1/2} + 6s \ ^2S_{1/2}$ transition at 194.2 nm with sufficient power to provide laser cooling, optical pumping, and fluorescence detection. A specific scheme for observing the clock transition might be the following: (we will assume that when the ions are cold, the widths of the Doppler-broadened optical lines are approximately equal to the natural width (~ 70 MHz)).

(1) We tune the laser about 35 MHz below the $6p \ ^2P_{1/2} (1,-1) + 6s \ ^2S_{1/2} (2,-2)$ optical transition. This laser tuning gives the maximum cooling possible,²² but rapidly pumps the ions out of the $(2,-2)$ ground state. (For example, the $(1,-1)$ excited state decays to the $(1,-1)$ ground state with a probability equal to 0.329.) For cooling and detection, we require each ion to scatter many photons. Unfortunately, the simple schemes^{15,16,23} for multiple scattering that have been realized with ions like $^{25}\text{Mg}^+$ do not exist for Hg^+ . There-

fore, for the initial cooling, we must mix all the ground states with microwave radiation. This effectively reduces the cooling by a factor of 8 from the two-level ion case, since only $1/8$ of the ions are in the (2,-2) ground state, but should not be a problem given enough laser power (see below).

(2) Once cooling is accomplished, we can pump all the ions into one of the clock levels by, for example, mixing all the ground-state levels except the (1,1) level. This pumping occurs because we are exciting the ions in the wings of other optical transitions; for example, we are pumping in the wings of the (1,0) + (2,-1) optical transition (about 3.5 GHz away) and the (1,0) excited state decays into the (1,1) ground state with a probability of 0.039. (Note that the (1,-1) excited state cannot decay to the (1,1) ground state.) We remark that we have neglected the decay of the ions from the $2P_{1/2}$ excited state to either the $2D_{3/2}$ or $2D_{5/2}$ states. That this is a good approximation is shown in Appendix B. The ratio of the scattering rate on the (1,-1) + (2,-2) optical transition to the pumping rate into the (1,1) ground-state level is about 6×10^4 , i.e., about 6×10^4 photons are scattered by each ion before it is pumped into the (1,1) ground-state clock level. This number can be reduced by tuning the laser to another optical transition; this may be necessary if the laser power is too small. As discussed below, it is desirable for detection purposes for this number to be large.

(3) After the pumping is achieved, the laser and ground-state mixing rf are turned off (to avoid ac Stark shifts and relaxation) and the clock transition is driven. If we use the Ramsey interference method as was done for $^{25}\text{Mg}^+$,¹⁶ the resulting linewidth is about one-half as wide as if we use continuous excitation (the Rabi method). Therefore, the Ramsey method will be assumed.

(4) After the rf cycle is complete, the laser is turned back on as well as the mixing rf (excluding the (1,1) ground-state level) and the fluorescence scattering is observed. It should not be too difficult to detect the scattered photons with about 10^{-3} overall efficiency.

This would mean that about 60 photons would be collected for each ion that had made the transition (before it is repumped to the (1,1) level) insuring that the noise would only be due to the statistical fluctuations in the number of ions that had made the transition (see Appendix A).

In order to lock a local oscillator to the center of the clock transition, one would first complete one of the above cycles with the local oscillator tuned to the half-intensity point (where the transition probability for each ion is one half) on, say, the low side of the central Ramsey peak. These photon counts could then be stored and the cycle repeated with the local oscillator tuned to the high-frequency side of the line. These resulting counts could then be subtracted from the first to give an error signal which can be used to force the mean frequency of the local oscillator to be at the center of the clock transition. We will assume that the time for fluorescence observation and repumping is much less than the clock transition time.

Systematic Frequency Shifts

We have already mentioned the stringent requirements on magnetic field stability and homogeneity. Using a superconducting magnet, it is possible to stabilize the magnetic field to better than 10^{-7} . (This may require locking the field to an NMR probe adjacent to the trap over the time of the clock transition). The field homogeneity requirements will be more difficult to satisfy (assuming a 1 cm diameter spherical working volume inside the trap), but are still feasible.

The electric fields from the applied trap potentials and from Coulomb interactions between ions can cause second-order Stark shifts, but the resulting fractional frequency shifts are estimated to be much less than 10^{-15} . The black body ac Zeeman shift³⁸ is estimated to be $\Delta\nu/\nu_0 \cong 1.3 \times 10^{-17} (T/300)^2$ and is therefore neglected. The black body ac Stark shift³⁹ is estimated to be $\Delta\nu/\nu_0 \cong 2 \times 10^{-16} (T/300)^4$ and therefore must be accounted for or reduced environmental temperatures are required.

In spite of the laser cooling that has been achieved, we must still be concerned with the second-order Doppler frequency shift. In the Penning trap, the cyclotron-axial temperature of $^{201}\text{Hg}^+$ ions needs to be cooled to below 1.45 K to insure that the second-order Doppler shifts (on these degrees of freedom) is less than 10^{-15} . These low temperatures should be easy to obtain. A more serious problem exists for the magnetron rotation of the cloud; the kinetic energy in this degree of freedom will probably limit how small the second-order Doppler shift can be.²⁴ In the limit of very small numbers of ions, the magnetron kinetic energy should be negligible,²⁵ but in the case discussed here, we would like to use the maximum number of ions possible and this will cause problems as described below.

The "magnetron" rotation in a Penning trap is simply a form of circular $\vec{E} \times \vec{B}$ drift; that is, the radial electric fields in the trap from the applied potentials on the electrodes and from space charge act in a direction perpendicular to the magnetic field. This causes the ions to drift in circular "magnetron" orbits about the axis of the trap. If we assume that we must keep the ions inside a 1 cm diameter spherical working volume, then qualitatively, the nature of the problem is as follows: if we add more ions to this volume, then the magnetron frequency increases due to two effects. First, we must increase the applied trap potentials to overcome the increased space charge repulsion along the z axis, which tends to elongate the cloud in this direction. Consequently, the magnetron frequency increases due to the increased potentials and the increased space charge fields in the radial direction. In Appendix C, we estimate the maximum number of ions contained in a 1 cm diameter sphere assuming that the second-order Doppler shift is 10^{-15} for ions on the perimeter of the cloud at $z = 0$. We obtain $N_{\text{max}} = 8.2 \times 10^4$ and note that the applied trap voltage is only 71 mV for $z_0 = r_0/1.64 = 0.8 \text{ cm}$.¹

Frequency Stability

At optimum power (transition probability is equal to one at line center), we can closely

approximate the number of detected photon counts for each experimental cycle as

$$N = N_i n_d \left(\frac{1 + \cos(\omega - \omega_0) T}{2} \right) \quad (4)$$

where, as in Appendix A, N_i is the number of ions in the trap and n_d is the average number of detected photons for each ion that has made the transition. ω and ω_0 are the frequency of the applied rf and "clock" center frequency; T is the time between the rf pulses at the beginning and end of the rf period. (We assume that the time of the rf pulses is much less than T .) As described above, the interrogating oscillator is switched between $\omega - \pi/2T$ and $\omega + \pi/2T$ (where we assume $|\omega - \omega_0| \ll \pi/2T$), and the resulting counts subtracted to give an error signal. The sensitivity to mistuning of ω is given by calculating the slope of the signal in Eq. 4 at the half-intensity points ($|\omega - \omega_0| = \pi/2T$). We have

$$\left| \frac{dN}{d\omega} \right|_{|\omega - \omega_0| = \pi/2T} = \frac{N_i n_d T}{2}$$

After one full switching cycle (taking the difference of the counts from both sides of the line), the error signal is

$$\delta N = 2 \left| \frac{dN}{d\omega} \right|_{|\omega - \omega_0| = \pi/2T} \times \delta \omega$$

where $\delta \omega \equiv \omega - \omega_0$. Since N fluctuates statistically, these fluctuations (δN) give rise to frequency fluctuations in the locked local oscillator:

$$(\delta \omega)_{\text{rms}}^2 = 4 \frac{\delta N^2}{\left| \frac{dN}{d\omega} \right|^2}_{|\omega - \omega_0| = \pi/2T}$$

Maximum frequency stability is thus given by

$$\sigma_y^2(2T) \equiv \frac{1}{2} \frac{(\delta \omega)_{\text{rms}}^2}{\omega_0^2}$$

Assuming $n_d \gg 2$ (Appendix A), we have²⁶

$$\sigma_y(\tau) = \frac{1}{2T\omega_0 \sqrt{N_i}} \sqrt{\frac{2T}{\tau}} \quad \tau > 2T$$

For $N_j = 8.2 \times 10^4$ and $T = 50$ s,

$$\sigma_y(\tau) = 2 \times 10^{-15} \tau^{-\frac{1}{2}} \quad \tau > 100 \text{ s}$$

and

$$Q = \frac{\omega_0 T}{\pi} \cong 2.6 \times 10^{12}$$

Lasers

Perhaps the single reason that such a proposal has not been made previously is that the required narrowband tunable laser has not been available at 194.2 nm. However, it appears that two possible approaches lend themselves to initial experiments in this system. Briefly, the first approach might be to use an externally narrowband filtered ($\cong 100$ MHz) pulsed ArF excimer laser. We estimate that it should be possible to achieve saturating intensity from such a filtered laser. However, the pulse lengths of these lasers are quite short ($\lesssim 10$ ns), so that only about two photons per ion will be effective in each laser shot to drive the optical transition. (The lifetime of the upper $^2P_{\frac{1}{2}}$ (1,-1) state is about 2.3 ns and decays with 0.46 probability to the (2,-2) ground state.) The potential advantage of excimer laser systems is that the repetition rates can be quite high (KrF lasers have been built with 1 kHz repetition rates). However, at the present time, it is probably only feasible to realize 150 Hz repetition rates for ArF lasers. This should allow reasonable signal to noise in the above scheme when the ions are cold; however, we estimate cooling times of order 20 minutes, which is uncomfortably long.

A second scheme using frequency mixing of cw lasers in nonlinear crystals is presently being pursued at NBS. Tunable coherent radiation in the 194 nm region has previously been produced by phase-matched sum frequency mixing of pulsed lasers in a potassium pentaborate (KB5) crystal.²⁷ The second harmonic of the 514 nm Ar⁺ single frequency cw laser line, when mixed with radiation near 790 nm from a cw dye laser, will generate single frequency cw radiation at 194 nm.

The estimated efficiency of this process for a 3 cm crystal is given by

$$P_3 \cong 8 \times 10^{-5} P_1 P_2,$$

where P_3 is the output power at 194 nm, P_1 is the input power at 257 nm from the doubled Ar⁺ laser, and P_2 is the input power at 790 nm.^{28,29} All powers are expressed in watts. The second harmonic of 514 nm radiation can be generated in 90° phase matched temperature tuned KDP or ADP crystals with an efficiency (for a 5 cm crystal) given by

$$P_1 \cong 2.5 \times 10^{-3} P_0^2,$$

where P_1 is the output power at 257 nm and P_0 is the input power at 514 nm. Thus, about 10 mW can be produced with a 2 W input. The output power can be increased considerably by using a cavity to build up the circulating power. As much as 300 mW of cw power at 257 nm has been produced in this way.³⁰ Assuming that 200 mW at 257 nm and 500 mW at 790 nm are available, about 8 μ W at 194 nm could be produced. From the experience with Mg⁺ ions,^{13,15,16} this should be adequate power for initial experiments. The output could be further increased by building a cavity around the KB5 crystal to increase the circulating power at 790 nm, 257 nm, or both. Finally, the output power at the ions could be increased by building a ring cavity around the trap. The frequency of the Ar⁺ laser can be stabilized to an I₂ absorption. The dye laser can be stabilized and tuned using standard techniques. The temperature of the KB5 may have to be shifted slightly from room temperature in order to satisfy the phase-matching conditions. We estimate from the observed temperature tuning at 201.6 nm³¹ that the required shift is less than 25 °C.

Two-Photon Optical Frequency Standard in ²⁰¹Hg⁺

We will briefly describe the properties of a ²⁰¹Hg⁺ optical frequency standard that has been suggested previously.³² (¹⁹⁹Hg⁺ should, of course, also be considered because of its simpler

structure.) Using two-photon Doppler-free spectroscopy,³³ it should be possible to excite $^{201}\text{Hg}^+$ ions from a ground-state sublevel to a particular $2D_{5/2}$ sublevel using a dye laser tuned to approximately 563.2 nm. An excited state and magnetic field could be chosen so that the transition frequency could be independent of magnetic field to first order. For the case of this optical transition, the second-order dependence of fractional frequency offset due to magnetic field would be reduced by approximately the ratio of the optical frequency (5.33×10^{14} Hz) to the ground-state hyperfine frequency. This represents a reduction in sensitivity of about four orders of magnitude which would greatly relax the constraints on magnetic field. The ground and excited states could be chosen such that the ground-state level would be depopulated by the two-photon transition; therefore, detection could be accomplished in essentially the same manner as described for the microwave case above. The lifetime of the excited states³⁵ is about 0.11 s, so that the Q of this transition is about 7.4×10^{14} !

A drawback to this scheme is the accompanying ac Stark shift³³; this shift is formally equivalent to the "light shift" in rubidium frequency standards. We have roughly estimated the transition probability per unit time to be $W \cong 0.3 I^2/\delta\nu$ where $\delta\nu$ is the larger of the (doubled) laser linewidth or the natural linewidth (1.4 Hz) and I is the laser intensity in each direction in W/cm². We have also estimated the accompanying light shift to be $\Delta\nu \cong -I$ (Hz). If the (doubled) laser linewidth is less than the natural width and if we drive the transition near saturating intensity ($W \cong 1/s$), then $I \cong 2.2$ W/cm², which implies a fractional frequency shift of 2×10^{-15} .

The black body ac Stark shift³⁸ is estimated to be $\Delta\nu/\nu_0 \cong 10^{-16} (T/300)^4$. The frequency shift⁴⁰ due to the interaction of the quadrupole moment of the atomic D levels with the applied quadrupole field and fields due to ion-ion collision is estimated to be less than 10^{-16} for the conditions described here.

In initial experiments, it will very likely not be possible to obtain (doubled) laser line-

widths less than 1.4 Hz; however, laser linewidths of a few tens of hertz should be achievable. Therefore, the above projections may not be too optimistic.

Assuming the same conditions as for the microwave case, predicted stabilities are also quite dramatic (assuming laser linewidths are sufficiently narrow). If we assume that the (Rabi) interaction time is 1 s and that the detection and repumping time is much less than 1 s, this would imply (for $N_i = 8.2 \times 10^4$)

$$\sigma_y(\tau) \cong 2 \times 10^{-18} \tau^{-\frac{1}{2}} \quad \tau \geq 2 \text{ s}$$

$$\text{For } N_i = 1, \sigma_y(\tau) \cong 6 \times 10^{-16} \tau^{-\frac{1}{2}}.$$

Conclusions

Some of the problems associated with a stored-ion frequency standard have been addressed by making a specific proposal around the $^{201}\text{Hg}^+$ ion. Although other interesting candidates exist, this system appears feasible enough that experimental work has begun at NBS. Current efforts are aimed at producing the 194.2 nm laser light, producing narrowband 563.2 nm laser light for the two-photon transition, studying the ion cloud dynamics in order to produce the rather diffuse, spatially stable ion clouds and making ion traps with significantly increased collection efficiency.

Acknowledgments

The authors wish to acknowledge the continued support from the Air Force Office of Scientific Research and the Office of Naval Research. We thank H. Dehmelt, C. Pollock, and H. Robinson for critical comments and we thank R. Ray and B. Barrett for manuscript preparation.

APPENDIX A

Statistical Fluctuations in Detected Photon Counts

For simplicity, we will assume the conditions shown in Fig. 2. The actual conditions discussed in this paper and in Refs. 15 and 16 are somewhat

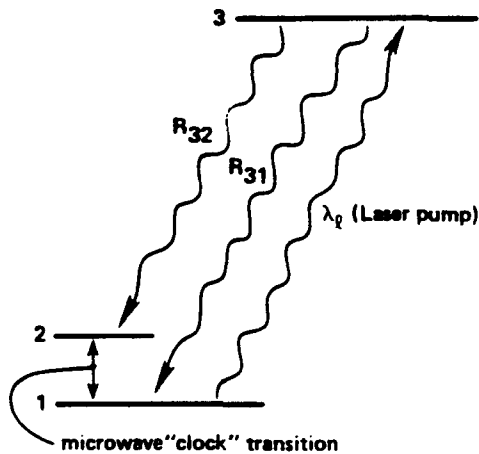


Figure 2. "Model" 3 level system to show the effects of statistical fluctuations in an optical pumping, double resonance experiment.

more complicated, but the basic result still applies. We assume that a laser is tuned to the $3 \rightarrow 1$ transition wavelength and that we can neglect excitation in the wings of the $3 \rightarrow 2$ transition by this laser. We also assume that the decay branching ratios R_{32} and R_{31} are such that $R_{31} \gg R_{32}$.

The basic scheme for an optical-pumping double-resonance experiment in this simple example is the following: (1) If the number of scattering events (for each ion) is sufficiently large, then essentially all the ions are pumped into the 2 level. (2) The laser is now turned off and the "clock" ($1 \rightarrow 2$) transition is driven. (3) The ions that have made the transition are then detected by turning the laser back on and observing the fluorescence scattering by collecting the light in a phototube.

For each ion that has made the clock transition, let the average number of detected photons be n_d ; the rms fluctuation in the number of detected photons per ion is $\sqrt{n_d}$. Because of inefficiencies in collection and detection, typically $n_d \ll R_{31}/R_{32}$, but the interesting case will be when n_d is still significantly greater than one. We will assume that the clock transition is driven with optimum power, so that when we are tuned to

the half-intensity point on the line (for maximum frequency sensitivity), the probability, p , that each ion has made a transition is 0.5. In this case, if the total number of ions is N_i , then the average number that have made the transition is $pN_i = N_i/2$ and the rms fluctuations in the number of ions that have made the transition on each experimental cycle is

$$\Delta N_i = \sqrt{N_i p(1-p)} = \sqrt{N_i}/2.$$

For one photon counting cycle, the average number of photons detected is $N_{TOT} = n_d N_i/2$. The fluctuations in the number of detected photons (ΔN_{TOT}) is due to two causes: (1) The fluctuations in the number of photons counted (Δn_{TOT})_d due to fluctuations in the counted photons for each ion. Since these are statistically independent:

$$(\Delta n_{TOT})_d = \sqrt{\sum^{N_i/2} (\Delta n_d)^2} = \sqrt{n_d N_i/2}$$

(2) The fluctuation in the number of photons counted (Δn_{TOT})_i due to the fluctuations in the number of ions that have made the transition:

$$(\Delta n_{TOT})_i = \Delta N_i n_d = n_d \sqrt{N_i}/2$$

Since these two processes are also statistically independent, the total fluctuations in N_{TOT} are given by:

$$\begin{aligned} \Delta N_{TOT} &= \sqrt{(\Delta n_{TOT})_d^2 + (\Delta n_{TOT})_i^2} \\ &= \frac{n_d \sqrt{N_i}}{2} \sqrt{1 + \frac{2}{n_d}} \end{aligned}$$

Therefore when $n_d \gg 2$, the fluctuations in the photon counts are given by the statistical fluctuations in the number of ions that have made the transition. We must note, of course, that the above arguments assume that the laser intensity and cloud of ions is stable, and therefore, fluctuations in signal due to changes in laser-cloud spatial overlap are negligible.

Appendix B

${}^2P_{3/2} \rightarrow {}^2D_{3/2, 5/2}$ Decay Rates

Decay from the $5d^{10} 6p {}^2P_J$ levels to the $5d^9 6s^2 {}^2D_J$ levels is allowed through configuration interaction, which can mix some $5d^{10} 6d$ amplitude into the D states and some $5d^9 6s 6p$ amplitude into the P states.³⁵ Crandell, et al.³⁶ have determined that the decay rate from the ${}^2P_{3/2}$ state to the ${}^2S_{1/2}$ ground state is $350 \pm 30\%$ times greater than the decay rate to the ${}^2D_{5/2}$ state. If LS coupling is valid, the ${}^2P_{3/2}$ state decays to the ${}^2D_{3/2}$ with probability 3×10^{-7} . This decay is highly suppressed because the energy difference is only 933 cm^{-1} , which corresponds to a wavelength of $11 \mu\text{m}$. (The decay rate is proportional to the cube of the energy difference.) Decay of the ${}^2P_{3/2}$ state to the ${}^2D_{5/2}$ state is forbidden by the electric dipole selection rules, since it requires J to change by 2. Hyperfine and Zeeman interactions mix different J states, making this decay slightly allowed. However, we estimate this probability to be less than 10^{-11} at a magnetic field of 0.5 T. The ${}^2D_{3/2}$ state decays to the ${}^2D_{5/2}$ state at a rate of about 54 s^{-1} and to the ${}^2S_{1/2}$ state at a rate of about 42 s^{-1} . The ${}^2D_{5/2}$ state decays to the ${}^2S_{1/2}$ at a rate of about 9.5 s^{-1} .³⁵ If the laser-induced ${}^2S_{1/2}$ to ${}^2P_{3/2}$ transition is denoted by γ_L , the ions reach the ${}^2D_{3/2}$ state at a rate of $3 \times 10^{-7} \cdot \gamma_L$ from which they decay, with probability about 0.56, to the ${}^2D_{5/2}$ state, where they stay for an average of about 0.11 s before decaying back to the ${}^2S_{1/2}$ state. If γ_L is less than $6 \times 10^6 \text{ s}^{-1}$, the ions spend less than 10% of their time in the metastable D states, so that this trapping does not cause a problem for the cooling. Transitions to the D states occur at a rate which is much less than the optical pumping rates between ground-state sublevels, so their neglect in the previous discussion on optical pumping is justified.

Appendix C

Maximum Number of Stored Ions

Since the cyclotron and axial kinetic energies are assumed cold, we will assume a uniform charge distribution for the ions.³⁷ For a spherical ion cloud, the magnetron rotation frequency of the cloud (ω_m) is given from the equations of motion as:

$$\omega_m = \frac{\omega_c}{2} - \sqrt{\left(\frac{\omega_c}{2}\right)^2 - \left(\frac{\omega_z^2}{2} + \frac{4\pi e\rho}{3M}\right)} \quad (\text{C.1})$$

where ω_c is the unperturbed ion cyclotron frequency $\omega_c = eB/Mc$, ω_z is the axial oscillation frequency derived from the applied trap voltage (V_0) as:¹

$$\omega_z^2 = 4e V_0 / M(r_0^2 + 2z_0^2)$$

and ρ is the space charge density. We have for the space charge potential from the ions (inside the cloud)

$$\phi_i = \frac{2}{3} \pi \rho (r^2 + z^2)$$

and the trap potential may be expressed as

$$\phi_T = \frac{V_0 (r^2 - 2z^2)}{r_0^2 + 2z_0^2}$$

When the axial-cyclotron motion is cold, we have $\phi_i(z) = \phi_T(z) = 0$; this implies

$$\rho = \frac{3}{4\pi} \frac{M}{e} \omega_z^2 \quad (\text{C.2})$$

If we assume we want the maximum second-order Doppler shift $\left(\frac{1}{2} \left(\frac{v}{c}\right)^2\right)$ less than ϵ , then we require $\omega_m = c \sqrt{2\epsilon} / r_{c\ell}$ where $r_{c\ell}$ is the radius of the cloud. If we want to maximize the number of ions $N = 4\pi\rho(r_{c\ell})^3 / (3e)$, then we want to maximize this expression subject to the above constraints on ω_m . Substituting Eqs. (C.1) and (C.2) into this expression for N we have:

$$N = 2 \frac{\sqrt{2} M c}{3e^2} r_{c\ell} \sqrt{\epsilon} \left(\omega_c r_{c\ell} - c \sqrt{2\epsilon} \right) \quad (\text{C.4})$$

(Values of r_{cl} where this expression is negative are unphysical because we assume that ϵ is a fixed value on the perimeter of the cloud (at $z = 0$) no matter what its size is. For very small clouds, this requires V_0 large enough that the ions are unbounded—the case for $N \leq 0$.)

From (C.2) and the expression for ω_z^2 ,

$$V_0 = \pi(r_0^2 + 2z_0^2) \rho / 3 \quad (C.5)$$

For the conditions assumed in the text, $r_{cl} = 0.5$ cm, $\omega_c = 40.5$ kHz, and $\epsilon = 10^{-15}$ we have $N \approx 8.2 \times 10^4$. Assuming $z_0 = r_0 / 1.64 = 0.8$ cm, then $V_0 = 0.071$ V.

References

1. H. G. Dehmelt, *Advan. Atomic and Mol. Physics* **3**, 53 (1967) and **5**, 109 (1969).
2. F. G. Major, NASA Report X-521.69.167, Goddard Space Flight Center (1969).
3. H. A. Schuessler, E. N. Fortson, and H. G. Dehmelt, *Phys. Rev.* **187**, 5 (1969).
4. H. A. Schuessler, *Metrologia* **7**, 103 (1971).
5. F. G. Major and G. Werth, *Phys. Rev. Lett.* **30**, 1155 (1973) and *Appl. Phys.* **15**, 201 (1978).
6. R. Ifflander and G. Werth, *Metrologia* **13**, 167 (1977).
7. M. D. McGuire, R. Petsch, and G. Werth, *Phys. Rev. A* **17**, 1999 (1978).
8. F. Strumia, *Proc. 32nd Ann. Symp. on Freq. Control (Fort Monmouth, NJ, May 1978)* p. 444.
9. F. L. Walls, D. J. Wineland, and R. E. Drullinger, *ibid.* p. 453.
10. M. Jardino, M. Desaintfuscién, R. Barillet, J. Viennet, P. Petit, and C. Audoin, *Proc. 34th Ann. Symp. on Freq. Control (Fort Monmouth, NJ, June 1980)* p. 353 and *Appl. Phys.* **24**, 1 (1981).
11. M. D. McGuire, *Bull. Am. Phys. Soc.* **26**, 615 (1981).
12. D. A. Church and H. G. Dehmelt, *J. Appl. Phys.* **40**, 3421 (1969).
13. D. J. Wineland, R. E. Drullinger, and F. L. Walls, *Phys. Rev. Lett.* **40**, 1639 (1978).
14. W. Neuhauser, M. Hohenstatt, P. Toschek, and H. Dehmelt, *Phys. Rev. Lett.* **41**, 233 (1978).
15. D. J. Wineland, J. C. Bergquist, Wayne M. Itano, and R. E. Drullinger, *Opt. Lett.* **5**, 245 (1980).
16. Wayne M. Itano and D. J. Wineland, *Phys. Rev. A*, to be published.
17. See also: H. G. Dehmelt, *Bull. Am. Phys. Soc.* **18**, 1521 (1973) and **20**, 60 (1975), and D. J. Wineland and H. G. Dehmelt, *Bull. Am. Phys. Soc.* **20**, 637 (1975).
18. J. L. Hall, *Science* **202**, 147 (1978).
19. D. J. Wineland, *Proc. 11th PTI, (NASA Publ. 2129, Nov., 1979)* p. 81.
20. J. L. Hall, *Proc. Int. Conf. on Atomic Phys., Boston, Mass. (Aug. 1980)*.
21. The ground-state hyperfine separation was taken from the measurements of Y. Guern, A. Bideau-Méhu, R. Abjean, and A. Johannin-Gilles, *Physica Scripta* **14**, 273 (1977).
22. D. J. Wineland and Wayne M. Itano, *Phys. Rev. A* **20**, 1521 (1979).
23. Wayne M. Itano and D. J. Wineland, *Bull. Am. Phys. Soc.* **24**, 1185 (1979).
24. A similar limitation for the rf trap is imposed by the kinetic energy in the forced "micromotion" of ions not at the center of the trap. See D. J. Wineland, *Proc. 2nd Int. Conf. on Precision Meas. and Fundamental Constants, Gaithersburg, MD, June 1981*, to be published.
25. D. J. Wineland and Wayne M. Itano, *Phys. Lett.* **82A**, 75 (1981).
26. The basic scheme proposed for $^{137}\text{Ba}^+$ in Ref. 9 should be possible; however, two important errors in this paper should be noted: first, the number of scattered photons before repumping was overestimated because pumping in the wings of the other optical lines was not considered. Second, although the improvement in signal-to-noise ratio due to multiple scattering was noted, it was overestimated because it was not assumed that the fluctuations would be limited to the statistical variations in the number of ions that made the clock transition. (See Appendix A).
27. R. E. Stickel, Jr. and F. B. Dunning, *Appl. Opt.* **17**, 981 (1978).
28. G. D. Boyd and D. A. Kleinman, *J. Appl. Phys.* **39**, 3597 (1968).
29. F. B. Dunning and R. E. Stickel, Jr., *Appl. Opt.* **15**, 3131 (1976).
30. P. Huber, *Opt. Commun.* **15**, 196 (1975).
31. R. E. Stickel, Jr. and F. B. Dunning, *Appl. Opt.* **16**, 2356 (1977).
32. P. L. Bender, J. L. Hall, R. H. Garstang, F. M. J. Pichanick, W. W. Smith, R. L. Barger, and J. B. West, *Bull. Am. Phys. Soc.* **21**, 599 (1976).
33. See for example: V. S. Letokhov and V. P. Chebotayev, *Nonlinear Laser Spectroscopy*, (Springer-Verlag, New York) 1977.
34. Ye. V. Baklanov, V. P. Chebotayev, and B. Ya. Dubetskii, *Appl. Phys.* **11**, 201 (1976).
35. R. H. Garstang, *National Bureau of Standards J. Research* **68A**, 61 (1964).
36. D. H. Crandall, R. A. Phaneuf, and G. H. Dunn, *Phys. Rev. A* **11**, 1223 (1975).
37. See for example: S. A. Prasad and T. M. O'Neil, *Phys. Fluids* **22**, 278 (1979). T. M. O'Neil and C. F. Driscoll, *Phys. Fluids* **22**, 260 (1979).
38. T. F. Gallagher and W. E. Cooke, *Phys. Rev. Lett.* **42**, 835 (1979).
39. L. L. Lewis, Wayne M. Itano, and D. J. Wineland, to be published.
40. H. G. Dehmelt, paper in these proceedings.

Precision measurement of the ground-state hyperfine constant of $^{25}\text{Mg}^+$

Wayne M. Itano and D. J. Wineland

Time and Frequency Division, National Bureau of Standards, Boulder, Colorado 80303

(Received 13 April 1981)

The ground-state hyperfine constant A and the nuclear-to-electronic g -factor ratio g_I/g_J of $^{25}\text{Mg}^+$ have been measured by a laser optical-pumping double-resonance technique. The ions were stored in a Penning trap at a magnetic field of about 1 T. The results are $A = -596.254\,376(54)$ MHz and $g_I/g_J = 9.299\,484(75) \times 10^{-5}$. The magnetic field at the ions was stabilized by servoing it to an ($\Delta m_I = 0, \Delta m_J = \pm 1$) electronic Zeeman transition. Other hyperfine ($\Delta m_I = \pm 1, \Delta m_J = 0$) transitions were detected while the field was thus stabilized. The derivative of the $(m_I, m_J) = (-3/2, 1/2)$ to $(-1/2, 1/2)$ transition frequency with respect to magnetic field B_0 goes to zero at $B_0 \approx 1.24$ T. The corresponding resonance was observed at this field with linewidths as small as 0.012 Hz ($Q = 2.4 \times 10^{10}$) by implementing the Ramsey interference method with two coherent rf pulses separated in time by up to 41.4 s.

I. INTRODUCTION

The ground-state magnetic-dipole hyperfine constants (A values) of the neutral alkali atoms have been measured to high precision by optical-pumping and atomic beam magnetic resonance techniques.^{1,2} A variety of theoretical methods have been used to calculate these quantities.³ By comparison, much less experimental and theoretical work has been done on the singly ionized alkali-earth atoms, which are isoelectronic to the alkalis. Purely optical measurements generally suffer from low resolution. Direct and indirect optical-pumping methods have been used to measure the ground-state A values of several alkaline-earth ions and some other ions that have a $^2S_{1/2}$ ground state,⁴ either in buffer-gas cells [Ba⁺, Cd⁺, Be⁺, Mg⁺ (Ref. 5)] or in ion traps [He⁺, Hg⁺ (Ref. 6), Ba⁺ (Ref. 7)]. Also, electron-spin resonance (ESR) spectroscopy has been used to study Mg⁺ (Ref. 8) and Cd⁺ (Ref. 9) trapped in solid rare-gas matrices, where the A values may be shifted from their free-ion values by a significant amount. This shift is typically a few percent for the neutral alkalis.¹⁰ The ground-state A value of Li-like fluorine has been measured by the method of perturbed angular correlations.¹¹ A few calculations of the ground-state A values of alkalilike positive ions have been published, especially for the Li series.^{3,12}

In this paper, we report on the first high-precision determination of the ground-state A value of the free $^{25}\text{Mg}^+$ ion. The nuclear-to-electronic g -factor ratio g_I/g_J was also determined. A preliminary report on these measurements has appeared previously.¹³

Our experimental techniques have several unusual features:

(1) The ions were stored in a Penning ion trap in ultrahigh vacuum. Perturbations to energy

levels caused by collisions with neutral molecules or other ions or by the trapping fields were very small, except for the Zeeman shift due to the large applied magnetic field. Relaxation times were many seconds so that very narrow resonances could be observed.

(2) Resonant light pressure from a frequency-doubled dye laser was used to reduce the ion temperature to less than 1 K, thus reducing all Doppler effects, and to confine the ions to a small volume around the trap center, which reduced magnetic-field inhomogeneity effects.¹⁴⁻¹⁸

(3) Laser optical-pumping, double-resonance techniques can achieve good signal-to-noise ratios, even with very small ion numbers.¹⁷ In fact, double-resonance signals can be observed from a single ion.^{14,18}

(4) The experiments were carried out in a high magnetic field, which was needed to confine the ions. In this case, the transition frequencies depend upon A , the g factors, and the magnetic field. Short-term fluctuations (~ 1 s) of the magnetic field imposed the main limitation on the determinations of A and g_I/g_J .

The details of the experimental method are discussed in Sec. II. The values of A and g_I/g_J are calculated from the data and their uncertainties are estimated in Sec. III. In Sec. IV these values are compared with the results of other experiments and with theory, and applications and extensions of our experimental techniques are discussed.

II. EXPERIMENTAL METHOD

A. $^{25}\text{Mg}^+$ level structure

Singly ionized Mg is isoelectronic to neutral Na. The ground state is labeled $3s\ ^2S_{1/2}$, and the first excited states are labeled $3p\ ^2P_J$ ($J = \frac{1}{2}, \frac{3}{2}$). Light of wavelength 279.6 nm was used to drive the

transition from the ground state to the $3p^2P_{3/2}$ level. The ^{25}Mg nucleus has nuclear spin $I = \frac{5}{2}$, so the ground and excited states have hyperfine structure. The experiments were carried out in a magnetic field of about 1 T, so that the nuclear and electronic angular momenta \vec{I} and \vec{J} were essentially decoupled. Figure 1 shows the ground-state energy levels as a function of magnetic field. The hyperfine constants of the $3p^2P_{3/2}$ state have not been measured. However, they can be estimated¹⁹ from the known $3p^2P_j$ fine structure splitting²⁰ and the known magnetic dipole²¹ and electric quadrupole²² moments of the ^{25}Mg nucleus. These values are $A \cong -18$ MHz and $B \cong 22$ MHz. A value for the effective nuclear charge $Z_1 = 10$ was assumed.

B. Apparatus

The basic experimental apparatus has been described previously.^{15,16} A Penning-style ion trap, which uses a uniform magnetic field and a quadrupolar electrostatic potential,²³ was used to store the ions. The characteristic dimensions of the trap were $r_0 = 1.64z_0 = 0.63$ cm. Typical operating parameters were $V_0 = 7$ V and $B_0 = 1$ T. $^{25}\text{Mg}^+$ ions were loaded into the trap in the following way: An electron beam coincident with the trap axis created positive ions by collisions with background gas, which were confined by the trap. An oven containing ^{25}Mg of 98% isotopic purity was heated, and the ^{25}Mg neutrals underwent charge-exchange reactions with the trapped positive ions to yield trapped $^{25}\text{Mg}^+$ ions. The magnetron radii of the ions

increased slowly due to collisions with background gas. The storage time has been observed to be about one day without light pressure cooling or confinement. The number of ions initially stored could be varied from about 10^4 down to about one by varying the current and duration of the electron beam. Typical numbers for the experiments reported here were about 10 to 100 ions. The reason for using such small numbers was that in order to get experimentally convenient optical-pumping time constants of no more than a few seconds, relatively high light intensity was required. Since the total available power was low (< 40 μW), it was necessary to focus the beam to a small spot size (about 50- μm diameter). The maximum ion density is limited by space-charge effects, so in order for the ion cloud to be small enough to have good overlap with the focused beam, the total ion number had to be small. During the resonance experiments, the background pressure was maintained below 1.3×10^{-7} Pa (10^{-9} Torr).

The source of 279.6 nm radiation was the second harmonic of the output of a single-mode cw rhodamine 110 dye laser. The frequency doubling took place in a 90°-phase-matched AD*P (deuterated ammonium dihydrogen phosphate) crystal, operated at a temperature of about 117 °C. The uv power generated was typically between 5 and 30 μW . The bandwidth of the dye laser was about 1 MHz and could be frequency stabilized in a long term to about ± 200 kHz by locking it to a saturated absorption hyperfine feature in I_2 . If the laser frequency was fixed in this way, fine tuning could be accomplished by varying the trap magnetic field to Zeeman shift the Mg^+ levels.

The second harmonic radiation was separated from the fundamental by a prism and focused into the trap, passing through 3-mm holes drilled into the ring electrode. The beam entered and exited from the vacuum enclosure through Brewster-angle windows. Resonance fluorescence photons emitted into the backward direction inside an $f/4$ cone were collected by a flat mirror set at 45° to the incident beam and imaged by lenses onto a photomultiplier tube (PMT). (The incident beam passed through a hole in this mirror.) Two stages of spatial filtering were used to reduce background due to light scattered from the windows. An interference filter centered at 280 nm and a Corning 7-54 glass filter reduced background due to light at other wavelengths. The net detection efficiency for a photon emitted from an ion, taking into account the detection solid angle, mirror reflectivity, transmission of the lenses and filters, and PMT quantum efficiency, was about 2×10^{-5} .

Data collection was controlled by a minicomputer, which swept the rf or microwave frequency

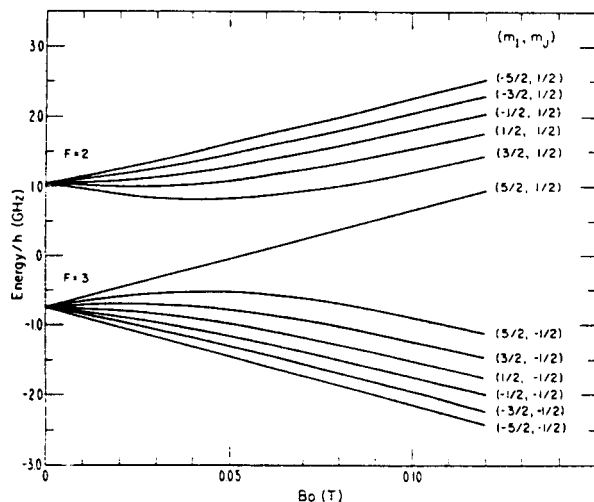


FIG. 1. Ground-state energy levels of $^{25}\text{Mg}^+$ as a function of the magnetic field B_0 . Note the transition from low field, where \vec{I} and \vec{J} are coupled to form the total angular momentum \vec{F} , to high field, where they are decoupled. All of the experiments were done at high field.

used to drive the $^{25}\text{Mg}^+$ ground-state transitions and recorded the number of photons detected by the PMT. The output of various frequency synthesizers was applied to a probe near the gap between the endcap and ring electrode and used to drive the nuclear spin flip ($\Delta m_J = 0$, $\Delta m_I = \pm 1$) rf transitions at about 300 MHz. The output of a klystron was directed at the trap from the end of a waveguide positioned outside one of the Brewster windows and used to drive the electronic spin flip ($\Delta m_J = \pm 1$, $\Delta m_I = 0$) microwave transitions at about 30 GHz. The klystron was phase locked to the third harmonic of a microwave frequency synthesizer. For high-accuracy work, the frequency synthesizers were phase locked to the output of a cesium atomic beam frequency standard. The computer also controlled an rf switch and a light shutter, which were necessary for some of the resonance schemes.

C. Resonance methods

The basic principles of the optical-pumping, double-resonance methods have been outlined previously.¹⁷ Resonant light pressure was used to cool the ions to roughly 1 K and to confine them to a small volume near the trap center. The electronic Zeeman splitting was much greater than the Doppler width. With light polarized perpendicular to the magnetic field and slightly lower in frequency than the ($^2S_{1/2}$, $m_I = -\frac{5}{2}$, $m_J = -\frac{1}{2}$) to ($^2P_{3/2}$, $m_I = -\frac{5}{2}$, $m_J = -\frac{3}{2}$) transition frequency, the steady-state population of the ($^2S_{1/2}$, $m_I = -\frac{5}{2}$, $m_J = -\frac{1}{2}$) level was about 94% and the ($^2S_{1/2}$, $m_I = -\frac{5}{2}$, $m_J = \frac{1}{2}$) population was about 6%, as a result of competition between relatively weak off-resonance transition rates.¹⁷ The frequency detuning from the resonance center, typically about 30 to 50 MHz, was necessary in order to provide cooling.^{14,15} At the light intensities used, these weak pumping rates were about 1 s^{-1} , much faster than any other relaxation rate between ground-state sublevels.

The optical-pumping mechanism is unusual in that the ($m_I = -\frac{5}{2}$, $m_J = -\frac{1}{2}$) ground-state sublevel, which is driven to the excited state at the highest rate, retains the highest steady-state population. The optical transition frequencies are shown in Fig. 2. Optical pumping into the $m_J = -\frac{1}{2}$ ground-state manifold takes place by the same mechanism as for $^{24}\text{Mg}^+$, which has zero nuclear spin. The m_I quantum number can be ignored for this part of the discussion. For light polarized perpendicular to the magnetic field, m_J must change by ± 1 in a transition from the ground state to the excited state. In spontaneous decay from the excited state to the ground state, m_J can change by 0 or ± 1 . Thus, the $-\frac{1}{2} \rightarrow -\frac{3}{2}$ transition, which is strongly driven by the laser, and the $+\frac{1}{2} \rightarrow -\frac{1}{2}$ tran-

sition do not optically pump the ground state. The first and second numbers refer to the ground- and excited-state m_J values. The other allowed transitions, $+\frac{1}{2} \rightarrow -\frac{1}{2}$ and $-\frac{1}{2} \rightarrow +\frac{1}{2}$, do cause optical pumping because the ion can decay to either ground-state m_J manifold. These transitions are driven weakly in their Lorentzian wings. Since the second harmonic of the laser frequency is close to the $-\frac{1}{2} \rightarrow -\frac{3}{2}$ transition frequency, its detuning from the $-\frac{1}{2} \rightarrow +\frac{1}{2}$ transition is four times as great as its detuning from the $+\frac{1}{2} \rightarrow -\frac{1}{2}$ transition (see Fig. 2). Hence, the $m_J = +\frac{1}{2}$ ground-state manifold is depopulated 16 times faster than the $m_J = -\frac{1}{2}$ manifold. In the steady state, the $m_J = -\frac{1}{2}$ manifold has 16 times the population of the $m_J = +\frac{1}{2}$ manifold, provided that the optical-pumping rate is much faster than competing relaxation rates. Optical pumping into the ($m_I = -\frac{5}{2}$) ground-state sublevels occurs because of hyperfine coupling in the excited state. The excited-state sublevels, which are labeled (m_I , $m_J = -\frac{3}{2}$), actually contain small admixtures of states with lower m_I , except for ($m_I = -\frac{5}{2}$, $m_J = -\frac{3}{2}$), which is pure. For example, the state which is nominally ($m_I = -\frac{5}{2}$, $m_J = -\frac{3}{2}$) contains a small amplitude (about 1.4×10^{-3} at $B_0 = 1 \text{ T}$) of the ($m_I = -\frac{5}{2}$, $m_J = -\frac{1}{2}$) state, etc. Hence, if an ion in the (m_I , $m_J = \frac{1}{2}$) ground-state sublevel is driven to the (m_I , $m_J = -\frac{3}{2}$) excited-state sublevel, it has a small probability of decaying to a ground-state sublevel with lower m_I , unless $m_I = -\frac{5}{2}$. Eventually, the ions are trapped in the $m_I = -\frac{5}{2}$ sublevels. The process by which an ion absorbs and emits a photon and is left in a different ground-state sublevel has been treated as if the absorption and emission were separate events. It would be more accurate to describe this process in terms of spontaneous resonance Raman scattering, but this distinction is actually of no importance, since neither the coherence nor the time delay between the two events is of interest.

The fluorescence level was proportional to the ($^2S_{1/2}$, $m_I = -\frac{5}{2}$, $m_J = -\frac{1}{2}$) population. Hence, a transition which changed this population could be detected as a change in fluorescence. In the following, let the ($^2S_{1/2}$, m_I , m_J) state be denoted by (m_I , m_J). Both the $(-\frac{5}{2}, -\frac{1}{2})$ to $(-\frac{5}{2}, -\frac{3}{2})$ nuclear spin-flip transition and the $(-\frac{5}{2}, -\frac{1}{2})$ to $(-\frac{5}{2}, \frac{1}{2})$ electronic spin-flip transition were detected by a decrease in fluorescence when rf at the resonance frequency was applied. When the rf transition was saturated, the fluorescence dropped by about 50%. This technique was previously used to detect the ground-state electronic spin-flip transition of $^{24}\text{Mg}^+$, which has zero nuclear spin.¹⁷ When light was tuned close to the ($^2S_{1/2}$, $m_I = \frac{5}{2}$, $m_J = \frac{1}{2}$) to ($^2P_{3/2}$, $m_I = \frac{5}{2}$, $m_J = \frac{3}{2}$) transition, most of the population was pumped into the $(\frac{5}{2}, \frac{1}{2})$ state. The $(\frac{5}{2},$

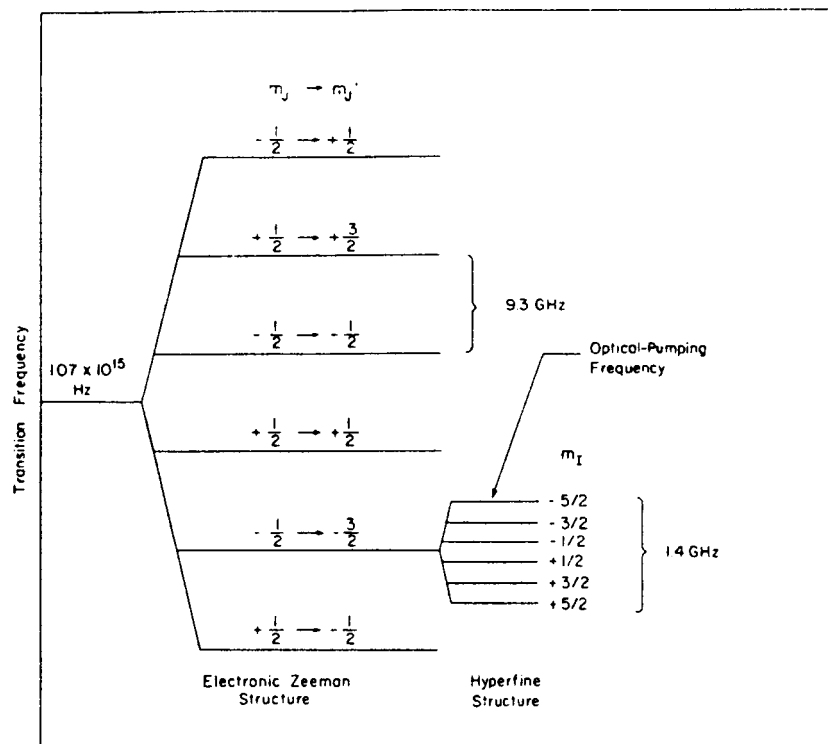


FIG. 2. Structure of the $^{25}\text{Mg}^+ 3s\ ^2S_{1/2}$ to $3p\ ^2P_{3/2}$ 279.6-nm line at a magnetic field $B_0 = 1$ T. The quantum numbers m_j and m_j' refer to the ground and excited states, respectively. The frequency splitting between adjacent electronic Zeeman components is approximately $\frac{2}{3}\mu_B B_0/h$. At high magnetic field, m_I is a good quantum number which is conserved in the optical transition process. Hence, each electronic Zeeman component splits into six hyperfine components corresponding to different values of m_I . This splitting is shown for the $(m_j \rightarrow m_j') = (-\frac{1}{2} \rightarrow -\frac{3}{2})$ component. The hyperfine splitting is drawn to a different scale than the electronic Zeeman splitting. The natural linewidth is 43 MHz, and the Doppler width is typically 100 MHz when the ions are cold. For most of the optical pumping experiments, the laser was tuned so that its second harmonic was about 30 to 50 MHz lower than the $(^2S_{1/2}, m_I = -\frac{5}{2}, m_j = -\frac{1}{2})$ to $(^2P_{3/2}, m_I = -\frac{5}{2}, m_j = -\frac{3}{2})$ transition, which is marked with an arrow.

$\frac{1}{2}$) to $(\frac{3}{2}, \frac{1}{2})$ and $(\frac{3}{2}, \frac{1}{2})$ to $(\frac{5}{2}, -\frac{1}{2})$ transitions were then detected by a decrease in fluorescence when rf was applied.

Other transitions were detected by more complex resonance schemes. The $(-\frac{5}{2}, \frac{1}{2})$ to $(-\frac{3}{2}, \frac{1}{2})$ transition was detected by a triple resonance method. The ions were optically pumped into the $(-\frac{5}{2}, -\frac{1}{2})$ state, the $(-\frac{5}{2}, -\frac{1}{2})$ to $(-\frac{5}{2}, \frac{1}{2})$ transition was saturated by frequency modulating the klystron through the resonance at a rate of about 10 Hz, and a decrease in fluorescence was observed as a frequency synthesizer was swept through the $(-\frac{5}{2}, \frac{1}{2})$ to $(-\frac{3}{2}, \frac{1}{2})$ resonance. The $(-\frac{3}{2}, \frac{1}{2})$ to $(-\frac{1}{2}, \frac{1}{2})$ transition was also detected by a quadruple resonance method. The ions were optically pumped into the $(-\frac{5}{2}, -\frac{1}{2})$ state and both the $(-\frac{5}{2}, -\frac{1}{2})$ to $(-\frac{5}{2}, \frac{1}{2})$ transition and the $(-\frac{5}{2}, \frac{1}{2})$ to $(-\frac{3}{2}, \frac{1}{2})$ transition were saturated. A decrease in fluorescence was observed as the frequency of another oscillator was swept through the $(-\frac{3}{2}, \frac{1}{2})$ to $(-\frac{1}{2}, \frac{1}{2})$ resonance. The reason for going to such lengths to observe this transition is that the first derivative

of its frequency with respect to magnetic field goes to zero at about 1.24 T, so that broadening and shifts of the resonance due to magnetic-field instability are essentially eliminated. The $(-\frac{5}{2}, \frac{1}{2})$ to $(-\frac{3}{2}, \frac{1}{2})$ transition frequency becomes field independent at about 1.9 T, which was higher than our electromagnet could reach. These methods could be extended to observe other transitions with further reduction in signal.

D. Resonance shifts and broadenings

The rf and microwave resonances can be broadened and shifted by magnetic-field fluctuations and drift and by interaction with the uv radiation and with additional rf fields. At $T = 20$ K, which was higher than was reached in any of the resonance experiments, the fractional frequency shift due to the second-order Doppler effect is -1.1×10^{-13} , which is negligible. Frequency shifts due to collisions with ions and neutral molecules were also negligible. At low temperatures, the repulsive

Coulomb force kept positive ions from approaching each other very closely. At a temperature T , the distance of closest approach R is given roughly by $k_B T = e^2/R$. For $T = 20$ K, $R = 8.4 \times 10^{-5}$ cm, so that spin exchange reactions between ions did not occur. The maximum electric field for this case is $e/R^2 = 21$ V/cm, and the rms field is much lower, so Stark shifts of the hyperfine structure are too small to be observable. Electrons and negative ions were expelled from the Penning trap because the potentials were set to trap positive ions. Collisions with background neutrals took place at a rate of less than about $(5 \text{ min})^{-1}$, which was determined from the ion temperature relaxation rate. Spin depolarization rates, which would increase the resonance linewidths, should be much lower.⁴ Fractional hyperfine density (pressure) shifts, estimated from the known shift for the $^{137}\text{Ba}^+$ ion,⁴ were less than 10^{-15} .

In general, the magnetic-field instability caused the greatest uncertainty in determining the resonance frequencies. The fractional fluctuations, measured with an NMR probe, were about 2×10^{-7} in 1 s and 10^{-6} in several seconds, with occasional sudden jumps of about 10^{-6} . The electronic spin-flip transition frequencies are essentially proportional to the magnetic field B_0 , so that typically, a 10^{-6} shift in B_0 causes a 30 kHz frequency shift at 30 GHz. The nuclear spin-flip transition frequencies have field sensitivities that vary with B_0 . A 10^{-6} shift in B_0 at $B_0 = 1.14$ T causes a 16-Hz shift of the $(-\frac{5}{2}, -\frac{1}{2})$ to $(-\frac{3}{2}, -\frac{1}{2})$ transition at 287.7 MHz and a 6-Hz shift of the $(-\frac{3}{2}, \frac{1}{2})$ to $(-\frac{1}{2}, \frac{1}{2})$ transition frequency at 286.7 MHz. For some experiments, the magnetic field was stabilized to an NMR probe. Because of the space limitations, the probe had to be located in a region where the field was not very homogeneous. This resulted in a fractional NMR linewidth of about 10^{-3} with a sample of diameter approximately 1 cm. The field fluctuations were at best about 1×10^{-6} over short time periods, as determined by the resonance linewidths. However, long-term drifts of about 10^{-5} , due primarily to changes with temperature of the tuned circuit in the NMR probe, were observed over periods of about 1 h. This field stabilization method was used to obtain the data reported previously.¹³ Another field stabilization method, based on sensing the electronic spin-flip transition of the ions, will be discussed later.

The light used for state preparation and detection causes resonances to be shifted and broadened.²⁴ These effects can be eliminated by shutting the light off while the transition is driven. When the light was chopped, the linewidth of the $(-\frac{5}{2}, -\frac{1}{2})$ to $(-\frac{3}{2}, \frac{1}{2})$ electronic spin-flip transition was observed to be as narrow as 15 kHz, which is con-

sistent with the measured short-term magnetic-field stability. The light was chopped on and off with a 50% duty cycle at a rate typically between 10 and 100 Hz. When the light was not chopped, linewidths as wide as 1.3 MHz were observed. The narrowing of the resonances when the light was chopped indicates that the transitions were driven primarily when the light was off.

The light-broadened line shape can be understood by applying the Bloch equations²⁵ to the effective two-level system consisting of the $(-\frac{5}{2}, -\frac{1}{2})$ and $(-\frac{3}{2}, \frac{1}{2})$ states. The ions spend very little time in any of the other ground-state or excited-state sublevels. In the absence of the microwave radiation, the state populations relax to their steady-state values with a time constant T_1 , which can be measured by first saturating the microwave transition, then suddenly shutting off the microwave power, and observing the fluorescence return to its normal level, as shown in Fig. 2 of Ref. 16. Typically, T_1 was about 1 s, which corresponds to an average light intensity of about 3.5 mW/cm². The transverse relaxation time T_2 was much shorter, since every optical scattering event destroyed the coherence of the effective two-level system. The resonance linewidth in the limit of zero microwave power is $1/(\pi T_2)$. This was observed to vary from about 40 kHz or less to 250 kHz, depending upon laser intensity and overlap of the light beam and ion cloud. For steady, uniform illumination $2/T_2 = \gamma_s$, where γ_s is the average scattering rate. If the overlap of the beam with the cloud is poor, then the light is effectively chopped on and off as the magnetron motion²³ takes the ions into and out of the beam. In this case, the effective scattering rate which determines T_2 saturates at about the magnetron frequency ν_m as the light intensity increases.

The resonance linewidths were observed to increase with microwave power in accordance with theory.²⁵ This increase gave an absolute calibration of the microwave magnetic field amplitude at the ions. Under typical operating conditions, this was about 2×10^{-8} T (0.2 mG). Similar light broadening effects were seen on the $(-\frac{5}{2}, -\frac{1}{2})$ to $(-\frac{3}{2}, -\frac{1}{2})$ nuclear spin-flip transition, but were not studied in detail. They were eliminated by chopping the light, so that linewidths of about 30 Hz were observed, due to magnetic-field fluctuations during the time required to sweep the resonance.

In most cases, light shifts²⁴ of resonances were difficult to observe because of field fluctuations and light broadening effects. However, in one case, a light shift was definitely observed. The $(-\frac{3}{2}, \frac{1}{2})$ to $(-\frac{1}{2}, \frac{1}{2})$ field insensitive transition at $B_0 = 1.24$ T was observed by the quadruple resonance

method described previously. This transition was driven with the light on and with it off. In both cases, the rf pulses at the $(-\frac{3}{2}, \frac{1}{2})$ to $(-\frac{1}{2}, \frac{1}{2})$ and the $(-\frac{1}{2}, \frac{1}{2})$ to $(-\frac{3}{2}, \frac{1}{2})$ transition frequencies were separated in time in order not to broaden the resonance. The resonance frequency was shifted down by about 3.5 Hz when the light was on relative to its value when the light was off. This shift implies an average light intensity of about 10 mW/cm², which is in reasonable agreement with the value inferred from T_1 .

Bloch-Siegert and other rf line-pulling effects²⁶ were negligible because of the low powers used. Line broadenings or shifts due to real or virtual transitions induced by the auxiliary rf fields in the triple and quadruple resonance methods can be eliminated by shutting them off while the main transition is driven.

E. Zeeman resonance magnetic-field stabilization

A system was developed which servoed the magnetic field by keeping the frequency of the $(-\frac{3}{2}, -\frac{1}{2})$ to $(-\frac{1}{2}, \frac{1}{2})$ electronic spin-flip transition resonant with a fixed microwave frequency. Other rf transition frequencies were measured while the field was thus stabilized. The field stabilization scheme worked as follows: The light was tuned close to resonance with the ($^2S_{1/2}$, $m_I = -\frac{3}{2}$, $m_J = -\frac{1}{2}$) to ($^2P_{3/2}$, $m_I = -\frac{3}{2}$, $m_J = -\frac{1}{2}$) transition frequency. A microwave frequency ν , with which to stabilize the electronic spin-flip transition, was chosen. The microwave radiation was shut off for 0.2 s, so that the rf transition could be driven without broadening from this source. The ions were subjected to microwave radiation of frequency $\nu + 10$ kHz for 0.8 s. Scattered photons were counted during this period and the number was stored. The microwave radiation was shut off for 0.2 s. It was turned on again for 0.8 s at frequency $\nu - 10$ kHz and the scattered photons were counted. This number was digitally subtracted from the one stored previously. If the result was positive, the field was too low, and vice versa. This number was sent to a digital-to-analog converter which was connected to an analog integrator. The output of the integrator controlled the magnet power supply and corrected the field. The cycle was then repeated. Either the $(-\frac{3}{2}, -\frac{1}{2})$ to $(-\frac{1}{2}, -\frac{1}{2})$ or the $(-\frac{1}{2}, \frac{1}{2})$ to $(-\frac{3}{2}, \frac{1}{2})$ nuclear spin-flip transitions could be detected by a decrease in the average photon scattering rate when rf at the resonance frequency was introduced. The light was chopped at about 8 Hz to reduce light broadenings and shifts of the resonances. A typical nuclear spin-flip resonance curve is shown in Fig. 3. Unfortunately, the field stability achieved with this

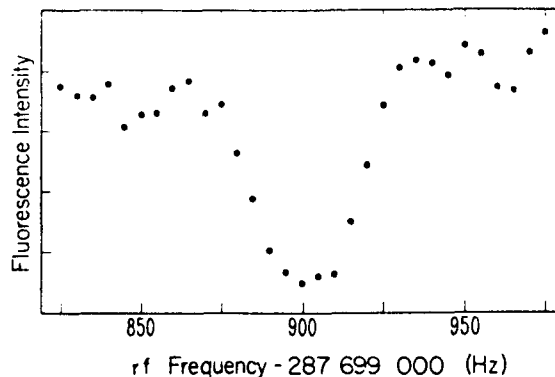


FIG. 3. rf resonance curve for the $(m_I, m_J) = (-\frac{5}{2}, -\frac{1}{2})$ to $(-\frac{3}{2}, -\frac{1}{2})$ hyperfine transition. The magnetic field B_0 was actively stabilized by keeping the $(-\frac{5}{2}, -\frac{1}{2})$ to $(-\frac{5}{2}, +\frac{1}{2})$ electronic spin-flip resonance centered at 33 466.187 MHz, which corresponds to $B_0 \cong 1.1405$ T. The 35-Hz linewidth is due primarily to the remaining short-term fractional fluctuations in B_0 of about 10^{-6} . Each point represents an integration time of 4 s.

system was limited by the low signal-to-noise ratio and the relatively poor short-term stability of the magnet. The fractional field fluctuations, estimated from the widths and reproducibility of the nuclear spin-flip resonances, were about 1×10^{-6} . These experiments were all carried out at $B_0 \cong 1.14$ T. This was experimentally convenient because the dye laser could be locked to a strong I_2 hyperfine feature.

F. Field independent transition

The first derivative with respect to the magnetic field of the $(-\frac{3}{2}, \frac{1}{2})$ to $(-\frac{1}{2}, \frac{1}{2})$ transition frequency goes to zero at a field of approximately 1.24 T. The fractional frequency shift $\delta\nu/\nu$ for a fractional field shift $\delta B/B$ from this field is $-0.012 (\delta B/B)^2$. This transition was detected by the quadruple resonance scheme outlined briefly in Sec. IIC. The $(-\frac{3}{2}, -\frac{1}{2})$ to $(-\frac{1}{2}, \frac{1}{2})$ electronic spin-flip frequency for this field could be predicted from previous data with an uncertainty of less than 10^{-5} . The microwave source was set to this frequency and the magnetic field adjusted until the decrease in fluorescence corresponding to the double resonance was observed. The field was left unstabilized, but was periodically reset by this method. The drift, after warmup, was on the order of $(1-2) \times 10^{-5}$ over 30 min, so it was not a serious problem. The microwave source was frequency swept at a rate of about 8 Hz by ± 750 kHz, so that the ions would still be in resonance during part of the sweep, even if the field drifted by $\pm 2 \times 10^{-5}$. This field shift corresponds to a frequency shift $\delta\nu$ of 1.4×10^{-3} Hz on the $(-\frac{1}{2}, \frac{1}{2})$ to $(-\frac{3}{2}, \frac{1}{2})$ transition. The necessary dye laser fre-

quency for this field was about 25 MHz away from the nearest hyperfine feature in I_2 . The laser frequency was stabilized to this feature by frequency shifting part of the beam by 25 MHz with an acousto-optic modulator and passing it through the I_2 cell.

The measurement sequence was as follows: The microwave source was left on continuously. We estimate that this caused an rf Stark shift of the $(-\frac{3}{2}, \frac{1}{2})$ to $(-\frac{1}{2}, \frac{1}{2})$ transition frequency of less than 10^{-4} Hz. The light was then blocked with an electromechanical shutter to eliminate light shifts and broadenings. An rf oscillator was switched on for a period of about 1 s to drive the $(-\frac{5}{2}, \frac{1}{2})$ to $(-\frac{3}{2}, \frac{1}{2})$ transition. The oscillator was frequency modulated by about 600 Hz at a rate of about 9 Hz to eliminate any sensitivity to field drifts. After this first rf oscillator was shut off, the $(-\frac{3}{2}, \frac{1}{2})$ to $(-\frac{1}{2}, \frac{1}{2})$ transition was then driven. Both the Rabi single-pulse method and the Ramsey two-pulse method were used.²⁷ For the Rabi method, the rf was switched on for a period t . For the Ramsey method, the rf was turned on for a period τ , off for a period T , and on again for a period τ . The two pulses were coherent in phase because the oscillator ran continuously during the period T , but was attenuated by 130 dB. At the end of this resonance period, the first rf oscillator was switched on for about 1 s to drive the $(-\frac{5}{2}, \frac{1}{2})$ to $(-\frac{3}{2}, \frac{1}{2})$ transition. The light was then unblocked and the scattered photons were counted. The initial fluorescence level was lower if ions had been driven to the $(-\frac{1}{2}, \frac{1}{2})$ level, than if they had not. The fluorescence level then rose to the previous steady-state value as the ions were optically pumped.¹⁷ The initial fluorescence level (first 2 to 4 s) was divided by the final level (next 4 to 10 s) in order to obtain a signal that was less sensitive to long-term laser intensity fluctuations. This cycle was repeated several times for each frequency setting of the $(-\frac{3}{2}, \frac{1}{2})$ to $(-\frac{1}{2}, \frac{1}{2})$ rf oscillator in order to improve the signal-to-noise ratio.

With the Rabi method, one obtains a linewidth (in Hz) of $(1.25t)^{-1}$ at optimum rf power. Linewidths as small as 40 mHz were observed with $t = 20$ s. With the Ramsey method with $\tau \ll T$ and optimum rf power, one obtains an oscillating line shape with a central minimum of width of $(2T)^{-1}$. The central minimum can be identified by the fact that it does not change for different T or by using the Rabi method, which yields only one deep minimum. Linewidths as small as 12 mHz were observed with $T = 41.4$ s. Since the frequency was about 292 MHz, this corresponds to a Q of 2.4×10^{10} . Typical curves are shown in Figs. 4 and 5. No evidence was seen for re-

laxations between ground-state sublevels, even for these long values of T . However, the initial scattering rate (and hence, the signal) became low for $T \geq 40$ s due to heating of the ions while the light was off, which increased the Doppler width.

III. RESULTS

The transition frequencies between (m_I, m_J) sublevels are given in closed form by the Breit-Rabi formula.²⁷ There are only three independent parameters in this formula: A , g_I/g_J , and $g_J \mu_B B_0/h$, where μ_B is the Bohr magnetron and B_0 is the magnetic field. Hence, it is sufficient to measure three different transition frequencies at the same magnetic field to determine all three parameters. In order to decorrelate the three parameters, it is helpful to measure one $\Delta m_I = 0$, $\Delta m_J = \pm 1$ transition frequency, which depends mostly on $g_J \mu_B B_0/h$, and two $\Delta m_I = \pm 1$, $\Delta m_J = 0$ transition frequencies, which depend primarily on A and secondarily on the other parameters. One of the two $\Delta m_I = \pm 1$, $\Delta m_J = 0$ transitions should have $m_J = -\frac{1}{2}$ and the other should have $m_J = \frac{1}{2}$ in order to decorrelate A and g_I/g_J . The absolute g factors can be determined if an independent measurement of magnetic field (actually

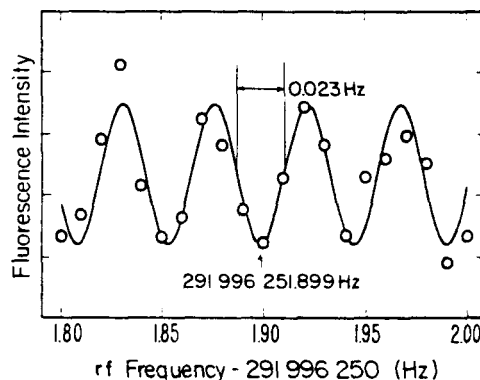


FIG. 4. rf resonance curve for the $(m_I, m_J) = (-\frac{3}{2}, \frac{1}{2})$ to $(-\frac{1}{2}, \frac{1}{2})$ hyperfine transition. Each circle represents the average of four measurements (total detection fluorescence integration time of 8 s). The solid curve is a theoretical fit. The quadruple resonance technique described in the text was used. The oscillatory line shape results from the use of the Ramsey method to drive the transition. Two coherent rf pulses of duration $\tau = 1.02$ s separated by $T = 20.72$ s were applied. The vertical arrow marks the central minimum, which corresponds to the resonance frequency. The magnetic field B_0 was set so that the $(-\frac{5}{2}, -\frac{1}{2})$ to $(-\frac{3}{2}, \frac{1}{2})$ electronic spin-flip resonance was in the range of $36\,248.374 \pm 0.750$ MHz, which corresponds to $B_0 \approx 1.2398$ T.

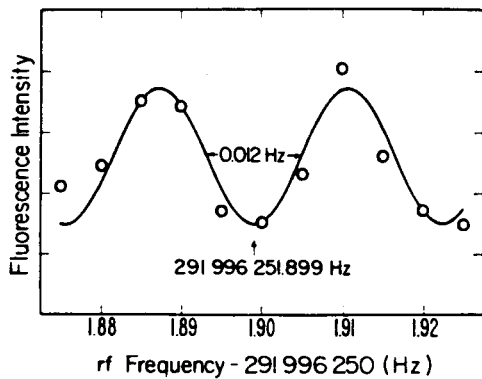


FIG. 5. rf resonance curve for the $(m_I, m_J) = (-\frac{3}{2}, \frac{1}{2})$ to $(-\frac{1}{2}, \frac{1}{2})$ hyperfine transition. Each circle represents the average of four measurements (total detection fluorescence integration time of 16 s). The pulse separation time T was 41.40 s. The experimental conditions were otherwise the same as for the curve shown in Fig. 4. The vertical arrow marks the central minimum.

$\mu_B B_0/h$ is made at the same time. However, this was not done.

At the time of our first experiments, the value of A was not very well known.^{5,16,28} The $^{25}\text{Mg}^+$ $(-\frac{5}{2}, -\frac{1}{2})$ to $(-\frac{3}{2}, \frac{1}{2})$ transition was found after searching a frequency range corresponding to A values from -628 to -595 MHz. The value of $g_J \mu_B B_0/h$ had been determined from the electronic spin-flip transition frequency of $^{24}\text{Mg}^+$, before loading $^{25}\text{Mg}^+$ into the trap. After allowing for drift of the magnetic field between measurements, A could be determined with a fractional uncertainty of 2×10^{-3} by taking g_I from previous NMR measurements and assuming g_J was equal to the free-electron g factor.

The positions of the other transitions could then be predicted and were observed by the methods described previously. Several transition frequencies were measured at each of several magnetic-field settings between 1.0 and 1.2 T, and were used to determine A and g_I/g_J .¹³

Our final determinations of A and g_I/g_J are based on a combination of the $(-\frac{5}{2}, -\frac{1}{2})$ to $(-\frac{3}{2}, -\frac{1}{2})$ transition frequency measured with the Zeeman resonance field stabilization scheme at magnetic field $B(1)$ and the $(-\frac{3}{2}, \frac{1}{2})$ to $(-\frac{1}{2}, \frac{1}{2})$ field-independent transition frequency at magnetic field $B(2)$. There are thus four parameters to be determined: A , g_I/g_J , $g_J \mu_B B(1)/h$, and $g_J \mu_B B(2)/h$. Four independent equations are provided by the Breit-Rabi formula expressions for the four frequencies $\nu(1)$ through $\nu(4)$. Here $\nu(1)$ and $\nu(2)$ are, respectively, the $(-\frac{5}{2}, -\frac{1}{2})$ to $(-\frac{3}{2}, -\frac{1}{2})$ and the $(-\frac{5}{2}, -\frac{1}{2})$ to $(-\frac{3}{2}, -\frac{1}{2})$ transition frequencies at $B(1)$ and $\nu(3)$ and $\nu(4)$ are, respectively, the $(-\frac{5}{2},$

$-\frac{1}{2})$ to $(-\frac{3}{2}, \frac{1}{2})$ and the $(-\frac{3}{2}, \frac{1}{2})$ to $(-\frac{1}{2}, \frac{1}{2})$ transition frequencies at $B(2)$. The experimental results (in MHz) are

$$\begin{aligned} \nu(1) &= 33\,466.187\,13, \\ \nu(2) &= 287.699\,897(48), \\ \nu(3) &= 36\,248.374, \\ \nu(4) &= 291.996\,251\,899(3). \end{aligned} \quad (1)$$

No uncertainty is shown for $\nu(1)$ or $\nu(3)$, since they were fixed experimentally. [Uncertainties in $\nu(1)$ or $\nu(3)$ due to magnetic-field fluctuations would show up as fluctuations in $\nu(2)$ or $\nu(4)$, respectively.] The uncertainty of $\nu(2)$ due to the lack of reproducibility of the line centers from run to run was only about 19 Hz. The uncertainty of $\nu(2)$ has been increased to reflect possible offsets of the field servo system due to light shifts of the electronic spin-flip transition frequency or to the magnetic-field inhomogeneity. These effects were reduced by chopping the light, but may not have been completely eliminated, because the microwave power and the light were not chopped alternately. Thus, the microwave resonance line shapes may have consisted of a broad, shifted component, due to transitions made while the light was on, and a narrow, unshifted component due to transitions made while the light was off. The microwave power was adjusted so that the linewidths were about 40 kHz, due largely, if not totally, to short-term field fluctuations. We estimate that the offset from the light-shifted component should have caused a fractional shift in the field of less than 10^{-6} , which would cause a shift in $\nu(2)$ of less than 16 Hz. The field inhomogeneity over a typical ion cloud diameter of about 150 μm is estimated to be less than 3×10^{-6} , and to a high degree the effect on the resonances is averaged away as the individual ions circulate through the volume. A direct light shift of the $\nu(2)$ resonance would be accompanied by a broadening of several kHz, which we did not observe. No uncertainty is shown for $\nu(3)$, which was swept by ± 750 kHz around this center value. The uncertainty shown for $\nu(4)$ reflects, in about equal parts, the statistical uncertainty of determining the line center and possible magnetic-field drift within the limits set by the frequency modulation of $\nu(3)$. The results of the fit are

$$\begin{aligned} A &= -596.254\,376(54) \text{ MHz}, \\ g_I/g_J &= 9.299\,484(75) \times 10^{-5}. \end{aligned} \quad (2)$$

These results are in agreement with, and about a factor of 4 more precise than our previously reported values. Essentially all of the uncertainty of the fit is due to the uncertainty of $\nu(2)$. Also

determined were $g_J \mu_B B(1)/h = 31\,962.151\,585$ MHz and $g_J \mu_B B(2)/h = 34\,745.375\,447$ MHz. The corresponding value of the magnetic field at the position of the ions in terms of its value at the position of the NMR probe was not known very precisely. Hence, we are only able to say that g_J is approximately equal to the g value of the free electron g_e , e.g., $g_J = 2.002(2)$.

We have estimated that all perturbations to A and g_I/g_J , such as pressure, Stark, and diamagnetic shifts are negligible compared to the stated uncertainties. If the diamagnetic shift of A has a coefficient comparable to the measured value for ^{85}Rb ,²⁹ then its contribution to $\nu(4)$ is around 0.3 Hz, which is much greater than the uncertainty of $\nu(4)$. However, this does not affect the determinations of A and g_I/g_J , since their uncertainties are dominated by the uncertainty of $\nu(2)$.

IV. DISCUSSION

The present result for A is generally in agreement with the previous less precise measurements. An observation of the $3s^2S_{1/2}$ to $3p^2P_{3/2}$ resonance line has been made by Crawford *et al.*, using an atomic beam source and Fabry-Perot etalons.²⁸ Their reported value for A is $-693(38)$ MHz, which differs from ours by 16%. The only other reported optical measurement of A is that of Drullinger *et al.*,¹⁶ using the method of laser fluorescence, stored ion spectroscopy. The isotope shifts and hyperfine structure of the ($3s^2S_{1/2}$, $m_J = -\frac{1}{2}$) to ($3p^2P_{3/2}$, $m_J = -\frac{3}{2}$) Zeeman component in a magnetic field of about 0.98 T were observed. The value obtained was $A = -608(50)$ MHz, in good agreement with the present result. Both of the optical determinations depend on assumptions about the isotope shift (the mass-shift formula is assumed) and on an estimate of the $^2P_{3/2}$ hyperfine structure. However, the uncertainties of these effects are small compared with the experimental precision. Weber and Grägel⁵ measured A by optical pumping in a buffer-gas cell. Their result, $A = -616(50)$ MHz, is in good agreement with the present result. Brom and Weltner⁹ have observed the electron spin resonance (ESR) spectrum of $^{25}\text{Mg}^+$ trapped in a solid argon matrix at 4 K. Their result was $A = -595.0(3)$ MHz, which indicates that A is reduced by 0.21(5)% under these conditions relative to its free-ion value (present determination). This is less than typical shifts for alkali atoms under similar conditions.¹⁰

Ab initio calculations of A in $^{25}\text{Mg}^+$ should be possible with about the same accuracy as for ^{23}Na ,³⁰ since the two systems are isoelectronic.

The only such calculation that has been carried out so far is by Lindgren,³¹ who obtains $A = -456$ MHz in the restricted Hartree-Fock approximation (-463 MHz with relativistic corrections) and $A = -545$ MHz when core polarization is included (-553 MHz with relativistic corrections). The remaining 7% difference between the relativistic calculation including core polarization and the experimental result is presumably due to pure correlation effects involving double excitations.

The semiempirical Fermi-Segrè formula^{19,32} predicts $A = -627.8$ MHz, which is 5% too high in magnitude. The NMR measurement of g_I ,²¹ uncorrected for diamagnetic effects, is used. Relativistic correction factors are left out. The derivative of the quantum defect with respect to quantum number which appears in this formula was evaluated from the extended Ritz formula given by Risberg.²⁰ If this term is left out, leaving the Goudsmit formula, the result ($A = -606.4$ MHz) is actually in better agreement with experiment.

Veseth has carried out a Hartree-Fock calculation of g_J of Mg^+ .³³ The values obtained for the individual correction terms, in the notation of Ref. 34, are $\delta_2 = -7.91 \times 10^{-5}$, $\delta_3 = 9.70 \times 10^{-5}$, and $\delta_4 = -7.66 \times 10^{-5}$. The final result is $g_J = 2.002\,260\,6$, with an estimated fractional uncertainty of 3×10^{-6} .

Hegstrom, using a simple hydrogenic approximation for the valence electron, obtains $g_I/g_e = (1-31) \times 10^{-6}$, or $g_J = 2.002\,257$.³⁵ The g_J value of $^{25}\text{Mg}^+$ trapped in a solid argon matrix at 4 K was reported by Brom and Weltner⁹ to be 2.006(4). The shift from the free-ion value is consistent with theory.

Our result for g_I/g_J can be combined with Veseth's calculated value of g_J to obtain g_I for the free $^{25}\text{Mg}^+$ ion. This can be combined with the NMR result for g_I of $^{25}\text{Mg}^{2+}$ ions in H_2O (Ref. 21) to obtain the shielding difference

$$\begin{aligned} \sigma^* &= 1 - g_I(\text{NMR})/g_I(\text{free ion}) \\ &= -9.9(9) \times 10^{-5}. \end{aligned}$$

The corresponding shielding differences for the alkali atoms (free atoms versus hydrated ions) have been measured.³⁶ They also are negative and increase monotonically in magnitude with atomic number Z . For ^{23}Na , $\sigma^* = -6.05(10) \times 10^{-5}$.

The absolute accuracy of our measurements could, of course, be substantially improved if the magnetic-field stability and homogeneity were improved. Accurate measurements of g_J could be made by comparing the electronic spin-flip frequency in the ion, $g_J \mu_B B_0/h$, to, for example, the cyclotron frequency of free electrons,³⁷ $2\mu_B B_0/h$.

h , in the same magnetic field.

These same experimental techniques could be extended to measure hyperfine constants and g factors of other ions,³⁸ such as $^9\text{Be}^+$. The high resolution with small perturbations which can be obtained may make it possible to study small effects not previously observed, such as the diamagnetic susceptibility of the nucleus,²⁹ or to realize new types of frequency standards.

ACKNOWLEDGMENTS

We wish to thank J. C. Bergquist and R. E. Drullinger for experimental assistance during the early part of the work. This work was supported in part by the Air Force Office of Scientific Research and the Office of Naval Research. One of us (W.M.I.) acknowledges the financial support of the NRC in the form of a Postdoctoral Research Associateship during this work.

- ¹For reviews, see E. Arimondo, M. Inguscio, and P. Violino, *Rev. Mod. Phys.* **49**, 31 (1977); G. H. Fuller, *J. Chem. Phys. Ref. Data* **5**, 835 (1976).
- ²For recent work on radioactive alkalis, including francium, see S. Liberman, J. Pinard, H. T. Duong, P. Juncar, P. Pillet, J.-L. Vialle, P. Jacquinet, F. Touchard, S. Büttgenbach, C. Thibault, M. de Saint-Simon, R. Klapisch, A. Pesnelle, and G. Huber, *Phys. Rev. A* **22**, 2732 (1980) and references therein.
- ³For examples of recent work and reviews, see M. Vajed-Samii, S. N. Ray, T. P. Das, and J. Andriessen, *Phys. Rev. A* **20**, 1787 (1979); S. Garpman, I. Lindgren, J. Lindgren, and J. Morrison, *Z. Phys. A* **276**, 176 (1976); I. Lindgren, *Phys. Scr.* **11**, 111 (1975).
- ⁴For a review, see E. W. Weber, *Phys. Rep.* **32**, 123 (1977).
- ⁵E. W. Weber and R. Grägel, private communication.
- ⁶F. G. Major and G. Werth, *Phys. Rev. Lett.* **30**, 1155 (1973); *Appl. Phys.* **15**, 201 (1978); M. D. McGuire, R. Petsch, and G. Werth, *Phys. Rev. A* **17**, 1999 (1978).
- ⁷R. Blatt and G. Werth, *Z. Phys. A* **299**, 93 (1981).
- ⁸J. M. Brom and W. Weltner, *J. Chem. Phys.* **58**, 5322 (1973).
- ⁹P. H. Kasai, *Phys. Rev. Lett.* **21**, 67 (1968).
- ¹⁰C. K. Jen, V. A. Bowers, E. L. Cochran, and S. N. Foner, *Phys. Rev.* **126**, 1749 (1962).
- ¹¹W. L. Randolph, J. Asher, J. W. Koen, P. Rowe, and E. Matthias, *Hyper. Interact.* **1**, 145 (1975).
- ¹²J. Hata and M. Sakai, *Phys. Lett.* **57A**, 419 (1976); S. N. Ray, J. E. Rodgers, and T. P. Das, *Phys. Rev. A* **13**, 1983 (1976); S. Ahmad, J. Andriessen, K. Raghunathan, and T. P. Das, *Bull. Am. Phys. Soc.* **26**, 481 (1981).
- ¹³W. M. Itano, D. J. Wineland, R. E. Drullinger, and J. C. Bergquist. Abstracts of the 7th International Conference on Atomic Physics, MIT, Cambridge, 1980 (unpublished), p. 238.
- ¹⁴W. Neuhauser, M. Hohenstatt, P. E. Toschek, and H. Dehmelt, *Phys. Rev. Lett.* **41**, 233 (1978); *Appl. Phys.* **17**, 123 (1978); *Phys. Rev. A* **22**, 1137 (1980).
- ¹⁵D. J. Wineland, R. E. Drullinger, and F. L. Walls, *Phys. Rev. Lett.* **40**, 1639 (1978).
- ¹⁶R. E. Drullinger, D. J. Wineland, and J. C. Bergquist, *Appl. Phys.* **22**, 365 (1980).
- ¹⁷D. J. Wineland, J. C. Bergquist, W. M. Itano, and R. E. Drullinger, *Opt. Lett.* **5**, 245 (1980).
- ¹⁸D. J. Wineland and W. M. Itano, *Phys. Lett.* **82A**, 75 (1981).
- ¹⁹H. Kopfermann, *Nuclear Moments* (Academic, New York, 1958).
- ²⁰P. Risberg, *Ark. Fys.* **9**, 483 (1955).
- ²¹O. Lutz, A. Schwenk, and A. Uhl, *Z. Naturforsch.* **30a**, 1122 (1975).
- ²²A. Lurio, *Phys. Rev.* **126**, 1768 (1962); J. Bauche, G. Couarraze, and J.-J. Labarthe, *Z. Phys.* **270**, 311 (1974).
- ²³H. Dehmelt, in *Advances in Atomic and Molecular Physics*, edited by D. R. Bates and I. Estermann (Academic, New York, 1967, 1969), Vols. 3 and 5.
- ²⁴W. Happer, *Rev. Mod. Phys.* **44**, 169 (1972).
- ²⁵A. Abragam, *The Principles of Nuclear Magnetism* (Oxford University Press, London, 1961).
- ²⁶M. Mizushima, *Phys. Rev.* **133**, A414 (1964).
- ²⁷N. F. Ramsey, *Molecular Beams* (Oxford University Press, London, 1956).
- ²⁸M. F. Crawford, F. M. Kelly, A. L. Schawlow, and W. M. Gray, *Phys. Rev.* **76**, 1527 (1949).
- ²⁹N. P. Economou, S. J. Lipson, and D. J. Larson, *Phys. Rev. Lett.* **38**, 1394 (1977).
- ³⁰T. Lee, N. C. Dutta, and T. P. Das, *Phys. Rev. A* **1**, 995 (1970).
- ³¹I. Lindgren, private communication.
- ³²L. L. Foldy, *Phys. Rev.* **111**, 1093 (1958).
- ³³L. Veseth, private communication.
- ³⁴L. Veseth, *Phys. Rev. A* **22**, 803 (1980).
- ³⁵R. Hegstrom, private communication.
- ³⁶A. Beckmann, K. D. Böklen, and D. Elke, *Z. Phys.* **270**, 173 (1974).
- ³⁷See for example, H. G. Dehmelt and F. L. Walls, *Phys. Rev. Lett.* **21**, 127 (1968); R. M. Jopson and D. J. Larson, *Bull. Am. Phys. Soc.* **25**, 1133 (1980).
- ³⁸W. M. Itano and D. J. Wineland, *Bull. Am. Phys. Soc.* **24**, 1185 (1979).

Laser cooling of ions stored in harmonic and Penning traps

Wayne M. Itano and D. J. Wineland

*Frequency and Time Standards Group, Time and Frequency Division, National Bureau of Standards,
Boulder, Colorado 80303*

(Received 17 August 1981)

Laser (light-pressure) cooling of two-level ions stored in a Penning trap is treated theoretically, in the limit that the frequencies of motion of the ions are much smaller than the natural linewidth of the optical transition. Rate equations for the mean-squared amplitudes of motion are derived from a semiclassical analysis, which is confirmed by quantum-mechanical perturbation theory. Simultaneous cooling of all three modes of motion is shown to require a spatially nonuniform laser-beam profile, unlike the case of the harmonic trap. Comparison is made with recent experiments. Also, the three-dimensional harmonic trap is treated by two simple methods. One is based on the energy rate equations and the other on Langevin-type equations. Identical results are obtained by the two methods for the steady-state energies. These results are compared with the works of others.

I. INTRODUCTION

Laser (light-pressure) cooling of atoms and atomic ions has been demonstrated in recent experiments which were stimulated by the original proposals for laser cooling of free atoms¹ and of ions bound in electromagnetic traps.² Cooling is of interest for high-resolution spectroscopy largely because all Doppler effects are fundamentally reduced. Cooling of Na atoms in an atomic beam has been reported by Balykin *et al.*³

Two types of electromagnetic traps⁴ have been used for the laser-cooling experiments on ions. Cooling of Ba⁺ ions stored in an rf quadrupole trap was demonstrated by a group at Heidelberg^{5,6} and of Mg⁺ ions stored in a Penning trap by a group at the National Bureau of Standards (NBS).⁷⁻⁹ The rf quadrupole trap uses an alternating inhomogeneous electric field, whose average effect is to create a three-dimensional harmonic potential well. The Penning trap uses a static uniform magnetic field. The ions undergo harmonic motion along the magnetic field and a superposition of circular motions in the plane perpendicular to the field.

Laser cooling of neutral atoms has been treated theoretically by several authors.^{1,10-17} Various proposals have been made for trapping neutral

atoms in potential wells created by nearly resonant optical fields,¹⁰⁻¹² by static electric fields,¹⁸ and by static magnetic fields,¹⁹ all of which include laser cooling. Previous theoretical treatments of laser cooling of trapped ions have been restricted to harmonic potential wells.^{6,16,20-23}

The purposes of this paper are twofold. First, we augment the work of Ref. 16 by explicitly including the effects of light and atomic polarization and of the angular distribution of scattered photons. Unpolarized atoms and isotropic scattering of reemitted photons were usually assumed in Ref. 16. Cooling limits are derived from energy rate equations and also from a simple force fluctuation model. These results are briefly compared with the work of others.

Second, we discuss laser cooling of ions stored in a Penning trap. The natural linewidth of the optical transition used for cooling is assumed to be much greater than any of the frequencies of motion of the trapped ions. This is the case which is most easily realized experimentally. Rate equations are obtained for the mean-squared values of the amplitudes of motion of the ion. Saturation effects are not included, so the results are valid only for low light intensity. Configurations of light beams which can cool all three modes of oscillation are described. For the Penning trap, un-

like the harmonic trap, this requires a spatially nonuniform laser beam profile. Some of the general methods were discussed in our previous paper,¹⁶ in which they were applied only to laser cooling of free and harmonically bound atoms. Some of the results of the calculations presented here have been quoted in a previous publication,⁹ in which the laser cooling of a single Mg^+ ion in a Penning trap was reported.

Laser cooling of an atom bound in a harmonic well is treated in Sec. II, in order to illustrate the basic ideas in some simple cases. A model of laser cooling of an ion in a Penning trap in which the motion of the ion is treated classically is given in Sec. III. These results are briefly compared with experiment. A quantum-mechanical treatment is given in Sec. IV. The results are discussed in Sec. V.

II. LASER COOLING IN A HARMONIC TRAP

A. Formulation of the problem

The problem to be considered here is the laser cooling of a two-level atom bound in a three-dimensional harmonic well. The term atom includes atomic ions. The ground electronic state $|g\rangle$ is assumed to be stable; the excited electronic state $|e\rangle$ is assumed to decay only to $|g\rangle$ by a one-photon electric-dipole transition at a rate γ . The energy difference between $|g\rangle$ and $|e\rangle$ is $\hbar\omega_0$.

Two-level atoms do not exist, but in practice they can be approximated. In zero external field, either the ground or excited states have some Zeeman degeneracy, since a ($J=0$)-to-($J'=0$) transition is forbidden for any one-photon process. (J and J' are the electronic angular momentum quantum numbers in the ground and excited states, respectively.) If a strong magnetic field is applied so that the Zeeman splitting of the optical transition is greater than either the Doppler or natural broadenings, then the laser can be tuned close to resonance with one Zeeman component. The corresponding magnetic sublevels of the ground and excited states will form a two-level system, provided that the excited-state sublevel cannot decay to any other ground-state sublevel. The simplest case involves $J=0$ and $J'=1$. More generally, if $J'=J+1$, then the $M=J$ ground-state sublevel and the $M'=J+1$ excited-state sublevel or the $M=-J$ ground-state sublevel and the $M'=-J-1$ excited-state sublevel will form two-

level systems.⁷ There are also possibilities when hyperfine structure is present. If the Zeeman splitting is not large compared to the Doppler broadening, it is still possible to form an effective two-level system, but only for certain polarizations and directions of propagation of the light. Systems which are not effectively two level, including those in which hyperfine and Zeeman structure must be taken into account, can be treated by straightforward extension of the two-level methods. For such cases, it may be necessary to introduce additional optical or rf frequencies to ensure that the atoms continue to interact with the laser beam or beams used for cooling. For the Ba^+ experiments,^{5,6} the magnetic field is zero and the $6s\ ^2S_{1/2} \rightarrow 6p\ ^2P_{1/2}$ transition is used ($J=J'=\frac{1}{2}$), so four levels are involved (for $I=0$ isotopes), aside from the metastable D states, but this case can be treated with only minor modifications to a two-level theory.²³

The harmonic potential causes the atom, which has mass M , to oscillate in the x , y , and z directions at angular frequencies Ω_x , Ω_y , and Ω_z . These frequencies are assumed to be much less than the natural linewidth γ , which is much less than the optical transition frequency ω_0 . This is the "weak binding" case of Ref. 16. This case is easily satisfied in practice, since, for a typical resonance line, $\gamma/2\pi \geq 20$ MHz, and for an rf quadrupole trap, $\Omega_i/2\pi \lesssim 2$ MHz ($i=x,y,z$).

The atom interacts with one or more monochromatic polarized laser beams. The electric field of such a beam is assumed to be given by a classical plane-wave solution:

$$\vec{E}(\vec{r}, t) = \hat{\epsilon} \text{Re} E_0 \exp(i\vec{k} \cdot \vec{r} - i\omega t), \quad (1)$$

where Re stands for the real part, $\hat{\epsilon}$ is a unit polarization vector perpendicular to \vec{k} , and $|\vec{k}| \equiv k = \omega/c$.

Consider a scattering event in which a free atom, moving with velocity \vec{v} , absorbs a photon of wave vector \vec{k} , emits a photon of wave vector \vec{k}_s , and has its velocity changed to \vec{v}' . From conservation of energy and momentum in the nonrelativistic ($v/c \ll 1$) limit,

$$\Delta\vec{v} \equiv \vec{v}' - \vec{v} = \hbar(\vec{k} - \vec{k}_s)/M, \quad (2)$$

$$\Delta E \equiv \frac{1}{2}M(v')^2 - \frac{1}{2}Mv^2 = \hbar^2(\vec{k} - \vec{k}_s)^2/2M + \hbar(\vec{k} - \vec{k}_s) \cdot \vec{v}, \quad (3)$$

$$\Delta E_i \equiv \frac{1}{2}M(v'_i)^2 - \frac{1}{2}Mv_i^2 = \hbar^2(k_i - k_{si})^2/2M + \hbar(k_i - k_{si})v_i \quad (i=x,y,z). \quad (4)$$

The subscripts i denote Cartesian components of vectors, except in ΔE_i , which is the kinetic energy due to motion in the i direction. These relations were derived for a free atom, but they also hold for the harmonically bound atom if the scattering takes place in a time much shorter than the period of oscillation, since the atom behaves as a free particle for such short times. Since resonance scattering takes place in a time roughly equal to γ^{-1} , this condition is equivalent to our weak binding assumption. The conservation laws which led to Eqs. (2)–(4) do not depend on the photon scattering being near a resonance. However, we wish to consider only the near-resonance case, where ω is within roughly the combined Doppler and natural broadening of the optical transition frequency. Since it was assumed that $v/c \ll 1$ and that $\gamma \ll \omega_0$, this implies that $k \cong \omega_0/c \cong k_0$. We will also assume that $R \ll \hbar\gamma$, where $R \equiv (\hbar k)^2/2M \cong (\hbar k_0)^2/2M$. This is easily satisfied for an allowed optical electric-dipole transition. For example, for the $6s\ ^2S_{1/2} \rightarrow 6p\ ^2P_{1/2}$ 493-nm resonance line in $^{138}\text{Ba}^+$, $R = h \times 5.9$ kHz, $\gamma = 2\pi \times 21$ MHz,²⁴ and $R/\hbar\gamma = 2.8 \times 10^{-4}$. For the $3s\ ^2S_{1/2} \rightarrow 3p\ ^2P_{3/2}$ 280-nm resonance line in $^{24}\text{Mg}^+$, $R = h \times 106$ kHz, $\gamma = 2\pi \times 43$ MHz,²⁵ and $R/\hbar\gamma = 2.5 \times 10^{-3}$. Since the fractional change in k , $|k - k_s|/k$, is at most about $2v/c + 2\hbar k/Mc$, we can also assume $k \cong k_s$. Equation (4) can be rewritten as

$$\Delta E_i = R(\hat{k}_i^2 - 2\hat{k}_i\hat{k}_{si} + \hat{k}_{si}^2) + \hbar(k_i - k_{si})v_i, \quad (5)$$

where \hat{k}_i and \hat{k}_{si} are the i components of the unit vectors $\hat{k} = \vec{k}/k$ and $\hat{k}_s = \vec{k}_s/k_s$.

The angular distribution of the scattered photons depends only on the orientation of the electric-dipole moment of the transition $\vec{d}_{ge} \equiv \langle g | \vec{d} | e \rangle$. We note here that the ground and excited states we consider are single M states and that an effective two-level system has been created by, for example, applying a magnetic field large enough to resolve the Zeeman structure. The probability that a photon is emitted into a solid angle $d\Omega$ in the \hat{k}_s direction is

$$P_s(\hat{k}_s)d\Omega = (3/8\pi) \sum_j |\hat{d}_{ge} \cdot \hat{\epsilon}_j(\hat{k}_s)^*|^2 d\Omega, \quad (6)$$

where

$$\hat{d}_{ge} = \vec{d}_{ge} / |\vec{d}_{ge}|,$$

and the summation is over the two unit polarization vectors for propagation in the \hat{k}_s direction. These vectors must satisfy

$$\hat{\epsilon}_k(\hat{k}_s)^* \cdot \hat{\epsilon}_j(\hat{k}_s) = \delta_{kj}, \quad (7)$$

$$\hat{\epsilon}_k(\hat{k}_s) \cdot \hat{k}_s = 0,$$

where δ_{ij} is the Kronecker delta, but are otherwise arbitrary. The normalization is such that $\int P_s(\hat{k}_s)d\Omega = 1$. Equation (6) applies to a non-moving atom, but it is approximately true for a moving atom, provided $v/c \ll 1$, which has been assumed. This treatment could be generalized to include other types of multipole radiation, such as magnetic dipole or electric quadrupole. The decay rates for such transitions are usually so slow ($\leq 10^3$ s⁻¹) that it becomes difficult to satisfy the weak binding condition, so they are not treated here. Equation (6) can be evaluated if $|g\rangle$ and $|e\rangle$ are eigenstates of the component of the total angular momentum along a quantization axis defined, for example, by a magnetic field. For a $\Delta M = 0$ transition (M is the eigenvalue of the total angular momentum in the \hat{B} direction) we have

$$P_s(\hat{k}_s) = (3/8\pi) \sin^2\theta_s. \quad (8a)$$

For a $\Delta M = \pm 1$ transition

$$P_s(\hat{k}_s) = (3/16\pi)(1 + \cos^2\theta_s). \quad (8b)$$

Here θ_s is defined by $\hat{B} \cdot \hat{k}_s = \cos\theta_s$. The isotropic distribution, which has been used in much of the previous work,^{12,15,16} corresponds to letting $P_s = 1/4\pi$. This is not of the form of Eq. (6). Given P_s , we can average Eq. (5) over all angles of the scattered photon

$$\langle \Delta E_i \rangle_s = \int P_s(\hat{k}_s) \Delta E_i d\Omega = R(f_i + f_{si}) + \hbar k_i v_i, \quad (9)$$

where

$$f_i \equiv \hat{k}_i^2 \quad (10a)$$

and

$$f_{si} \equiv \int P_s(\hat{k}_s) \hat{k}_{si}^2 d\Omega. \quad (10b)$$

The terms linear in \hat{k}_{si} drop out because $P_s(\hat{k}_s) = P_s(-\hat{k}_s)$ for any P_s of the form of Eq. (6) or for the isotropic distribution. The total energy change per scattering event, averaged over all angles of the scattered photon, is

$$\begin{aligned} \langle \Delta E \rangle_s &= \langle \Delta E_x \rangle_s + \langle \Delta E_y \rangle_s + \langle \Delta E_z \rangle_s \\ &= 2R + \hbar \vec{k} \cdot \vec{v}. \end{aligned} \quad (11)$$

This is the same as Eq. (3) of Ref. 16.

The average rate of energy change is obtained by multiplying the scattering rate by the average energy change per scattering event. The scattering rate γ_s is equal to the product of the number of photons per unit area per unit time $I/\hbar\omega$ and the absorption cross section for photons of that particular polarization and propagation direction ($I = c |E_0|^2/8\pi$). For a particular atomic velocity \vec{v} , the cross section can be obtained from perturbation theory,¹⁶ provided the intensity is below saturation. This is proportional to the Doppler-shifted natural line shape

$$\sigma(\omega, \vec{v}) = \sigma_0(\gamma/2)^2 / [(\omega_0 + \vec{k} \cdot \vec{v} + R/\hbar - \omega)^2 + (\gamma/2)^2], \quad (12)$$

where

$$\sigma_0 = 6\pi\lambda_0^2 |\hat{\epsilon} \cdot \hat{d}_{eg}|^2, \quad \lambda_0 \equiv c/\omega_0. \quad (13)$$

This is Eq. (24) of Ref. 16. Terms of order $(v/c)^2$ and $(v/c)(R/\hbar\omega)$ are neglected (see Secs. IV A and IV B of Ref. 16). If we take $|\hat{\epsilon} \cdot \hat{d}_{eg}|^2 = \frac{1}{3}$, which is the average over all polarizations $\hat{\epsilon}$, then $\sigma_0 = 2\pi\lambda_0^2$. As a more realistic example, for the $3p^2P_{3/2} (M_J = \pm \frac{3}{2}) \leftarrow 3s^2S_{1/2} (M_J = \pm \frac{1}{2})$ transitions in $^{24}\text{Mg}^+$ excited by light polarized perpendicular to the magnetic field, $\sigma_0 = 3\pi\lambda_0^2$. (Note that the expression given in Ref. 7 is too small by a factor of 2.) The rate equations for the energies in the x , y , and z vibrational modes, which in the absence of collisions are separately conserved, are

$$\frac{dE_i}{dt} + (I/\hbar\omega) \langle \sigma(\omega, \vec{v}) [\hbar k_i v_i + R(f_i + f_{si})] \rangle_v \quad (i = x, y, z). \quad (14)$$

Here the velocity average $\langle g(\vec{v}) \rangle_v$ of an arbitrary function $g(\vec{v})$ is defined in terms of the velocity probability function $P(\vec{v})$ as $\langle g(\vec{v}) \rangle_v \equiv \int P(\vec{v}) \times g(\vec{v}) d^3\vec{v}$. If a form for $P(\vec{v})$ as a function of $\{E_i\}$ is assumed, then Eq. (14) can be solved to obtain $\{E_i\}$ as a function of time. This might, for example, be a product of Maxwell-Boltzmann distributions for motion in the x , y , and z directions, characterized by three temperatures, which need not be equal,^{16,23} unless there is rapid energy transfer between modes by collisions between bound atoms. A special case of Eq. (14), with additional collisional relaxation terms, was discussed in Sec. V F of Ref. 16. If more than one laser beam is present, this can be taken into account by adding additional terms of the same form, with different $\hat{\epsilon}$, E_0 , \vec{k} , and ω , to the right-hand side of Eq. (14). Equation (14) holds for a single atom or for the ensemble average of a cloud of noninteracting atoms. If collisions between atoms are important, they can be taken into account by introducing phenomenological relaxation constants which tend to equalize the energies in the different modes.¹⁶ If the evolution of the entire velocity distribution, and not of just the average kinetic energy, is of interest, methods based on the Fokker-Planck or another kinetic equation can be used.^{13-15, 20-23, 26}

B. Cooling limits derived from energy rate equations

1. One laser beam along x axis

Consider a single laser beam propagating along the x axis ($\vec{k} = k\hat{x}$). Equation (14) becomes

$$\frac{dE_x}{dt} = (I/\hbar\omega) \langle \sigma(\omega, \vec{v}) [\hbar k v_x + R(1 + f_{xx})] \rangle_v, \quad (15a)$$

$$\frac{dE_y}{dt} = (I/\hbar\omega) \langle \sigma(\omega, \vec{v}) \rangle_v R f_{yy}, \quad (15b)$$

$$\frac{dE_z}{dt} = (I/\hbar\omega) \langle \sigma(\omega, \vec{v}) \rangle_v R f_{zz}. \quad (15c)$$

For negative laser detuning ($\omega < \omega_0 + R/\hbar \equiv \omega_0$), $\sigma(\omega, \vec{v})$ is larger for negative v_x than for positive v_x so that the right-hand side of Eq. (15a) is negative, until very low temperatures are reached. This is the basic principle of laser cooling. If considerable cooling has already taken place, so that the Doppler broadening is much less than the natural linewidth or the detuning, i.e., $k(v_x)_{\text{rms}} \ll \gamma/2$ or $k(v_x)_{\text{rms}} \ll (\omega_0 + R/\hbar - \omega)$, then Eq. (12) for the cross section can be approximated by

$$\sigma(\omega, \vec{v}) \approx \sigma_0(\gamma/2)^2 [(\gamma/2)^2 + (\omega_0 - \omega)^2]^{-1} \{1 - 2(\omega_0 - \omega)\vec{k} \cdot \vec{v} / [(\gamma/2)^2 + (\omega_0 - \omega)^2]\}. \quad (16)$$

R has been dropped, because it is assumed that $R/\hbar \ll (\omega_0 - \omega)$. Note that

$$\langle \sigma(\omega, \vec{v}) \rangle_v \cong \sigma_0 (\gamma/2)^2 [(\gamma/2)^2 + (\omega_0 - \omega)^2]^{-1}, \quad (17)$$

provided $P(\vec{v}) = P(-\vec{v})$, which we assume to be true. Let γ_s be the average scattering rate:

$$\gamma_s \equiv (I/\hbar\omega) \langle \sigma(\omega, \vec{v}) \rangle_v. \quad (18)$$

Equations (15a)–(15c) now become

$$\frac{dE_x}{dt} = \gamma_s \{ -2(\omega_0 - \omega) \hbar k^2 \langle v_x^2 \rangle_v / [(\gamma/2)^2 + (\omega_0 - \omega)^2] + R(1 + f_{sx}) \}, \quad (19a)$$

$$\frac{dE_y}{dt} = \gamma_s R f_{sy}, \quad (19b)$$

$$\frac{dE_z}{dt} = \gamma_s R f_{sz}. \quad (19c)$$

The motion in the y and z directions is heated by recoil and does not reach a steady state.¹⁶ The kinetic energy in the x direction reaches a steady-state value when the right-hand side of Eq. (19a) is zero:

$$\begin{aligned} E_{Kx} &\equiv \frac{1}{2} M \langle v_x^2 \rangle_v \\ &= \hbar(1 + f_{sx}) [(\gamma/2)^2 + (\omega_0 - \omega)^2] / 8(\omega_0 - \omega). \end{aligned} \quad (20)$$

The minimum value is obtained by setting $(\omega_0 - \omega) = \gamma/2$:

$$E_{Kx} = (1 + f_{sx}) \hbar \gamma / 8. \quad (21)$$

For isotropic scattering, $f_{sx} = \frac{1}{3}$, so the minimum $E_{Kx} = \hbar \gamma / 6$. This agrees with the result of Javanainen and Stenholm,²⁰ in the unsaturated limit. They treated this situation by using a Fokker-Planck equation. If the atomic electric-dipole moment is oriented along a quantization axis perpendicular to the x axis, corresponding to a $\Delta M = 0$ transition, then from Eqs. (8a) and (10),

$$f_{sx} = (3/8\pi) \int_{-1}^1 \int_0^{2\pi} \sin^2 \theta (\sin \theta \cos \phi)^2 d\phi d \cos \theta = \frac{2}{5}, \quad (22)$$

where θ and ϕ are spherical polar angles, so the minimum $E_{Kx} = 7\hbar\gamma/40$. This is in agreement with the results obtained by Cook,¹⁴ who used a Fokker-Planck equation, for the one-dimensional cooling of an unbound atom in a weak standing wave, when the dipole is perpendicular to the light propagation direction. This is essentially the same problem that we have treated here. For an unbound atom, a standing wave is required in order that the average radiation pressure force be zero, so that is not accelerated continuously in one direction. Cooling from a single running wave can occur for the harmonically bound atom, since a steady force only shifts the equilibrium point in the potential well. The harmonic restoring force was required in order to ensure that $P(\vec{v}) = P(-\vec{v})$, which led to the cancellation of a term in deriving Eq. (16) from Eq. (14). The method we have used here and in Ref. 16, which is

based on calculating the average energy imparted to the atom in the photon scattering process, takes into account heating due to both induced fluctuations (recoil on absorption) and spontaneous fluctuations (recoil on emission), at least in the low-intensity limit. These two sources of fluctuations were introduced separately in Ref. 14. In our treatment, the induced fluctuations are associated with the term proportional to f_i and the spontaneous fluctuations with the term proportional to f_{si} in Eq. (14).

The treatment of the atomic motion has been essentially classical. This should be valid in the limit of large harmonic oscillator quantum numbers. The mean occupation number for motion in the x direction is $\langle n_x \rangle \cong 2E_{Kx}/\hbar\Omega_x \geq \gamma/3\Omega_x$, so in the weak binding approximation the motion remains in the classical regime.

2. Laser beams along x , y , and z axes

In Sec. II B 1 it was shown that a single laser beam parallel to one of the principal axes of the harmonic potential cools motion parallel to the beam but heats the perpendicular motion by recoil. One simple configuration which is capable of cooling all modes of oscillation consists of three laser beams, one along each of the x , y , and z axes. Denote the laser frequencies by ω_i ($i=x,y,z$) and assume that all are tuned below resonance ($\omega_i < \omega_0$). Then the atoms are cooled, and, assuming that the Doppler widths are small compared with either the natural linewidth or the detunings, [$k_i(v_i)_{\text{rms}} \ll \gamma/2$ or $k_i(v_i)_{\text{rms}} \ll (\omega_0 - \omega_i)$, where $k_i \equiv \omega_i/c$],

$$\frac{dE_i}{dt} = -2\gamma_{si}(\omega_0 - \omega_i)\hbar k_i^2 \langle v_i^2 \rangle_v / [(\gamma/2)^2 + (\omega_0 - \omega_i)^2] + R[\gamma_{si} + (\gamma_s)_{\text{tot}} f_{si}], \quad (23)$$

where γ_{si} is the average scattering rate due to the laser beam along the i axis and $(\gamma_s)_{\text{tot}} = \gamma_{sx} + \gamma_{sy} + \gamma_{sz}$. In the steady state,

$$\begin{aligned} E_{Ki} &\equiv \frac{1}{2} M \langle v_i^2 \rangle_v \\ &= \hbar [1 + f_{si}(\gamma_s)_{\text{tot}}/\gamma_{si}] [(\gamma/2)^2 + (\omega_0 - \omega_i)^2] / 8(\omega_0 - \omega_i). \end{aligned} \quad (24)$$

This is minimized, [for constant $(\gamma_s)_{\text{tot}}/\gamma_{si}$], by setting $(\omega_0 - \omega_i) = \gamma/2$:

$$E_{Ki} = [1 + f_{si}(\gamma_s)_{\text{tot}}/\gamma_{si}] \hbar \gamma / 8. \quad (25)$$

The total mean kinetic energy can be minimized by adjusting the relative laser powers so that

$$(\gamma_{si})/(\gamma_s)_{\text{tot}} = (f_{si})^{1/2} / [(f_{sx})^{1/2} + (f_{sy})^{1/2} + (f_{sz})^{1/2}]. \quad (26)$$

For the isotropic case, the minimum kinetic energy in each mode is $\hbar\gamma/4$, which agrees with Ref. 16 (Sec. VE 2).

3. One laser beam at oblique angle to axes

Another method of cooling all three modes of oscillation is with a single laser beam which is not parallel to any of the principal axes. Equation (14) can be used to obtain the cooling rate. As has been pointed out previously, it is necessary that all of the motional frequencies (Ω_x , Ω_y , and Ω_z) be different.^{6,16,23} Otherwise there is at least one mode of oscillation perpendicular to the laser beam which is not cooled, but rather is heated by recoil, like the y and z modes discussed in Sec. II B 1. In the low Doppler limit [$(\vec{k} \cdot \vec{v})_{\text{rms}} \ll \gamma/2$ or $(\vec{k} \cdot \vec{v})_{\text{rms}} \ll (\omega_0 - \omega)$],

$$\frac{dE_i}{dt} = \gamma_s \{ -2(\omega_0 - \omega)\hbar k^2 f_i \langle v_i^2 \rangle_v / [(\gamma/2)^2 + (\omega_0 - \omega)^2] + R(f_i + f_{si}) \}, \quad (27)$$

where we have assumed that $\langle v_i v_j \rangle_v = 0$ if $i \neq j$. This should be valid if the frequencies are sufficiently different and the intensity is sufficiently low. In the steady state,

$$E_{Ki} = \hbar(1 + f_{si}/f_i) [(\gamma/2)^2 + (\omega_0 - \omega)^2] / 8(\omega_0 - \omega), \quad (28)$$

and this is minimized by setting $(\omega_0 - \omega) = \gamma/2$. Then

$$E_{Ki} = (1 + f_{si}/f_i) \hbar \gamma / 8. \quad (29)$$

If one has control over the direction of the beam, then the total average kinetic energy can be minimized if

$$f_i = (f_{si})^{1/2} / [(f_{sx})^{1/2} + (f_{sy})^{1/2} + (f_{sz})^{1/2}]. \quad (30)$$

For an isotropic angular distribution, this can be

accomplished by pointing the laser along the $\hat{x} + \hat{y} + \hat{z}$ direction, in which case, $E_{Ki} = \hbar\gamma/4$. This is close to the configuration used by Neuhauser *et al.*⁶ Equation (29) is equivalent to the low-intensity limit of Eq. (31) of Javanainen.²³

C. Cooling limit derived from force fluctuations

The steady-state cooling limits derived in Sec. II B can also be obtained from a simple classical

model, in which the effect of the scattered photons on the atomic motion is divided into an average damping force and a random, fluctuating force. The advantage of this approach is its great simplicity; it uses concepts which are familiar from the theory of noise in electronic circuits.

The one-dimensional cooling case, which was solved by the energy rate equation method in Sec. II B 1, will be treated, in order to demonstrate the basic method in the simplest case. The method can also be applied to the other cases treated in Sec. II B.

The equation of motion (Newton's second law) for the x coordinate of the atom is

$$M\ddot{x} + M\Omega_x^2 x = F_x(t), \quad (31)$$

where $F_x(t)$ is the x component of the force on the atom due to photon scattering. Each scattering event imparts a momentum impulse $\hbar(\vec{k} - \vec{k}_s)$ in a time less than about γ^{-1} , which we have assumed to be very short compared to the period of oscillation. Therefore we can represent $F_x(t)$ by a sum of Dirac delta functions:

$$F_x(t) = \sum_l \delta(t - t_l) \hbar[k - k_{sx}(l)], \quad (32)$$

where $k_{sx}(l)$ is the value of k_{sx} for the l th scattering. The scattering events take place at random times at an average rate $I\sigma(\omega, \vec{v})/\hbar\omega$. The time-averaged force on an atom of velocity \vec{v} is

$$\langle F_x \rangle = (I/\hbar\omega)\sigma(\omega, \vec{v})\hbar k, \quad (33)$$

since the $k_{sx}(l)$ terms average to zero. In the low Doppler limit,

$$\begin{aligned} \langle F_x \rangle &= \gamma_s \{1 - 2(\omega_0 - \omega)k\dot{x} / [(\gamma/2)^2 + (\omega_0 - \omega)^2]\} \hbar k \\ &\equiv \gamma_s \hbar k - M\Gamma\dot{x}. \end{aligned} \quad (34)$$

The equation of motion can now be written as

$$M\ddot{X} + M\Gamma\dot{X} + M\Omega_x^2 X = F'(t) \equiv F_x(t) - \langle F_x \rangle, \quad (35)$$

which describes a damped harmonic oscillator driven by a random force $F'(t)$. We have eliminated the constant force $\gamma_s \hbar k$ by shifting the origin, so that $X(\text{new}) = x(\text{old}) - \gamma_s \hbar k / M\Omega_x^2$. This equation has the same form as the one which describes the response of a series RCL (resistance-capacitance-inductance) circuit to a fluctuating emf.

The fluctuations in X can be calculated by standard methods.²⁷ Let $G(f)$ be the complex gain function which describes the steady-state response X to a sinusoidal F' with frequency f , and which is

defined by

$$X(f)\exp(2\pi ift) = G(f)F'(f)\exp(2\pi ift). \quad (36)$$

Here the physical quantities $X(t)$ and $F'(t)$ are given by the real parts of $X(f)\exp(2\pi ift)$ and $F'(f)\exp(2\pi ift)$, respectively. Let $w(f)$ be the one-sided power spectral density of $F'(t)$, defined by

$$w(f) = 4 \int_0^\infty \langle F'(t)F'(t+\tau) \rangle \cos 2\pi f\tau d\tau.$$

Then the mean-squared value of X is

$$\langle X^2 \rangle = \int_0^\infty |G(f)|^2 w(f) df. \quad (37)$$

For the system described by Eq. (35),

$$G(f) = 1/M[\Omega_x^2 - (2\pi f)^2 + i2\pi\Gamma f]. \quad (38)$$

The spectral density function can be calculated by following the standard derivation for the power spectrum of shot noise.²⁸ The only difference is that the impulses vary in size because of the random direction of the emitted photon. A derivation is given in the Appendix. We have

$$\begin{aligned} w(f) &= 2\gamma_s \hbar^2 \langle (k - k_{sx})^2 \rangle_s \\ &= 2\gamma_s \hbar^2 (k^2 + \langle k_{sx}^2 \rangle_s) \\ &= 4M\gamma_s R (1 + f_{sx}), \end{aligned} \quad (39)$$

which is valid for frequencies f less than about $\gamma/2\pi$. The fact that Eq. (39) is plausible can be seen by examining the more familiar expression for the spectral density of current for shot noise, $w_I(f) = 2eI = 2e^2 N$, where I is the average current, and N is the average number of electrons per second passing through a temperature limited diode. Substituting the rms change in momentum for e and the average scattering rate for N , we arrive at Eq. (39).

The term $|G(f)|^2$ in the integrand in Eq. (37) is sharply peaked around $f = \Omega_x/2\pi$, where $w(f)$ is nearly constant, so

$$\begin{aligned} \langle X^2 \rangle &\equiv w(\Omega_x/2\pi) \int_0^\infty |G(f)|^2 df \\ &= \frac{4\gamma_s R}{M} (1 + f_{sx}) \int_0^\infty \frac{df}{[\Omega_x^2 - (2\pi f)^2]^2 + (2\pi\Gamma f)^2} \\ &= \gamma_s R (1 + f_{sx}) / M\Gamma\Omega_x^2. \end{aligned} \quad (40)$$

The average kinetic energy is

$$\begin{aligned} E_{Kx} &= \frac{1}{2} M \langle v^2 \rangle = \frac{1}{2} M \Omega_x^2 \langle X^2 \rangle = \frac{1}{2} \gamma_s R (1 + f_{sx}) / \Gamma \\ &= \hbar (1 + f_{sx}) [(\gamma/2)^2 + (\omega_0 - \omega)^2] / 8(\omega_0 - \omega). \end{aligned} \quad (41)$$

In the last step Eq. (34) was used to express Γ in terms of other parameters. This is the same result obtained previously from the energy rate equation [see Eq. (20)], and the minimum energy is obtained when $(\omega_0 - \omega) = \gamma/2$ [see Eq. (21)]. Equation (35) is the Langevin equation, with the addition of the harmonic restoring force. Therefore the theory developed for the solution of the Langevin equation could be applied to the present problem.^{12,26}

III. LASER COOLING IN A PENNING TRAP (SEMICLASSICAL TREATMENT)

A. Classical motion of an ion in a Penning trap

The classical motion of a single ion in a Penning trap has been treated previously.^{4,29} Here we summarize the important results.

The idealized Penning trap consists of a uniform magnetic field $\vec{B} = B_0 \hat{z}$ along the z axis and a quadrupole electrostatic potential of the form

$$V(x, y, z) = A_0(2z^2 - x^2 - y^2). \quad (42)$$

Consider an ion of mass M and charge q . The equation of motion for the ion position \vec{r} is

$$M\dot{\vec{v}} = -q\vec{\nabla}V(\vec{r}) + (q/c)\vec{v} \times \vec{B} \quad (\vec{v} \equiv \dot{\vec{r}}) \quad (43)$$

and the equations for the Cartesian components (x, y, z) of \vec{r} are

$$\dot{v}_x = (2qA_0/M)x + (qB_0/Mc)v_y, \quad (44a)$$

$$\dot{v}_y = (2qA_0/M)y - (qB_0/Mc)v_x, \quad (44b)$$

$$\dot{v}_z = -(4qA_0/M)z. \quad (44c)$$

The general solutions to these equations are

$$x(t) = r_m \cos(\omega_m t + \theta_m) + r_c \cos(\omega'_c t + \theta_c), \quad (45a)$$

$$y(t) = -r_m \sin(\omega_m t + \theta_m) - r_c \sin(\omega'_c t + \theta_c), \quad (45b)$$

$$z(t) = r_z \cos(\omega_z t + \theta_z). \quad (45c)$$

We can also write the expressions for x and y in the complex form²⁹

$$x(t) + iy(t) = r_m \exp[-i(\omega_m t + \theta_m)] + r_c [-i(\omega'_c t + \theta_c)]. \quad (45d)$$

We have assumed that q , A_0 , and B_0 are all positive. The amplitudes (r_m, r_c, r_z) , defined to be greater than or equal to zero, and the phases $(\theta_m, \theta_c, \theta_z)$ are determined by the initial conditions. The frequencies are the magnetron frequency ω_m , the modified cyclotron frequency ω'_c , and the axial frequency ω_z , where

$$\omega_z = (4qA_0/M)^{1/2}, \quad (46a)$$

$$\omega_m = \omega_c/2 - (\omega_c^2/4 - \omega_z^2/2)^{1/2}, \quad (46b)$$

$$\omega'_c = \omega_c/2 + (\omega_c^2/4 - \omega_z^2/2)^{1/2}. \quad (46c)$$

Here $\omega_c = qB_0/Mc$ is the ordinary cyclotron frequency. These solutions assume that $\omega_c^2 > 2\omega_z^2$, since otherwise the motion is unstable. A typical experimental configuration might have $M = 25u$, $q = e$, $B_0 = 1$ T (10 kG), and $A_0 = 10$ V/cm². For these values of the parameters, $\omega_z \cong 2\pi \times 197.7$ kHz, $\omega_m \cong 2\pi \times 33.7$ kHz, and $\omega'_c \cong 2\pi \times 580.6$ kHz. The ion executes simple harmonic motion at frequency ω_z in the z direction and a superposition of circular motions at frequencies ω'_c and ω_m in the xy plane. Figure 1 shows a typical xy orbit for the case $\omega_m \ll \omega'_c$ and $r_m > r_c$. In this case the magnetron motion can be interpreted as an $\vec{E} \times \vec{B}$ drift of the center of the cyclotron orbit around the trap axis.

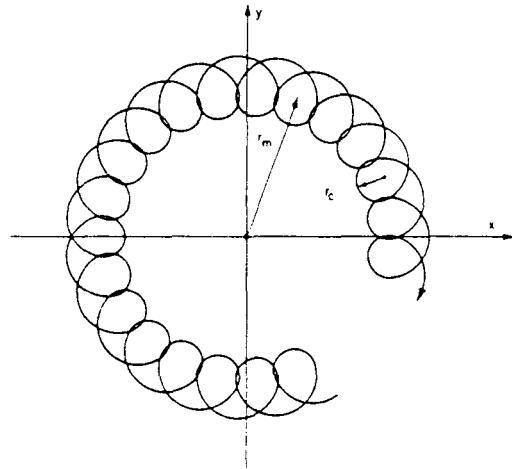


FIG. 1. Orbit of an ion in a Penning trap, projected onto the xy plane. The magnetic field direction is out of the drawing and the charge of the ion is assumed to be positive.

The kinetic energy of the ion is

$$E_K \equiv \frac{1}{2} M v^2 = \frac{1}{2} M r_m^2 \omega_m^2 + \frac{1}{2} M r_c^2 \omega_c^2 + M r_m r_c \omega_m \omega_c \cos(\omega_m t - \omega_c t + \theta_m - \theta_c) + \frac{1}{2} M r_z^2 \omega_z^2 \sin^2(\omega_z t + \theta_z). \quad (47)$$

The potential energy is

$$E_P \equiv qV(\vec{r}) = \frac{1}{2} M \omega_z^2 [r_z^2 \cos^2(\omega_z t + \theta_z) - \frac{1}{2}(r_m^2 + r_c^2) - r_m r_c \cos(\omega_m t - \omega_c t + \theta_m - \theta_c)]. \quad (48)$$

The total energy is a constant of the motion,

$$E = E_K + E_P = \frac{1}{2} M r_z^2 \omega_z^2 + M \Omega (\omega_c' r_c^2 - \omega_m r_m^2), \quad (49)$$

where

$$\Omega = \frac{1}{2} (\omega_c' - \omega_m). \quad (50)$$

We are interested primarily in reducing E_K , rather than E , since this will reduce Doppler shifts. The time-averaged kinetic energies in the axial, magnetron, and cyclotron modes are

$$\langle E_{Kz} \rangle = \frac{1}{4} M r_z^2 \omega_z^2, \quad (51a)$$

$$\langle E_{Km} \rangle = \frac{1}{2} M r_m^2 \omega_m^2, \quad (51b)$$

$$\langle E_{Kc} \rangle = \frac{1}{2} M r_c^2 \omega_c^2. \quad (51c)$$

Hence, we are interested in reducing r_z , r_m , and r_c . Note, however, that an increase in r_m leads to a decrease in the total magnetron energy, because of the potential energy contribution. Therefore, the orbit is unstable toward an increase of r_m if the ion is perturbed, for example, by collisions with neutral molecules. In the following, the term "cooling" will refer to the reduction of the kinetic energy,⁹ regardless of what happens to the total energy.

We note that the canonical momentum \vec{p} is defined by $\vec{p} = M\vec{v} + (q/c)\vec{A}$, where \vec{A} is the vector potential. We choose the symmetric gauge, where $\vec{A}(\vec{r}) = \frac{1}{2}\vec{B} \times \vec{r}$. In this gauge, the axial component of the canonical angular momentum is a constant of the motion given by

$$L_z \equiv x p_y - y p_x = M \Omega (r_m^2 - r_c^2). \quad (52)$$

B. Effect of photon interactions

We treat the effect of a laser beam on the motion of an ion with essentially the same assumptions that were made for the case of a harmonically bound atom. The ion is assumed to have only two internal energy levels, which are connected by an electric-dipole transition. The decay rate of the upper state is assumed to be much greater than any of the frequencies of motion (ω_c' , ω_m , and ω_z). Hence a photon scattering event can be considered to take place instantaneously, as far as the motion of the ion is concerned. In this semiclassical treatment, the ion moves according to the classical equations of motion between scattering events, which perturb its velocity. The scattering events occur at a rate determined by quantum-mechanical perturbation theory. We consider only the limit of low laser intensity. The various quantities ω_0 , γ , R , f_i , f_{si} , \vec{d}_{ge} , P_s , and σ_0 are defined as in Sec. II.

Consider an event in which an ion moving according to Eqs. (45a)–(45c) absorbs a photon of wave vector \vec{k} and emits a photon of wave vector \vec{k}_s at time t_0 . For $t < t_0$, the motion is described by the amplitudes r_i and the phases θ_i ($i = m, c, z$); for $t > t_0$ they are modified to r_i' and θ_i' . Let $\Delta\vec{v} \equiv \hbar(\vec{k} - \vec{k}_s)/M$. Then

$$\Delta r_z^2 \equiv (r_z')^2 - r_z^2 = (\Delta v_z / \omega_z)^2 - (2r_z \Delta v_z / \omega_z) \sin(\omega_z t_0 + \theta_z), \quad (53a)$$

$$\Delta r_m^2 \equiv (r_m')^2 - r_m^2 = [(\Delta v_x)^2 + (\Delta v_y)^2] / 4\Omega^2 + (r_m / \Omega) [\sin(\omega_m t_0 + \theta_m) \Delta v_x + \cos(\omega_m t_0 + \theta_m) \Delta v_y], \quad (53b)$$

$$\Delta r_c^2 \equiv (r_c')^2 - r_c^2 = [(\Delta v_x)^2 + (\Delta v_y)^2] / 4\Omega^2 - (r_c / \Omega) [\sin(\omega_c' t_0 + \theta_c) \Delta v_x + \cos(\omega_c' t_0 + \theta_c) \Delta v_y]. \quad (53c)$$

These equations are derived from combinations of Eqs. (45a)–(45c) and their time derivatives. Equation (53a) is, of course, equivalent to Eq. (4), since the axial mode is harmonic. From Eqs. (53b) and (53c) it can be shown that the magnetron radius is reduced if $\Delta\vec{v}$ is tangential to and in the same direction as the magnetron motion, while the cyclotron radius is reduced if $\Delta\vec{v}$ is tangential to and in the opposite direction as the cyclotron motion. The radii are increased for the opposite cases. This behavior has been noted previous-

ly.⁷⁻⁹ The requirements for cooling the cyclotron mode are similar to those for a harmonic oscillator, while those for the magnetron mode are different.

C. Rate equations for mean-squared amplitudes

1. Uniform laser beams

Here we consider the effect of a plane-wave laser beam of the form given by Eq. (1). We assume the intensity to be constant over the orbit of the ion. Consider a laser beam parallel to the z axis. If the laser frequency ω is less than ω_0 , the axial motion is cooled. Throughout the rest of Sec. III we neglect R/\hbar compared with $(\omega_0 - \omega)$ or γ . The magnetron and cyclotron modes are heated by recoil. As far as the axial mode is concerned, this is the same as the problem treated in Sec. II B 1. In the steady state

$$\langle E_{Kz} \rangle = \hbar(1 + f_{sz})[(\gamma/2)^2 + (\omega_0 - \omega)^2]/8(\omega_0 - \omega),$$

and for the optimum detuning,

$$(\omega_0 - \omega) = \gamma/2, \quad \langle E_{Kz} \rangle = (1 + f_{sz})\hbar\gamma/8.$$

The second terms on the right-hand sides of Eqs. (53b) and (53c) average to zero; therefore, the heating rates of the magnetron and cyclotron modes are given by

$$\frac{d\langle r_m^2 \rangle}{dt} = \frac{d\langle r_c^2 \rangle}{dt} = \gamma_s R (f_{sx} + f_{sy})/2M\Omega^2. \quad (54)$$

The brackets around r_m^2 and r_c^2 denote ensemble averages. Now consider a laser beam propagating along the x direction ($\vec{k} = k\hat{x}$). Assume that the system has somehow been cooled, so that $k(v_y)_{rms} \ll \gamma/2$ or $k(v_y)_{rms} \ll |\omega_0 - \omega|$. Then, using Eqs. (16), (45a), and (45b), the scattering cross section is

$$\sigma(\omega, \vec{v}) \cong \sigma_0(\gamma/2)^2 [(\gamma/2)^2 + (\omega_0 - \omega)^2]^{-1} \{ 1 + 2(\omega_0 - \omega)k[r_m \omega_m \sin(\omega_m t + \theta_m) + r_c \omega_c' \sin(\omega_c' t + \theta_c)] / [(\gamma/2)^2 + (\omega_0 - \omega)^2] \}. \quad (55)$$

For an individual ion, the amplitudes and phases ($r_m, r_c, \theta_m, \theta_c$) are perturbed by each scattering event. To find the average rate of change of $\langle r_z^2 \rangle, \langle r_m^2 \rangle, \langle r_c^2 \rangle$, we multiply $(I/\hbar\omega)$ by the cross section [Eq. (55)] and by the change per scattering [Eqs. (53a)–(53c)] and average over $r_m, r_c, \theta_m, \theta_c$, and \hat{k}_s :

$$\frac{d\langle r_z^2 \rangle}{dt} + 2\gamma_s R f_{sz} / M\omega_z^2, \quad (56a)$$

$$\frac{d\langle r_m^2 \rangle}{dt} = \gamma_s \{ (\omega_0 - \omega)\hbar k^2 \omega_m \langle r_m^2 \rangle / M\Omega [(\gamma/2)^2 + (\omega_0 - \omega)^2] + R(1 + f_{sx} + f_{sy})/2M\Omega^2 \}, \quad (56b)$$

$$\frac{d\langle r_c^2 \rangle}{dt} = \gamma_s \{ -(\omega_0 - \omega)\hbar k^2 \omega_c' \langle r_c^2 \rangle / M\Omega [(\gamma/2)^2 + (\omega_0 - \omega)^2] + R(1 + f_{sx} + f_{sy})/2M\Omega^2 \}. \quad (56c)$$

For negative laser detuning, ($\omega < \omega_0$), Eq. (56c) predicts that $\langle r_c^2 \rangle$ is reduced until it reaches a steady-state value, while Eq. (56b) predicts that $\langle r_m^2 \rangle$ increases without limit. This is because the Doppler shift causes the scattering rate to increase when either the cyclotron or magnetron contribution to the velocity is opposed to \vec{k} . For positive laser detuning, ($\omega > \omega_0$), the opposite occurs. The Doppler shift due to the heated mode will eventually cause the approximation for the cross section [Eq. (55)] to break down, which will modify the heating and cooling rates, but not change these qualitative features. The axial motion is heated regardless of detuning. It could be cooled by intro-

ducing a laser beam with some component along z , with negative detuning. However, there is no combination of uniform laser beams which is capable of cooling all three modes.

2. Nonuniform beam along x and uniform beam along z

Cooling of both the magnetron and cyclotron modes can be accomplished with a laser beam whose direction of propagation is in the xy plane and whose intensity increases on the side of the z axis on which the magnetron velocity is along the direction of propagation. The photon scattering

then tends to cool the magnetron motion. With negative laser detuning, the cyclotron motion will be cooled, due to Doppler effect velocity selection. This method has been demonstrated experimentally.^{8,9} The axial motion can be cooled with a separate beam or by tilting the nonuniform beam so that it has a component along the z axis.

Here we treat the case of a nonuniform beam of frequency ω_1 and wave vector $k_1\hat{x}$ and a uniform beam of frequency ω_2 and wave vector $k_2\hat{z}$ which cools the axial motion. The laser intensity of the nonuniform beam is assumed to be a function of y with value I_1 at $y=0$ and a positive slope I_1/y_0 at $y=0$ (see Fig. 2). We approximate the intensity profile by $I(y)=I_1(1+y/y_0)$ for $|y| \ll y_0$. The rms magnetron and cyclotron radii are assumed to be much less than y_0 , so that this linear approximation is valid. Let I_2 be the intensity of the laser beam along z . Let the scattering cross sections for the beams along the x and z axes, which depend upon the light polarizations through Eq. (13), be $\sigma_1(\omega_1, \vec{v})$ and $\sigma_2(\omega_2, \vec{v})$, respectively, with resonant ($\vec{v}=0, \omega=\omega_0$) cross sections σ_{01} and σ_{02} . The rate equations for the mean-squared amplitudes are

$$\begin{aligned} \frac{d\langle r_z^2 \rangle}{dt} &= (I_2/\hbar\omega_2)\langle \sigma_2(\omega_2, \vec{v}) \Delta r_z^2 \rangle \\ &+ (I_1/\hbar\omega_1)\langle (1+y/y_0)\sigma_1(\omega_1, \vec{v}) \Delta r_z^2 \rangle, \end{aligned} \quad (57a)$$

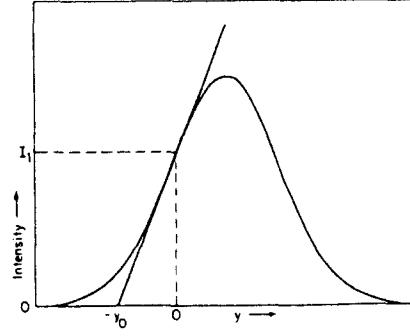


FIG. 2. Intensity profile of nonuniform laser beam. I_1 is the intensity at $y=0$ and I_1/y_0 is its slope. The tangent to the curve is used as an approximation to the actual profile in the calculation.

$$\begin{aligned} \frac{d\langle r_i^2 \rangle}{dt} &= (I_1/\hbar\omega_1)\langle (1+y/y_0)\sigma_1(\omega_1, \vec{v}) \Delta r_i^2 \rangle \\ &+ (I_2/\hbar\omega_2)\langle \sigma_2(\omega_2, \vec{v}) \Delta r_i^2 \rangle, \end{aligned} \quad (57b)$$

where $i = m, c$. The Δr_z^2 and Δr_i^2 are evaluated from Eqs. (53a)–(53c) using the \vec{k} appropriate to each laser beam. We now make the low Doppler approximation to the cross section and perform the ensemble average. The average scattering rates γ_{sl} ($l = 1, 2$) are given by

$$\gamma_{sl} = (I_l \sigma_{0l} / \hbar \omega_l) (\gamma/2)^2 / [(\gamma/2)^2 + (\omega_0 - \omega_l)^2]. \quad (58)$$

The rate equations become

$$\frac{d\langle r_z^2 \rangle}{dt} = -2\gamma_{s2}(\omega_0 - \omega_2)\hbar k_z^2 \langle r_z^2 \rangle / M [(\gamma/2)^2 + (\omega_0 - \omega_2)^2] + (2\gamma_{s2}R / M \omega_2^2) [1 + (1 + \gamma_{s1}/\gamma_{s2})f_{sz}], \quad (59a)$$

$$\begin{aligned} \frac{d\langle r_m^2 \rangle}{dt} &= -\gamma_{s1}\hbar k_1 \langle r_m^2 \rangle / 2M\Omega y_0 + \gamma_{s1}(\omega_0 - \omega_1)\hbar k_1^2 \omega_m \langle r_m^2 \rangle / M\Omega [(\gamma/2)^2 + (\omega_0 - \omega_1)^2] \\ &+ (\gamma_{s1}R / 2M\Omega^2) [1 + (1 + \gamma_{s2}/\gamma_{s1})(f_{sx} + f_{sy})], \end{aligned} \quad (59b)$$

$$\begin{aligned} \frac{d\langle r_c^2 \rangle}{dt} &= \gamma_{s1}\hbar k_1 \langle r_c^2 \rangle / 2M\Omega y_0 - \gamma_{s1}(\omega_0 - \omega_1)\hbar k_1^2 \omega_c \langle r_c^2 \rangle / M\Omega [(\gamma/2)^2 + (\omega_0 - \omega_1)^2] \\ &+ (\gamma_{s1}R / 2M\Omega^2) [1 + (1 + \gamma_{s2}/\gamma_{s1})(f_{sx} + f_{sy})]. \end{aligned} \quad (59c)$$

The axial motion can be cooled if $\omega_2 < \omega_0$ [see Eq. (59a)]. The first term on the right-hand side of Eq. (59b) shows cooling of the magnetron motion due the intensity gradient (for $y_0 > 0$), the second shows heating due to Doppler selection (for $\omega_1 < \omega_0$), and the third shows heating due to recoil. For $y_0 > 0$ and $\omega_1 < \omega_0$, the first term on the right-hand side of Eq. (59c) shows heating of the cyclotron motion due the intensity gradient, the second shows cooling due to Doppler selection, and the third shows heating due to recoil. Some

terms have been neglected in Eqs. (59b) and (59c) because they are at most of relative order $(k_1 v_x / \gamma)(y/y_0)$ compared to the recoil heating term. The term in the first set of parentheses is small, by the low Doppler assumption, while the term in the second set is small because $(r_m)_{\text{rms}}$ and $(r_c)_{\text{rms}}$ are assumed to be much less than y_0 . The condition for simultaneous cooling of the magnetron and cyclotron modes, for $y_0 > 0$ and $\omega_1 < \omega_0$, is

$$\omega_m < [(\gamma/2)^2 + (\omega_0 - \omega_1)^2] / 2k_1 y_0 (\omega_0 - \omega_1) < \omega'_c. \quad (60)$$

Assuming this condition is satisfied, as can be obtained experimentally, the steady state is given by

$$\langle r_z^2 \rangle = \hbar [1 + (1 + \gamma_{s1}/\gamma_{s2}) f_{sz}] [(\gamma/2)^2 + (\omega_0 - \omega_2)^2] / 2M\omega_z^2 (\omega_0 - \omega_2), \quad (61a)$$

$$\langle r_m^2 \rangle = \frac{\hbar k_1 y_0 [1 + (1 + \gamma_{s2}/\gamma_{s1})(f_{sx} + f_{sy})]}{2M\Omega \{1 - 2k_1 y_0 (\omega_0 - \omega_1) \omega_m / [(\gamma/2)^2 + (\omega_0 - \omega_1)^2]\}}, \quad (61b)$$

$$\langle r_c^2 \rangle = \frac{\hbar k_1 y_0 [1 + (1 + \gamma_{s2}/\gamma_{s1})(f_{sx} + f_{sy})]}{2M\Omega \{k_1 y_0 (\omega_0 - \omega_1) \omega'_c / [(\gamma/2)^2 + (\omega_0 - \omega_1)^2] - 1\}}. \quad (61c)$$

The average kinetic energy can be obtained by inserting these values into Eqs. (51a)–(51c). The parameters γ_{s2}/γ_{s1} , $(\omega_0 - \omega_1)$, $(\omega_0 - \omega_2)$, and y_0 can be adjusted in order to minimize the kinetic energy. In the general case, this is complicated.

We consider a simple case which can be experimentally realized. For this case, the Doppler selection cooling rate of the cyclotron motion is much greater than the intensity gradient heating rate, and the Doppler selection heating rate of the magnetron motion is less than and not too close to the intensity gradient cooling rate. These conditions are most easily satisfied when $\omega'_c/\omega_m \gg 1$, which is obtained by reducing the electric potential. Also, y_0 must fall within a certain range, so that $k_1 y_0 \omega'_c/\gamma \gg 1$ and $(1 - 2k_1 y_0 \omega_m/\gamma)$ is not too small, assuming that $(\omega_0 - \omega_1) \cong \gamma/2$. Then the magnetron kinetic energy is much less than the cyclotron kinetic energy. We have

$$\langle E_{Kz} \rangle = \hbar [1 + (1 + \gamma_{s1}/\gamma_{s2}) f_{sz}] \times [(\gamma/2)^2 + (\omega_0 - \omega_2)^2] / 8(\omega_0 - \omega_2). \quad (62a)$$

$$\langle E_{Kc} \rangle \cong \hbar [1 + (1 + \gamma_{s2}/\gamma_{s1})(f_{sx} + f_{sy})] \times [(\gamma/2)^2 + (\omega_0 - \omega_1)^2] / 4(\omega_0 - \omega_1), \quad (62b)$$

and we neglect $\langle E_{Km} \rangle$. For constant γ_{s1} and γ_{s2} , the kinetic energies are minimized if we set $(\omega_0 - \omega_2) = (\omega_0 - \omega_1) = \gamma/2$:

$$\langle E_{Kz} \rangle = [1 + (1 + \gamma_{s1}/\gamma_{s2}) f_{sz}] \hbar \gamma / 8, \quad (63a)$$

$$\langle E_{Kc} \rangle \cong [1 + (1 + \gamma_{s2}/\gamma_{s1})(f_{sx} + f_{sy})] \hbar \gamma / 4. \quad (63b)$$

The total kinetic energy can be minimized by adjusting the relative laser beam intensities so that

$$\gamma_{s1}/\gamma_{s2} = [2(f_{sx} + f_{sy})/f_{sz}]^{1/2}. \quad (64)$$

For the isotropic angular distribution, this condition is $\gamma_{s1}/\gamma_{s2} = 2$, in which case, $\langle E_{Kz} \rangle \cong \frac{1}{2} \langle E_{Kc} \rangle \cong \hbar \gamma / 4$. This gives the same average kinetic energy in the x , y , and z directions as for the harmonic trap discussed in Secs. II B 2 and II B 3. The minimum energies are slightly different for an anisotropic distribution, as is the case for the harmonic trap.

3. Nonuniform beam in xz plane

Cooling of all three modes can be accomplished by rotating the direction of the nonuniform beam

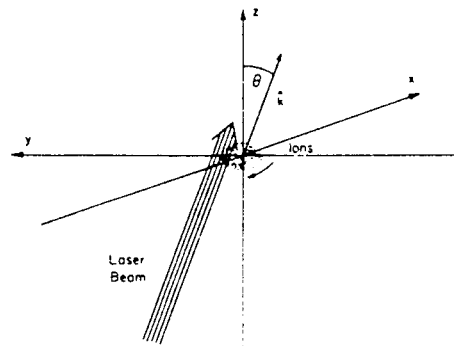


FIG. 3. Nonuniform laser beam configuration which is capable of cooling all three modes of motion of an ion in a Penning trap. The trap coordinate axes are indicated. The ion cloud is at the origin, and the direction of the magnetron rotation is indicated by an arrow. The laser light propagates in the \hat{k} direction, which lies in the xz plane. The laser beam is focused so that it is more intense for $y > 0$ than for $y < 0$.

described in Sec. III C 2 so that it has a component along z and eliminating the uniform beam. Let $\vec{k} = k \sin\theta \hat{x} + k \cos\theta \hat{z}$, ($0 < \theta < \pi/2$), be the wave vector for the nonuniform beam, which has fre-

quency ω . The geometry is shown in Fig. 3. Let γ_s be the average scattering rate. In the low Doppler approximation,

$$\frac{d\langle r_z^2 \rangle}{dt} = -2\gamma_s(\omega_0 - \omega)\hbar k^2 \cos^2\theta \langle r_z^2 \rangle / M[(\gamma/2)^2 + (\omega_0 - \omega)^2] + (2\gamma_s R / M\omega_z^2)(\cos^2\theta + f_{sz}), \quad (65a)$$

$$\begin{aligned} \frac{d\langle r_m^2 \rangle}{dt} = & -\gamma_s \hbar k \sin\theta \langle r_m^2 \rangle / 2M\Omega y_0 + \gamma_s(\omega_0 - \omega)\hbar k^2 \sin^2\theta \omega_m \langle r_m^2 \rangle / M\Omega[(\gamma/2)^2 + (\omega_0 - \omega)^2] \\ & + (\gamma_s R / 2M\Omega^2)(\sin^2\theta + f_{sx} + f_{sy}), \end{aligned} \quad (65b)$$

$$\begin{aligned} \frac{d\langle r_c^2 \rangle}{dt} = & \gamma_s \hbar k \sin\theta \langle r_c^2 \rangle / 2M\Omega y_0 - \gamma_s(\omega_0 - \omega)\hbar k^2 \sin^2\theta \omega'_c \langle r_c^2 \rangle / M\Omega[(\gamma/2)^2 + (\omega_0 - \omega)^2] \\ & + (\gamma_s R / 2M\Omega^2)(\sin^2\theta + f_{sx} + f_{sy}). \end{aligned} \quad (65c)$$

Some small terms have been neglected. The axial motion can be cooled if $\omega < \omega_0$. The condition for simultaneous cooling of the magnetron and cyclotron modes, assuming $y_0 > 0$ and $\omega < \omega_0$, is given by Eq. (60), with $k \sin\theta$ substituted for k_1 . If this condition is met, which is feasible experimentally, the steady-state mean-squared amplitudes are given by

$$\langle r_z^2 \rangle = \hbar(1 + f_{sz}/\cos^2\theta)[(\gamma/2)^2 + (\omega_0 - \omega)^2] / 2M\omega_z^2(\omega_0 - \omega), \quad (66a)$$

$$\langle r_m^2 \rangle = \frac{\hbar k y_0 (\sin^2\theta + f_{sx} + f_{sy})}{2M\Omega \sin\theta \{1 - 2k \sin\theta y_0 (\omega_0 - \omega) \omega_m / [(\gamma/2)^2 + (\omega_0 - \omega)^2]\}}, \quad (66b)$$

$$\langle r_c^2 \rangle = \frac{\hbar k y_0 (\sin^2\theta + f_{sx} + f_{sy})}{2M\Omega \sin\theta \{2k \sin\theta y_0 (\omega_0 - \omega) \omega'_c / [(\gamma/2)^2 + (\omega_0 - \omega)^2] - 1\}}. \quad (66c)$$

We consider the same limit as in Sec. III C 3, i.e., the Doppler selection cooling rate of the cyclotron motion is much greater than the intensity gradient heating rate, and the Doppler selection heating rate of the magnetron motion is less than and not too close to the intensity gradient cooling rate. Then

$$\langle E_{Kz} \rangle = \hbar(1 + f_{sz}/\cos^2\theta)[(\gamma/2)^2 + (\omega_0 - \omega)^2] / 8(\omega_0 - \omega), \quad (67a)$$

$$\langle E_{Kc} \rangle \cong \hbar[1 + (f_{sx} + f_{sy})/\sin^2\theta][(\gamma/2)^2 + (\omega_0 - \omega)^2] / 4(\omega_0 - \omega), \quad (67b)$$

and $\langle E_{Km} \rangle$ is negligible. These quantities are minimized by setting $(\omega_0 - \omega) = \gamma/2$:

$$\langle E_{Kz} \rangle = (1 + f_{sz}/\cos^2\theta)\hbar\gamma/8, \quad (68a)$$

$$\langle E_{Kc} \rangle \cong [1 + (f_{sx} + f_{sy})/\sin^2\theta]\hbar\gamma/4. \quad (68b)$$

The total kinetic energy is minimized with respect to θ for

$$\tan^4\theta = 2(f_{sx} + f_{sy})/f_{sz}. \quad (69)$$

For the isotropic angular distribution, this condition is, $\theta = \tan^{-1}(\sqrt{2}) \cong 54.74^\circ$, in which case, $\langle E_{Kz} \rangle \cong \frac{1}{2}\langle E_{Kc} \rangle \cong \hbar\gamma/4$. This is the same limit obtained in Sec. III C 3.

4. Comparison with experimental data

The most unambiguous comparison between theory and experiment can be made for the case of a single ion. The details of energy exchange due to collisions are not precisely understood for the case of a cloud of ions; moreover the frequencies of oscillation ω_z , ω'_c , and ω_m are all shifted by the presence of space charge. Both of these problems are absent for a single ion, and the simple theory discussed above should apply.

Laser cooling of a single $^{24}\text{Mg}^+$ ion in a Penning trap has been performed previously.⁹ The cooling achieved was such that the Doppler

broadening was significantly less than the natural linewidth of the transition, so the results of the last section should apply. For this experiment,⁹ a single $^{24}\text{Mg}^+$ ion was stored in the trap and cooled. The trap parameters were $B_0 \cong 1.01$ T and $A_0 = V_0 / (r_0^2 + 2z_0^2) \cong 2.95$ V/cm², where the interelectrode voltage was $V_0 \cong 2$ V and the electrode dimensions, in the notation of Ref. 4, were such that $r_0^2 + 2z_0^2 \cong 0.678$ cm². This gave approximate observed frequencies of $\omega'_c \cong 2\pi \times 638.5$ kHz, $\omega_z \cong 2\pi \times 106.9$ kHz, and $\omega_m \cong 2\pi \times 8.95$ kHz. The laser beam intensity profile in the vicinity of the ion was measured to be $I(y) \cong I' \exp[-2(y-d)^2 / w_0^2]$, where $d \cong 15$ μm and $w_0 \cong 25$ μm .

From this expression, we estimate

$$\frac{1}{y_0} = \frac{1}{I(y=0)} \frac{dI}{dy} \Big|_{y=0} = \frac{1}{10.4 \mu\text{m}}.$$

The transition involved in the laser cooling was the $^{24}\text{Mg}^+ (3p^2P_{3/2}, M_J = -\frac{3}{2}) \leftarrow (3s^2S_{1/2}, M_J = -\frac{1}{2})$ transition at $\lambda = 279.6$ nm; for this case [see Eqs. (8b) and (10b)] $f_{sz} = \frac{2}{5}$ and $f_{sx} + f_{sy} = \frac{3}{5}$. From Eq. (69), the angle of laser propagation that minimizes the total kinetic energy is $\theta = \tan^{-1}(3^{1/4}) \cong 52.77^\circ$. Experimentally, θ could be varied between 82° and 90° , and it was set at 82° . The laser detuning was such that $(\omega_0 - \omega) \cong 2\pi \times 25$ MHz.

From Eqs. (66a)–(66c) we predict $\langle r_z^2 \rangle = (4.17 \times 10^{-4} \text{ cm})^2$, $\langle r_c^2 \rangle = (2.07 \times 10^{-5} \text{ cm})^2$, and $\langle r_m^2 \rangle = (5.25 \times 10^{-5} \text{ cm})^2$. An important parameter in very high resolution spectroscopy is the second-order Doppler shift $\Delta\omega_0 / \omega_0 \cong -\frac{1}{2} \langle v^2 \rangle / c^2$. Because this shift is proportional to the kinetic energy of the ions, it is convenient to define a “temperature” in terms of the kinetic energy. The concept of a temperature may not be valid for a single ion, but it is reasonable to define temperatures for the axial and cyclotron degrees of freedom in terms of the time-averaged kinetic energies as $\langle E_{Kz} \rangle \cong \frac{1}{2} k_B T_z$ and $\langle E_{Kc} \rangle \cong k_B T_c$, where k_B is Boltzmann’s constant. For the magnetron degree of freedom, there is an additional problem since the total energy is negative (when the electric potential is defined to be zero at the origin) and decreases to minus infinity as $\langle r_m^2 \rangle$ goes to plus infinity. However, it is still useful to define, by analogy with the cyclotron motion, $\langle E_{Km} \rangle \cong k_B T_m$. Using these definitions, we find for the experiment of Ref. 9, $T_z \cong 11$ mK, $T_c \cong 1.0$ mK, and $T_m \cong 1.3 \times 10^{-6}$ K. From the residual Doppler broadening of the optical lines measured in Ref. 9

we estimated that $T_c = (50 \pm 30)$ mK and $T_m \leq 1$ mK. At the present time we do not understand why the measured temperatures are higher than predicted. One difficulty not mentioned previously is the possible collisional heating due to impurity ions, such as NH_3^+ , H_3O^+ , N_2H^+ , and HCO^+ , that might be simultaneously trapped.

IV. LASER COOLING IN A PENNING TRAP (QUANTUM-MECHANICAL TREATMENT)

A. Quantum states of an ion in a Penning trap

The Hamiltonian operator for a single ion in the same idealized Penning trap which was treated classically in Sec. II A, is

$$H = [\vec{p} - (q/c)\vec{A}(\vec{r})]^2 / 2M + qV(\vec{r}) \equiv H_{xy} + H_z, \quad (70)$$

where

$$H_{xy} = (p_x^2 + p_y^2) / 2M + \frac{1}{2} M \Omega^2 (x^2 + y^2) - \frac{1}{2} \omega_c L_z, \quad (71a)$$

and

$$H_z = p_z^2 / 2M + \frac{1}{2} M \omega_z^2 z^2. \quad (71b)$$

Here \vec{r} and \vec{p} are operators and L_z is an operator defined by $L_z \equiv xp_y - yp_x$. This Hamiltonian has been dealt with by other authors.^{30,31} Here we summarize the useful results. H_z is the Hamiltonian of a one-dimensional simple harmonic oscillator. Therefore it can be rewritten as

$$H_z = (N_z + \frac{1}{2}) \hbar \omega_z, \quad (72)$$

where

$$N_z = a_z^\dagger a_z, \quad (73a)$$

$$z = z_0 (a_z^\dagger + a_z), \quad (73b)$$

$$p_z = iz_0 M \omega_z (a_z^\dagger - a_z), \quad (73c)$$

$$z_0 = (\hbar / 2M \omega_z)^{1/2}. \quad (73d)$$

H_{xy} is the Hamiltonian of a two-dimensional isotropic oscillator, plus a term proportional to L_z . It can be rewritten as

$$H_{xy} = (N_c + \frac{1}{2}) \hbar \omega'_c - (N_m + \frac{1}{2}) \hbar \omega_m, \quad (74)$$

where

$$N_i = a_i^\dagger a_i \quad (i = c, m) \quad (75a)$$

$$a_c = (a_x + ia_y) / 2^{1/2}, \quad (75b)$$

$$a_m = (a_x - ia_y)/2^{1/2}, \quad (75c)$$

$$x = r_0(a_x^\dagger + a_x)/2^{1/2}, \quad y = r_0(a_y^\dagger + a_y)/2^{1/2}, \quad (75d)$$

$$p_j = r_0 M \Omega (a_j^\dagger - a_j)/2^{1/2} \quad (j = x, y) \quad (75e)$$

$$r_0 = (\hbar/M\Omega)^{1/2}. \quad (75f)$$

The three sets of raising and lowering operators satisfy the commutation relations

$$[a_i, a_j] = 0, \quad (76a)$$

$$[a_i^\dagger, a_j^\dagger] = 0, \quad (76b)$$

$$[a_i, a_j^\dagger] = \delta_{ij} I \quad (i = z, c, m) \quad (76c)$$

where I is the identity operator. The axial component of the angular momentum operator can be written in the form

$$L_z = (N_m - N_c)\hbar. \quad (77)$$

The complete set of eigenstates of H is given by the set of simultaneous eigenstates of N_z , N_m , and N_c . We label these states $|n_z, n_m, n_c\rangle$, where n_z , n_m , and n_c are the eigenvalues of N_z , N_m , and N_c and can be any set of nonnegative integers. They can be generated from the $|0, 0, 0\rangle$ state by applying the raising operators. The normalized states are

$$|n_z, n_m, n_c\rangle = (n_z! n_m! n_c!)^{-1/2} (a_z^\dagger)^{n_z} (a_m^\dagger)^{n_m} (a_c^\dagger)^{n_c} |0, 0, 0\rangle. \quad (78)$$

the coordinate-space representation of $|0, 0, 0\rangle$ is

$$\langle x, y, z | 0, 0, 0\rangle = \pi^{-3/4} (2^{1/2} z_0 r_0^2)^{-1/2} \exp[-z^2/2z_0^2 - (x^2 + y^2)/2r_0^2]. \quad (79)$$

Explicit expressions for the wave functions for arbitrary quantum numbers have been given by Sokolov and Pavlenko.³¹ By comparing the classical expressions for the energy [Eq. (49)] and the axial angular momentum component [Eq. (52)] with the corresponding quantum-mechanical operators, [Eqs. (72), (74), and (77)], one obtains the following correspondences between classical amplitudes of motion and the quantum numbers:

$$r_c^2 \sim (n_c + \frac{1}{2}) r_0^2, \quad (80a)$$

$$r_m^2 \sim (n_m + \frac{1}{2}) r_0^2, \quad (80b)$$

$$r_z^2 \sim 4(n_z + \frac{1}{2}) z_0^2. \quad (80c)$$

B. Transition rates

We treat the interaction of the ion with the electromagnetic field by second-order time-dependent perturbation theory, in the form of the "golden rule." The motion of the ion as a whole, as well as its internal structure, is described by wave functions. In Sec. III, only the internal structure was treated quantum mechanically. Consider the transition rate from $|n_z^i, n_m^i, n_c^i\rangle \equiv |\{n^i\}\rangle$ to $|\{n^f\}\rangle$ induced by a near-resonant uniform laser beam described by Eq. (1). The ion is in its ground electronic state $|g\rangle$ before and after the transition. This is a kind of spontaneous resonance Raman scattering, through the intermediate electronic state $|e\rangle$. The cross section for this process is given by Eq. (19) of Ref. 16. We make the electric-dipole approximation and sum over all polarizations and directions of the scattered photon.

This cross section is

$$\sigma(\{n^i\} \rightarrow \{n^f\}) = \sigma_0 (\gamma/2)^2 \int \left| \sum_{\{n^j\}} \frac{\langle \{n^f\} | \exp(-i\vec{k}_s \cdot \vec{r}) | \{n^j\} \rangle \langle \{n^j\} | \exp(i\vec{k} \cdot \vec{r}) | \{n^i\} \rangle}{\omega_0 - \omega - i\gamma/2 + \omega(\{n^j\}) - \omega(\{n^i\})} \right|^2 P_s(\hat{k}_s) d\Omega, \quad (81)$$

where $\omega(\{n^i\}) \equiv (n_z^i + \frac{1}{2})\omega_z + (n_c^i + \frac{1}{2})\omega_c - (n_m^i + \frac{1}{2})\omega_m$, and the other terms have been defined previously. We have replaced \vec{x} of Ref. 16 with \vec{r} here. The transition rate is obtained by multiplying this cross section by $I/\hbar\omega$.

The transition rate due to a nonuniform laser beam can also be calculated by perturbation theory. The only difference is that the electric field vector due to the laser perturbation $-\vec{d}\cdot\vec{E}(\vec{r},t)$, which induces transitions to the intermediate state, is no longer a uniform plane wave of the form of Eq. (1). We consider only the low-intensity limit, in which case the transition from the intermediate state to the final state is induced by the zero-point field. Consider a nonuniform beam like the one treated in Sec. III C 3, which has an intensity gradient in the y direction and has a wave vector $\vec{k}=k\sin\theta\hat{x}+k\cos\theta\hat{z}$, ($0<\theta<\pi/2$). Let the electric field be

$$\vec{E}(\vec{r},t)=\hat{e}(1+y/2y_0)\text{Re}E_0\exp(i\vec{k}\cdot\vec{r}-i\omega t), \quad (82)$$

which gives the intensity profile

$$I(y)=I_0[1+y/y_0+(y/2y_0)^2]\cong I_0(1+y/y_0) \quad (83)$$

for $|y|\ll y_0$. We can use this \vec{E} in the perturbation matrix element to reproduce the case treated classically in Sec. III C 3, provided that the wave functions are localized in the region $|y|\ll y_0$. The transition rate is

$$\gamma(\{n^i\}\rightarrow\{n^f\})=(I_0/\hbar\omega)\sigma^*(\{n^i\}\rightarrow\{n^f\}), \quad (84)$$

where the effective cross section σ^* is given by

$$\sigma^*(\{n^i\}\rightarrow\{n^f\}) = \sigma_0(\gamma/2)^2 \int \left| \sum_{\{n^j\}} \frac{\langle\{n^f\}|\exp(-i\vec{k}_s\cdot\vec{r})|\{n^j\}\rangle\langle\{n^j\}|(1+y/2y_0)\exp(i\vec{k}\cdot\vec{r})|\{n^i\}\rangle}{\omega_0-\omega-i\gamma/2+\omega(\{n^j\})-\omega(\{n^i\})} \right|^2 P_s(\hat{k}_s)d\Omega. \quad (85)$$

C. Rate equations for average quantum numbers

We calculate the rate equations for the ensemble averages of the quantum numbers $\langle n_z \rangle$, $\langle n_m \rangle$, and $\langle n_c \rangle$. We do not consider coherences between $|n_z, n_m, n_c\rangle$ states. Let $P(\{n^i\})$ be the probability that the ion has the set of quantum numbers $\{n^i\}$. We can derive the rate equations for any of the cases considered in Sec. III. For the sake of brevity we consider only the case of the nonuniform laser beam propagating in the xz plane [Sec. III C 3], using the effective cross section defined by Eqs. (84) and (85). The rate equations are given by¹⁶

$$\frac{d\langle n_i \rangle}{dt} = \sum_{\{n^i\}, \{n^f\}} P(\{n^i\})\gamma(\{n^i\}\rightarrow\{n^f\})(n_i^f - n_i^i), \quad (86)$$

where

$$i=z, m, c.$$

We make the low Doppler approximation. In this limit we can make the approximation

$$[\omega_0-\omega-i\gamma/2+\omega(\{n^j\})-\omega(\{n^i\})]^{-1} \cong (\omega_0-\omega-i\gamma/2)^{-1} [1+[\omega(\{n^i\})-\omega(\{n^j\})]/(\omega_0-\omega-i\gamma/2)] \quad (87)$$

in Eq. (85). Equation (87) is valid for

$$|[\omega(\{n^i\})-\omega(\{n^j\})]/(\omega_0-\omega-i\gamma/2)| \ll 1.$$

This condition is violated for some terms in Eq. (85), which correspond to large differences in quantum numbers, since the summation is over all possible $\{n^j\}$, but these terms are of negligible size, because the matrix elements are very small. With this approximation, Eq. (86) can be evaluated by straightforward algebra. We outline the important steps here. The method was previously used for the harmonic trap in Ref. 16. We note that

$$\langle \{n^j\} | A | \{n^l\} \rangle [\omega(\{n^l\}) - \omega(\{n^j\})] = \langle \{n^j\} | [A, H/\hbar] | \{n^l\} \rangle \quad (88)$$

for any operator A . The summations in Eq. (86) over $\{n^j\}$ and $\{n^l\}$ can be carried out using the closure property, and we obtain

$$\frac{d\langle n_i \rangle}{dt} = \gamma_s \sum_{\{n^l\}} P(\{n^l\}) \int \langle \{n^l\} | A^\dagger [N_i, A] | \{n^l\} \rangle P_s(\hat{k}_s) d\Omega. \quad (89)$$

Here

$$A \equiv \exp(-i\vec{k}_s \cdot \vec{r}) \{ (1 + y/2y_0) \exp(i\vec{k} \cdot \vec{r}) + [(1 + y/2y_0) \exp(i\vec{k} \cdot \vec{r}), H/\hbar(\omega_0 - \omega - i\gamma/2)] \}, \quad (90)$$

and

$$\gamma_s = (I_0 \sigma_0 / \hbar \omega) (\gamma/2)^2 / [(\omega_0 - \omega)^2 + (\gamma/2)^2] \quad (91)$$

is the average scattering rate. We define the ensemble averages $\langle r_i^2 \rangle$, using Eqs. (80a)–(80c) by

$$\langle r_z^2 \rangle \equiv 4z_0^2 \langle n_z + \frac{1}{2} \rangle \equiv 4z_0^2 \sum_{\{n^l\}} P(\{n^l\}) (n_z^l + \frac{1}{2}), \quad (92a)$$

$$\langle r_i^2 \rangle \equiv r_0^2 \langle n_i + \frac{1}{2} \rangle \equiv r_0^2 \sum_{\{n^l\}} P(\{n^l\}) (n_i^l + \frac{1}{2}) \quad (i = m, c). \quad (92b)$$

The rate equations for $\langle r_i^2 \rangle$ ($i = z, m, c$), obtained by evaluating Eq. (89) and dropping small terms, are identical with Eqs. (65a)–(65c). This is not surprising, because the average quantum numbers are large. The other cases treated in Sec. II C can be treated by the same methods. The rate equations obtained are identical to those obtained from the classical analysis. Here the following quantities are regarded as small: r_m/y_0 , r_c/y_0 , ω_m/γ , ω'_c/γ , ω_z/γ , $R/\hbar\gamma$, $k\omega_m r_m/\gamma$, $k\omega'_c r_c/\gamma$, and $1/ky_0$.

The quantities kz_0 and kr_0 are assumed to be not too large, so that when multiplied by a small quantity, the result is still small.

V. DISCUSSION

We have carried out a semiclassical calculation of the laser cooling of an ion in a Penning trap, for the case where the frequencies of motion are much less than the natural linewidth of the optical transition. The results are confirmed by a quantum-mechanical calculation based on perturbation theory. Also, some simple calculations of laser cooling in a harmonic trap are presented. Where a direct comparison can be made, the results agree with those obtained by more formal methods.^{20,23}

Experiments have confirmed the qualitative features of the present analysis.^{7–9} Cooling to average kinetic energies so low that the Doppler broadening of the optical transition is smaller than

the natural linewidth has been observed.⁹ However, the ultimate limits predicted by the theory have not been achieved in these experiments.

Useful improvements to the theory would include taking into account Coulomb forces between ions and assuming a more realistic laser beam profile. Saturation of the optical transition has not been included. However, this is not a severe restriction, especially for the final stages of cooling, since we would expect the minimum energies to be obtained in the low-intensity limit, as for the harmonic trap.²⁰ It would be interesting to apply the Fokker-Planck formalism to the Penning trap as has been done for the harmonic trap.^{20–23}

In this paper, the case of resolved sidebands ($\omega'_c, \omega_z, \omega_m \gg \gamma$) has not been treated but should be quite straightforward and could follow the development of Ref. 16 and this paper. We remark that when the mean occupation numbers $\langle n_i \rangle$ are small enough, then all sidebands can be well resolved. This means that cooling can be achieved using spatially *uniform* plane waves provided the lasers are tuned to the correct sidebands.

Motional sideband cooling of the magnetron motion of an electron in a Penning trap³² has been demonstrated and is closely related to laser cooling. Here the axial resonance, which is analogous to the optical transition of the two-level ion, is driven by an inhomogeneous rf field at the sideband frequency $\omega_z + \omega_m$. The modes are coupled by the field in such a way that the magnetron motion is cooled.

We also remark that, in general, the reduction of the magnetron orbits can be achieved by other means which add (total) energy to the magnetron degree of freedom.³³ This could be achieved, for example, by coupling the magnetron motion to a negative resistance or by collisions with atomic beams that preferentially interact with the side of the cloud where the magnetron motion is in the same direction as the beam. This effect could be important in certain collision experiments.³⁴

All previous detailed theoretical treatments of laser cooling of trapped ions have assumed harmonic potential wells. The experiments which most closely approach this situations are performed with rf quadrupole traps, in which the motion of an ion consists of the high frequency, small amplitude "micromotion" superimposed on the low frequency, large amplitude "secular motion."⁴ Approximating such a trap by a harmonic potential neglects the micromotion. The average kinetic energy in the micromotion, averaged over an rf cycle, is just an effective potential energy for the secular motion. A formalism which could take account of the micromotion, either classically or quantum mechanically, might be useful for the interpretation of the experiments.

Finally, we wish to point out that Einstein,³⁵ in the same paper in which the A and B coefficients for spontaneous and stimulated emission were introduced, treated a problem which is closely related to laser cooling. He showed that a gas of two-level atoms comes into thermal equilibrium with radiation having the Planck spectrum, as a result of light pressure forces. In this case, since the radiation is broad band and isotropic, the average damping force is mostly due to an effect that we have neglected: The apparent intensity of a light source increases if the observer moves toward the source, as a result of the transformation law for the electric and magnetic fields. The Doppler shift and angular aberration of the light must also be taken into account. The damping force due to the average light pressure competes with the fluctuating force due to photon recoil so that, in the steady state and in the nonrelativistic limit, $E_{Kx} = \frac{1}{2} k_B T$, if the radiation has the Planck spectrum for tem-

perature T . Recently, the calculation has been extended to demonstrate that the gas has the relativistic Boltzmann distribution after it comes into thermal equilibrium with the radiation.³⁶

This work was supported in part by the Air Force Office of Scientific Research and the Office of Naval Research.

APPENDIX: SPECTRAL DENSITY OF A RANDOM SERIES OF IMPULSES

We calculate here the one-sided (i.e., defined for positive frequencies) power spectral density of $G(t)$, where $G(t)$ is a stationary, random function of time consisting of a series of Dirac delta functions. These impulses occur at an average rate γ and they may vary in amplitude. This calculation follows that of Rice.³⁷

First we calculate the correlation function,

$$R(\tau) \equiv \langle G(t)G(t+\tau) \rangle, \quad (\text{A1})$$

where the angular brackets denote an ensemble average, and R is independent of t , by the assumption of stationarity. We consider $G(t)$ during the time interval $0 < t < T$, where T is arbitrary. We denote a particular member of the ensemble by $G_{Kk}(t)$, where K is the number of impulses that occur in the period, and k uniquely identifies the member. This function takes the following form:

$$G_{Kk}(t) = \sum_{l=1}^K g_{Kkl} \delta(t - t_{Kkl}). \quad (\text{A2})$$

The amplitudes g_{Kkl} can vary, but are not correlated in any way with t_{Kkl} , K , or l . The l index does not indicate an order in time. For fixed K and l , t_{Kkl} can be anywhere in the interval from 0 to T with equal probability. We define ensemble averages over the index k as

$$\langle g_{Kkl} \rangle_k \equiv \langle g \rangle, \quad (\text{A3})$$

$$\langle g_{Kkl}^2 \rangle_k \equiv \langle g^2 \rangle, \quad (\text{A4})$$

where $\langle g \rangle$ and $\langle g^2 \rangle$ are independent of l and K . The product $G_{Kk}(t)G_{Kk}(t+\tau)$ takes the form

$$\begin{aligned} G_{Kk}(t)G_{Kk}(t+\tau) &= \sum_{l=1}^K \sum_{l'=1}^K g_{Kkl}g_{Kkl'} \delta(t - t_{Kkl}) \delta(t + \tau - t_{Kkl'}) \\ &= S_1 + S_2, \end{aligned} \quad (\text{A5})$$

where

$$S_1 = \sum_{l=1}^K (g_{Kkl})^2 \delta(t - t_{Kkl}) \delta(t + \tau - t_{Kkl}) \quad (\text{A6})$$

and

$$S_2 = \sum_{l \neq l'} g_{Kkl} g_{Kkl'} \delta(t - t_{Kkl}) \delta(t + \tau - t_{Kkl'}) \quad (\text{A7})$$

Now we carry out the ensemble averages over the index k for fixed K :

$$\begin{aligned} \langle S_1 \rangle_k &= \sum_{l=1}^K (\langle g^2 \rangle / T) \int_0^T \delta(t - t_{Kkl}) \delta(t + \tau - t_{Kkl}) dt_{Kkl} \\ &= \sum_{l=1}^K (\langle g^2 \rangle / T) \delta(\tau) = K (\langle g^2 \rangle / T) \delta(\tau) \end{aligned} \quad (\text{A8})$$

and

$$\begin{aligned} \langle S_2 \rangle_k &= \sum_{l \neq l'} (\langle g \rangle / T)^2 \int_0^T \delta(t - t_{Kkl}) dt_{Kkl} \int_0^T \delta(t + \tau - t_{Kkl'}) dt_{Kkl'} \\ &= \sum_{l \neq l'} (\langle g \rangle / T)^2 = K(K-1) (\langle g \rangle / T)^2. \end{aligned} \quad (\text{A9})$$

The ensemble average over K is carried out using the Poisson distribution function

$$p(K) = (\gamma T)^K e^{-\gamma T} / K!, \quad (\text{A10})$$

where $p(K)$ is the probability that K impulses occur during the period T . Finally, we have

$$R(\tau) = \sum_{K=0}^{\infty} p(K) (\langle S_1 \rangle_k + \langle S_2 \rangle_k) = \gamma \langle g^2 \rangle \delta(\tau) + \gamma^2 \langle g \rangle^2. \quad (\text{A11})$$

The spectral density is given by

$$w(f) = 4 \int_0^{\infty} R(\tau) \cos 2\pi f \tau d\tau = 2\gamma \langle g^2 \rangle + 2\gamma^2 \langle g \rangle^2 \delta(f), \quad (\text{A12})$$

which is defined for frequencies $f \geq 0$. The first (white noise) term corresponds to the spectral density calculated in Eq. (39). The second (dc) term comes from the average value of G , which correspond to $\langle F_x \rangle$ defined in Eq. (33).

¹T. W. Hänsch and A. L. Schawlow, *Opt. Commun.* **13**, 68 (1975).

²D. J. Wineland and H. Dehmelt, *Bull. Am. Phys. Soc.* **20**, 637 (1975).

³V. I. Balykin, V. S. Letokhov, and V. I. Mishin, *Pis'ma Zh. Eksp. Teor. Fiz.* **29**, 614 (1979) [*JETP Lett.* **29**, 560 (1979)]; *Zh. Eksp. Teor. Fiz.* **78**, 1376 (1980) [*Sov. Phys.—JETP* **51**, 692 (1980)].

⁴H. G. Dehmelt, in *Advances in Atomic and Molecular Physics*, edited by D. R. Bates and I. Esterman (Academic, New York, 1967), Vol. 3.

⁵W. Neuhauser, M. Hohenstatt, P. Toschek, and H. Dehmelt, *Phys. Rev. Lett.* **41**, 233 (1978); *Appl. Phys.* **17**, 123 (1978).

⁶W. Neuhauser, M. Hohenstatt, P. Toschek, and H. Dehmelt, *Phys. Rev. A* **22**, 1137 (1980).

⁷D. J. Wineland, R. E. Drullinger, and F. L. Walls,

Phys. Rev. Lett. **40**, 1639 (1978).

⁸R. E. Drullinger, D. J. Wineland, and J. C. Bergquist, *Appl. Phys.* **22**, 365 (1980).

⁹D. J. Wineland and W. M. Itano, *Phys. Lett.* **82A**, 75 (1981).

¹⁰A. Ashkin, *Phys. Rev. Lett.* **40**, 729 (1978); A. Ashkin and J. P. Gordon, *Opt. Lett.* **4**, 161 (1979); A. Ashkin, *Science* **210**, 1081 (1980).

¹¹J. P. Gordon and A. Ashkin, *Phys. Rev. A* **21**, 1606 (1980).

¹²V. S. Letokhov, V. G. Minogin, and B. D. Pavlik, *Zh. Eksp. Teor. Fiz.* **72**, 1328 (1977) [*Sov. Phys.—JETP* **45**, 698 (1977)]; V. S. Letokhov and V. G. Minogin, *ibid.* **74**, 1318 (1978) [*ibid.* **47**, 690 (1978)].

¹³R. J. Cook, *Phys. Rev. A* **20**, 224 (1979); **21**, 268 (1980); **22**, 1078 (1980).

¹⁴R. J. Cook, *Phys. Rev. Lett.* **44**, 976 (1980).

- ¹⁵J. Javanainen and S. Stenholm, *Appl. Phys.* **21**, 35 and 163 (1980).
- ¹⁶D. J. Wineland and W. M. Itano, *Phys. Rev. A* **20**, 1521 (1979).
- ¹⁷A. P. Kazantsev, *Usp. Fiz. Nauk.* **124**, 113 (1978) [*Sov. Phys. Usp.* **21**, 58 (1978)].
- ¹⁸W. H. Wing, *Phys. Rev. Lett.* **45**, 631 (1980).
- ¹⁹V. S. Letokhov and V. G. Minogin, *Opt. Commun.* **35**, 199 (1980).
- ²⁰J. Javanainen and S. Stenholm, *Appl. Phys.* **21**, 283 (1980).
- ²¹J. Javanainen and S. Stenholm, *Appl. Phys.* **24**, 71 (1980).
- ²²J. Javanainen and S. Stenholm, *Appl. Phys.* **24**, 151 (1981).
- ²³J. Javanainen, *Appl. Phys.* **23**, 175 (1980).
- ²⁴F. M. Kelly and M. S. Mathur, *Phys. Rev. A* **18**, 2135 (1978).
- ²⁵W. L. Wiese, M. W. Smith, and B. M. Miles, *Atomic Transition Probabilities*, Vol. II, Natl. Bur. Stand. (U.S.), Natl. Stand. Ref. Data Ser. 22 (U.S. G.P.O., Washington, D. C., 1969), p. 30.
- ²⁶For discussions of the classical and quantum Fokker-Planck and Langevin equations, see M. Sargent III, M. O. Scully, and W. E. Lamb, Jr., *Laser Physics* (Addison-Wesley, Reading, Mass., 1974).
- ²⁷See, for example, F. N. H. Robinson, *Noise in Electrical Circuits* (Oxford University Press, London, 1962), Chap. II.
- ²⁸See, for example, *Threshold Signals*, edited by James L. Lawson and George E. Uhlenbeck (Dover, New York, 1965), pp. 79–83.
- ²⁹J. Byrne and P. S. Farago, *Proc. Phys. Soc., London* **86**, 801 (1965).
- ³⁰G. Gräff and E. Klempt, *Z. Naturforsch.* **22a**, 1960 (1967); G. Gräff, E. Klempt, and G. Werth, *Z. Phys.* **222**, 201 (1969).
- ³¹A. A. Sokolov and Yu. G. Pavlenko, *Opt. Spectrosc.* (USSR) **22**, 1 (1967).
- ³²H. G. Dehmelt, *Nature* **262**, 777 (1976); R. S. Van Dyck, Jr., P. B. Schwinberg, and H. G. Dehmelt, in *New Frontiers in High-Energy Physics*, edited by B. M. Kursunoglu, A. Perlmutter, and L. F. Scott (Plenum, New York, 1978), p. 159; D. J. Wineland, *J. Appl. Phys.* **50**, 2528 (1979).
- ³³D. J. Wineland, R. E. Drullinger, J. C. Bergquist, and W. M. Itano, *Bull. Am. Phys. Soc.* **24**, 1185 (1979).
- ³⁴M. D. McGuire and E. N. Fortson, *Phys. Rev. Lett.* **33**, 737 (1974).
- ³⁵A. Einstein, *Phys. Z.* **18**, 121 (1917); English translation in *Sources of Quantum Mechanics*, edited by B. L. van der Waerden (North-Holland, Amsterdam, 1967).
- ³⁶V. Ben-Ya'acov, *Phys. Rev. D* **23**, 1441 (1981); C. H. Braden, R. F. Fox, and H. A. Gersch, *ibid.* **23**, 1455 (1981); A. Peres, *ibid.* **23**, 1458 (1981).
- ³⁷S. O. Rice, *Bell Syst. Tech. J.* **23**, 282 (1944).

Shift of $^2S_{1/2}$ hyperfine splittings due to blackbody radiation

Wayne M. Itano, L. L. Lewis, and D. J. Wineland

Frequency and Time Standards Group, Time and Frequency Division, National Bureau of Standards, Boulder, Colorado 80303

(Received 27 October 1981)

Frequency shifts of hyperfine splittings of $^2S_{1/2}$ states due to the blackbody radiation field are calculated. It is shown that they can be estimated from the dc hyperfine Stark shifts, which have previously been measured in the ground states of hydrogen and the alkali atoms. The shift at 300 K is large enough to be significant in primary Cs atomic beam frequency standards, and should be measurable. A simple method of calculating the hyperfine Stark shifts is described, which is based on the Bates-Damgaard method for determining radial matrix elements and the Fermi-Segrè formula for determining the contact hyperfine matrix elements. It is applied to Ba^+ and Hg^+ , for which no experimental data are yet available, and which are currently of interest for frequency standards.

The most accurate and stable atomic frequency standards are based on hyperfine transition frequencies in $^2S_{1/2}$ ground states, such as in ^{133}Cs , 1H , and ^{87}Rb . In this Communication, we estimate the temperature-dependent shift of $^2S_{1/2}$ hyperfine splittings due to the blackbody radiation field. We note that this effect is large enough to be observable in a Cs atomic beam apparatus. The shift of the Cs hyperfine splitting at $T = 300$ K from the unperturbed ($T = 0$ K) value causes a frequency offset which is significant for primary frequency standards.

According to the Planck radiation law,

$$E^2(\omega)d\omega = B^2(\omega)d\omega = \frac{8\alpha^3}{\pi} \frac{\omega^3 d\omega}{\exp(\omega/kT) - 1}, \quad (1)$$

where $E^2(\omega)d\omega [B^2(\omega)d\omega]$ is the squared amplitude of the blackbody electric (magnetic) field in a bandwidth $d\omega$ around ω . [Atomic units (a.u.) are used unless otherwise specified ($\hbar = m_e = e = 1$).] The mean-squared fields are

$$\begin{aligned} \langle E^2(t) \rangle &= \frac{1}{2} \int_0^\infty E^2(\omega) d\omega = \frac{4\pi^3}{15} \alpha^3 (kT)^4 \\ &= (8.319 \text{ V/cm})^2 [T(\text{K})/300]^4 \end{aligned} \quad (2)$$

and

$$\begin{aligned} \langle B^2(t) \rangle &= \frac{1}{2} \int_0^\infty B^2(\omega) d\omega \\ &= (2.775 \times 10^{-6} \text{ T})^2 [T(\text{K})/300]^4 \end{aligned} \quad (3)$$

Gallagher and Cooke¹ pointed out that these fields induce temperature-dependent shifts of transition frequencies in atoms and molecules through the ac Zeeman and Stark effects.^{2,3} They estimated the shifts in high- n Rydberg levels and some other systems. Blackbody frequency shifts have not yet been observed in any system.

The fractional blackbody ac Zeeman shift of the ground-state hyperfine splitting in H or Cs was estimated in Ref. 1 to be about 10^{-16} at $T = 300$ K. We have derived the following expression for this shift in any $^2S_{1/2}$ ground state, which is valid at zero dc magnetic field and at temperatures such that the peak of the blackbody spectrum is at a much higher frequency than the hyperfine frequency. We find

$$\begin{aligned} \frac{\delta\omega_{\text{hfs}}}{\omega_{\text{hfs}}} &\cong -\frac{\alpha^2}{24} (g_J - g_I)^2 \int_0^\infty \frac{B^2(\omega)}{\omega^2} d\omega \\ &= -(\pi/18) (g_J - g_I)^2 \alpha^5 (kT)^2 \\ &\cong -1.304 \times 10^{-17} [T(\text{K})/300]^2, \end{aligned} \quad (4)$$

where g_J and g_I are the electronic and nuclear g factors, respectively. In the last line, we have assumed that $g_J = 2$ and that $|g_I/g_J| \ll 1$.

At laboratory temperatures, the blackbody ac Stark shift of the hyperfine splitting, which has previously been neglected, is generally larger than the ac Zeeman shift. The ac hyperfine Stark shift due to an electric field of frequency ω is approximately equal to the dc hyperfine Stark shift due to a static field with the same rms values, if $\omega \ll \omega_{\text{res}}$, where ω_{res} is the lowest allowed electric dipole transition frequency. The correction is of order $(\omega/\omega_{\text{res}})^2$ and will be considered in more detail below. For the ground states of any of the alkali atoms, $(\omega/\omega_{\text{res}})^2 \leq 3 \times 10^{-3}$, where ω is the frequency corresponding to the peak of the blackbody spectrum at 300 K. Therefore, at 300 K, the blackbody ac hyperfine shift is approximately equal to the shift caused by a dc field of 8.3 V/cm.

The dc hyperfine Stark shift was first observed in Cs by Haun and Zacharias.⁴ Later, it was observed in

H (see Ref. 5) and other alkali atoms.⁶ These experiments measured the Stark shift of the $(F = I + \frac{1}{2}, M_F = 0) \rightarrow (F = I - \frac{1}{2}, M_F = 0)$ transition. They can be considered to be measurements of the scalar hyperfine polarizabilities, which are independent of M_F and the orientation of the electric field, since the contributions from the tensor polarizabilities can be estimated and are less than the experimental uncertainties.⁷ Only the scalar polarizability contributes to the blackbody ac Stark shift, because of the isotropy of the blackbody radiation. The fractional ac Stark shift of the Cs hyperfine splitting can be estimated from the measured dc hyperfine polarizability (see Table I of Ref. 6) and Eq. (2) to be $-1.69(4) \times 10^{-14} [T(\text{K})/300]^4$. This shift is large enough to affect the calibration of primary Cs frequency standards and therefore should be taken into account. For example, the fractional uncertainty of one primary Cs frequency standard (Cs 1 of the Physikalisch-Technische Bundesanstalt) is stated to be 6.5×10^{-15} , but has not been corrected for the blackbody shift.⁸

The theory of the dc hyperfine Stark shift of $^2S_{1/2}$ ground states is quite well developed, and the calculations are in good agreement with the experiments. The shift appears in the third order of perturbation theory, where the electric-field interaction is taken twice and the hyperfine interaction is taken once. For hydrogenic atoms and ions, an analytic solution has been obtained.^{9,10} Numerical calculations have been made for the neutral alkali atoms.¹¹⁻¹⁴ The shift in Li has been calculated without using perturbation theory by the spin-optimized self-consistent field method, with the electric field included in the Hamiltonian.¹⁵

We write the third-order perturbation expression for the scalar fractional dc hyperfine Stark shift of the $ns^2S_{1/2}$ state of an alkalilike atom or ion in the following form, which is independent of the spin and magnetic moment of the nucleus,

$$\delta\omega_{\text{hfs}}/\omega_{\text{hfs}} = -kE^2 = -(k_1 + k_2)E^2, \quad (5)$$

where

$$k_1 = \sum_{n''J} \frac{(n^2S_{1/2} || r || n''^2P_J)^2}{6[W(n''PJ) - W(nS)]^2} \quad (6a)$$

and

$$k_2 = - \sum_{n'',J,n',s} \frac{(n^2S_{1/2} || r || n''^2P_J)}{3[W(n''PJ) - W(nS)]} \times \frac{(n'^2S_{1/2} || r || n''^2P_J)\psi_{n',s}(0)}{[W(n'S) - W(nS)]\psi_{ns}(0)}. \quad (6b)$$

The reduced matrix elements of \vec{r} , the position operator of the valence electron, are defined with the conventions of Edmonds.¹⁶ We choose the phases of

the radial wave functions so that they are real. $W(n''PJ)$ and $W(nS)$ are the energies (not including the hyperfine interaction) of the n''^2P_J and the $ns^2S_{1/2}$ states, respectively, and $\psi_{ns}(0)$ is the value of $ns^2S_{1/2}$ wave function at the origin. The dc magnetic field is assumed to be so small that the Zeeman splitting is much less than the hyperfine splitting.

These formulas were derived by following the method of Feichtner *et al.*,¹³ in which the $ns^2S_{1/2}$ wave functions and energies are calculated to first order in the contact hyperfine interaction and the Stark shifts are then calculated by second-order perturbation theory. We ignore the spin-dipolar and quadrupole hyperfine interactions, since they contribute only to the tensor hyperfine polarizability. The terms k_1 and k_2 correspond, respectively, to the diagrams drawn in Figs. 1(a) and 1(b) of Lee *et al.*¹¹ and the "hfs" and "wave function" terms of Feichtner *et al.*¹³

We have developed a simple method of approximately evaluating Eqs. (6a) and (6b). We calculate the radial matrix elements using the Coulomb (Bates-Damgaard) approximation¹⁷ and the values of the s -state wave functions at the origin using the Fermi-Segré formula.¹⁸ We have used this method to calculate the scalar fractional ground-state hyperfine polarizabilities of Li, Na, K, Rb, and Cs and have obtained agreement with experiment to within 12% or better in all cases. The lowest three p states and the lowest five s states were included in the basis. In using the Bates-Damgaard method, the experimental term values were used to calculate the n^* values. For the p states, the centers of gravity of the two fine-structure levels were used for the term values. Table 3 of Ref. 17 was used with linear interpolation. In evaluating Eq. (6b), the phases of the wave functions must be kept consistent. If we define the s -state wave functions to be positive at the origin, then the sign of the radial integral involving the ns wave function, obtained from Table 3 of Ref. 17, must be reversed if n is even. This is because the Coulomb wave functions used by Bates and Damgaard, which are good approximations to the true wave functions outside the core, are positive for r greater than the last node [see Eq. (10) of Ref. 17] and the true ns wave functions have $n - 1$ nodes.

This method can be used for other atoms, for which no experimental data or calculations have yet been published, such as the singly ionized alkaline earths. We have carried out the calculations for the ground states of Hg^+ and Ba^+ , which are currently of interest for applications in stored-ion frequency standards.^{19,20} In atomic units, $k = 37.9$ for Hg^+ and $k = 902$ for Ba^+ . The conversion between atomic and laboratory units of E^2 is given by

$$E^2(\text{a.u.}) = 3.782 \times 10^{-20} E^2[(\text{V/cm})^2]. \quad (7)$$

At 300 K, the fractional blackbody ac hyperfine Stark Shifts are -9.9×10^{-17} and -2.4×10^{-15} for Hg^+ and Ba^+ , respectively. In rf trap experiments, the ac Stark shift due to the trapping fields may be larger.

The ground-state hyperfine shift due to an ac electric field of magnitude $E(t) = E(\omega) \cos \omega t$ can be obtained by the same method that was used to derive Eqs. (6a) and (6b), except that the formula for ac Stark shift is used. We assume that $\omega \ll \omega_{\text{res}}$, where ω_{res} is taken to be the frequency of the center of gravity of the fine-structure components of the first resonance line. If we assume that only the first excited p state makes a significant contribution, which is a good approximation for the alkali atoms, the shift is

$$\begin{aligned} \delta\omega_{\text{hfs}}/\omega_{\text{hfs}} &= -\frac{1}{2} [k_1[1 + 3(\omega/\omega_{\text{res}})^2] + k_2[1 + (\omega/\omega_{\text{res}})^2]] E^2(\omega) \\ &= -k \langle E^2(t) \rangle [1 + (3k_1/k + k_2/k)(\omega/\omega_{\text{res}})^2] \end{aligned} \quad (8)$$

The effect of the frequency distribution of the blackbody electric field is thus to increase $|\delta\omega_{\text{hfs}}/\omega_{\text{hfs}}|$ by the fractional amount

$$\epsilon = (3k_1/k + k_2/k) \langle \omega^2 \rangle / \omega_{\text{res}}^2 \quad (9)$$

relative to its value for a dc electric field of the same rms value. The mean-squared frequency of the

blackbody electric field $\langle \omega^2 \rangle$ is given by

$$\begin{aligned} \langle \omega^2 \rangle &= \int_0^\infty \omega^2 E^2(\omega) d\omega / \int_0^\infty E^2(\omega) d\omega \\ &= \frac{40\pi^2}{21} (kT)^2 \end{aligned} \quad (10)$$

Among the alkali atoms, ϵ is the largest for Cs, which has the lowest value of ω_{res} . If we take k_1 and k_2 from Ref. 11, then for Cs,

$$\epsilon = 1.4 \times 10^{-2} [T(\text{K})/300]^2, \quad (11)$$

which, at 300 K, is smaller than the experimental uncertainty in the dc hyperfine polarizability.

The blackbody shift could be observed in a Cs frequency standard which was modified so that the temperature of a tube surrounding the atoms in the resonance region could be varied. If the temperature were changed, for example, from 300 to 400 K, the fractional frequency shift would be 3.7×10^{-14} . If the frequency standard had the same frequency stability as NBS-6, the primary frequency standard of the United States,²¹ this shift could be determined to 30% or better in an averaging time of several hours.

This work was supported in part by the Air Force Office of Scientific Research and the Office of Naval Research.

¹T. F. Gallagher and W. E. Cooke, Phys. Rev. Lett. **42**, 835 (1979).

²M. Mizushima, Phys. Rev. **133**, A414 (1964).

³C. H. Townes and A. L. Schawlow, *Microwave Spectroscopy* (McGraw-Hill, New York, 1955), pp. 273-279.

⁴R. D. Haun and J. R. Zacharias, Phys. Rev. **107**, 107 (1957).

⁵E. N. Fortson, D. Kleppner, and N. F. Ramsey, Phys. Rev. Lett. **13**, 22 (1964); P. C. Gibbons and N. F. Ramsey, Phys. Rev. A **5**, 73 (1972); J. G. Stuart, D. J. Larson, and N. F. Ramsey, *ibid.* **22**, 2092 (1980).

⁶J. R. Mowat, Phys. Rev. A **5**, 1059 (1972).

⁷H. Gould, E. Lipworth, and M. C. Weisskopf, Phys. Rev. **188**, 24 (1969).

⁸G. Becker, IEEE Trans. Instrum. Meas. **29**, 297 (1980).

⁹C. Schwartz, Ann. Phys. (N.Y.) **6**, 156 (1959).

¹⁰P. G. H. Sandars, Proc. Phys. Soc. London **92**, 857 (1967).

¹¹T. Lee, T. P. Das, and R. M. Sternheimer, Phys. Rev. A **11**, 1784 (1975).

¹²N. L. Manakov, V. D. Ovsyannikov, and L. P. Rapoport, Opt. Spektrosk. **38**, 424 (1975) [Opt. Spectrosc. (USSR) **38**, 242 (1975)].

¹³J. D. Feichtner, M. E. Hoover, and M. Mizushima, Phys. Rev. **137**, A702 (1965).

¹⁴H. P. Kelly, R. L. Chase, G. R. Daum, and J. J. Chang,

Phys. Rev. A **8**, 2777 (1973).

¹⁵U. Kaldor, J. Phys. B **6**, 71 (1973).

¹⁶A. R. Edmonds, *Angular Momentum in Quantum Mechanics*, 2nd ed. (Princeton University, Princeton, N.J., 1974).

¹⁷D. R. Bates and A. Damgaard, Philos. Trans. R. Soc. London Ser. A **242**, 101 (1949).

¹⁸H. Kopfermann, *Nuclear Moments* (Academic, New York, 1958).

¹⁹F. G. Major and G. Werth, Phys. Rev. Lett. **30**, 1155 (1973); M. D. McGuire, R. Petsch, and G. Werth, Phys. Rev. A **17**, 1999 (1978); M. Jardino, M. Desaintfuscien, R. Barillet, J. Viennet, P. Petit, and C. Audoin, Appl. Phys. **24**, 107 (1981); M. D. McGuire, Bull. Am. Phys. Soc. **26**, 615 (1981); D. J. Wineland, W. M. Itano, J. C. Bergquist, and F. L. Walls, in *Proceedings of the 35th Annual Symposium on Frequency Control* (U.S. Army Electronics Command, Fort Monmouth, N.J., 1981).

²⁰R. Blatt and G. Werth, Z. Phys. A **299**, 93 (1981); F. L. Walls, D. J. Wineland, and R. E. Drullinger, in *Proceedings of the 32nd Annual Symposium on Frequency Control* (U.S. Army Electronics Command, Fort Monmouth, N.J., 1978).

²¹D. J. Wineland, D. W. Allan, D. J. Glaze, H. W. Hellwig, and S. Jarvis, IEEE Trans. Instrum. Meas. **25**, 453 (1976).

LASER COOLED, STORED ION EXPERIMENTS AT NBS AND POSSIBLE APPLICATIONS TO MICROWAVE AND OPTICAL FREQUENCY STANDARDS

D.J. Wineland, J.C. Bergquist, R.E. Drullinger, H. Hemmati, W.M. Itano and F.L. Walls

Frequency and Time Standards Group, Time and Frequency Division, National Bureau of Standards, Boulder, Colorado 80303, U.S.A.

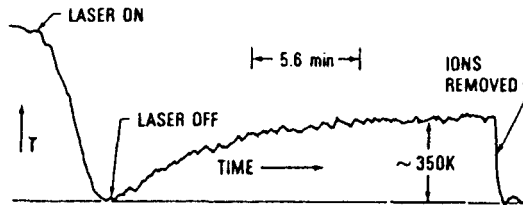
Abstract. - Research on stored ion frequency standards at the United States National Bureau of Standards is briefly discussed. We summarize past work and indicate directions of future research.

Introduction. - The purpose of this paper is to briefly summarize the work at the National Bureau of Standards (NBS) which has been directed towards realizing a frequency standard based on stored ions. The similar work of other groups [1] is not discussed here. This summary briefly describes past work and indicates future directions of research at NBS.

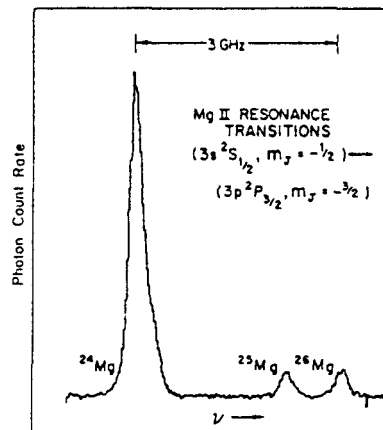
The stored ion work at NBS was initiated in the Fall of 1977. The goal of this work has been to devise a technique for realizing a frequency standard whose accuracy would be significantly better than that of the Cs atomic beam frequency standard. With this in mind, the ion storage method [2] was pursued because it can provide long confinement times without the usual perturbations associated with confinement (e.g., the wall shift in the H-maser).

The initial work was directed toward realizing laser cooling of ions [3], since this would provide a way to substantially suppress the frequency shift due to the second-order Doppler or time-dilation effect. For these initial experiments, Mg^+ ions were stored in a Penning trap. Mg^+ ions were chosen, since the electronic structure is fairly simple (i.e., like that of neutral alkali atoms) and required a laser source at 280 nm. The Penning trap was chosen because the residual heating mechanisms (at least for a cloud of ions) are less than for the rf trap.

In the first experiments [4], the temperature of the ions was monitored directly by the bolometric technique [5]. Figure 1 shows the Mg^+ ion temperature vs. time for a fixed laser detuning of about -2 GHz from the $3s\ ^2S_{1/2} (M_J = -1/2) \rightarrow 3p\ ^2P_{3/2} (M_J = -3/2)$ transition frequency. The sensitivity of these temperature measurements was limited by noise in the electronic detection. Therefore, subsequent measurements detected the temperature by observing the fluorescence light scattered by the ions and measuring the Doppler widths of the optical lines [6].



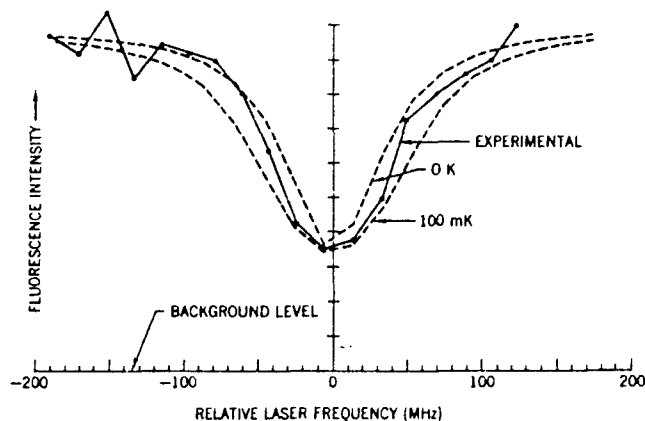
1. Ion temperature vs. time when laser cooling is applied for fixed laser detuning of -2 GHz. The ions were initially heated above equilibrium temperature with the laser. Laser cooling was then applied on the $3s\ 2S_{1/2}\ (M_J = -1/2) \rightarrow 3p\ 2P_{3/2}\ (M_J = -3/2)$ transition for a fixed time until a temperature approaching 0 K (< 40 K) was achieved. After the laser is turned off, the ions rethermalize to the ambient temperature.



2. Spectra of one Zeeman component of laser cooled $^{24,25,26}\text{Mg}^+$. The room temperature Doppler width of these lines is about 3 GHz. Only the $^{24}\text{Mg}^+$ is directly laser cooled. The $^{25}\text{Mg}^+$ hyperfine structure has been optically pumped resulting in the observation of only the $(M_J = -1/2, M_I = -5/2) \leftrightarrow (M_J = -3/2, M_I = -5/2)$ component.

Figure 2 shows the fluorescence light from a "low" power laser which is swept in frequency across the $3s\ 2S_{1/2}\ (M_J = -1/2) \rightarrow 3p\ 2P_{3/2}\ (M_J = -3/2)$ optical transitions of the three naturally occurring Mg^+ isotopes. At the same time, a higher power (approximately 10 times higher power) fixed-frequency laser is tuned to the low frequency side of the $^{24}\text{Mg}^+$ transition to keep the sample cold. (Note that the $^{25}\text{Mg}^+$ and $^{26}\text{Mg}^+$ isotopes are not directly laser cooled, but are cooled by Coulomb collisions with the cooled $^{24}\text{Mg}^+$.)

Lowest temperatures have so far been obtained for single ions [7] where cyclotron-magnetron "temperatures" of approximately 0.05 K have been obtained for a single $^{24}\text{Mg}^+$ ion. Figure 3 shows the double-resonance detection of the $^2S_{1/2} (M_J = -\frac{1}{2}) \rightarrow ^2P_{3/2} (M_J = -\frac{1}{2})$ optical transition in a single $^{24}\text{Mg}^+$ ion. Our theoret-

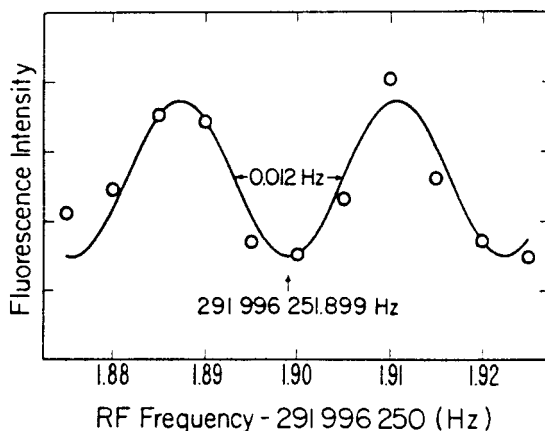


3. Double-resonance curve of a single $^{24}\text{Mg}^+$ ion. On the vertical axis is the fluorescence from a fixed-frequency laser (power approximately $5 \mu\text{W}$) tuned to the $(^2P_{3/2}, M_J = -3/2) \leftarrow (^2S_{1/2}, M_J = -1/2)$ transition. Each point represents a 10 s integration; the connecting lines are only for clarity. The horizontal axis is the frequency of the low-power ($\ll 5 \mu\text{W}$) laser which is continuously scanned across the $(^2P_{3/2}, M_J = -1/2) \leftarrow (^2S_{1/2}, M_J = -1/2)$ transition. The dashed curves are simulations of fluorescence at $T = 0 \text{ K}$ and 100 mK (no added noise). The solid curve is experimental data. From these data, we conclude $T = 50 \pm 30 \text{ mK}$.

tical predictions [8, also Itano, Wayne M., and Wineland, D. J., to be published] indicated that lower temperatures should be obtained; possible limitations may be caused by the presence of impurity ions in the trap. Future experimental investigations are planned; a new apparatus with improved fluorescence collection efficiency is being constructed.

In the Penning trap, ions are unstable with respect to collisions with background gas; that is, collisions cause the magnetron orbits to increase in size and this leads to ion loss. This process can be reversed by a technique which is formally equivalent to the usual laser cooling [4,6, also Itano, Wayne M., and Wineland, D. J., to be published]; specifically, the magnetron energy is increased and the orbit size reduced by laser scattering by spatially tailoring the laser beam. The result is that infinite confinement times are in principle possible in the Penning trap.

The ground-state structure of Mg^+ ions has been measured by double-resonance schemes where changes in the laser fluorescence can be used to monitor ground-state rf and microwave transitions [9,10]. This has led to a measurement of the ground-state hyperfine constant ($A = -596.254\ 376(54)$ MHz) and g_I/g_J ($= 9.299\ 484(75) \times 10^{-5}$) in $^{25}Mg^+$. For this ion, the derivative of the ground-state $(M_I, M_J) = (-3/2, 1/2)$ to $(-1/2, 1/2)$ transition with respect to magnetic field B_0 goes to zero at $B_0 \cong 1.24$ T. The corresponding resonance ($\nu \cong 292$ MHz) was observed at this field with linewidths as small as 0.012 Hz ($Q \cong 2.4 \times 10^{10}$) by implementing the Ramsey interference method with two coherent rf pulses separated in time by 41.4 s (see figure 4). We expect that such narrow resonance lines (and even narrower lines) can be observed in other ions (e.g., Hg^+) with higher ground-state transition frequencies. This could then yield extremely high Q ($> 10^{12}$) in microwave transitions which would be valuable for frequency standard applications.

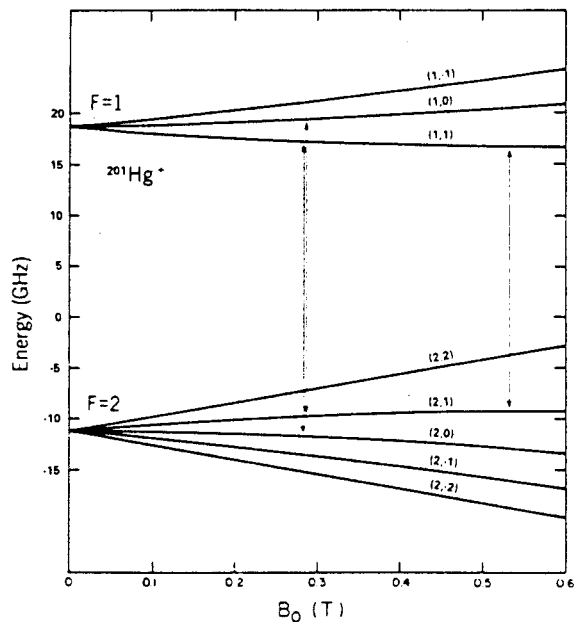


4. Rf resonance curve for the $(m_I, m_J) = (-3/2, 1/2)$ to $(-1/2, 1/2)$ ground-state hyperfine transition in $^{25}Mg^+$. Each circle represents the average of four measurements (total detection fluorescence integration time of 16 s). The oscillatory lineshape results from the use of the Ramsey method to drive the transition. Two coherent rf pulses of duration $\tau = 1.02$ s separated by $T = 41.4$ s were applied. The vertical arrow marks the central minimum, which corresponds to the resonance frequency.

In some double-resonance schemes, it is possible to scatter many photons for each microwave or optical "clock" photon absorbed. (In Ref. 10, a factor of about 10^6 was achieved.) This "quantum multiplication" should allow the signal-to-noise ratio in double-resonance detection schemes to be limited only by the statistical noise in the number of ions that have made the "clock" transition [9,11]. This will be extremely important for frequency standards based on ions where the number of ions is necessarily rather small.

Because of the above results, we have initiated work at NBS to realize microwave [11] and optical [11,12] frequency standards based on Hg^+ ions stored in a Penning trap.

The proposed microwave frequency standard is based on the $(F, M_F) = (1,1) \leftrightarrow (2,1)$ ground-state hyperfine transition in $^{201}\text{Hg}^+$, which is field-independent to first order at $B_0 \cong 0.534$ T, with frequency $\cong 25.9$ GHz (see figure 5). If B_0 can be controlled to slightly better than 0.1 ppm over the ion cloud, the fractional frequency shift can be kept below 10^{-15} . (At the "field-independent" point $\Delta\nu/\nu_0 = (\Delta B/B_0)^2/6$). The velocity in the magnetron motion will give a second-order Doppler shift; it should be controllable to 10^{-15} (see below). All other systematic shifts, such as those due to collisions, the trap electric fields, or thermal radiation appear to be less than 10^{-15} [11]. It should be possible to observe the transition with a Q of 2.6×10^{12} or better, by using optical pumping and detection techniques similar to those demonstrated with $^{25}\text{Mg}^+$. The accuracy of this standard could be better than 10^{-15} .



5. Ground-state hyperfine energy levels of $^{201}\text{Hg}^+$ vs. magnetic field. States are designated by the (F, M_F) representation. Three transitions are indicated at the fields where the transition frequencies are independent of magnetic field to first order.

The proposed optical frequency standard [11,12] is based on the two-photon-allowed $5d^{10} \tilde{e} \ ^2S_{1/2} \rightarrow 5d^9 6s^2 \ ^2D_{5/2}$ Hg^+ transition, which has a natural Q of 7.4×10^{14} . The second-order Doppler effect can be eliminated by driving the transi-

tion with counter-propagating 563.2 nm laser beams. Hyperfine-Zeeman components, whose magnetic field derivatives vanish at particular values of B_0 , exist in $^{199}\text{Hg}^+$ and $^{201}\text{Hg}^+$. The two-photon transition can be detected with high efficiency by using the 194.2 nm fluorescence intensity as a probe of the ground-state population. Taking full advantage of the high Q transition would require a laser with linewidth less than 1 Hz, which does not exist at present. However, linewidths $\lesssim 100$ Hz appear feasible and could be used for initial experiments. If the laser linewidth is less than the natural linewidth, then the ac Stark shift is about 2×10^{-15} near saturation. All other systematic shifts appear to be less than 10^{-15} . We note that the ac Stark shift can be made negligibly small by driving the single photon $^2S_{1/2} \rightarrow 2D_{5/2}$ quadrupole transition. In this case, it will be desirable to use a single ion that can be confined to approximately realize the Dicke criterion in order to suppress first-order Doppler effects.

The method currently being investigated for generating the required 194.2 nm radiation for laser cooling and optical detection is sum-frequency mixing in a KB5 crystal of the output of a 792 nm single-mode cw ring dye laser and the second harmonic, generated in an ADP crystal, of the output of a 514 nm stabilized, single-mode cw Ar^+ laser.

For the microwave frequency standard, it is especially desirable to use the largest possible number of ions in order to increase signal to noise. Unfortunately, as the number of ions is increased, the second-order Doppler shift due to magnetron rotation also increases, which will, therefore, limit the number of ions to about 10^5 or less for 10^{-15} accuracy [11]. (A similar problem exists for the rf trap due to the kinetic energy in the micromotion [13]). Therefore, studies will also be devoted to methods of controlling the density and shape of the ion clouds.

We gratefully acknowledge the support of the United States Air Force Office of Scientific Research and the Office of Naval Research.

References.

- [1] See for example the following references and other references therein: Major, F. G., and Werth, G., Phys. Rev. 30 (1973) 1115; Dehmelt, H., Proc. 35th Ann. Symp. Freq. Control, Philadelphia, Pa., June 1981; McGuire, M. D., Petsch, R., and Werth, G., Phys. Rev. A. 17 (1978) 1999; McGuire, M. D., Bull. Am. Phys. Soc. 26 (1981) 615; Jardino, M., Desaintfuscién, M., Barillet, R., Viennet, J., Petit, P., and Audoin, C., Appl. Phys. 24 (1981) 1. Neuhauser, W., Hohenstatt, M., Toschek, P. E., and Dehmelt, H., Phys. Rev. A22 (1980) 1137; Javanainen, J., and Stenholm, S., Appl. Phys. 24 (1981) 151.
- [2] Dehmelt, H. G., Advances At. Mol. Phys. 3 (1967) 53 and 5 (1969) 109.
- [3] Wineland, D. J., and Dehmelt, H. G., Bull. Am. Phys. Soc. 20 (1975) 637; Hänsch, T. W., and Schawlow, A. L., Opt. Commun. 13 (1975) 68.
- [4] Wineland, D. J., Drullinger, R. E., and Walls, F. L., Phys. Rev. Lett. 40 (1978) 1639.

- [5] Dehmelt, H., and Walls, F., Phys. Rev. Lett. 21 (1968) 127. Wineland, D. J., and Dehmelt, H. G., J. Appl. Phys. 46 (1975) 919.
- [6] Drullinger, R. E., Wineland, D. J., Bergquist, J. C., Appl. Phys. 22 (1980) 365.
- [7] Wineland, D. J., and Itano, Wayne M., Phys. Lett. 82A (1981) 75.
- [8] Wineland, D. J., and Itano, Wayne M., Phys. Rev. A20 (1979) 1521.
- [9] Wineland, D. J., Bergquist, J. C., Itano, Wayne M., and Drullinger, R. E., Opt. Lett. 5 (1980) 245.
- [10] Itano, Wayne M., and Wineland, D. J., Phys. Rev. A24, (1981) 1364.
- [11] Wineland, D. J., Itano, Wayne M., Bergquist, J. C., and Walls, F. L., Proc. 35th Ann. Symp. Freq. Control, Philadelphia, Pa., June, 1981.
- [12] Bender, P. L., Hall, J. L., Garstang, R. H., Pichanick, F. M. J., Smith, W. W., Barger, R. L., and West, J. B., Bull. Am. Phys. Soc. 21 (1976) 599.
- [13] Wineland, D. J., Proc. Conf. on Prec. Meas. and Fundamental Constants, Gaithersburg, Md. June, 1981.

Spectroscopy of Stored Ions

D. J. Wineland

Frequency and Time Standards Group, Time and Frequency Division
National Bureau of Standards, Boulder, CO 80303

The benign environment and long confinement times obtained with ion storage techniques have led to some unique experiments in the area of precision measurements and fundamental constants. This is perhaps epitomized by the single electron g factor measurements at the University of Washington in which a precision of 4 parts in 10^{11} has been attained. Now, use of lasers to cool stored ions has allowed the experimentalist to approach the goal of unperturbed atomic ions nearly at rest; most recently, spectroscopy has been performed on single "cold" trapped ions. Stored ion experiments in the area of precision measurements and fundamental constants will be briefly reviewed. These include experiments on e^-/e^+ g factors, mass spectroscopy, lifetimes, and atomic spectroscopy. The intent is to emphasize the unique environment provided by ion storage techniques for these measurements.

Key words: atomic ion spectroscopy; electron g factor; fundamental constants; ion storage; mass spectroscopy; precision measurements.

1. Introduction

The purpose of this paper is twofold. The first purpose is to outline "trapped ion" experiments of the last decade which have contributed to the area of precision measurements and fundamental constants. The second purpose is to emphasize why the stored ion "environment" is particularly well suited to the area of precision measurements.

The main advantage of the stored ion technique is that the ideal of an unperturbed species at rest in space is approached to a high degree. Specifically, charged particles such as electrons and atomic ions can be stored for long periods of time (essentially indefinitely) without the usual perturbations associated with confinement (for example the perturbations due to collisions with walls or buffer gasses in a traditional optical pumping experiment). These unique properties were exploited most notably by Dehmelt and co-workers [1] before 1970; since then, that group and others have continued to extend these techniques with dramatic results.

Unfortunately, there is a price to be paid for this property of long storage times with small perturbations—the number of particles that can be stored is typically small ($\leq 10^6$ for a "trap" with centimeter dimensions); the resulting low densities are governed by the competition between space charge repulsion and the confining electromagnetic forces obtained under normal laboratory conditions. These low numbers, of course, require very sensitive detection techniques and preclude many types of experiments—for example spectroscopic experiments on complex molecular ions where only a small fraction of the ions is in a given state. Although some effort has been made to increase the number of ions by space charge neutralization [2, 3] and trap "arrays" [4], these methods introduce other experimental complications. In spite of the low numbers obtained, sensitive techniques have been developed to detect simple species such as electrons and atomic ions so that *single* electrons [5, 6] and ions [7, 8] have been observed.

Since the intent is to discuss experiments relating to precision measurements and fundamental constants,

many interesting experiments using stored ion techniques are not discussed in this paper. The reader is referred elsewhere to experiments on, for example, photo-detachment [9, 10], chemical reactions [11], electron-ion recombination [12], charge transfer [13, 14], and non-neutral plasma studies [15]. Also, more general reviews are available [1, 16, 17].

In Sec. 2, methods of trapping are briefly reviewed. In Secs. 3–6, experiments on electrons/positrons, mass spectroscopy, atomic spectroscopy, and lifetime measurements are described with emphasis on the ion's environment. In the last section, speculations about other future experiments are made.

2. Ion Trapping Methods

Four types of traps have been useful: the rf (or Paul) trap, the Penning trap, and electrostatic and magnetostatic traps. These traps and their relevant properties are briefly described here. More detailed descriptions are given elsewhere [1, 16].

2.1 The rf Quadrupole Trap

The ideal rf or Paul [18] trap uses hyperbolic electrodes in a vacuum apparatus as shown in Fig. 1. These electrodes are symmetric about the z axis, so we can describe the potential in cylindrical coordinates. If an alternating voltage of frequency Ω is applied between the endcaps and ring electrode, then the instantaneous potential inside the trap is given by (following the notation of Ref. [1]):

$$\phi(r, z) = A(r^2 - 2z^2), \quad A = A_0 \cos \Omega t. \quad (1)$$

An ion experiences an rf electric field such that its motion (the "micromotion") is 180° out of phase with respect to the electric force. Because the electric field is inhomogeneous, the force averaged over one period ($T = 2\pi/\Omega$) of the micromotion is in a direction of weaker field amplitude (independent of the sign of the charge), i.e.,

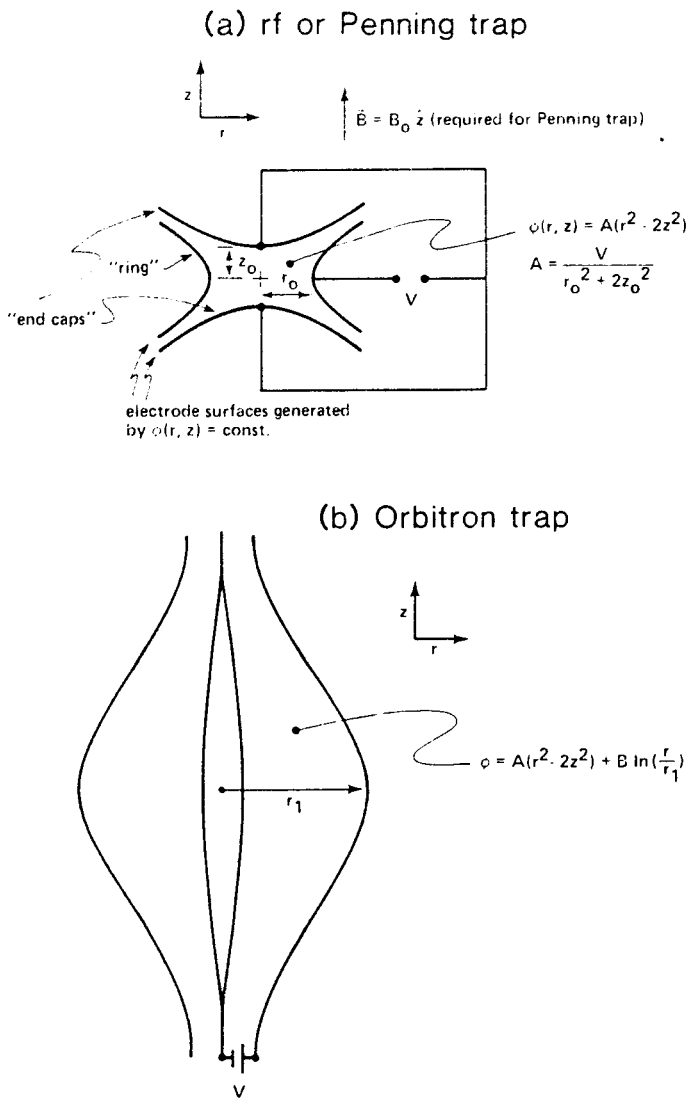


FIGURE 1. Electrode configuration for rf, Penning, and orbitron ion traps. All electrode surfaces are figures of revolution about the axial (z) direction. In a practical orbitron trap, it is desirable to make the center electrode as thin as possible to reduce ion loss from collisions.

towards the center of the trap. For Ω sufficiently high, this restoring force gives rise to a pseudopotential

$$\Psi(r, z) = \frac{eA_0^2}{M\Omega^2} [(\bar{r})^2 + 4(\bar{z})^2]$$

where \bar{r} and \bar{z} are the positions of the ion averaged over T , e is the ion charge, and M is the ion mass. The resulting "secular" motion is

$$\begin{aligned} \bar{z} &= \bar{z}_0 \cos(\bar{\omega}_z t + \phi_z) \\ \bar{x} &= \bar{x}_0 \cos(\bar{\omega}_r t + \phi_x) \quad \bar{\omega}_z = 2\bar{\omega}_r = \frac{2\sqrt{2}eA_0}{M\Omega} \\ \bar{y} &= \bar{y}_0 \cos(\bar{\omega}_r t + \phi_y) \end{aligned}$$

In more detail, we have for the z motion:

$$z = \bar{z}_0 \left[1 + \frac{\sqrt{2}\bar{\omega}_z}{\Omega} \cos \Omega t \right] \cos \bar{\omega}_z t,$$

where we require $\Omega/\bar{\omega}_z \gg 1$.

For ease of comparison with the Penning trap, it will be useful to consider the case of a spherical pseudo-potential well in the rf trap. This is accomplished by

simultaneously applying a static potential between the ring and endcaps so that

$$\phi = (U_0 + A_0 \cos \Omega t)(r^2 - 2z^2).$$

If we choose

$$\begin{aligned} U_0 &= \frac{e}{M\Omega^2} A_0^2, \quad \text{then} \\ \Psi(r, z) &= \frac{2eA_0^2}{M\Omega^2} [(\bar{r})^2 + (\bar{z})^2]. \end{aligned} \quad (2)$$

In this case:

$$\begin{aligned} z &= \bar{z}_0 \left[1 + \frac{2\bar{\omega}_z}{\Omega} \cos \Omega t \right] \cos \bar{\omega}_z t \\ \begin{Bmatrix} \bar{x} \\ \bar{y} \end{Bmatrix} &= \begin{Bmatrix} \bar{x}_0 \\ \bar{y}_0 \end{Bmatrix} \left[1 + \frac{\bar{\omega}_z}{\Omega} \cos \Omega t \right] \cos \bar{\omega}_r t, \end{aligned} \quad (3)$$

where $\bar{\omega}_z = \bar{\omega}_r = \frac{2eA_0}{M\Omega}$.

Approximate experimental values for stored atomic ions are such that $r_0 \approx 1$ cm, A_0 is a few hundred volts/cm², $\Omega/2\pi$ is a few MHz, and $\Omega/\bar{\omega}_z \approx 10$.

If the secular motion is "cold" then we expect the maximum density of ions to be given when the force from the space charge potential ϕ_i cancels that due to the trap. In this case, for the pseudo-potential given by Eq. (2), the ion cloud is a uniformly charged sphere of charge density ρ with internal potential

$$\phi_i = (2/3) \pi \rho (r^2 + z^2).$$

Therefore for a well with $2eA_0^2/M\Omega^2 = 10$ V/cm², the condition $\phi_i = -\Psi(r, z)$ gives a density $n = 3.3 \times 10^7$ /cm³. In practice, attainable densities are approximately 1 to 2 orders of magnitude lower due to "rf heating"—a process which couples kinetic energy from the micromotion into the secular motion. One way this happens is through collisions with background gas. However, at high vacuum other coupling mechanisms can occur partly due to the presence of impurity ions or imperfections in the trap electrodes. This process can give kinetic energies of ions of as much as electron volts and shortened storage times of less than 1 s. If one uses a light buffer gas such as He to provide viscous damping [1] then storage times of many days can be achieved [19, 20]. However, this increases perturbations due to collisions; therefore, for experiments on large numbers of ions in an rf trap, there appears to be a practical trade-off between the temperature of the ions and possible perturbations due to collisions with a cooling buffer gas. However, this is not a fundamental limitation and one hopes it will be solved in the future.

We note that in principle, densities could be increased by increasing the rf field strengths; in practice, higher densities (close to 10^9 /cm³ [21]) have been achieved by decreasing the electrode dimensions. This, of course, may not increase the ion number and it also may increase the rf heating because the field imperfections may be relatively larger.

It is interesting to note that the methods proposed for trapping of neutral particles in laser beams [22] are very analogous to the rf trapping of charged particles. In the laser beam case, the outer atomic electron experiences net forces in the (inhomogeneous) laser field. But since the electron is bound to the nucleus, dispersive effects

occur. If the laser is tuned above the frequency of an electronic transition, similar to an ion in a rf trap, the atom is forced to regions of low field intensity. If the laser is tuned below resonance, the atom is forced to regions of high field intensity.

2.2 The Penning Trap

The Penning trap [23] uses the same electrode configuration as the rf trap (Fig. 1) but now A in Eq. (1) is a constant U_0 such that the charged species see a static potential well along the z axis. We have $\phi_T = U_0(r^2 - 2z^2)$. This causes a repulsive potential in the $x-y$ plane which can be overcome by superimposing a static magnetic field along z ($B = B_0\hat{z}$). For a single ion in the trap, the equations of motion are [1, 24]

$$\begin{aligned} \ddot{z} + \omega_z^2 z &= 0, \\ \omega_z^2 &= \frac{4eU_0}{M} = \frac{4eV_0}{M(r_0^2 + 2z_0^2)}, \\ \ddot{\mathbf{r}} &= \frac{1}{2}\omega_z^2 \mathbf{r} - i\omega_c \dot{\mathbf{r}}, \\ \omega_c &= \frac{eB_0}{Mc}, \end{aligned}$$

where

$$\mathbf{r} = x + iy.$$

Therefore

$$z = z_0 \cos \omega_z t \text{ and } \mathbf{r} = \mathbf{r}_c e^{-i\omega_c t} + \mathbf{r}_m e^{-i\omega_m t} \quad (4)$$

where

$$\begin{Bmatrix} \omega_c \\ \omega_m \end{Bmatrix} = \frac{1}{2} \omega_c \begin{Bmatrix} + \\ - \end{Bmatrix} [(\omega_c/2)^2 - \omega_z^2/2]^{1/2}. \quad (5)$$

Some useful expressions are:

$$\omega^2 + \omega_z^2/2 = \omega_c \omega \quad (\omega = \omega_m \text{ or } \omega_c), \quad (6a)$$

$$\omega_c' + \omega_m = \omega_c, \quad (6b)$$

$$\omega_c' \omega_m = \omega_z^2/2. \quad (6c)$$

Typical operating conditions in a Penning trap are such that for electrode spacings about 1 cm, V_0 is a few volts and B_0 is larger than a few tenths of a tesla. The required large magnetic field can either be an advantage or disadvantage, depending on the experiment. It should be noted that the magnetron motion (the $\mathbf{r}_m e^{-i\omega_m t}$ term) is in an unstable equilibrium in the trap. For example, if collisions with background neutrals occur, the ions will diffuse out of the trap. (When the magnetron velocity is much less than the velocity of the neutrals, \mathbf{r}_m random walks in the $x-y$ plane with step size $\sim r_c$.) This is a potential disadvantage when compared to the rf trap for which all three degrees of freedom (x, y, z) are in stable equilibrium. In practice however, this is not a limitation because ions can be stored for days in a room temperature apparatus [25] and electrons for weeks [5] in an 80 K apparatus. Moreover, the technique of sideband or radiation pressure cooling [6, 21, 25, 26] can reverse this diffusion process.

If the voltage V_0 applied to the electrodes becomes too high, then the radial electric field is high enough to overcome the $e\mathbf{v} \times \mathbf{B}/c$ magnetic force and the ions strike the ring electrode in exponentially increasing orbits (argument of square root in Eq. (5) becomes negative). For singly ionized atoms, the voltage where this occurs is

given by $V_c \approx 1200 B_0^2 (r_0^2 + 2z_0^2)/M$ where V_c is in volts, B_0 in tesla, M in u (atomic mass units) and dimensions in cm. This same mechanism limits the densities achievable in the Penning trap since space charge also gives radial electric fields. If the axial and cyclotron temperatures are low enough, then we can approximate the equilibrium distribution of the ion cloud [27] by a uniformly charged ellipsoid which has an (internal) potential of:

$$\phi_i(r) = (2/3) \pi \rho (ar^2 + bz^2)$$

where a and b are constants. The \mathbf{r} motion of an individual ion is now given by Eq. (4) with

$$\begin{Bmatrix} \omega_c' \\ \omega_m \end{Bmatrix} = \frac{\omega_c}{2} \begin{Bmatrix} + \\ - \end{Bmatrix} \left[\left[\frac{\omega_c}{2} \right]^2 - \frac{\omega_z^2}{2} - \frac{4\pi e \rho a}{3M} \right]^{1/2} \quad (7)$$

where ω_z is the axial frequency for a single ion in the trap. For a spherical distribution, $a = b = 1$; and the maximum density allowable (argument of square root term kept positive) is given by (using $\phi_i(z) = -\phi_T(z)$):

$$n = \frac{\rho}{e} < \frac{B_0^2}{8\pi c^2 M}$$

or

$$n < 2.7 \times 10^9 B_0^2 / M$$

where B_0 is in tesla and M in u. For $B_0 = 1$ T, $M = 100$ u, $n < 2.7 \times 10^7/\text{cm}^3$ which is similar to the rf trap case. In experiments at the National Bureau of Standards (NBS), densities within a factor of about 3 of the theoretical maximum have been observed as indicated by the space charge shifted magnetron rotation frequency.

2.3 Electrostatic Traps

The orbitron trap [28] has the advantage of simplicity and although lifetimes are observed to be relatively short, precision lifetime and spectroscopic measurements have been made by Prior and his colleagues at Berkeley [29, 30].

The orbitron trap is purely electrostatic and has axial symmetry as shown in Fig. 1b. A potential which is useful is given by the general form [31]:

$$\phi = A(r^2 - 2z^2) + B \ln(r/r_1),$$

because a harmonic well is provided along the z axis. The equations of motion for the $x-y$ plane are not solvable analytically, but the motion is basically composed of precessing orbits about the z axis [32]. Storage times in such a trap should be shorter because a single collision with a background neutral is sufficient to cause an ion to collide with the center electrode and be lost. Also the cooling discussed in Sec. 6 would be more difficult to realize. Nevertheless, with a trap whose electrodes approximate equipotentials of this function, trapping times of about one second were achieved by Knight [31] at a pressure of 10^{-6} Pa ($\approx 10^{-8}$ Torr). (The center electrode was a 100 μm dia. wire.)

An axial magnetic field superimposed along the z axis has been investigated theoretically [33]; in this case, storage times should increase dramatically. Ions will eventually be lost by diffusing in towards the center electrode; therefore, storage times should be comparable to that of the Penning trap. However, the frequency of the drift motion about the center of the trap will depend on the distance from the z axis; for the Penning trap this drift (magnetron) frequency is independent of radial posi-

tion (neglecting space charge) and may be part of the reason for the slow evolution of the ion cloud under the influence of the ion-ion collisions. A possible advantage over the Penning trap is that experiments may be possible at much lower magnetic fields [33].

2.4 Magnetostatic Traps

Magnetic bottles are of course used extensively for plasma confinement and also in ion spectroscopy. The disadvantage in terms of spectroscopy appears to be that rather large magnetic field inhomogeneities are required for trapping, thus causing inhomogeneities and broadening in paramagnetic ion line shapes. The main application in terms of precision measurements has been the Michigan e^+/e^- experiments [34]; these are reviewed by A. Rich at this conference.

3. e^+/e^- $g-2$ Measurements in a Penning Trap

This experiment has been pursued primarily by the groups of Dehmelt at the University of Washington, and Gräff at Mainz [35-37]. Only the Washington single electron experiment [6] will be discussed here, since its accuracy significantly exceeds that of the experiments on clouds of electrons [35-38]. Experiments on clouds of electrons are susceptible to rather large and difficult to measure space charge shifts. For example, the fractional shift of the cyclotron frequency of one electron due to another electron a distance r away (in a direction perpendicular to the magnetic field) is approximately given by [39]

$$\frac{\Delta\omega}{\omega_0} = \frac{1}{2} \frac{e}{m\omega_c^2} \left[\frac{1}{r} \frac{\partial}{\partial r} (rE_r) \right]$$

where m is the electron mass, ω_c is the cyclotron frequency, and E_r is the electric field at one electron from the other. For a magnetic field of 1 T, and $r = 100 \mu\text{m}$, $\Delta\omega/\omega_0 = 4.1 \times 10^{-9}$ which gives a shift of about 4 ppm in $g-2$. In 1971, the Michigan group had measured the electron $g-2$ to 3 ppm [40]; this result and the problems associated with the space charge shifts led the Washington group to develop an experiment based on single electrons. A complete account of this experiment is given in Refs. [6, 41]. A simpler account is given in Ref. [42].

Briefly, a single electron can be detected [5, 42, 43] by monitoring the currents induced in the electrodes by the axial (z) oscillation at frequency ω_z . The harmonically bound electron is equivalent to a series L-C circuit which shunts the electrodes [5]; this L-C oscillator can be phase locked to an external oscillator by feeding back on the trap voltage V_0 [6]. It is useful to think of the single electron bound to the Penning trap as a one electron pseudo atom whose "nucleus" is the earth (to which the Penning trap is fixed), thus the name "geonium" [6]. The quantum mechanical solution for the energy levels of this "atom" are given by:

$$E/h = m\nu_s + (n + 1/2)\nu_c + (k + 1/2)\nu_z - (q + 1/2)\nu_m$$

where m is the spin quantum number ($m = \pm 1/2$) and n , k , and q are the cyclotron, axial and magnetron quantum numbers ($n, k, q = 0, 1, 2 \dots$). (The magnetron energy is mostly potential energy and is negative.)

In the $g-2$ and e^+/e^- mass ratio experiments it is necessary to detect the occurrence of spin flip and cyclotron transitions. This can be accomplished by superimposing a weak magnetic bottle centered on the trap such that the field is [6]:

$$B = (B_0 + \beta(z^2 - r^2/2))\hat{z} - \beta zy\hat{y} - \beta zx\hat{x}$$

The spin, cyclotron, and magnetron magnetic moments interact with this magnetic bottle to shift the axial frequency by an amount

$$\delta\nu_z = [m + n + 1/2 + (\nu_m/\nu_c)q]\delta$$

$$\delta = \mu_B \beta / (2\pi^2 m \nu_z)$$

For $\nu_z = 60$ MHz and $\beta = 0.012$ T/cm², $\delta = 1$ Hz, therefore for example, spin flip transitions would show up as 1 Hz changes in ν_z or as an accompanying step increase in feedback voltage to the locked axial resonance [6].

For reproducibility, it was desirable to have the electron at the center of the trap. This could be accomplished by sideband excitation [6, 26, 44, 45] as follows: with the (damped) axial motion driven by an inhomogeneous rf field of frequency $\nu_z + \nu_m$, the electron sees a sideband at ν_z because of the magnetron motion through the rf field. Therefore the electron absorbs quanta of energy $h(\nu_z + \nu_m)$ and reradiates (by the damping) quanta of energy $h\nu_z$. The deficit, $h\nu_m$, goes into the magnetron energy which shrinks the magnetron orbit. In principle, this technique allows for infinite storage times.

The electron $g-2$ has now been measured with an accuracy of 0.04 ppm [46] and the positron $g-2$ to 0.05 ppm [47]. The details of these remarkable experiments are described in Ref. [6]; rather than give a complete description of the experiments, only the experimental environment is described here. From Ref. [6], the cyclotron degree of freedom was radiatively thermalized to 4 K. The axial temperature was somewhat higher. Pressure was estimated to be as low as 10^{-12} Pa so that collisions with background gas could be neglected. At temperatures near 4 K, axial excursions of 0.1 mm and cyclotron orbit sizes of ~ 60 nm would be obtained. During cyclotron excitation to $n = 15$, this gave a corresponding relativistic shift of only -6×10^{-9} . Using sideband excitation, $r_m = 14 \mu\text{m}$. From Eq. (6b), there is, of course a large systematic shift ($\sim 6 \times 10^{-4}$ in $g-2$) between the observed and free space cyclotron frequencies. Due to imperfections in the trap, a direct measurement of ν_m (by magnetron excitation) and the calculated value from Eq. (6c) can disagree slightly. However, it can be shown that the error in ν_m is much less [6, 48] than the above difference which was measured to be $10^{-4} \nu_m$. Thus the error in $g-2$ was negligible. Errors in the present experiments are estimated from field jitter and drift and dependence of $g-2$ on applied spin flip power [47]. Ultimately, the experiment will be limited by systematic shifts associated with the superimposed magnetic bottle. To eliminate this problem, new ways have been proposed to detect the spin flips [6, 49]. For example, it might be possible to use a switchable magnetic bottle so that while the cyclotron and $g-2$ resonances are driven, the bottle would be off and transitions would be detected by turning the bottle on [50]. Even without a magnetic bottle, the axial motion is still linked to the cyclotron degrees of freedom via the relativistic mass shift [6, 51]. This coupling is about an order of magnitude smaller than for the magnetic bottle; the required increase in axial well depth stability might be provided with a reference electron in an adjacent trap whose axial frequency is locked to a particular value [52].

4. Mass Spectroscopy

With the long storage times and high vacuums in the traps, one could expect extremely narrow motional resonances. In the Washington electron experiments cyclotron excitation resonances reproducible to a few parts in 10^9 have been observed [53], and in principle the resolution should only be limited by effects due to inhomogeneous or time varying fields. Using the methods described in Sec. 3, the electron/positron mass ratio has recently been measured to about 0.1 ppm [63]. This very important experiment represents an improvement by more than two orders of magnitude over previous experiments. In addition, the cyclotron resonances of both atomic ions and electrons can be measured in the same magnetic field and in the same apparatus. This rather unique feature has led to experiments designed to make a direct measurement of the electron/proton mass ratio in a Penning trap.

The three current experiments using this method [53–55] all basically measure the (shifted) cyclotron frequencies of electrons and protons in the same magnetic field. In the experiment of Gärtner and Klempt [54], resonances were detected by electron/proton loss; the largest uncertainty was due to a space charge shift in the proton cyclotron resonance. In the Van Dyck and Schwinberg experiment, resonances were detected in several (non-destructive) ways [53]; the limit here was the uncertainty in the relative positions of the electrons and protons in the trap and also possibly ion number (space charge) dependent shifts. In the experiment of Gräff, Kalinowsky, and Traut, resonances were detected by an energy dependent time of flight technique [55]. The experiment of Van Dyck and Schwinberg has the smallest uncertainty (0.14 ppm) and substantial improvements can be expected.

With regard to space charge shifts, it is worth noting that in an ideal trap described by a quadratic electric potential and uniform magnetic field, if only one species is trapped and if the cyclotron motion is excited by a uniform electric field, then *no* space charge shifts can occur because only the center of mass mode is excited [26, 56]. Unfortunately, deviations from the ideal trap fields can occur, impurity ions can be present, and the excitation usually occurs from non-uniform fields. All of these things can lead to (partial) excitation of the internal modes which then results in space charge shifts. These systematic shifts increase with the mass of the ion and therefore are much more important for protons and atomic ions than for electrons.

After the initial single electron work, it became apparent that it should be possible to observe single ion cyclotron resonances by observing the induced currents in the ring electrode if it is divided in half [57] or into quadrants [53]; the key advantage here is that space charge shifts are totally absent. Since the cyclotron frequency of protons in a field of 4 T is about 60 MHz, electronic detection should be similar to the detection of the axial resonance of single electrons.

Other, related mass spectroscopy experiments should be possible. First, using techniques as those referred to above, mass ratios of various atomic (molecular) ions could be measured. It should also be possible to observe the cyclotron resonance of single atomic ions by laser techniques. For example, if a single cold Be^+ ion is localized at the center of the trap [8] with a laser beam whose diameter is approximately $3 \mu\text{m}$, then it should be possible to observe cyclotron excitation which increases the

orbit radius to about $3 \mu\text{m}$ by the decrease in fluorescence scattering. This corresponds to a temperature ($k_B T = (1/2) M (\omega_c')^2 r_c^2$) of 14 K in a field of 5 T and a relativistic shift of 1.4×10^{-13} . The axial and magnetron frequencies could be measured in a similar fashion. If the electron cyclotron frequency were measured in the same magnetic field, the accuracy in M_e/M_p from this indirect experiment would be limited by the accuracy of M_{Be}/M_p which is about 0.04 ppm [58].

In preliminary experiments at NBS, the axial resonance ($\nu_z \approx 200 \text{ kHz}$) of a small cloud (<10) of $^{25}\text{Mg}^+$ ions has been measured in this way; however significant broadening (a few parts in 10^4) is observed—presumably due to impurity ions. For an initial experiment on Be^+ , the electron cyclotron frequency can be measured indirectly by measuring the spin flip frequency on the same ion; since $g_J(\text{Be}^+)$ may be calculable to as good as a few parts in 10^8 [59], the error in M_e/M_p could still be limited by the error in M_{Be}/M_p . Ultimately when M_e/M_p is known better by other means, such measurements should lead to better experimental determinations of $g_J(\text{Be}^+)$ and M_{Be}/M_p .

We conclude by remarking that the extreme confinement possible with the stored ion techniques considerably relaxes the requirements on magnetic field homogeneity in these experiments.

5. Radiative Lifetime Measurements

Although perhaps not “high precision” in an absolute sense, the radiative lifetime measurements of Prior and colleagues at Berkeley should be included in this review because these measurements, made on simple atomic ions, can be compared with various theories. Lifetimes of $2^1\text{S}_0 \text{Li}^+$ ($\tau \approx 503 \mu\text{s}$) in a Penning trap [60], 2s He^+ ($\tau \approx 1.92 \text{ ms}$) in an orbitron [29], and $2^3\text{S}_1 \text{Li}^+$ ($\tau \approx 58.6 \text{ s}$) in an rf trap [61] have been measured. One should also include the $5^2\text{D}_{3/2} \text{Ba}^+$ ($\tau \approx 17.5 \text{ s}$) measurement in an rf trap by Schneider and Werth [62] and the $5^2\text{D}_{5/2} \text{Ba}^+$ ($\tau \approx 47 \text{ s}$) measurement in an rf trap by Plumelle *et al.* [19]. The key advantage of the traps in these measurements is the very long storage times and the benign environment which minimizes the effects of other relaxations. For the very long lifetimes, perhaps no other method is available.

6. Atomic Spectroscopy

As discussed in Sec. 1, the small number of ions involved makes it desirable to study simple atomic ions, but this does not preclude the study of simple molecular ions [1, 64]. As we will see, the potential accuracy and precision for atomic spectroscopy using ion storage techniques is quite remarkable. This was apparent from the early experiments on the $^3\text{He}^+$ ground state hyperfine structure [1, 65] where linewidths of about 10 Hz at 8.7 GHz were obtained. Since that time the $2\text{s } ^3\text{He}^+$ hyperfine structure (hfs) has been measured in an orbitron trap by Prior and Wang [66]. The importance of this measurement is that a comparison between the 1s and 2s hfs suppresses the effects of nuclear structure corrections and allows an accurate check of the QED corrections; such experimental/theoretical comparisons are most meaningful for hydrogenic ions.

A significant interest in stored atomic ion spectroscopy stems from the desire to make a frequency standard. Stimulated by the He^+ experiments, various proposals [65, 67–78] have been made for microwave and optical stored ion frequency standards. For a microwave stand-

ard, considerable attention has been given to the $^{199}\text{Hg}^+$ ion because (1) its ground state hyperfine frequency (~ 40 GHz) may be the largest of any conveniently usable ion, (2) its large mass gives a relatively small second order Doppler shift at a given temperature ($\sim 2 \times 10^{-13}$ at 300 K), and (3) a $^{202}\text{Hg}^+$ lamp source (194 nm) is available for optical pumping. Starting with the work of Major and Werth [69], groups at Mainz [74], Orsay [76], and at least one commercial company [74] have sought to develop a frequency standard based on $^{199}\text{Hg}^+$ ions stored in an rf trap. This work has been developed to a fairly high level; the group at Orsay [76] has made a working standard whose stability compares favorably with that of a commercial cesium beam frequency standard.

However, the full potential of the stored ion technique has yet to be realized. Historically, it appears that this has been due to two problems. (1) Because it has been difficult to cool the ions, second order Doppler or time dilation shifts can be sizeable (e.g.: $\sim 10^{-11}$ in Ref. [74], $\sim 4 \times 10^{-10}$ in Ref. [65]). (2) Signal-to-noise ratio has been poor due to the small number of stored ions.

In the past two or three years, both of these problems have been addressed. In 1978, groups at NBS and Heidelberg demonstrated [21, 25] that radiation pressure from lasers [44, 70, 79] could be used to cool ions to temperatures < 0.1 K, thereby reducing the second-order Doppler shift by more than three orders of magnitude below the room temperature case. As discussed below, the reduction of kinetic energy is most favorable for very small numbers of ions (down to one ion), so that there is a trade-off between the maximum number of ions we can use and the minimum second-order Doppler shift that can be achieved.

With regard to signal-to-noise ratio, in certain optical-pumping, double-resonance experiments, it is possible to scatter many optical photons from each ion for each microwave or optical "clock" photon absorbed [70, 73, 79-81]. This can allow one to make up for losses in detection efficiency due to small solid angle, small quantum efficiency in the photon detector, etc., so that the transition probability for each ion can be measured with *unity* detection efficiency. This means that the signal-to-noise ratio need be limited only by the statistical fluctuations in the number of ions that have made the transition [78, 81]. Therefore the signal-to-noise ratio can be maximized for the given number of ions. The ability to sensitively detect the fluorescence from ions is emphasized by experiments on single ions [7, 8] where it is even possible to make photographs as shown in Fig. 2.

More recently, the narrow linewidths anticipated for the stored ion technique have been observed; a resonance linewidth of about 0.012 Hz at 292 MHz has been observed [82] for the $(m_I, m_J) = (-3/2, 1/2) \leftrightarrow (-1/2, 1/2)$ hyperfine transition of $^{25}\text{Mg}^+$ at a magnetic field of about 1.24 T where the first derivative of the transition frequency with respect to magnetic field is zero. (The Ramsey interference method was implemented by applying two rf pulses of 1 s duration separated by 41 s.) These narrow linewidths should be preserved with hyperfine transitions of higher frequency, such as in Hg^+ , but, of course, more attention must be paid to field homogeneity and stability. In any case, the above results allow one to contemplate microwave frequency standards with $Q > 10^{12}$ and inaccuracies $< 10^{-15}$ [78]. Of course, in addition to the interest in frequency standards, very high precision hyperfine and optical spectroscopy on Hg^+ [74], Ba^+ [20, 82], Mg^+ [25, 82, 83], and other alkali-like ions [75] is possible.

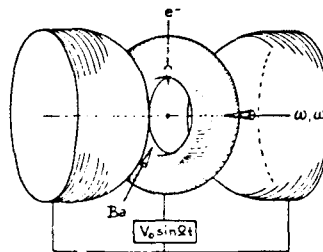
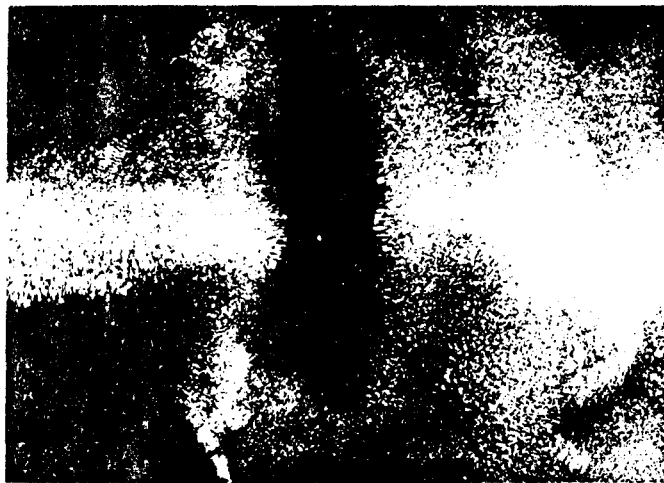


FIGURE 2. Photograph of fluorescence from single Ba^+ ion in an rf trap ($T \approx 10\text{-}36$ mK; from Ref. [86]). The schematic diagram of the rf trap from same view. Inner diameter of ring is 0.7 mm.

The possibilities for an optical frequency standard are even more dramatic [70, 71, 77, 78, 84, 85]. For a given interaction time, the Q of a transition will scale with the frequency. Therefore, in principle, an optical frequency standard would have clear advantages over a microwave frequency standard. The increased Q would allow one to work with smaller numbers, even down to one ion [70, 77, 78], and therefore obtain the "ultimate" atomic frequency standard. Example optical frequency standard candidates are the $^3\text{P}_0 \leftarrow ^1\text{S}_0$ transition in Tl^+ , Al^+ or Ga^+ [70], the $^3\text{P} \leftarrow ^1\text{S}$ transition in B^+ [85], the $\text{D} \leftarrow \text{P} \leftarrow \text{S}$ Raman transitions in Ba^+ [77], the $\text{S} \rightarrow \text{D}$ two photon transition in Hg^+ [71, 78], and the $^2\text{P}_{3/2} \leftarrow ^2\text{P}_{1/2}$ transition in Pb^+ [72]. All have $Q \geq 10^{14}$. Unfortunately, before the full potential of an ion-storage optical frequency standard can be realized, tunable lasers with suitable spectral purity must become available. This problem may be nearing solution [84]. Also, if an optical frequency standard is to provide time, the phase of the radiation must be measured. This appears to present a much more formidable problem [84, 85]. Therefore it is expedient to continue to pursue a microwave frequency standard where both of these problems have been solved.

Rather than concentrate on the details of the various experiments it is useful to examine the environment of the stored ions in order to identify possible systematic effects. We will be primarily concerned with Stark and second order Doppler shifts. Usually only second order Stark shifts will be important; therefore we will be interested only in $\langle E^2 \rangle$. As an example, for the strongly polarizable cesium (neutral) atom, the ground state hyperfine shift [88] is equal to: $\delta\nu/\nu = -2.5 \times 10^{-16} E^2$ (E in volts/cm); therefore electric fields of volts/cm become

important in very high accuracy experiments [90]. Magnetic field shifts due to instabilities and inhomogeneities are of course important in the Penning trap but can be made negligible in many experiments. (See for example Refs. [78, 82].) Other effects such as electric quadrupole frequency shifts could be important in certain experiments [70, 78].

For single ions, laser cooling has already achieved temperatures between 10 mK and 100 mK [7, 8]. Theoretically, when the motional oscillation frequencies Ω_i (ω_z and ω_r for the rf trap and ω_z , ω_c , and ω_m for the Penning trap) are less than the natural linewidth ($\Delta\nu = \gamma/2\pi$) of the optical cooling transition, then the limiting "temperature" (governed by photon recoil) in each degree of freedom is given by $k_B T = \hbar\gamma/2$ [21, 25, 44, 87]. (For a single ion, the precise minimum temperature depends on the angle of incidence of the laser beam and on the spatial distribution of recoil photons [87].) For strongly allowed transitions as in Ba^+ or Mg^+ , this limiting temperature is about 1 mK. For more weakly allowed transitions the temperature is correspondingly less but other limits such as thermodynamic limits can come into play [44]. When the condition $\Omega_i \gg \gamma$ is fulfilled then the limiting energy [44, 86] is given by $E_i = \hbar\Omega_i (\langle n_i \rangle + 1/2)$ where $\langle n_i \rangle = 5\gamma^2/(16\Omega_i^2)$. Therefore the limiting kinetic energy is given by $E_{ki} = \hbar\Omega_i/4$ but the uncertainty in energy (and therefore second order Doppler effect) is much less [44]. For simplicity we will assume only the case $\Omega_i \ll \gamma$ below, however even better results are potentially obtained for the opposite condition. For a single ion in an rf trap, when $U_0 = 0$ the nonthermal micromotion has an average kinetic energy equal to that of the secular motion [1]; this is also true in the spherical trap. In the Penning trap the kinetic energy in the nonthermal magnetron motion can be much

less than in the cyclotron or axial modes. Therefore, the minimum second order Doppler shifts are given approximately by:

$$\frac{\Delta\nu_D}{\nu_0} = \frac{E_k}{Mc^2} = \begin{cases} \frac{3}{2} \hbar\gamma/Mc^2 & \text{rf trap} \\ \frac{3}{4} \hbar\gamma/Mc^2 & \text{Penning trap} \end{cases}$$

For a single ion in an rf trap (assuming the spherical trap of Eqs. (2) and (3)), $\langle E^2 \rangle$ is primarily due to the oscillating rf fields and is largest for the z motion. A simple calculation gives $\langle E^2 \rangle_z = M\Omega^2\hbar\gamma/e^2$ for maximum laser cooling or $\langle E^2 \rangle_z = 2M\Omega^2k_B T/e^2$ for a given temperature in the z secular motion. For a single ion in a Penning trap, it is usually possible to make $r_m, r_c \ll z$ [8, 87], therefore Stark shifts from the static fields are primarily due to the z motion. We find $\langle E^2 \rangle_z = \hbar\gamma M\omega_z^2/(2e^2)$ for maximum laser cooling or $\langle E^2 \rangle_z = k_B T M\omega_z^2/e^2$ at temperature T . In the Penning trap, a larger effect can be caused by the motional electric field $\mathbf{E} = \mathbf{v} \times \mathbf{B}/c$. We have $\langle E^2 \rangle_M = \hbar\gamma B_0^2/(Mc^2)$ (maximum laser cooling) and $\langle E^2 \rangle_M = 2k_B T B_0^2/(Mc^2)$. In Table 1 are shown examples of the second order Doppler shift and $\langle E^2 \rangle$ for single ions in rf and Penning traps.

For clouds of identical ions, we first consider the electric fields due to collisions between ions. For the rf trap, we neglect the energy in the micromotion since the ions are driven in phase, therefore ion collisional effects in the rf and Penning traps are treated the same. $\langle E^2 \rangle$ will of course depend on the cloud density and temperature but some idea of the magnitude can be given by calculating the electric field for one ion on another at the distance of closest approach. Assuming the maximum energy available for closest approach is given by $3k_B T$, we have $E_{\text{max}} = 6.7 \times 10^{-8}$ V/cm ($\gamma/2\pi = 10$ MHz and max-

TABLE 1. Fractional second order Doppler shifts, Stark fields, and classical rms axial amplitudes (z_{rms}) for single ions in rf and Penning traps. When $\gamma/2\pi$ is given, we assume maximum theoretical laser cooling ($\Omega_i \ll \gamma$). For both traps we assume $M = 100$ u. For the rf trap $\Omega/2\pi$ (rf drive frequency) = 1 MHz, $A_0 = 300$ V/cm². For the Penning trap, $\omega_z/2\pi = 20$ kHz, $B = 1$ T. T is the temperature of the secular motion for the rf trap and the temperature of the cyclotron and axial motion for the Penning trap. $\langle E^2 \rangle_z$ is the mean square electric field for motion along the z axis, $\langle E^2 \rangle_M$ is the mean square "motional" electric field for the $\mathbf{v} \times \mathbf{B}/c$ force. Note that z_{rms} for the Penning trap can be reduced at the expense of increasing $\langle E^2 \rangle_z$.

	$\gamma/2\pi$	—	—	10 MHz	1 kHz
rf	T (K)	300	4	2.4×10^{-4}	2.4×10^{-8}
	$\Delta\nu_D/\nu_0$	8.3×10^{-13}	1.1×10^{-14}	6.6×10^{-19}	6.6×10^{-23}
	$\langle E^2 \rangle_z$ (V ² /cm ²)	210	2.8	1.7×10^{-4}	1.7×10^{-8}
	z_{rms} (μm)	170	20	0.15	1.5×10^{-3}
Pen.	$\Delta\nu_D/\nu_0$	4.2×10^{-13}	5.5×10^{-15}	3.3×10^{-19}	3.3×10^{-23}
	$\langle E^2 \rangle_z$ (V ² /cm ²)	4.2×10^{-2}	5.7×10^{-4}	3.4×10^{-8}	3.4×10^{-12}
	$\langle E^2 \rangle_M$ (V ² /cm ²)	4.99	0.067	4.0×10^{-6}	4.0×10^{-10}
	z_{rms} (μm)	1300	145	1.1	0.011

imum laser cooling) and $E_{\max} = 7.4$ V/cm at $T = 4$ K. Therefore at modest temperatures, ion-ion collision induced Stark shifts can be quite small.

For clouds of ions, other effects can contribute to Stark and second order Doppler shifts. We will consider only theoretical limits and therefore neglect effects such as rf heating which may be the real limitation in a practical experiment. We will assume that the secular motion in an rf trap and the axial and cyclotron modes in a Penning trap have been cooled to negligible values. For both traps we will assume that it is desirable to maximize the number of ions N .

Then in an rf trap we must consider the effects of the micromotion and corresponding electric fields for ions on the edge of the cloud. We impose the constraint that the maximum fractional second order Doppler shift not exceed a certain value (ϵ). Therefore for the rf spherical well we set $\Psi(r, z) = -\phi_i$, and with the condition on ϵ (the maximum second order Doppler effect is due to ions at $z = r_i, r = 0$) we find

$$N_{\max} = 6.48 \times 10^{15} r_i M \epsilon$$

when M is in u, and r_i is the cloud radius.

For the Penning trap, the maximum second order Doppler effect is due to the magnetron motion of ions on the edge of the cloud ($r_m = r_i, z = 0$). We set $\phi_i(z) = -\phi_T(z)$ and for a spherical cloud we find from Eqs. (5-7),

$$N_{\max} = 1.96 \times 10^{13} B \sqrt{\epsilon} \left[r_i^2 - \frac{440 M \sqrt{\epsilon}}{B} r_i \right]$$

where B is in tesla, M in u. Negative solutions are unphysical because they correspond to parameters where the magnetron second order Doppler shift cannot be made as large as ϵ (for a spherical cloud).

For very small values of ϵ , very low density ion clouds are required which implies very small applied potentials. From the condition $\phi_i = -\Psi_T$ for the rf trap we have (for the spherical well):

$$\frac{2eA_0^2}{M \Omega^2} = 7.2 \times 10^{-8} \frac{N_{\max}}{r_i^3} \left[\frac{V}{\text{cm}^2} \right]$$

and similarly, for the Penning trap we have:

$$A = 3.6 \times 10^{-8} \frac{N_{\max}}{r_i^3} \left[\frac{V}{\text{cm}^2} \right].$$

We can also calculate the corresponding electric fields. As before, for the rf trap, the maximum fields occur on ions for $z = r_i$ and $r = 0$ and we have

$$\langle E^2 \rangle_{z(\max)} = 8 r_i^2 A_0^2 = \frac{2M \Omega^2 N_{\max}}{r_i}.$$

In the Penning trap, the electric fields cancel along the z axis. Along the radial direction,

$$\langle E^2 \rangle_{r(\max)} = (2Mc^2 \epsilon / (er_i))^2.$$

In Table 2 are shown some representative values of maximum numbers of stored ions, trap potentials, and Stark shifts for various values of ϵ and r_i on clouds of ions. In certain configurations, second order Doppler and Stark shifts could still be a problem; however, with small enough numbers of ions these can be overcome. We note that in many cases, the electric fields from black-body radiation ($\langle E^2 \rangle_{bb} \approx (10 \text{ V/cm})^2$) can be much larger than those due to trapping conditions [78, 89, 90]. Therefore, operation at reduced environmental temperatures may ultimately be required.

TABLE 2. Maximum numbers, pseudopotential well depths for rf traps, applied potentials for Penning traps, and electric fields for "cold" spherical ion clouds in rf and Penning traps. A maximum fractional second order Doppler shift ϵ is assumed. The secular motion for the rf trap and the axial and cyclotron motion for the Penning trap are assumed to be frozen out (i.e., cooled to negligible values). r_i = ion cloud radius: $M = 100$ u, $\Omega/2\pi = 1$ MHz, $B = 1$ T.

ϵ		10^{-12}	10^{-12}	10^{-15}	10^{-15}
rf	r_i (cm)	0.5	0.01	0.5	0.01
	N_{\max}	3.2×10^5	6500	320	~6
	$\frac{2eA_0^2}{M \Omega^2} \left[\frac{V}{\text{cm}^2} \right]$	0.19	470	1.9×10^{-4}	0.47
	$\langle E^2 \rangle_z \left[\frac{V^2}{\text{cm}^2} \right]$	760	760	0.76	0.76
Pen.	N_{\max}	4.5×10^6	—	1.5×10^5	53
	$A_0 \left[\frac{V}{\text{cm}^2} \right]$	1.3	—	0.043	1.9
	$\langle E^2 \rangle_{r_i} \left[\frac{V^2}{\text{cm}^2} \right]$	0.14	—	1.4×10^{-7}	3.5×10^{-4}

7. Other Possibilities

With the special features of the ion traps in mind, it is worthwhile speculating on possible future experiments. A very interesting class of experiments has already been initiated on multiply charged ions. Electron capture rates of Ne^{q+} ($1 \leq q \leq 10$) in an orbitron trap have recently been measured [14] and Penning traps are being developed for high Z ion storage [91]. These experiments may pave the way for interesting spectroscopy on for example high Z hydrogenic ions where precise theoretical calculations are available. Various energy separations become higher; for example the $^{235}\text{U}^{91+}$ ground state hfs transition may be in the visible [92]. In the future, more exotic species may be available for study such as anti-protons, e^-/e^- pairs in a Penning trap or e^+/e^- , e^+/p^- , e^-/p^+ or p^+/p^- pairs in an rf trap [92].

The Penning trap may be an ideal place to measure g_J factors in certain atomic ions. First, because very small samples ($<100 \mu\text{m}$) can be used, the effects of inhomogeneous fields are greatly reduced [81]. Second, atomic g_J factors could be measured in terms of the Bohr magnetron by measuring the cyclotron frequency of free electrons in the same magnetic field. This technique has already been used to measure the g_J factor in S^- [93]. More generally, these features plus the very high resolutions possible [82] should allow precise measurements of other magnetic-field-dependent structure. For example, deviations in the Breit-Rabi formula for hfs could be measured and it may be possible to measure the effects of nuclear diamagnetism [94].

From Tables 1 and 2, it is evident that Stark shifts can be very small on cooled ions; this suggests that the spectroscopy of Rydberg ions with minimal Stark shifts may be possible. With this in mind, perhaps a measurement of the Rydberg along the lines of Kleppner's proposal [95] is possible in an ion.

Finally, ion storage techniques might also be used for measurement devices, for example, to measure magnetic fields [96] or frequencies of lasers [45, 97].

Quite generally, it is now feasible to think of experiments on stored ions where the perturbations are extremely small. Hopefully, this can lead to many new precision experiments other than the ones discussed here.

The preparation of this paper was supported in part by the Air Force Office of Scientific Research and the Office of Naval Research. The author thanks W. M. Itano, G. Dunn, J. C. Bergquist, R. E. Drullinger and F. L. Walls for a critical reading of the manuscript and R. Ray and B. Barrett for manuscript typing.

References

- [1] H. G. Dehmelt, *Adv. At. Mol. Phys.* 3, 53 (1967); 5, 109 (1969).
- [2] F. G. Major and J. P. Schermann, *Bull. Am. Phys. Soc.* 16, 838 (1971).
- [3] C. Audoin, private communication (1979).
- [4] F. G. Major, *J. de Phys. (Paris)* 38, L-221 (1977).
- [5] D. Wineland, P. Ekstrom, and H. Dehmelt, *Phys. Rev. Lett.* 31, 1279 (1973).
- [6] R. S. Van Dyck, Jr., P. B. Schwinberg, and H. G. Dehmelt, in *New Frontiers in High-Energy Physics*, Ed. by B. M. Kursunoglu, A. Perlmutter, and L. F. Scott (Plenum, New York, 1978), p. 159; H. G. Dehmelt, in *Atomic Physics 7*, Ed. by D. Kleppner and P. M. Pipkin (Plenum, New York, 1981), p. 337.
- [7] W. Neuhauser, M. Hohenstatt, P. E. Toschek, and H. Dehmelt, *Phys. Rev. A* 22, 1137 (1980).
- [8] D. J. Wineland and W. M. Itano, *Phys. Lett.* 82A, 75 (1981).
- [9] W. A. M. Blumberg, R. M. Jopson, and D. J. Larson, *Phys. Rev. Lett.* 40, 1320 (1978).
- [10] W. A. M. Blumberg, W. M. Itano, and D. J. Larson, *Phys. Rev. A* 19, 139 (1979).
- [11] R. T. McIver, Jr. in *Lecture Notes in Chemistry*, Vol. 7, Ed. by H. Hartmann and K. P. Wanczek (Springer-Verlag, New York, 1978), p. 97.
- [12] F. L. Walls and G. H. Dunn, *Phys. Today* 27(8), 30 (August, 1974).
- [13] H. A. Schuessler, *Metrologia* 13, 109 (1977); D. A. Church and H. M. Holzscheiter, *Chem. Phys. Lett.* 76, 109 (1980).
- [14] C. R. Vane, M. H. Prior, and Richard Marrus, *Phys. Rev. Lett.* 46, 107 (1981).
- [15] J. H. Malmberg and C. F. Driscoll, *Phys. Rev. Lett.* 44, 654 (1980); T. M. O'Neil, *Proc. Inter. Conf. on Plasma Physics*, II (April 1980).
- [16] H. A. Schuessler, in *Progress in Atomic Spectroscopy Part B*, Ed. by W. Hanle and H. Kleinpoppen (Plenum, New York, 1979), p. 999.
- [17] G. Werth, *Acta Phys. Polon.* A61, 213 (1982).
- [18] W. Paul, O. Osberghaus, and E. Fisher, *Forschungsber. Wirtsch. Verkehrsministeriums Nordrhein-Westfalen* No. 415 (1958).
- [19] F. Plumelle, M. Desaintfuscien, J. L. Duchene, and C. Audoin, *Optics Commun.* 34, 71 (1980); F. Plumelle, Thesis, Universite de Paris-Sud, Orsay (1979).
- [20] R. Blatt and G. Werth, *Z. Phys.* 299, 94 (1981). Also see these proceedings.
- [21] W. Neuhauser, M. Hohenstatt, P. Toschek, and H. G. Dehmelt, *Phys. Rev. Lett.* 41, 233 (1978); W. Neuhauser, M. Hohenstatt, P. Toschek, and H. G. Dehmelt, *Appl. Phys.* 17, 123 (1978).
- [22] For a review see A. Ashkin, *Science* 210, 1081 (1980).
- [23] F. M. Penning, *Physica* 3, 873 (1936).
- [24] J. Byrne and P. S. Farago, *Proc. Phys. Soc. (London)* 86, 801 (1965).
- [25] D. J. Wineland, R. E. Drullinger, and F. L. Walls, *Phys. Rev. Lett.* 40, 1639 (1978); R. E. Drullinger, D. J. Wineland, and J. C. Bergquist, *Appl. Phys.* 22, 365 (1980).
- [26] D. J. Wineland and H. G. Dehmelt, *Int. J. Mass. Spectr. Ion Phys.* 16, 338 (1975); and erratum, 19, 251 (1976); H. G. Dehmelt, *Nature* 262, 777 (1976).
- [27] See for example: S. A. Prasad and T. M. O'Neil, *Phys. Fluids* 22, 278 (1979).
- [28] K. H. Kingdon, *Phys. Rev.* 21, 408 (1923).
- [29] M. H. Prior, *Phys. Rev. Lett.* 29, 611 (1972).
- [30] M. H. Prior and E. C. Wang, *Phys. Rev. Lett.* 35, 29 (1975).
- [31] R. D. Knight, *Appl. Phys. Lett.* 38, 221 (1981).
- [32] The case of a purely logarithmic potential has been investigated by R. H. Hooverman, *J. Appl. Phys.* 34, 3505 (1963). See also R. R. Lewis, *J. Appl. Phys.* 53, 3975 (1982).
- [33] C. E. Johnson, private communication.
- [34] A. Rich and J. C. Wesley, *Rev. Mod. Phys.* 44, 250 (1972). Also see the review by A. Rich, these proceedings.
- [35] G. Gräff, E. Klempt, and G. Werth, *Z. Phys.* 222, 201 (1969).
- [36] G. Gräff and M. Holzscheiter, *Phys. Lett.* 79A, 380 (1980).
- [37] D. A. Church and B. Mokri, *Z. Phys.* 244, 6 (1971).
- [38] F. L. Walls and T. Stein, *Phys. Rev. Lett.* 31, 975 (1973).
- [39] S. Liebes, Jr., and P. A. Franken, *Phys. Rev.* 116, 633 (1959).
- [40] J. C. Wesley and A. Rich, *Phys. Rev. A* 4, 1341 (1971).
- [41] R. S. Van Dyck, Jr., P. B. Schwinberg, and H. G. Dehmelt, *Phys. Rev. Lett.* 38, 310 (1977).
- [42] P. Ekstrom and D. Wineland, *Scientific American* 243, August (1980).
- [43] R. S. Van Dyck, Jr., D. J. Wineland, P. A. Ekstrom, and H. G. Dehmelt, *Appl. Phys. Lett.* 28, 446 (1976).
- [44] D. J. Wineland and W. M. Itano, *Phys. Rev. A* 20, 1521 (1979).
- [45] D. J. Wineland, *J. Appl. Phys.* 50, 2528 (1979).
- [46] R. S. Van Dyck, Jr., P. B. Schwinberg, and H. G. Dehmelt, *Bull. Am. Phys. Soc.* 24, 758 (1979).

- [47] P. B. Schwinberg, R. S. Van Dyck, Jr., and H. G. Dehmelt, *Phys. Rev. Lett.* **24**, 1679 (1981). Also see these proceedings.
- [48] G. Gabrielse and R. S. Van Dyck, Jr., *Bull. Am. Phys. Soc.* **26**, 598 (1981).
- [49] H. Dehmelt, R. Van Dyck, P. Schwinberg, and G. Gabrielse, *Bull. Am. Phys. Soc.* **24**, 675 (1979); and H. G. Dehmelt and G. Gabrielse, *Bull. Am. Phys. Soc.* **24**, 758 (1979).
- [50] P. B. Schwinberg and R. S. Van Dyck, Jr., *Bull. Am. Phys. Soc.* **24**, 1202 (1979); *Bull. Am. Phys. Soc.* **26**, 598 (1981).
- [51] G. Gabrielse and H. G. Dehmelt, *Bull. Am. Phys. Soc.* **25**, 1149 (1980). Also see these proceedings.
- [52] P. B. Schwinberg and R. S. Van Dyck, Jr., *Bull. Am. Phys. Soc.* **23**, 40 (1978).
- [53] R. S. Van Dyck, Jr., P. B. Schwinberg, and S. H. Bailey, in *Atomic Masses and Fundamental Constants 6*, Ed. by J. A. Nolen, Jr., and W. Benenson (Plenum, New York, 1980), p. 173; R. S. Van Dyck, Jr., and P. B. Schwinberg, these proceedings.
- [54] G. Gärtner and E. Klempt, *Z. Phys. A* **287**, 1 (1978).
- [55] G. Gräff, H. Kalinowsky, and J. Traut, *Z. Phys.* **296**, 35 (1980). Also see these proceedings.
- [56] D. J. Wineland and H. G. Dehmelt, *J. Appl. Phys.* **46**, 919 (1975).
- [57] D. J. Wineland, *Bull. Am. Phys. Soc.* **18**, 1573 (1973).
- [58] A. M. Wapstra and K. Bos, *Atomic Data and Nuc. Data Tables* **19**, 177 (1977).
- [59] R. Hegstrom, private communication.
- [60] M. H. Prior and H. A. Shugart, *Phys. Rev. Lett.* **27**, 902 (1971).
- [61] R. D. Knight and M. H. Prior, *Phys. Rev.* **21**, 179 (1980).
- [62] R. Schneider and G. Werth, *Z. Phys.* **293**, 103 (1980).
- [63] P. B. Schwinberg, R. S. Van Dyck, Jr., and H. G. Dehmelt, *Phys. Lett.* **81A**, 119 (1981).
- [64] S. C. Menasian and H. G. Dehmelt, *Bull. Am. Phys. Soc.* **18**, 408 (1973); F. J. Grieman, B. H. Mahan, and A. O'Keefe, *J. Chem. Phys.* **72**, 4246 (1980).
- [65] H. A. Schuessler, E. N. Fortson, and H. G. Dehmelt, *Phys. Rev.* **187**, 5 (1969).
- [66] M. H. Prior and E. C. Wang, *Phys. Rev. Lett.* **35**, 29 (1975); and *Phys. Rev. A* **16**, 6 (1977).
- [67] F. G. Major, NASA Report X-521.69.167, Goddard Space Flight Center (1969).
- [68] H. A. Schuessler, *Metrologia* **7**, 103 (1971).
- [69] F. G. Major and G. Werth, *Phys. Rev. Lett.* **30**, 1155 (1973); F. G. Major and G. Werth, *Appl. Phys.* **15**, 201 (1978).
- [70] H. Dehmelt, *Bull. Am. Phys. Soc.* **18**, 1521 (1973); H. Dehmelt, *Bull. Am. Phys. Soc.* **20**, 60 (1975); D. J. Wineland and H. Dehmelt, *Bull. Am. Phys. Soc.* **20**, 637 (1975); H. Dehmelt, *IEEE Trans. Instrum. Meas.* **IM-31**, 83 (1982).
- [71] P. L. Bender, J. L. Hall, R. H. Garstang, F. M. J. Pichanick, W. W. Smith, R. L. Barger, and J. B. West, *Bull. Am. Phys. Soc.* **21**, 599 (1976).
- [72] F. Strumia, *Proc. 32nd Ann. Symp. Freq. Control.* June 1978, p. 444. (Copies available from Electronic Industries Assn., 2001 Eye St., NW., Washington, DC 20006.)
- [73] F. L. Walls, D. J. Wineland, and R. E. Drullinger, *Proc. 32nd Ann. Symp. Freq. Control.* June 1978, p. 453. (Copies available from Electronic Industries Assn., 2001 Eye St., NW., Washington, DC 20006.)
- [74] M. D. McGuire, R. Petsch, and G. Werth, *Phys. Rev. A* **17**, 1999 (1978). M. D. McGuire, *Bull. Am. Phys. Soc.* **26**, 615 (1981).
- [75] W. M. Itano and D. J. Wineland, *Bull. Am. Phys. Soc.* **24**, 1185 (1979).
- [76] M. Jardino, M. Desaintfuscien, R. Barillet, J. Viennet, P. Petit, and C. Audoin, *Appl. Phys.* **24**, 1 (1981).
- [77] P. E. Toschek and W. Neuhauser, in *Atomic Physics 7*, Ed. by D. Kleppner and F. M. Pipkin (Plenum, New York, 1981), p. 529.
- [78] D. J. Wineland, W. M. Itano, J. C. Bergquist, and F. L. Walls, *Proc. 35th Ann. Symp. Freq. Control.* June, 1981. (Copies available from Electronic Industries Assn., 2001 Eye St., NW., Washington, DC 20006.) Also see W. M. Itano, D. J. Wineland, J. C. Bergquist and F. L. Walls, these proceedings.
- [79] T. W. Hänsch and A. L. Schawlow, *Opt. Commun.* **13**, 68 (1975).
- [80] M. H. Prior and R. D. Knight, *Opt. Comm.* **35**, 54 (1980).
- [81] D. J. Wineland, J. C. Bergquist, W. M. Itano, and R. E. Drullinger, *Opt. Lett.* **5**, 245 (1980).
- [82] W. M. Itano and D. J. Wineland, *Phys. Rev. A* **24**, 1364 (1981).
- [83] W. Nagourney and H. Dehmelt, *Bull. Am. Phys. Soc.* **26** (1981).
- [84] J. L. Hall, *Science* **202**, 147 (1978); in *Atomic Physics 7*, Ed. by D. Kleppner and F. M. Pipkin (Plenum, New York, 1981), p. 267.
- [85] D. J. Wineland, *Proc. 11th Ann. Precise Time and Time Interval Meeting (NASA Publ. 2129, Nov. 1979)*, p. 81.
- [86] W. Neuhauser, M. Hohenstatt, P. Toschek, and H. Dehmelt, *Proc. 5th Int. Conf. on Spectral Lineshapes*, West Berlin, July 1980.
- [87] W. M. Itano and D. J. Wineland, *Phys. Rev. A* **25**, 35 (1982).
- [88] R. D. Haun, Jr., and J. R. Zacharias, *Phys. Rev.* **107**, 107 (1957).
- [89] T. F. Gallagher and W. E. Cooke, *Phys. Rev. Lett.* **42**, 835 (1979).
- [90] W. M. Itano, L. L. Lewis, and D. J. Wineland, *Phys. Rev. A* **25**, 1233 (1982).
- [91] D. A. Church, in *Physics of Electron and Atomic Collisions*, Ed. by S. Datz (North Holland, 1982), p. 533.
- [92] H. G. Dehmelt, R. S. Van Dyck, Jr., P. B. Schwinberg, and G. Gabrielse, *Bull. Am. Phys. Soc.* **24**, 757 (1979).
- [93] R. M. Jopson and D. J. Larson, *Phys. Rev. Lett.* **47**, 789 (1981).
- [94] N. P. Economou, S. J. Lipson, and D. J. Larson, *Phys. Rev. Lett.* **38**, 1394 (1977).
- [95] D. Kleppner, *Bull. Am. Phys. Soc.* **20**, 1458 (1975).
- [96] P. B. Schwinberg and R. S. Van Dyck, *Bull. Am. Phys. Soc.* **24**, 35 (1979).
- [97] J. C. Bergquist and D. J. Wineland, *Proc. 33rd Ann. Symp. Freq. Control.* June 1979. (Copies available from Electronic Industries Assn., 2001 Eye St., NW., Washington, DC 20006.)

Abstract Submitted
for the Philadelphia, PA meeting of the
American Physical Society
3-5 Nov. 1982

Physics and Astronomy
Classification Scheme
Number 32

Bull. Am. Phys. Soc. 27, 864 (1982)

Suggested title of session
in which paper should be
placed
Spectroscopy, Optics and
Photoionization

Magnetic Field Dependence of (s,l) Electron
Configurations.* D. J. WINELAND and WAYNE M. ITANO, NBS.
Using the modified Breit-Wills theory¹ (for hfs of (s,l)
electron configurations) in second order perturbation
theory, we have calculated the magnetic field dependence
of ³L_j states. Our main interest is in predicting the
field^j dependence of intercombination lines of group III₃A
ions for possible use in optical frequency standards.^{2,3}

For example, the $(5s^2)^1S_0(M_I=-9/2) \rightarrow (5s\ 5p)^3P_0(M_I=-9/2)$
transition frequency ($\nu_0=1.3 \times 10^{15}$ Hz) in In II is indepen-
dent of magnetic field(B) in first order at $B_0=25 \pm 5$ kG, with
second order field dependence of $\Delta\nu/\nu_0 \approx -2 \times 10^{-8} (\Delta B/B)^2$.
This suggests an In II (or other ion) fre-
quency standard in a Penning trap or rf trap with super-
imposed magnetic field. For In II, coherent radiation
(power >10 μ W) for laser cooling/optical⁴ pumping could
be accomplished by sum frequency mixing⁴ in ADP.

*Supported by ONR and AFOSR

1 A. Lurio, Phys. Rev. 142, 46 (1966).

2 H.G. Dehmelt, IEEE Trans. Instr. Meas. IM-31, 83 (1982)

3 R.L. Barger, J.C. Bergquist, T.C. English, and D.J.
Glaze, Appl. Phys. Lett. 34, 850 (1979).

4 H. Hemmati, J.C. Bergquist, and Wayne M. Itano, to be
published.

() Prefer Standard Session

Signature of APS Member

D. J. Wineland
National Bureau of Standards
325 Broadway
Boulder, CO 80303

Laser Cooling and Double Resonance Spectroscopy of Stored Ions

W.M. Itano and D.J. Wineland

Frequency and Time Standards Group, Time and Frequency Division
National Bureau of Standards, 325 S. Broadway
Boulder, CO 80303, USA

1. Introduction

The use of ion storage techniques for spectroscopy is motivated by the fact that ions can be confined by electric and magnetic fields for long periods of time without suffering the large perturbations which usually accompany other methods of confinement, such as those due to collisions with buffer gas molecules. Linewidths as small as a few Hz and Q's as high as 10^{10} have been observed on ground-state hyperfine transitions of atomic ions stored in rf quadrupole traps [1-3]. The accuracy of these measurements has been limited largely by the second-order Doppler shift. The signal-to-noise ratios have been limited by the small number of ions that can be stored (about 10^5 - 10^6) and by the difficulty of detecting transitions. Hyperfine and Zeeman transitions have been detected by charge exchange [1], fluorescence [2,3], photodetachment [4], and photodissociation [5].

In this paper we discuss recent work at the National Bureau of Standards (NBS) in this area. The second-order Doppler shift can be reduced by laser (resonant light pressure) cooling. This technique has been demonstrated in experiments on stored ions by our group at NBS [6-8] and also by a group at Heidelberg [9]. Other work at NBS has been directed toward the realization of high-efficiency laser-optical-pumping, double-resonance detection techniques [10]. These techniques have been used to make the first highprecision hyperfine structure measurements of $^{25}\text{Mg}^+$ [11]. We anticipate that the laser cooling and double resonance techniques will find practical application in the development of frequency standards based on stored ions [12].

Laser Spectroscopy V, eds. A.R.W. McKellar, T. Oka, and B.P. Stoicheff.
(Springer Verlag, N.Y., 1981).

2. Apparatus

A block diagram of the apparatus is shown in Fig.1. The Mg^+ ions are confined in a Penning-style ion trap. They are irradiated by light resonant with the $3s\ ^2S_{1/2} \rightarrow 3p\ ^2P_{3/2}$ 280 nm transition and also by rf and microwave radiation resonant with various transitions between ground-state sublevels. Scattered 280 nm photons are collected by a mirror and counted by a photomultiplier tube, with a net detection efficiency of about 10^{-5} .

A Penning trap confines ions by a combination of a uniform static magnetic field, $\vec{B} = B_0 \hat{z}$, and a quadrupolar electrostatic potential. The magnetic field causes the ions to move in circular "cyclotron" orbits in the x-y plane. The electric fields provide a harmonic restoring force for the axial (z) motion and cause the centers of the cyclotron orbits to move in the x-y plane in circular "magnetron" orbits around the trap symmetry axis. The angular frequencies corresponding to the axial, cyclotron, and magnetron motions are denoted by ω_z , ω_c' , and ω_m respectively. For typical operating conditions, $\omega_z \cong 2\pi \cdot 200$ kHz, $\omega_c' \cong 2\pi \cdot 800$ kHz, and $\omega_m \cong 2\pi \cdot 25$ kHz. Typically, $B_0 \cong 1$ T, and a potential $V_0 \cong 7$ V is applied across the trap electrodes, which have inside dimensions of about 1 cm. The axial and cyclotron motions are thermal and stable. The magnetron motion is nonthermal and unstable, since an increase in the size of the magnetron orbit leads to a decrease in the total (kinetic plus potential) energy. However, storage times of about 1 day have been observed, even without laser cooling. The background pressure is typically $\leq 10^{-8}$ Pa.

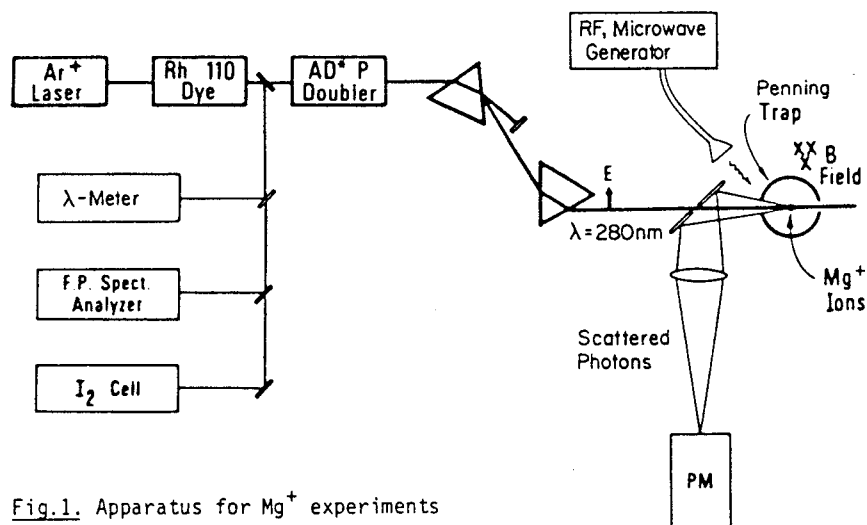


Fig.1. Apparatus for Mg^+ experiments

The 280 nm radiation was produced by frequency doubling the output of a single-mode cw Rhodamine 110 dye laser in a 90° phase-matched AD*P crystal. Between 5 and 30 μ W of UV radiation was generated in a bandwidth of about 1 MHz. The dye laser could be long-term stabilized to discrete frequencies to less than 1 MHz by locking it to saturated absorption features in I_2 . Fine tuning could be done by varying the trap magnetic field to Zeeman shift the Mg^+ levels. For efficient laser cooling, the UV linewidth must be less than the Doppler width of the transition (3 GHz at 300K), but need not be much less than the natural linewidth (43 MHz).

3. Laser Cooling in a Penning Trap

The basic principle of laser cooling is that light pressure can be used to damp the velocity of an atom or ion if the light frequency is tuned slightly below that of a strong optical transition. The process is easily described for the case of free or harmonically bound atoms [9,13-16]. Atoms whose velocities are directed toward the light source see a frequency Doppler shifted closer to resonance; if their velocities are directed away from the source, the frequency shift is away from resonance. Therefore, the atoms tend to absorb photons when their velocity is directed toward the source. This cools them, since the momentum of the absorbed photons reduces the atomic momentum. (The photons are re-emitted in random directions.) Three-dimensional cooling can be obtained with six laser beams directed along the $\pm x$, $\pm y$, and $\pm z$ directions. A single beam suffices to cool all oscillational modes of an atom bound in a three-dimensional harmonic potential, if the modes are nondegenerate and if the beam is not directed along one of the principal axes.

Cooling of the axial and cyclotron modes of an ion in a Penning trap takes place by the process just described for free or harmonically bound atoms, if the light is tuned below resonance [17]. Cooling of the magnetron mode can be accomplished by focusing the light beam so that it is more intense on the side of the trap axis on which the magnetron motion recedes from the light source [6-8,17]. By "cooling" of a mode, we mean the reduction of the average kinetic energy in that mode, regardless of what happens to the potential energy. In order to efficiently cool all modes, the angle between the beam and the z axis should be about 45°; the optimum angle depends on the angular distribution of the scattered photons [17]. We have derived rate equations for the laser cooling of an ion in a Penning trap by

a single nonuniform light beam [17]. Solving these equations, we find that it should be possible to cool an ion to a "temperature" T given by $k_B T \approx \hbar \gamma / 2$, where k_B is Boltzmann's constant and γ is the natural linewidth of the upper state. The "temperature" is defined in terms of the mean kinetic energy and may be different for the different modes. For Mg^+ , this minimum temperature is about 1 mK.

4. Optical Pumping and Double Resonance

The extremely long ground-state relaxation times possible for stored ions make it possible to observe very narrow transition linewidths and to observe very weak optical pumping processes. An ion must scatter about 10^4 optical photons in order to be cooled significantly below room temperature. Therefore, even weak depopulation pumping processes would have an adverse effect on the cooling. Cooling, in turn, influences the optical pumping by reducing the Doppler broadening until it is less than the natural linewidth. This makes it possible for a monochromatic laser to interact strongly with all of the ions and not just with a small velocity class.

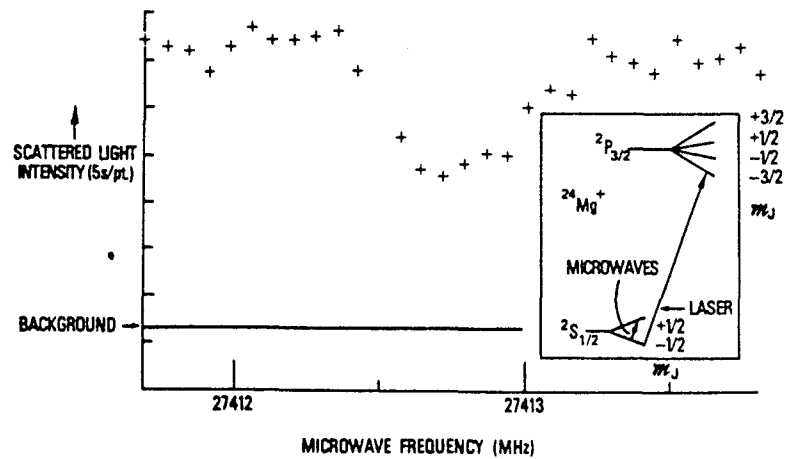


Fig.2. Optical pumping and double resonance of $^{24}Mg^+$

Generally, the $(^2S_{1/2}, M_J = -1/2) \rightarrow (^2P_{3/2}, M_J = -3/2)$ Zeeman component was used for laser cooling of $^{24}Mg^+$, which has $I=0$ (see Fig.2). This transition does not lead to depopulation pumping of the ground state, since the $M_J = -3/2$ excited state sublevel must decay to the $M_J = -1/2$ ground state

sublevel. When this transition is driven near resonance with light polarized perpendicular to the magnetic field, the $(^2S_{1/2}, M_J = -1/2) + (^2P_{3/2}, M_J = +1/2)$ and $(^2S_{1/2}, M_J = +1/2) + (^2P_{3/2}, M_J = -1/2)$ transitions are driven weakly in their Lorentzian wings (the Zeeman splitting is much greater than the Doppler broadening). In the steady state, which is achieved in ≤ 1 s, 16/17 \approx 94% of the population is in the $M_J = -1/2$ ground-state sublevel [10].

The ground-state Zeeman transition $(^2S_{1/2}, M_J = -1/2 \rightarrow +1/2)$ can be detected by a decrease in the fluorescence intensity. This "flop-out" detection method can be very efficient, since a transition due to a single microwave photon interrupts the flow of scattered optical photons until the ion is pumped back to the $M_J = -1/2$ sublevel by weak, off-resonance scattering. Since the decrease in the number of scattered photons per ion can be very large, it is possible to make up for poor light collection and detector quantum efficiency, so that the transition can be detected with nearly unit efficiency. Similar detection methods have been proposed previously [18].

The $(^2S_{1/2}, M_I = -5/2, M_J = -1/2) \rightarrow (^2P_{3/2}, M_I = -5/2, M_J = -3/2)$ hyperfine-Zeeman component was generally used for laser cooling of $^{25}\text{Mg}^+$ ($I = 5/2$). In the steady state, about 16/17 of the population is pumped into the $(M_I = -5/2, M_J = -1/2)$ ground-state sublevel. Pumping into the $M_J = -1/2$ manifold takes place by the same mechanism as in $^{24}\text{Mg}^+$. Pumping into the $M_I = -5/2$ sublevels takes place because of hyperfine coupling in the excited state [10]. Any transition which decreases the population in the $(M_I = -5/2, M_J = -1/2)$ ground-state sublevel can be detected by a decrease in the fluorescence intensity.

5. Results

In the Penning trap, low temperatures become easier to achieve as the ion density is reduced. This is because the radial electric field due to space charge increases the magnetron velocity. This problem does not exist for a single, isolated ion, and the lowest temperatures were observed for this case [8].

Figure 3 shows the fluorescence from a small number of $^{24}\text{Mg}^+$ ions as a function of time. After the ions were cooled and localized at trap center, an oven containing ^{25}Mg (98% isotopic purity) was heated in order to induce the resonant charge exchange reaction $(^{24}\text{Mg}^+ + ^{25}\text{Mg} \rightarrow ^{24}\text{Mg} + ^{25}\text{Mg}^+)$. The

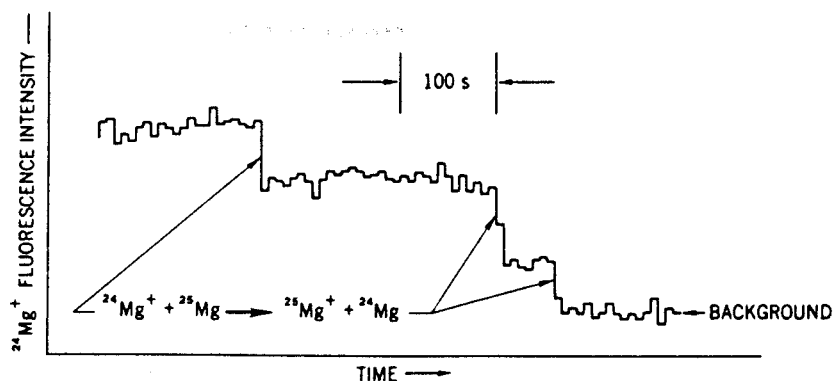


Fig.3. Fluorescence from 3, 2, and 1 $^{24}\text{Mg}^+$ ions

resulting $^{25}\text{Mg}^+$ ions were ejected from the trap by resonant cyclotronmagneton rf excitation. The three large step decreases in fluorescence are due to loss of the $^{24}\text{Mg}^+$ ions, one at a time, and the last plateau above background is the fluorescence from a single ion. The signal was about 50 photons/s per ion.

The "temperature" of a single $^{24}\text{Mg}^+$ ion was determined from the Doppler width by optical-optical double resonance (see Fig.4). One laser was tuned slightly below the $(^2S_{1/2}, M_J = -1/2) + (^2P_{3/2}, M_J = -3/2)$ transition, to provide cooling and fluorescence detection. A low power laser was swept continuously across the $(^2S_{1/2}, M_J = -1/2) + (^2P_{3/2}, M_J = -1/2)$ transition, which was detected by a decrease in the fluorescence. The resulting lineshape reflects both the natural and Doppler broadenings. The data points represent 10s integrations; the connecting lines are only for clarity. Simulated curves are shown for temperatures of 0 K and 1000 mK. We estimate that $T = 50 \pm 30$ mK. Since the light was incident at 82° with respect to the z axis, this is essentially a measurement of the cyclotron-magneton (x-y) temperature. The axial (z) temperature was estimated to be about 600 mK by probing the axial excursions with a focused laser beam. According to our calculations, it should be possible to obtain a cyclotron-magneton temperature of about 1 mK and an axial temperature of about 11 mK for these conditions [17]. At present, the discrepancy is not understood, but may be due to the presence of impurity ions in the trap.

Ground-state Zeeman and hyperfine transitions were detected by the optical-pumping, double-resonance methods outlined previously. The only transition in $^{24}\text{Mg}^+$ is the electronic spin flip transition (see Fig.2). Several

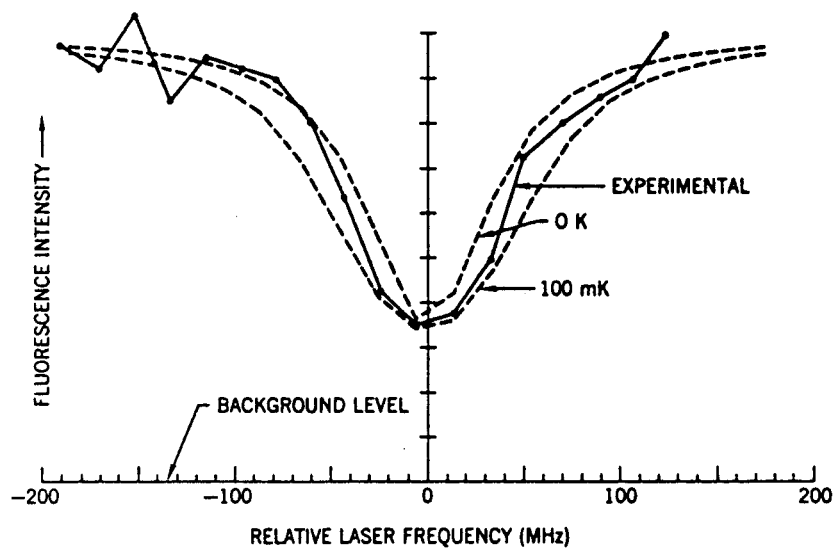


Fig.4. Optical-optical double resonance of a single $^{24}\text{Mg}^+$ ion

transitions in $^{25}\text{Mg}^+$, corresponding to both nuclear and electronic spin flip transitions, were observed. Most transitions were broadened by the instability of B_0 , which was, at best, about 1 ppm in a few seconds. The magnetic field derivative of the $(M_I, M_J) = (-3/2, +1/2) \leftrightarrow (-1/2, +1/2)$ transition goes to zero at $B_0 \approx 1.2398$ T. Near this field, the transition was observed with linewidths as narrow as 0.012 Hz (see Fig.5). The oscil-

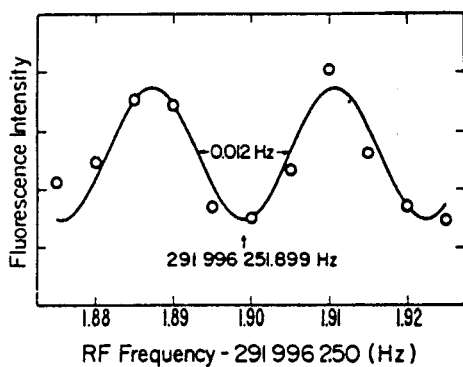


Fig.5. $^{25}\text{Mg}^+$ $(M_I, M_J) = (-3/2, +1/2) \leftrightarrow (-1/2, +1/2)$ ground-state hyperfine resonance

latory lineshape results from the use of the Ramsey interference method [19], which was implemented by driving the transition with two coherent rf pulses of 1.02 s duration separated by 41.4 s. The center of the resonance can be determined with an uncertainty of about 10^{-11} . Several different transition frequencies were measured in order to obtain separately the hyperfine constant ($A = -596.254\ 376\ (54)$ MHz) and the nuclear-to-electronic g factor ratio ($g_I/g_J = 9.299\ 484\ (75) \times 10^{-5}$) [11].

6. Future Possibilities

Work is being initiated at NBS on the development of a microwave frequency and time standard based on a hyperfine transition in $^{201}\text{Hg}^+$ and of an optical frequency standard based on a two-photon transition to a metastable state in $^{199}\text{Hg}^+$ or $^{201}\text{Hg}^+$. Both proposed standards are based on a cloud of Hg^+ ions stored in a Penning trap and use the $6s\ ^2S_{1/2} \rightarrow 6p\ ^2P_{1/2}$ 194 nm transition for laser cooling.

The proposed microwave frequency standard is based on the $(F, M_F) = (1,1) \leftrightarrow (2,1)$ transition, which is field-independent to first order at $B_0 \approx 0.534$ T, with frequency ≈ 25.9 GHz. If B_0 can be controlled to slightly better than 0.1 ppm over the ion cloud, the fractional frequency shift can be kept below 10^{-15} . All other systematic shifts, such as those due to the second-order Doppler effect, collisions, the trap electric fields, or thermal radiation, appear to be less than 10^{-15} . It should be possible to observe the transition with a Q of 2.6×10^{12} or better, by using optical pumping and detection techniques similar to those demonstrated with $^{25}\text{Mg}^+$. The accuracy of this standard could be as good as 10^{-15} , which is about 100 times better than that of the best frequency standards now available.

The proposed optical frequency standard is based on the two-photon-allowed $5d^{10}\ 6s\ ^2S_{1/2} \rightarrow 5d^9\ 6s^2\ ^2D_{5/2}$ Hg^+ transition, which has a natural Q of 7.4×10^{14} [12]. The first-order Doppler effect can be eliminated by driving the transition with counter-propagating 563.2 nm laser beams. Hyperfine-Zeeman components whose magnetic field derivatives vanish at particular values of B_0 exist in $^{199}\text{Hg}^+$ and $^{201}\text{Hg}^+$. The two-photon transition can be detected with high efficiency by using the 194.2 nm fluorescence intensity as a probe of the ground state population. Taking full advantage of the high Q transition would require a laser with linewidth less than 1 Hz, which does not exist at present. However, linewidths ≤ 100 Hz appear feasible and could be used for

initial experiments. If the laser linewidth is less than the natural linewidth, then the ac Stark shift is about 2×10^{-15} near saturation. All other systematic shifts appear to be less than 10^{-15} .

The method currently being investigated for generating the required 194.2 nm radiation is sum-frequency mixing in a K85 crystal of the output of a 792 nm single-mode cw ring dye laser and the second harmonic, generated in an ADP crystal, of the output of a 514 nm stabilized, single-mode cw Ar⁺ laser. The method has been demonstrated previously with pulsed lasers [21]. Further details of these proposed Hg⁺ frequency standards are published elsewhere [12].

Acknowledgments. We wish to acknowledge experimental assistance by Drs. J.C. Bergquist and R.E. Drullinger. This work was supported in part by the Air Force Office of Scientific Research and the Office of Naval Research.

References

1. H.A. Schuessler, E.N. Fortson, H.G. Dehmelt: *Phys. Rev.* *187*, 5-38 (1969)
2. F.G. Major, G. Werth: *Phys. Rev. Lett.* *30*, 1155-1158 (1973)
3. R. Blatt, G. Werth: *Z. Phys. A* *299*, 93 (1981)
4. R.M. Jopson, D.J. Larson: *Bull. Am. Phys. Soc.* *25*, 1133 (1980)
5. C.B. Richardson, K.B. Jefferts, H.G. Dehmelt: *Phys. Rev.* *165*, 80-87 (1968)
6. D.J. Wineland, R.E. Drullinger, F.L. Walls: *Phys. Rev. Lett.* *40*, 1639-1642 (1978)
7. R.E. Drullinger, D.J. Wineland, J.C. Bergquist: *Appl. Phys.* *22*, 365-368 (1980)
8. D.J. Wineland, W.M. Itano: *Phys. Lett.* *82A*, 75-78 (1981)
9. W. Neuhauser, M. Hohenstatt, P.E. Toschek, H. Dehmelt: *Phys. Rev. Lett.* *41*, 233-236 (1978); *Appl. Phys.* *17*, 123-129 (1978); *Phys. Rev. A* *22*, 1137-1140 (1980)
10. D.J. Wineland, J.C. Bergquist, W.M. Itano, R.E. Drullinger: *Opt. Lett.* *5*, 245-247 (1980)
11. W.M. Itano, D.J. Wineland: *Phys. Rev. A*, to be published
12. D.J. Wineland, W.M. Itano, J.C. Bergquist, F.L. Walls: *Proc. 35th Ann. Symp. on Freq. Control* (U.S. Army Electronics Command, Fort Monmouth, NJ, 1981)
13. T.W. Hansch, A.L. Schawlow: *Opt. Commun.* *13*, 68-69 (1975)
14. D.J. Wineland, H. Dehmelt: *Bull. Am. Phys. Soc.* *20*, 637 (1975)
15. D.J. Wineland, W.M. Itano: *Phys. Rev. A* *20*, 1521-1540 (1979)
16. J. Javanainen: *Appl. Phys.* *23*, 175-182 (1980)
17. W.M. Itano, D.J. Wineland: *Phys. Rev. A*, submitted
18. H. Dehmelt: *Bull. Am. Phys. Soc.* *20*, 60 (1975)
19. N.F. Ramsey: *Molecular Beams* (Oxford Univ. Press, London 1956) pp.124-134
20. P.L. Bender, J.L. Hall, R.H. Garstang, F.M.J. Pichanick, W.W. Smith, R.L. Barger, J.B. West: *Bull. Am. Phys. Soc.* *21*, 599 (1976)
21. R.E. Stickei, F.B. Dunning: *Appl. Opt.* *17*, 981-982 (1978)

Generation of continuous-wave 194-nm radiation by sum-frequency mixing in an external ring cavity

H. Hemmati, J. C. Bergquist, and Wayne M. Itano

Time and Frequency Division, National Bureau of Standards, Boulder, Colorado 80303

Received November 4, 1982

Several microwatts of tunable cw radiation near 194 nm in a linewidth of less than 2 MHz have been generated by sum-frequency mixing the radiation from a frequency-doubled argon-ion laser with the radiation from a ring dye laser in a crystal of potassium pentaborate. An external ring cavity resonant with the dye laser gives an enhancement factor of about 14 in the sum-frequency-generated radiation power. The Doppler-limited absorption spectrum of the $6s\ ^2S_{1/2}-6p\ ^2P_{1/2}$ first resonance line of natural Hg II has been resolved, and the vacuum wave number for the mass-202 isotope has been measured to be $51485.904(20)\text{ cm}^{-1}$.

High-resolution spectroscopy of atomic and molecular lines in the UV region of the spectrum requires tunable sources of radiation. Many of the tunable UV sources can only be obtained by second-harmonic generation (SHG) or sum-frequency mixing (SFM). For radiation pressure cooling and optical pumping of electromagnetically confined mercury ions, which have great potential in optical and microwave frequency standards,¹ a narrow-band tunable cw laser near the $6s\ ^2S_{1/2}-6p\ ^2P_{1/2}$ first resonance line (194.2 nm) is required. For optimum cooling, the frequency, linewidth, and stability of the radiation source must be less than the natural linewidth of the resonance line of Hg^+ (about 70 MHz) with a minimum cw power requirement, which is estimated, from experiments on Mg^+ ions,² to be about $1\ \mu\text{W}$.

In this Letter we describe a method for producing 194-nm radiation by SFM, in a potassium pentaborate (KB5) crystal, the 257-nm second harmonic of the output of a cw 515-nm argon-ion laser with the output of a tunable cw dye laser in the 792-nm region. Previously, Stickel and Dunning,³ using pulsed dye lasers, generated coherent radiation tunable between 185 and 217 nm by SFM in KB5. However, cw sources of radiation can demonstrate better frequency stability and smaller linewidths. The shortest-wavelength cw radiation that was previously produced by SFM in a crystal is approximately 211 nm.⁴ The only other technique that has been demonstrated for generation of coherent cw radiation below 200 nm is four-wave mixing in strontium vapor, at approximately 170 nm, by Freeman *et al.*⁵

A schematic of the experimental setup is shown as Fig. 1. The primary radiation sources are a ring dye laser operating with the dye LD700 near 792 nm and a 257-nm source that is the frequency-doubled output of the 515-nm line of an argon-ion laser. The 257-nm second harmonic is generated in an ammonium dihydrogen phosphate (ADP) crystal, which is placed in an external ring cavity that is resonant at the fundamental frequency.⁶ Both lasers operate in a single-frequency

mode and are frequency stabilized to separate reference cavities. For the argon-ion laser, additional long-term stabilization is provided by locking the reference cavity to a hyperfine component of a corresponding molecular iodine line. A 30-mm \times 5-mm \times 5-mm Brewster-cut KB5 crystal is used for SFM. To enhance the 792-nm radiation power inside the crystal, this crystal is placed inside an external ring cavity, similar to the frequency-doubling cavity, which is locked on resonance with the dye laser. The Brewster-cut crystal minimizes Fresnel losses for the input beams and compensates for beam astigmatism inside the ring cavity. The 792- and 257-nm input beams are polarized along the a axis of the crystal. The 194-nm beam is polarized along the c axis, and all three beams propagate along the b axis. For the biaxial KB5 crystal, this is the 90° phase-matched condition. The dye-laser beam is introduced into the cavity through a partially reflecting mirror ($R \cong 90\%$). The sum-frequency radiation is well separated from the 792-nm radiation at 15 cm from the KB5 crystal since the refraction angles for these radiations differ by $\sim 2.5^\circ$. Because of this, no special mirrors or dichroic beam splitters are necessary inside the 792-nm enhancement ring cavity to extract the 194-nm radiation. Maximum

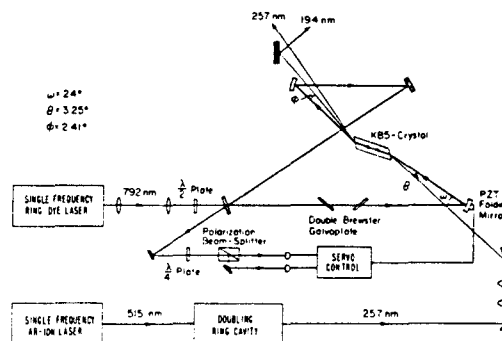


Fig. 1. Experimental setup for generation of 194-nm radiation in an external ring cavity.

TN-117

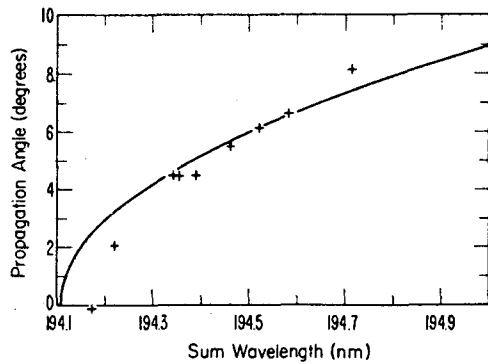


Fig. 2. Angle tuning in KB5 crystal. The crosses represent our data; the solid curve is from calculations.

enhancement is obtained inside the cavity by stabilizing the cavity on resonance, using the polarization technique discussed by Hänsch and Couillaud.⁷ A similar enhancement cavity was recently used by Couillaud *et al.* for SFM in an ADP crystal.⁸

As was previously discussed for SHG of the 257-nm radiation,⁶ the external ring cavity offers several attractive features, including the possibility of achieving higher enhancement factors than is generally possible with laser intracavity SFM. In this experiment, buildup factors as high as 14 were obtained using an input mirror with a reflectivity of about 90%. This buildup factor is presumably limited by the quality of the surface polish of our KB5 crystal.

The KB5 crystal is located inside a small housing that is equipped with electrical heaters to provide the temperature tuning necessary for the 90° phase-matched condition. This crystal is positioned in the beam waist of the cavity, which is about 50 μm in diameter and is close to the optimum spot size for sum-frequency generation. The 257-nm radiation is focused to about the same diameter and superposed with the 792-nm radiation for maximum UV generation.

With input powers of 25 and 220 mW at 257 and 792 nm, respectively, and a buildup factor of 12 in the enhancement cavity, about 2 μW of single-frequency 194-nm radiation is obtained. This corresponds to an efficiency parameter of about $3 \times 10^{-5} \text{ W}^{-1}$ for the SFM process. This is about a factor of 2 smaller than the value calculated from the previously measured nonlinear coefficients of KB5.⁹ The output radiation was measured by a calibrated EMR Type 541F-05M-14 solar-blind photomultiplier tube (PMT). About 80 mW of 257-nm and 300 mW of 792-nm radiation were obtained previously in our experiments. At these input power levels, a fourfold improvement to 8 μW of 194-nm radiation is expected. At the 2- μW power level, we see no degradation of the 194-nm radiation power with time. Since the 257- and 792-nm radiation beams are also well separated outside the crystal, again because of different refraction angles, a second ring cavity may be added to enhance the power of the 257-nm radiation, which would further increase the 194-nm radiation power. The linewidth of the 194-nm output is less than 2 MHz, inferred from the linewidth of the primary beams, each of which is about 1 MHz.

Figure 2 shows the propagation angle for the input beams in the a - b plane, relative to the b axis, versus the wavelength for which angle phase-matched SFM occurs at a temperature of about 25°C. The solid curve is calculated from the published indices of refraction.¹⁰

Figure 3 shows the wavelength for which 90° phase-matched SFM occurs, as a function of temperature. In both cases (Figs. 2 and 3) the 257-nm wavelength is fixed and the 792-nm wavelength is varied. The greatest conversion efficiency occurs when the 90° condition is met. For the mercury-ion resonance line at 194 nm, the required 90° phase-matching temperature is about 34°C.

A preliminary study was made of the isotope shift and hyperfine structure of the $6s^2 S_{1/2}$ - $6p^2 P_{1/2}$ 194.2-nm transition of singly ionized mercury by absorption spectroscopy. The argon-ion laser was stabilized at a fixed frequency while the dye laser was tuned in frequency. The dye laser could be continuously scanned over 40 GHz. The external enhancement ring cavity is locked and synchronously scanned with the dye laser. Both cavities are frequency scanned by double tipping Brewster plates, which have nearly zero insertion loss and do not cause any beam displacement as the cavities are tuned.

The absorption spectrum is obtained by probing the ground state of the singly ionized Hg ions that are created in a glass cell excited by an electrodeless rf discharge, using 150-MHz rf radiation with power of less than 10 W. The cell contained the naturally occurring Hg isotopes with Xe gas (10^{17} cm^{-3}) as the buffer and was heated to about 70°C to increase the density of the Hg atoms. To eliminate laser intensity noise, the signal was differentially detected by using two photomultiplier tubes. A fraction of the 194-nm beam was split off and directed into one PMT. The remaining radiation was directed through the Hg cell and subsequently detected by the second PMT. By using a differential amplifier, the gains of the two PMT's were adjusted to balance the intensity fluctuations of the 194-nm radiation. No attempt was made to normalize the spectrum against laser-power variations.

To calibrate the frequency scan, a portion of the 792-nm dye laser beam was directed into a 250-MHz free-spectral-range confocal interferometer. This in-

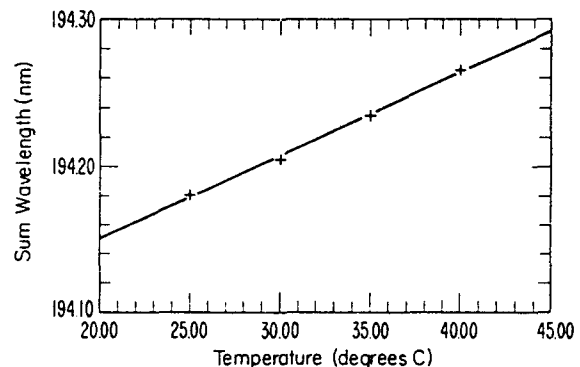


Fig. 3. Temperature tuning in KB5 crystal. The crosses represent our data; the line is a linear least-squares fit.

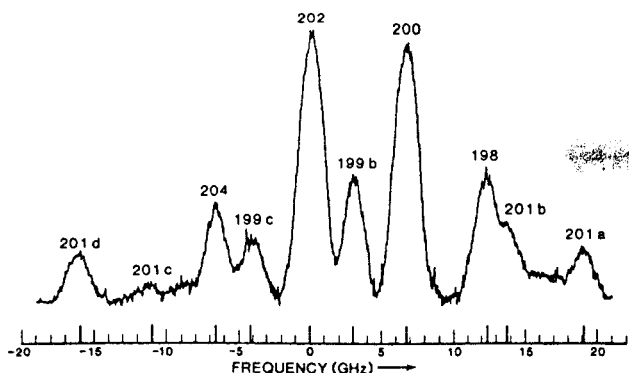


Fig. 4. Isotope and hyperfine-structure components of the 194.2-nm resonance line in natural Hg II.

terferometer gave simultaneous frequency markers with the recording of the atomic-absorption spectrum as a function of the dye-laser frequency. A single scan of the isotope and hyperfine structure of the 194-nm transition recorded in approximately 24 sec is shown in Fig. 4. The most abundant isotopes of mercury are masses 202 (30%), 200 (23%), 199 (17%), 198 (10%), 201 (13%), and 204 (7%), which appear clearly in our scan. The contribution from the 199a hyperfine component, which is located at about 24.7 GHz, to the blue of the 201a hyperfine component is not included in this figure. The relative line spacing of the absorption spectra is in good agreement with the previous work by Guern *et al.*, in which Fabry-Perot interferometric techniques were used.¹¹

The wavelength of the $^{202}\text{Hg}^+$ component was determined from the wavelengths of the input lasers. The argon-ion laser was locked to the a_2 component of the 43-0, $P(13)$ transition of $^{127}\text{I}_2$, whose vacuum wavelength is known to be 514.67352 nm.¹² An interferometric wavelength meter,¹³ which has an accuracy of a few parts in 10^7 , was used to measure the wavelength of the dye laser. The reference for the wavelength meter was a He-Ne laser stabilized to the h component of the 11-5, $R(127)$ transition of $^{127}\text{I}_2$, which has a vacuum wavelength of 632.99137 nm. Proper corrections were made for the refractive index of air for our laboratory physical conditions, using the formulas of Edlén.¹⁴ The dye-laser vacuum wavelength necessary to generate UV radiation in resonance with the $^{202}\text{Hg}^+$ component was measured to be 791.9965 ± 0.0002 nm, where the accuracy is limited by our inability to determine the line center. This corresponds to the UV sum-frequency wave number of 51485.904 ± 0.020 cm^{-1} . The uncertainty in the UV wave number has been increased because of possible line shifts caused by the electric fields of electrons and ions in the discharge. The measured width of an individual component is 1.8 GHz. If we assume that the line profile is the convolution of a Lorentzian line shape and a Gaussian Doppler profile, calculated for the temperature measured at the cell walls, we find that the width of the Lorentzian is 620 MHz, compared with the natural width of 70 MHz. The line shift can be of the same order.

In conclusion, we have demonstrated the possibility

of generating narrow-band tunable cw coherent radiation below 200 nm by SFM in KB5. If the argon-ion laser were replaced with a tunable dye laser, or if other ion laser lines were used, tunable cw UV radiation could be generated at even shorter wavelengths, possibly down to 165 nm or below. The 194-nm radiation produced by the SFM was used to resolve the isotope and hyperfine structure of the $6s\ ^2S_{1/2}-6p\ ^2P_{1/2}$ transition in Hg II and to measure the absolute wave number for this line in $^{202}\text{Hg}^+$.

We wish to thank D. J. Wineland, R. E. Drullinger, F. L. Walls, and K. B. Persson for many stimulating and useful discussions. We also thank J. Faller for the loan of the National Bureau of Standards iodine-stabilized He-Ne laser. We gratefully acknowledge the support of the U.S. Air Force Office of Scientific Research and the Office of Naval Research.

References

1. D. J. Wineland, W. M. Itano, J. C. Bergquist, and F. L. Walls, in *Proceedings of 35th Annual Symposium on Frequency Control* (Electronic Industries Associates, Washington, D.C., 1981), pp. 602-611; F. G. Major and G. Werth, *Phys. Rev. Lett.* **30**, 1155-1158 (1973); M. D. McGuire, R. Petsch, and G. Werth, *Phys. Rev. A* **17**, 1999-2004 (1978); M. Jardino, M. Desaintfusien, R. Barillet, J. Viennet, P. Petit, and C. Audoin, *Appl. Phys.* **24**, 107-112 (1981); L. S. Cutler, R. F. Gifford, and M. D. McGuire, in *Proceedings of Thirteenth Annual Precise Time and Time Interval Applications and Planning Meeting, Washington, D.C., 1981*, NASA Conf. Pub. 2220 (National Aeronautics and Space Administration, Washington, D.C., 1982), pp. 563-578; P. L. Bender, J. L. Hall, R. H. Garstang, F. M. J. Pichanick, W. W. Smith, R. L. Barger, and J. B. West, *Bull. Am. Phys. Soc.* **21**, 599 (1976).
2. D. J. Wineland, R. E. Drullinger, and F. L. Walls, *Phys. Rev. Lett.* **40**, 1639-1642 (1978).
3. R. E. Stickel, Jr., and F. B. Dunning, *Appl. Opt.* **17**, 981-982 (1978).
4. R. E. Stickel, Jr., S. Blit, G. F. Hildebrandt, E. D. Dahl, F. B. Dunning, and F. K. Tittle, *Appl. Opt.* **17**, 2270 (1978).
5. R. R. Freeman, G. C. Bjorklund, N. P. Economou, P. F. Liao, and J. E. Bjorkholm, *Appl. Phys. Lett.* **33**, 739-742 (1978).
6. J. C. Bergquist, H. Hemmati, and W. M. Itano, *Opt. Commun.* (to be published).
7. T. W. Hänsch and B. Couillaud, *Opt. Commun.* **35**, 441-444 (1980).
8. B. Couillaud, Ph. Dabkiewicz, L. A. Bloomfield, and T. W. Hänsch, *Opt. Commun.* **7**, 265-267 (1982).
9. H. J. Dewey, *IEEE J. Quantum Electron.* **QE-12**, 303-306 (1976).
10. W. R. Cook, Jr., and L. M. Hubby, Jr., *J. Opt. Soc. Am.* **66**, 72-73 (1976); F. B. Dunning and R. E. Stickel, Jr., *Appl. Opt.* **15**, 3131-3134 (1976).
11. Y. Guern, A. Bideau-Méhu, R. Abjean, and A. Johann-Gilles, *Phys. Scr.* **14**, 273-276 (1977).
12. F. Spieweck, *IEEE Trans. Instrum. Meas.* **IM-29**, 361-363 (1980).
13. J. L. Hall and S. A. Lee, *Appl. Phys. Lett.* **29**, 367-369 (1976).
14. B. Edlén, *Metrologia* **2**, 71-80 (1966).

Laser-Fluorescence Mass Spectroscopy

D. J. Wineland, J. J. Bollinger, and Wayne M. Itano

Time and Frequency Division, National Bureau of Standards, Boulder, Colorado 80303

(Received 29 December 1982)

Measurements of ion cyclotron-resonance frequencies in a Penning trap, by a laser fluorescence technique, are described. This technique has been applied to indirect measurements of the proton-to-electron mass ratio and the ${}^9\text{Be}^+$ electron g_J factor. It is found that $m_p/m_e = 1836.152\,38(62)$ (0.34 ppm) and $g_J({}^9\text{Be}^+) = 2.002\,262\,06(42)$ (0.21 ppm). Ultimately, ion cyclotron-resonance accuracies near 1 part in 10^{13} should be possible.

PACS numbers: 06.20.Jr, 07.75.+h, 35.10.-d

The possibility of performing high-resolution mass spectroscopy in a Penning electromagnetic trap has been realized for some time.¹ Recently, experiments²⁻⁴ have determined the proton-electron mass ratio m_p/m_e by alternately storing protons and electrons in the same Penning trap apparatus and comparing their cyclotron frequencies. In Ref. 2, cyclotron resonance is detected by measuring ion loss from the trap after resonant excitation. In Ref. 3, resonant excitation of cyclotron motion is detected by the increase of the ion's orbital magnetic moment; this appears as a change in the time-of-flight spectrum when ions are ejected from the trap into an axially symmetric inhomogeneous magnetic field. In Ref. 4, ion cyclotron resonance is detected by synchronously observing induced currents in the ring electrode, which is split into quadrants. The respective accuracies of m_p/m_e in these experiments are ± 2.9 ppm, ± 0.60 ppm, and ± 0.14 ppm. Here we demonstrate an alternative technique for precision mass spectroscopy in a Penning trap and apply it to an indirect measurement of m_p/m_e .

In our experiment, we measure the axial (ν_z), magnetron (ν_m), and electric-field-shifted cyclotron (ν_c') frequencies of a small cloud of atomic ions stored in a Penning trap by observing the changes in ion fluorescence scattering from a laser beam which is focused onto the ion cloud as shown schematically in Fig. 1. That is, when the ion motional frequencies are excited by an externally applied oscillating electric field, the ion orbits increase in size causing a decrease in laser fluorescence. To a good approximation, the electric field excites only the collective cen-

ter-of-mass modes, whose frequencies are equal to those of a single isolated ion in the trap.⁵ The three measured frequencies can then be combined to yield the free-space cyclotron frequency (ν_c) from the expression⁶

$$qB_0/2\pi m = \nu_c = [(\nu_c')^2 + \nu_z^2 + \nu_m^2]^{1/2} \text{ (SI units), } (1)$$

where B_0 is the (uniform) applied magnetic field, q is the ion charge, and m is the ion mass. Therefore, if ν_c is measured for different ions, mass comparisons can be made.

As a demonstration of the technique, we have compared the cyclotron frequency to magnetic-field-dependent nuclear-spin-flip hyperfine

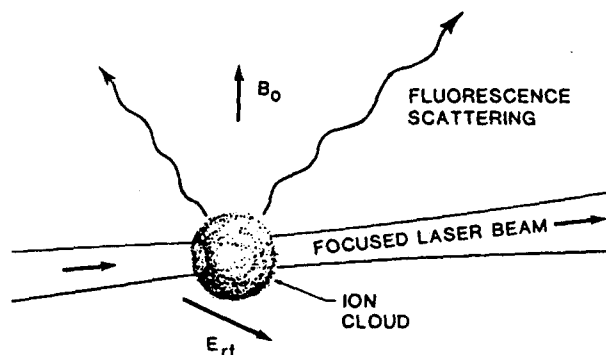


FIG. 1. Basic technique. A small sample of ions is confined by static magnetic and electric fields (not shown). A laser beam is focused onto the sample and the fluorescence scattering is observed. When the cyclotron motion is excited by an externally applied electric field (\vec{E}_{rf}) the ion orbits increase in size which results in a decrease in fluorescence.

$|\Delta M_I| = 1$ transition frequencies in the ${}^9\text{Be}^+ 2s^2S_{1/2}$ ground state. Approximately twenty ${}^9\text{Be}^+$ ions (spherical cloud of diam $\cong 100 \mu\text{m}$) were stored in a Penning trap⁴ with $1.64z_0 = r_0 = 0.417 \text{ cm}$. Typical conditions were $B_0 = 1.134 \text{ T}$ and applied trap voltage $V_0 = 1 \text{ V}$, giving $\nu_c' = 1.922 \text{ MHz}$, $\nu_s = 198 \text{ kHz}$, and $\nu_m = 10.2 \text{ kHz}$. The trap was made of gold mesh end caps and a molybdenum-mesh ring electrode. The center of the trap was at one focus of an ellipsoidal mirror; the second focus was outside the vacuum system. A lens was used to collimate the fluorescence light into a photomultiplier tube. The ions were laser cooled, compressed, and pumped into the $(M_I, M_J) = (-\frac{3}{2}, -\frac{1}{2})$ ground state by a laser tuned to the $2s-2S_{1/2}(-\frac{3}{2}, -\frac{1}{2}) - 2p^2P_{3/2}(-\frac{3}{2}, -\frac{3}{2})$ ($\lambda \cong 313 \text{ nm}$) transition.⁷ The size of the cloud was determined by using a second probe laser. The density was determined by measuring the space-charge-shifted $\vec{E} \times \vec{B}$ cloud-rotation frequency via the change in Doppler shift across the cloud by means of the probe laser.⁸ We note that this cloud-rotation frequency is $> \nu_m$; only when space charge is negligible are these frequencies equal. From these measurements of cloud size and density, ion number was determined. The magnetic-field-dependent $(-\frac{3}{2}, -\frac{1}{2}) - (-\frac{1}{2}, -\frac{1}{2})$ ground-state spin flip hyperfine transition frequency (ν_s) was measured by an rf-optical double-resonance technique described elsewhere.⁷ In some cases, the $(\frac{3}{2}, \frac{1}{2}) - (\frac{1}{2}, \frac{1}{2})$ transition was measured. The spin flip frequency and cyclotron frequency were measured nearly simultaneously on the same ion cloud by stepping rf oscillators in frequency across ν_s and ν_c' . That is, the cyclotron resonance was probed at one frequency near ν_c' and then the spin resonance probed at a frequency near ν_s . Then the cyclotron and spin oscillators were incremented (by typically 0.25 and 2 Hz, respectively) and the cycle repeated. For each step of the spin and cyclotron resonances, the laser was shut off while the resonance was driven to avoid light shifts. Resonance curves taken in this fashion are shown in Fig. 2. This simultaneous sweeping reduced the effect of slow fluctuations in B_0 (ca. $\pm 1.5 \text{ ppm/min}$). Axial and magnetron resonances could be taken separately by using the same frequency-stepping technique; however, much better axial resonance curves were observed by leaving the laser on continuously. Potentially this causes a light shift as discussed below. From the measured values of ν_s and the values for the ${}^9\text{Be}^+$ hyperfine constant (A) and nuclear-to-electron g -factor ratio (g_I/g_J), the

Breit-Rabi formula was used to determine

$$\nu_e({}^9\text{Be}^+) \cong g_J({}^9\text{Be}^+) e B_0 / (4\pi m_e), \quad (2)$$

where $g_J({}^9\text{Be}^+)$ is the electron g factor in ${}^9\text{Be}^+$ and e is the electron charge. Since $\nu_c({}^9\text{Be}^+)$ and $\nu_e({}^9\text{Be}^+)$ are measured under essentially the same conditions we have

$$R \equiv 2\nu_e({}^9\text{Be}^+) / \nu_c({}^9\text{Be}^+) \\ = g_J({}^9\text{Be}^+) m({}^9\text{Be}^+) / m_e, \quad (3)$$

where $m({}^9\text{Be}^+)$ is the ${}^9\text{Be}^+$ mass. To determine A and g_I/g_J , we have measured the $(-\frac{3}{2}, +\frac{1}{2}) - (-\frac{1}{2}, +\frac{1}{2})$ and $(\frac{3}{2}, -\frac{1}{2}) - (\frac{1}{2}, -\frac{1}{2})$ ground-state transition frequencies at field-independent points.⁷ We obtain the preliminary values $A = -625008-837.048(10) \text{ Hz}$ and $g_I/g_J = 2.134779853(2) \times 10^{-4}$. The only significant deviation from the Breit-Rabi formula is a shift in the effective value of A , proportional to B_0^2 and approximately equal to -0.017 Hz at $B_0 = 1 \text{ T}$.⁹ This has a negligible effect on the present experiment.

In our determination of R we have considered the following systematic effects:

(1) Deviations of the electric potential from a pure quadratic ($r^2 - 2z^2$). The only clearly observable systematic effect was an axial anharmonicity of approximately $(\partial\nu_s/\partial E_z)\nu_s^{-1} \cong -0.1/\text{eV}$ ($V_0 = 1 \text{ V}$). This is about 10 times larger than that observed with a trap of solid uncompensated electrodes.¹⁰ However, because of the small excitation required to observe the axial resonance, typical linewidths were $< 4 \text{ Hz}$. We have also ob-

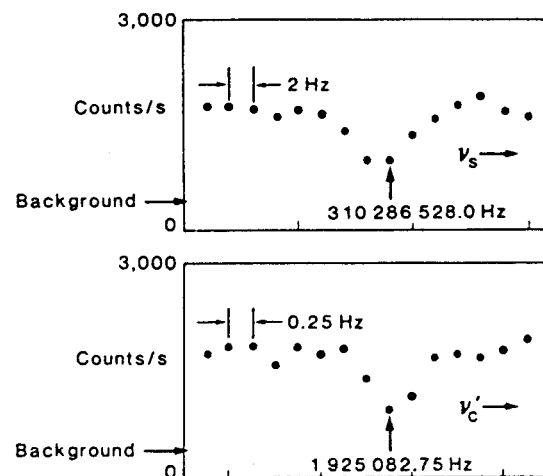


FIG. 2. Example cyclotron (ν_c') and spin (ν_s) resonances. These curves were taken nearly simultaneously by the technique described in the text. $B_0 \cong 1.134 \text{ T}$, $\nu_s \cong 215 \text{ kHz}$.

served a slight (<0.1 ppm) negative cyclotron anharmonicity which agrees in sign and approximate magnitude with the axial anharmonicity. For fixed V_0 , an error in ν_c' or ν_z due to a fourth-order anharmonic term in the electric potential causes an error in R proportional to B_0^{-2} . An error in our measurement of ν_c' which is independent of B_0 causes an error in $R \propto B_0^{-1}$.

(2) Induced-charge frequency shifts.⁵ From the measured numbers of ions this shift should be <0.1 ppm and causes an error in $R \propto B_0^{-2}$ for constant ion number.

(3) Optical-well shift. Since a focused laser beam creates an optical potential well,¹¹ we might expect a shift in ν_z . For the conditions realized here, we estimate $\Delta\nu_z/\nu_z \cong 10^{-7}$ and measure $\Delta\nu_z/\nu_z < 10^{-7}$. For fixed ν_z this shift causes an error in $R \propto B_0^{-2}$.

(4) Magnetic bottle shift.⁴ The trap could contribute to the magnetic field inhomogeneity through its susceptibility. Because the amount of material constituting the electrodes is small, we estimate this shift to be small. It causes an error in $R \propto B_0^{-1}$.

(5) Light shift on spin transitions. Although the laser is off while the ν_z power is applied we typically repeated the ν_z cycle two or four times on each point to increase the signal-to-noise ratio. This might cause a spin coherence between spin pulses which could then be light shifted. Measurements indicated that such a shift was $<0.5 \times 10^{-7}$. This shift is independent of B_0 .

(6) Space charge. Other kinds of ions were driven from the trap with strong cyclotron excitation; therefore no space-charge shifts should occur.⁵

Values of R vs B_0^{-2} and B_0^{-1} were extrapolated to the limit $B_0 \rightarrow \infty$. Axial frequencies of 292 and 215 kHz at magnetic fields of 0.673 T [$(\frac{3}{2}, \frac{1}{2}) - (\frac{1}{2}, \frac{1}{2})$ transition], 0.764 T, and 1.134 T were used. The total spread of unextrapolated values was 0.4 ppm and the total spread of extrapolated values was approximately 0.15 ppm. From these extrapolations and our estimates of systematic effects we find

$$g_J(^9\text{Be}^+)m(^9\text{Be}^+)/m_e = 32891.5710(49) \quad (0.15 \text{ ppm}). \quad (4)$$

The numbers in parentheses represent estimates of one standard deviation. We note that we have checked this result to 2 ppm accuracy by comparing $\nu_e(^9\text{Be}^+)$ to the cyclotron frequency of elec-

trons which are alternately stored in the trap.

This result, with a theoretical value^{12,13} of $g_J(^9\text{Be}^+)$ and the value¹⁴ of $m(^9\text{Be}^+)/m_p$, can be used to give an indirect determination of m_p/m_e . Using Veseth's value¹² for $g_J(^9\text{Be}^+)$, we obtain

$$m_p/m_e = 1836.15238(62) \quad (0.34 \text{ ppm}). \quad (5)$$

This value agrees with but is (0.34 ± 0.37) ppm lower than the most precise direct determination.⁴ If we assume the value of m_p/m_e from Ref. 4, we obtain

$$g_J(^9\text{Be}^+) = 2.00226206(42) \quad (0.21 \text{ ppm}). \quad (6)$$

The potential accuracy for direct mass comparisons with use of this method is extremely high. Assume that cyclotron resonance is performed on a single Be^+ ion in a trap with $z_0 = r_0/\sqrt{2} = 1$ cm, $B_0 = 6$ T, $\nu_z \cong 150$ kHz. If maximum laser cooling¹⁵ is achieved, then $z_{\text{max}} \cong 1 \mu\text{m} \gg r_c(\text{max}), r_m(\text{max})$; this implies that the effects of anharmonicities are greatly suppressed. The third- and fourth-order axial corrections to the electric potential can be nulled by proper biasing of the end cap and guard electrodes on a compensated trap.⁴ The largest uncompensated terms in the electric potential appear to be due to residual third- and fourth-order terms which violate axial symmetry. Using perturbation theory,¹⁶ we estimate these terms to be at the level of a few parts in 10^{13} (and proportional to B_0^{-2}). The induced-charge frequency shift would be at the level of a few parts in 10^{13} (proportional to B_0^{-2}). Magnetic bottle effects could be nulled¹⁷ and relativistic shifts would be negligible.

Eventually, precision mass comparisons could be made between isotopes of the same species or, more interestingly, between different nuclear isomers. In the case of nuclear isomers, if the energy difference could also be determined in terms of γ -ray wavelengths, a conversion factor from wavelength to atomic mass unit would be obtained.¹⁸ Such techniques could also be employed to study radiation pressure forces.¹¹

We gratefully acknowledge the support of the U. S. Office of Naval Research and the U. S. Air Force Office of Scientific Research. We thank R. D. Deslattes, B. N. Taylor, and R. S. Van Dyck, Jr., for helpful comments. Special thanks go to L. Veseth, R. Hegstrom, and S. J. Lipson for sending us their unpublished results.

¹D. J. Wineland, Bull. Am. Phys. Soc. 18, 1573 (1973).

- ²G. Gartner and E. Klempt., *Z. Phys. A* **287**, 1 (1978).
- ³G. Gräff, H. Kalinowsky, and J. Traut, *Z. Phys. A* **297**, 35 (1980).
- ⁴R. S. Van Dyck, Jr., and P. B. Schwinberg, *Phys. Rev. Lett.* **47**, 395 (1981).
- ⁵L. S. Brown and G. Gabrielse, *Phys. Rev. A* **25**, 2423 (1982).
- ⁶W. M. Itano and D. J. Wineland, *Phys. Rev. A* **24**, 1364 (1981).
- ⁷J. J. Bollinger and D. J. Wineland, to be published.
- ⁸W. M. Itano, unpublished calculations; S. J. Lipson, unpublished calculations; see also N. P. Economou, S. J. Lipson, and D. J. Larson, *Phys. Rev. Lett.* **38**, 1394 (1977).
- ⁹D. J. Wineland, P. A. Ekstrom, and H. G. Dehmelt, *Phys. Rev. Lett.* **31**, 1279 (1973).
- ¹⁰D. J. Wineland and H. G. Dehmelt, *J. Appl. Phys.* **46**, 919 (1975).
- ¹¹A. Ashkin, *Science* **210**, 1081 (1980).
- ¹² $g_J = 2.002\,262\,73(60)$. L. Veseth, private communication.
- ¹³ $g_J = 2.002\,262\,84(80)$. R. Hegstrom, to be published.
- ¹⁴ $m(^9\text{Be}^+)/m_p = 8.946\,534\,34(43)$ (0.048 ppm), B. N. Taylor, private communication (based on the January 1982 midstream atomic mass adjustment of A. H. Wapstra and K. Bos).
- ¹⁵W. M. Itano and D. J. Wineland, *Phys. Rev. A* **25**, 35 (1982).
- ¹⁶L. D. Landau and E. M. Lifshitz, *Mechanics* (Pergamon, New York, 1960), p. 86.
- ¹⁷G. Gabrielse and H. Dehmelt, *Bull. Am. Phys. Soc.* **26**, 598 (1981).
- ¹⁸R. D. Deslattes, private communication; see also R. D. Deslattes, E. G. Kessler, W. C. Sauder, and A. Henins, *Ann. Phys. (N.Y.)* **129**, 378 (1980).

ERRATUM

LASER-FLUORESCENCE MASS SPECTROSCOPY.
D. J. Wineland, J. J. Bollinger, and Wayne M.
Itano [Phys. Rev. Lett. 50, 628 (1983)].

The second sentence under the heading "Optical-well shift" on p. 630 should read as follows: "For the conditions realized here, we estimate an error $\Delta R/R \cong 10^{-7}$ and measure $\Delta R/R < 10^{-7}$ due to this effect." The second to the last sentence under the heading "Light shift on spin transitions" should read as follows: "Measurements indicated that a shift in R due to this effect was $< 0.5 \times 10^{-7}$."

Some of the references listed at the end of the paper are out of order. References 5, 6, 7, 8, 9, and 10 should be renumbered 6, 7, 8, 9, 10, and 5, respectively.

TIME AND FREQUENCY STANDARDS BASED ON CHARGED PARTICLE TRAPPING

Wayne M. Itano, D. J. Wineland, H. Hemmati, J. C. Bergquist, and J. J. Bollinger
Time and Frequency Division
National Bureau of Standards
Boulder, Colorado 80303

Summary

Microwave or optical frequency standards based on internal resonance transitions of ions confined in electromagnetic traps have the fundamental advantages of long observation times and small perturbations. These advantages are somewhat offset by low signal to noise ratios. Work at NBS has concentrated on microwave hyperfine transitions of atomic ions stored in Penning-type ion traps. The use of narrowband, tunable light sources for state selection and detection and for reducing the average kinetic energy of the ions (laser cooling) is an important feature of this work. Results to date include the fluorescence detection and cooling to about 50 mK of a single Mg⁺ ion and the observation of a 0.012 Hz linewidth on a 300 MHz ²⁵Mg⁺ hyperfine transition. A frequency standard based on ²⁰¹Hg ions is under development. Related work, mostly based on RF-type ion traps, is underway at several other labs.

Introduction

At present, the most accurate (reproducible) frequency standards are based on microwave transitions of atoms or molecules. The stability of a frequency standard increases with increased Q (transition frequency divided by linewidth) and increased signal to noise ratio. The reproducibility depends upon control of environmental factors. Standards based on narrow optical transitions have the advantage of higher Q for a given interaction time, for cases where the linewidth is limited by interaction time. However, the use of such a frequency standard to generate precise time, one of the chief applications of frequency standards, is very difficult with current technology. The main difficulty is dividing an optical frequency down to the RF region. Also, high-stability optical sources are not easy to produce.

An atomic frequency standard can be either active or passive in nature. In an active device, such as a self-oscillating hydrogen maser, excited

atoms decay, emitting radiation with a stable frequency. In a passive device, such as a cesium atomic beam, the atomic resonance frequency is probed by radiation derived from an oscillator whose frequency is controlled in a feedback loop so that the frequency of the radiation matches that of the atoms. All of the proposed frequency standards based on stored ions to be discussed in this paper are passive devices.

Ions can be confined for long periods (as long as days) under ultrahigh vacuum conditions in ion traps by electric and magnetic fields. For frequency standard applications, stored ions have the combined advantages of long interaction times (hence narrow resonance lines), because both the storage and relaxation times can be long, and small perturbations to transition frequencies. Atoms in atomic beams also have small perturbations, but the interaction time is limited to the flight time through the apparatus (≤ 0.01 s). Atoms can be stored without relaxation in buffer gases or coated cells for times up to about 1 s, but the transition frequencies are significantly perturbed by collisions. The fundamental disadvantage of ion traps is the low signal to noise ratio, due to the small number of ions that can be stored (typically 10^6 or less in a trap of cm dimensions).

Several laboratories have worked on developing a frequency standard based on the 40.5 GHz ground state hyperfine splitting of ¹⁹⁹Hg ions stored in a trap of the RF quadrupole (Paul) type.¹⁻⁵ State selection and detection is by optical pumping. Resonance light from a lamp containing ²⁰²Hg pumps ions from the F=1 level to the F=0 level. Resonant microwave radiation repopulates the F=1 level and is detected by an increase in the resonance fluorescence intensity. Resonance linewidths of about 1 Hz have been observed.⁴ At present, the main accuracy limitation is the second-order Doppler (time dilation) shift, which is relatively high (about 10^{-11}) because the average ion kinetic energy is a few eV. In a similar experiment on trapped ¹⁷¹Yb⁺ ions, Blatt et al.⁶ have observed a 0.06 Hz linewidth on a 12.6 GHz hyperfine transition, corresponding to a Q

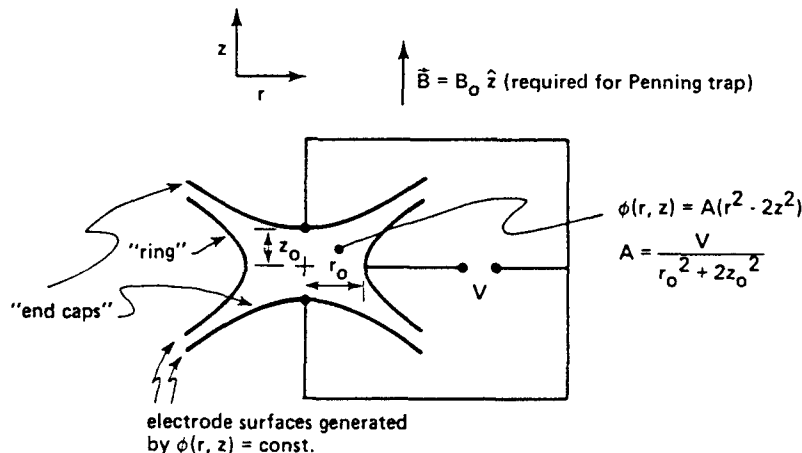


Figure 1. Electrode configuration for RF or Penning trap.

of 2×10^{11} , the highest yet obtained in microwave spectroscopy. Various proposals have been made for optical frequency standards based on narrow transitions in atomic ions,⁹ but none of them have yet been experimentally realized.

Experimental Methods and Results

The stored ion experiments at the National Bureau of Standards (NBS)¹⁰⁻¹⁵ have all used Penning traps. In a Penning trap, an outline of which is shown in Fig. 1, ions are confined by a quadrupole electric potential and a uniform magnetic field. Since only static fields are used, cooling the ions to reduce the second-order Doppler shift is much easier than in an RF trap, which uses oscillating inhomogeneous electric fields. Confinement of an ion in a Penning trap is unstable, because collisions with residual gas molecules increase the radial extent of the orbit. In practice, however, ions can be confined for days even without laser cooling (to be explained below), and indefinitely with laser cooling.

Laser cooling (also called optical sideband cooling or radiation pressure cooling) is a method by which a beam of light can be used to damp the velocity of an atom or ion. The basic mechanism for cooling of a trapped ion by a laser beam tuned slightly lower in frequency than a strongly allowed resonance transition is as follows: when the velocity of the ion is directed against the laser beam, the light frequency in the ion's frame is Doppler shifted closer to resonance so that the light scattering takes place at a higher rate than when the velocity is along the laser beam. Since the photons are reemitted in random directions, the net effect, over a motional cycle, is to damp the ion's velocity, due to absorption of photon momentum. If the laser frequency is tuned above resonance, it causes heating. The effects of frequency detuning, orientation, and intensity profile of the laser beam on laser cooling of an ion in a Penning trap have been calculated.¹⁶

Laser cooling of $Mg^{+10,11,13}$ and Be^{+15} ions has been achieved, using the strongly allowed first resonance lines. For both ions, the light sources were the second harmonics, generated in nonlinear crystals, of CW dye lasers. It is easier to reach very low temperatures with low ion densities, because of space charge induced motion. Single ions can be detected by fluorescence, as shown in Fig. 2. The four plateaus are due to the presence in the trap of three, two, one, and zero ^{24}Mg ions, which were neutralized, one by one, by ^{25}Mg atoms coming from an oven.¹³ Optical Doppler broadening measure-

ments on a single ion indicated that the effective temperature for motion parallel to the laser beam was about 50 mK.¹³ Laser cooling and detection of a single trapped ion has also been reported by Neuhauser *et al.*^{17,18}

Long relaxation times for hyperfine and Zeeman sublevels make possible a very sensitive double resonance technique.¹² In some cases, the laser polarization and frequency can be adjusted so that most of the ions are transferred to the sublevel which is coupled most strongly to the excited state and which scatters photons at a high rate. A transition from this level induced, for example, by microwaves, results in an interruption of the photon scattering until the ion is pumped back to the original sublevel by weak, off-resonance transitions. The number of photons not scattered during this period can be very large, in fact greater than 10^6 , so that the microwave transition can be detected with nearly 100% quantum efficiency, even though only a small fraction of scattered photons are counted. This is important for maximizing the signal to noise ratio in a frequency standard.

Figure 3 shows a hyperfine resonance obtained on a small cloud of laser cooled ^{25}Mg ions.¹⁴ The oscillatory lineshape results from the use of the Ramsey separated oscillatory field technique, applied in the time domain. Two coherent 1.02 s RF pulses separated by 41.4 s were used to drive the transition. This resonance demonstrates the long relaxation times possible with stored ions. Line broadening due to magnetic field variations was eliminated by operating the trap near a magnetic field at which the derivative of the transition frequency with respect to field is zero. Figure 4 shows a similar hyperfine resonance of ^{9}Be . Two 2 s RF pulses separated by 4 s were applied.¹⁹

Future Work

Details of a specific proposal for a microwave frequency standard based on a hyperfine transition of ^{201}Hg ions stored in a Penning trap have been published previously.²⁰ The main advantage of Hg is the high frequency of the transition (26 GHz). The potential accuracy is estimated to be about 1 part in 10^{15} . (At present, the most accurate frequency standards are laboratory Ca atomic beams, with an accuracy of 1 part in 10^{13} to 10^{14} .) For laser cooling and optical pumping of Hg, a narrowband, tunable, CW 194 nm source is required. Such a source has recently been developed at NBS.²¹ The second harmonic of an argon ion 515 nm laser, generated in an ADP (ammonium dihydrogen phosphate) crystal, is sum frequency mixed with a 792 nm dye

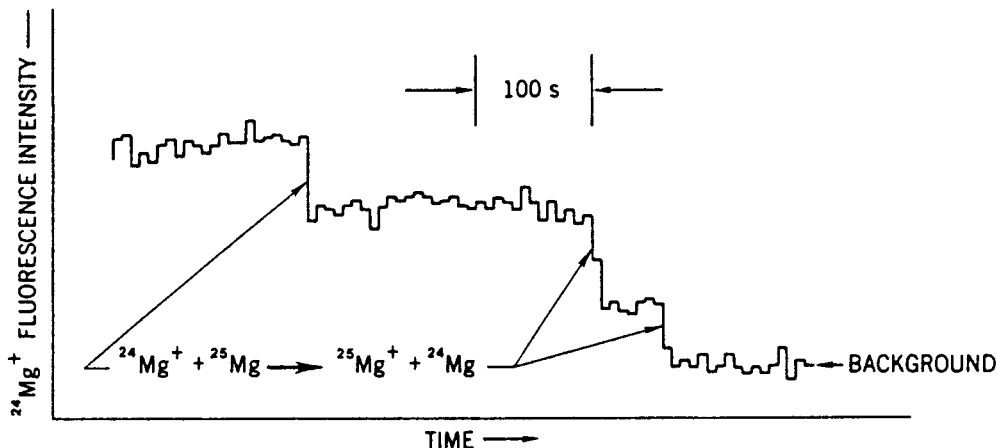


Figure 2. Fluorescence from a small cloud of $^{24}Mg^{+}$ ions. The three large steps are due to the loss of individual ions.

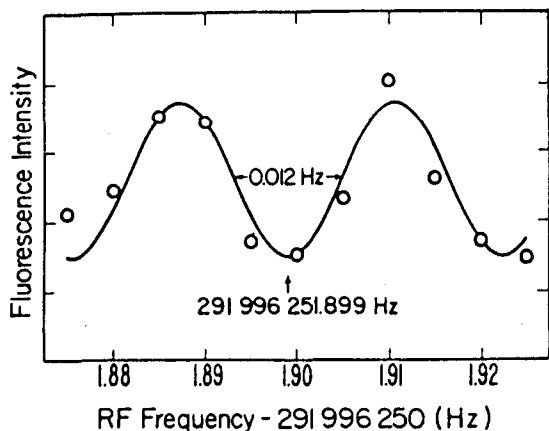


Figure 3. $^{25}\text{Mg}^+$ hyperfine resonance.

laser in a KB5 (potassium pentaborate) crystal. The output at 194 nm is about 2 μW , which should be enough for preliminary experiments.

Acknowledgments

We wish to thank the Air Force Office of Scientific Research and the Office of Naval Research for their support of this work.

References

1. F. G. Major and G. Werth, "High-Resolution Magnetic Hyperfine Resonance in Harmonically Bound Ground-State ^{199}Hg Ions," *Phys. Rev. Lett.* **30**, 1155 (1973).
2. M. D. McGuire, R. Petsch, and G. Werth, "Precision Determination of the Ground-State Hyperfine Separation in ^{199}Hg Using the Ion-Storage Technique," *Phys. Rev. A* **17**, 1999 (1978).
3. M. Jardino, M. Desaintfuscien, R. Barillet, J. Viennet, P. Petit, and C. Audoin, "Frequency Stability of a Mercury Ion Frequency Standard," *Appl. Phys.* **24**, 107 (1981).
4. L. S. Cutler, R. P. Gifford, and M. D. McGuire, "A Trapped Mercury 199 Ion Frequency Standard," *Proc. 13th Annual Precise Time and Time Interval Applications and Planning Meeting, Washington, D. C., 1981 (NASA Conf. Publ. 2220, NASA Scientific and Tech. Info. Branch, 1982) pp. 563-578.*
5. L. Maleki, "Recent Developments and Proposed Schemes for Trapped Ion Frequency Standards," *Proc. 13th Annual Precise Time and Time Interval Applications and Planning Meeting, Washington, D. C., 1981 (NASA Conf. Publ. 2220, NASA Scientific and Tech. Info. Branch, 1982) pp. 593-607.*
6. R. Blatt, H. Schnatz, and G. Werth, "Ultra-high-Resolution Microwave Spectroscopy on Trapped ^{171}Yb Ions," *Phys. Rev. Lett.* **48**, 1601 (1982).
7. H. G. Dehmelt, "Mono-Ion Oscillator as Potential Ultimate Laser Frequency Standard," *IEEE Trans. Instrum. Meas.* **IM-31**, 83 (1982).
8. F. Strumia, "Analysis of New Microwave and Optical Frequency Standards Based on Ion Storage," *Proc. 32nd Annual Symposium on Frequency Control, U. S. Army Electronics Command, Fort Monmouth, N. J., 1978 (Electronic Industries Assoc., 2001 Eye St., N. W., Washington, D. C. 20006, 1978) pp. 444-452.*
9. P. L. Bender, J. L. Hall, R. H. Garstang, F. M. J. Pichanick, W. W. Smith, R. L. Barger, and J. B. West, "Candidates for Two-Photon Absorption Optical Frequency Standards," *Bull. Am. Phys. Soc.* **21**, 599 (1976).

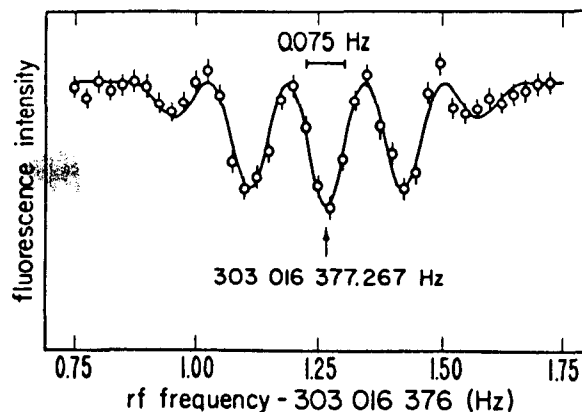


Figure 4. $^9\text{Be}^+$ hyperfine resonance.

10. D. J. Wineland, R. E. Drullinger, and F. L. Walls, "Radiation-Pressure Cooling of Bound Resonant Absorbers," *Phys. Rev. Lett.* **40**, 1639 (1978).
11. R. E. Drullinger, D. J. Wineland, and J. C. Bergquist, "High-Resolution Optical Spectra of Laser Cooled Ions," *Appl. Phys.* **22**, 365 (1980).
12. D. J. Wineland, J. C. Bergquist, W. M. Itano, and R. E. Drullinger, "Double-Resonance and Optical-Pumping Experiments on Electromagnetically Confined, Laser-Cooled Ions," *Opt. Lett.* **5**, 245 (1980).
13. D. J. Wineland and W. M. Itano, "Spectroscopy of a Single Mg^+ Ion," *Phys. Lett.* **82A**, 75 (1981).
14. W. M. Itano and D. J. Wineland, "Precision Measurement of the Ground-State Hyperfine Constant of ^{25}Mg ," *Phys. Rev. A* **24**, 1364 (1981).
15. D. J. Wineland and W. M. Itano, "Spectroscopy of Laser Cooled Be Ions," *Bull. Am. Phys. Soc.* **27**, 471 (1982); J. J. Bollinger and D. J. Wineland, unpublished.
16. W. M. Itano and D. J. Wineland, "Laser Cooling of Ions Stored in Harmonic and Penning Traps," *Phys. Rev. A* **25**, 35 (1982).
17. W. Neuhauser, M. Hohenstatt, and P. Toschek, "Optical-Sideband Cooling of Visible Atom Cloud Confined in Parabolic Well," *Phys. Rev. Lett.* **41**, 233 (1978).
18. W. Neuhauser, M. Hohenstatt, and P. Toschek, "Localized Visible Ba Mono-Ion Oscillator," *Phys. Rev. A* **22**, 1137 (1980).
19. D. J. Wineland, W. M. Itano, and J. J. Bollinger, unpublished.
20. D. J. Wineland, W. M. Itano, J. C. Bergquist, and F. L. Walls, "Proposed Stored ^{201}Hg Ion Frequency Standards," *Proc. 35th Annual Symposium on Frequency Control, U. S. Army Electronics Command, Fort Monmouth, N. J., 1981 (Electronic Industries Assoc., 2001 Eye St., N. W., Washington, D. C., 20006, 1981) pp. 602-611.*
21. H. Hemmati, J. C. Bergquist, and W. M. Itano, "Generation of CW 194 nm Radiation by Sum Frequency Mixing in an External Ring Cavity," unpublished.

FREQUENCY STANDARD RESEARCH USING STORED IONS

D. J. WINELAND, WAYNE M. ITANO, J. C. BERGQUIST, J. J. BOLLINGER and
H. HEMMATI

National Bureau of Standards, Boulder, Colorado 80303, U.S.A.

Abstract—We summarize research undertaken to develop time and frequency standards based on stored ions. The ion storage method for high resolution spectroscopy is also briefly compared to the methods for stored neutrals and slow atomic beams.

Key words—Atomic clocks, atomic spectroscopy, frequency standards, high resolution spectroscopy, laser spectroscopy.

1. INTRODUCTION

The possibility of producing very cold atomic beams and stored neutrals is exciting. Certainly these experiments are interesting by themselves but they also point the way to some new experiments in high resolution spectroscopy and may result in new schemes for atomic frequency standards. The technique of stored ions also has great promise in these applications and therefore it is useful to compare these techniques so that potential problems can be addressed in the future. In the case of trapped ions, practical frequency standards techniques have already been demonstrated. Stabilities comparable to or better than some commercial standards have been achieved and the potential is clear to obtain long term stability and accuracy of 10^{-15} in a practical device. This paper is biased toward the stored ion technique but certainly this method is not without difficult problems; moreover the potential problems with slow atomic beams and stored neutrals might be made small in the future.

1.1. *Stored Ions vs Stored Neutrals or Atomic Beams*

Probably the main attraction of the stored ion techniques for high resolution spectroscopy is that the ideal of an unperturbed species at rest in space is approached to a high degree. Specifically, charged particles such as electrons and atomic ions can be stored for long periods of time (essentially indefinitely) without the usual perturbations associated with confinement (for example the perturbations due to collisions with walls or buffer gasses in a traditional gas cell optical pumping experiment). This advantage would also appear to carry over when the stored ion technique is compared to the present schemes for stored neutrals. The current proposals for neutral trapping rely on strongly perturbing the internal structure of the atom (or molecule) to provide binding. This is especially clear for magnetostatic⁽¹⁾ and electrostatic⁽²⁾ trapping where there is a direct trade off between the atom's kinetic energy and internal energy. In the case of laser traps this trade off is not quite as clear, but in traps using either induced dipole forces⁽³⁾ or radiation pressure forces,⁽⁴⁾ rather strong ac Stark shifts accompany the trapping process. In all cases, these internal energy shifts associated with trapping may cause unwanted systematic frequency shifts in high resolution spectroscopy. This problem can be overcome if the trap is turned off while the "clock" transitions are driven, but even if maximum laser cooling is achieved on strongly allowed transitions, minimum velocities are on the order of 10 cm/s which would limit the time the trap could be off (therefore limiting Q) and would cause an additional heating mechanism. Of course, the confining fields of electromagnetic traps for ions can cause shifts but these appear to be controllable down to below 10^{-15} .⁽⁵⁻⁷⁾

In principle, atoms in an atomic beam can be totally free of external fields; this is perhaps the principal advantage of the method. We note however, that typical residual fields due to contact potentials etc. in an atomic beam apparatus can be several mV/cm. These fields might cause

observable systematic frequency shifts in certain experiments. A trapped ion on the other hand seeks the region of zero electric field; for cooled ions the average magnitude of electric field can be below 1 mV/cm.⁽⁶⁾ Perhaps the chief limitation of the atomic beam method is caused by the net linear motion of atoms; even if Doppler cancellation schemes are used, residual first order Doppler shifts can be the limiting systematic effect. This is, for example, true for the cesium beam frequency standard, the most accurate frequency and time standard available. For the case of trapped ions, the same ions can be confined nearly indefinitely; therefore the net velocity averages to zero and first order Doppler shifts are nearly absent.

The primary disadvantage of the stored ion technique is that the number of trapped ions is typically small—approximately 10^6 ions or less for a trap of centimeter dimensions. Therefore one is usually restricted to use simple atomic systems where signal to noise can be maximized.

1.2. Scope of Paper

The remainder of the paper discusses stored ion experiments whose goal is very high resolution spectroscopy—i.e. stored ion frequency standards: present status and future goals.

2. STORED IONS AND FREQUENCY STANDARDS

2.1. Microwave Frequency Standards

At present, the most accurate (reproducible) frequency standards are based on microwave transitions of atoms or molecules. The stability of a frequency standard increases with increased Q (transition frequency divided by linewidth) and increased signal to noise ratio. The reproducibility depends upon control of environmental factors. Standards based on narrow optical transitions have the advantage of higher Q for a given interaction time, for cases where the linewidth is limited by interaction time. However, the use of such a frequency standard to generate precise time, one of the chief applications of frequency standards, is very difficult with current technology. The main difficulty is dividing an optical frequency down to the RF region. Also, high-stability optical sources are not easy to produce.

An atomic frequency standard can be either active or passive in nature. In an active device, such as a self-oscillating hydrogen maser, excited atoms decay, emitting radiation with a stable frequency. In a passive device, such as a cesium atomic beam, the atomic resonance frequency is probed by radiation derived from an oscillator whose frequency is controlled in a feedback loop so that the frequency of the radiation matches that of the atoms. All of the proposed frequency standards based on stored ions to be discussed in this paper are passive devices.

Ions can be confined for long periods (as long as days) under ultrahigh vacuum conditions in ion traps by electric and magnetic fields. For frequency standard applications, stored ions have the combined advantages of long interaction times (hence narrow resonance lines), because both the storage and relaxation times can be long, and small perturbations to transition frequencies. Atoms in atomic beams also have small perturbations, but the interaction time is limited to the flight time through the apparatus (≤ 0.01 s for room temperature atoms). Atoms can be stored without relaxation in buffer gases or coated cells for times up to about 1 s, but the transition frequencies are significantly perturbed by collisions. A possible disadvantage of ion traps is the low signal to noise ratio (S/N), due to the small number of ions that can be stored. However this disadvantage can be offset by obtaining very high Q , since the stability $\sigma_y(\tau)$ of an oscillator locked to an atomic transition scales as $(S/N \cdot Q)^{-1}$. For example, if an oscillator is locked to the 26 GHz hyperfine transition in $^{201}\text{Hg}^+$ and a linewidth of 0.01 Hz is obtained, then 100 stored ions can potentially give a stability $\sigma_y(\tau) = 6 \times 10^{-14} \tau^{-1/2}$ ⁽⁸⁾ This would exceed any existing passive atomic frequency standard.

Several laboratories have worked on developing a frequency standard based on the 40.5 GHz ground state hyperfine splitting of $^{199}\text{Hg}^+$ ions stored in a trap of the rf quadrupole (Paul) type.⁽⁹⁻¹³⁾ State selection and detection is by optical pumping. Resonance light from a lamp

containing $^{202}\text{Hg}^+$ pumps ions from the $F = 1$ level to the $F = 0$ level. Resonant microwave radiation repopulates the $F = 1$ level and is detected by an increase in the resonance fluorescence intensity. Resonance linewidths of about 1 Hz have been observed.⁽¹²⁾ At present, the main accuracy limitation is the second-order Doppler (time dilation) shift, which is relatively high (about 10^{-11}) because the average ion kinetic energy is a few eV. In a similar experiment on trapped $^{171}\text{Yb}^+$ ions, Blatt *et al.*⁽¹⁴⁾ have observed a 0.06 Hz linewidth on a 12.6 GHz hyperfine transition, corresponding to a Q of 2×10^{11} , the highest yet obtained in microwave spectroscopy.

2.2. Laser Cooling and Microwave Frequency Standards

Perhaps the chief advantage of applying laser cooling to stored ions is the suppression of Doppler effects. Even without laser cooling, first order Doppler effects are highly suppressed because of the long term storage. However, without laser cooling, second order Doppler shifts can be relatively large (approximately 2×10^{-13} for room temperature Hg^+ ions) and since the velocity distributions are non-Maxwellian—these shifts are difficult to precisely characterize.

With laser cooling, temperatures < 1 K are easily obtained. The lowest temperatures (approximately 0.01 K) have been obtained for single ions.⁽¹⁵⁻¹⁷⁾ However for a microwave frequency standard, many ions are required in order to keep the signal to noise ratio high enough to maintain desired stability.^(6,8) So far the only reported experiments with the goal of a laser cooled microwave frequency standard are those of NBS.^(18,19) These experiments are based on the storage of many ions (10^2 – 10^5) in a Penning trap where residual heating mechanisms⁽²⁰⁾ are apparently much less than in the rf trap. The Penning trap⁽²⁰⁾ requires static electric and magnetic fields for trapping. Since the required magnetic fields are rather large (~ 1 T), one uses extremum points in the clock transition frequency vs magnetic field; for these conditions, stabilities below 10^{-15} should be obtained.^(8,18,19) Linewidths of approximately 0.01 Hz have been obtained on 300 MHz nuclear spin flip hyperfine transitions in⁽²¹⁾ $^{25}\text{Mg}^+$ and an oscillator has been locked to a similar transition in $^9\text{Be}^+$, giving a stability approaching 10^{-13} . Operation on a 26 GHz transition in $^{201}\text{Hg}^+$ is anticipated; inaccuracy of $< 10^{-15}$ and stabilities better than 10^{-16} appear possible.⁽⁸⁾

2.3 Optical Frequency Standards

The potential accuracy and stability of optical frequency standards, where a single isolated ion can be used to advantage (i.e. signal to noise ratio is sacrificed in favor of very high Q), are extremely high. Anticipated accuracies of 10^{-18} do not seem unreasonable provided that sufficiently narrow band lasers (≤ 10 Hz) are eventually obtained.

Optical frequency standards have the basic advantage of higher Q for fixed coherent interaction time. Dehmelt has proposed optical frequency standards based on forbidden transitions of single, laser cooled group III A ions (Tl^+ , In^+ , Ga^+ , Al^+ , or B^+) stored in small rf traps.⁽⁷⁾ Penning traps or Penning/rf trap combinations might also be used.⁽²²⁾ The $6^2\text{S}_{1/2}$ – $6^2\text{P}_{1/2}$ – $5^2\text{D}_{3/2}$ Raman transition in Ba^+ could be used as a reference to generate a stable infrared difference frequency in a nonlinear crystal.^(7,23) Also in Ba^+ , the $5^2\text{D}_{5/2}$ to $5^2\text{D}_{3/2}$ 12 μm transition⁽²⁴⁾ and the quadrupole-allowed $6^2\text{S}_{1/2}$ to $5^2\text{D}_{5/2}$ 1.8 μm transition⁽²⁵⁾ have been proposed as standards. Other high Q optical transitions in Sr^+ ,⁽²⁶⁾ Pb^+ , I^+ , and Bi^+ ⁽²⁷⁾ have been suggested for stored ion frequency standards. The two-photon^(28,8) or single photon quadrupole⁽¹⁸⁾ $5\text{d}^{10}6\text{s}^2\text{S}_{1/2}$ to $5\text{d}^96\text{s}^2\text{D}_{5/2}$ transition in Hg^+ has also been suggested. Two-photon transitions have the advantage of being first-order Doppler free even for a cloud of many ions, where it is impossible to satisfy the Dicke criterion at optical wavelengths. They have the disadvantage that the large fields required to drive the transition cause ac Stark shifts.

3. REFERENCES

1. W. PAUL and U. TRINKS, *Inst. Phys. Conf. Ser.* **42**, 18 (1978).
2. W. H. WING, *Phys. Rev. Lett.* **45**, 631 (1980).
3. See for example: A. ASHKIN, *Science* **210**, 1081 (1980); V. S. LETOKHOV and V. G. MINOGIN, *Phys. Rep.* **73**, 1 (1981), and references therein.

4. V. G. MINOGIN and J. JAVANAINEN, *Optics Commun.* **43**, 119 (1982).
5. WAYNE M. ITANO, L. L. LEWIS and D. J. WINELAND, *Phys. Rev.* **A25**, 1233 (1982).
6. D. J. WINELAND, in *Precision Measurements and Fundamental Constants II*, edited by B. N. TAYLOR and W. D. PHILLIPS, National Bur. Stds. (U.S.), Spec. Publ. 617, (in press).
7. H. DEHMELT, *I.E.E.E. Trans. Instrum. Meas.* **IM31**, 83 (1982).
8. D. J. WINELAND, W. M. ITANO, J. C. BERGQUIST and F. L. WALLS, *Proc. 35th Annual Symposium on Frequency Control*, U.S. Army Electronics Command, Fort Monmouth, NJ, 1981 (Electronic Industries Assoc., 2001 Eye St., N. W., Washington, D. C., 20006, 1981) pp. 602-611.
9. F. G. MAJOR and G. WERTH, *Phys. Rev. Lett.* **30**, 1155 (1973).
10. M. D. MCGUIRE, R. PETSCH and G. WERTH, *Phys. Rev.* **A17**, 1999 (1978).
11. M. JARDINO, M. DESAINTEFUSCIEN, R. BARILLET, J. VIENNET, P. PETIT and C. AUDOIN, *Appl. Phys.* **24**, 107 (1981).
12. L. S. CUTLER, R. P. GIFFARD and M. D. MCGUIRE, *Proc. 13th Annual Precise Time and Time Interval Applications and Planning Meeting*, Washington, D. C., 1981 (NASA Conf. Publ. 2220, NASA Scientific and Tech. Info. Branch, 1982) pp. 563-578.
13. L. MALEKI, *Proc. 13th Annual Precise Time and Time Interval Applications and Planning Meeting*, Washington, D.C., 1981 (NASA Conf. Publ. 2220, NASA Scientific and Tech. Info. Branch, 1982) pp. 593-607.
14. R. BLATT, H. SCHNATZ and G. WERTH, *Phys. Rev. Lett.* **48**, 1601 (1982).
15. W. NEUHAUSER, M. HOHENSTATT, P. TOSCHEK and H. DEHMELT, *Phys. Rev.* **A22**, 1137 (1980).
16. D. J. WINELAND and WAYNE M. ITANO, *Phys. Lett.* **82A**, 75 (1981).
17. W. NAGOURNEY, G. JANIK, and H. DEHMELT, *Proc. Natl. Acad. Sci. U.S.A.*, **80**, 643 (1983).
18. D. J. WINELAND, J. C. BERGQUIST, R. E. DRULLINGER, H. HEMMATI, W. M. ITANO and F. L. WALLS, *J. de Physique* **42**, C8-307 (1981).
19. WAYNE M. ITANO, D. J. WINELAND, H. HEMMATI, J. C. BERGQUIST and J. J. BOLLINGER, *I.E.E.E., Trans. Nuc. Sci.* **NS30**, 1521 (1983).
20. D. J. WINELAND, WAYNE M. ITANO and R. S. VAN DYCK, Jr., in *Advances in Atomic and Molecular Physics*, Vol. 19, p. 135, edited by BEDERSON and BATES, Academic Press, New York.
21. WAYNE M. ITANO and D. J. WINELAND, *Phys. Rev.* **A24**, 1364 (1981).
22. D. J. WINELAND and W. M. ITANO, *Bull. Am. Phys. Soc.* **27**, 864 (1982).
23. W. NEUHAUSER, M. HOHENSTATT, P. TOSCHEK and H. DEHMELT, *Proc. 5th Int. Conf. on Spectral Lineshapes*, West Berlin (1980).
24. H. DEHMELT, W. NAGOURNEY and G. JANIK, *Bull. Am. Phys. Soc.* **27**, 402 (1982).
25. H. G. DEHMELT, *J. de Physique* **42**, C8-299 (1981).
26. H. G. DEHMELT and H. WALTHER, *Bull. Am. Phys. Soc.* **20**, 61 (1975).
27. F. STRUMIA, *Proc. 32nd Ann. Symp. Freq. Control*, Fort Monmouth, New Jersey, Electronic Industries Assoc., 2001 Eye St., N. W. Washington, D.C., p. 444 (1978).
28. P. L. BENDER, J. L. HALL, R. H. GARSTANG, F. M. J. PICHANICK, W. W. SMITH, R. L. BARGER and J. B. WEST, *Bull. Am. Phys. Soc.* **21**, 599 (1976).

Precision Measurements of Laser Cooled ${}^9\text{Be}^+$ Ions

J.J. Bollinger, D.J. Wineland, W.M. Itano, and J.S. Wells
Time and Frequency Division, National Bureau of Standards
Boulder, CO 80303, USA

1. Introduction

The long confinement times with minimal perturbations of ion storage techniques provide a basis for high resolution spectroscopy [1,2]. Line Q's greater than 10^{10} and linewidths smaller than a few Hz have been obtained on ground-state hyperfine transitions in atomic ions stored in rf quadrupole traps [3-7]. The accuracy of these measurements has been limited, to a large extent, by the second-order Doppler shift. Radiation pressure from lasers has been used to reduce the second-order Doppler shift by cooling ion temperatures below 1 K for single Ba^+ and Mg^+ ions in an rf trap [8,9] and for single Mg^+ ions and small clouds of Mg^+ ions in a Penning trap [10-12]. ${}^9\text{Be}^+$ ions have an electronic structure similar to Mg^+ ions and are consequently easy to cool with a frequency-doubled dye laser ($\lambda=313$ nm). This paper discusses measurements of cyclotron frequencies, g-factors, hyperfine constants, and ion cloud parameters which have been made on clouds of laser-cooled ${}^9\text{Be}^+$ ions.

The ${}^9\text{Be}^+$ ions are confined by the static magnetic and electric fields of a Penning trap and stored for hours. The trap is made of gold mesh endcaps and a molybdenum mesh ring electrode. The center of the trap is at one focus of an ellipsoidal mirror; the second focus is outside the vacuum system. A lens is used to collimate the fluorescence light into a photomultiplier tube. The ions are cooled and compressed by a 313 nm narrowband source tuned to the $2s^2S_{1/2} (M_L, M_J) = (-3/2, -1/2) \rightarrow 2p^2P_{3/2} (-3/2, -3/2)$ transition. The 313 nm light source is obtained by generating the second harmonic of the output of a single mode cw dye laser in a 90° phase-matched crystal of rubidium dihydrogen phosphate (RDP). The resulting power is typically 20 μW . In addition to cooling, the 313 nm light also optically pumps the ions into the $(M_L, M_J) = (-3/2, -1/2)$ ground state [10,11].

2. Laser-Fluorescence Mass Spectroscopy

The axial (ν_z), magnetron (ν_m), and electric-field-shifted cyclotron (ν_c') frequencies of a small cloud of ${}^9\text{Be}^+$ ions stored in a Penning trap are measured by observing the changes in ion fluorescence scattering from the laser beam which is focused onto the ion cloud [13]. When the ion motional frequencies are excited by an externally applied oscillating electric field, the ion orbits increase in size, causing a decrease in laser fluorescence due to a decrease in overlap between the ion cloud and laser beam. To a good approximation, the electric field excites only the collective center-of-mass modes, whose frequencies are equal to those of a single, isolated ion in the trap [14]. The three measured frequencies can then be combined to yield the free-space cyclotron frequency (ν_c) from the expression [15]

168

Laser Spectroscopy VI, ed. by H.P.
Weber and W. Luthy, (Springer Verlag)
1983

$$qB_0/2\pi m = \nu_c = [(\nu_c^1)^2 + \nu_z^2 + \nu_m^2]^{1/2} \quad (1)$$

where B_0 is the applied magnetic field, q is the ion charge, and m is the ion mass. Mass comparisons can be made by measuring ν_c for different ions.

This technique was demonstrated by comparing the cyclotron frequency to magnetic-field-dependent nuclear-spin-flip hyperfine $|\Delta M_J| = 1$ transition frequencies in the ${}^9\text{Be}$ ground state. This, along with the Breit-Rabi formula, yielded the ratio [13]

$$R = g_J({}^9\text{Be}^+)m({}^9\text{Be}^+)/m_e \quad (2)$$

to 0.15 ppm. This result, with a theoretical value of $g_J({}^9\text{Be}^+)$ [16] and the known value [17] of $m({}^9\text{Be}^+)/m_p$, can be used to give an indirect determination of m_p/m_e ,

$$m_p/m_e = 1836.152\ 38(62) \ (0.34 \text{ ppm}) \quad (3)$$

This value agrees with the most precise direct determination [18]. If the recent value of m_p/m_e from Ref. 18 is used, an indirect determination,

$$g_J({}^9\text{Be}^+) = 2.002\ 262\ 63 \ (33) \ (0.16 \text{ ppm}), \quad (4)$$

is obtained which agrees with the theoretical calculations [16]. Because of the small cloud sizes and small excitation required to observe the motional resonance, the potential accuracy of the laser fluorescence method for mass spectroscopy is extremely high due to suppression of field inhomogeneity and trap anharmonicity effects. It is estimated that ion cyclotron resonance accuracies near 1 part in 10^{13} may ultimately be possible [13].

3. Cloud Temperature, Density, and Size

The cloud temperature, density, and size can be determined by using a second focused, frequency-doubled dye laser as a probe laser. If the probe laser is tuned from the optically pumped $(-3/2, -1/2)$ ground state to the $2p^2P_{3/2}(-3/2, +1/2)$ state, some of the ion population is removed from the $(-3/2, -1/2)$ ground state. This results in a decrease in the fluorescence light intensity. The size of this signal depends on the overlap of the probe beam with the cloud. The spatial extent of the cloud can be determined by measuring where the depopulation transition signal disappears as the probe laser is moved across the cloud. In this way the shape of the clouds is measured to be approximately ellipsoidal with typical dimensions ranging from 100 to 300 μm .

The ion cloud undergoes a slow $\vec{E} \times \vec{B}$ drift rotation about the z axis. The cloud rotation frequency differs from the single ion magnetron frequency due to the space charge of the other ions. It can be determined by measuring the change in the Doppler shift of the depopulation transition as the probe laser is moved in the radial direction. The ion number density is then obtained from the measured cloud rotation frequency. Measured densities are $1-2 \times 10^7$ ions/cm³ and are relatively independent of the number of ions in the cloud, the trap voltage, and other trap parameters. For the small and large cloud sizes, this gives total ion numbers ranging from a few ions to nearly 1000 ions.

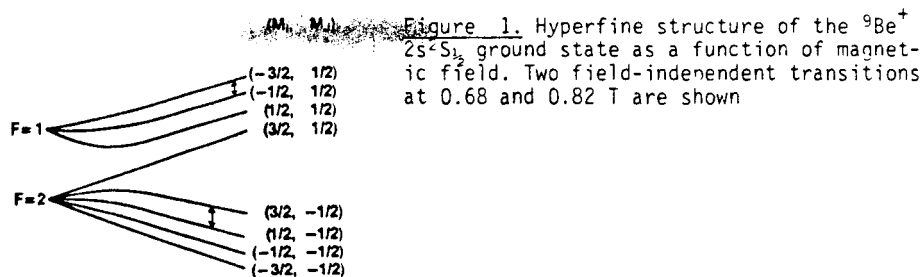
The temperature of the cyclotron motion can be determined from the full width at half maximum (fwhm) of the depopulation transition. Cyclotron temperatures of 20 to 100 mK were obtained for almost all of the clouds. From the measurements of the cloud size and rotation frequency, the magnetron kinetic energy averaged over the cloud can be determined and an effective magnetron temperature can be calculated. This temperature increases with the size of the cloud, but even for the larger clouds, it is less than 200 mK. Because the probe laser is directed perpendicular to the magnetic field, a direct measurement of the axial temperature cannot be made. The axial motion is indirectly cooled by collisional coupling to the cyclotron motion but is directly heated by the recoil of the scattered photons [19]. The equilibration time between the axial and cyclotron motions is determined to be less than 100 ms for the clouds in this experiment. The axial temperature is measured by turning off the cooling laser, waiting a variable length of time, and then measuring the temperature of the cyclotron motion. In this way axial temperatures are measured to be hotter than typical cyclotron temperatures, but not more than 200 to 300 mK for most of the clouds. A typical average temperature of 200 mK gives a second-order Doppler shift of 3 parts in 10^{15} .

In a frame of reference rotating with the cloud, the ion cloud behaves like a one-component plasma; that is, the positive charged ions behave as if they were moving in a uniform density background of negative charge [20]. The properties of such a plasma are determined by the coupling constant Γ . Γ equals the potential energy of nearest neighbors divided by the thermal energy of the ions. For Γ 's approaching 1, the plasma is called strongly coupled. Theoretical calculations predict that for $\Gamma > 2$, the plasma should have characteristics associated with those of a liquid, and at $\Gamma \approx 155$, a liquid-solid phase transition should take place [21]. We have measured Γ 's on the order of 3 or 4 for many clouds and as high as 10-15 for a few clouds. It may eventually be possible to obtain Γ 's where an ordering of the cloud into a lattice structure may take place [22].

4. Hyperfine Structure Measurements

By measuring the frequency difference between depopulation transitions when the probe laser is tuned to different $2p^2P$ states, a determination of the $2p^2P$ hyperfine structure and the $2p^2P$ fine structure separation is made [23]. The $2p^2P_{1/2}$ A value is determined to be -114.4(6.0) MHz. This is the first experimental measurement of the $2p^2P_{1/2}$ A value and it is in agreement with the theoretical calculation of -116.8(2.4) MHz [24]. The zero field $2p^2P_{1/2} - 2p^2P_{3/2}$ fine structure interval is determined to be 197.151(75) GHz. In addition, the zero field $2p^2P_{3/2} + 2s^2S_1$ and $2p^2P_{1/2} + 2s^2S_1$ optical transitions are determined to be $31\,935.3198(45)$ cm^{-1} and $31\,928.7435(40)$ cm^{-1} respectively.

The ground state hyperfine structure is determined by measuring the $(-3/2, 1/2) \rightarrow (-1/2, 1/2)$ and $(3/2, -1/2) \rightarrow (1/2, -1/2)$ ground state transition frequencies at magnetic field independent points [11] (see Fig. 1). Microwaves are used to transfer population from the optically pumped ground state to one of the states of a field independent transition. The transition is detected by a decrease in the fluorescence light intensity when the field-independent transition is probed. Figure 2 shows the signal obtained for the $(-3/2, 1/2) \rightarrow (-1/2, 1/2)$ transition. The oscillatory lineshape results from the use of the Ramsey interference method, which is implemented by driving the transition with two coherent rf pulses of 0.5 s duration separated by 19 s. The performance of an



oscillator locked to this transition is measured [25] to be comparable to the performance of a commercial Cs standard. In addition, the $(-3/2, 1/2) \rightarrow (-1/2, 1/2)$ field independent transition frequency is determined to 4×10^{-13} accuracy. Work on the $(3/2, -1/2) \rightarrow (1/2, -1/2)$ field-independent transition is not completed, but preliminary measurements have determined its frequency to 4×10^{-12} accuracy. From these two measurements, preliminary ground-state values of $A = -625\,008\,837.048(4)$ Hz (6×10^{-12}) and $g_I/g_J = 2.134\,779\,853(1) \times 10^{-4}$ (5×10^{-10}) are obtained.

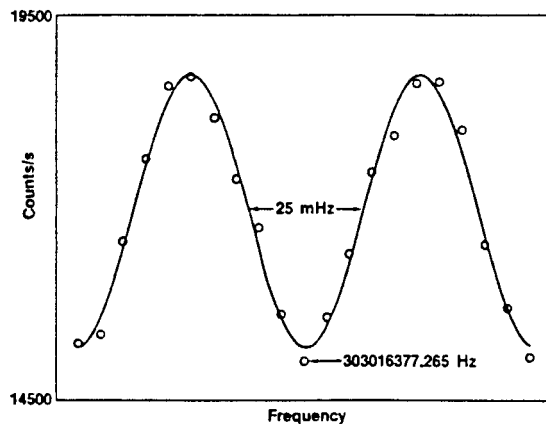


Figure 2. Signal obtained on the $(-3/2, 1/2) \rightarrow (-1/2, 1/2)$ field-independent transition. The sweep width is 100 mHz and the frequency interval between points is 5 mHz. The dots are experimental and are the average of ten sweeps; the curve is a least-squares fit

Acknowledgments

This work was supported in part by the Air Force Office of Scientific Research and the Office of Naval Research.

References:

1. H. G. Dehmelt: *Advan. Atomic and Mol. Phys.* 3, 53 (1967) and 5, 109 (1969)
2. D. J. Wineland, W. M. Itano, and R. S. Van Dyck, Jr.: *Advan. Atomic and Mol. Phys.* 19, to be published
3. H. A. Schuessler, E. N. Fortson, and H. G. Dehmelt: *Phys. Rev.* 187, 5 (1969)

4. F. G. Major and G. Werth: Phys. Rev. Lett. 30, 1155 (1973)
5. R. Blatt, H. Schnatz, and G. Werth: Phys. Rev. Lett. 48, 1601 (1982)
6. M. Jardino, M. Desaintfuscien, R. Barillet, J. Viennet, P. Petit, and C. Audoin: Appl. Phys. 24, 107 (1981)
7. L. S. Cutler, R. P. Giffard, and M. D. McGuire: "Mercury -199 Trapped Ion Frequency Standard: Recent Theoretical Progress and Experimental Results," in Proc. 37th Ann. Symp. on Freq. Control, 1983 (Systematics General Corporation, RD1 Box 352 Rt 38 Brinley Plaza, Wall Township, NJ 07719) to be published
8. W. Neuhauser, M. Hohenstatt, P. Toschek, and H. Dehmelt: Phys. Rev. Lett. 41, 233 (1978) and Phys. Rev. A 22, 1137 (1980)
9. W. Nagourney, G. Janik, and H. Dehmelt: Proc. Nat. Acad. Sci. USA 80, 643 (1983)
10. R. E. Drullinger, D. J. Wineland, and J. C. Bergquist: Appl. Phys. 22, 365 (1980)
11. W. M. Itano and D. J. Wineland: Phys. Rev. A 24, 1364 (1981)
12. D. J. Wineland and W. M. Itano: Phys. Lett. 82A, 75 (1981)
13. D. J. Wineland, J. J. Bollinger, and W. M. Itano: Phys. Rev. Lett. 50, 628 (1983) and erratum 50, 1333 (1983)
14. D. J. Wineland and H. G. Dehmelt: J. Appl. Phys. 46, 919 (1975)
15. L. S. Brown and G. Gabrielse: Phys. Rev. A 25, 2423 (1982)
16. $g_J = 2.002\ 262\ 73(60)$, L. Veseth, private communication; and $g_J = 2.002\ 262\ 84(80)$, R. Hegstrom, to be published
17. $m(^9\text{Be})/m_p = 8.946\ 534\ 34(43)$ (0.048 ppm), B. N. Taylor, private communication (based on the January 1982 midstream atomic mass adjustment of A. H. Wapstra and K. Bos)
18. R. S. Van Dyck, Jr. and P. B. Schwinberg: Phys. Rev. Lett. 47, 395 (1981) and R. S. Van Dyck, F. L. Moore, and P. B. Schwinberg: Bull. Am. Phys. Soc. 28, 791 (1983)
19. D. J. Wineland and W. M. Itano: Phys. Rev. A 20, 1521 (1979) and W. M. Itano and D. J. Wineland: Phys. Rev. A 25, 35 (1982)
20. J. H. Malmberg and T. M. O'Neil: Phys. Rev. Lett. 39, 1333 (1977)
21. S. Ichimaru: Rev. Mod. Phys. 54, 1017 (1982)
22. The behavior of the small ion clouds in this experiment may not be exactly the same as that calculated in the thermodynamic limit. Specifically, the liquid-solid phase transition may take place at a value different from $\Gamma = 155$
23. J. J. Bollinger, J. S. Wells, and D. J. Wineland: to be published
24. S. Garpman, I. Lindgren, J. Lindgren, and J. Morrison: Z. Phys. A 276, 167 (1976)
25. J. J. Bollinger, W. M. Itano, and D. J. Wineland: "Laser Cooled ^9Be Accurate Clock," in Proc. 37th Ann. Symp. on Freq. Control, 1983 (Systematics General Corporation, RD1 Box 352 Rt 38 Brinley Plaza, Wall Township, NJ 07719) to be published

Hyperfine structure of the $2p^2P_{1/2}$ state in ${}^9\text{Be}^+$

J. J. Bollinger, J. S. Wells, D. J. Wineland, and Wayne M. Itano

*Time and Frequency Division, National Bureau of Standards,
Boulder, Colorado 80303*

(Received 17 October 1984)

An optical-optical double resonance technique has been used on beryllium ions stored in a Penning trap to measure the magnetic dipole hyperfine interaction constant $A_{1/2}$ of the $2p^2P_{1/2}$ level in ${}^9\text{Be}^+$. The measured value of $A_{1/2} = -118.6(3.6)$ MHz is in good agreement with theoretical calculations. The $2p^2P$ fine-structure splitting and the $2s^2S_{1/2} \rightarrow 2p^2P_{3/2,1/2}$ optical transition frequencies have also been measured.

The $2p^2P$ hyperfine structure of the LiI electronic sequence has attracted much theoretical interest over the past two decades (see, for example, Refs. 1-4 and references contained in Ref. 5). This is because of the computational feasibility in a three-electron system, the importance of and interest in polarization and correlation effects, and the availability of good experimental measurements⁵⁻⁷ in ${}^7\text{Li}$. The $A_{1/2}$, $A_{3/2}$, and $A_{3/2,1/2}$ hyperfine constants of the $2p^2P$ state in ${}^7\text{Li}$ have been measured; these constants determine the individual spin-dipolar, orbital, and contact contributions to the $2p^2P$ hyperfine structure. Agreement with theoretical calculations is on the order of a few percent.¹ Measurements of the $A_{3/2}$ hyperfine constant of the $2p^2P$ state have been made in ${}^9\text{Be}^+$ (Ref. 8) and ${}^{11}\text{B}^{2+}$ (Ref. 9). In ${}^9\text{Be}^+$, $|A_{3/2}|$ has been measured to be less than 0.6 MHz.⁸ A Hartree-Fock central field calculation yields the value $A_{3/2} \cong -18.7$ MHz, but polarization and correlation effects contribute +17.2 MHz and produce a final value of $A_{3/2} = -1.5(1.2)$ MHz in agreement with the experimental measurements.¹ Measurements of the $A_{1/2}$ and $A_{3/2,1/2}$ hyperfine constants of the $2p^2P$ state in ${}^9\text{Be}^+$ are useful for further tests of the theoretical calculations and are needed to determine the individual spin-dipolar, orbital, and contact contributions to the $2p^2P$ hyperfine structure. This paper reports the first measurement of the $A_{1/2}$ hyperfine constant of the $2p^2P$ state in ${}^9\text{Be}^+$. The measured value of $A_{1/2} = -118.6(3.6)$ MHz is in agreement with the theoretical calculation of Ref. 1 of $-116.8(2.4)$ MHz.

Much of the experimental apparatus used in this measurement has been described in other reports.^{10,11} ${}^9\text{Be}^+$ ions were confined by the static magnetic and electric fields of a Penning trap in ultrahigh vacuum ($< 10^{-7}$ Pa). The uniform magnetic field of approximately 1.1 T nearly decoupled the nuclear spin from the total electronic angular momentum. The confining electric field (≤ 1 V/cm) had a negligible perturbation (< 1 Hz) on the $2s^2S_{1/2}$ and $2p^2P_J$ energy levels of the ions. The benign environment and long confinement times of electromagnetic traps have been used to make numerous high-precision rf and microwave measurements of the hyperfine structure in the ground state of ions.¹² Here, however, an optical measurement of the first excited state hyperfine structure was accomplished by using laser cooling to reduce the ion temperature below a few K so that the hyperfine components of the optical transition were resolved. A narrow-band (< 4 MHz) radiation source (power $\cong 20$ μW) tuned to the low-frequency side of the

$$2s^2S_{1/2}(M_J, M_J) = (-\frac{3}{2}, -\frac{1}{2}) \rightarrow 2p^2P_{3/2}(-\frac{3}{2}, -\frac{3}{2})$$

($\lambda = 313$ nm)

transition of ${}^9\text{Be}^+$ was used to cool and spatially compress the ions and optically pump them into the $(-\frac{3}{2}, -\frac{1}{2})$ ground state.¹¹ The 313-nm source was obtained by frequency doubling the output of a single-mode cw dye laser. The resonance fluorescence induced by this "cooling" laser was used to detect the ions.¹¹ Typical ion "clouds" consisted of at most several hundred ions with cloud densities of 2×10^7 ions/cm³ and cloud diameters of 100-300 μm .

The $2p^2P_{1/2}$ hyperfine structure was measured by an optical-optical double resonance technique with a second frequency-doubled dye laser, denoted the probe laser (power $\ll 1$ μW).¹³ When the probe laser was tuned in resonance with the

$$2s^2S_{1/2}(-\frac{3}{2}, -\frac{1}{2}) \rightarrow 2p^2P_{1/2}(-\frac{3}{2}, +\frac{1}{2})$$

transition (transition A), some of the ion population was removed from the $(-\frac{3}{2}, -\frac{1}{2})$ ground state. This resulted in a decrease in the observed fluorescence induced by the cooling laser. The $2s^2S_{1/2}(-\frac{3}{2}, -\frac{1}{2}) \rightarrow 2p^2P_{1/2}(-\frac{3}{2}, -\frac{1}{2})$ transition (transition B) was detected in a similar way. Radio-frequency (rf) radiation (frequency approximately equal to 300 MHz) tuned to the ground-state $(-\frac{3}{2}, -\frac{1}{2}) \rightarrow (-\frac{1}{2}, -\frac{1}{2})$ transition was used to mix the $(-\frac{3}{2}, -\frac{1}{2})$ and $(-\frac{1}{2}, -\frac{1}{2})$ ground states. Owing to this rf mixing, a decrease in the fluorescent light intensity was also observed when the probe laser was tuned from the $(-\frac{1}{2}, -\frac{1}{2})$ ground state to the $2p^2P_{1/2}(-\frac{1}{2}, +\frac{1}{2})$ state (transition C). Figure 1 shows the transitions driven by the probe laser. Figure 2(a) shows the depopulation signals obtained when the probe laser was frequency swept through transitions A and C.

Part of the probe dye laser beam, before doubling, was picked off and sent into an ${}^{127}\text{I}_2$ cell. ${}^{127}\text{I}_2$ saturated absorption spectra were simultaneously recorded as the probe laser was frequency swept through the optical transitions to the $2p^2P_{1/2}$ state (see Fig. 2). At the magnetic field used in this experiment, line number 955 of the ${}^{127}\text{I}_2$ atlas¹⁴ and the next higher-frequency line (uncataloged) approximately coincided with the ${}^9\text{Be}^+$ transitions to the $M_J = -\frac{1}{2}$ and $M_J = +\frac{1}{2}$ states of the $2p^2P_{1/2}$ manifold, respectively. The frequency differences between the I_2 hyperfine components were measured by stabilizing two dye lasers to different I_2 hyperfine components and making heterodyne difference frequency measurements on a p - i - n diode. This provided the frequency scale from which measurements of the frequency differences between the transitions detected by the

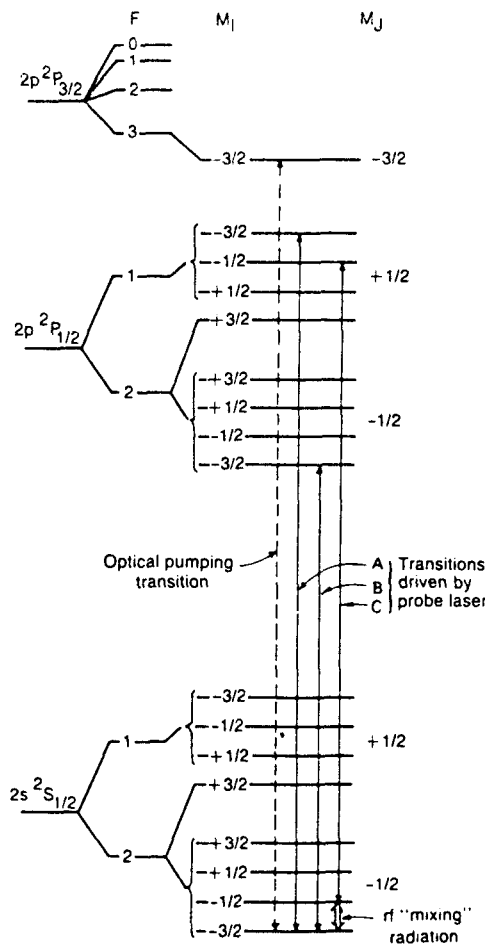


FIG. 1. Sketch of the energy levels of the $2s^2S_{1/2}$ and $2p^2P_J$ states of Be^+ . The cooling/optical pumping transition is indicated by the dotted line. The transitions detected by the probe laser are marked by solid lines and are labeled A, B, and C. The rf mixing radiation serves to populate both the $(M_l, M_j) = (-\frac{3}{2}, -\frac{1}{2})$ and $(-\frac{1}{2}, -\frac{1}{2})$ ground states.

probe laser were made. From data like that shown in Fig. 2, the frequency difference between transitions A and C was measured to be 360.4(2.4) MHz. (Error estimates in this paper are one standard deviation uncertainties.) The measured frequency difference between transitions A and B was 10787.7(5.4) MHz. In addition to random error, the error estimates include uncertainties in systematic shifts due to background slopes, overlap of neighboring transitions, and calibration of the frequency scale. By alternately chopping the probe and cooling laser beams (at about 30 Hz), potential light shifts were eliminated. Any ac Stark or ac Zeeman shifts produced by the ground-state rf mixing were estimated to be negligible.

The 360.4(2.4)-MHz difference between transitions A and C is the sum of $2p^2P_{1/2}$ hyperfine-structure contributions and the $(-\frac{3}{2}, -\frac{1}{2}) \rightarrow (-\frac{1}{2}, -\frac{1}{2})$ ground-state splitting. The ground-state contribution was separately measured by an rf-optical double resonance technique^{10,11} to be 310.286815(30) MHz. The splitting between the $2p^2P_{1/2}(-\frac{3}{2}, +\frac{1}{2})$ and $2p^2P_{1/2}(-\frac{1}{2}, +\frac{1}{2})$ states is then 50.1(2.4) MHz. In addition, the measured value of the

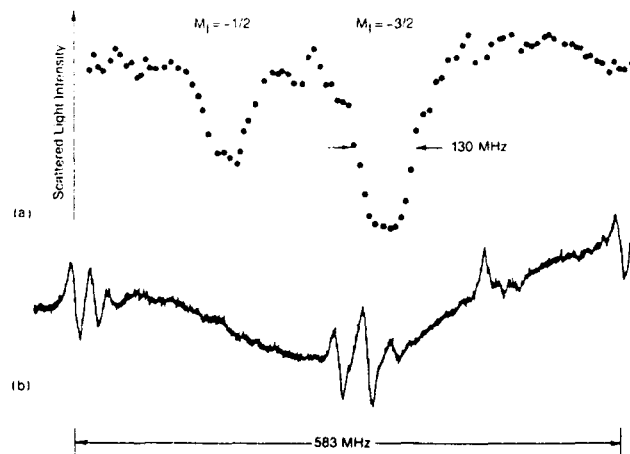


FIG. 2. (a) Depopulation signals obtained when the probe laser was frequency swept through transitions A and C. The data are the average of eight sweeps. (b) $^{127}\text{I}_2$ saturated absorption spectra ($^{127}\text{I}_2$ scattered light intensity vs frequency) simultaneously recorded with the depopulation signals. The frequency scale of the $^{127}\text{I}_2$ saturated absorption spectra is half the frequency scale of the $^9\text{Be}^+$ depopulation signals. These $^{127}\text{I}_2$ hyperfine components belong to the next higher frequency line (uncataloged) above line number 955 in the $^{127}\text{I}_2$ atlas (see Ref. 14).

$(-\frac{3}{2}, -\frac{1}{2}) \rightarrow (-\frac{1}{2}, -\frac{1}{2})$ ground-state transition was used, along with measured values of the ground-state hyperfine constant and g factors,^{10,15} to determine the magnetic field, $B = 1.1368277(22)$ T.

The absolute frequencies of the optical $2s^2S_{1/2} \rightarrow 2p^2P_{1/2}$ transitions were determined (to less precision than the frequency differences) from the simultaneous recordings of the $^9\text{Be}^+$ signals and the $^{127}\text{I}_2$ saturated absorption signals along with the tabulated frequencies¹⁴ of the $^{127}\text{I}_2$ lines. Transitions A, B, and C were measured relative to line number 954 [R91(3-8)] of the $^{127}\text{I}_2$ atlas because it was the nearest unblended line. Similarly, the $2s^2S_{1/2}(-\frac{3}{2}, -\frac{1}{2}) \rightarrow 2p^2P_{3/2}(-\frac{3}{2}, -\frac{3}{2})$ cooling transition was also measured relative to line number 960 [P89(4-10)]. These measurements, along with the measured magnetic field, the ground-state hyperfine constant and g factors,^{10,15} and the Landé g factors for the $2p^2P_{1/2}$ and $2p^2P_{3/2}$ states, determine the $2p^2P$ zero-field fine-structure interval ΔE , and the $2s^2S_{1/2} \rightarrow 2p^2P_{1/2}$ and $2s^2S_{1/2} \rightarrow 2p^2P_{3/2}$ zero-field optical transition frequencies. We obtained

$$\Delta E/h = 197\,150(64) \text{ MHz} ,$$

$$\nu(2s^2S_{1/2} \rightarrow 2p^2P_{1/2}) = 31\,928.7436(40) \text{ cm}^{-1} ,$$

$$\nu(2s^2S_{1/2} \rightarrow 2p^2P_{3/2}) = 31\,935.3198(45) \text{ cm}^{-1} .$$

These values agree with the previous, less precise measurements of Ref. 16. A many-body perturbation theory calculation^{17,18} of $\Delta E/h = 6.412 \text{ cm}^{-1} = 192\,227 \text{ MHz}$ is within 2.5% of the experimental measurement.

The Hamiltonian for the $2p^2P$ manifold is given by

$$H = H_{fs} + H_{Ze} + H_{Zn} + H_{hfs} + H'_{Ze} .$$

$H_{fs} = (\frac{2}{3})\Delta E L \cdot S$ is the fine-structure interaction. $H_{Ze} = (g_L L_x + g_S S_x)\mu_B B$ is the Zeeman interaction of the exter-

nal magnetic field with the electron orbital and spin magnetic moments. We take $g_S = 2.0023193$ (free-electron value) and $g_L = 1$ (reduced mass corrections are included in H'_{Ze}). $H_{Zn} = -g_I \mu_N I_z B$ is the Zeeman interaction of the external magnetic field with the nuclear magnetic moment. μ_B and μ_N are the Bohr and nuclear magnetons. g_I is the nuclear g factor in the $2p^2P$ state of $^9\text{Be}^+$. For the precision of these measurements, g_I can be taken equal to the g factor of the bare nucleus,¹⁹ $g_I = -0.784955(2)$. H_{hfs} is the hyperfine-structure interaction. $H_{\text{hfs}} = H_{\text{hfsm}} + H_Q$ consists of a magnetic dipole interaction H_{hfsm} and an electric quadrupole interaction H_Q . The electric quadrupole interaction does not couple the nuclear quadrupole moment with the $2p^2P_{1/2}$ states and, for the purposes of this experiment, can be neglected. H_{hfsm} can be parametrized by the three constants^{1,5}

$$A_J = \frac{\langle J, M_J = J, I, M_I = I | H_{\text{hfsm}} | J, M_J = J, I, M_I = I \rangle}{hIJ}$$

$$= \frac{\langle J, M_J = J, I, M_I = I | hA_J \mathbf{I} \cdot \mathbf{J} | J, M_J = J, I, M_I = I \rangle}{hIJ}$$

for $J = \frac{3}{2}, \frac{1}{2}$, and the off-diagonal element

$$A_{J,J-1} = \frac{\langle J, M_J, I, M_I | H_{\text{hfsm}} | J-1, M_J, I, M_I \rangle}{hM_J(J^2 - M_J^2)^{1/2}}$$

$$(E_{-3/2, 1/2} - E_{-1/2, 1/2})/h = 50.1(2.4) \text{ MHz (experiment)}$$

$$= -(1 - \alpha^2) A_{1/2} / 2 - A_{3/2}^2 / 4U + \alpha 2\sqrt{2} A_{3/2, 1/2} + g_I \mu_N B / h \quad (1)$$

$$(E_{-3/2, 1/2} - E_{-3/2, -1/2})/h = 10787.7(5.4) \text{ MHz (experiment)}$$

$$= U + \delta g_{1/2} \mu_B B / h - 3[1 - (\alpha^2 + \beta^2)/2] A_{1/2} / 2 + 3A_{1/2}^2 / 4U + (\alpha - \beta) 3\sqrt{2} A_{3/2, 1/2} \quad (2)$$

$\delta g_{1/2}$ is the sum of the corrections to the $2p^2P_{1/2}$ g_J factor due to H'_{Ze} . Its value was calculated by many-body perturbation theory to be $-10.95(3) \times 10^{-5}$.¹⁸

The quantity $A_{1/2} = -118.6(3.6)$ MHz was determined from Eqs. (1) and (2) and is in good agreement with the theoretical calculation of $A_{1/2} = -116.8(2.4)$ MHz.¹ The uncertainty is due mainly to the experimental uncertainty in the measured frequencies. A rather poor value for $A_{3/2, 1/2}$ of $A_{3/2, 1/2} = -19.2(28.6)$ MHz was also determined from Eqs. (1) and (2). The calculation of Ref. 1 predicts $A_{3/2, 1/2} = -23.2(1.0)$ MHz. The precision of the $A_{3/2, 1/2}$ measurement was limited by the small 0.04 amplitude admixture of the $2p^2P_{3/2}$ states in the $2p^2P_{1/2}$ manifold.

Increased accuracy in the hyperfine constants and an independent determination of the $2p^2P_{1/2}$ g_J factor can be obtained by measuring more transitions at higher magnetic

for $J = \frac{3}{2}$. H'_{Ze} is the relativistic, diamagnetic, and finite nuclear mass correction to the Zeeman interaction H_{Ze} .^{20,21}

If H_{Zn} , H_{hfs} , and H'_{Ze} are at first neglected, the energies and eigenstates of $H_{fs} + H_{Ze}$ can be determined analytically. Let $|J, M_J\rangle$ denote an eigenstate of J^2 and J_z . The $2p^2P_{1/2}$ $M_J = +\frac{1}{2}$ and $M_J = -\frac{1}{2}$ eigenstates of $H_{fs} + H_{Ze}$ are, respectively,

$$(1 - \alpha^2)^{1/2} |\frac{1}{2}, \frac{1}{2}\rangle - \alpha |\frac{3}{2}, \frac{1}{2}\rangle$$

and

$$(1 - \beta^2)^{1/2} |\frac{1}{2}, -\frac{1}{2}\rangle - \beta |\frac{3}{2}, -\frac{1}{2}\rangle$$

With the experimental values $B = 1.1368277(22)$ T and $(\Delta E/h) = 197150(64)$ MHz, the theoretically determined $J = \frac{3}{2}$ amplitude admixtures are $\alpha = 0.03706(1)$ and $\beta = 0.03910(1)$, and the states are theoretically split by a frequency $U = 10610.57(1)$ MHz. The effects of $H_{Zn} + H_{\text{hfsm}} + H'_{Ze}$ were treated by perturbation theory. Terms with estimated contributions of much less than 0.1 MHz were neglected. The following two equations were obtained for the measured frequency differences, $(E_{M_J, M_J} - E_{M'_J, M'_J})/h$, in the $2p^2P_{1/2}$ manifold:

fields. At approximately 6.26 T, the $2p^2P_{3/2}$, $M_J = -\frac{3}{2}$ and $2p^2P_{1/2}$, $M_J = +\frac{1}{2}$ levels cross and the $2p^2P_{3/2}$ amplitude admixture in the $2p^2P_{1/2}$ manifold is approximately 4.5 times larger than at 1.1 T. At a magnetic field of approximately 9.39 T, the $2p^2P_{3/2}$, $M_J = -\frac{3}{2}$ and $2p^2P_{1/2}$, $M_J = -\frac{1}{2}$ levels cross and the hyperfine interaction strongly couples states with $\Delta M_J = -\Delta M_J$. These antilevel crossings are particularly sensitive to the off diagonal hyperfine constant $A_{3/2, 1/2}$.^{5,6}

We gratefully acknowledge the support of the U.S. Air Force Office of Scientific Research and the U.S. Office of Naval Research. We thank J. D. Prestage and R. Blatt for carefully reading the manuscript and for helpful comments.

¹S. Garpman, I. Lindgren, J. Lindgren, and J. Morrison, Z. Phys. A 276, 167 (1976); Phys. Rev. A 11, 758 (1975).

²D. R. Beck and C. A. Nicolaides, in *The Fourth International Conference on Beam-Foil Spectroscopy, September 15-19, 1975, Gatlinburg, Tennessee*, edited by I. A. Sellin and D. J. Pegg (Plenum, New York, 1976), Vol. 2, p. 105.

³R. K. Nesbet, Phys. Rev. A 2, 661 (1970).

⁴J. D. Lyons, R. T. Pu, and T. P. Das, Phys. Rev. 178, 103 (1969).

⁵H. Orth, H. Ackermann, and E. W. Otten, Z. Phys. A 273, 221 (1975).

⁶K. C. Brog, T. G. Eck, and H. Wieder, Phys. Rev. 153, 91 (1967); H. Wieder and T. G. Eck, *ibid.* 153, 103 (1967).

⁷G. J. Ritter, Can. J. Phys. 43, 770 (1965).

⁸O. Poulsen, T. Andersen, and N. Skouboe, J. Phys. B 8, 1393 (1975).

⁹O. Poulsen, P. S. Ramanujam, and D. B. Iversen, J. Phys. B 8, L450 (1975).

¹⁰D. J. Wineland, J. J. Bollinger, and W. M. Itano, Phys. Rev. Lett. 50, 628 (1983); 50, 1333(E) (1983).

¹¹W. M. Itano and D. J. Wineland, Phys. Rev. A 24, 1364 (1981).

- ¹²D. J. Wineland, W. M. Itano, and R. S. Van Dyck, Jr., *Adv. At. Mol. Phys.* **19**, 135 (1983).
- ¹³D. J. Wineland, J. C. Bergquist, W. M. Itano, and R. E. Drullinger, *Opt. Lett.* **5**, 245 (1980).
- ¹⁴S. Gerstenkorn and P. Luc, *Atlas du spectre d'absorption de la molécule de l'iode entre 14 800–20 000 cm^{-1}* (Editions du CNRS, Paris, 1978); *Rev. Phys. Appl.* **14**, 791 (1979).
- ¹⁵W. M. Itano, D. J. Wineland, and J. J. Bollinger, *Bull. Am. Phys. Soc.* **28**, 780 (1983).
- ¹⁶L. Johansson, *Ark. Fys.* **20**, 489 (1961).
- ¹⁷L. Veseth, *J. Phys. B* **16**, 2913 (1983).
- ¹⁸L. Veseth (private communication).
- ¹⁹W. M. Itano, *Phys. Rev. B* **27**, 1906 (1983).
- ²⁰A. Abragam and J. H. Van Vleck, *Phys. Rev.* **92**, 1448 (1953).
- ²¹L. Veseth, *Phys. Rev. A* **22**, 803 (1980); *J. Phys. B* **16**, 2891 (1983).

Trapped Ions, Laser Cooling, and Better Clocks

D. J. Wineland

In a recent experiment (1) at the National Bureau of Standards (NBS) in Boulder, Colorado, the frequency of a particular hyperfine transition in the ground state of beryllium atomic ions was measured with an inaccuracy of only about one part in 10^{13} . In this experiment, the ions were confined or "trapped" in a small region of space by

tenths of a percent. On the experimental side, about 8 years ago a measurement (3) of beryllium ion hyperfine structure to an accuracy of 3 ppm (parts per million) was made. Since the accuracy of this previous measurement is presumably good enough to satisfy the theorists for quite some time in the future, one can logically ask why anyone would want to

Summary. Ions that are stored in electromagnetic "traps" provide the basis for extremely high resolution spectroscopy. By using lasers, the kinetic energy of the ions can be cooled to millikelvin temperatures, thereby suppressing Doppler frequency shifts. Potential accuracies of frequency standards and clocks based on such experiments are anticipated to be better than one part in 10^{15} .

using static electromagnetic fields and their kinetic temperature was lowered to less than 1 K by a process sometimes called "laser cooling." In all of physics, only a few measurements can boast a higher accuracy; those experiments measure similar transitions in neutral cesium atoms.

Experimental spectroscopy (the study of the interaction between radiation and matter) has traditionally provided a means of checking the theory of quantum mechanics which predicts the internal energy structure of atoms and molecules. In the case of hyperfine structure, which represents the magnetic coupling between the nucleus and atomic electrons, the theory quickly becomes very complicated. For alkali-like ions, the most sophisticated calculations (2) agree with experiment at a level of only a few

make a better measurement. Briefly, I will give three of the reasons.

1) The primary driver in several laboratories (including NBS) is to provide better clocks and frequency standards. The principal use of atomic clocks is in navigation and communications, where requirements have continued to press the state of the art. The way an atomic clock works is perhaps apparent in the internationally agreed on definition of the second: "The second is the duration of 9,192,631,770 periods of the radiation corresponding to the transition between the two hyperfine levels of the ground state of the cesium-133 atom." A simplified model for the practical realization of the second involves making a device (an atomic beam apparatus) which allows one to induce and detect transitions between the two ground-state hyperfine energy levels. When the frequency of the radiation for maximum transition probability is attained, the cycles are electroni-

cally counted; when 9,192,631,770 cycles have occurred, 1 second has passed. Several laboratories are trying to apply this same idea to the internal energy levels of ions; there is reason to believe that the inaccuracy of a time standard based on stored ions can eventually be much smaller than that of the cesium clock, which can have an accuracy of about one part in 10^{13} or less (4).

2) With the extreme accuracy attained with stored ion techniques, it may be possible to measure various small effects which would otherwise be masked by measurement imprecision. As an example, it should be possible to measure nuclear magnetic susceptibility as a small perturbation to atomic hyperfine structure (5). Nuclear magnetic susceptibility, which has not been measured previously, could give a new kind of information about nuclear structure. Trapped ions may provide a way to make the required precise measurements.

3) The system itself, laser-cooled stored ions, is intrinsically interesting and may provide the basis for other experiments which are only peripherally related to spectroscopy. An example is the study of strongly coupled three-dimensional plasmas (6).

For brevity, this article will only touch on some aspects of stored ion spectroscopy where laser cooling is employed and how they are related to better clocks and frequency standards. A recent review article (7) includes many interesting trapped ion experiments which are not discussed here.

Trapped Ions

The principal attraction of the stored ion technique is that charged particles, including electrons and atomic ions, can be stored for long periods of time (days are not uncommon) without the usual perturbations associated with confinement [for example, the frequency shifts associated with the collisions of ions with buffer gases in a more traditional optical pumping experiment (8)].

Storage has principally been accomplished in four types of "traps": the RF (radio frequency) or Paul trap, the Pen-

The author is a research physicist in the Time and Frequency Division of the National Bureau of Standards, Boulder, Colorado 80303.

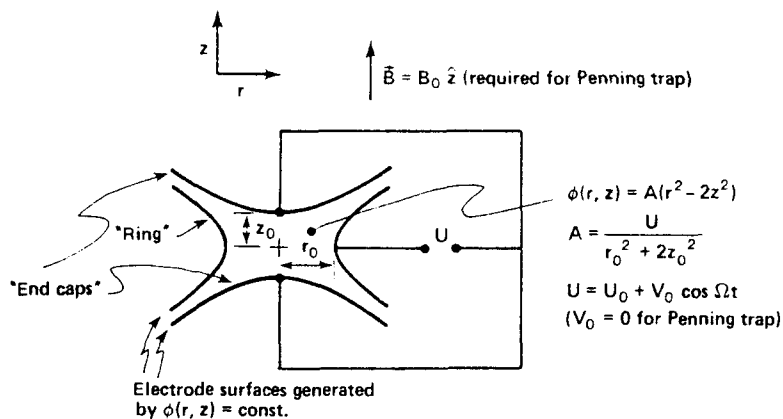


Fig. 1. Schematic representation of the electrode configuration for the "ideal" Paul (RF) or Penning trap. Electrode surfaces are figures of revolution about the z axis and are equipotentials of $\phi(r, z) = A(r^2 - 2z^2)$. (Cylindrical coordinates are used with the origin at the center of the trap.) Typical dimensions are $\sqrt{2} z_0 = r_0 \approx 1$ cm. Typical operating parameters are: for the Paul trap, $V_0 \approx 300$ V/cm, $\Omega/2\pi \approx 1$ MHz; for the Penning trap, $U_0 \approx 1$ V, $B \approx 1$ T.

ning trap, the Kingdon (electrostatic) trap, and the magnetostatic trap ("magnetic bottle"). Magnetic bottles have had limited use in high-resolution work because the trapping relies on spatially inhomogeneous magnetic fields, which can cause shifts and broadening of magnetic field-dependent lines. A notable exception is the electron g factor measurements at the University of Michigan by H. R. Crane, A. Rich, and their colleagues (9). The Kingdon trap (10) is perhaps the simplest, using only static electric fields for trapping. Since an electrostatic potential minimum cannot exist in a charge-free region, the Kingdon trap relies on a dynamical equilibrium for trapping (ions orbit around an attractive wire). Kingdon traps have been used in spectroscopic experiments by Prior and his colleagues (11), but so far neither Kingdon traps nor magnetic bottles have been used in laser cooling experiments, and therefore they will not be discussed further here.

The Paul (12) or RF trap uses inhomogeneous RF electric fields to provide confinement in a pseudopotential well (7, 13). It is the three-dimensional analog of the Paul quadrupole mass filter. To see how it works, we first note that in a (homogeneous) sinusoidal RF electric field, ion motion is sinusoidal but is 180° out of phase with respect to the electric force. If the field is somewhat inhomogeneous, it is easy to show that the force on the ion averaged over one cycle of the driven motion is toward the region of weaker field. Since an electric field minimum can exist in a charge-free region, stable trapping can be accomplished. Such a trap is shown schematically in Fig. 1, where the three trap electrodes are shaped to provide an electric poten-

tial of the form $(r^2 - 2z^2)$ inside the trap. For this "ideal" trap shape, an ion is bound in a nearly harmonic well: detection of the ion well frequencies can then be used to perform mass analysis.

The "ideal" Penning (14) trap uses the same electrode configuration as in Fig. 1 but uses static electric and magnetic fields. A harmonic potential well is provided along the z axis by static electric fields. This, however, results in a radial electric field, which forces the ions toward the "ring" electrode. This effect can be overcome if a static magnetic field \mathbf{B} is superimposed along the z axis. In this case the x - y motion of the ions is a composite of circular cyclotron orbits (primarily due to the \mathbf{B} field) and a circular $\mathbf{E} \times \mathbf{B}$ drift magnetron motion about the trap axis.

Both the Paul and Penning traps can provide long-term confinement. Storage times of days are not uncommon: in the first single-electron (Penning trap) experiments (15) the same electron was used in experiments for several weeks! This long-term storage is important in spectroscopy because (i) "transit time" broadening (the broadening of transitions due to the time-energy uncertainty relation associated with the time the ion stays in the trap) can be made negligible and (ii) the average velocity $\langle v \rangle$ of the ions approaches zero. The latter is important because it can make averaged first-order Doppler frequency shifts negligible. Suppression of such first-order Doppler shifts is perhaps the chief advantage over the atomic beam method; for example, residual first-order Doppler shifts (due to the net velocity of the atomic beam) are the main limitation to accuracy for the cesium beam frequency standard. (Actually, even though

$\langle v \rangle \rightarrow 0$ for the traps, the first-order Doppler effect is proportional to $\langle \mathbf{k} \cdot \mathbf{v} \rangle$, where \mathbf{k} is the wave vector of the radiation. For spatially inhomogeneous radiation fields, shifts can occur. If the lifetime of the ion's internal transition is long compared to the periods of ion motion, these effects result in asymmetric sidebands at the ion motional frequencies; however, the "pulling" caused by these sidebands can be extremely small.)

The perturbation of the ions' internal structure due to trapping can be extremely small. Perhaps the most troublesome frequency shifts are caused by electric fields. Shifts which are linearly dependent on the electric field are absent because the average electric field $\langle \mathbf{E} \rangle = 0$. (We know that because if $\langle \mathbf{E} \rangle \neq 0$ the ions would leave the trap.) Second-order shifts can be quite small. As an example, the shift of the ground-state hyperfine frequency of Hg^+ ions, ν_0 (Hg^+), has been calculated (16) as $\delta\nu/\nu_0$ (Hg^+) $\approx -1.4 \times 10^{-18} E^2$, where E is in volts per centimeter. Radio-frequency electric fields in an RF trap may be as high as 300 V/cm; this could give a fractional shift of 10^{-13} . However, for small samples of laser-cooled ions electric fields can be smaller than 1 mV/cm (17), yielding negligible shifts. (The restoring electric forces become less as the ion's kinetic energy is reduced.) Of course, there are also shifts associated with electric fields due to ion-ion collisions, but these are expected to be smaller than the trapping fields (17).

In most cases the magnetic field (\mathbf{B}) of the Penning trap (typically about 1 T or 10^4 gauss) causes large frequency shifts to the ions' internal structure. The energy separation of the beryllium hyperfine transition mentioned in the introduction goes to zero at zero magnetic field (1); therefore, in some sense, the energy separation is entirely due to the external magnetic field. This might be regarded as a severe disadvantage, except that this transition and some others become independent of magnetic field to first order at certain magnetic fields. Second-order field dependence can be small; for the beryllium example $\Delta\nu/\nu_0 = -0.017 (\Delta B/B)^2$, so if the field is held to 10^{-8} of the nominal field (this can be done with a superconducting magnet), the fractional shifts are only 1.7×10^{-18} . Thus, magnetic fields can strongly perturb the internal structure but these perturbations may only be a philosophical disadvantage. For the clock application we do not care about their existence if they can be made reproducible and stable; more-

over, these perturbations are physically interesting since they can sometimes be calculated with high precision.

A third feature of the traps may be regarded as either a disadvantage or advantage. Typically, the number of ions that can be trapped is rather small. Densities in the range of 10^5 to 10^7 cm^{-3} are typical; therefore the total number of ions may be quite small. Fortunately, atomic ions can be sensitively detected; this is apparent in the single-ion experiments discussed below. In many spectroscopic experiments it is anticipated that the signal-to-noise ratio can approach the theoretical limit (18)—that is, that it can be limited only by the statistical fluctuations in the number of ions that make the transition. We note that if we could obtain much higher densities by using larger confining fields then we would lose one of the advantages of the technique because electric field frequency shifts would become troublesome in very high resolution work.

The small sample sizes can actually be regarded as an advantage in a couple of ways. First, the small numbers imply that the ions can be confined to a small region of space—down to dimensions on the order of $1 \mu\text{m}$ or less for single ions (19, 20). This means that field imperfections—deviations from the quadratic electric potential or deviation from uniformity of the magnetic field in Penning traps—can be quite small over the ion sample. Therefore accuracy in magnetic field-dependent studies (mass spectroscopy, g factor measurements) can be extremely high. Second, in single-photon absorption spectra it is desirable to satisfy the Lamb-Dicke criterion (21)—that is, confinement to dimensions $\leq \lambda/2\pi$, where λ is the wavelength of the radiation. When the Lamb-Dicke criterion is satisfied, first-order Doppler effects (broadening or sideband generation) are suppressed. For optical wavelengths this condition can be met only for single confined ions.

For high-resolution spectroscopy, Paul and Penning traps have many desirable features in common, but they differ in some important respects. The magnetic field of the Penning trap may be a disadvantage in some experiments but it may also be the clear choice for magnetic field-dependent studies. The RF trap is able to provide tighter spatial confinement and may be the best choice for optical frequency standards (where it is desirable to satisfy the Lamb-Dicke criterion), although the Penning trap can nearly satisfy the Lamb-Dicke criterion on optical transitions in certain cases.

Heating mechanisms in the Paul trap (due to the large RF fields) are typically more severe than in the Penning trap. This can be an important problem for large numbers of stored ions.

Laser Cooling

The experiments of Dehmelt and collaborators (13) in the 1960's showed the ability of the stored ion technique to obtain very high resolution in atomic spectra. Prior to 1970, the ground-state hyperfine transition in the $^3\text{He}^+$ ($\nu_0 \cong 8.7$ GHz) ion was measured in an RF trap with a line width of only 10 Hz (22), but the accuracy was limited by the second-order Doppler shift ($\Delta\nu/\nu_0 = -1/2 \langle v^2 \rangle / c^2$) to 10 Hz (c = speed of light). The second-order Doppler effect is due to relativistic time dilation. Because the atoms are moving, their time proceeds slower than a laboratory observer; this effect must be accounted for. The relatively large second-order Doppler frequency shifts imposed by the high velocities of the stored ions and the difficulty of measuring their velocity distribution have historically been the main limitation to achieving high accuracy in stored ion spectra.

In 1975 proposals were made (23, 24) to get around this general problem of the second-order Doppler shift by a process commonly called laser (or sideband) cooling. The idea is outlined for the case of an atom with internal (optical) transition frequency ν_a having natural (radiative) line width $\Delta\nu_a$. Assume that the atom is constrained to move in a harmonic well along the z axis (one-dimensional model of the ion trap). Therefore its velocity is given by $v_z = v_0 \cos 2\pi\nu_\nu t$, where ν_ν is its oscillation frequency in the well and we assume $\nu_\nu \gg \Delta\nu_a$. When observed along the direction of the motion, the spectrum in the laboratory contains the central resonance line (at frequency ν_a) with sidebands generated by the first-order Doppler effect at frequencies $\nu_a + n\nu_\nu$ having intensity $J_n^2(\nu_0\nu_a/c\nu_\nu)$ (with n a positive or negative integer); here, J_n is the Bessel function of order n . This spectrum is a simple frequency modulation (FM) spectrum where the frequency modulation is supplied by the first-order Doppler effect (21). If we irradiate the atom with photons of frequency $\nu_L = \nu_a + n\nu_\nu$, the frequencies of the resonantly scattered photons occur at ν_a and nearly symmetrically around ν_a at the sideband frequencies $\nu_a \pm \nu_\nu, \nu_a \pm 2\nu_\nu, \dots$. Therefore, although photons of energy $h(\nu_a + n\nu_\nu)$

are absorbed, on the average photons of energy $h\nu_a$ are reemitted; when n is negative, this energy difference causes the kinetic energy of the atom to decrease by $n h \nu_\nu$ per scattering event.

This explanation in terms of sidebands (24) is easily visualized for $\nu_\nu \gg \Delta\nu_a$. For all experiments done so far $\Delta\nu_a \gg \nu_\nu$; however, the above conclusion is still valid. An alternative explanation (23) for this limit (note that when $\nu_\nu \rightarrow 0$ the atoms are free) is that when $\nu_L < \nu_a$, the atom predominantly interacts with the incident radiation when it moves toward the source of radiation and Doppler shifts the frequency into resonance—that is, when $\nu_L(1 + v_z/c) = \nu_a$. In the absorption process, the photon momentum is first transferred to the atom, causing its momentum to change by h/λ , where h is Planck's constant. Since the reemission occurs nearly symmetrically in the $\pm z$ directions, the net effect is to change the velocity of the atom by $\Delta v_z = h/M\lambda$ (M = mass of the atom). If $\Delta v_z \ll v_z$, then the kinetic energy of the absorber decreases by an amount $Mv_z\Delta v_z = nh\nu_\nu$. The cooling process is weak in that it takes about 10^4 scattering events to do substantial cooling below room temperature; it is strong in that, for allowed transitions, the resonant scattering rate can approach 10^8 sec^{-1} . Clearly, however, we require a situation where a two-level system is approached in order to have 10^4 scattering cycles; hence we usually think in terms of simple atomic systems.

Laser cooling was first observed in 1978 in experiments at both NBS (Boulder) and Heidelberg University. In the NBS experiments (25), the temperature of Mg^+ ions was monitored by observing the induced currents (26) in the trap electrodes of a Penning trap. At magnetic fields of about 1 T a two-level system is formed in $^{24}\text{Mg}^+$ (the most abundant isotope) by driving the $3s^2S_{1/2}$ ($M_J = -1/2$) \leftrightarrow $3p^2P_{3/2}$ ($M_J = -3/2$) transition with linearly polarized light (see inset in Fig. 2). From the selection rule $\Delta M_J = 0, \pm 1$, the ion must fall back to the original ground state. In addition, because other allowed transitions are driven weakly, about 16/17 of the ions are pumped into the $M_J = -1/2$ ground state (27). In these experiments, cooling to $\cong 40$ K was observed and was limited by the noise in the induced current detection.

In the first Heidelberg experiments (28), cooling was observed through the increased storage time of Ba^+ ions in a miniature Paul trap. (Separation between the end caps $2z_0 \cong 0.5$ mm.) The line

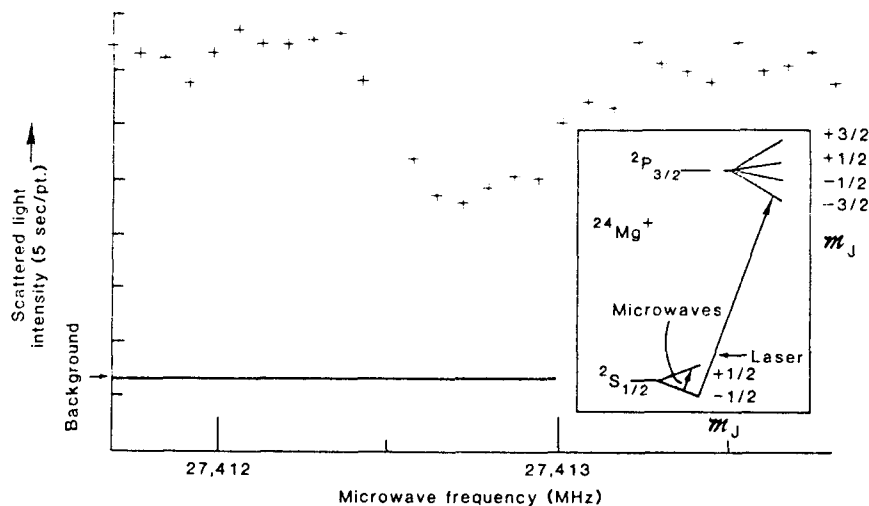


Fig. 2. Microwave/optical double resonance spectrum of $^{24}\text{Mg}^+$. Inset shows relevant energy levels of $^{24}\text{Mg}^+$ in a magnetic field. With the laser tuned to the transition shown, the ions are pumped into the $^2S_{1/2}$ ($M_J = -1/2$) ground state and a two-level system is formed with this ground state and the excited $^2P_{3/2}$ ($M_J = -3/2$) state. When incident microwaves are tuned to the ($M_J = -1/2$) \leftrightarrow ($M_J = +1/2$) ground-state Zeeman transition, these levels are nearly equally populated, which causes a decrease in fluorescence scattering from the ions. Transitions in other ions are detected in a similar way to this example. [From (27)]

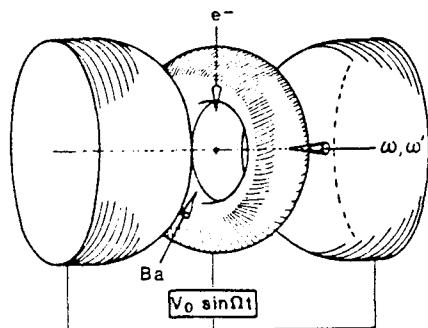
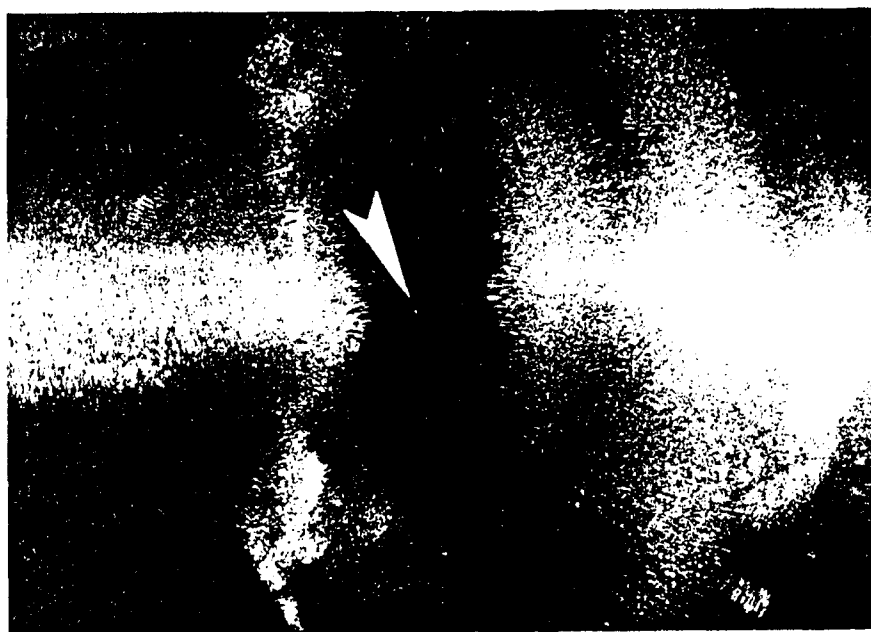


Fig. 3. Photographic image of a single Ba^+ ion (indicated by arrow) localized at the center of a miniature RF trap ($z_0 \cong 0.25$ mm). The lower part of the figure is a drawing of the trap electrodes in the same orientation as in the photograph. [From (19)]

that was used for cooling was the $6s^2S_{1/2} - 6p^2P_{1/2}$ transition ($\lambda = 493$ nm). A second laser ($\lambda = 650$ nm) was required to empty the metastable $^2D_{3/2}$ state to which atoms could decay from the $^2P_{1/2}$ state. More recently, laser cooling experiments on trapped ions have been carried out at Seattle (20) and Orsay (29). In addition, laser cooling on neutral atomic beams has also been observed (30).

In both kinds of traps, it has become customary to describe the resulting ion kinetic energy in terms of temperature; however, this must be interpreted with caution. For a cloud of ions in a Penning trap it is theoretically possible (31) to cool the cyclotron and axial energy to approximately $h\Delta\nu_a/2$. Equating this energy to $k_B T$ where k_B is Boltzmann's constant, we get $T \cong 1$ mK for $\Delta\nu_a = 43$ MHz (Mg^+). However, the kinetic energy in the magnetron motion depends on the space charge density and size of the cloud (6) and can be much larger than this for more than a few ions in the trap. In a similar vein, for a cloud of ions in an RF trap, the energy of motion in the pseudopotential well can be cooled to the same limit as the cyclotron or axial motion in a Penning trap (28). However space charge repulsion tends to push the ions toward the edge of the cloud where the energy in the driven motion can be much larger than this. These problems (17) which can cause undesirable second-order Doppler shifts can be suppressed in both traps by going to very small numbers of ions—down to one.

Single Ions

In subsequent Heidelberg experiments (19) single ions were observed in an RF trap by laser fluorescence scattering. Figure 3 is a photograph of a single Ba^+ ion. The size of the image determined the extent of the ion motion; therefore the temperature in the pseudopotential well was measured to be between 10 and 36 mK. [The driven motion "temperature" will be equal to or larger than this (13, 17).] Laser cooling of single Mg^+ ions in Penning (32) and RF (20) traps has also been accomplished. The lowest temperatures attained are those of the Seattle group (20), where the temperature in at least two directions of the pseudopotential motion was determined to be less than 20 mK. [Cooling in all directions will be straightforward (19).] In both of the magnesium experiments, the temperature was determined from the Doppler broadening on the optical cooling

transition. For temperatures below about 0.1 K this Doppler broadening contributes only a small part of the total line width, which is now primarily due to radiative decay. Therefore, very low temperature becomes difficult to measure. In the future this problem may be circumvented by probing narrow optical transitions as described below. In any case, the amount of cooling that has already been achieved gives a significant reduction in the second-order Doppler shift correction. If we can assume, for example, that magnesium ions have been cooled to 10 mK, then the second-order Doppler shift correction is about one part in 10^{16} .

Spectra

Strongly allowed transitions, which are desirable for the laser cooling, are perhaps not so interesting for high-resolution spectroscopy since the resolutions are limited by the radiative line width (as in the case of Mg^+ above). For high-resolution spectroscopy we usually think in terms of optical pumping/double-resonance detection schemes. A simple example which is characteristic of the method is shown in Fig. 2. In this case, the object was to detect the ($M_J = -1/2$) \leftrightarrow ($M_J = +1/2$) ground-state Zeeman transition. The ions are both laser-cooled and pumped into the $^2S_{1/2}$ ($M_J = -1/2$) ground state as discussed above. The fluorescence (scattered) light intensity is monitored while a microwave generator whose output is directed at the ions is frequency swept through the Zeeman transition. When the resonance condition is satisfied the ground-state populations are nearly equalized; this causes a decrease in the scattered light, which is then the signature of the microwave resonance. This example is illustrative of the various detection schemes used but it is not so interesting for high-resolution spectroscopy since here the line width of the transition was limited by magnetic field fluctuations.

A more interesting example is given by the ground state ($M_I = -3/2$, $M_J = +1/2$) \leftrightarrow ($M_I = -1/2$, $M_J = +1/2$) nuclear spin flip hyperfine transition of $^{25}Mg^+$. At a field of about 1.24 T, the first derivative of this transition frequency with respect to magnetic field goes to zero; therefore the transition frequency becomes highly insensitive to magnetic field fluctuations. At this field, the resonance shown in Fig. 4 was measured (33) with a line width of only 0.012 Hz. The oscillatory line shape results from the

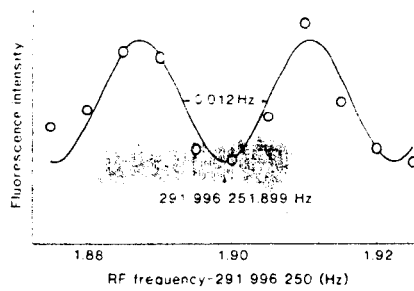


Fig. 4. Graph of a hyperfine resonance of trapped $^{25}Mg^+$ ions. The oscillatory line shape results from the use of the Ramsey resonance method, implemented by applying two coherent RF pulses 1.02 seconds long, separated by 41.4 seconds. The solid curve is a theoretical line shape [From (32)]

use of the Ramsey method (34) in the time domain: two phase coherent RF pulses 1.02 seconds long separated in time by 41.4 seconds were used to drive the transition. In order to avoid light shifts, the laser was shut off while the RF transition was driven.

A similar transition was used for the beryllium "clock" mentioned in the introduction. For the beryllium case, the most important limitation to accuracy was caused by a second-order Doppler shift. This resulted because when the laser was off during the RF transition period (about 20 seconds), the ions were heated slightly due to background gas collisions. This problem can be suppressed in the future by using cryogenic pumping.

Frequency Standards and Clocks

In a frequency standard or clock, measurement imprecision ($\delta\nu_{\text{error}}/\nu_0$) is approximately equal to $(Q S/N)^{-1}$, where $Q \equiv \nu_0/\Delta\nu_0$ and S/N is the signal-to-noise ratio for detecting the number of ions that have made the transition. If the radiative line width is small enough, then the experimentally observed line width ($\Delta\nu_0$) need only be limited by the length of time taken to induce the transition. Because of this, $\Delta\nu_0$ is probably independent of the species of trapped ion used. Therefore, we would like to use as high a frequency (ν_0) as possible in order to increase Q and reduce measurement imprecision. This is the single disadvantage of either Mg^+ or Be^+ ions, since the interesting "clock" transitions are only around 300 MHz ($Q \approx 10^{10}$). A better ion for a laser-cooled microwave clock is perhaps Hg^+ (18) ($\nu_0 \approx 40$ GHz for $^{199}Hg^+$). Very important frequency standard work has already been accom-

plished with this ion (35), but laser cooling is much harder to achieve than for Be^+ or Mg^+ (partly because the 194-nm cooling radiation is difficult to produce), and has not been done yet.

A logical extension of this idea is to go to much higher frequency—for example, to use a narrow optical transition. The anticipated Q in this case can be extremely high, 10^{15} or more. A number of transitions in various ions have been proposed (7); Dehmelt (36) was the first to suggest that such extremely high resolution spectroscopy could be carried out by using single-photon transitions in, for example, single group IIIA ions. For instance (36), the $^1S_0 \leftrightarrow ^3P_0$ transition in Tl^+ ($\lambda = 202$ nm) has a $Q \approx 5 \times 10^{14}$. For such single-photon optical transitions, it is desirable to approximately satisfy the Lamb-Dicke criterion; this is most easily accomplished with single trapped ions. Others (37) have proposed using two-photon Doppler-free transitions, for example the $^2S_{1/2} \rightarrow ^2D_{5/2}$ transitions in Hg^+ ($\lambda = 563$ nm, $Q = 7 \times 10^{14}$). Two-photon optical transitions with equal frequency photons have the advantage of eliminating the first-order Doppler effect for a cloud of many ions, where it is impossible to satisfy the Lamb-Dicke criterion. They ultimately have the disadvantage that the rather large optical fields necessary to drive the transition cause undesirable a-c Stark shifts.

Already, in experiments at Heidelberg and Washington (38), the two-photon $^2S_{1/2} \rightarrow ^2P_{1/2} \rightarrow ^2D_{3/2}$ stimulated Raman transition in Ba^+ has been observed. In these transitions, the first-order Doppler effect is present; its magnitude (for copropagating beams) is the same as that of a single laser beam at the difference frequency. Present results (38) are limited by laser line width broadening, but such transitions should also be extremely narrow; the lifetime of the $^2D_{3/2}$ state in Ba^+ is 17.5 seconds (39), which would give an intrinsic Q of 1.6×10^{16} .

For single ions, optical spectra should give precise temperature information through the intensity of the motional sidebands generated by the Doppler effect (35, 40). In the near future, the resolution of the sideband structure in the transitions noted above will probably be limited by the laser line widths. This problem might be alleviated by driving a stimulated Raman transition between two nearly degenerate levels in the electronic ground state of the ion. In $^{24}Mg^+$, for example, the $^2S_{1/2}$ ($M_J = -1/2$) \rightarrow $^2P_{1/2}$ ($M_J = -1/2$) \rightarrow $^2S_{1/2}$ ($M_J = -1/2$) transition could be driven by using two

laser beams separated in frequency by the $M_J = -1/2$, and $M_J = +1/2$ ground-state frequency difference. The effects of the laser line width would be suppressed by generating the two laser lines with a phase modulator (41): the line width of the overall transition would be limited by the ground-state lifetime. The intensity of the motional sidebands would depend on $v \cdot (\mathbf{k}_1 - \mathbf{k}_2)$, where \mathbf{k}_1 and \mathbf{k}_2 are the wave vectors of the two laser beams and v is the ion velocity. Thus the angle between the beams could be chosen to optimize the temperature information.

Conclusions

The projected accuracy for optical frequency standards is extremely high. As an example, in In^+ , the line width of the $^1S_0 \rightarrow ^3P_1$ "cooling" transition is about 1.3 MHz; this implies a second-order Doppler shift of 10^{-19} or lower. Other systematic shifts can occur (1, 7, 13, 16, 18, 33, 35-38, 42) but it is not unreasonable to think they will be controllable to this level. These extreme accuracies make important the problem of measurement imprecision, since the signal-to-noise ratio on a single ion will be about one for each measurement cycle. Practically speaking, this means that a long averaging time will be required to reach a measurement precision equal to these accuracies. In fact, for a while, the accuracy and resolution may be limited by laser line width characteristics (line width and line width symmetry); however, the potential for extremely narrow lasers also exists (43).

With the great potential for the optical frequency standards, one can logically ask why we bother thinking about RF or microwave frequency standards, where the desired large numbers of ions (to increase signal-to-noise and measurement precision) causes unwanted second-order Doppler effects (17). At present, the answer concerns the utility of optical frequency standards within current technological limitations. To use such devices as clocks as in communications and navigation, one must count cycles of the radiation. At microwave frequencies this is straightforward. At

optical frequencies it is technically feasible but very hard (44); it has not been done yet. To illustrate further, one might also have asked why we do not push the frequency even higher, that is, make a clock based on narrow Mössbauer transitions in bound nuclei. Here, however, the technological problems become even more apparent. In spite of the technical problems of making an optical "clock," optical frequency standards will, of course, find many immediate uses. An obvious class of experiments are cosmological in nature; for example, more precise measurements of the gravitational red shift will arise. In any case, the potential accuracy for stored ion spectroscopy in all spectral regions seems extremely high. Frequency standards and clocks with inaccuracy of one part in 10^{15} appear very reasonable; eventually they could be orders of magnitude better than this.

References and Notes

- J. J. Bollinger, W. M. Itano, D. J. Wineland, *Proc. 37th Annu. Symp. Freq. Control* (1983), p. 37 (copies available from Systematics General Corporation, Brinley Plaza, Route 38, Wall Township, N.J. 07719).
- S. Garpman, I. Lindgren, J. Lindgren, J. Morrison, *Z. Phys. A* 276, 167 (1976); S. Ahmad *et al.*, *Phys. Rev. A* 27, 2790 (1983).
- J. Vetter, H. Ackermann, G. ZuPutlitz, E. W. Weber, *Z. Phys. A* 276, 161 (1976).
- A. G. Mungall and C. C. Costain, *IEEE Trans. Instrum. Meas.* IM-32, 224 (1983); G. Becker, *Proc. 10th Int. Congr. Chronometry* 2, 33 (1979); D. J. Wineland, D. W. Allan, D. J. Glaze, H. Hellwig, S. Jarvis, Jr., *IEEE Trans. Instrum. Meas.* IM-25, 453 (1976).
- D. J. Larson, *Bull. Am. Phys. Soc.* 19, 1193 (1974).
- J. J. Bollinger and D. J. Wineland, *Phys. Rev. Lett.* 53, 348 (1984).
- D. J. Wineland, W. M. Itano, R. S. Van Dyck, Jr., *Adv. At. Mol. Phys.* 19, 135 (1983).
- E. W. Weber, *Phys. Rep.* 32, 123 (1977).
- A. Rich and J. C. Wesley, *Rev. Mod. Phys.* 44, 250 (1972).
- K. H. Kingdon, *Phys. Rev.* 21, 408 (1923).
- M. H. Prior and E. C. Wang, *Phys. Rev. A* 16, 6 (1977).
- E. Fisher, *Z. Phys.* 156, 1 (1959); R. F. Wuerker, H. Shelton, R. V. Langmuir, *J. Appl. Phys.* 30, 342 (1959).
- H. G. Dehmelt, *Adv. At. Mol. Phys.* 3, 53 (1967); *ibid.* 5, 109 (1969).
- F. M. Penning, *Physica* 3, 873 (1936).
- P. Ekstrom and D. Wineland, *Sci. Am.* 243 (No. 2), 104 (1980); D. J. Wineland, P. Ekstrom, H. Dehmelt, *Phys. Rev. Lett.* 31, 1279 (1973).
- W. M. Itano, L. L. Lewis, D. J. Wineland, *Phys. Rev. A* 25, 1233 (1982).
- D. J. Wineland, *Natl. Bur. Stand. (U.S.) Publ.* 617, in press.
- D. J. Wineland, W. M. Itano, J. C. Bergquist, F. L. Walls, *Proc. 35th Annu. Symp. Freq. Control* (1981), p. 602 (copies available from Electronic Industries Association, 2001 Eye Street, NW, Washington, D.C. 20006).
- W. Neuhauser, M. Hohenstatt, P. Toschek, H. Dehmelt, *Phys. Rev. A* 22, 1137 (1980).

- W. Nagourney, G. Janik, H. Dehmelt, *Proc. Natl. Acad. Sci. U.S.A.* 80, 643 (1983).
- R. H. Dicke, *Phys. Rev.* 89, 472 (1953).
- H. A. Schuessler, E. N. Fortson, H. G. Dehmelt, *ibid.* 187, 5 (1969).
- T. W. Hansch and A. L. Schawlow, *Opt. Commun.* 13, 68 (1975).
- D. J. Wineland and H. G. Dehmelt, *Bull. Am. Phys. Soc.* 20, 637 (1975).
- D. J. Wineland, R. E. Drullinger, F. L. Walls, *Phys. Rev. Lett.* 40, 1639 (1978).
- H. G. Dehmelt and F. L. Walls, *ibid.* 21, 127 (1968); D. A. Church and H. G. Dehmelt, *J. Appl. Phys.* 40, 3421 (1969).
- D. J. Wineland, J. C. Bergquist, W. M. Itano, R. E. Drullinger, *Opt. Lett.* 5, 245 (1980).
- W. Neuhauser, M. Hohenstatt, P. Toschek, H. Dehmelt, *Phys. Rev. Lett.* 41, 233 (1978).
- F. Plumelle, Abstracts for the 15th European Group on Atomic Spectroscopy Conference, Madrid, 5 to 8 July 1983.
- S. V. Andreev, V. I. Balykin, V. S. Letokhov, V. G. Minogin, *JETP Lett.* 34, 442 (1981); J. V. Prodan, W. D. Phillips, H. J. Metcalf, *Phys. Rev. Lett.* 49, 1149 (1982); J. L. Hall, W. Ertmer, R. Blatt, in preparation; W. D. Phillips, Ed., "Laser-cooled and trapped atoms," *Natl. Bur. Stand. (U.S.) Spec. Publ.* 653 (1983).
- W. M. Itano and D. J. Wineland, *Phys. Rev. A* 25, 35 (1982).
- D. J. Wineland and W. M. Itano, *Phys. Lett. A* 82, 75 (1981).
- W. M. Itano and D. J. Wineland, *Phys. Rev. A* 24, 1364 (1981).
- N. F. Ramsey, *Molecular Beams* (Oxford Univ. Press, London, 1956).
- F. G. Major and G. Werth, *Phys. Rev. Lett.* 30, 1155 (1973); M. D. McGuire, R. Petsch, G. Werth, *Phys. Rev. A* 17, 1999 (1978); M. Jardino *et al.*, *Appl. Phys.* 24, 107 (1981); L. S. Cutler, R. P. Giffard, M. D. McGuire, *Proc. 37th Annu. Symp. Freq. Control* (1983), p. 32 (copies available from Systematics General Corporation, Brinley Plaza, Route 38, Wall Township, N.J. 07719); M. Jardino, F. Plumelle, M. Desaintfuscién, J. L. Duchène, *Proc. 38th Annu. Symp. Freq. Control* (Philadelphia, 1984), in press.
- H. Dehmelt, *IEEE Trans. Instrum. Meas.* IM-31, 83 (1982).
- P. L. Bender *et al.*, *Bull. Am. Phys. Soc.* 21, 599 (1976).
- W. Neuhauser, M. Hohenstatt, P. E. Toschek, H. Dehmelt, in *Spectral Line Shapes*, B. Wende, Ed. (deGruyter, Berlin, 1981); W. Nagourney, *Bull. Am. Phys. Soc.* 29, 815 (1984).
- R. Schneider and G. Werth, *Z. Phys. A* 293, 103 (1979).
- H. A. Schuessler, *Appl. Phys. Lett.* 18, 117 (1971); F. G. Major and J. L. Duchène, *J. Phys. (Orsay)* 36, 953 (1975); H. S. Lakkaraju and H. A. Schuessler, *J. Appl. Phys.* 53, 3967 (1982); M. Jardino, F. Plumelle, M. Desaintfuscién, in *Laser Spectroscopy VI*, H. P. Weber and W. Lüthy, Eds. (Springer-Verlag, New York, 1983), p. 173.
- J. E. Thomas *et al.*, *Phys. Rev. Lett.* 48, 867 (1982).
- D. J. Wineland and W. M. Itano, *Bull. Am. Phys. Soc.* 27, 864 (1982).
- J. L. Hall, L. Hollberg, Ma Long-Shen, T. Baer, H. G. Robinson, *J. Phys. (Orsay)* 42, C8-59 (1981); A. Yariv and K. Vahala, *IEEE J. Quant. Electron.* QE-19, 889 (1983); R. W. P. Drever *et al.*, *Appl. Phys. B* 31, 97 (1983); J. Hough *et al.*, *ibid.* 33, 179 (1984).
- See Proceedings of the Third Symposium on Frequency Standards and Metrology, *J. Phys.* 42, Colloque C-8, December 1981; V. P. Chebotayev *et al.*, *Appl. Phys. B* 29, 63 (1982); D. A. Jennings *et al.*, *Opt. Lett.* 8, 136 (1983); K. M. Baird, *Phys. Today* 36 (No. 1), 52 (1983).
- I gratefully acknowledge the support of the Office of Naval Research and the Air Force Office of Scientific Research. I also thank J. J. Bollinger, J. C. Bergquist, J. Cooper, W. M. Itano, J. D. Prestage, and S. R. Stein for helpful comments on the manuscript.

SPECTROSCOPY OF STORED ATOMIC IONS

D. J. Wineland, Wayne M. Itano, J. C. Bergquist,
J. J. Bollinger and J. D. Prestage
Time and Frequency Division
National Bureau of Standards
325 Broadway
Boulder, Colorado 80303

I. INTRODUCTION

In this paper, we briefly review measurements of atomic ion spectra made with the stored ion technique in the last few years. By design, its scope is limited; for example, in these proceedings G. Werth will review experiments specifically relating to high resolution microwave spectra of stored ions and R. S. Van Dyck Jr. and D. A. Church will discuss applications of the stored ion technique to $g-2$ measurements and collision studies respectively. We will also omit the interesting excited state lifetime measurements made using traps¹⁻³ and measurements of molecular spectra³. More comprehensive reviews are given elsewhere³⁻¹⁶; we also refer the reader to the abstracts for this conference.

The ion storage technique for studies of atomic spectra is actually quite general and could in principle be used on all atomic and molecular ions; in practice, however, we find that its applicability is more limited. The number of ions that can be stored is typically rather small (densities $\lesssim 10^6/\text{cm}^3$, trap volume $\lesssim 10\text{ cm}^3$) and therefore the signal to noise ratio in many experiments is rather small. This problem is compounded if the ion population is distributed over many states as in the case of molecules, but in spite of these difficulties, trapped molecular ion spectra have been obtained by laser induced fluorescence³. The low densities of course yield the main advantage of the technique - that is, the perturbations on the ions' internal structure (due to ion-ion collisions for example) are extremely small. This coupled with long storage times and methods for obtaining cold samples can lead to very high resolution and accuracy.

II. TRAPPING

The basic methods of trapping have been discussed in the various reviews referred to in the introduction. The Paul (or rf) trap is the most popular method; both it and the Penning trap can provide very long trapping times ($>$ hours). The Kingdon trap is finding increased use (partially because of its simplicity) but the

Atomic Physics 9, R.S. Vandyck Jr.
and E.N. Fortson, eds., (World
Scientific, Singapore, 1985)

magnetostatic trap or magnetic bottle has not been used very much in spectroscopy because of the inhomogeneous fields required for trapping. Combinations of the above traps have been studied but not extensively used. A summary of trap methods has been given in a recent review³ and in other papers in these proceedings.

III. STATE PREPARATION AND DETECTION

Optical Pumping/Double Resonance

In the past several years the dominant method of state selection and detection of stored atomic ions has been via optical means. More conventional optical pumping and detection with lamps¹⁷ and lasers¹⁸ has been used for example to measure hyperfine spectra¹⁹. In addition, some novel optical pumping and detection effects have been realized using lasers with trapped ions; we illustrate this with a few examples.

In Fig. 1, we show the $3^2S_{1/2}$ and $3^2P_{3/2}$ level structure of $^{24}\text{Mg}^+$ ions in a magnetic field. If a laser is tuned to the $(-1/2) \rightarrow (-3/2)$ transition (numbers in parentheses refer to the ground $3^2S_{1/2}$ and excited $3^2P_{3/2}$ values of M_J respectively) then we note that ions must decay to the $M_J = -1/2$ ground level because of the selection rule $\Delta M_J = 0, \pm 1$. At first, one might think that after many photon scattering events the ions are gradually pumped from the $M_J = -1/2$ to $M_J = +1/2$ ground state level because of excitation in the wings of

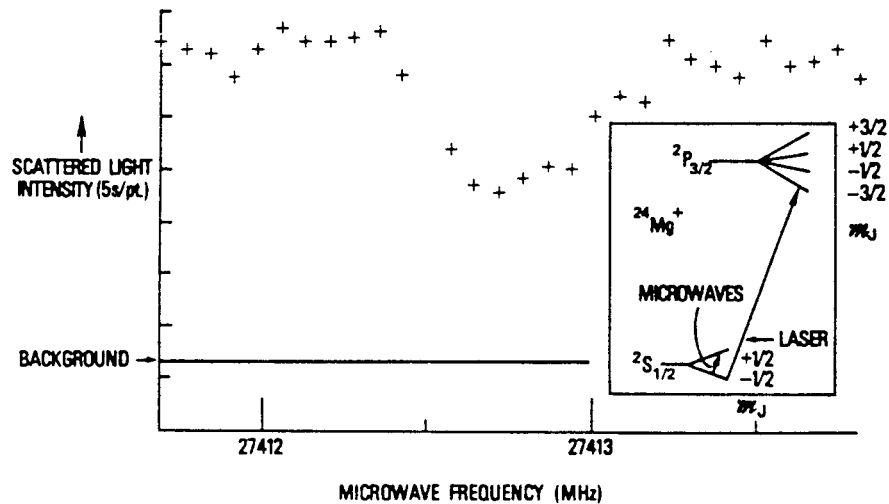


Fig. 1. Microwave/optical double resonance spectrum of $^{24}\text{Mg}^+$. Inset shows relevant energy levels of $^{24}\text{Mg}^+$ in a magnetic field. With the laser tuned to the transition shown, 16/17 of the ions are pumped into the $^2S_{1/2}$ ($M_J = -1/2$) ground state and a quasi two level system is formed with this ground state and the excited $^2P_{3/2}$ ($M_J = -3/2$) state. When incident microwaves are tuned to the $(M_J = -1/2) \leftrightarrow (M_J = +1/2)$ ground state Zeeman transition, these levels are nearly equally populated which causes a decrease in fluorescence scattering from the ions. Transitions in other ions can be detected in a similar way. (From ref. 20).

other allowed transitions (Assume the laser is linearly polarized perpendicular to the magnetic field so that only $\Delta M_J = \pm 1$ transitions are allowed). In fact just the opposite occurs. Although excitation in the wings of the $(-1/2) \rightarrow (+1/2)$ transition pumps ions out of the $(-1/2)$ ground state, excitation in the wings of the $(+1/2) \rightarrow (-1/2)$ transition also occurs which tends to pump ions from the $(+1/2)$ to $(-1/2)$ ground state. Since this latter transition is four times closer in frequency to the laser than the former one, the net result is that about 16/17 of the population is pumped into the $(-1/2)$ ground state.²⁰ This pumping is very weak, but because of the very long relaxation times of the ions in the trap it can be very efficient. Similar optical pumping can also be observed when hyperfine structure is present; for example²¹, in the case of $^{25}\text{Mg}^+$ and $^9\text{Be}^+$. Novel hyperfine pumping effects have also been observed²² in the excited $^3\text{S}_1$ states of Li^+ . This kind of pumping is far from universal. For example "depopulation" pumping occurs if one excites any of the $3^2\text{S}_{1/2} \rightarrow 3^2\text{P}_{1/2}$ transitions in $^{24}\text{Mg}^+$. In this case, which is perhaps more typical, one must redistribute or mix the ground state population in order to see additional scattering from the laser. In this instance one of the advantages of the traps for high resolution spectroscopy (weak relaxation) becomes a disadvantage in terms of observation. Solutions to this problem are: (1) provide a buffer gas for relaxation. For example, Ruster et al.²³, observed fluorescence from single Ba^+ ions in an rf trap by relaxing the ions against an H_2 buffer gas. (2) If the number of ground (and metastable) states is not too large, artificial relaxation can be provided by auxiliary microwave or laser radiation.

This kind of pumping described above is important for laser cooling and also establishes a population imbalance necessary to observe other internal transitions in the ions. In the Mg^+ example above, if the scattered fluorescence light from the ions is monitored, the $(M_J = -1/2)$ to $(M_J = +1/2)$ ground state Zeeman transition (induced by microwave radiation) can be detected by observing the decrease in fluorescence as the microwave oscillator is swept through resonance. (Fig. 1) An interesting feature of this optical pumping, double resonance detection scheme is that each microwave photon absorbed causes a change of about $\Delta N^* = 24B(-1/2, -3/2)/17B(-1/2, +1/2)$ in the number of scattered photons where $B(M_J, M_J')$ is the transition rate from the M_J ground state to the M_J' excited state.²⁰ For Mg^+ ions in a magnetic field of about 1 T, ΔN^* can be as high as 2×10^6 . This technique has sometimes been referred to as "electron shelving" because the ion's electron is temporarily "shelved" in a state from which the laser scattering is essentially absent.⁷ It has been used in all the optical pumping double resonance experiments on Mg^+ and Be^+ ions stored in Penning traps. Not only is the detection sensitivity increased by this photon number amplification effect but also by the photon energy upconversion. Perhaps noteworthy is the case of detecting absorbed 303 MHz photons in Be^+ hyperfine transitions (see below) where an energy enhancement factor of $\Delta N^* \lambda(303 \text{ MHz})/\lambda(\text{laser}) > 10^{12}$ is obtained. These impressive numbers are of course not realized in practice since fluorescence collection efficiencies are typically significantly less than 100%. However, a more important statement is that if (the absence of) enough scattered photons per ion (typically ≥ 2) are observed before repumping takes place, then the signal to noise ratio in such experiments need only be limited by the statisti-

cal fluctuations in the number of ions that make the transition²⁴. This is the maximum signal to noise ratio possible.

Because of the extremely high detection sensitivity in such quasi-two level systems, the ability to detect very small numbers of ions exists: in fact single ions have been detected by several groups^{23,25-28}. This is perhaps not so surprising if we consider for example a Mg^+ ion which is cooled down (see below) to where the Doppler broadening is smaller than the natural width and is localized to say less than a few μm in the trap. In this case, a $0.05 \mu W$ laser beam ($\lambda = 280 \text{ nm}$) focused to a beam waist $\omega_0 = 5 \mu m$ can scatter about 10^7 photons/s - an easily detectable signal even with modest collection efficiency.

Recently, another interesting optical pumping scheme has been developed for trapped negative ions²⁹⁻³¹; here a population imbalance in Zeeman substates has been created using polarization dependent photodetachment. In these experiments, changes in trapped ion number were detected by driving the ion motions and detecting the induced currents. This method of state selection and detection is similar to that used in past experiments on H_2^+ where polarization dependent photodissociation was employed⁵.

Cooling

The technique of radiation pressure³² or sideband³³ cooling was first demonstrated^{34,35} in 1978 (see also refs. 27 and 36). It has become a key element in experiments whose goal is high resolution spectroscopy because both first and second order Doppler effects are suppressed. Frequency shifts in spectra due to the second order Doppler effect (time dilation of the ions which are moving with respect to the lab) have historically been the main limitation to obtaining high accuracy because of the relatively high temperatures of the ions in the trap - up to about 1 eV for ions in an rf trap. A kinetic energy of 1 eV for ions with mass $M = 50 \text{ u}$ (atomic mass units) yields a fractional second order Doppler frequency shift of 2×10^{-11} . The kinetic energy of the ions can be determined by observing first order Doppler effect generated sidebands in microwave spectral lines³⁷⁻⁴². It can be reduced by cooling the ions with a light buffer gas such as He^{4,5,7,23,43-51}. With these techniques, accuracies near one part in 10^{13} should be obtained^{40,42} but if one hopes to obtain an accuracy significantly better than the best existing frequency standards (a few parts in 10^{14} for cesium beams) laser cooling may be necessary.

The best experimental results on laser cooling (and those most easily compared to theory) have been obtained using single ions. This is because for many trapped ions, rf heating in Paul traps (due to the driven motion) and the kinetic energy in the magnetron motion for Penning traps gives rise to higher effective temperatures. In the first single ion experiments, done at Heidelberg on Ba^+ ions, photographs were made of the trapped ion²⁵. The size of the image determined the extent of the ion motion; therefore the temperature in the pseudopotential well was measured to be between 10 and 36 mK. The kinetic energy in the driven motion will be approximately the same^{4,52}. Laser cooling of single Mg^+ ions in Penning²⁶ and rf²⁷ traps has also been accomplished. The lowest temperatures measured are those of the Seattle group²⁷ where the temperature for at least

two directions of the pseudopotential motion was determined to be less than 20 mK (Fig. 5). (Cooling in all directions will be straightforward). In both of the magnesium experiments, the temperature was determined from the observed Doppler broadening on optical transitions. For temperatures below about 0.1 K this Doppler broadening contributes only a small part of the total linewidth which is now primarily due to radiative decay. Therefore, very low temperature becomes difficult to measure. In the future this problem can be circumvented by measuring the first order Doppler effect generated sidebands in optical spectra as was done for microwave spectra above. In any case, for Mg^+ ions cooled to 20 mK, the second order Doppler effect is only about 2 parts in 10^{16} !

The theory of laser cooling of trapped ions has been elaborated for a large number of cases, starting with the original proposal³³, which introduced the "optical sideband" picture. Calculations based on this picture are included in refs. 25, 35, and 53. The fundamental process is the absorption of a photon with frequency less than that of an optical transition, followed by the emission of a photon whose frequency, on the average, is about equal to the transition frequency, the deficit coming out of the kinetic energy of the ion. Some of the more recent general discussions of the state of the theory are given by Javanainen⁵⁴ and Stenholm⁵⁵. For reasons of theoretical simplicity, the ions are usually considered to be two-level systems confined by harmonic potentials, and interactions between ions are generally ignored. This situation corresponds fairly closely to the experiments carried out with a single ion in an rf trap.

Of particular interest from an experimental point of view is the Lamb-Dicke regime or limit, which corresponds to the ion being confined to dimensions much less than an optical wavelength. In this limit, the broadening of the optical transition due to the first-order Doppler effect disappears.

Wineland and Itano⁵³ calculated cooling rates and limiting temperatures using perturbation theory and rate equations. They considered the limiting cases of the trap oscillation frequency being much greater than or much less than the natural linewidth (γ) of the optical transition, calling them the "strong binding" and "weak binding" cases, respectively. Experiments, so far, correspond to the weak binding case. In this limit, the minimum temperature is on the order of $\hbar\gamma/2k_B$. They also treated laser cooling in a Penning trap for the weak binding case and compared the results with experiment⁵⁶. All of these calculations were limited to low laser intensities.

André et al.⁵⁷ calculated numerically the equilibrium energy distributions for the weak binding case. In later work⁵⁸, the kinetic energy due to the micromotion in an rf trap was included, using a semiclassical method.

In a series of papers, Javanainen and Stenholm⁵⁹⁻⁶¹ and Javanainen⁶²⁻⁶⁴ have used quantum statistical methods to study various limiting cases. The Fokker-Planck equation for the Wigner function was solved in the "heavy particle" limit, which corresponds roughly to the weak binding case, for one-dimensional⁵⁹ and three-dimensional⁶² traps. The "fast particle" limit, which corresponds to high excitation of the ionic motion, was treated by solving a Fokker-Planck equation in the n (harmonic oscillator quantum number) representation, for both the strong binding and weak

binding cases⁶⁰. The Lamb-Dicke limit was treated by solving the coupled rate equations for the populations, for both the strong binding and weak binding cases⁶¹. Recently, results have been obtained for the steady state⁶⁵ and the dynamics⁶⁶, which are exact in the Lamb-Dicke limit. These results extend and correct the earlier work.

Laser Sources

A troublesome obstacle that is generally encountered in optical studies of atomic ions is the radiation source. This is because the wavelength of the requisite radiation frequently lies in the ultraviolet (UV). While reliable continuous-wave (cw) lasers are readily available throughout the visible, there are but a few cw lasers in the U.V. region. Presently, most of the narrowband cw UV sources are generated by some nonlinear process that requires high powers at the fundamental wavelength(s) in order to reach useful levels of UV power. And so it is only with the development of high power tunable dye lasers and power enhancement cavities that narrowband and tunable UV sources with useable powers are possible⁶⁷. Fortunately, very little power is required to radiatively cool ions that are confined in electromagnetic traps at high vacuum; usually no more than several microwatts.

At present the most prominent method of generating UV radiation is by the interaction of high power laser radiation with an optically transparent material presenting a non-linear response. The two dominant methods are second harmonic generation (SHG), which is the doubling of laser radiation, and sum frequency mixing (SFM), which is the generation of a higher frequency source by the mixing of the outputs of two lower frequency lasers⁷¹. The phase matching condition

$$n_3\omega_3 = n_1\omega_1 + n_2\omega_2$$

must be met in order to efficiently produce radiation at ω_3 by mixing lasers at frequencies ω_1 and ω_2 ($\omega_3 = \omega_1 + \omega_2$). n_1 is the refractive index of the nonlinear medium for the frequency ω_1 . For second harmonic generation, $\omega_1 = \omega_2$ and the phase matching condition reduces to $n(\omega) = n(2\omega)$. Since all optical materials have spectral dispersion, properly oriented uniaxial or biaxial crystals are required to satisfy the phase matched condition to give efficient mixing. In experiments on the ions Mg^+ and Be^+ , tunable UV radiation has been generated near the first resonance lines (280 nm & 313 nm respectively) by SHG in KDP isomorphs (AD*P & RDP respectively). These crystals were temperature tuned to phase match the UV and fundamental indices (90° phase matched). In both cases the conversion efficiency exceeded $5 \times 10^{-4} W^{-1}$ so that tens of microwatts of UV radiation could be obtained by single-passing the light from the tunable dye laser through the crystal. For radiation pressure cooling and optical pumping of trapped mercury ions, narrowband and tunable radiation near the $6s \ ^2S_{1/2} - 6p \ ^2P_{1/2}$ first resonance line at 194 nm is required. One method for producing cw radiation at 194 nm is by SFM in a potassium pentaborate (KB5) crystal, the 257 nm second harmonic of the output of a cw 515 nm argon-ion laser with the output of a tunable cw dye laser in the 792 nm region⁶⁸ (Fig. 2). The 257

nm second harmonic is generated in a ADP crystal that is placed in an external ring cavity which is held in resonance at the fundamental frequency⁶⁹. To amplify the 194 nm power, the KB5 crystal is placed into two intersecting power enhancement cavities. One of these cavities increases by 15 the circulating 792 nm power and the second cavity increases by 7 the 257 nm power. By this method 8-10 microwatts of tunable cw 194 nm power has been generated. Thermal lensing caused by heating in the KB5 crystal due to absorption of light at 792 nm is the present limit to achieving higher powers at 194 nm⁷⁰.

Sympathetic Cooling

So far, optical pumping and laser cooling have been achieved on only a few different ions. Laser cooling could be extended to certain other ions but in practice this may be difficult to accomplish because of the required laser wavelengths or "trapping" in metastable states. Ions which are difficult to cool directly can be cooled by collisional coupling with other stored ions which are easy to cool³⁴. This has been demonstrated⁷² in experiments on Mg^+ where $^{24}Mg^+$ was laser cooled and by collisions "sympathetically" cooled $^{25}Mg^+$ and $^{26}Mg^+$. (We note that in subsequent experiments at NBS, it was possible to sympathetically cool $^{24}Mg^+$ by laser cooling $^{25}Mg^+$; this result is more definitive because the laser was tuned to the heating side of the $^{24}Mg^+$ transition.) For ions in a Penning trap, lighter ions should be held near the center of the trap by heavier ions which are laser cooled⁷³. Qualitatively, this should occur because the magnetron frequency is slightly higher for heavy mass

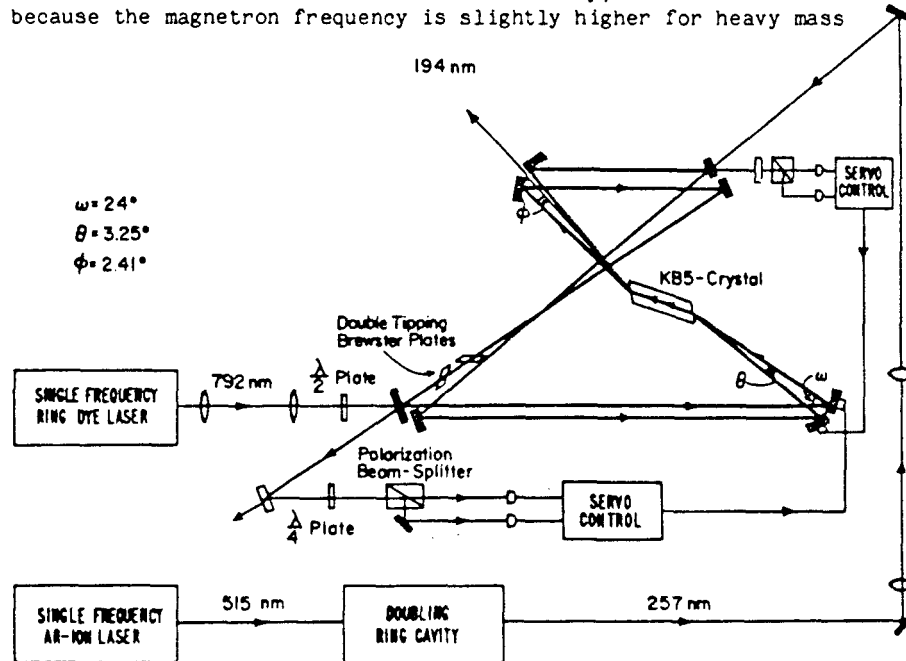


Fig. 2. 194 nm laser source. (From ref. 68)

ions; this causes a friction force on the lighter ions which should push them towards the center of the trap^{56,75}. At low temperatures, the separation between species should be nearly complete⁷³. As an example, spectroscopy could be done on ${}^9\text{Be}^+$ ions which are held at the center of the trap and sympathetically cooled by an outer annulus of ${}^{24}\text{Mg}^+$ ions which are laser cooled. The cooling laser could be applied so that it would not spatially overlap the ${}^9\text{Be}^+$ ions and therefore light shifts on the ${}^9\text{Be}^+$ energy levels could be avoided. In this way, extremely narrow linewidths ($\ll 1$ MHz) and high accuracy spectra on Be^+ (or other ions) might be obtained. For ions in an rf trap, sympathetic cooling may be limited by rf heating.

IV. rf AND OPTICAL SPECTRA

Radiofrequency Spectra

The ion storage method is capable in principle of achieving extremely narrow resonance linewidths on either rf or optical transitions. It is much easier experimentally to observe narrow lines on rf transitions because the natural linewidths are negligible and because stable, tunable oscillators are readily available. Sub-hertz linewidths on hyperfine transitions have been observed on several different atomic ions.

Early work on the hyperfine structures of H_2^+ and the 1s and 2s states of ${}^3\text{He}^+$ has been reviewed previously^{5,6}. Recent work on the determination of ground state hyperfine structure separations by microwave-optical double resonance is reviewed elsewhere in these Proceedings¹⁹. We restrict our discussion to studies of negative ions and to the high-accuracy work at the National Bureau of Standards (NBS) on laser cooled ions.

Microwave spectra of negative atomic ions have been obtained in a series of experiments by Larson and coworkers. These experiments were carried out with Penning traps in magnetic fields of about 1 T. State preparation and detection were carried out by utilizing the polarization dependence of the photodetachment cross section. Microwave transitions between Zeeman components of the ground ${}^2\text{P}_{3/2}$ states of ${}^{32}\text{S}^-$ and ${}^{16}\text{O}^-$ were observed^{29,30} (Fig. 3). The observable transitions were from $M_J = +1/2$ to $M_J = +3/2$ and from $M_J = -1/2$ to $M_J = -3/2$. The two transition frequencies are separated due to the perturbation by the ${}^2\text{P}_{1/2}$ state. The average of the two transition frequencies yields the atomic g_J factor, while the frequency splitting yields an indirect value for the fine structure separation. The magnetic field was calibrated by detecting the cyclotron resonance of electrons in the same trap. The accuracy obtained for the g_J factors was sufficient to show the deviations from the Landé value after correction for the anomalous moment of the electron. In further studies, different M_I components of the $M_J = -3/2$ to $M_J = -1/2$ transition in the ${}^2\text{P}_{3/2}$ state of ${}^{33}\text{S}^-$ were observed³¹. The dipole and quadrupole hyperfine parameters were determined from the frequency splittings.

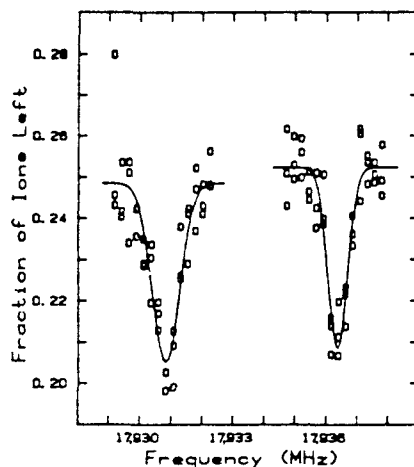


Fig. 3. Microwave resonances between magnetic sublevels of the $2p_{3/2}$ ground state of $^{32}\text{S}^-$ at about 0.96 T. (From ref. 29).

The ground state hyperfine constants (A) and nuclear-to-electronic g factor ratios (g_I/g_J) of $^{25}\text{Mg}^+$ and $^9\text{Be}^+$ have been measured with high accuracy in a series of experiments at NBS. In these experiments, the ions were stored for long periods (hours) in Penning traps. The ions were optically pumped and laser cooled by light from a frequency-doubled dye laser. Radiofrequency transitions between ground-state hyperfine Zeeman sublevels were detected by a change in the fluorescence intensity. In most cases, the resonances are broadened by magnetic field instabilities and inhomogeneities. However, for certain transitions, and at certain values of the magnetic field, the first derivatives of the transition frequencies with respect to the field are zero. If the magnetic field is sufficiently close to one of these values, a resonance can be observed with a linewidth limited only by the finite observation time.

In $^{25}\text{Mg}^+$, the first derivative of the ($M_I = -3/2, M_J = 1/2$) to ($M_I = -1/2, M_J = 1/2$) transition goes to zero at a value of the magnetic field near 1.24 T. Near this field, a resonance with a width of 0.012 Hz and a center frequency of 291.996 251 899(3) MHz was observed²¹ (Fig. 4). A and g_I/g_J were determined with much less accuracy, because the other transitions observed were field-dependent. The results are $A = -596\,254\,376(54)$ Hz and $g_I/g_J = 9.299\,484(75) \times 10^{-5}$.

Similar spectroscopy has been performed with $^9\text{Be}^+$ ions with an even higher degree of accuracy⁷⁵. Two field-insensitive transitions have been observed. They are ($M_I = -3/2, M_J = 1/2$) to ($M_I = -1/2, M_J = 1/2$) at about 0.82 T and ($M_I = 3/2, M_J = -1/2$) to ($M_I = 1/2, M_J = -1/2$) at about 0.68 T. The first of these has been used as a reference for a frequency standard. The results for the constants are $A = -625\,008\,837.048(4)$ Hz and $g_I/g_J = 2.134\,779\,853(1) \times 10^{-4}$. The accuracy of these constants is currently limited by the theoretical uncertainty of the diamagnetic shift of the hyperfine structure. The determination of the actual values (as opposed to the

ratios) of the g factors by measuring the cyclotron frequency of the ions is discussed in the section on mass spectroscopy.

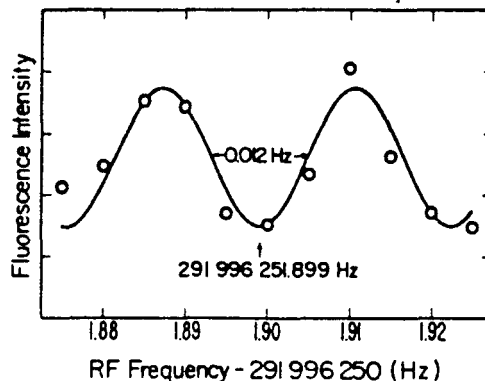


Fig. 4. The ($M_I = -3/2, M_J = 1/2$) to ($M_I = -1/2, M_J = 1/2$) resonance in $^{25}\text{Mg}^+$ at about 1.24 T. The oscillatory lineshape results from the use of the Ramsey separated oscillatory field method, implemented by applying two phase-coherent rf pulses 1.02 s long, separated by 41.4 s. (From ref. 21).

The repeatability from run to run of the frequency standard based on the $^9\text{Be}^+$ hyperfine transition is less than 1 part in 10^{13} . Possible sources of systematic errors have been carefully investigated. At present, the largest source of error is the second-order (relativistic time dilation) shift, equal to $-(1/2)\langle v^2 \rangle / c^2$. While the cooling laser is on, this shift is only about -3×10^{-15} . However, the light and the state-preparation microwaves must be shut off while the rf resonance is driven, in order to prevent resonance shifts and broadenings. The ions heat up during this period, which is typically 20 s. The average shift is about -3×10^{-13} and can be calibrated by optical Doppler width measurements of the ion temperature. The magnetic field instability of a few parts in 10^6 leads to a random error of about 3×10^{-14} . Shifts due to thermal radiation, electric fields, and microwave switch leakage are estimated to be below 10^{-14} . Shifts due to collisions with residual gas molecules are estimated to be below 10^{-15} . A light shift can exist, even though the light is shut off during the rf resonance period, if coherence survives the optical pumping period. In order to eliminate a shift of this type, the rf phase is randomized before the beginning of each rf resonance period.

Even better frequency standard performance might be expected if a hyperfine transition in $^{201}\text{Hg}^+$ were used, because of the higher transition frequency²⁴. As a preliminary step toward this goal, the ground-state Zeeman resonance of $^{198}\text{Hg}^+$ ions stored in a Penning trap has been observed at NBS by microwave-optical double resonance. The value obtained for the g factor is 2.003 1743(74), which agrees with a theoretical calculation¹³¹.

Optical Spectra

In this section we review optical spectroscopy that has been performed with atomic ions in traps. Very few such studies have been

performed, if spectroscopy is narrowly defined as the determination of energy level separations. The first observation of laser-induced fluorescence of trapped ions was made by Iffländer and Werth¹⁸. They observed the 493 nm $6^2S_{1/2}$ to $6^2P_{1/2}$ (D1) line of Ba^+ ions in an rf trap, using a pulsed tunable dye laser as a source. In later work, they observed a saturation dip in the D1 fluorescence when the ions were illuminated by counterpropagating laser beams⁷⁶. This feature is not broadened nor shifted by the first-order Doppler effect. The hyperfine splitting of the D1 line of the $^{137}Ba^+$ isotope was resolved by Blatt et al.⁷⁷. The average kinetic energy of the trapped ions in these experiments was a few eV, so the first-order Doppler broadening was large (typically about 5 GHz).

Experiments at several laboratories have now demonstrated the Doppler narrowing that can be achieved by laser cooling^{14,27,36,72}. We note again that laser cooling, unlike some other Doppler reduction techniques, can be used to eliminate second-order as well as first-order Doppler effects. Optical transitions have been observed for which the widths are dominated by the natural linewidths, due to the reduction of the first-order Doppler broadening by laser cooling. This degree of line narrowing has been observed on single Mg^+ ions in a Penning trap at NBS²⁶ and on single Mg^+ and Ba^+ ions in rf traps at the University of Washington (U.W.)^{27,28}. The U.W. group obtained a value for the natural linewidth of the 280 nm $3^2S_{1/2}$ to $3^2P_{3/2}$ (D2) line, which agreed with previously published Hanle-effect measurements, by fitting the observed resonance profiles. (Fig. 5)

A narrow spectral feature in a single, trapped Ba^+ ion due to two-photon excitation of the $6^2S_{1/2} - 6^2P_{1/2} - 5^2D_{3/2}$ Raman resonance was first observed in experiments at the University of Heidelberg¹⁴. This feature is potentially very narrow, since its natural linewidth is on the order of the inverse of the $5^2D_{3/2}$ lifetime, which has been measured to be 17.5 (4.0) s⁷⁸.

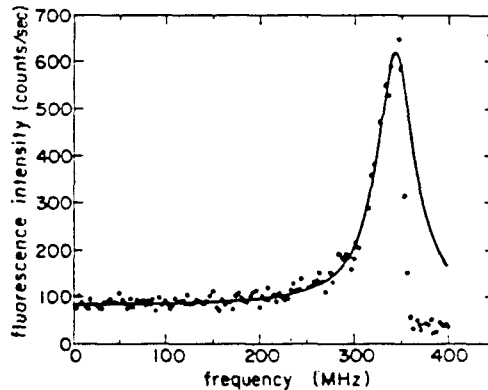


Fig. 5. Fluorescence of a single laser-cooled $^{24}Mg^+$ ion in an rf trap as a function of the relative optical frequency. The sharp decrease in signal above the line center is due to laser-induced heating. The fitted linewidth is equal to the natural linewidth to within the measurement error. (From ref. 27)

In recent work at U.W. this feature has been observed with greatly increased resolution²⁸. In these experiments, the blue (493

nm) laser is tuned to the low side of the $6\ ^2S_{1/2}$ to $6\ ^2P_{1/2}$ transition and the red (650 nm) laser is swept across the $5\ ^2D_{3/2}$ to $6\ ^2P_{1/2}$ transition while fluorescence at the blue wavelength is observed. What is observed is a broad resonance due to the one-photon transition centered at the $5\ ^2D_{3/2}$ to $6\ ^2P_{1/2}$ transition with a narrow dip which occurs at the two-photon resonance (i.e., when the frequency difference between the blue and red lasers is equal to the $6\ ^2S_{1/2}$ to $5\ ^2D_{3/2}$ transition frequency). The two-photon resonance is broadened, but to a high degree not shifted by the laser intensities¹³². The observed linewidth of the dip is about 5 MHz and is due to the laser frequency widths. This is less than the natural linewidth of the $6\ ^2P_{1/2}$ state, which is about 21 MHz. This type of two-photon resonance has been observed previously in other atomic systems¹⁹.

The isotope and hyperfine shifts of the D2 line of Mg^+ were measured in experiments at NBS⁷². In these experiments, which were carried out in a Penning trap, one laser was tuned to the low side of the $24Mg^+$ component, to continuously cool the ion cloud, while the fluorescence induced by a lower-power laser was observed as its frequency was swept. Laser cooling was particularly useful for this measurement because it allowed full resolution of the optical isotope structure which is normally obscured by the room temperature Doppler width. These measurements are in agreement with those made by other methods.

The first measurement of the magnetic dipole hyperfine constant of the $2\ ^2P_{1/2}$ excited state of $9Be^+$ was made recently at NBS^{75,80}.

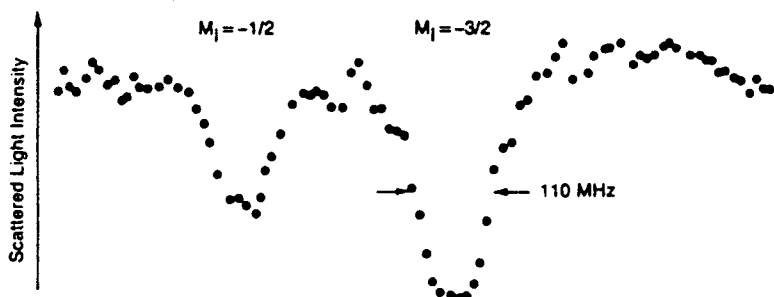


Fig. 6. Optical-optical double resonance signals corresponding to the $2\ ^2S_{1/2}$ ($M_I = -3/2$, $M_J = -1/2$) to $2\ ^2P_{1/2}$ ($M_I = -3/2$, $M_J = +1/2$) and the $2\ ^2S_{1/2}$ ($M_I = -1/2$, $M_J = -1/2$) to $2\ ^2P_{1/2}$ ($M_I = -1/2$, $M_J = +1/2$) transitions at about 1.14 T in a cloud of laser-cooled $9Be^+$ ions. The signal observed is the fluorescence due to a laser tuned to the $2\ ^2S_{1/2}$ ($M_I = -3/2$, $M_J = -1/2$) to $2\ ^2P_{3/2}$ ($M_I = -3/2$, $M_J = -3/2$) transition as a function of the frequency of another, lower-power laser. Note that the room temperature Doppler width would be about 4 GHz. (From ref. 80)

The ions were confined in a Penning trap at a magnetic field of about 1.14 T and laser-cooled to about 0.5 K by excitation of a hyperfine-Zeeman component of the 313 nm $2^2S_{1/2}$ to $2^2P_{3/2}$ (D2) line with a frequency-doubled dye laser. Several hyperfine-Zeeman components of the $2^2S_{1/2}$ to $2^2P_{1/2}$ (D1) line were probed with a second frequency-doubled dye laser (Fig. 6). The resonance frequencies of these components were measured by comparing the dye laser frequencies to the frequencies of $^{127}\text{I}_2$ hyperfine components. The relative frequencies of the $^{127}\text{I}_2$ components were determined by laser heterodyne measurements. The laser cooling was required in order to resolve the hyperfine components of the D1 line. The value obtained for $A(2^2P_{1/2})$ was -118.3(3.6) MHz, which is in good agreement with theoretical calculations.

Certainly, the few experiments described here have only just begun to exploit the possibilities for high resolution optical spectroscopy with trapped ions. The fundamental advantages are the same as for microwave spectroscopy (long observation times with small perturbations and elimination of Doppler effects by laser cooling). There is the additional advantage of higher fractional resolution for a given measurement period, due to the higher transition frequencies.

V MASS SPECTROSCOPY

In addition to the study of spectra due to the internal energy levels in atomic ions, the possibility also exists to perform mass spectrum analysis using the traps. The Paul (or rf) trap is the three dimensional analogue of the Paul rf quadrupole mass spectrometer which is commonly used for residual gas analysis. For high resolution studies, measuring mass ratios by comparing the cyclotron frequencies of different ions in the same magnetic field has been more successful.

For several years, trapped ion cyclotron resonance (ICR) spectrometers have been used by chemists to yield mass spectra⁸¹⁻⁸⁴. Trapped ICR spectrometers are basically Penning traps with rectangular shaped electrodes. If semiempirical fits are made to the cyclotron resonances in order to account for ion number dependent effects such as space charge, mass determinations near 1 ppm accuracy are possible⁸⁵. However, Penning traps with hyperbolic electrodes would seem to be better for very high resolution work for the following reason: To the extent that the electric potential inside the trap is quadratic and the magnetic field (B) homogeneous, the (modified) cyclotron, axial, and magnetron motions are harmonic (neglecting relativistic effects) and their frequencies (ν_c' , ν_z and ν_m respectively) are related by⁸⁶:

$$\nu_c'^2 = \nu_c^2 + \nu_z^2 + \nu_m^2. \quad (1)$$

where ν_c is the "unmodified" cyclotron frequency in a magnetic field B. In principle, a quadratic electric potential is guaranteed if the electrodes are equipotentials of the function $\phi = A(r^2 - 2z^2)$. This case is more nearly satisfied for the Penning traps with hyperbolic electrodes than for the typical ICR cells. Therefore, we could expect higher resolutions and accuracy in the Penning traps because the higher order terms in the potential (which give rise to anharmonic frequency shifts and corresponding uncertainties) would be

less. Additionally, sample sizes for ions and electrons in Penning traps can be quite small ($\ll \text{mm}^3$), therefore suppressing the effects of magnetic field inhomogeneities and electric field imperfections.

Five recent experiments have demonstrated the usefulness of the Penning trap for mass spectroscopy. In the three experiments of refs. 87-89, direct measurements of the electron/proton mass ratio (m_e/m_p) were made by comparing the cyclotron frequencies of electrons and protons in the same Penning trap apparatus; this direct measurement of such widely different masses would be nearly impossible in a more conventional mass spectrometer.⁹⁰

These three experiments are very similar in principle; they differ in the method of detection. For example Gärtner and Klempf (2.9 ppm accuracy) detect electron/ion cyclotron resonance by measuring electron/ion loss from the trap after resonant excitation⁸⁷. In the work of Gräff et al. (0.6 ppm accuracy), resonant excitation of electron/proton cyclotron motion is detected by the increase of the electron/proton orbital magnetic moment; this appears as a change in the time of flight spectrum when the electrons/protons are ejected out one endcap into an axially symmetric inhomogeneous magnetic field.

The most accurate measurements (0.04 ppm) are those of Van Dyck et al.^{89,91}. This accuracy comes about primarily because the experiment is more sensitive to cyclotron excitation, therefore anharmonic and relativistic effects in the spectra are less. In this experiment, ν_c' , ν_z and ν_m are separately determined yielding ν_c via Eq. 1. ν_z is measured by observing the spectrum of induced currents in the endcap electrodes. The proton cyclotron resonance is observed by splitting the ring electrode into quadrants, exciting the cyclotron motion by applying ac voltage across two of the quadrants and detecting the induced currents in the other two quadrants in a bridge arrangement. A resulting 76.4 MHz synchronously detected signal is shown in Fig. 7 where the line is only 0.2 Hz (2.5 ppb) wide. Recently linewidths on the order of 30 mHz have been observed⁹¹. Electron cyclotron resonance is detected using the magnetic bottle technique⁹² and ν_m is measured via sideband structure on the ν_z and ν_c' spectra⁸⁹. The present uncertainty in m_e/m_p (0.04 ppm) is limited by the uncertainty in the respective positions of the electrons and protons (and therefore the respective average magnetic field) when they are alternately stored in the trap.

In the experiments of Wineland et al.⁹³, ν_c' , ν_z and ν_m for ${}^9\text{Be}^+$ ions in a Penning trap were determined by observing the changes in ion fluorescence scattering from a laser beam which is focused onto the cooled ion cloud. That is, when the ion motional frequencies are excited by an externally applied oscillating electric field, the ion orbits increase in size causing a decrease in ion cloud/laser beam overlap which results in a decrease in laser fluorescence. In these experiments, the resulting value of ν_c (from Eq. 1) was compared to the ${}^9\text{Be}^+$ electron spin flip frequency to 0.15 ppm accuracy, limited by a rather large anharmonic term in the electric potential. This result could be viewed as giving an indirect measurement of m_e/m_p (to 0.2 ppm) if a theoretical value of $g_J({}^9\text{Be}^+)$ is assumed or it could be viewed as yielding a measurement of $g_J({}^9\text{Be}^+)$ (to 0.15 ppm) by using the Van Dyck et al., measurement of m_e/m_p .

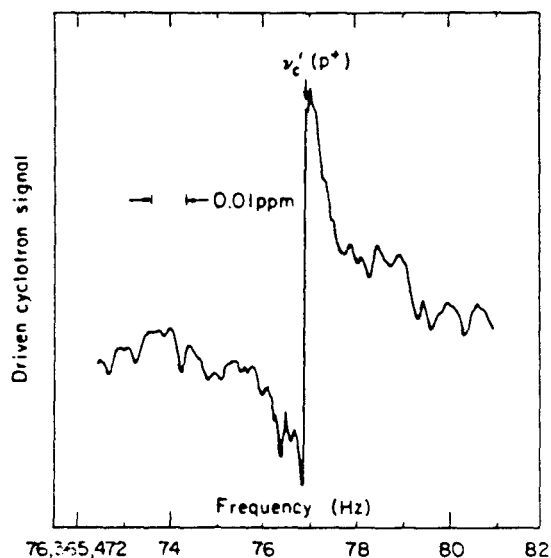


Fig. 7. Graph of proton cyclotron resonance in a Penning trap. This narrow dispersion-shaped curve is the result of direct synchronous detection of the resonance at $\nu_c'(p^+) = 76,365,476.9$ Hz using the split quadrupole design in a well-compensated Penning trap (for $V_0 = 54.4$ V). The linewidth, limited primarily by observation time, represents fewer than 40 protons. (From ref. 89)

In the experiments of Schwinberg et al.⁹⁴ the electron/positron mass ratio was measured to a precision of about 0.1 ppm. The cyclotron frequency detection method is the same as for the g-2 experiments.⁹²

Discussion

It appears that several orders of magnitude improvement can be expected if the effects of magnetic and electric field imperfections can be reduced. (Relativistic effects can also be very important; see Van Dyck, these proceedings). Two ways this can be done are (1) directly reduce the field imperfections. Higher order terms in the electric potential can be reduced by using compensation electrodes and magnetic bottles could be eliminated⁹². One must worry about distortions of the magnetic field by the electrodes; these could be suppressed by appropriate machining⁹⁵. (2) Increase the sensitivity to ion motion. If much smaller ion motions can be detected, the ions sample field imperfections to a lesser extent. These effects usually scale as some high power (≥ 2) of the ion amplitude so that improvement here could be substantial. (Frequency shifting effects of third and fourth order anharmonic terms have been discussed by Landau and Lifshitz⁹⁶; these arguments can be extended to higher order terms). Ideally, one would like to use single ions at very low temperature since the extent of ion orbits can be extremely small. Detection sensitivity to induced currents can be increased by using SQUID amplifiers⁹⁷ and therefore can be extended to heavier ions

(including molecular ions) which are more difficult to detect. Accuracies near 1 part in 10^{13} are not unrealistic for the laser fluorescence method⁹³; this is primarily a statement that if the ions can be laser cooled, they can be confined (and detected) in extremely small regions of space where field imperfection effects are minimized.

For more than one ion in the trap, space charge effects can show up in several ways; for simplicity we only discuss the effect on the axial resonance here but similar arguments could be made for the other degrees of freedom. For a single ion species near the center of the trap where the coupling to the endcap electrodes for all ions is the same (i.e. the electric field from a voltage applied to one endcap is uniform over the cloud) no space charge shift in ν_z is observed since only the center of mass motion couples to the electrodes⁹⁸. This was demonstrated in the work of Ref. 93 where for example, observed magnetron frequencies were consistent with the free space value (accuracy $\approx 0.5\%$) but the magnetron frequency of individual ions was shifted by about a factor of 3 because of space charge⁹⁹. If the cloud is spread out radially (e.g. shaped like a pancake whose diameter approaches the trap diameter) then the internal modes of oscillation in addition to the center of mass mode are observable because the z coupling to the endcaps depends on the ion's radius in the trap¹⁰⁰. Internal modes also become observable if the ions are only weakly coupled together and the trap is imperfect so that for example ν_z depends on r. If two species of ions are present in the trap, different effects come into play. For dilute clouds the center of mass oscillation of one species is space charge shifted by the other ions⁴. This property was used in ref. 74 to measure ion density. In the experiment of ref.93, the presence of single BeH^+ ions would broaden the Be^+ cyclotron resonances by more than 100 ppm.

To further illustrate the above remarks, we present a simple example: that of two ions in a Penning trap. If the axial excursions of the ions (z_1 and z_2) are small compared to their separation r in the radial direction, then the equations of motion in the z direction can be approximately written

$$m_1 \ddot{z}_1 + k_1 z_1 = k_3(z_1 - z_2)$$

$$m_2 \ddot{z}_2 + k_2 z_2 = k_3(z_2 - z_1)$$

where $\omega_{zi} = (k_i/m_i)^{1/2}$ ($i = 1,2$) are the respective oscillation frequencies of the ions (with the other ion removed from the trap) and $k_3 = q_1 q_2 / r^3$. These equations can be solved exactly¹⁰¹. Some limiting cases are interesting to examine.

Case 1: $k_1 = k_2$, $m_1 = m_2$. The center of mass oscillates at the unshifted value $\omega_z = \omega_{z1} = \omega_{z2}$. If the coupling to the endcaps is different for the two ions (eg. suppose one ion is at the center of the trap and the other at a nominal radius r) then some current is induced at the internal mode frequency $\omega_z' = (\omega_z^2 - 2k_3/m)^{1/2}$. The strength of the induced current due to the internal mode will scale with the difference in endcap coupling between the two ions.

Case 2: $m_1 = m_2$, $k_1 \neq k_2$, $k_3 \ll |k_1 - k_2|$ (weak coupling limit). Observed induced currents are at $\omega_{z1}' = (\omega_{z1}^2 - k_3/m_1)^{1/2} = \omega_{z1}$, ions are nearly independent.

Case 3: $m_1 = m_2$, $k_1 = k_2$, $k_3 \gg |k_1 - k_2|$ (strong coupling limit). Dominant part of the center of mass oscillation is at frequency $\omega_z' = (\omega_{z1} + \omega_{z2})/2$; particles appear locked together.

Case 4: $m_1 = m_2$, $k_1 \neq k_2$, $k_3 \approx |k_1 - k_2|$ (intermediate coupling). Oscillations near ω_{z1} and ω_{z2} ; qualitatively not significantly different than case 2.

The most straightforward solution to space charge problems is to use single ions. Short of this, different ion species can be eliminated from the trap by: (1) driving the unwanted ions out of the trap using strong motional excitation^{89,93,102}. (2) Operate the trap in a mass selective mode. For rf traps both high and low masses can be excluded. For the Penning trap, particles with lower charge to mass ratio can be ejected by exceeding the critical voltage³ for these ions. This was used in ref. 93 to eject ions with $M \geq 15$ u. (3) Selective ionization. In ref. 93, Be^+ ions were created but H_2^+ and He^+ formation was prevented by using an electron beam energy just slightly above the ionization potential of neutral Be.

The problem of space charge frequency shifts will depend on the particular experiment and can of course be quite complicated. In general, it will not be enough to consider the space charge frequency shift of one ion due to the other ions. For example, in the method of observing induced currents in the electrodes, the observable is the sum of the induced currents due to all ions. In the simple case of a small cloud of identical ions near the center of the trap, space charge frequency shifts in the spectrum of the total current are absent.

VI APPLICATIONS

The ion storage technique will continue to find varied applications. We illustrate here with a few examples; other applications are mentioned in the reviews referred to in the introduction and in the accompanying papers^{19,92,102}.

Frequency Standards and Clocks

In several laboratories, the primary motivation for doing high resolution spectroscopy is to use such spectra as references for frequency standards and clocks. Clocks are frequency standards where it is possible to count cycles of the radiation so that time intervals can be generated. This distinction is an important one in practice; for example, it will probably be much more difficult to obtain a laser "clock" than a microwave "clock" even though the performance of laser frequency standards should eventually be superior¹⁰³.

In a frequency standard or clock operating at frequency ν_0 , measurement imprecision ($\delta\nu_{\text{error}}/\nu_0$) is approximately limited to $(Q \cdot S/N)^{-1}$ where $Q \equiv \nu_0/\Delta\nu_0$ and S/N is the signal to noise ratio for detecting the number of ions that have made the transition. If the

radiative linewidth is small enough then the experimental linewidth ($\Delta\nu_0$) is probably independent of the trapped ion that is used (eg. determined by interrogation time). Therefore we would like to use as high a frequency (ν_0) as possible in order to increase Q. This is the single disadvantage of either Mg^+ or Be^+ ions since the interesting "clock" transitions are only around 300 MHz ($Q \approx 10^{10}$). In spite of this limitation, the accuracy achieved with a beryllium clock¹⁰⁴ approaches that of the best cesium standards and significant improvement could be expected. A better ion for a laser cooled microwave clock²⁴ is perhaps Hg^+ ($\nu_0 \approx 40$ GHz for $^{199}\text{Hg}^+$.) Very important frequency standard work has already been accomplished using this ion^{19,40,105-107}, but laser cooling is much harder to achieve than for Be^+ or Mg^+ . A logical extension of this idea is to go to much higher frequency; for example, to use a narrow optical transition. A number of transitions in various ions have been proposed³; Dehmelt¹⁰⁸ was the first to suggest that such extremely high resolution spectroscopy could be carried out using single photon transitions in for example single group IIIA ions. For instance¹⁰⁸ the $6^1\text{S}_0 \leftrightarrow 6^3\text{P}_0$ transition in Tl^+ ($\lambda = 202$ nm) has a $Q \approx 5 \times 10^{14}$. For such single photon optical transitions, it is desirable to approximately satisfy the Lamb-Dicke criterion; this is most easily accomplished with single trapped ions. In experiments at Heidelberg and Seattle, the present resolution of the two photon $6^2\text{S}_{1/2} \rightarrow 6^2\text{P}_{1/2} + 6^2\text{D}_{3/2}$ stimulated Raman transition in Ba^+ is limited by laser linewidth broadening, but this transition could be extremely narrow¹³²; the lifetime of the $^2\text{D}_{3/2}$ state in Ba^+ is 17.5 s which would give an intrinsic Q of 1.6×10^{16} .

The accuracy for optical frequency standards could be extremely high. As an example, in In^+ , the linewidth of the $5^1\text{S}_0 \rightarrow 5^3\text{P}_1$ "cooling" transition is about 1.3 MHz, this implies a second order Doppler shift of 10^{-19} or lower. Other systematic shifts can occur^{3-5,13,19,21,24,40,104-111} but it is not unreasonable to think they will be smaller than or controllable to this level. These extreme accuracies make important the problem of measurement imprecision since the signal to noise ratio on a single ion will be about one for each measurement cycle. Practically speaking, this means that a long averaging time will be required to reach a measurement precision equal to these accuracies. In fact, for a while, it may be that the accuracy and resolution will be limited by laser linewidth characteristics (linewidth and linewidth symmetry). However the potential for extremely narrow tunable lasers also exists^{103,112,113}.

Search for Spatial Anisotropy

Frequency standards, including those based on atomic or nuclear (Mössbauer) transitions, have traditionally played an important role in testing gravitational theories. One example is measurements of the gravitational red shift. In addition, the very high resolution attained in trapped ion spectroscopy enables other sensitive tests of the Einstein Equivalence Principle (EEP). All metric theories of gravity (including General Relativity) are founded on the EEP, according to which, any nongravitational physics experiment done in a local freely falling frame near a strongly gravitating mass will have the same outcome when done in a freely falling frame far away from

all such masses. Also included in the EEP is local Lorentz invariance which states that the outcome of the experiment is independent of the velocity of the freely falling frame^{114,115}. In particular, two different atomic clocks (i.e., clocks based on transitions in two different kinds of atoms) located at the same point in space-time will have relative rates which are independent of (1) the velocity of the freely falling lab, and (2) the position and mass of strongly gravitating bodies. As a test of the EEP the frequency of the ${}^9\text{Be}^+$ "clock" transition ($M_J = 1/2, M_I = -3/2$) + ($M_J = 1/2, M_I = -1/2$) has been compared to the frequency of a passive hydrogen maser¹³³ to see if a correlation can be found with orientation in space.

Two gravitational interactions have been proposed which violate the EEP and shift the ${}^9\text{Be}^+$ "clock" transition relative to the hydrogen transition. The first is a direct coupling of a nucleon's spin to the gravitational field,¹¹⁶

$$U_g = U(r) \bar{I} \cdot \hat{r} = U(r) I_2 P_1(\cos \beta),$$

where $U(r)$ is the strength of the coupling, \hat{r} is the unit vector pointing from the particle to the source of the field and β is the angle between the magnetic field used to confine the ${}^9\text{Be}^+$ ions (the quantization axis) and the direction \hat{r} . In the second model¹¹⁷ the inertial mass of a nucleon in ${}^9\text{Be}^+$ depends upon the orientation of its orbit relative to the direction toward nearby massive bodies in the universe (e.g., the Milky Way Galaxy or the Virgo Supercluster of galaxies). This mass anisotropy is a quadrupolar effect and thus produces a shift of the ${}^9\text{Be}^+$ transition proportional to $P_2(\cos \beta)$. These experiments are also sensitive to a quadrupolar coupling between a nucleon's velocity (in the laboratory frame) and the velocity of the earth through the cosmic microwave background^{114,118}. Thus it is possible to test local Lorentz invariance by investigating the extent to which the mean rest frame of the universe acts as a preferred frame.

These experiments have searched for a sidereal time variation in the ${}^9\text{Be}^+$ "clock" transition which is proportional to $P_\ell(\cos \beta)$ ($\ell = 1, 2, 3$) for three directions of the unit vector \hat{r} : the direction of the galactic center, the direction of the Virgo supercluster center and the direction of motion through the apparent mean rest frame of the universe. Preliminary experiments have achieved resolution better than 1 mHz and see no such variation. These first results have decreased the limits set by Hughes¹¹⁹ and Drever¹²⁰ on a $P_2(\cos \beta)$ variation by a factor of about 50. Ultimately, one could expect an increase in resolution of an additional factor of 100 or more.

Non Neutral Plasmas

At sufficiently high ion densities and sufficiently low ion temperatures such that the Debye length is small compared to the ion cloud dimensions, the ion cloud in a Penning or rf trap can be described as a non-neutral plasma¹²¹. Experiments on ions and electrons stored in Penning-type traps have studied a variety of plasma and cooperative effects. Examples include the spectra of plasma and diocotron waves in three dimensional plasmas¹²¹⁻¹²³ and the detection of waves similar to the drumhead modes of a vibrating

membrane, in a nearly two dimensional cloud of ions stored in a hyperbolic Penning trap¹⁰⁰. Radiation pressure from lasers can be used to cool and compress stored ions and study non-neutral plasmas in a state where the thermal energy per ion is less than the Coulomb energy per ion. Such a plasma is called strongly coupled¹²⁴. A strongly coupled plasma is characterized by the Coulomb coupling constant $\Gamma \equiv q^2/ak_B T$ where $a = (4\pi n/3)^{-1/3}$, q is the ion charge, T is the ion temperature, and n is the ion number density. Extensive theoretical calculations exist for a strongly coupled one component plasma (OCP)¹²⁴. An OCP consists of a single charge species embedded in a uniform density background of opposite charge. These calculations¹²⁴ predict that at $\Gamma = 2$, the pair correlation function should begin to show oscillations characteristic of a liquid, and at much larger values^{125,126} of Γ ($\Gamma = 170$), crystallization may take place. Crystallization has been observed¹²⁷ in a two dimensional OCP ($\Gamma = 137$) and in a system of charged aluminum particles (several microns in size) stored in an rf trap¹²⁸. In a frame of reference rotating with the ($\vec{E} \times \vec{B}$) rotation frequency of an ion cloud in a Penning trap, the ions can be viewed as being embedded in a uniform charge distribution of opposite sign. Specifically, the spatial correlations and the values of Γ for the onset of liquid and solid behavior are the same for the OCP and the non-neutral plasma in a Penning trap¹²⁹. A value of Γ on the order of 2 has been estimated for a pure electron plasma stored in a long cylindrical Penning trap and cooled to near the 4K temperature of its surroundings.¹³⁰ In a small plasma of laser cooled ${}^9\text{Be}^+$ ions stored in a Penning trap, a value of Γ as large as 10 (indicating liquid behavior) has been measured⁹⁹. In this latter experiment, a second laser was used to probe the ion plasma and measure the temperature of the ions from the Doppler broadening of the optical probe transition. The ion number density was determined by measuring the ($\vec{E} \times \vec{B}$) cloud rotation frequency. Because the trap electric field and magnetic field were known, the space charge electric field was extracted from the cloud rotation frequency and used to determine the ion number density. Ion number densities of $\approx 2 \times 10^7/\text{cm}^3$ and temperatures of ≤ 75 mK produced values of $\Gamma = 10$. Values of Γ large enough to observe a liquid-solid phase transition should be accessible in future versions of this experiment. If the theoretical cooling and density limits can be obtained, values of Γ as large as 15,000 are perhaps possible for Be^+ ions. Because experimental information on three dimensional, strongly coupled plasmas is almost non-existent, these experiments can provide some useful tests of the theoretical calculations.

Acknowledgments

The NBS experiments and the preparation of this manuscript were supported by the Office of Naval Research and the Air Force Office of Scientific Research. We thank E. C. Beaty, G. Leuchs and H. U. Daniel for suggestions and comments on the manuscript.

1. P. L. Smith, B. C. Johnson, H. S. Kwong, W. H. Parkinson, and R. D. Knight, *Physica Scripta*, Topical Issue T8 (1984).
2. B. C. Johnson, P. L. Smith, and R. D. Knight, *Astrophys. J.* 281 (in press).
3. D. J. Wineland, W. M. Itano, and R. S. Van Dyck Jr., *Adv. At.*

- Mol. Phys. 19, 135 (1983) and references therein.
4. H. G. Dehmelt, Adv. At. Mol. Phys. 3, 53 (1967).
 5. H. G. Dehmelt, Adv. At. Mol. Phys. 5, 109 (1969).
 6. H. A. Schuessler, In "Physics of Atoms and Molecules, Progress in Atomic Spectroscopy" (W. Hanle and H. Kleinpoppen, eds.), Plenum, New York, 999 (1979)
 7. H. G. Dehmelt, In "Advances in Laser Spectroscopy" (F. T. Arecchi, F. Strumia, and H. Walther, eds.). Plenum, New York, (1983) p. 153.
 8. J. F. J. Todd, G. Lawson, and R. F. Bonner, In "Quadrupole Mass Spectroscopy and its Applications" (P. H. Dawson, ed.), Chapter VIII. Elsevier, Amsterdam (1976).
 9. H. G. Dehmelt, In "The Physics of Electronic and Atomic Collisions" (J. S. Risley and R. Geballe, eds.) Univ. of Washington Press, Seattle (1975) p. 857.
 10. H. G. Dehmelt, At. Phys. 7, 337 (1981).
 11. H. G. Dehmelt, J. Phys. (Orsay, Fr.) 42, C8-299 (1981).
 12. V. G. Minogin, Usp. Fiz. Nauk 137, 173 [Sov. Phys. Usp. 25, 359 Engl. Transl.] (1982).
 13. W. Neuhauser, M. Hohenstatt, P. Toschek, and H. Dehmelt, In "Spectral Line Shapes" (B. Wende, ed.), 5 (De Gruyter, Hawthorne, New York, 1981) p. 1045.
 14. P. E. Toschek and W. Neuhauser, At. Phys. 7, 529 (1981).
 15. G. Werth, Acta Phys. Polonica A61, 213 (1982).
 16. D. J. Wineland, J. C. Bergquist, R. E. Drullinger, H. Hemmati, W. M. Itano, and F. L. Walls, J. Phys. (Orsay, Fr.) 42, C8-307 (1981).
 17. J. L. Duchêne, C. Audoin, and J. P. Schermann, Metrologia 13, 157 (1977).
 18. R. Iffländer and G. Werth, Metrologia 13, 167 (1977).
 19. G. Werth, these proceedings.
 20. D. J. Wineland, J. C. Bergquist, W. M. Itano, and R. E. Drullinger, Opt. Lett. 5, 245 (1980).
 21. W. M. Itano and D. J. Wineland, Phys. Rev. A 24, 1364 (1981).
 22. M. H. Prior and R. D. Knight, Opt. Commun. 35, 54 (1980).
 23. W. Ruster, J. Bonn, P. Peuser, and N. Trautmann, Appl. Phys. B30, 83 (1983).
 24. D. J. Wineland, W. M. Itano, J. C. Bergquist, and F. L. Walls, Proc. 35th Annu. Symp. Freq. Control, (1981) p. 602 (copies available from Electronic Industries Assoc., 2001 Eye St., NW, Washington, DC 20006).
 25. W. Neuhauser, M. Hohenstatt, P. Toschek, and H. G. Dehmelt, Phys. Rev. A22, 1137 (1980).
 26. D. J. Wineland and W. M. Itano, Phys. Lett. 82A, 75 (1981).
 27. W. Nagourney, G. Janik, and H. Dehmelt, Proc. Natl. Acad. Sci. USA, 80, 643 (1983).
 28. W. Nagourney, Bull. Am. Phys. Soc. 29, 815 (1984).
 29. R. M. Jopson, and D. J. Larson, Opt. Lett. 5, 531 (1980).
 30. D. J. Larson, and R. M. Jopson, in Laser Spectroscopy V, eds. A. R. W. McKellar, T. Oka, and B. P. Stoicheff. (Springer-Verlag, NY, 1983) p. 369.
 31. R. M. Jopson, R. Trainham, and D. J. Larson, Bull. Am. Phys. Soc., 26, 1306 (1981).
 32. T. W. Hänsch and A. L. Schawlow, Opt. Commun. 13, 68 (1975).
 33. D. J. Wineland and H. G. Dehmelt, Bull. Am. Phys. Soc. 20, 637 (1975).

34. D. J. Wineland, R. E. Drullinger, and F. L. Walls, *Phys. Rev. Lett.* 40, 1639 (1978).
35. W. Neuhauser, M. Hohenstatt, P. Toschek, and H. G. Dehmelt, *Phys. Rev. Lett.* 41, 233 (1978).
36. F. Plumelle, Abstract for 15th EGAS Conf. Madrid, July 5-8 (1983).
37. H. A. Schuessler, *Appl. Phys. Lett.* 18, 117 (1971).
38. F. G. Major and J. L. Duchêne, *J. Phys. (Orsay, Fr.)* 36, 953 (1975).
39. H. S. Lakkaraju and H. A. Schuessler, *J. Appl. Phys.* 53, 3967 (1982).
40. L. S. Cutler, R. P. Giffard, and M. D. McGuire, *Proc. 37th Annu. Symp. Freq. Control*, (1983) p. 32 (copies available from Systematics General Corp., Brinley Plaza, Rt. 38, Wall Township, NJ 07719).
41. M. Jardino, F. Plumelle, and M. Desaintfuscién, in *Laser Spectroscopy VI*, eds. H. P. Weber and W. Lüthy, (Springer-Verlag, NY 1983) p. 173.
42. M. Jardino, F. Plumelle, M. Desaintfuscién, and J. L. Duchêne, *Proc. 38th Annu. Symp. Freq. Control*, Phil. PA, (1984) to be published.
43. M. Vedel, *J. Phys. (Orsay, Fr.)* 37, L-339 (1976).
44. P. H. Dawson, *Adv. Electron. Electron Phys. Suppl.* 13B, 173 (1980).
45. F. Plumelle, M. Desaintfuscién, J. J. Duchêne, and C. Audoin, *Opt. Commun.* 34, 71 (1980).
46. H. Schaaf, U. Schmeling, and G. Werth, *Appl. Phys.* 25, 249 (1981).
47. J. André and F. Vedel, *J. Phys. (Orsay, Fr.)* 38, 1381 (1977).
48. J. André, F. Vedel, and M. Vedel, *J. Phys. (Orsay, Fr.)* 40, L-633 (1979).
49. F. Vedel, J. André, and M. Vedel, *J. Phys. (Orsay, Fr.)* 42, 1611 (1981).
50. F. Vedel, J. André, M. Vedel, and G. Brincourt, *Phys. Rev.* A27, 2321 (1983).
51. M. Vedel, J. André, S. Chaillat-Negrel, and F. Vedel, *J. Phys. (Orsay, Fr.)* 42, 541 (1981).
52. D. J. Wineland, In "Precision Measurements and Fundamental Constants II" (B.N. Taylor and W. D. Phillips, eds.). NBS Spec. Publ. (U.S.) 617 (in press).
53. D. J. Wineland, and W. M. Itano, *Phys. Rev.* A20, 1521 (1979).
54. J. Javanainen, *Acta Phys. Pol.* A61, 271 (1982).
55. S. Stenholm, *Phys. Rev. A* 27, 2513 (1983).
56. W. M. Itano, and D. J. Wineland, *Phys. Rev. A* 25, 35 (1982).
57. J. André, A. Teboul, F. Vedel, and M. Vedel, *J. Phys. (Orsay, Fr.)* 42, C8-315 (1981).
58. J. André, A. Teboul, and F. Vedel, *J. Phys. Lett. (Paris)* 45, L-1 (1984).
59. J. Javanainen and S. Stenholm, *Appl. Phys.* 21, 283 (1980).
60. J. Javanainen and S. Stenholm, *Appl. Phys.* 24, 71 (1981).
61. J. Javanainen and S. Stenholm, *Appl. Phys.* 24, 151 (1981).
62. J. Javanainen, *Appl. Phys.* 23, 175 (1980).
63. J. Javanainen, *J. Phys. B* 14, 2519 (1981).
64. J. Javanainen, *J. Phys. B* 14, 4191 (1981).
65. M. Lindberg, *J. Phys. B* 17, 2129 (1984).

66. J. Javanainen, M. Lindberg, and S. Stenholm, *J. Opt. Soc. Am. B* 1, 111 (1984).
67. See for example the review article by B. Couillaud, *J. Phys. (Orsay, Fr)* 42, C8-115 (1981) & references therein.
68. H. Hemmati, J. C. Bergquist, and Wayne M. Itano, *Opt. Lett.* 8, 73 (1983).
69. J. C. Bergquist, H. Hemmati, and Wayne M. Itano, *Optics Comm.* 43, 437 (1982)
70. H. Hemmati and J. C. Bergquist, *Optics Comm.* 47, 157 (1983).
71. See for example Amnon Yariv, Introduction to Optical Electronics, 2nd Ed. (1976).
72. R. E. Drullinger, D. J. Wineland, and J. C. Bergquist, *Appl. Phys.* 22, 365 (1980).
73. T. M. O'Neil, *Phys. Fluids* 24, 1447 (1981).
74. H. A. Schuessler, E. N. Fortson, and H. G. Dehmelt, *Phys. Rev.* 187, 5 (1969).
75. J. J. Bollinger, D. J. Wineland, W. M. Itano, and J. S. Wells, in Laser Spectroscopy VI, eds. H. P. Weber and W. Lüthy, (Springer-Verlag, NY) 1983, p. 168.
76. R. Ifländer and G. Werth, *Opt. Commun.* 21, 411 (1977).
77. R. Blatt, U. Schmeling, and G. Werth, *Appl. Phys.* 20, 295 (1979).
78. R. Schneider, and G. Werth, *Z. Phys. A* 293, 103 (1979).
79. G. Alzetta, A. Gozzini, L. Moi, and G. Orriols, *Nuovo Cimento* 36B, 5(1976); E. Arimondo and G. Orriols, *Lett. Nuovo Cimento* 17, 333 (1976); H. R. Gray, R. M. Whitley, and C. R. Stroud Jr., *Opt. Lett.* 3, 218 (1978).
80. J. J. Bollinger, J. S. Wells, D. J. Wineland, W. M. Itano, to be published.
81. R. T. McIver Jr., *Rev. Sci. Instrum.* 41, 555 (1970).
82. R. T. McIver Jr., *Lect. Notes Chem.* 7, 97 (1978).
83. R. T. McIver Jr., *Rev. Sci. Instrum.* 49, 111 (1978).
84. M. B. Comisarow, *Int. J. Mass Spectrom. Ion Phys.* 37, 251 (1981).
85. T. J. Francis, M. G. Sherman, R. L. Hunter, M. J. Locke, W. D. Bowers, and R. T. McIver Jr., *Int. J. Mass. Spectrum and Ion Physics* 54, 189 (1983).
86. L. S. Brown and G. Gabrielse, *Phys. Rev. A* 25, 2423 (1982).
87. G. Gärtner and E. Klempt, *Z. Phys. A* 287, 1 (1978).
88. G. Gräff, H. Kalinowsky, and J. Traut, *Z. Phys.* 297, 35 (1980).
89. R. S. Van Dyck Jr. and P. B. Schwinberg, *Phys. Rev. Lett.* 47, 395 (1981).
90. L. G. Smith and A. H. Wapstra, *Phys. Rev. C* 11, 1392 (1975).
91. R. S. Van Dyck, Jr., F. L. Moore, D. L. Farnham, and P. B. Schwinberg, abstract this conference.
92. R. S. Van Dyck Jr., these proceedings.
93. D. J. Wineland, J. J. Bollinger, and W. M. Itano, *Phys. Rev. Lett.* 50, 628; erratum: 50, 1333 (1983).
94. P. B. Schwinberg, R. S. Van Dyck Jr., and H. G. Dehmelt, *Phys. Lett. A* 81A, 119 (1981).
95. G. Gabrielse, and H. G. Dehmelt, *Bull. Am. Phys. Soc.* 26, 598 (1981).
96. L. D. Landau, and E. M. Lifshitz, Mechanics (Pergamon, New York, 1960) p. 86.
97. D. A. Pritchard, Workshop on Ion Trapping, this meeting.

98. D. J. Wineland, and H. G. Dehmelt, *J. Appl. Phys.* 46, 919 (1975).
99. J. J. Bollinger and D. J. Wineland, *Phys. Rev. Lett.* to be published.
100. S. Barlow, Thesis, Univ. of Colorado, 1984, unpublished.
101. For example see K. R. Symon, *Mechanics* (Addison-Wesley, 1961) p. 192.
102. D. A. Church, these proceedings.
103. See for example the proceedings of the Third Symp. on Frequency Standards and Metrology, *J. Phys. (Orsay, Fr.)* Vol. 42, C8 (1981).
104. J. J. Bollinger, W. M. Itano, and D. J. Wineland, *Proc. 37th Annu. Symp. Freq. Control*, 37 (1983). (Copies available from Systematics General Corp., Brinley Plaza, Rt. 38 Wall Township, NJ 07719).
105. F. G. Major and G. Werth, *Phys. Rev. Lett.* 30, 1155 (1973).
106. M. D. McGuire, R. Petsch, and G. Werth, *Phys. Rev. A* 17, 1999 (1978).
107. M. Jardino, M. Desaintfuscien, R. Barillet, J. Viennet, P. Petit, and C. Audoin, *Appl. Phys.* 24, 107 (1981).
108. H. Dehmelt, *IEEE Trans. Instrum. Meas.* IM-31, 83 (1982).
109. W. M. Itano, L. L. Lewis, D. J. Wineland, *Phys. Rev. A* 25, 1233 (1982).
110. P. L. Bender, J. L. Hall, R. H. Garstang, F. M. Pichanick, W. W. Smith, R. L. Barger, and J. B. West, *Bull. Am. Phys. Soc.* 21, 599 (1976).
111. D. J. Wineland and W. M. Itano, *Bull. Am. Phys. Soc.* 27, 864 (1982).
112. A. Yariv and K. Vahala, *I.E.E.E. J. Quant. Electronics*, Vol. QE-19, 889 (1983).
113. R. W. P. Drever, J. L. Hall, F. V. Kowalski, J. Hough, G. M. Ford, A. J. Munley, and H. Ward, *Appl. Phys.* B31, 97 (1983).
114. C. M. Will, *Theory and Experiment in Gravitational Physics*, Cambridge University Press, Cambridge (1981).
115. J. C. Gallop and B. W. Petley, *Nature* 305, 53 (1983).
116. J. Leitner and S. Okubo, *Phys. Rev.* 136, B1542 (1964).
117. G. Cocconi and E. Salpeter, *Nuovo Cimento* 10, 646 (1958).
118. G. F. Smoot, M. V. Gorenstein, and R. A. Müller, *Phys. Rev.* 39, 898 (1977).
119. V. W. Hughes, H. G. Robinson, and V. Beltran-Lopez, *Phys. Rev. Lett.* 4, 342 (1961). W. L. Williams, Ph.D. Thesis, Yale (1966).
120. R. W. P. Drever, *Phil. Mag.* 6, 683 (1961).
121. J. H. Malmberg and J. S. deGrassie, *Phys. Rev. Lett.* 35, 577 (1975).
122. J. S. deGrassie and J. H. Malmberg, *Phys. Fluids* 23, 63 (1980).
123. G. Dimonte, *Phys. Rev. Lett.* 46, 26 (1981).
124. S. Ichimaru, *Rev. Mod. Phys.* 54, 1017 (1982).
125. W. L. Slattery, A. D. Doolen, and H. E. DeWitt, *Phys. Rev. A* 21, 2087 (1980).
126. J. P. Hansen, *Phys. Rev. A* 8, 3096 (1973).
127. C. C. Grimes and G. Adams, *Phys. Rev. Lett.* 42, 795 (1979).
128. R. F. Wuerker, H. Shelton, and R. V. Langmuir, *J. Appl. Phys.* 30, 342 (1959).
129. J. H. Malmberg and T. M. O'Neil, *Phys. Rev. Lett.* 39, 1333 (1977).

130. J. H. Malmberg, T. M. O'Neil, A. W. Hyatt, and C. F. Driscoll, Bull. Am. Phys. Soc. 28, 1155 (1983).
131. V. A. Dzuba, V. V. Flambaum, P. G. Silvestrov, and O. P. Sushkov, Phys. Scripta, to be published.
132. P. M. Radmore and P. L. Knight, J. Phys. B15, 561 (1982) and references therein.
133. D. Howe and F. L. Walls, IEEE Trans. Instrum. Meas. IM-32, 218 (1983).

Strongly Coupled Nonneutral Ion Plasma

J. J. Bollinger and D. J. Wineland

Time and Frequency Division, National Bureau of Standards, Boulder, Colorado 80303

(Received 7 May 1984)

Radiation pressure from a laser has been used to cool and compress small nonneutral plasmas of ${}^9\text{Be}^+$ ions confined by static electric and magnetic fields. A second laser has been used as a probe to measure ion densities of $2 \times 10^7 \text{ cm}^{-3}$ and ion temperatures below 100 mK. A Coulomb coupling constant, Γ , as large as 10 has been measured indicating that the plasma is strongly coupled. In the future, values of Γ large enough to observe a liquid-solid phase transition should be accessible.

PACS numbers: 52.25.Lp, 52.25.Ps, 52.70.Kz, 52.90.+z

This Letter reports measurements of the density and temperature of a small nonneutral plasma composed of ${}^9\text{Be}^+$ ions. The thermodynamic state of such a classical Coulomb system is determined by the coupling constant Γ (defined below) which is a measure of the ratio of the Coulomb energy to kinetic energy per particle.¹ For values of Γ on the order of 1 or larger, correlation effects become important and the plasma is called strongly coupled. Recently, values of Γ on the order of 2 have been estimated for a pure electron plasma cooled to near the 4 K temperature of its surroundings.² By use of electrodynamic storage, very large values of Γ have been obtained with highly charged aluminum particles several microns in size.³ Classical, two-dimensional, strongly coupled plasmas have been realized with the system of electrons on the surface of liquid helium. In this system, values of Γ as large as 200 are experimentally accessible, and a liquid-solid phase transition has been observed⁴ at $\Gamma \cong 137$. To the authors' knowledge, the experiments reported in this paper give the largest values of Γ reported in a steady-state, magnetically confined, three-dimensional plasma.

The experimental arrangement used here^{5,6} is similar to that used in other nonneutral-plasma studies.⁷⁻¹² It is different in that the spatial extent of the plasmas could be nondestructively mapped and in that it was possible to control the shape, density, internal temperature, and angular momentum (add or subtract) of the plasmas with radiation pressure from lasers. A uniform magnetic field $\vec{B} = B_0 \hat{z}$ ($B_0 \cong 0.8 \text{ T}$) provided confinement of the ${}^9\text{Be}^+$ ions perpendicular to the magnetic field. Static electric fields produced by three electrodes were used to provide confinement of the ions along the magnetic field. The only qualitative difference between this confinement geometry and that of Refs. 7-12 is that the electric potential produced by

the electrodes varied continuously over the confinement region and had the form $\phi_T(r,z) = m\omega_z^2(2z^2 - r^2)/4q$, where ω_z is the single-particle "axial" or z oscillation frequency, q is the charge, m is the ion mass, and (r,z) are cylindrical coordinates. This system has usually been called a Penning trap.^{13,14} A pressure below about 10^{-8} Pa was maintained in the confinement region. Radiation pressure from a laser was used to cool and compress the ion plasma.^{15,16} This was accomplished with a focused, frequency-doubled dye laser beam tuned to the low-frequency side of the $2s^2S_{1/2}(M_J = -\frac{3}{2}, M_J = -\frac{1}{2}) \rightarrow 2p^2P_{3/2}(-\frac{3}{2}, -\frac{3}{2})$ transition in ${}^9\text{Be}^+$ ($\lambda = 313 \text{ nm}$) and directed at the ion plasma perpendicular to the magnetic field. The beam had a waist of about $60 \mu\text{m}$ and a power of about $10 \mu\text{W}$. The ions were optically pumped in the $2s^2S_{1/2}(-\frac{3}{2}, -\frac{1}{2})$ ground state and detected by observing the ion fluorescence scattering induced by this cooling laser beam. The plasma radius was decreased by directing the cooling laser beam to the side of the plasma which receded from the laser beam because of the $\vec{E} \times \vec{B}$ rotation.¹⁵⁻¹⁷ On the average, each photon-scattering event decreased the canonical angular momentum [in the gauge where $\vec{A}(\vec{r}) = \frac{1}{2}\vec{B} \times \vec{r}$] of the system by dh/λ , where d is the distance between the laser beam and the trap axis and h/λ is the photon momentum. Since the scattering rate was large ($\cong 10^6$ scattered photons per second per ion) this effect could dominate other external torques on the ions such as collisions of the ions with the background gas. In practice, relatively high-density, stable plasmas were maintained for many hours.

The ions were expected to be in near thermal equilibrium with each other. The equilibrium state of a nonneutral plasma confined by static electric fields and a uniform magnetic field has been discussed by O'Neil and co-workers.^{11,12} The ion dis-

tribution function is

$$f(r, z, \nabla) = n_0 (m/2\pi k_B T)^{3/2} \exp\left\{-\left[\frac{1}{2} m (\nabla - \omega r \hat{\theta})^2 + q\phi(r, z) + \frac{1}{2} m \omega (\Omega - \omega) r^2\right] / k_B T\right\}, \quad (1)$$

where n_0 is the ion density at the center of the trap, $\Omega = qB_0/mc$ is the cyclotron frequency, ω is determined by the total canonical angular momentum of the system, and $\phi = \phi_I + \phi_T$ is the sum of the potential due to the ions (including the potential due to the induced charges on the trap electrodes) and the applied trap potential. The distribution function is a Maxwellian velocity distribution superimposed on a rigid rotation of frequency ω . This rotation is due to the $\vec{E} \times \vec{B}$ force on the ions and is often called the magnetron rotation. $\phi(r, z)$ and the spatial shape of the plasma are determined from Poisson's equation (Eq. 3, Ref. 11), $\nabla^2 \phi = -4\pi q n_0 e^\psi$, where $\psi = -[q\phi + \frac{1}{2} m \omega (\Omega - \omega) r^2] / k_B T$. In the limit $T \rightarrow 0$, this is satisfied when the plasma is a uniformly charged figure of revolution with $\phi_I(r, z) = -2\pi q n_0 (\alpha r^2 + \beta z^2) / 3$, where $n_0 = m\omega \times (\Omega - \omega) / 2\pi q^2$, $\beta = 3\omega_z^2 / 2\omega (\Omega - \omega)$, and $2\alpha + \beta = 3$. In the limit that the ratio of the plasma dimensions to the trap dimensions approaches zero (about 10^{-2} here) the plasma becomes a uniformly charged spheroid.

In a frame of reference rotating about the trap axis with frequency ω , the ion plasma behaves like a neutral one-component plasma.¹⁰ That is, the positively charged ions behave as if they are moving in a uniform, negatively charged background. The properties of a one-component plasma are expressed in terms of the Coulomb coupling constant¹

$$\Gamma \equiv q^2 / a k_B T, \quad (2)$$

where a is defined by $4\pi n_0 a^3 / 3 = 1$, and T is the temperature of the ions from the distribution of Eq. (1). Theoretical calculations¹ predict that at $\Gamma \approx 2$, the pair-correlation function should begin to show oscillations characteristic of a liquid, and at much larger values^{18,19} of Γ ($\Gamma \approx 170$), crystallization may take place. (For the small plasmas of this experiment, surface effects may be important; however, this is not expected to greatly alter the theoretical prediction.)

Values of Γ in this experiment were determined by separately measuring the density, n_0 , and temperature, T , of the ions. A second laser beam (beam waist $\approx 60 \mu\text{m}$) was used to probe the plasma. When the probe laser frequency was swept through the $2s^2S_{1/2}(-\frac{3}{2}, -\frac{1}{2}) \rightarrow 2p^2P_{3/2}(-\frac{3}{2}, +\frac{1}{2})$ transition, some of the ion population was removed from the optically pumped ground state, resulting in a decrease in the resonance fluores-

cence induced by the cooling laser as shown in Fig. 1. The size of this depopulation signal depended on the local density of the plasma at the intersection of the probe beam and the plasma. With the probe beam perpendicular to the magnetic field, spatial maps of the plasmas were taken by moving the probe beam across the plasma in both the radial and

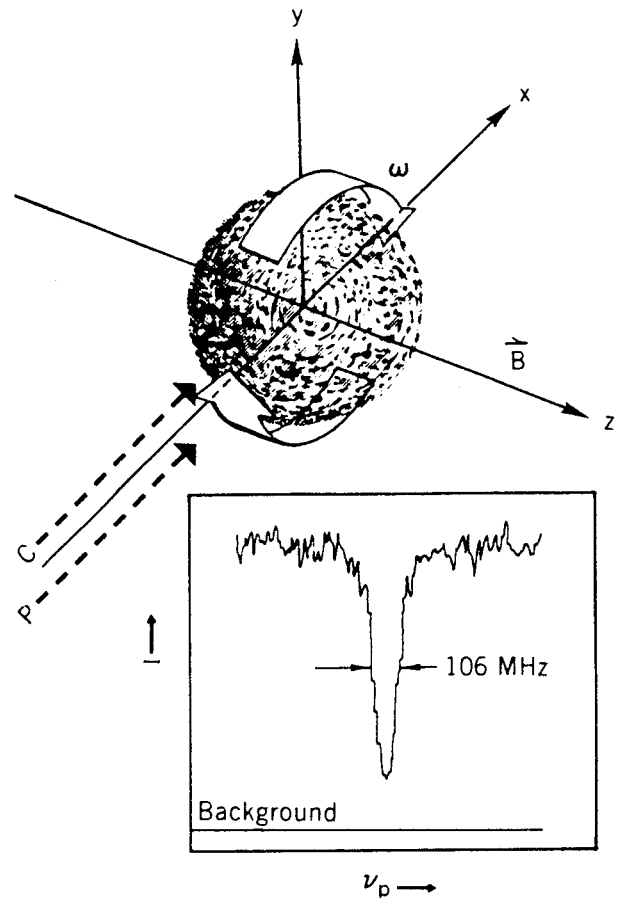


FIG. 1. Sketch of the plasma with the cooling (C) and probe (P) laser beams. The cooling beam was directed at the side of the plasma which receded from this beam. For much of the data, the probe beam was directed approximately parallel to the cooling beam. The rotation frequency, ω , was measured by translating the probe beam in the y direction (radially). Spatial maps of the plasma were obtained by translating the probe beam in both the y (radial) and z (axial) directions. The inset shows the depopulation signal obtained when the frequency (ν_p) of the probe laser was slowly swept through the $2s^2S_{1/2}(-\frac{3}{2}, -\frac{1}{2}) \rightarrow 2p^2P_{3/2}(-\frac{3}{2}, +\frac{1}{2})$ transition. I is the ${}^9\text{Be}^+$ fluorescence intensity from the cooling laser.

TABLE I. Summary of measurements on four nonneutral plasmas taken at three values of ω_z . All data were taken at a magnetic field of $B_0 = 0.819$ T. The coupling Γ and the Debye length λ_D were calculated with use of the axial temperature T_z . N is the number of ions and r_c is the rms radius of the cyclotron orbit.

$\omega_z/2\pi$ (kHz)	$10^{-7}n_0$ (cm^{-3})	a (μm)	N	T_c (mK)	T_z (mK)	Γ	λ_D (μm)	r_c (μm)
243	2.1(6)	23(2)	142(51)	45(12)	144(34)	5.1(1.3)	6(1)	1.1(1)
243	2.0(5)	23(2)	172(62)	56(13)	151(36)	4.9(1.2)	6(1)	1.2(1)
198	2.0(5)	23(2)	126(45)	10(12)	75(30)	9.7(3.9)	4(1)	0.5(3)
175	1.8(5)	24(2)	95(34)	19(12)	82(30)	8.6(3.2)	5(1)	0.7(2)

axial directions. The spatial maps were consistent with a uniform-density, spheroidal plasma (typical dimensions 100 to 300 μm) with a sharp drop in density (in less than a few Debye lengths) at the plasma edge. The rotation frequency ω was determined by measuring the change in the Doppler shift of the depopulation transition as the probe beam was moved radially across the plasma (see Fig. 1). n_0 was then determined from $n_0 = m\omega(\Omega - \omega)/2\pi q^2$ with use of the measured value of ω . (Ω was determined by auxiliary measurements.⁵) T was determined from the width of the depopulation signals. The 19.4-MHz natural width and the plasma rotation convoluted with the Gaussian spatial intensity profile of the probe beam contributed to the width of the depopulation signals. In addition there was a saturation broadening of the depopulation signals when the signal size approached the total fluorescence count rate. These broadening mechanisms were calculated and the Doppler broadening due to the nonzero temperature of the ions was extracted. With the probe laser beam perpendicular to the magnetic field, the temperature, T_c , of the cyclotron motion was measured.

The cooling laser beam, directed perpendicular to the magnetic field, only indirectly cooled the axial motion of the ions by collisional coupling of the axial motion with the cooled cyclotron motion. The axial motion was directly heated by the recoil of the scattered photons¹⁷; therefore, the axial temperature, T_z , was possibly higher than T_c . T_z was measured by passing the probe beam along a diagonal between the three electrodes. In this case, the depopulation signals contained a contribution due to the Doppler broadening by the axial (z) motion of the ions. Table I summarizes the measurements on four separate plasmas in this experiment. Γ was calculated by use of T_z , because it was the larger of the two temperatures. In future experiments, by directing the cooling beam along the diagonal and

cooling the axial motion directly, an axial temperature equal to the cyclotron temperature should be obtained.

The theoretical cooling limit¹⁷ depends on the linewidth, $\Delta\nu$, of the cooling transition and predicts a temperature equal to $h\Delta\nu/2k_B$, where h is Planck's constant. For ${}^9\text{Be}^+$, $\Delta\nu = 19.4$ MHz which gives a limiting temperature of 0.5 mK. At a magnetic field of 10 T, the density, limited by the Brillouin density,^{14,20} could be as high as $n_0 = 3 \times 10^{10}/\text{cm}^3$ for ${}^9\text{Be}^+$ ions. Therefore, values of Γ as large as 15000 are perhaps accessible and crystallization in a nonneutral ion plasma might be obtained. We note that fairly direct measurements of the pair-correlation function could be made by observing interferences in the low-angle laser scattering from the ions, similar to x-ray crystallographic techniques. Ion diffusion (or lack thereof) could be measured by spatially separating the cooling probe beams (along z) and pulsing the probe beam similar to that described by Stern, Hill, and Rymer.¹⁸ Classical mechanics has been assumed to give an adequate description in the preceding discussions. At temperatures below $\hbar\Omega/k_B$, the discreteness of the Landau (quantized cyclotron) levels becomes important. At slightly lower temperatures, $T \leq \hbar\omega_p/k_B$, where $\omega_p = [2\omega(\Omega - \omega)]^{1/2}$ is the plasma frequency of the ions, the collective motion of the ions should be treated quantum mechanically.¹⁰ Both of these interesting regions may be accessible with ${}^9\text{Be}^+$ or perhaps other ions which have a much smaller radiative linewidth $\Delta\nu$ where even lower temperatures could be expected.

We gratefully acknowledge the support of the U. S. Office of Naval Research and the U. S. Air Force Office of Scientific Research. We thank T. M. O'Neil, W. M. Itano, and S. Barlow for reading the manuscript and for helpful comments. Special thanks go to J. D. Prestage for his help with the final data acquisition.

- ¹S. Ichimaru, *Rev. Mod. Phys.* **54**, 1017 (1982), and references therein.
- ²J. H. Malmberg, T. M. O'Neil, A. W. Hyatt, and C. F. Driscoll, *Bull. Am. Phys. Soc.* **28**, 1155 (1983).
- ³R. F. Wuerker, H. Shelton, and R. V. Langmuir, *J. Appl. Phys.* **30**, 342 (1959).
- ⁴C. C. Grimes and G. Adams, *Phys. Rev. Lett.* **42**, 795 (1979).
- ⁵D. J. Wineland, J. J. Bollinger, and W. M. Itano, *Phys. Rev. Lett.* **50**, 628, 1333(E) (1983).
- ⁶J. J. Bollinger, D. J. Wineland, W. M. Itano, and J. S. Wells, in *Laser Spectroscopy VI*, edited by H. P. Weber and W. Luthy, Springer Series in Optical Sciences Vol. 40 (Springer, Berlin, 1983), p. 168.
- ⁷J. H. Malmberg and J. S. deGrassie, *Phys. Rev. Lett.* **35**, 577 (1975).
- ⁸C. F. Driscoll and J. H. Malmberg, *Phys. Rev. Lett.* **50**, 167 (1983), and references therein.
- ⁹G. Dimonte, *Phys. Rev. Lett.* **46**, 26 (1981).
- ¹⁰J. H. Malmberg and T. M. O'Neil, *Phys. Rev. Lett.* **39**, 1333 (1977).
- ¹¹S. A. Prasad and T. M. O'Neil, *Phys. Fluids* **22**, 278 (1979).
- ¹²T. M. O'Neil and C. F. Driscoll, *Phys. Fluids* **22**, 266 (1979).
- ¹³F. M. Penning, *Physica (Utrecht)* **3**, 873 (1936).
- ¹⁴H. G. Dehmelt, *Adv. At. Mol. Phys.* **3**, 53 (1967), and **5**, 109 (1969); D. J. Wineland, W. M. Itano, and R. S. Van Dyck, Jr., *Adv. At. Mol. Phys.* **19**, 135 (1983).
- ¹⁵R. E. Drullinger, D. J. Wineland, and J. C. Bergquist, *Appl. Phys.* **22**, 365 (1980).
- ¹⁶W. M. Itano and D. J. Wineland, *Phys. Rev. A* **24**, 1364 (1981).
- ¹⁷W. M. Itano and D. J. Wineland, *Phys. Rev. A* **25**, 35 (1982); D. J. Wineland and W. M. Itano, *Phys. Rev. A* **20**, 1521 (1979).
- ¹⁸W. L. Slatterly, G. D. Doolen, and H. E. DeWitt, *Phys. Rev. A* **21**, 2087 (1980).
- ¹⁹J. P. Hansen, *Phys. Rev. A* **8**, 3096 (1973).
- ²⁰R. C. Davidson, *Theory of Nonneutral Plasmas* (Benjamin, Reading Mass., 1974), p. 4.
- ²¹R. A. Stern, D. N. Hill, and N. Rynn, *Phys. Lett.* **93A**, 127 (1983).

Laser-Cooled-Atomic Frequency Standard

J. J. Bollinger, J. D. Prestage, Wayne M. Itano, and D. J. Wineland
Time and Frequency Division, National Bureau of Standards, Boulder, Colorado 80303
 (Received 5 December 1984)

The first frequency standard based on laser-cooled atoms is reported. Beryllium atomic ions were stored in a Penning trap and cooled by radiation pressure from a laser. The frequency of the ${}^9\text{Be}^+$ ($M_I, M_J = (-\frac{3}{2}, +\frac{1}{2}) \rightarrow (-\frac{1}{2}, +\frac{1}{2})$) ground-state hyperfine transition at its magnetic-field-independent point was determined to be 303 016 377.265 070(57) Hz. The accuracy of a frequency standard referenced to this transition was comparable to the best frequency standards, which are based on cesium atomic beams.

PACS numbers: 32.30.Bv, 06.30.Ft, 35.70.Fk

The principle of laser cooling was introduced^{1,2} as a way of suppressing both first- and second-order Doppler shifts in high-resolution spectroscopy. Aside from the interest in the physics of the cooling process itself, two of the primary goals of this technique are more accurate atomic spectroscopy and improved frequency standards. This has been noted in the experimental and theoretical reports on trapped ions,³⁻⁶ cooled atomic beams,⁷⁻⁹ and trapped neutrals.⁹⁻¹³ As a step toward these goals we report an accurate measurement of ${}^9\text{Be}^+$ ground-state hyperfine structure and present results on the first frequency (and time) standard based on laser-cooled atoms. Such experiments provide improved measurements of hyperfine constants and g -factor ratios.⁵ In addition, they could lead to measurements of previously undetected physical quantities and improvements in previous experimental tests. Examples include the measurement of deviations of atomic hyperfine structure from that predicted by the Breit-Rabi formula due, for example, to nuclear diamagnetism¹⁴ and various tests of gravitational interactions such as tests of spatial anisotropy (Hughes-Drever-type experiments).¹⁵

In the experiment reported here, ${}^9\text{Be}^+$ ions were confined in high vacuum ($< 10^{-7}$ Pa) by the static magnetic and electric fields of a Penning trap.⁵ The long confinement times and benign environment of the Penning trap are beneficial for high-resolution spectroscopy.⁵ The three axially symmetric electrodes of this trap provide an electrostatic potential of the form $\phi_T = A(2z^2 - r^2)$, where r and z are cylindrical coordinates. For $A > 0$, positive ions experience a harmonic restoring force along \hat{z} . A uniform magnetic field parallel to \hat{z} provides confinement in the radial direction. Ion radial motion is a superposition of circular cyclotron motion and a circular $\mathbf{E} \times \mathbf{B}$ drift "magnetron" motion about the axis of the trap.

An essential feature of this experiment was the reduction of the source of the largest systematic uncertainty, the second-order Doppler shift, by reduction of the ion kinetic energy with radiation pressure from a laser.¹⁻⁵ Cooling of the axial and cyclotron motions of a trapped ion by a laser beam tuned slightly lower in

frequency than a strongly allowed resonance transition can be understood by considering the following one-dimensional model. Suppose that the ions are constrained to move along the z axis in a harmonic well and assume that a laser is directed at the ions along \hat{z} . An ion absorbs and reemits photons predominantly when its velocity is directed against the laser beam, because the light frequency in the ion's frame is Doppler shifted into resonance. When averaged over all angles of reemission, the ion's momentum is reduced by h/λ per scattered photon, where λ is the laser wavelength. The "cooling" laser also couples with the magnetron motion and can be used to reduce the radius of the magnetron orbit and therefore compress the radius of the ion "cloud."^{3,16}

Specifically, in this experiment a narrow-band (< 4 MHz) radiation source (power $\approx 20 \mu\text{W}$) tuned to the low-frequency side of the

$$2s^2S_{1/2}(M_I = -\frac{3}{2}, M_J = -\frac{1}{2}) \\ - 2p^2P_{3/2}(-\frac{3}{2}, -\frac{3}{2})$$

($\lambda = 313$ nm) transition of ${}^9\text{Be}^+$ was used to cool and spatially compress the ions and optically pump them into the $(-\frac{3}{2}, -\frac{1}{2})$ ground state.¹⁶ The 313-nm source was obtained by frequency doubling of the output of a single-mode cw dye laser. The resonance fluorescence induced by this cooling laser was used to detect the ions.^{16,17} The size, density, and temperature of the ion clouds were determined by use of a similar radiation source as a probe.¹⁷ Typical clouds ranged from a few hundred to 2000 ions with cloud diameters from 300 to 500 μm and densities of about 3×10^7 ions/cm³. Cyclotron and axial temperatures of less than 100 mK and effective magnetron temperatures of less than 2 K were obtained with the cooling laser applied continuously. Ion storage times were many hours without the laser applied; with the laser applied, ion loss is negligible.

At a magnetic field of about 0.8194 T [ground state $(-\frac{3}{2}, -\frac{1}{2}) \rightarrow (-\frac{3}{2}, \frac{1}{2})$ electron spin-flip frequency of 23 914.01 MHz], the $(-\frac{3}{2}, \frac{1}{2}) \rightarrow (-\frac{1}{2}, \frac{1}{2})$ ground-state hyperfine transition, ν_1 (see Fig. 1),

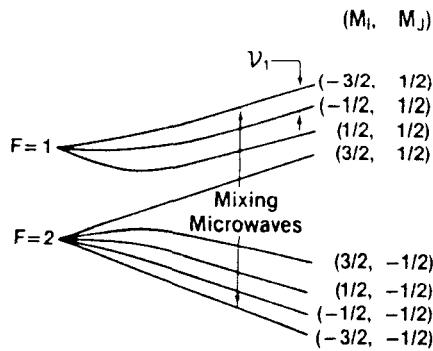


FIG. 1. Hyperfine structure (not drawn to scale) of the ${}^9\text{Be}^+ 2s^2S_{1/2}$ ground state as a function of magnetic field. ν_1 is independent of magnetic field to first order at $B = 0.8194$ T.

depends only quadratically on the magnetic field deviation, δB , as $\delta\nu_1/\nu_1 = -0.017(\delta B/B)^2$. The ν_1 transition was detected by optical-microwave-rf triple resonance. Microwave radiation tuned to the electron spin-flip resonance transferred half of the ion population from the optically pumped $(-\frac{3}{2}, -\frac{1}{2})$ state to the $(-\frac{3}{2}, +\frac{1}{2})$ state. Some of the $(-\frac{3}{2}, +\frac{1}{2})$ state population was transferred to the $(-\frac{1}{2}, +\frac{1}{2})$ state by application of rf near the 303-MHz ν_1 transition frequency. As a result of the microwave mixing this resulted in an additional decrease in the $(-\frac{3}{2}, -\frac{1}{2})$ state population and therefore a decrease in the observed fluorescence.

Ramsey's method of separated oscillatory fields¹⁸ was used to interrogate ν_1 . An rf pulse of duration t was applied, followed by a free precession interval of duration T and a second rf pulse of duration t coherent with the first pulse. Data were taken with $T = 10$ s and $t = 0.1, 0.5,$ and 2.0 s, and with $T = 19$ s and $t = 0.5$ s. Typically the cooling laser and mixing microwaves were on for a period of 3 s, during which the ${}^9\text{Be}^+$ ions were prepared in the $(-\frac{3}{2}, -\frac{1}{2})$ and $(-\frac{3}{2}, +\frac{1}{2})$ states. The cooling laser and mixing microwaves were then turned off in order to avoid light and ac Zeeman shifts during the interrogation period. After the interrogation period, the laser and microwaves were turned back on, and the signal was obtained from the fluorescence count rate during the first 0.3 s of this time interval. Figure 2 shows the signal obtained for the $(t, T) = (0.5 \text{ s}, 19 \text{ s})$ interrogation. The linewidth $\Delta\nu_1 = 25$ mHz gives a $Q \equiv \nu_1/\Delta\nu_1$ of 1.2×10^{10} on the 303-MHz ν_1 transition frequency.

A synthesized rf source near 303 MHz was used to probe ν_1 . A passive hydrogen maser [fractional frequency stability¹⁹ $\sigma_y(\tau) = 1.5 \times 10^{-12}\tau^{-1/2}$ for measurement time τ in seconds; frequency drift $< 3 \times 10^{-16}/\text{d}$] was used as the external reference for this source. A computer alternately stepped the rf frequency by $\pm \Delta\nu_1/2$ about a calculated frequency f_i . After each rf frequency step, a measurement of the

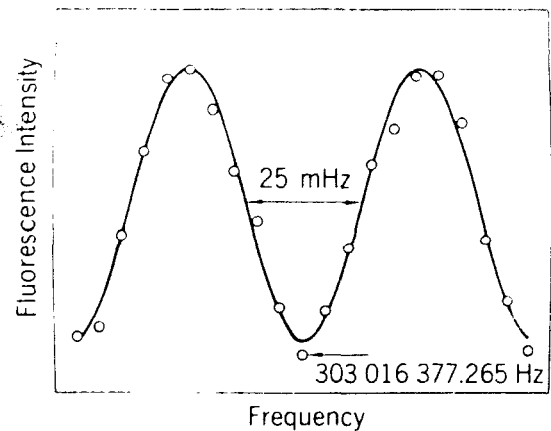


FIG. 2. Signal obtained on the ν_1 field-independent transition for $(t, T) = (0.5 \text{ s}, 19 \text{ s})$. The sweep width was 100 mHz and the frequency interval between points was 5 mHz. The dots are experimental and are the average of ten sweeps; the curve is a least-squares fit.

signal was made and a new frequency f_{i+1} was obtained about which the next rf step was made. f_{i+1} was obtained through a digital servo system which steered the frequencies $\{f_i\}$ to the ν_1 transition frequency in a way that was independent of a linear drift in the total count rate.²⁰⁻²²

Data were taken without interruption for a period of approximately 2 h. After this, the run was stopped and the magnetic field measured and reset if necessary. The average frequency and $\sigma_y(\tau)$ were calculated from the frequencies $\{f_i\}$. For each run, $\sigma_y(\tau)$ was fitted to a $\tau^{-1/2}$ dependence for τ greater than the servo attack time (~ 100 s). A total of sixty runs were used in the final determination of the ν_1 transition frequency. For the 29 runs with a $(0.5 \text{ s}, 19 \text{ s})$ Ramsey interrogation, $\sigma_y(\tau)$ ranged from $1.3 \times 10^{-11}\tau^{-1/2}$ to $4 \times 10^{-11}\tau^{-1/2}$. The statistical uncertainty of the average frequency of each run was estimated from the fitted $\sigma_y(\tau)$ at τ equal to the total measurement time of the run. A weighted-average frequency for each group of identical (t, T) interrogations was calculated.

In order to determine the frequency offset due to the second-order Doppler or time dilation effect, the cyclotron and axial temperatures of the ions were measured (via optical Doppler broadening) as a function of the time that the cooling laser was turned off by a technique similar to that discussed in Ref. 17. Figure 3 shows the results of these measurements on typical ion clouds. The heating shown in Fig. 3 produced a second-order Doppler shift, $-\langle v^2/2c^2 \rangle \nu_1$, of $-107(27) \mu\text{Hz}$ for the $(0.5 \text{ s}, 19 \text{ s})$ interrogation. The contribution of the magnetron rotation of the cloud to the second-order Doppler shift was almost an order of magnitude less. The weighted-average frequency of each (t, T) interrogation was corrected for the total second-order Doppler shift. The weighted average of the resulting frequencies provided (if further sys-

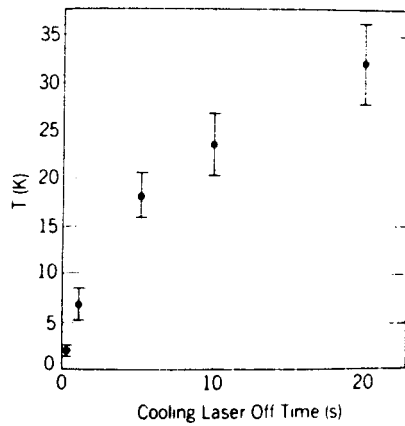


FIG. 3. Temperature, T , of the cyclotron and axial motions as a function of the length of time that the cooling laser is off.

tematic corrections are neglected) a $33\text{-}\mu\text{Hz}$ (1.1×10^{-13}) one-standard-deviation determination of the ν_1 transition frequency relative to the passive hydrogen maser reference.

Table I lists the estimated systematic errors. The 3 parts in 10^6 magnetic field fluctuations produced a small offset in the measured ν_1 frequency through the quadratic magnetic field dependence of ν_1 . Because ν_1 is a $\Delta m_F = \pm 1$ transition, there was a small shift due to the Earth's rotation. This shift arises because only one rotating component of the applied (linearly polarized) rf field was responsible for inducing the ν_1 transition. The ions may be viewed as being in an inertial frame with the laboratory (including the trap and applied rf field) rotating around the ions once per sidereal day. This produced a shift equal to $f_R \cos\beta$, where f_R is the rotation frequency of the Earth and β is the angle between the magnetic field and the Earth's rotation axis. Microwave leakage during the interrogation period could have produced a frequency shift in ν_1 as large as 1 part in 10^{14} . By stepping the rf synthesizer so that the sides of the ninth side lobes [in the (0.5 s, 19 s) interrogation], rather than the central Ramsey lobe, were sampled, a frequency shift in ν_1 due to a background slope was measured to be less than 5×10^{-15} . We estimated the frequency shift due to the blackbody electromagnetic field at 300 K to be $-3(3) \times 10^{-16}$.²³ Any frequency shift due to a coherence in the hyperfine states that survived the repumping period was eliminated by randomization of the phase of the rf before each interrogation period. Fractional shifts of the ground-state hyperfine frequency of $^{137}\text{Ba}^+$ (Vetter, Stuke, and Weber²⁴) and $^{199}\text{Hg}^+$ (Cutler, Giffard, and McGuire²⁵) due to He collisions have been measured to be about $5 \times 10^{-11}/\text{Pa}$ and $4 \times 10^{-11}/\text{Pa}$, respectively. On the basis of this, a frequency shift in ν_1 due to background neutral collisions with a vacuum better than 10^{-7} Pa was estimated to be much less than 1 part in 10^{15} . We have not considered

TABLE I. Estimated systematic errors. The size of the effect is the fraction of the transition frequency ν_1 .

Systematic effect	Size of effect
Second-order Doppler	$-38(9) \times 10^{-14}$
Magnetic field fluctuations	$-1.3(\pm 1.3) \times 10^{-14}$
Rotation of Earth	$-1.8(0.2) \times 10^{-14}$
Microwave leakage	$\leq 1 \times 10^{-14}$
Background slopes	$\leq 5 \times 10^{-15}$
Servo offsets	$\leq 5 \times 10^{-15}$
Blackbody radiation shift	$-3(3) \times 10^{-16}$
Coherence between cycles	$< 1 \times 10^{-15}$
Background gas collisions	$< 1 \times 10^{-15}$
Stark shifts	$< 1 \times 10^{-15}$
First-order Doppler	$< 1 \times 10^{-15}$
ac Zeeman shifts	$< 1 \times 10^{-15}$
Total systematic offset	$-41.1(9.4) \times 10^{-14}$

any possible frequency shifts due to the presence of nearby conducting surfaces.²⁶ The systematic uncertainty of 9.4×10^{-14} is comparable to that of the U.S. cesium standard (8.5×10^{-14}).²⁷ The combined uncertainty due to the random error and the systematic errors of Table I was $34 \mu\text{Hz}$ (1.1×10^{-13}). The final measured frequency of the ν_1 transition was

$$\nu_1 = 303\,016\,377.265\,070(57) \text{ Hz},$$

where the uncertainty includes the 1.5 parts in 10^{13} uncertainty of the passive hydrogen maser frequency relative to the SI second.

The accuracy of the present measurement was limited by the second-order Doppler shift due to the ion heating shown in Fig. 3. The slow heating near the end of the interrogation period was consistent with collisional heating by the room-temperature background gas. The rapid heating observed immediately after the cooling laser was turned off may be caused by asymmetry-induced transport.²⁸ With the cooling laser off, axial asymmetries of the trap can increase the total canonical angular momentum of the ions, resulting in an increase in the ion-cloud radius. As the ion cloud expands, electrostatic potential energy of the ions due to the space-charge and trap electric fields is converted into thermal energy of the ions. The observed heating can possibly be reduced by improvement of the trap axial symmetry, by use of ion clouds of lower density, and by improvement of the vacuum. The use of a second ion (e.g., $^{24}\text{Mg}^+$) to "sympathetically" cool^{3,29} the $^9\text{Be}^+$ ions could help prevent the heating, whatever

er its cause. The $^{24}\text{Mg}^+$ cooling-laser beam could be applied continuously throughout the interrogation period and could keep the $^9\text{Be}^+$ ions cold by Coulomb coupling with the cold $^{24}\text{Mg}^+$ ions. Because of the centrifugal separation of the $^9\text{Be}^+$ and $^{24}\text{Mg}^+$ ions,³⁰ the overlap of the $^9\text{Be}^+$ ions with the $^{24}\text{Mg}^+$ cooling-laser beam could be made very small and result in an ac Stark shift on the ν_1 transition of less than 1 part in 10^{15} . Use of these techniques might result in more than an order of magnitude improvement in the performance of the present $^9\text{Be}^+$ frequency standard or one based on other ions.⁵

We gratefully acknowledge the support of the U.S. Air Force Office of Scientific Research and the U.S. Office of Naval Research. We thank F. L. Walls for information on the passive hydrogen maser, S. R. Stein for many helpful discussions, and J. C. Bergquist, H.-U. Daniel, and G. Leuchs for carefully reading the manuscript.

¹T. W. Hänsch and A. L. Schawlow, *Opt. Commun.* **13**, 68 (1975).

²D. J. Wineland and H. G. Dehmelt, *Bull. Am. Phys. Soc.* **20**, 637 (1975).

³D. J. Wineland, R. E. Drullinger, and F. L. Walls, *Phys. Rev. Lett.* **40**, 1639 (1978).

⁴W. Neuhauser, M. Hohenstatt, P. Toschek, and H. G. Dehmelt, *Phys. Rev. Lett.* **41**, 233 (1978); H. G. Dehmelt, *IEEE Trans. Instrum. Meas.* **31**, 83 (1982).

⁵D. J. Wineland, W. M. Itano, and R. S. Van Dyck, Jr., *Adv. At. Mol. Phys.* **19**, 135 (1983).

⁶R. Blatt, H. Schnatz, and G. Werth, *Phys. Rev. Lett.* **48**, 1601 (1982).

⁷V. I. Balykin, V. S. Letokhov, and V. I. Mushin, *Pis'ma Zh. Eksp. Teor. Fiz.* **29**, 614 (1979) [*JETP Lett.* **29**, 560 (1979)].

⁸W. D. Phillips and H. Metcalf, *Phys. Rev. Lett.* **48**, 596 (1982).

⁹*Laser Cooled and Trapped Atoms*, edited by W. D. Phillips, U.S. National Bureau of Standards Special Publication No. 653 (U.S. GPO, Washington, D.C., 1983), and *Prog. Quantum Electron.* **8**, 115 (1984).

¹⁰A. Ashkin and J. P. Gordon, *Opt. Lett.* **4**, 161 (1979).

¹¹W. H. Wing, *Phys. Rev. Lett.* **45**, 631 (1980).

¹²D. E. Pritchard, *Phys. Rev. Lett.* **51**, 1336 (1983).

¹³J. Dalibard, S. Reynaud, and C. Cohen-Tannoudji, *Opt. Commun.* **47**, 395 (1983).

¹⁴D. J. Larson, *Hyperfine Interactions* (North-Holland, Amsterdam, 1978), Vol. 4, p. 73.

¹⁵C. M. Will, *Theory and Experiment in Gravitational Physics* (Cambridge Univ. Press, Cambridge, 1981), p. 30; J. D. Prestage, J. J. Bollinger, W. M. Itano, and D. J. Wineland, to be published.

¹⁶W. M. Itano and D. J. Wineland, *Phys. Rev. A* **24**, 1364 (1981).

¹⁷J. J. Bollinger and D. J. Wineland, *Phys. Rev. Lett.* **53**, 348 (1984).

¹⁸N. F. Ramsey, *Molecular Beams* (Oxford Univ. Press, London, 1956).

¹⁹ $\sigma_y^2(\tau) = \langle [f_{i+1}(\tau) - f_i(\tau)]^2 / 2\bar{f}^2 \rangle$, where $f_i(\tau)$ is the i th measurement of the average frequency over a measurement time interval τ , the brackets denote an average over all measurements i , $\bar{f} = \langle f_i \rangle$, and zero dead time is assumed between measurements. See J. A. Barnes *et al.*, *IEEE Trans. Instrum. Meas.* **20**, 105 (1971).

²⁰M. Jardino, M. Desaintfuscien, R. Barillet, J. Viennet, P. Petit, and C. Audoin, *Appl. Phys.* **24**, 107 (1981).

²¹L. S. Cutler, R. P. Giffard, and M. D. McGuire, in *Proceedings of the Thirteenth Annual PTTI Applications and Planning Meeting, Washington, D.C., 1981* (NASA, Washington, D.C., 1982), NASA Publication No. 2220, p. 563.

²²J. J. Bollinger, W. M. Itano, and D. J. Wineland, in *Proceedings of the Thirty-Seventh Symposium on Frequency Control, Philadelphia, 1983* (Systematics General Corp., Wall Township, N.J., 1983), p. 37.

²³W. M. Itano, L. L. Lewis, and D. J. Wineland, *Phys. Rev. A* **25**, 1233 (1982).

²⁴J. Vetter, M. Stuke, and E. W. Weber, *Z. Phys. A* **273**, 129 (1975).

²⁵L. S. Cutler, R. P. Giffard, and M. D. McGuire, in *Proceedings of the Thirty-Seventh Annual Symposium on Frequency Control, Philadelphia, 1983* (Systematics General Corp., Wall Township, N.J., 1983), p. 32.

²⁶M. Babiker and G. Barton, *Proc. Roy. Soc. London, Ser. A* **326**, 255 (1972); G. L. Guttrich and K. W. Billman, *Phys. Lett.* **24A**, 53 (1967).

²⁷D. J. Wineland, D. W. Allan, D. J. Glaze, H. W. Hellwig, and S. Jarvis, *IEEE Trans. Instrum. Meas.* **25**, 453 (1976).

²⁸C. F. Driscoll and J. H. Malmberg, *Phys. Rev. Lett.* **50**, 167 (1983); D. L. Eggleston, T. M. O'Neil, and J. H. Malmberg, *Phys. Rev. Lett.* **53**, 982 (1984).

²⁹R. E. Drullinger, D. J. Wineland, and J. C. Bergquist, *Appl. Phys.* **22**, 365 (1980).

³⁰T. M. O'Neil, *Phys. Fluids* **24**, 1447 (1981).

Limits for Spatial Anisotropy by Use of Nuclear-Spin-Polarized ${}^9\text{Be}^+$ Ions

J. D. Prestage, J. J. Bollinger, Wayne M. Itano, and D. J. Wineland
Time and Frequency Division, National Bureau of Standards, Boulder, Colorado 80303
 (Received 28 February 1985)

The frequency of a nuclear spin-flip ($|\Delta m_I| = 1$) transition in ${}^9\text{Be}^+$ has been compared to the frequency of a hydrogen maser transition ($|\Delta F| = 1$, $\Delta m_F = 0$) to see if the relative frequencies depend on the orientation of the ${}^9\text{Be}^+$ ions in space. The present null result represents a decrease in the limits set by Hughes and Drever on a spatial anisotropy by a factor of about 300.

PACS numbers: 04.80.+z, 35.10.-d

In metric theories of gravity the influence of external gravitational fields on atomic structure is governed by the Einstein equivalence principle (EEP).¹ All metric theories (including general relativity) are based on the EEP which states that (i) all bodies fall in a given gravitational field with the same acceleration (weak equivalence principle), (ii) the outcome of any local nongravitational experiment is independent of the velocity and orientation of the freely falling apparatus [local Lorentz invariance, (LLI)], and (iii) the outcome of any local nongravitational experiment is independent of where and when in the universe it is performed. It follows from LLI that two different atomic clocks located at the same point in space-time will have relative rates that are independent of the velocity and orientation of the freely falling lab.

As a test of LLI the frequency of the $2^2S_{1/2}(M_I, M_J) = (-\frac{3}{2}, +\frac{1}{2}) \rightarrow (-\frac{1}{2}, +\frac{1}{2})$ (see Fig. 1) ground-state hyperfine transition in ${}^9\text{Be}^+$ (hereafter called the "clock" transition) has been compared to the frequency of a passive hydrogen maser² to see if a correlation between the relative rates of the two clocks and the orientation of the ${}^9\text{Be}^+$ nuclear spin in space can be found. Such clock-comparison experiments are interpreted as the most precise tests of LLI.^{1,3}

Various proposals for violations of LLI have been made. One of these is a coupling of a particle's spin to the gravitational field,⁴ $U_g = U_n \mathbf{I} \cdot \hat{\mathbf{r}} + U_e \mathbf{S} \cdot \hat{\mathbf{r}}$, where U_n and U_e are the strengths of the coupling for a nucleon

and electron spin, respectively, and $\hat{\mathbf{r}}$ is the unit vector from the atom to the source of the field. This interaction violates parity (P) and time-reversal (T) invariance. Similarly, and LLI-violating and P -nonconserving coupling of a particle's spin to its motion with velocity \mathbf{V} relative to some preferred frame of reference of the form $U_v = K_n \mathbf{I} \cdot \mathbf{V} + K_e \mathbf{S} \cdot \mathbf{V}$ has been proposed.⁵ These couplings produce a shift of the ${}^9\text{Be}^+$ clock transition proportional to $\cos\beta$ where β is the angle between the quantization axis for the ions and the direction of $\hat{\mathbf{r}}$ or \mathbf{V} . The hydrogen maser transition ($F=1, M_F=0 \rightarrow F=0, M_F=0$) is not sensitive to these perturbations in first order because, in the low operating magnetic field of the maser ($\sim 100 \mu\text{G}$) the proton and electron spins couple together so that $\langle \mathbf{I} \cdot \hat{\mathbf{r}} \rangle = \langle \mathbf{S} \cdot \hat{\mathbf{r}} \rangle = 0$ for any direction $\hat{\mathbf{r}}$, where the averaging is done in either of the two maser states.

Another LLI-violating interaction which shifts the relative rates of the ${}^9\text{Be}^+$ and maser clocks was originally proposed by Cocconi and Salpeter as a model for inertial mass.⁶ The model is motivated by Mach's principle which states that a body's inertial mass is determined by the total distribution of matter in the universe. Since matter in the nearby universe is distributed anisotropically, inertial mass could show a corresponding anisotropy. Indeed, in this model the mass of an orbiting nucleon (orbital angular momentum $l \geq 1$) will depend upon the orientation of its orbit relative to the direction of the matter anisotropy. This interaction leads to a shift of the ${}^9\text{Be}^+$ clock transition proportional to $P_2(\cos\beta) = (3\cos^2\beta - 1)/2$, where β is now the angle between the quantization axis for the ${}^9\text{Be}^+$ ions and the direction of matter anisotropy in the nearby universe (e.g., the direction toward the galactic center or Virgo supercluster center). Searches for frequency shifts of NMR transitions in ${}^7\text{Li}$ which were correlated with the direction toward the galactic center were made by Hughes and co-workers⁷ and Drever⁸ and their null results ruled out the Cocconi-Salpeter model. It should be stated that in their model of inertial mass, Cocconi and Salpeter computed the change in kinetic energy of an orbiting nucleon induced by a spatial anisotropy. Others^{9,10} have pointed out that when anisotropic effects on both kinetic and potential

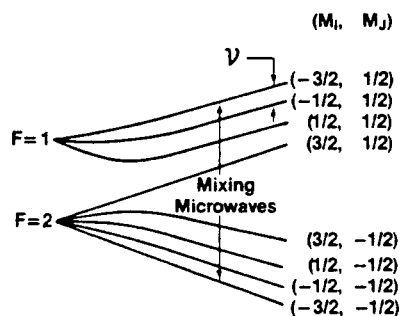


FIG. 1. Hyperfine structure (not drawn to scale) of the ${}^9\text{Be}^+ 2s^2S_{1/2}$ ground state as a function of magnetic field. ν is a first-order magnetic field-independent transition at 0.819 T.

energies are considered, the null results are to be expected provided that the anisotropy couples in the same way to both forms of energy. These experiments can thus be regarded as a test of the universal coupling of gravity to all forms of mass-energy.^{1,3}

Models of electrodynamics in a gravitational field which include the possibility of nonuniversal couplings are the Dicke-Peebles-Ni formalism^{10,11} and the $TH\epsilon\mu$ formalism.^{1,3,12} In the $TH\epsilon\mu$ formalism the parameters T_0 and H_0 describe the coupling of gravity to material particles while ϵ_0 and μ_0 describe gravity's coupling to electromagnetic fields. In this formalism the limiting speed for material particles is c_0 while the

speed of light is c_{light} , where $c_0/c_{\text{light}} = (T_0\epsilon_0\mu_0/H_0)^{1/2}$.

If $c_0 \neq c_{\text{light}}$ an electromagnetically bound system of charged particles experiences a coupling between its internal structure and center-of-mass motion. This produces a contribution $\delta E = \sum \delta m^{ij} V^i V^j$ to the electromagnetic part of the nuclear binding energy. δm^{ij} is the anomalous inertial mass tensor^{1,3} which depends upon the electromagnetic structure of the nucleus and \mathbf{V} is the velocity of the nucleus through some preferred frame. This could be the rest frame of the sun or the mean rest frame of the universe (defined as the frame in which the cosmic 3-K background radiation is isotropic).¹³

In the $TH\epsilon\mu$ formalism¹⁴

$$\delta E \cong -\frac{1}{4} \left[1 - \frac{T_0\epsilon_0\mu_0}{H_0} \right] \left\langle \frac{e^2}{c^2} \sum_{i \neq j} \frac{1}{r_{ij}^3} \left[(\mathbf{r}_{ij} \cdot \mathbf{V})^2 - \frac{r_{ij}^2 V^2}{3} \right] \right\rangle_{I, M_I}, \quad (1)$$

where \mathbf{r}_{ij} is the coordinate vector from the i th to j th nuclear proton, e is the proton charge, c is the speed of light, and the summation is over the Z protons. Use of the Wigner-Eckart theorem gives

$$\delta E \cong -\frac{1}{4} \left[1 - \frac{T_0\epsilon_0\mu_0}{H_0} \right] \frac{3M_I^2 - I(I+1)}{I(2I-1)} \frac{e^2}{c^2} \left\langle \sum_{i \neq j} \frac{(\mathbf{r}_{ij} \times \mathbf{r}_{ij})_0^{(2)}}{r_{ij}^3} \right\rangle_{I, M_I} (\mathbf{V} \times \mathbf{V})_0^{(2)}, \quad (2)$$

where $(\dots)_M^{(J)}$ denotes the J, M spherical component of the tensor in parenthesis. The resulting variation in the ${}^9\text{Be}^+$ clock transition frequency is

$$\delta\nu \cong \left[1 - \frac{T_0\epsilon_0\mu_0}{H_0} \right] \frac{(Z-1)e^2 Q}{6hR^3} \frac{V^2}{c^2} P_2(\cos\beta), \quad (3)$$

where Q and R are the electric quadrupole moment and charge radius of the ${}^9\text{Be}$ nucleus. We have used the following estimate for the nuclear matrix element¹⁵:

$$e^2 \left\langle \sum_{i \neq j} \frac{(\mathbf{r}_{ij} \times \mathbf{r}_{ij})_0^{(2)}}{r_{ij}^3} \right\rangle_{I, M_I} \cong \frac{(Z-1)e^2 Q}{\sqrt{6}R^3}. \quad (4)$$

These quadrupolar perturbations do not shift the hydrogen-maser transition frequency. Finally because the ${}^9\text{Be}^+$ nuclear spin is $I = \frac{3}{2}$, we are sensitive to shifts of the clock transition up to order $P_3(\cos\beta)$ but no higher.

A discussion of the Be^+ clock is given by Bollinger *et al.*¹⁶ A few hundred to 2000 ${}^9\text{Be}^+$ ions are stored in a Penning trap.¹⁷ The ions are cooled and optically pumped (95%) into the $2^2S_{1/2}(M_I, M_J) = (-\frac{3}{2}, -\frac{1}{2})$ ground state by radiation from a frequency-doubled dye laser ($\lambda = 313$ nm, power $\cong 20$ μW) which is tuned slightly below the $2^2S_{1/2}(-\frac{3}{2}, -\frac{1}{2}) \rightarrow 2^2P_{3/2}(-\frac{3}{2}, -\frac{3}{2})$ transition frequency.^{16,17} At this frequency the ions absorb radiation more strongly when their motion is toward the laser than when they move away from it. When averaged over all angles of reemission, the ion's momentum is reduced by h/λ per scattered photon where λ is the laser wavelength and h is Planck's constant. This results in a cooling of

the Be^+ cloud to about 1 K. The observed intensity of the scattered fluorescent light from the $2^2S_{1/2}(-\frac{3}{2}, -\frac{1}{2}) \rightarrow 2^2P_{3/2}(-\frac{3}{2}, -\frac{3}{2})$ transition is proportional to the population of the $(-\frac{3}{2}, -\frac{1}{2})$ ground state.

At a magnetic field of about 0.8194 T [ground-state $(-\frac{3}{2}, -\frac{1}{2}) \rightarrow (-\frac{3}{2}, \frac{1}{2})$ electron spin-flip frequency of 23 914.01 MHz], the clock transition frequency, ν , depends only quadratically on the magnetic field deviation, δB , as $\delta\nu/\nu = -0.017(\delta B/B)^2$. The clock transition is detected by optical-microwave-rf triple resonance. Microwave radiation tuned to the electron spin-flip resonance transfers half of the ion population from the optically pumped $(-\frac{3}{2}, -\frac{1}{2})$ state to the $(-\frac{3}{2}, +\frac{1}{2})$ state. Some of the $(-\frac{3}{2}, +\frac{1}{2})$ state population is transferred to the $(-\frac{1}{2}, +\frac{1}{2})$ state by application of rf near the 303-MHz clock transition frequency. Because of the microwave mixing this results in an additional decrease in the $(-\frac{3}{2}, -\frac{1}{2})$ state population and therefore a decrease in the observed fluorescence.

The clock transition is driven by a synthesizer using Ramsey's separated oscillatory fields technique¹⁸ with 0.5-s coherent Rabi pulses separated by a 19-s free-precession period. A computer adjusts the frequency of the synthesizer so that it remains centered on the clock transition. The time base for this synthesizer is provided by a passive hydrogen maser. Any shift of the ${}^9\text{Be}^+$ transition frequency relative to the maser transition will appear as a variation of the synthesizer's frequency. In a 2-h measurement period the signal-

to-noise ratio was sufficient to locate the center of the 25-mHz-wide clock resonance to better than 0.5%. The results of 29 such measurements taken between 7 May and 15 June, 1984 are shown plotted against sidereal time in Fig. 2.¹⁹

Because the Earth rotates, the angle β changes throughout the day. That is, $\beta = \beta(\tau)$ where τ is the sidereal time. For example, consider the direction of motion through the mean rest frame of the universe. Our laboratory is at 40° north latitude and our magnetic field is horizontal and directed 232° from geographic north (i.e., almost southeast). Thus, at 3^h sidereal time $\beta = 158^\circ$ while at 15^h, $\beta = 34^\circ$. Since the magnetic field direction is not changed with respect to the vertical we are insensitive to any shifts of the ${}^9\text{Be}^+$ transition caused by the Earth's gravitational field.

We have searched for a variation in the clock transition frequency of the form

$$\nu = \nu_0 + A_k P_k(\cos\beta(\tau)) \quad (5)$$

($k = 1, 2,$ or 3) where A_k measures the magnitude of any LLI violation. The results of a least-squares fit of the function of Eq. (5) to the data of Fig. 2 is shown in Table I. Also shown in that table is the direction in space which determines the angle $\beta(\tau)$. The errors are the quadrature sum of the statistical error (one sigma) and a 27- μHz uncertainty in the variation of the second-order Doppler shift of the clock transition over the 29 runs. This shift arises because, to avoid light shifts of the clock transition, during the 20-s Ramsey interrogation period the ions are not laser cooled and consequently heat up from about 1 K to about 30 K. Also, magnetic field measurements at the beginning and the end of each run indicate a field deviation of $\delta B/B \cong \pm 1.5 \times 10^{-6}$. This leads to a peak-to-peak frequency fluctuation of the clock transition of about 12 μHz over the 29 runs. These were the two largest systematic errors in this measurement, although several other effects were considered.¹⁶ Fluctuations

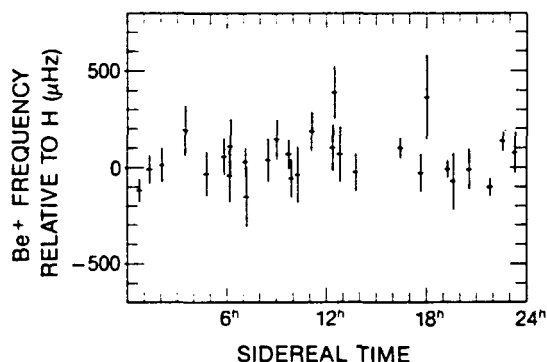


FIG. 2. Variation of the ${}^9\text{Be}^+$ clock transition frequency referenced to a passive hydrogen maser plotted against sidereal time. Tick marks on the vertical scale are 100 μHz apart.

in any of the systematic errors could potentially mimic a $P_k(\cos\beta(\tau))$ variation but the amplitude of such variations would be below our quoted uncertainty.

In addition to the directions listed in Table I we have also fitted the data of Fig. 2 for an arbitrary direction (excluding those directions within 10° of the Earth's rotational axis where our sensitivity is reduced). We find that all resulting values of A_k are consistent with zero at the 100- μHz level.

In the direction of the galactic center, our present limit on $|A_2|$ (in ${}^9\text{Be}^+$) of $50 + 42 = 92 \mu\text{Hz}$ is about a factor of 200 improvement over the limit of Hughes and co-workers⁷ and Drever⁸ on $|A_2|$ (in ${}^7\text{Li}$) for the same direction. For the direction of the Earth's motion through the mean rest frame of the universe, we take 81 μHz as the limit on $|A_2|$. Using Eq. (3) and $V^2/c^2 \cong 10^{-6}$ (Ref. 13) we place a limit on the $TH\epsilon\mu$ preferred-frame parameter^{1,3} of $|1 - T_0\epsilon_0\mu_0 \times H_0^{-1}| \leq 10^{-18}$. This is about 300 times smaller than the Hughes-Drever limit on this parameter if we use their limit on A_2 in the direction of the galactic center and the same method for estimating the nuclear matrix element [Eq. (4)]. The limits on A_1 are comparable with limits set by other workers²⁰ while the limits on A_3 are new. From the limit on A_1 we find that $U_n K_n |V| \leq 100 \mu\text{Hz}$ and because $\langle S_z \rangle$ differs for the two levels of the clock transition by about 2×10^{-4} , we find $U_e K_e |V| \leq 0.50 \text{ Hz}$. Although the limits established here can be regarded as a test of LLI, we wish to emphasize that they set an upper limit on *any* dependence of the relative clock rates on their orientation with respect to the sun or the fixed stars, whether from a breakdown of LLI or some other cause, such as a new interaction.

It should be possible to improve the sensitivity of the present measurement by more than an order of magnitude.¹⁶ A search for a $P_1(\cos\beta)$ interaction due to the Earth's gravitational field would be facilitated by orienting the experimental magnetic field along the

TABLE I. Variation of the ${}^9\text{Be}^+$ clock transition frequency, ν , measured relative to a passive hydrogen maser. A_k is a measure of any LLI violation, $\nu = \nu_0 + A_k P_k(\cos\beta(\tau))$, where β is the angle between the ${}^9\text{Be}^+$ quantization axis and the direction in space given in the table. τ is sidereal time.

Direction	A_k (μHz)		
	A_1	A_2	A_3
Motion through mean rest frame of the universe	35 ± 40	35 ± 46	13 ± 54
Motion through solar rest frame	36 ± 42	30 ± 51	9 ± 63
Galactic center	-49 ± 38	-50 ± 42	-15 ± 46
Virgo supercluster	20 ± 40	0 ± 49	9 ± 57
Sun	40 ± 39	-58 ± 43	16 ± 47

vertical. It should also be possible to make such measurements similar to the present one using nuclear magnetic resonance techniques on neutral atoms.^{20,21} In fact, relevant data may already exist from NMR gyroscope experiments.²²

We gratefully acknowledge the support of the U. S. Air Force Office of Scientific Research and the U. S. Office of Naval Research. We thank F. L. Walls for information on the passive hydrogen maser and gratefully acknowledge helpful discussions with M. P. Haugan. We thank C. M. Will, S. R. Stein, and D. W. Allan for carefully reading the manuscript.

¹C. M. Will, *Theory and Experiment in Gravitational Physics* (Cambridge Univ. Press, Cambridge, 1981).

²D. Howe and F. Walls, *IEEE Trans. Instrum. Meas.* **32**, 218 (1983).

³M. P. Haugan, *Ann. Phys. (N.Y.)* **118**, 156 (1979), and doctoral dissertation, Stanford University, 1978 (unpublished).

⁴J. Leitner and S. Okubo, *Phys. Rev.* **136**, B1542 (1964); N. D. Hari Dass, *Phys. Rev. Lett.* **36**, 393 (1976).

⁵P. R. Phillips and D. Woolum, *Nuovo Cimento* **64B**, 28 (1969).

⁶G. Cocconi and E. Salpeter, *Nuovo Cimento* **10**, 646 (1958).

⁷V. W. Hughes, H. G. Robinson, and V. Beltran-Lopez, *Phys. Rev. Lett.* **4**, 342 (1960); S. A. Lewis, W. L. Williams, and V. W. Hughes, *Bull. Am. Phys. Soc.* **11**, 121 (1966); W. L. Williams, doctoral dissertation, Yale University, 1966 (unpublished).

⁸R. W. P. Drever, *Philos. Mag.* **6**, 683 (1961).

⁹S. T. Epstein, *Nuovo Cimento* **16**, 587 (1960); R. H. Dicke, *Phys. Rev. Lett.* **7**, 359 (1961).

¹⁰W.-T. Ni, in *Proceedings of the 1983 International School Symposium on Precision Measurement and Gravitational Experiments*, edited by W.-T. Ni (National Tsing Hua University, Taiwan, China, 1983), p. 519.

¹¹P. J. Peebles and R. H. Dicke, *Phys. Rev.* **127**, 629 (1962).

¹²A. P. Lightman and D. L. Lee, *Phys. Rev. D* **8**, 364 (1973).

¹³P. M. Lubin, G. L. Epstein, and G. F. Smoot, *Phys. Rev. Lett.* **50**, 616 (1983); D. J. Fixsen, E. S. Cheng, and D. J. Wilkinson, *Phys. Rev. Lett.* **50**, 620 (1983).

¹⁴The interaction between two charged particles in the $TH\epsilon\mu$ formalism is given in Eq. (4.13) of Ref. 3. Equation (1) here is the total interaction for a collection of such particles.

¹⁵M. P. Haugan is currently making a more detailed calculation of this matrix element.

¹⁶J. J. Bollinger, J. D. Prestage, W. M. Itano, and D. J. Wineland, *Phys. Rev. Lett.* **54**, 1000 (1985).

¹⁷H. G. Dehmelt, *Adv. At. Mol. Phys.* **3**, 53 (1967), and **5**, 109 (1969); D. J. Wineland, W. M. Itano, and R. S. Van Dyck, Jr., *Adv. At. Mol. Phys.* **19**, 135 (1983).

¹⁸N. F. Ramsey, *Molecular Beams* (Oxford Univ. Press, London, 1956).

¹⁹Preliminary results of this experiment were presented at the Ninth International Conference on Atomic Physics Satellite Workshop on Ion Trapping, Seattle, Washington, July 1984 (unpublished).

²⁰D. J. Wineland and N. F. Ramsey, *Phys. Rev. A* **5**, 821 (1972); J. C. Gallop and B. W. Petley, *Nature (London)* **303**, 53 (1983).

²¹B. C. Grover, *Phys. Rev. A* **28**, 2521 (1983); F. J. Raab, in *Proceedings of the Ninth International Conference on Atomic Physics, Seattle, Washington, 1984*, edited by R. S. Van Dyck, Jr., et al. (World Scientific, Singapore, 1985); T. E. Chupp, private communication.

²²E. Kanegsberg, *Proc. SPIE-Int. Soc. Opt. Eng.* **157**, 73 (1978).

NBS *Technical Publications*

Periodical

Journal of Research—The Journal of Research of the National Bureau of Standards reports NBS research and development in those disciplines of the physical and engineering sciences in which the Bureau is active. These include physics, chemistry, engineering, mathematics, and computer sciences. Papers cover a broad range of subjects, with major emphasis on measurement methodology and the basic technology underlying standardization. Also included from time to time are survey articles on topics closely related to the Bureau's technical and scientific programs. Issued six times a year.

Nonperiodicals

Monographs—Major contributions to the technical literature on various subjects related to the Bureau's scientific and technical activities.

Handbooks—Recommended codes of engineering and industrial practice (including safety codes) developed in cooperation with interested industries, professional organizations, and regulatory bodies.

Special Publications—Include proceedings of conferences sponsored by NBS, NBS annual reports, and other special publications appropriate to this grouping such as wall charts, pocket cards, and bibliographies.

Applied Mathematics Series—Mathematical tables, manuals, and studies of special interest to physicists, engineers, chemists, biologists, mathematicians, computer programmers, and others engaged in scientific and technical work.

National Standard Reference Data Series—Provides quantitative data on the physical and chemical properties of materials, compiled from the world's literature and critically evaluated. Developed under a worldwide program coordinated by NBS under the authority of the National Standard Data Act (Public Law 90-396).

NOTE: The Journal of Physical and Chemical Reference Data (JPCRD) is published quarterly for NBS by the American Chemical Society (ACS) and the American Institute of Physics (AIP). Subscriptions, reprints, and supplements are available from ACS, 1155 Sixteenth St., NW, Washington, DC 20056.

Building Science Series—Disseminates technical information developed at the Bureau on building materials, components, systems, and whole structures. The series presents research results, test methods, and performance criteria related to the structural and environmental functions and the durability and safety characteristics of building elements and systems.

Technical Notes—Studies or reports which are complete in themselves but restrictive in their treatment of a subject. Analogous to monographs but not so comprehensive in scope or definitive in treatment of the subject area. Often serve as a vehicle for final reports of work performed at NBS under the sponsorship of other government agencies.

Voluntary Product Standards—Developed under procedures published by the Department of Commerce in Part 10, Title 15, of the Code of Federal Regulations. The standards establish nationally recognized requirements for products, and provide all concerned interests with a basis for common understanding of the characteristics of the products. NBS administers this program as a supplement to the activities of the private sector standardizing organizations.

Consumer Information Series—Practical information, based on NBS research and experience, covering areas of interest to the consumer. Easily understandable language and illustrations provide useful background knowledge for shopping in today's technological marketplace.

Order the above NBS publications from: Superintendent of Documents, Government Printing Office, Washington, DC 20402.

Order the following NBS publications—FIPS and NBSIR's—from the National Technical Information Service, Springfield, VA 22161.

Federal Information Processing Standards Publications (FIPS PUB)—Publications in this series collectively constitute the Federal Information Processing Standards Register. The Register serves as the official source of information in the Federal Government regarding standards issued by NBS pursuant to the Federal Property and Administrative Services Act of 1949 as amended, Public Law 89-306 (79 Stat. 1127), and as implemented by Executive Order 11717 (38 FR 12315, dated May 11, 1973) and Part 6 of Title 15 CFR (Code of Federal Regulations).

NBS Interagency Reports (NBSIR)—A special series of interim or final reports on work performed by NBS for outside sponsors (both government and non-government). In general, initial distribution is handled by the sponsor; public distribution is by the National Technical Information Service, Springfield, VA 22161, in paper copy or microfiche form.

U.S. Department of Commerce
National Bureau of Standards
Gaithersburg, MD 20899

Official Business
Penalty for Private Use \$300



POSTAGE AND FEES PAID
U.S. DEPARTMENT OF COMMERCE
COM-215

SPECIAL FOURTH-CLASS RATE
BOOK